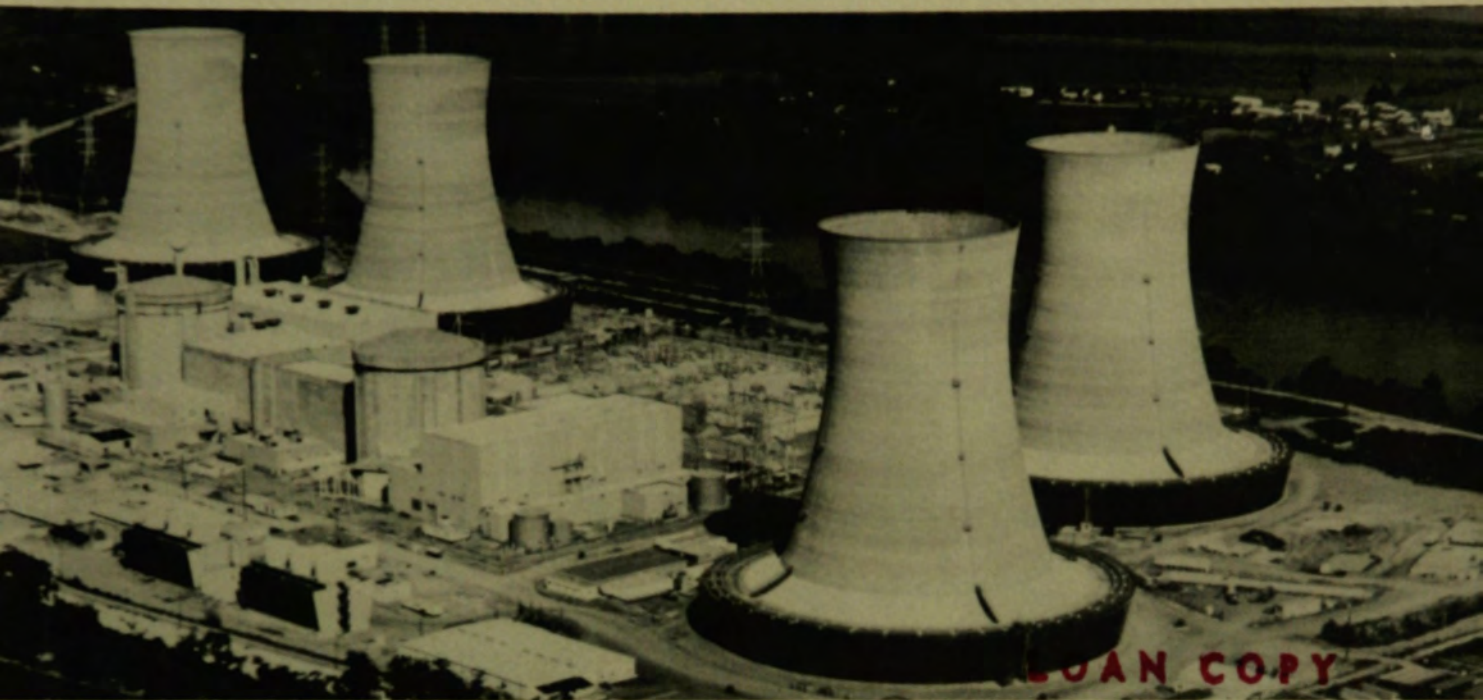


46
GEND-INF- 075-PT2
September 1986

CY-1



LOAN COPY

THIS REPORT MAY BE RECALLED
AFTER TWO WEEKS. PLEASE
RETURN PROMPTLY TO:

INEL TECHNICAL LIBRARY

This is an informal report intended for use as a preliminary or working document

GEND

General Public Utilities • Electric Power Research Institute • U.S. Nuclear Regulatory Commission • U.S. Department of Energy

TMI-2 CORE DEBRIS GRAB SAMPLES--

EXAMINATION AND ANALYSIS

PART 2

I. ESTEBAN	1-7-87
Thomas Young	6-21-89
Joe Palmer	4/29/90

D. W. Akers
E. R. Carlson
B. A. Cook

S. A. Ploger
J. O. Carlson

Prepared for the
U.S. Department of Energy
Three Mile Island Operations Office

DISCLAIMER

This book was prepared as an account of work sponsored by an agency of the United States Government. Neither the United States Government nor any agency thereof, nor any of their employees, makes any warranty, express or implied, or assumes any legal liability or responsibility for the accuracy, completeness, or usefulness of any information, apparatus, product or process disclosed, or represents that its use would not infringe privately owned rights. References herein to any specific commercial product, process, or service by trade name, trademark, manufacturer, or otherwise, does not necessarily constitute or imply its endorsement, recommendation, or favoring by the United States Government or any agency thereof. The views and opinions of authors expressed herein do not necessarily state or reflect those of the United States Government or any agency thereof.

TMI-2 CORE DEBRIS GRAB SAMPLES--
EXAMINATION AND ANALYSIS

PART 2

Douglas W. Akers
Eric R. Carlson
Beverly A. Cook
Scott A. Ploger
Johan O. Carlson

Published September 1986

EG&G Idaho, Inc.
Idaho Falls, Idaho 83415

Prepared for the
U.S. Department of Energy
Idaho Operations Office
Under DOE Contract No. DE-AC07-76ID01570

CONTENTS

APPENDIX A--EXAMINATION TECHNIQUES	A-1
APPENDIX B--PHOTOGRAPHS OF SAMPLES AND PARTICLES	B-1
APPENDIX C--METALLURGICAL EXAMINATIONS	C-1
APPENDIX D--ELEMENTAL ANALYSES	D-1
APPENDIX E--RADIOCHEMICAL ANALYSES	E-1
APPENDIX F--TMI-2 CORE NODULAR ORIGEN-2 CALCULATIONS	F-1
APPENDIX G--SURFACE AREA CALCULATION FOR PARTICLE SIZE FRACTIONS	G-1
APPENDIX H--THERMAL ANALYSIS OF TMI-2 CORE DEBRIS SAMPLES	H-1

DRAFT REPORT: TMI-2 CORE DEBRIS GRAB
SAMPLES--EXAMINATION AND ANALYSIS

PART 2

Due to its large volume, this report has been divided into two parts. Part 1 contains the main body of the report, and Part 2 contains the appendixes.

APPENDIX A

EXAMINATION TECHNIQUES

APPENDIX A

EXAMINATION TECHNIQUES

This appendix presents a brief overview of techniques used during examination of the TMI-2 core debris grab samples, including physical, metallurgical, chemical, and radiochemical examinations.

Physical Examinations

Visual/Photographic

The visual and photographic examinations of the bulk core debris grab samples were performed through a glove box window for Samples 1 through 6, and through a hot cell periscope for Samples 7 through 11. Individual particles were removed and examined in the glove box.

Weight

The samples were weighed in the hot cell using an electronic balance (Sartorius Model 1205 MP).

Bulk Tap Density

The gross volume of each sample was determined by placing the bulk sample in a graduated beaker, tapping the beaker to compact the material, and measuring the sample volume. The weight (g) was divided by the volume (cm^3) to obtain the bulk tap density. The uncertainty associated with this analysis is large (<25%) because the irregular top surface of the sample in the beaker prevented precise measurement of the volume.

Particle Size Distribution

The core debris grab samples were subjected to a particle size distribution analysis by sieving each bulk sample into progressively

smaller (4000 μm to 1680 μm , 1680 to 1000 μm , 1000 to 707 μm , 707 to 297 μm , 297 to 149 μm , 149 to 74 μm , 75 to 30 μm , 30 to 20 μm , and <20 μm) particle size fractions (9 to 10 groups in most cases). Sieve sizes were predetermined during visual examination of the samples, and new sieves (manufactured by Tyler, Inc.) were used for each sample to prevent cross contamination. Each bulk sample was placed in the top of the sieve column, and the larger (>1000 μm) particle size fractions were separated using dry, mechanical or hand-agitated sieving. Smaller (<1000 μm) particle size fractions were separated by wet sieving to prevent loss of particles by aerosol transport or adherence to sieve surfaces. Freon was selected as the wash solution because it is not chemically reactive. Each sieve fraction was visually examined, photographed, and weighed.

Sample 4 was not sieved because it consisted of large particles. Sample 5 consisted mostly of large particles and was sieved into only four particle size fractions. Sample 7 was sieved after being agitated for 5 min and then again after 1 h to determine whether or not the sieving technique had an effect on results of the particle size distribution.

Ferromagnetic Material Content

The quantity of ferromagnetic material present in each sieve fraction was determined for Sample 6 (E9, 56 cm). This analysis was performed by placing a small (2-lb pull) magnet in a small beaker and then placing the beaker in contact with each sieve fraction. After stirring the beaker in the sample material, the magnet, beaker, and attached magnetic material were removed and placed in a container. The magnet then was removed from the beaker, allowing the magnetic material to drop into the container. No material adhered to the beaker after removing the magnet; therefore, it was assumed that all material in the container had a ferromagnetic component.

Pyrophoricty

Pyrophoricty (pilot ignition) tests were performed on portions the core debris grab samples to evaluate potential safety hazards during core recovery operations. The test procedure was verified by igniting zirconium hydride powder, using a small Tesla coil (Fisher Scientific Model BD 10) rated at 50,000 volts. Ignition of the powder was recorded both by video tape and still photography before beginning the actual core debris pyrophoricty tests. An additional method used to produce higher temperatures (i.e., a propane torch) also was tested on the zirconium hydride powder before beginning the actual test on the core debris material. The sample material was tested dry; then a drop of water was added and the material was tested wet.

Metallurgical Examinations

Optical Metallography

This technique involved viewing highly polished particles using a light microscope at magnifications up to about 500X. In addition, the particles often were treated with etchants to highlight grain boundaries and second phases.

The following grinding and polishing sequence was used for the TMI-2 core debris particles:

1. Course grind with water-lubricated silicon carbide 120 grit paper in a whirlamat
2. Medium grind with 400 grit paper
3. Final grind with 600 grit paper
4. Initial polish with kerosene-type fluid lubricated by diamond grit on a hard paper in a whirlamat

5. Final polish with 1- μm diamond grit on a short nap nylon
6. Metallic (non-zircaloy) particles were further polished with 0.3- μm Al_2O_3 grit in a vibratory polisher.

In general, either an immersion or swab etching technique was used, depending on whether a heavy or light etch was appropriate. The following etchants were used on the various materials:

o Fuel	-	85% H_2O_2 , 15% H_2SO_4
o Zircaloy	-	55% lactic acid, 19% HNO_3 , 19% H_2O_2 , 7% HF
o Non-zircaloy metallic	-	9.5% HNO_3 , 90.5% methanol.

Scanning Electron Microscopy (SEM)

For this technique, a finely focused electron beam is swept in a raster across the surface of a sample. The types of signals which are produced when the focused electron beam impinges on a sample surface include secondary electrons, backscattered electrons, and characteristics x-rays. In SEM, the primary signal of interest is the variation in secondary electron emission that occurs. The variation is due to differences in surface topography. The secondary electrons are collected by a scintillator-photomultiplier system, and the resultant signal is displayed on a cathode ray tube (CRT). The scanning electron beam is synchronized with the scanning of the CRT such that images can be presented on a storage oscilloscope or a monitor oscilloscope for photographing. This procedure also is used for backscattered electron images. These electrons have a higher energy than secondary electrons, resulting in greater escape depths. The primary advantage of backscattered electron images is that they show different brightness values of phases of different composition.

Energy Dispersive X-ray Spectroscopy (EDS)

EDS analysis is performed by measuring characteristic detectable x-rays from elements above atomic number 10 on the periodic table which are excited by a scanning electron beam. The beam is typically 1 μm in diameter, but scattering produces x-rays over a region up to ten times wider. A SEM/EDS system is very convenient for speedy area surveys of elemental content and spectral uniformity, and produces superb images and photographic records. Other advantages are the low beam energy and relatively poor operating vacuum, both of which limit absorption of deposited molecules. However, the usefulness of this instrument is reduced by susceptibility to background radiation, inability to detect oxygen and carbon, and absence of binding energy information.

Scanning Auger Spectroscopy (SAS)

This instrument rasteres an electron beam over a sample region, ionizing surface atoms and generating characteristic x-rays and secondary electrons in the process. Rather than the x-rays, Auger spectroscopy collects and energy-analyzes the emitted Auger electrons from elements above atomic number 2. The double-focusing electron optics and tight energy resolution essentially eliminate interferences from background radiation. Moreover, the detected secondary electrons are only able to escape the outermost atomic or molecular layers, so depth resolution is extremely fine. Most SAS systems incorporate inert gas ion sputter-etching for both specimen cleaning and depth profiling; the positive ion flux counter balances charging by incident electrons. The elemental detection threshold is typically 0.1 at. % which is comparable to EDS. SAS spatial resolution is equal to the beam diameter, which varies between models from 0.1 to 20 μm .

Chemical Examinations

Inductively Coupled Plasma Spectrometry (ICP)

Liquid-based samples are nebulized and pulse-injected into an inductively (radio frequency) heated plasma, causing all elements present to emit characteristic light wavelengths. The light is separated on a diffraction-grating monochromator, and the wavelength intensities are sequentially measured by photomultiplier tube. [As such, ICP is a refinement of atomic emission spectroscopy.] This technique generally is free of elemental interferences, is highly accurate, and has a detection threshold of approximately 0.001 at. % (10 ppm). This analysis is performed on liquids (dissolved sample material). The equipment used was an ISA 2000 Scanning Spectrometer.

X-Ray Diffraction

Every crystalline substance scatters x-rays in its own unique diffraction pattern, producing a "fingerprint" of its atomic and molecular structure. The intensity of each reflection provides limited semiquantitative information on the molecular structures present. One unique feature of x-ray diffraction is that components are identified as specific compounds. Small (<10 mg) portions of the samples were placed in a powder camera, exposed to the x-ray beam, and characteristic x-ray diffraction patterns produced. The equipment used was a Phillips X-ray Diffractometer.

X-ray diffraction analysis was performed on several samples. However, the following problems were encountered in analyzing the samples:

- o Because of high radiation levels associated with the samples, only small (1-2 mg) portions could be analyzed. Therefore, several (up to 10) portions had to be analyzed and averaged to characterize a large (20-30 mg) sample.

- o The heterogeneity (many different phases structures) of the TMI-2 core debris grab samples made it difficult to characterize a sample because the lattice structure observed contained all phases present.
- o Crystalline structures of most importance are the mixed oxides (U,Zr). There are few or no materials standards for the variety of lattice structure observed, matrix determination of composition difficult.
- o Where U or Zr is a minor component, it is difficult to resolve the minor oxide species with available equipment. This makes identifying minor but important structures in the samples difficult.

Radiochemical Examinations

Gamma Spectroscopy

The initial radiochemical analysis performed was gamma spectroscopy. This technique is based on gamma-ray emissions which produce a spectrum specific to individual radionuclide species. The spectra were analyzed by a computerized gamma spectroscopy system using DEC DPD-15 and PDP-11/44 computers with a GAUSS VI analysis program.^a This program (a) identifies the radionuclides associated with the gamma-ray energy peaks and (b) determines their emission rates corrected for detector efficiency, random pulse summing, and decay during the count. The values were converted to disintegration rates by dividing them by the gamma-ray emission probability. The equipment used was fabricated at EG&G Idaho and calibrated using standards of the National Bureau of Standards.

Dissolved portions of samples were diluted and analyzed in 60-mL bottles at calibrated distances with a computerized Ge(Li) gamma spectroscopy system. They were analyzed as point source geometries at distances ranging up to 195 cm from the detector. The mass of each portion

analyzed was less than or equal to 100 mg to keep the specific radionuclide concentration low and minimize the effects of mass attenuation. The effects of mass attenuation were evaluated and corrections applied. The uncertainty of the gamma spectroscopy analysis method is less than 10%, with the exception of those radionuclides whose concentrations were determined using low energy gamma rays (^{152}Eu and ^{125}Sb). The uncertainty associated with these radionuclides is approximately 30%.

Neutron Activation/Delayed Neutron Analysis

The fissile/fertile material content was measured by neutron activation/delayed neutron analysis at the Coupled Fast Reactivity Measurement Facility (CFRMF) at the Idaho National Engineering Laboratory.^a The total fissile/fertile material content was measured by remotely exposing individual 1- by 5-cm cylinders containing sample material to a fast spectrum neutron flux in the central region of the CFRMF core. The cylinder was removed after a 1-min exposure, and the delayed neutrons were measured after about 40 s, using a ^3He detector in a hydrogen moderator.

The fissile material content was determined by exposing the cylinder to a thermal spectrum neutron flux, causing only the ^{235}U and ^{239}Pu within the material to fission and emit delayed neutrons. It was assumed that the quantity of ^{239}Pu was insignificant (<2 wt% based on theoretical predictions). However, a 5 to 8% bias may have resulted. The fertile material contents were determined by subtracting the measured fissile material content (^{235}U and ^{239}Pu) from the total fissile/fertile material content using appropriate calibrations. Calibration measurements were made using both mass and various enrichment standards (depleted U, natural U, 4.3% enriched U, and 93% enriched U).

a. J. E. Klein, M. H. Putnam, R. H. Helmer, GAUSS VI, A Computer Program for the Automatic Analysis of Gamma Rays from Germanium Spectrometers, ANRC-113, June 1973.

^{129}I , ^{90}Sr , and Tellurium Analyses

Analyses for ^{90}Sr and ^{129}I were performed on the dissolved sample material. After an organic separation, the volatile sample fraction was analyzed via neutron activation with a subsequent gamma spectroscopy analysis. The ^{129}I present in the dissolved material was activated to ^{130}I , a gamma-ray emitting radionuclide. The sample material then was analyzed via gamma spectrometry, and the ^{129}I concentration calculated from the measured ^{130}I .

The ^{90}Sr analysis was performed on the nonvolatile sample fractions by precipitating the Sr carrier and ^{90}Sr from the other radionuclides, followed by beta analysis performed in a liquid scintillation counter (Packard Tricarb 3385).

There is a total uncertainty associated with the ^{90}Sr and Te analyses of 10-15%. Uncertainties associated with these analyses result from the sample dissolution and individual analytical techniques. The uncertainty associated with the dissolution is due to potential material losses on glassware surfaces and the occasional presence of small (<10%) amounts of insoluble material after the dissolution. However, for some samples, the uncertainties are 30 to 50% due to uncertainties in the sample weight for small (<10 mg) portions and losses during dissolution as determined by comparison of the fissile/fertile and chemical analysis results.

Cesium Release and Settling Tests

Cesium release and settling (turbidity and airborne fission product release) tests were conducted on material from recombined bulk Sample 6. Tests were performed on both as-received and crushed materials. Crushing was intended to simulate the breakup of TMI-2 core material during reactor defueling. The material was mixed with simulated reactor coolant (adjusted to the correct chemistry and pH).

For the cesium release test, the quantity of fission products leached into the coolant was measured as a function of time (0 min, 5 min, 20 min, 1 h, 24 h, up to 3 days). Cesium was the main fission product of interest.

A two part settling test also was performed which measured (a) turbidity of the sample material/coolant mixture as a function of time and (b) airborne fission product release as a function of time with a continuous air flow (0.5 linear m/s) over the liquid. Aliquots were removed at the aforementioned times, and the turbidity was measured using a turbidimeter (H. F. Instruments Co., Model DR1-100D). The airborne fission product release test was performed on the liquid portion of the mixture after 40 h of leaching. Radionuclide concentrations present in the airstream were measured using a particulate air sampling system developed by Science Applications, Inc.

APPENDIX B

PHOTOGRAPHS OF SAMPLES AND PARTICLES

APPENDIX B

PHOTOGRAPHS OF SAMPLES AND PARTICLES

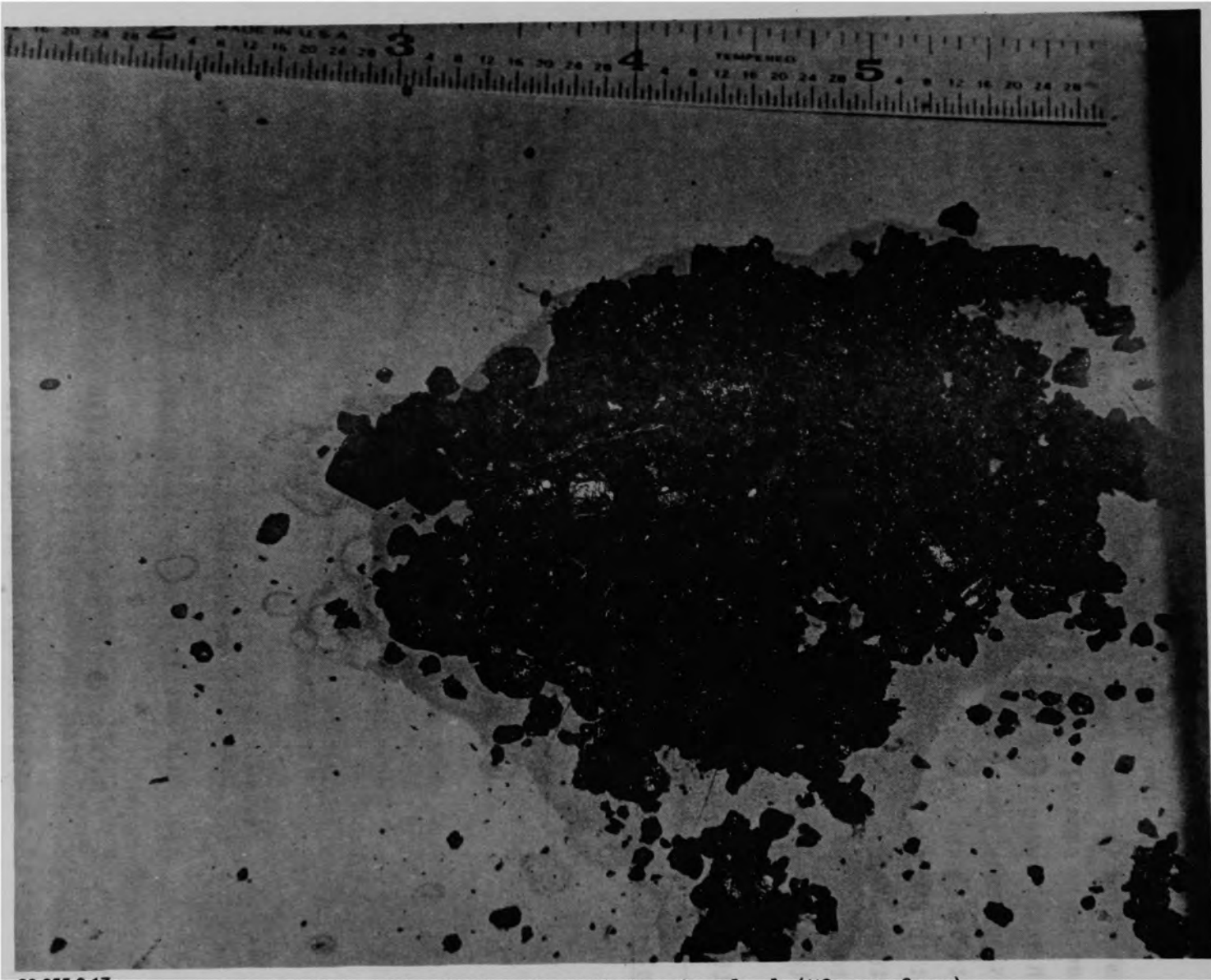
As part of the initial unloading and weighing activities, visual examination was undertaken, and photographs were made of the bulk samples after their removal. Several larger sized ($\geq 1000 \mu\text{m}$) particles from each sample were then selected for follow-up examination and analysis. This appendix contains photographs of the bulk samples and individual particles taken from all samples with the exception of number 2 which was sent to B&W and number 3 in which the large individual particles were not photographed.

Photographs of individual particles smaller than $1000 \mu\text{m}$ are not included in this report due to the lack of acuity in the photos.

TABLE B-1. SAMPLE CROSS REFERENCE INDEX

<u>Sample No.</u>	<u>Description</u>	<u>Figure(s)</u>
1	Bulk material/eleven particles	B-1 thru B-7
3	Bulk material	B-8 thru B-7
4	Bulk material/five particles	B-10 thru B-14
5	Bulk material/eleven particles	B-15 thru B-21
6	Bulk material/eleven particles	B-22 thru B-29
7	Bulk material/one particle size fraction/eleven particles	B-30 thru B-41
8	Bulk material/two particle size fraction/eleven particles	B-42 thru B-54
9	Bulk material/two particle size fraction/eleven particles	B-55 thru B-67
10	Bulk material/one particle size fraction/eleven particles	B-68 thru B-78
11	Bulk material/two particle size fraction/eleven particles	B-79 thru B-93

B-4



83-655-3-17

Figure B-1. The bulk material for Sample 1 (H8, surface).



84-216-2-22

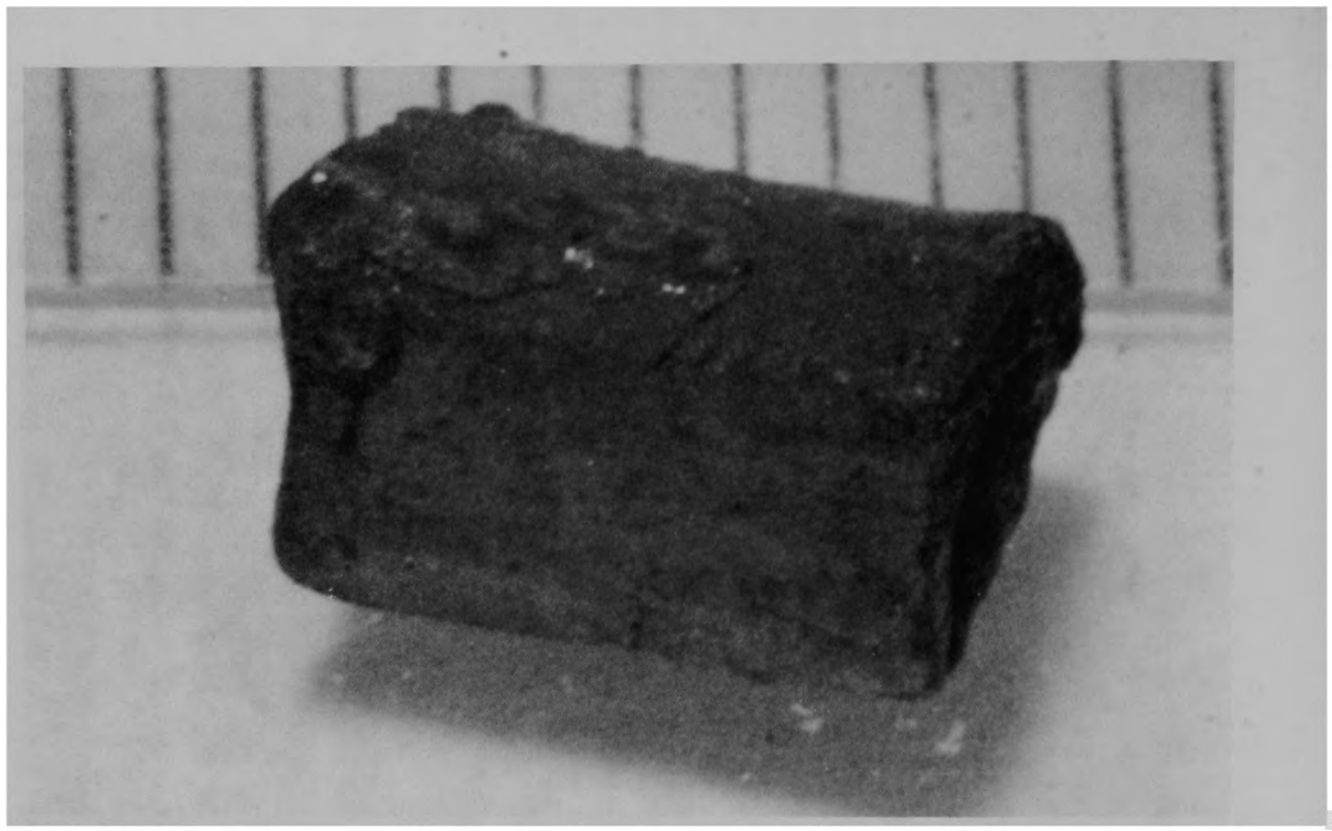
a) Front view of particle



84-216-2-30

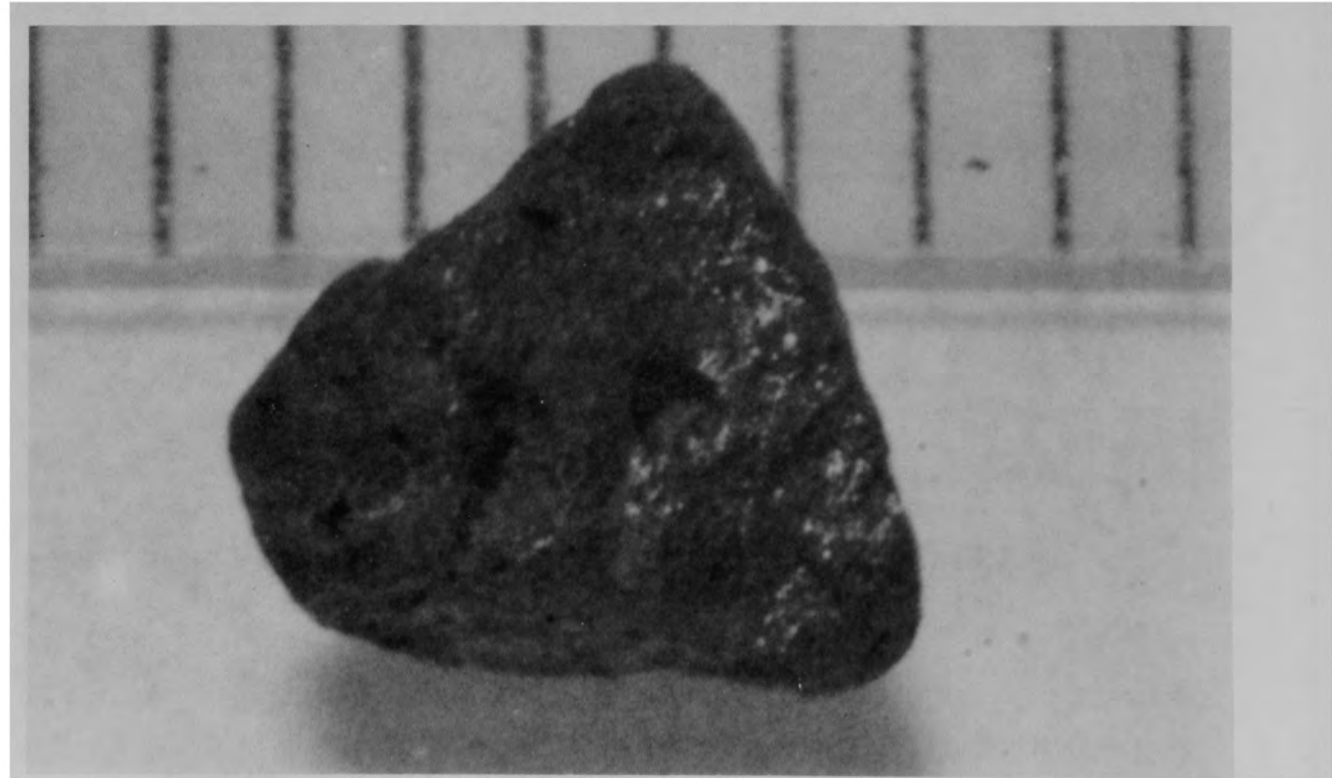
b) Back view of particle

Figure B-2. Particle 1A from Sample 1 (H8, surface), size range:
 $>4000 \mu\text{m}$.



84-216-3-4

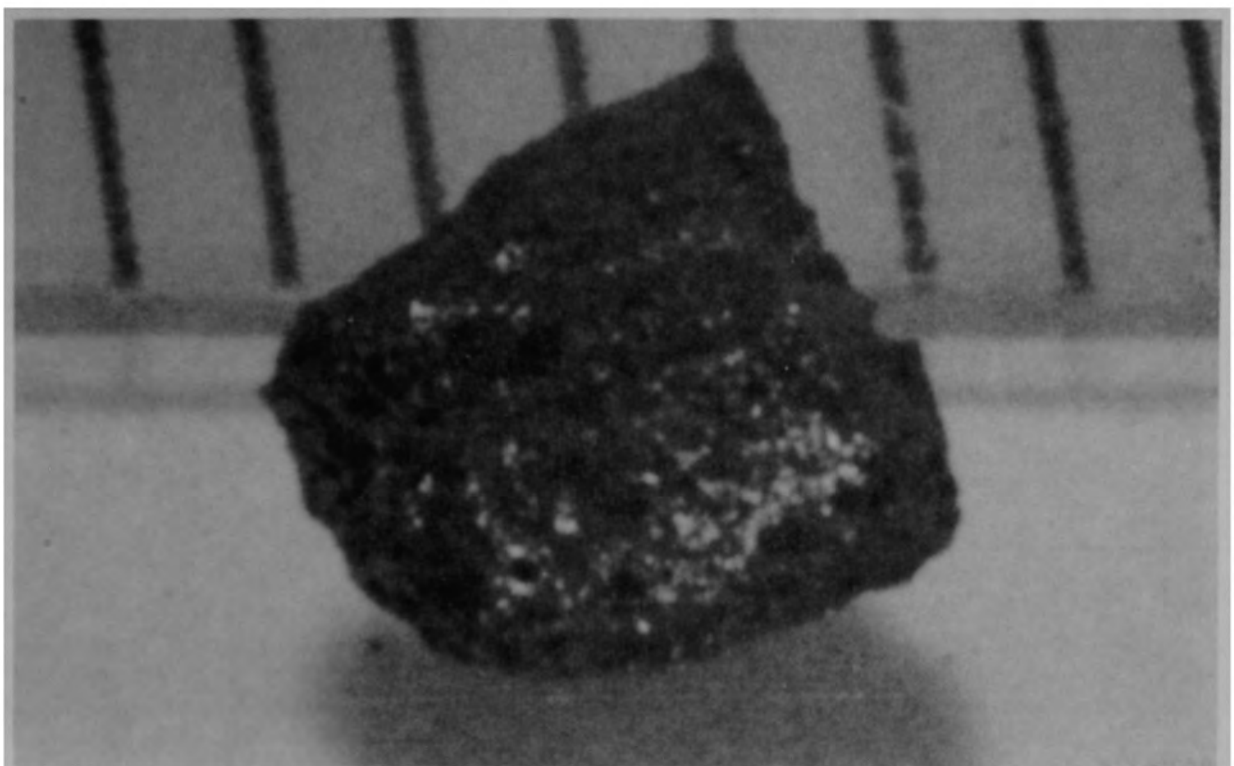
a) Particle 1B (size range: >4000 μm)



84-216-3-9

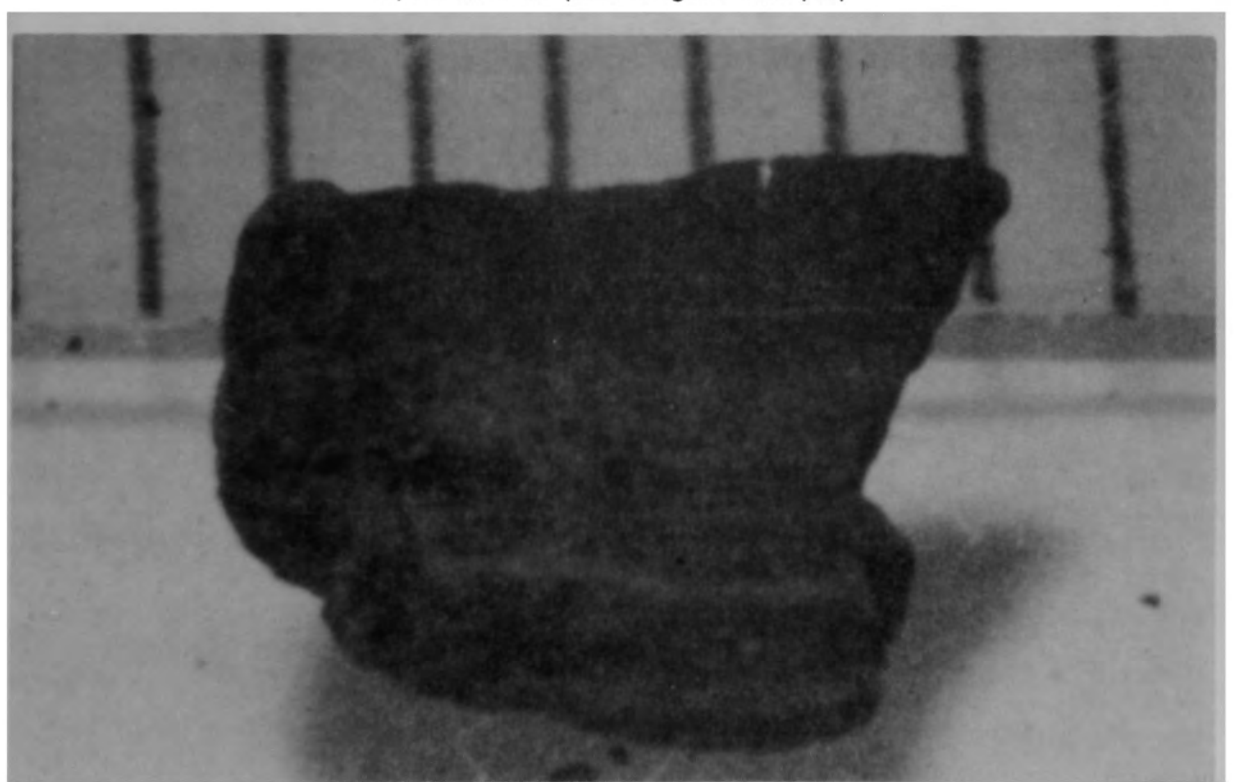
b) Particle 1C (size range: >4000 μm)

Figure B-3. Particles from Sample 1 (H8, surface).



83-216-3-12

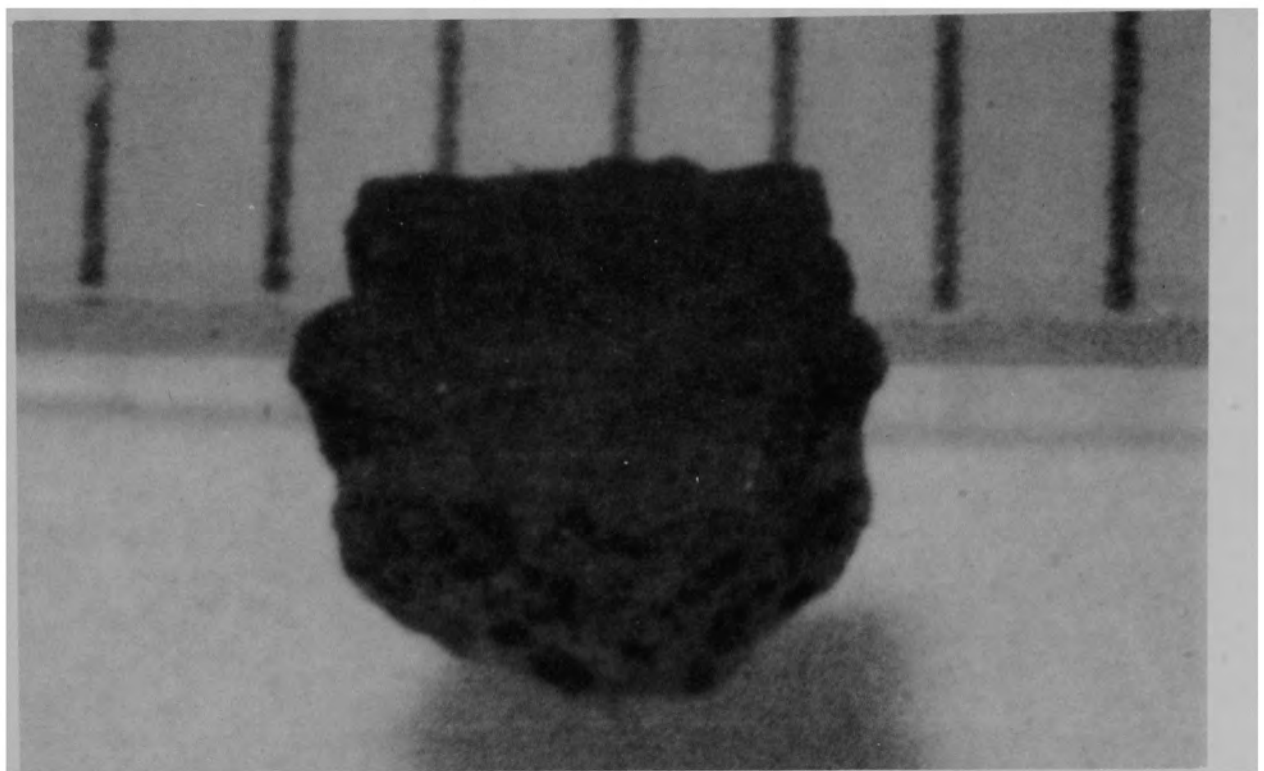
a) Particle 1D (size range: >4000 μm)



84-216-3-17

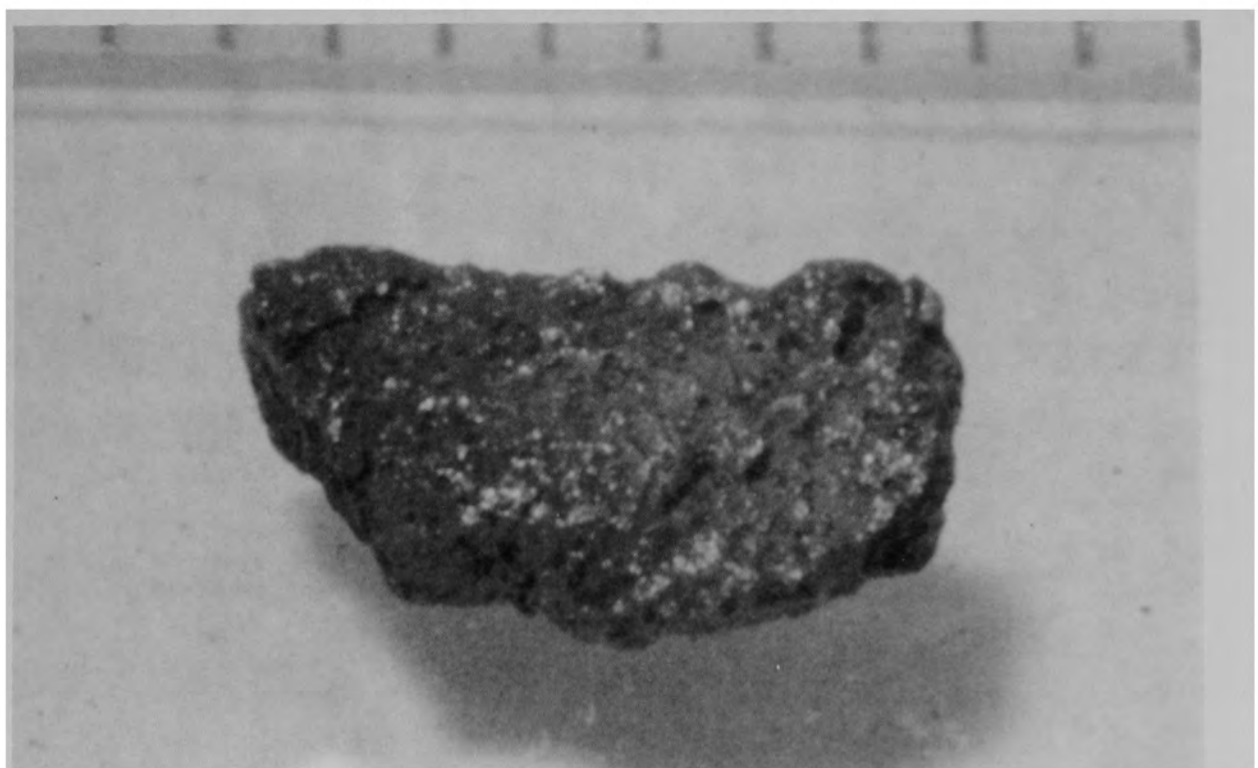
b) Particle 1E (size range: >4000 μm)

Figure B-4. Particles from Sample 1 (H8, surface)



84-216-3-18

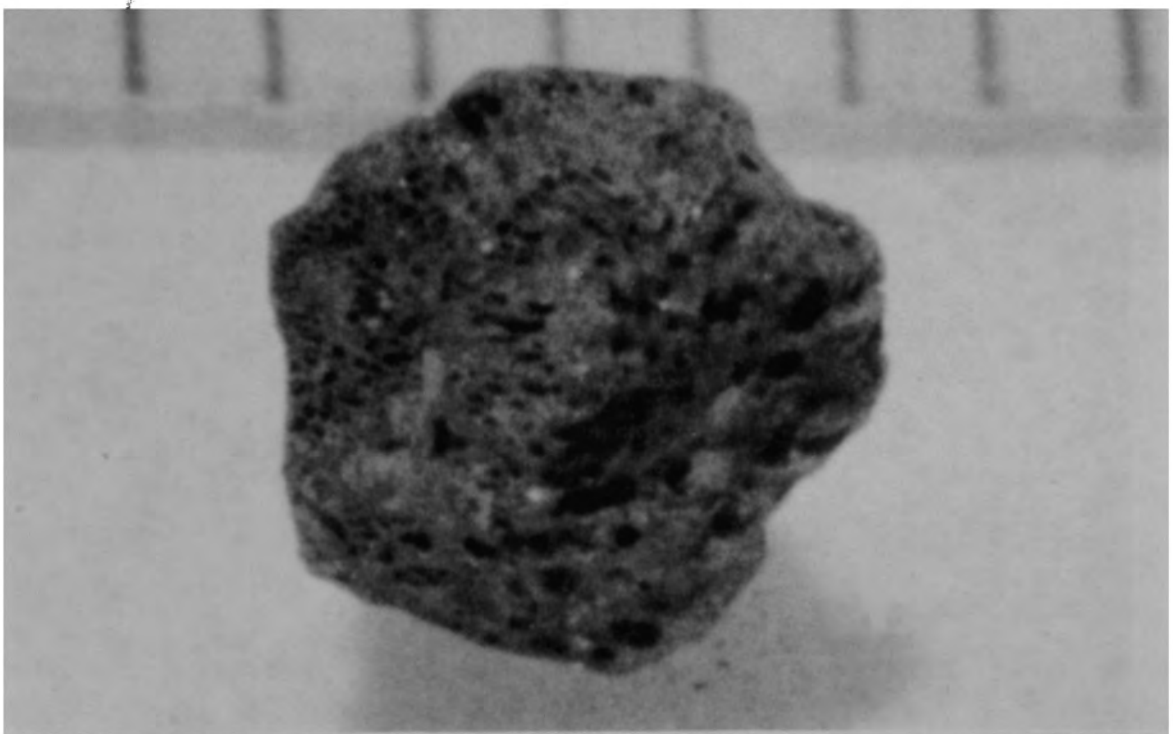
a) Particle 1F (size range: 1680-4000 μm)



84-216-3-21

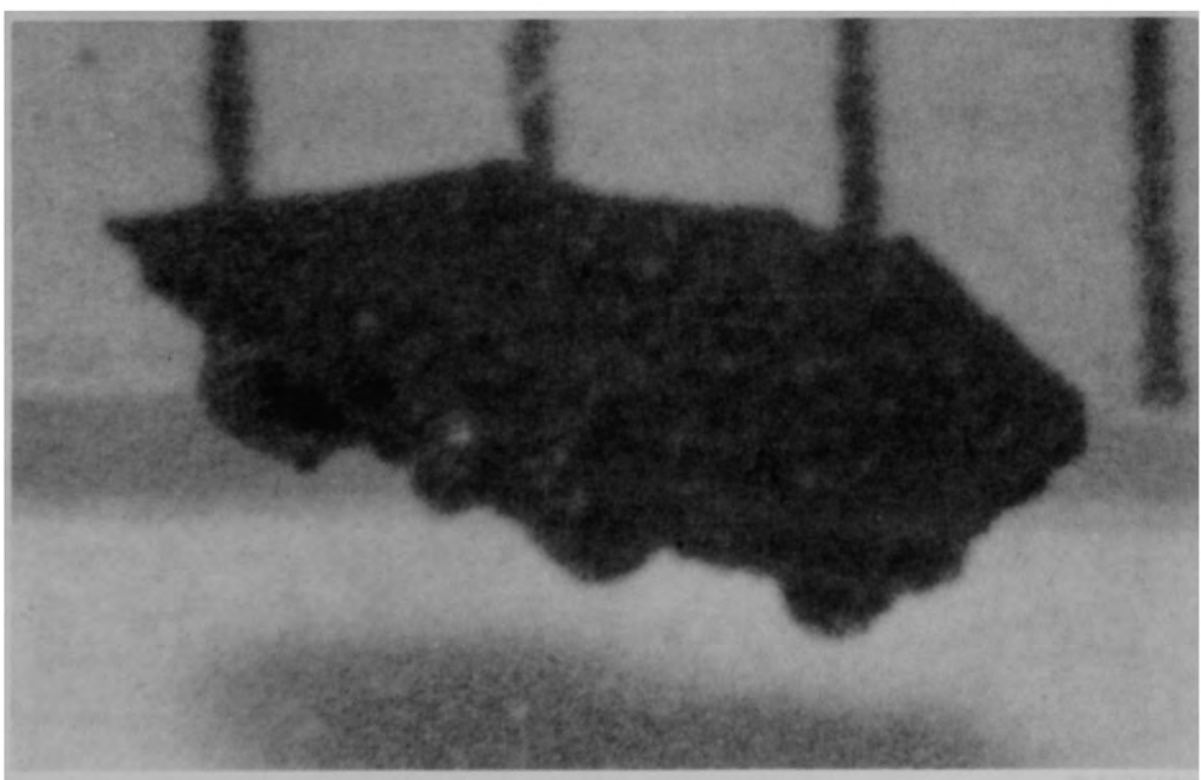
b) Particle 1G (size range: 1680-4000 μm)

Figure B-5. Particles from Sample 1 (H8, surface).



84-216-3-23

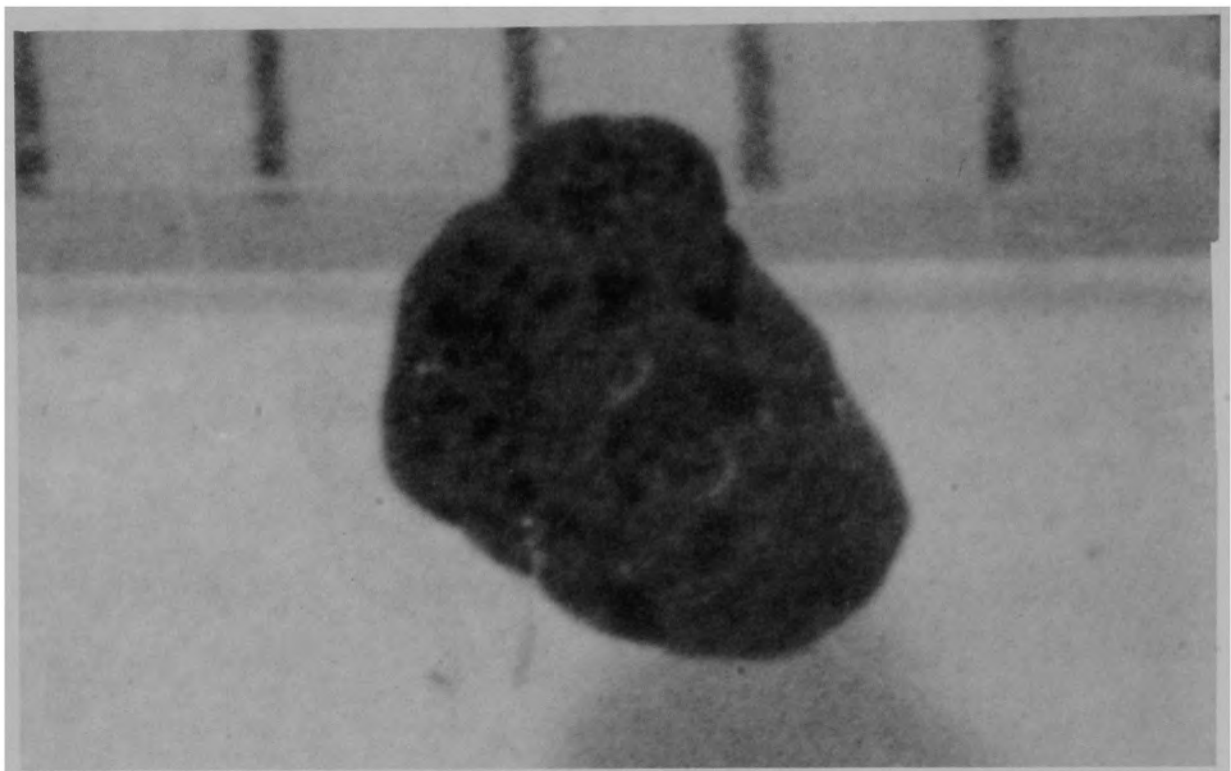
a) Particle 1H (size range: 1680-4000 μm)



84-216-3-24

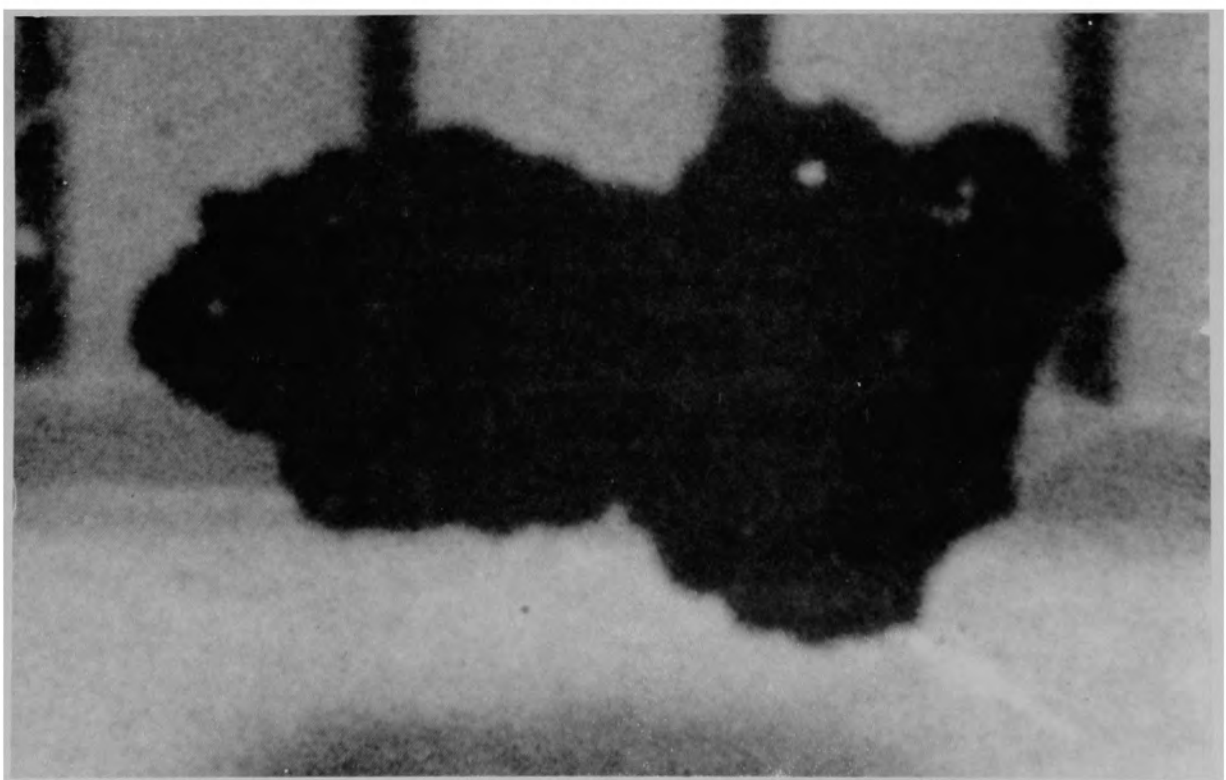
b) Particle 1I (size range: 1000-1680 μm)

Figure B-6. Particles from Sample 1 (H8, surface).



84-216-3-27

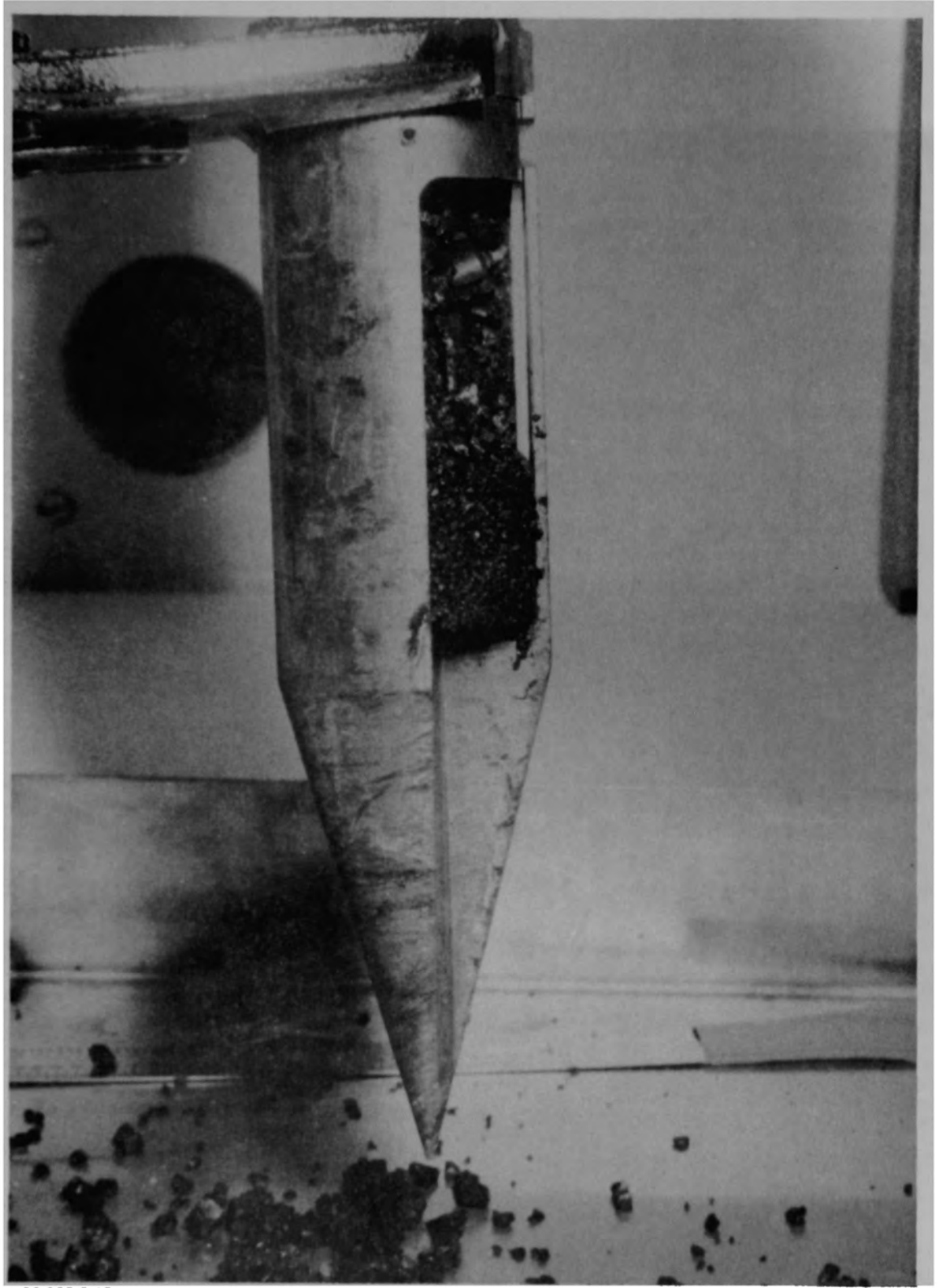
a) Particle 1J (size range: 1000-1680 μm)



84-216-3-28

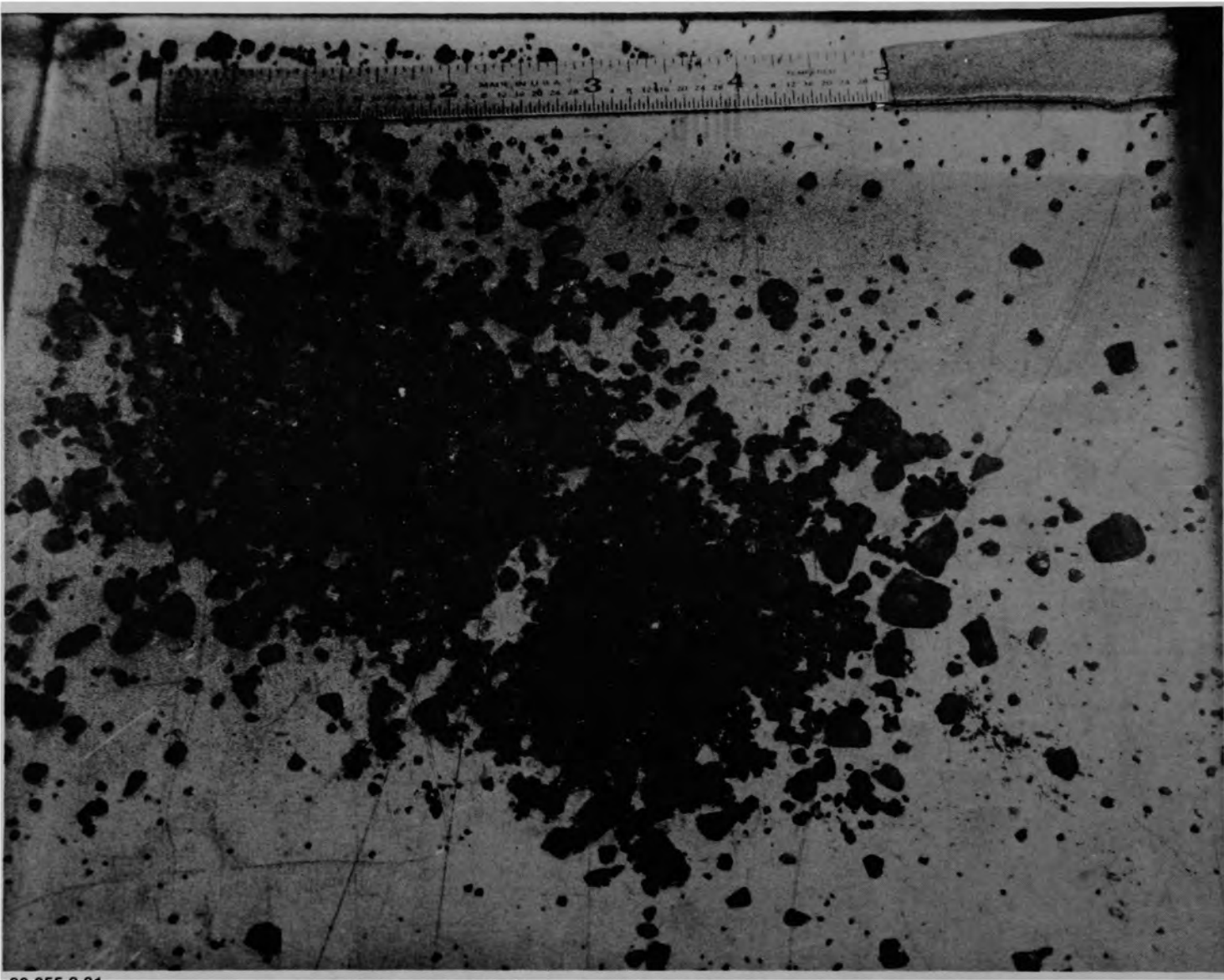
b) Particle 1K (size range: 1000-1680 μm)

Figure B-7. Particles from Sample 1 (H8, surface).



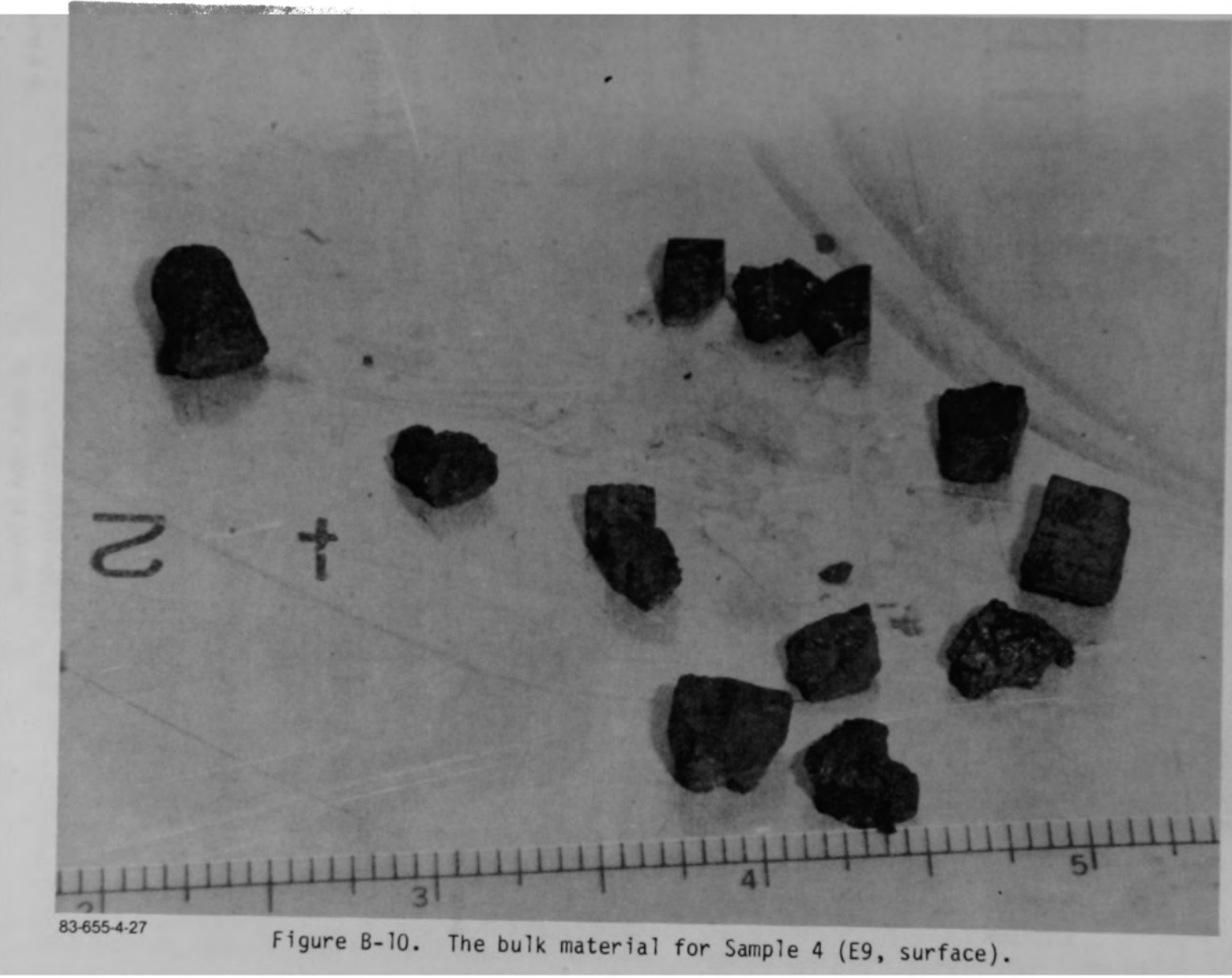
83-655-8-15

Figure B-8. Stratified material in sampling tool for Sample 3 (H8, 56 cm).



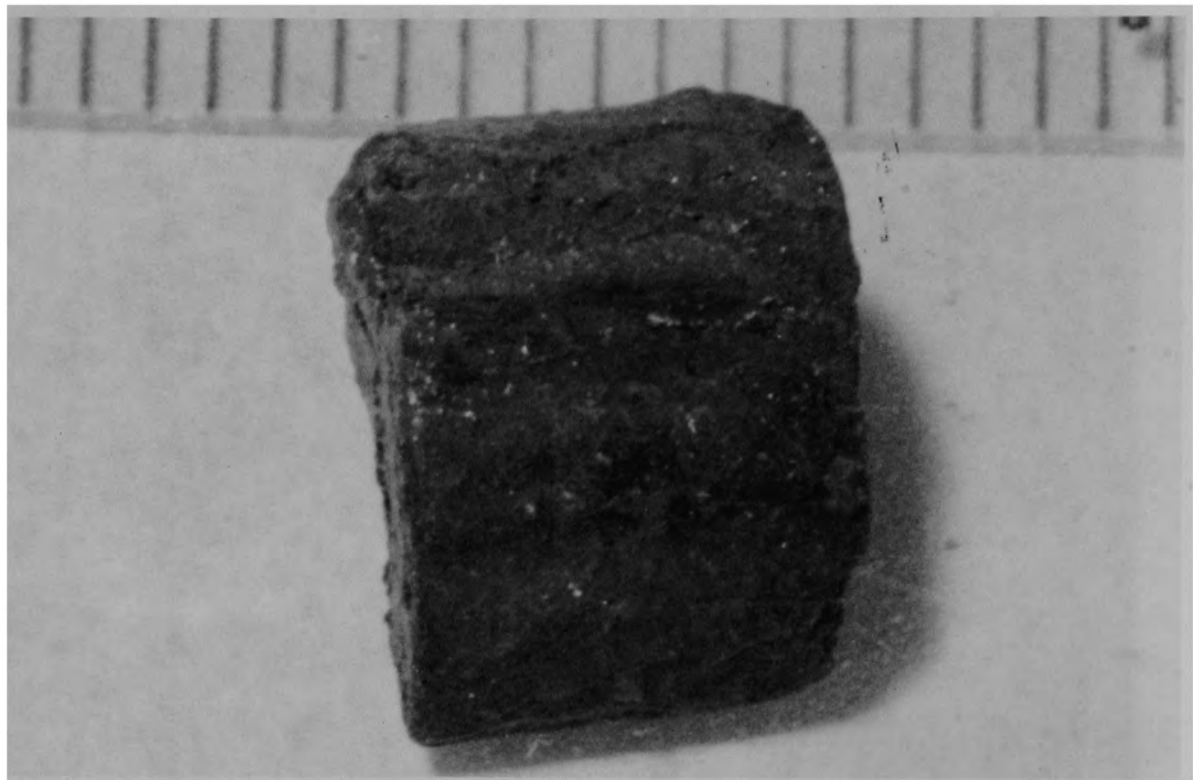
83-655-8-31

Figure B-9. The bulk material for Sample 3 (H8, 56 cm).



83-655-4-27

Figure B-10. The bulk material for Sample 4 (E9, surface).



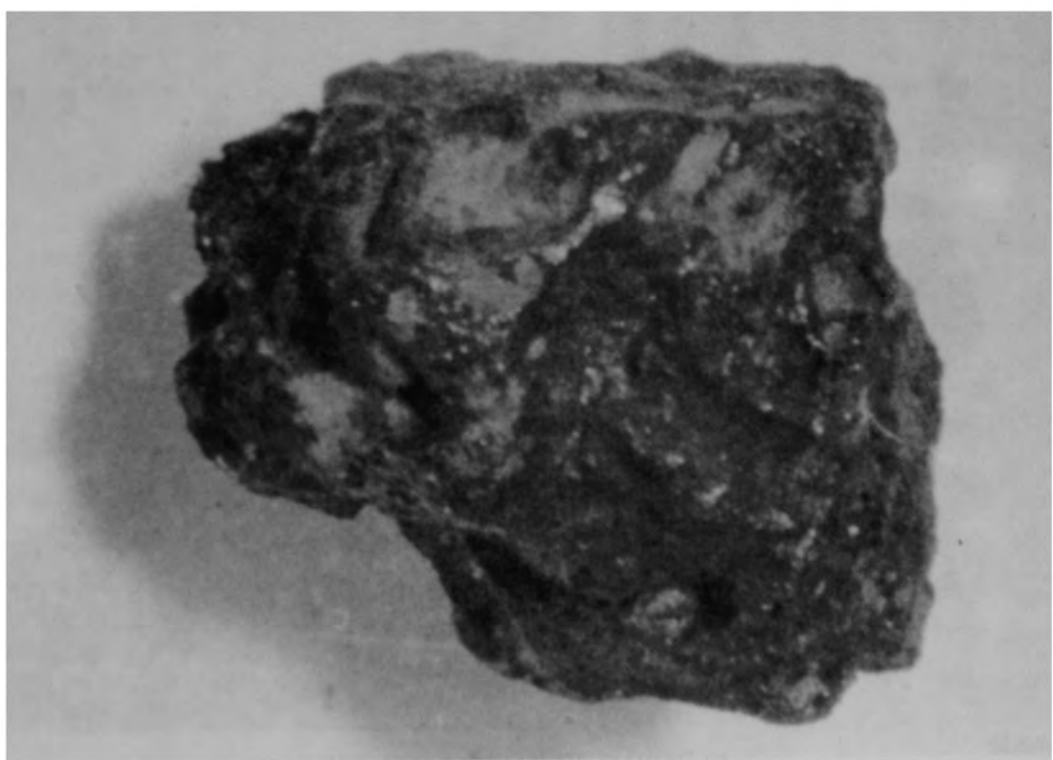
84-157-2-28

Figure B-11. Particle 4A from Sample 4 (E9, surface), size range:
 $>4000 \mu\text{m}$.



84-157-2-11

a) Front view of particle



84-157-2-16

b) Back view of particle

Figure B-12. Particle 4B from Sample 4 (E9, surface), size range:
 $>4000 \mu\text{m}$.



84-157-2-22

a) Particle 4C (size range: >4000 μm)



84-157-2-32

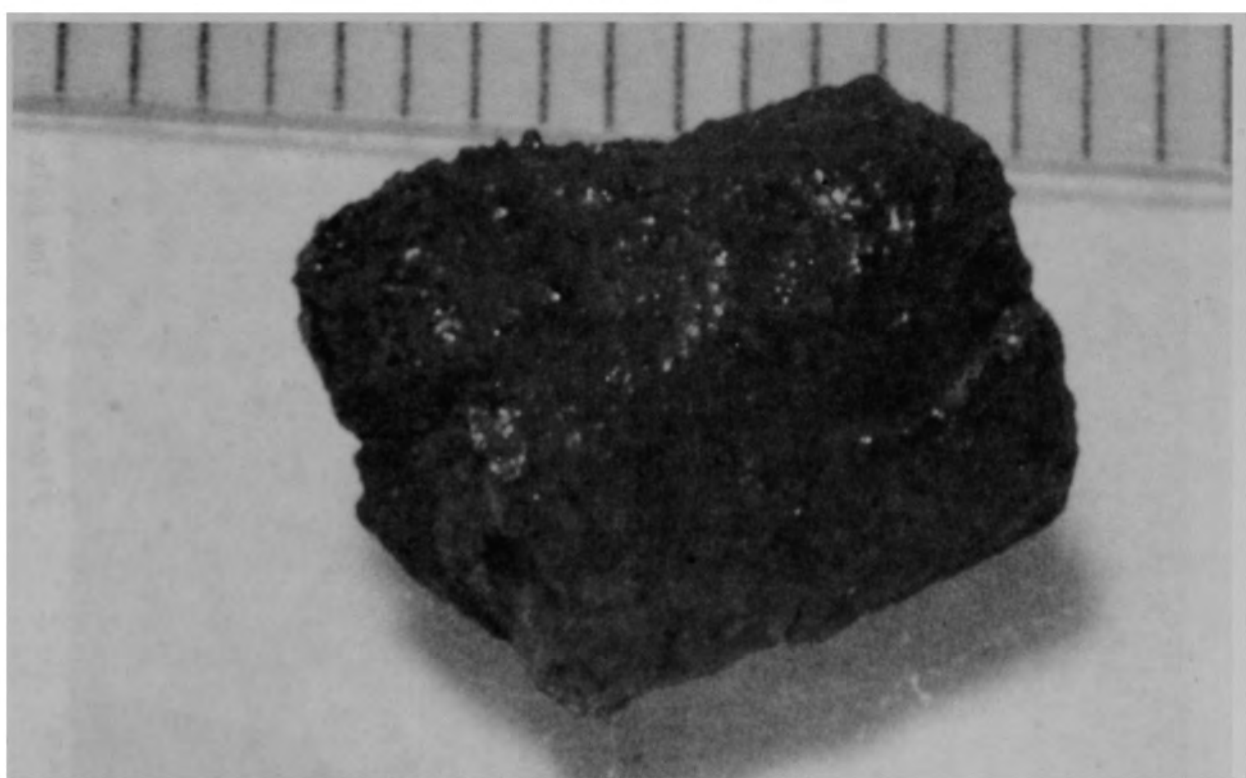
b) Particle 4D (size range: >4000 μm)

Figure B-13. Particles from Sample 4 (E9, surface).



84-157-3-4

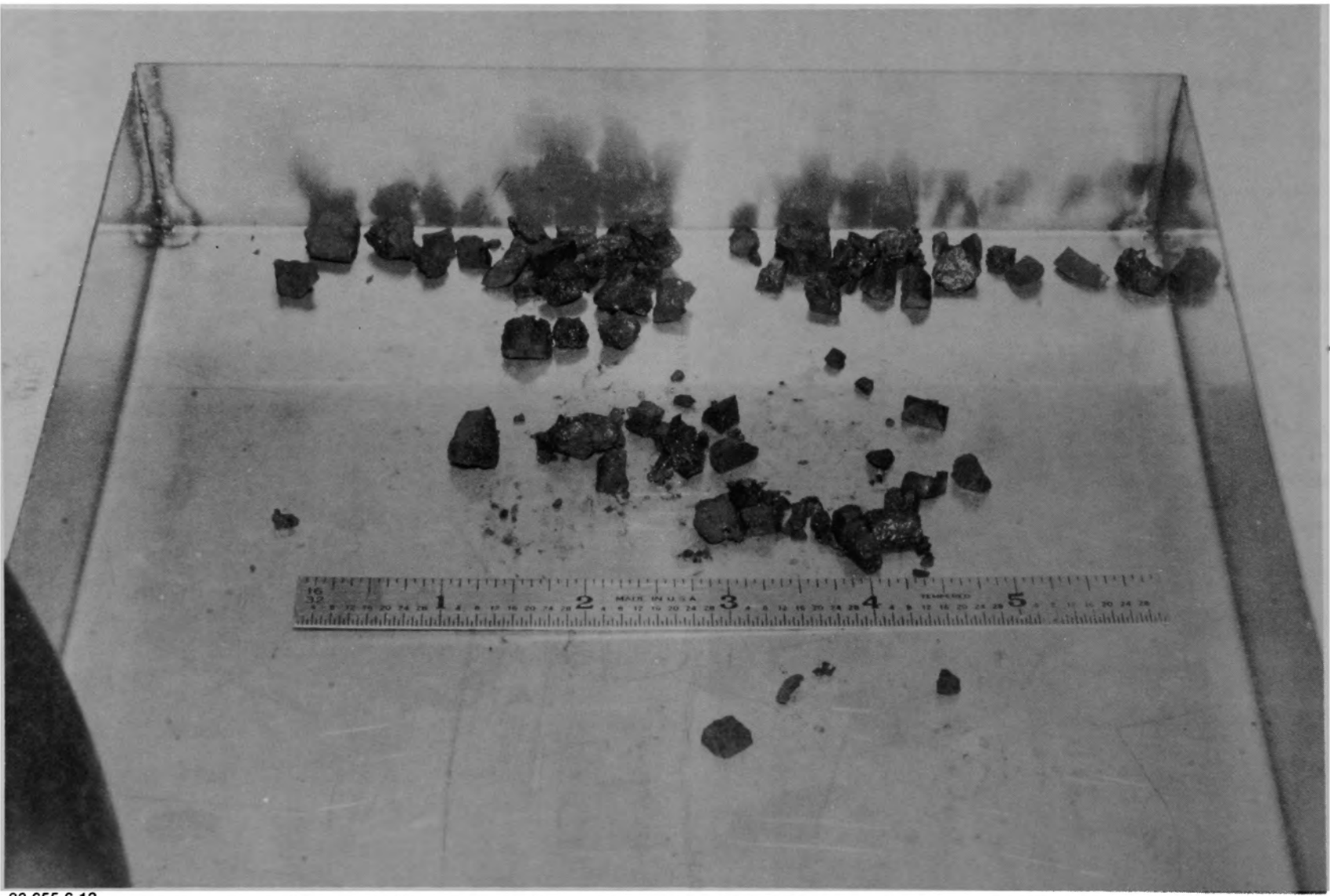
a) Front view of particle



84-157-3-6

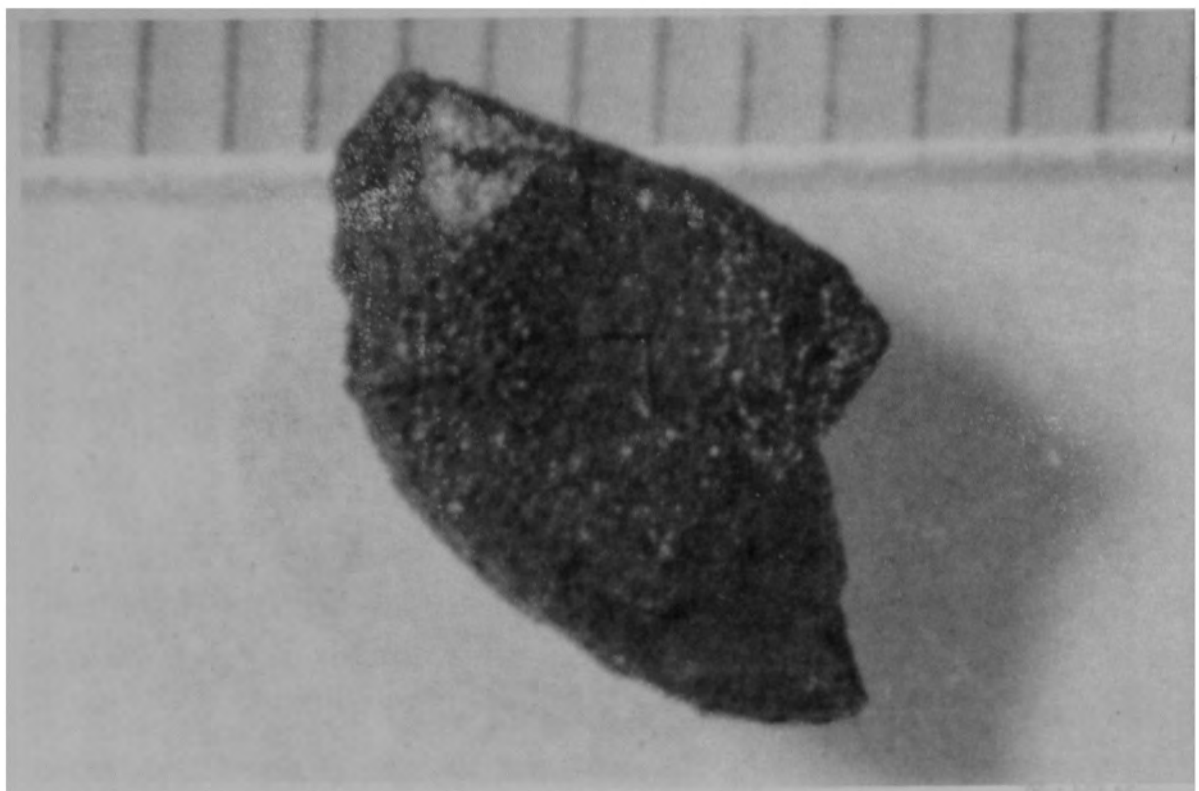
b) Back view of particle

Figure B-14. Particle 4E from Sample 4 (E9, surface), size range:
 $>4000 \mu\text{m}$.



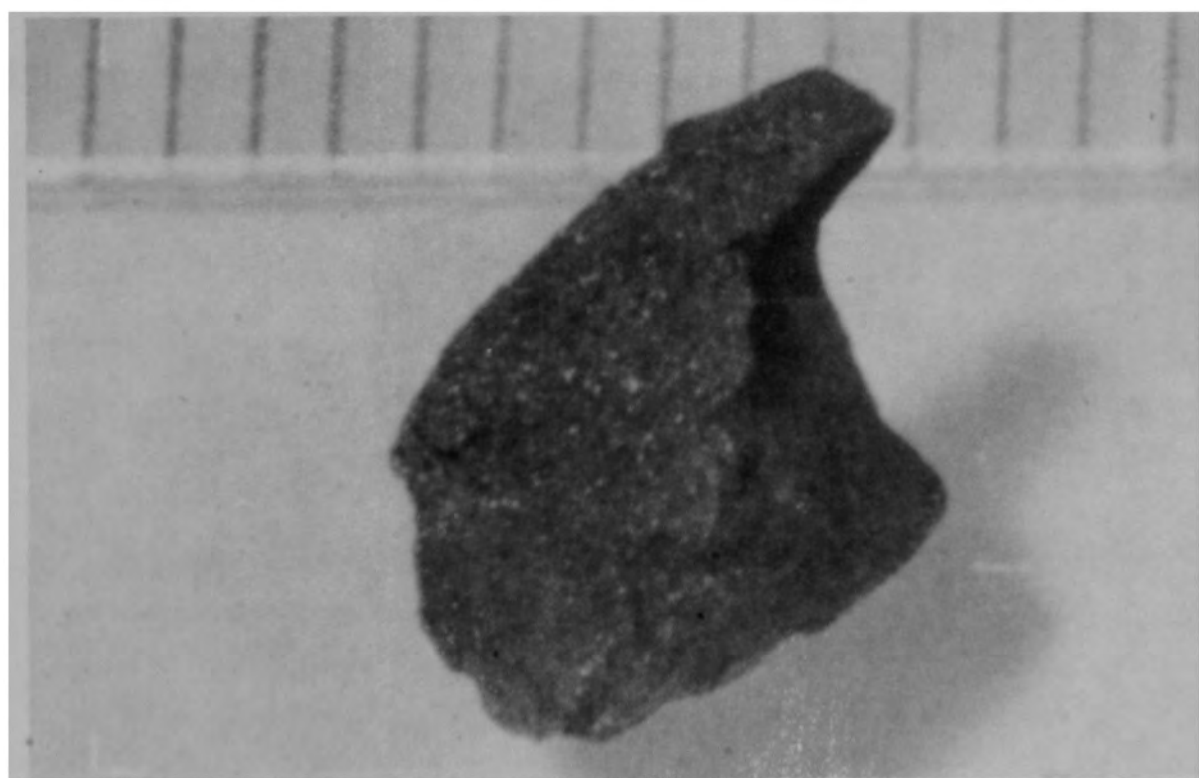
83-655-6-12

Figure B-15. The bulk sample material for Sample 5 (E9, 8 cm).



84-194-1-19

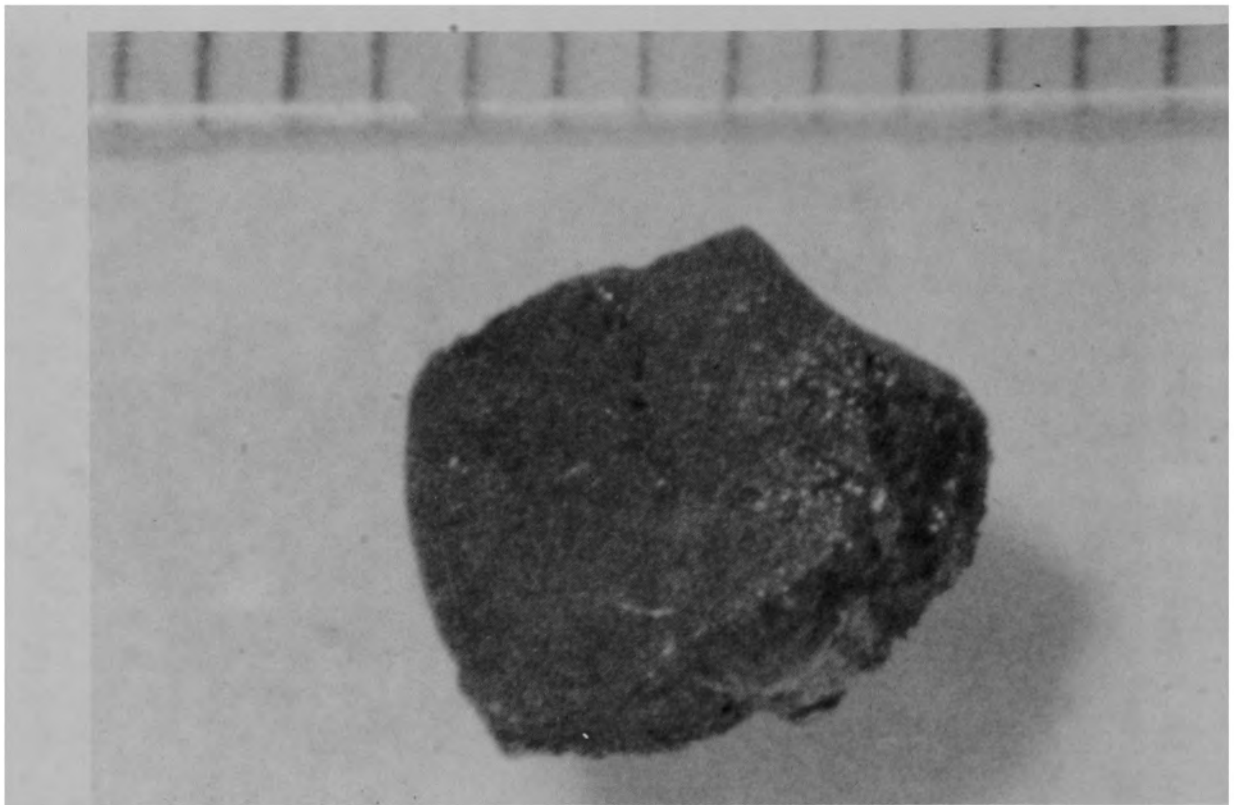
a) Front view of particle



84-194-1-27

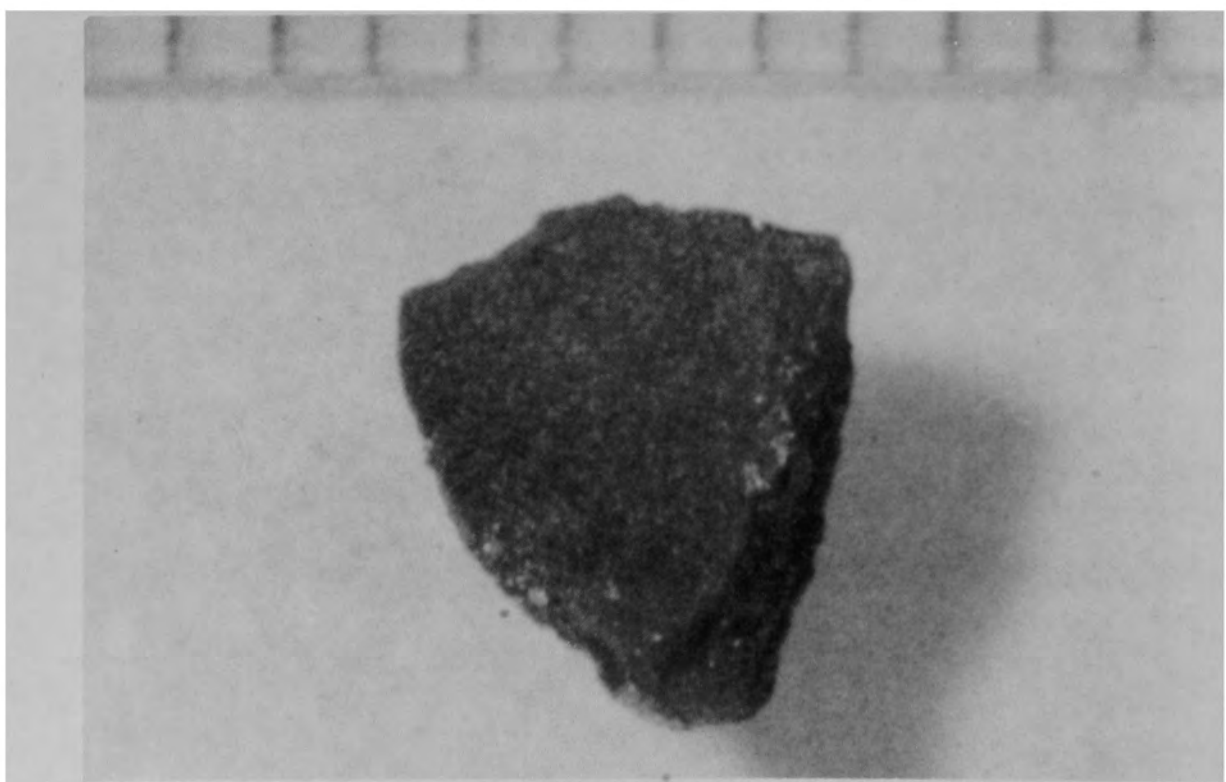
b) Back view of particle

Figure B-16. Particle 5A from Sample 5 (E9, 8 cm), size range:
 $>4000 \mu\text{m}$.



84-194-1-30

a) Particle 5B (size range: >4000 μm)



84-194-2-8

b) Particle 5C (size range: >4000 μm)

Figure B-17. Particles from Sample 5 (E9, 8 cm).



84-194-2-15

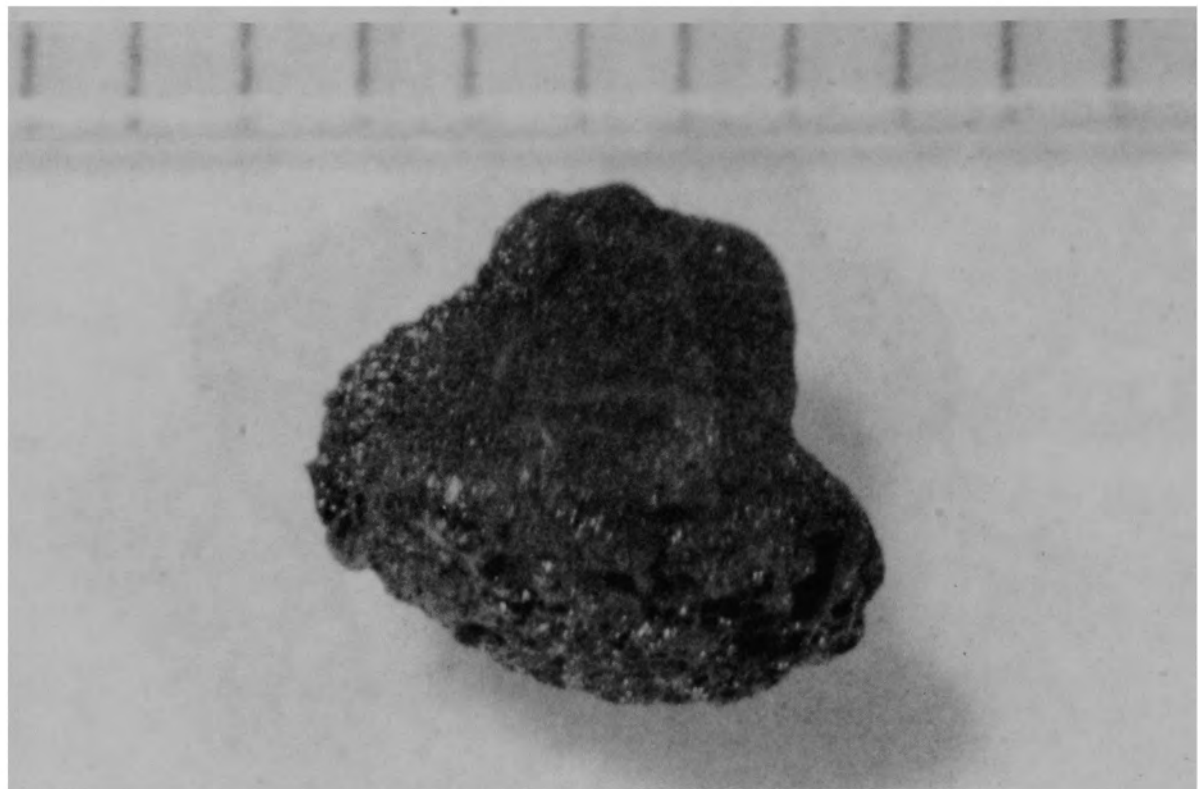
a) Particle 5D (size range: $>4000 \mu\text{m}$)



84-194-2-24

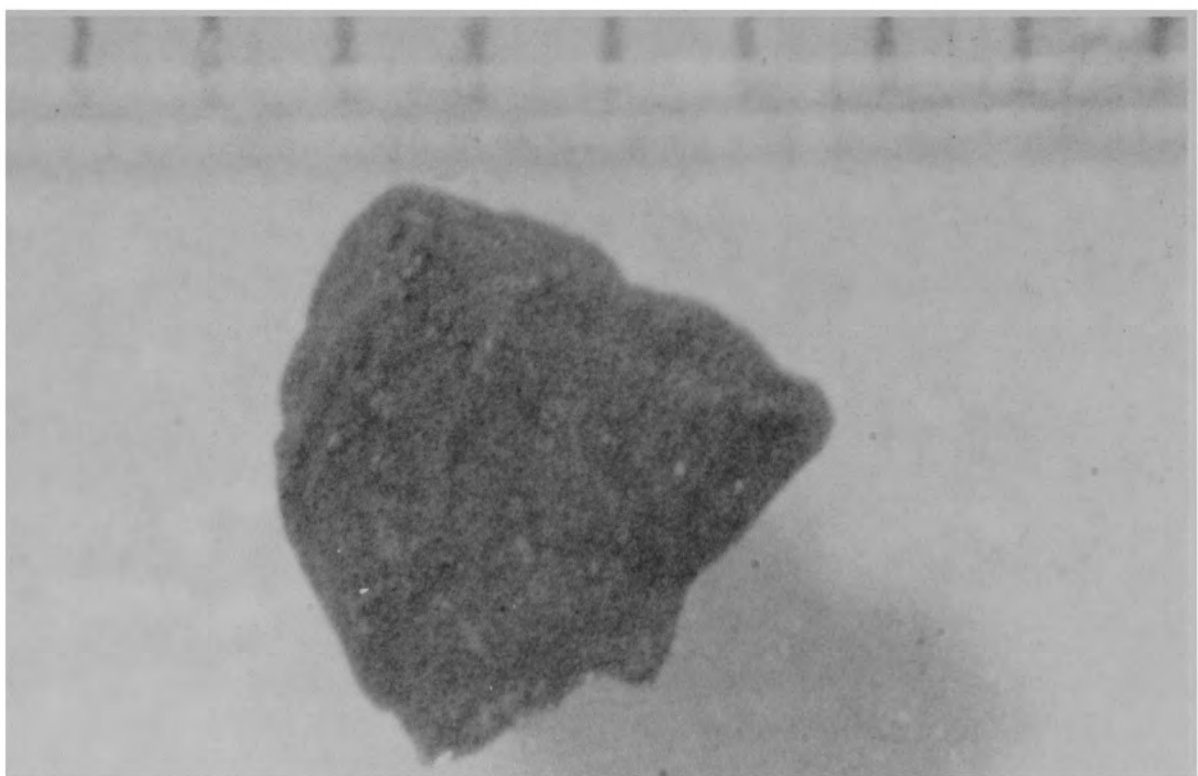
b) Particle 5E (size range: $>4000 \mu\text{m}$)

Figure B-18. Particles from Sample 5 (E9, 8 cm).



84-194-2-27

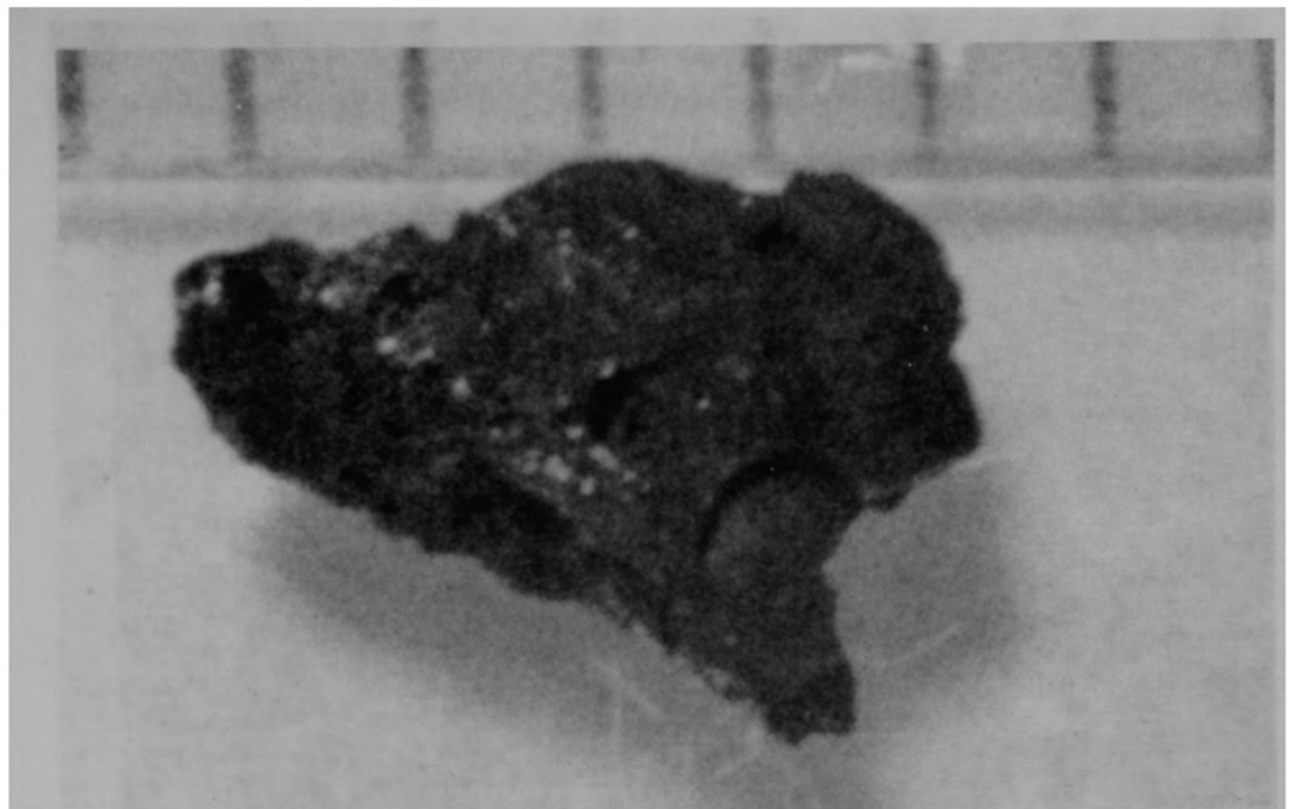
a) Particle 5F (size range: 1680-4000 μm)



84-194-3-4

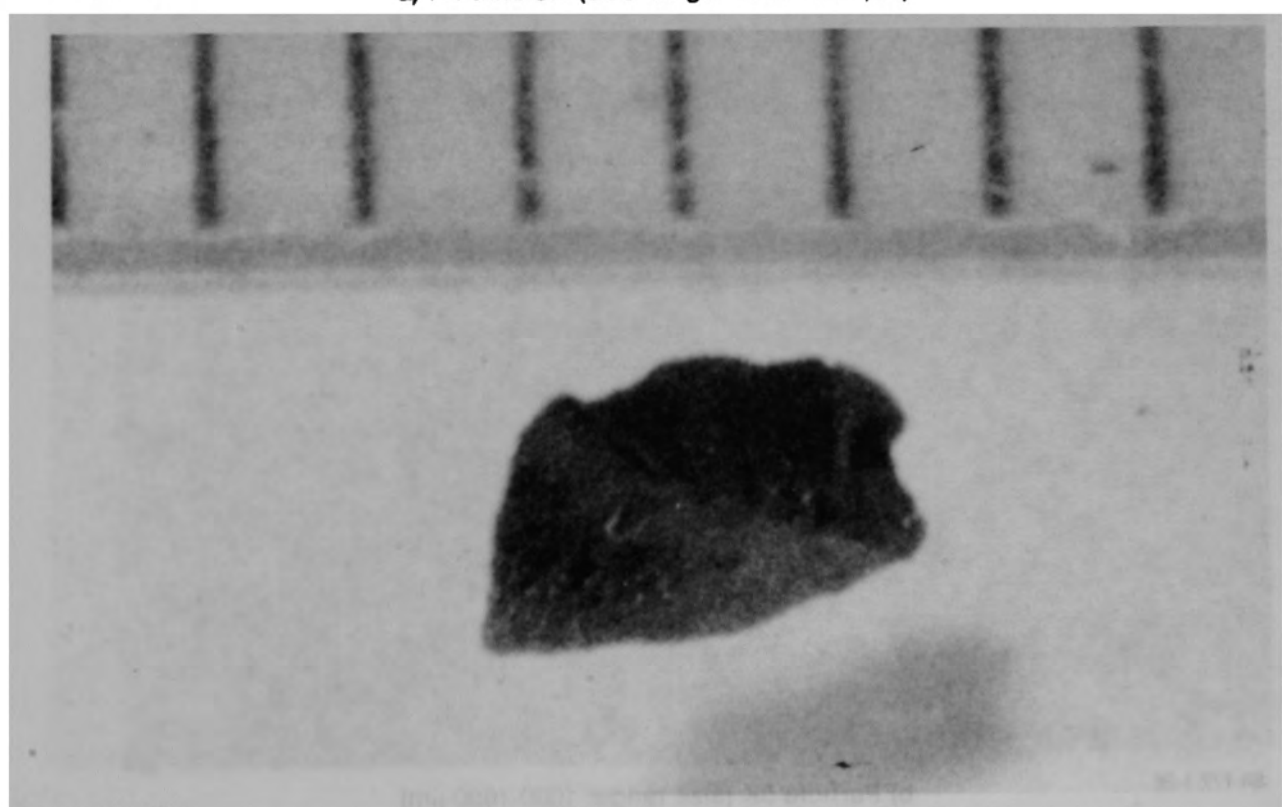
b) Particle 5G (size range: 1680-4000 μm)

Figure B-19. Particles from Sample 5 (E9, 8 cm).



RA 194 3-19

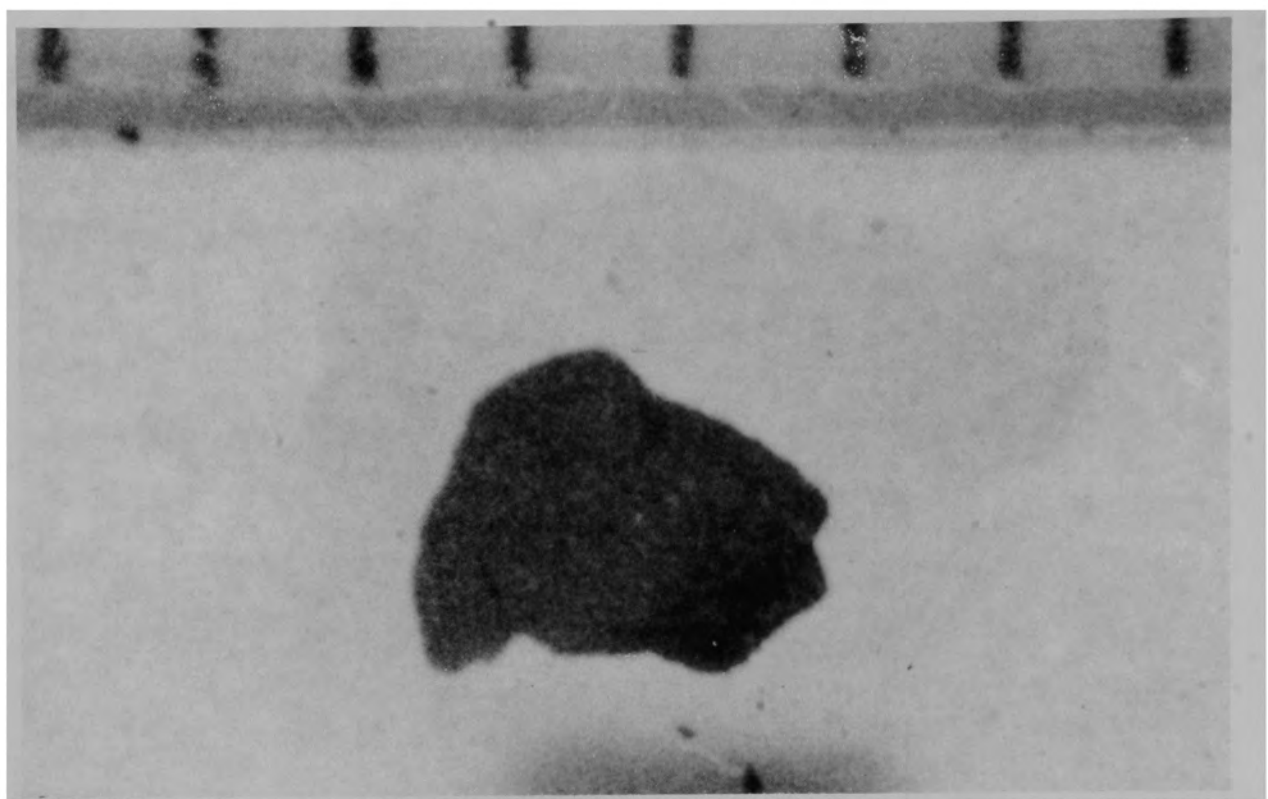
a) Particle 5H (size range: 1000-1680 μm)



84-172-1-22

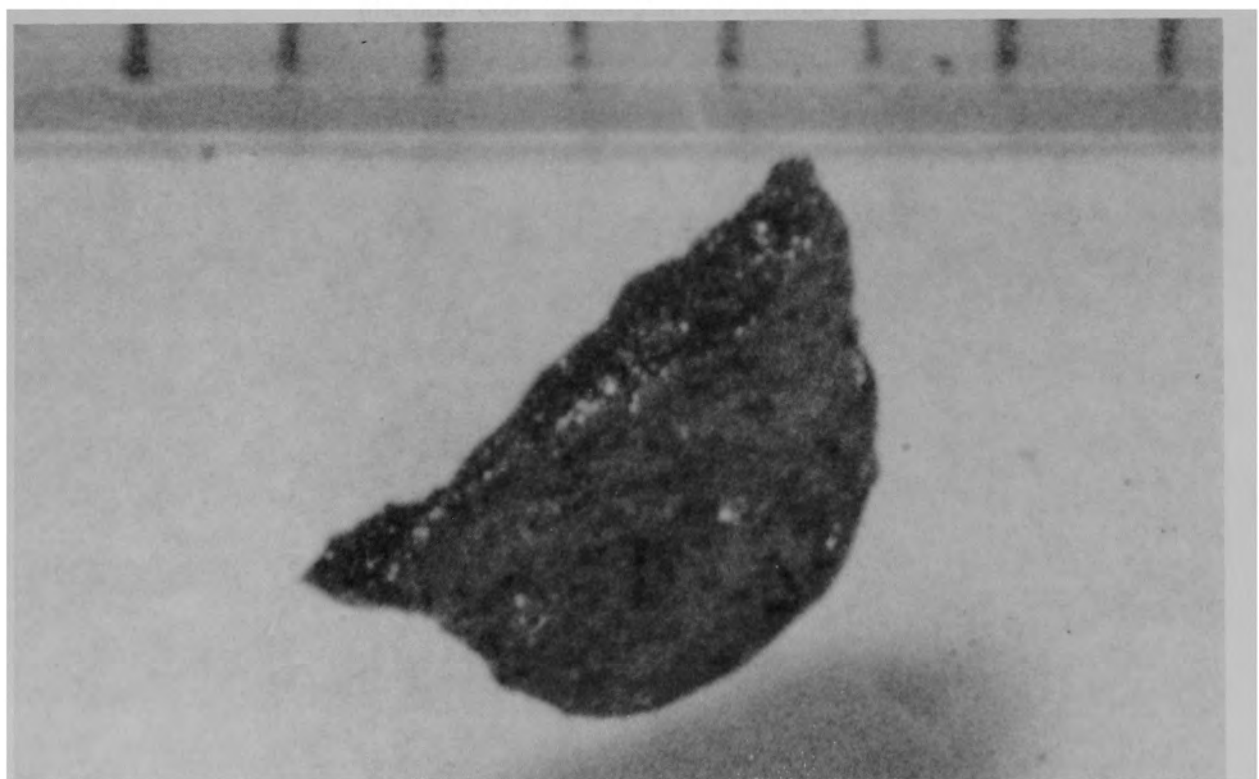
b) Particle 5I (size range: 1000-1680 μm)

Figure B-20. Particles from Sample 5 (E9, 8 cm).



84-172-1-24

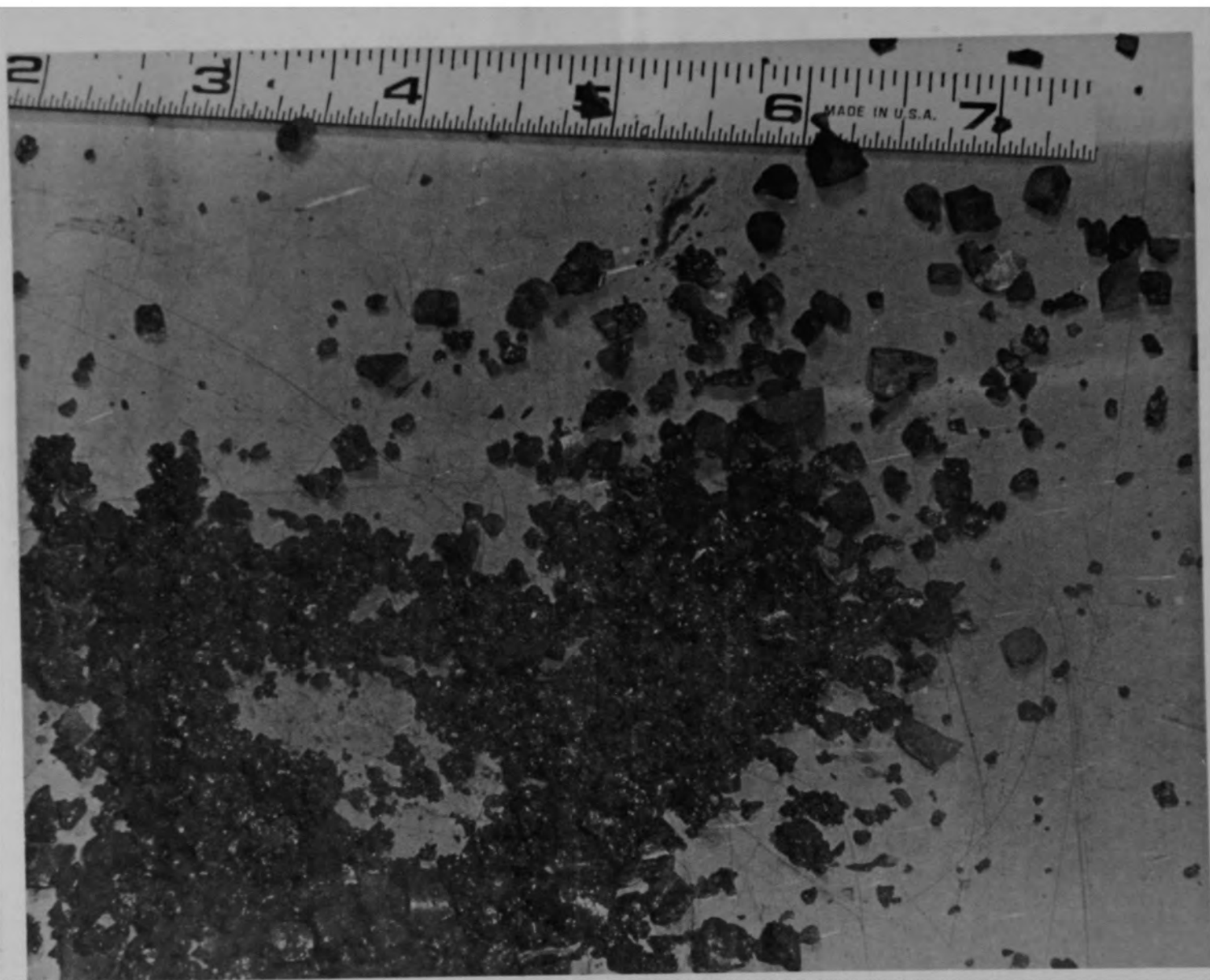
a) Particle 5J (size range: 1000-1680 μm)



84-172-1-26

b) Particle 5K (size range: 1000-1680 μm)

Figure B-21. Particles from Sample 5 (E9, 8 cm).



83-655-10-13

Figure B-22. The bulk material for Sample 6 (E9, 56 cm).



84-199-3-4

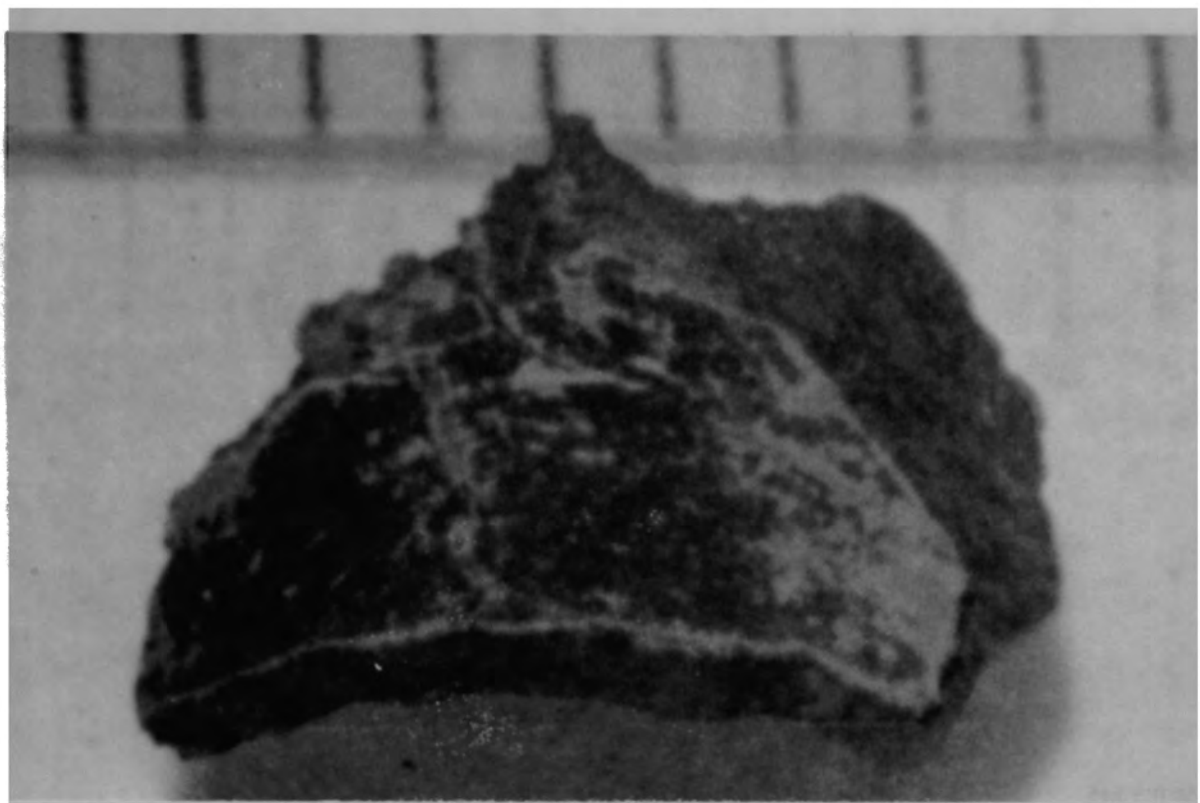
a) Front view of particle



84-199-3-6

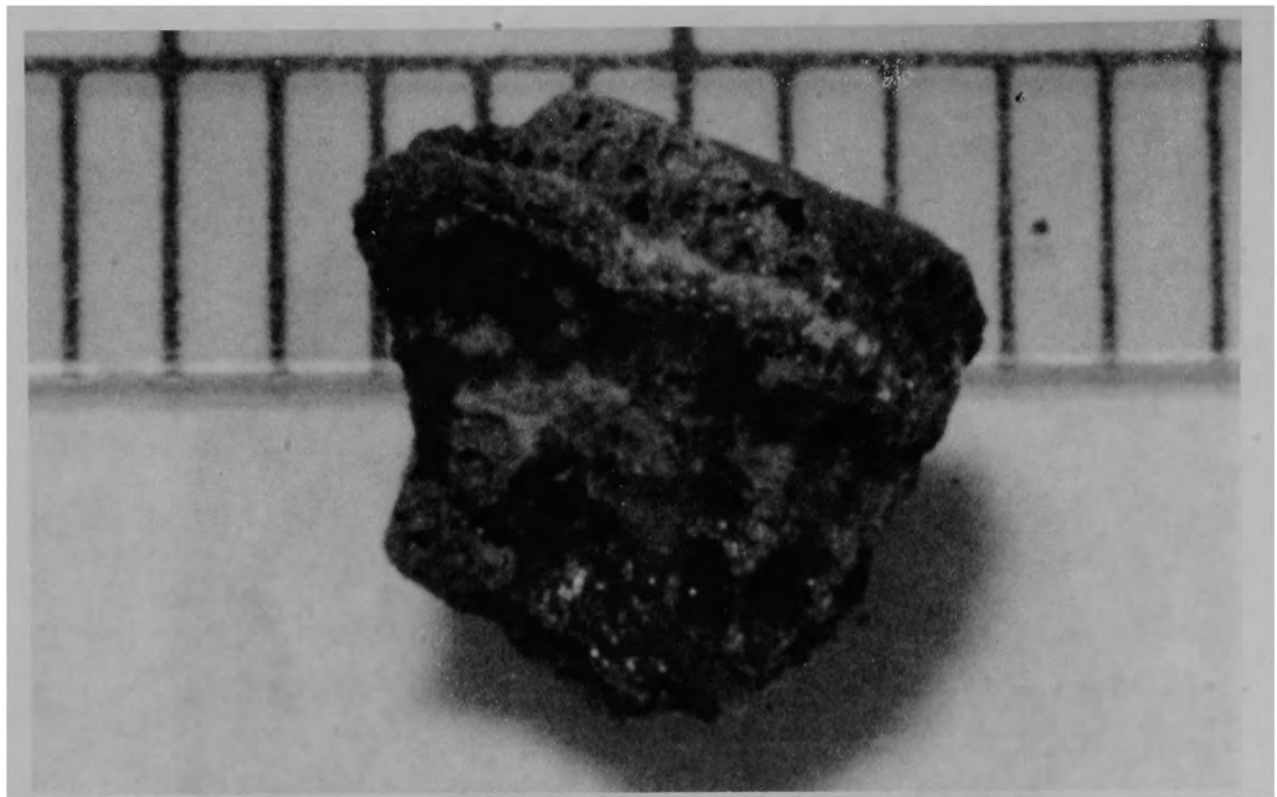
b) Back view of particle

Figure B-23. Particle 6A from Sample 6 (E9, 56 cm), size range:
 $>4000 \mu\text{m}$.



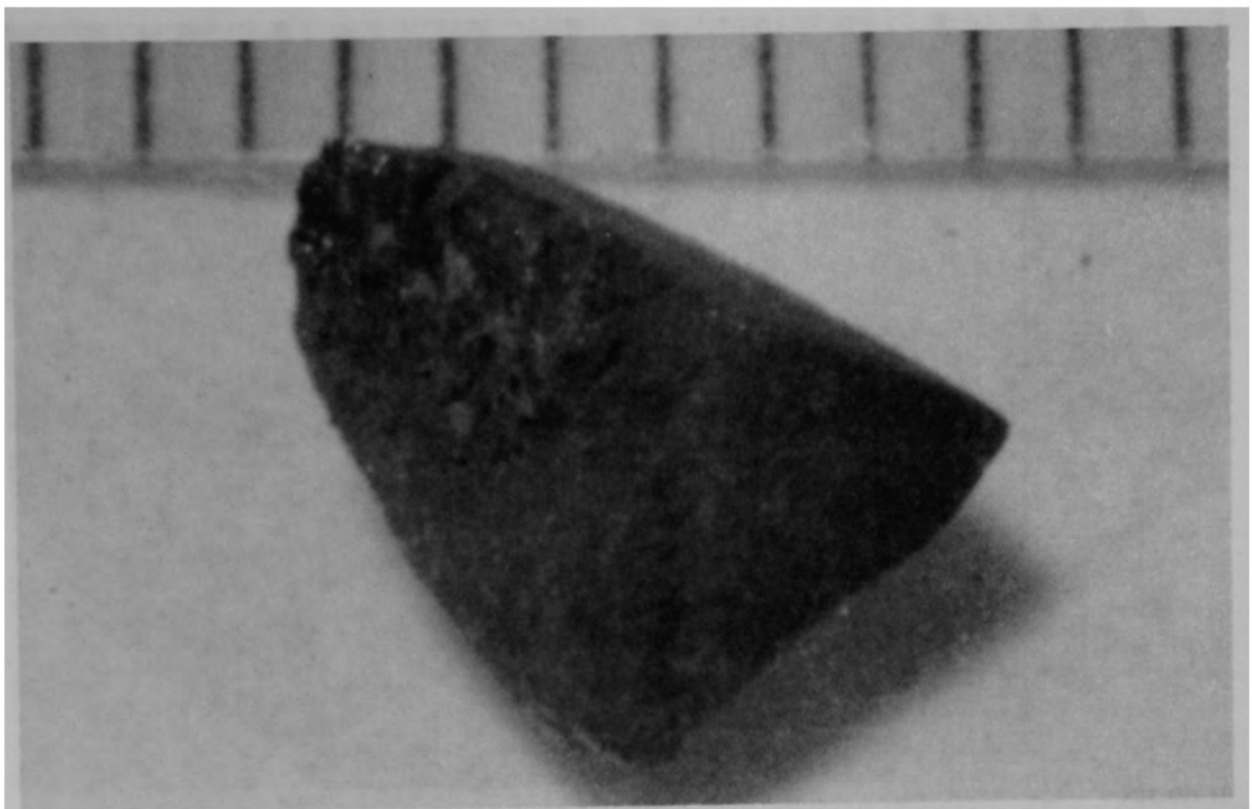
84-199-3-12

Figure B-24. Particle 6B from Sample 6 (E9, 56 cm), size range: >4000 μm .



84-199-3-15

Figure B-25. Particle 6C from Sample 6 (E9, 56 cm), size range: $>4000\mu\text{m}$.



84-199-3-19

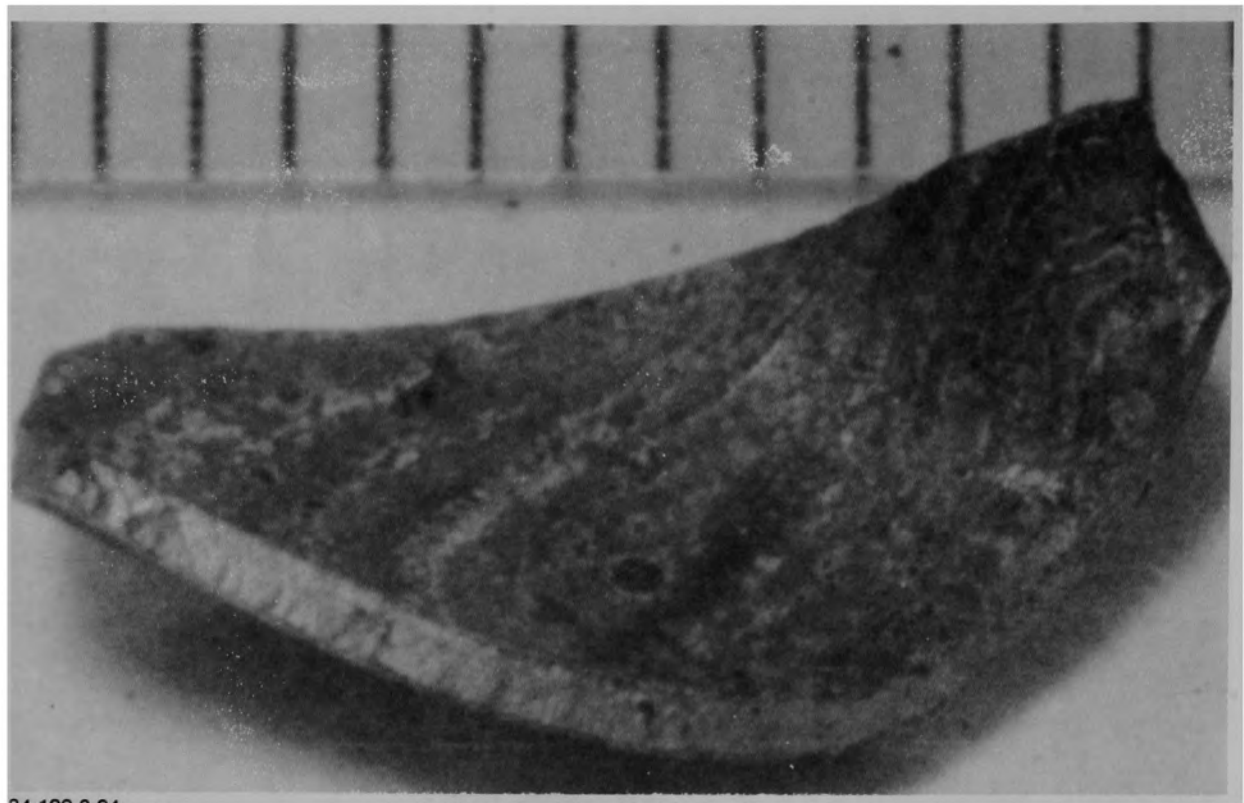
a) Front view of particle



84-199-3-21

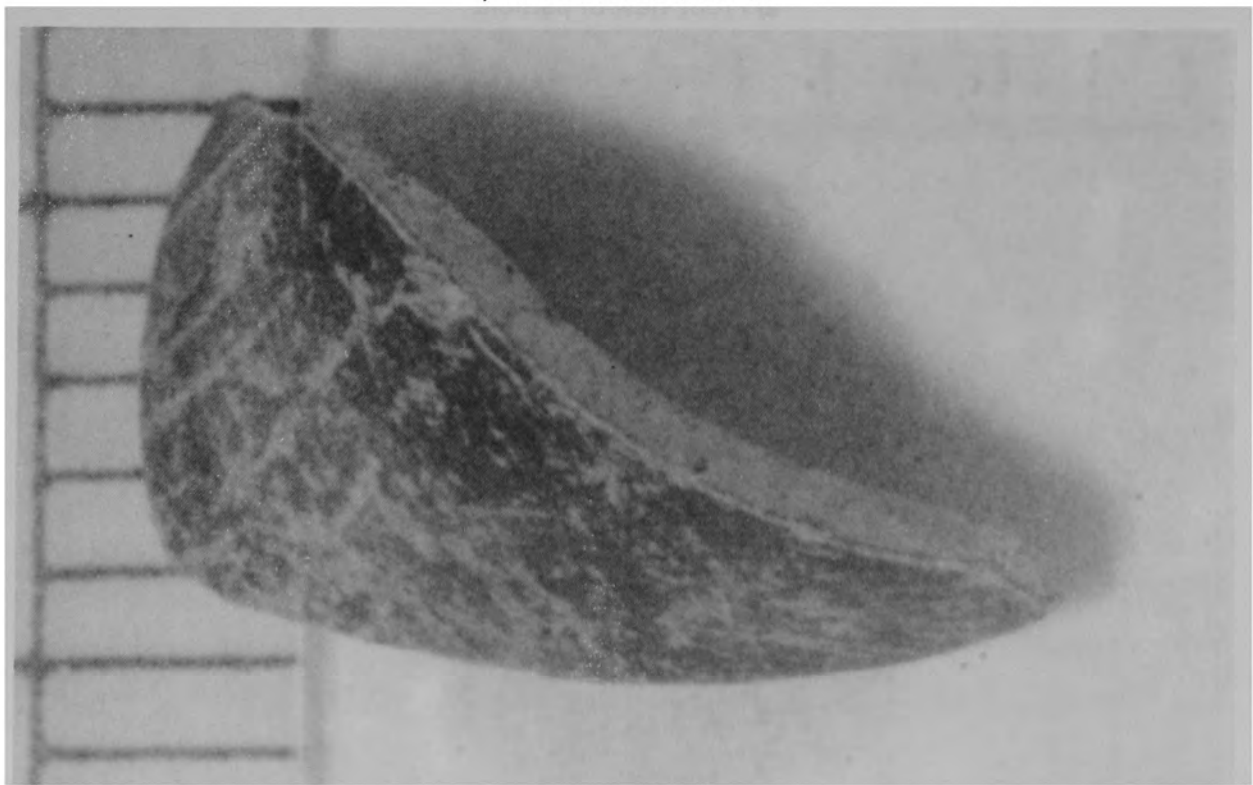
b) Back view of particle

Figure B-26. Particle 6D from Sample 6 (E9, 56 cm), size range:
 $>4000 \mu\text{m}$.



84-199-3-24

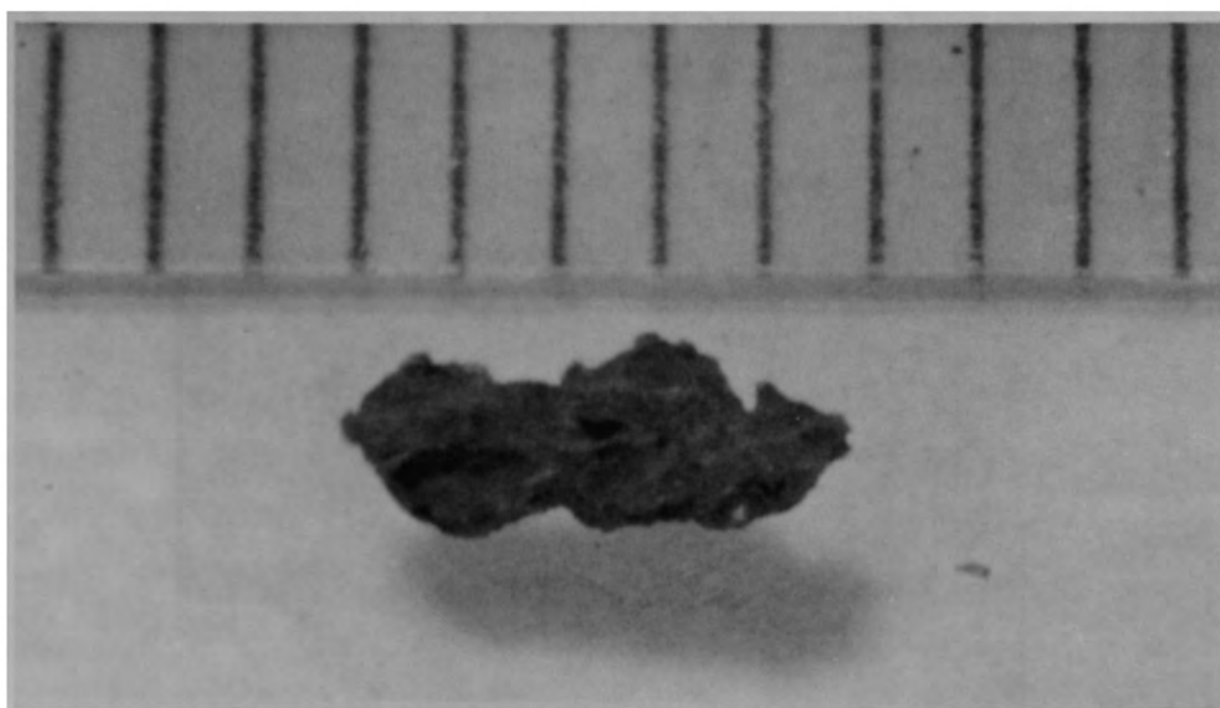
a) Front view of particle



84-199-3-26

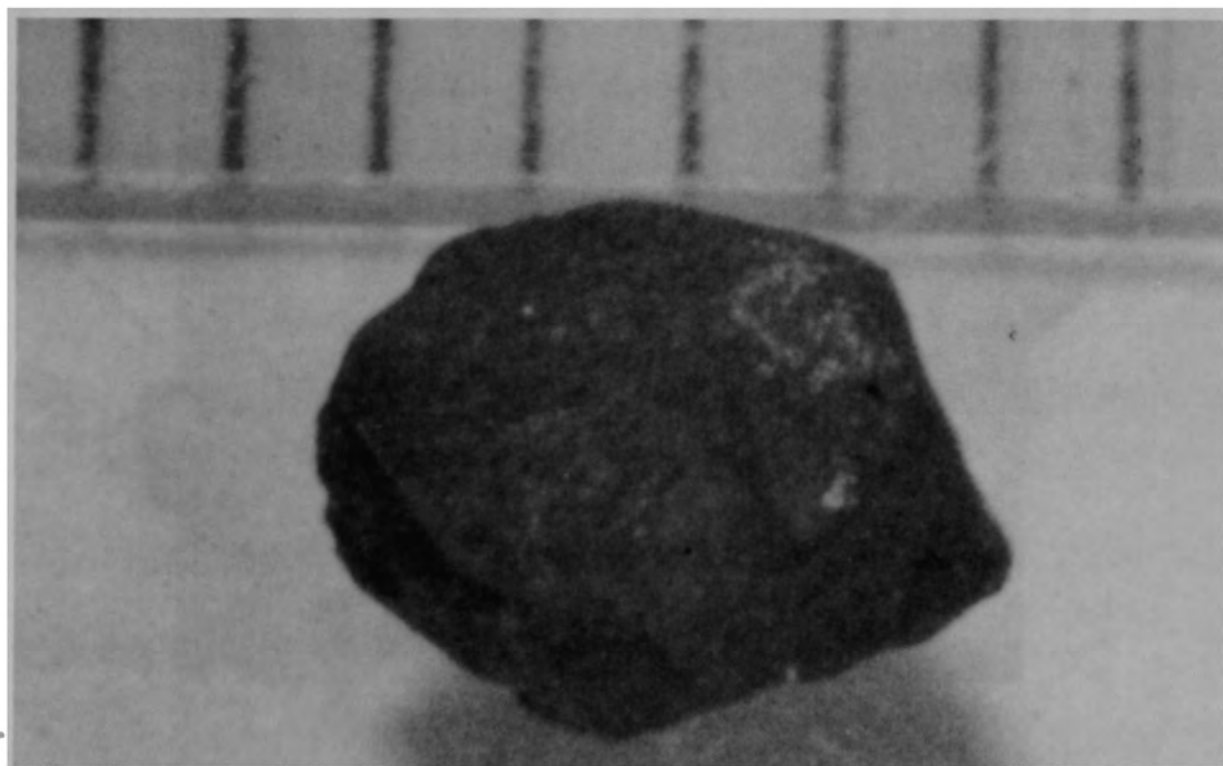
b) Back view of particle

Figure B-27. Particle 6E from Sample 6 (E9, 56 cm), size range:
 $>4000 \mu\text{m}$.



84-199-4-6

a) Particle 6F (size range: >1680-4000 μm)



84-199-4-8

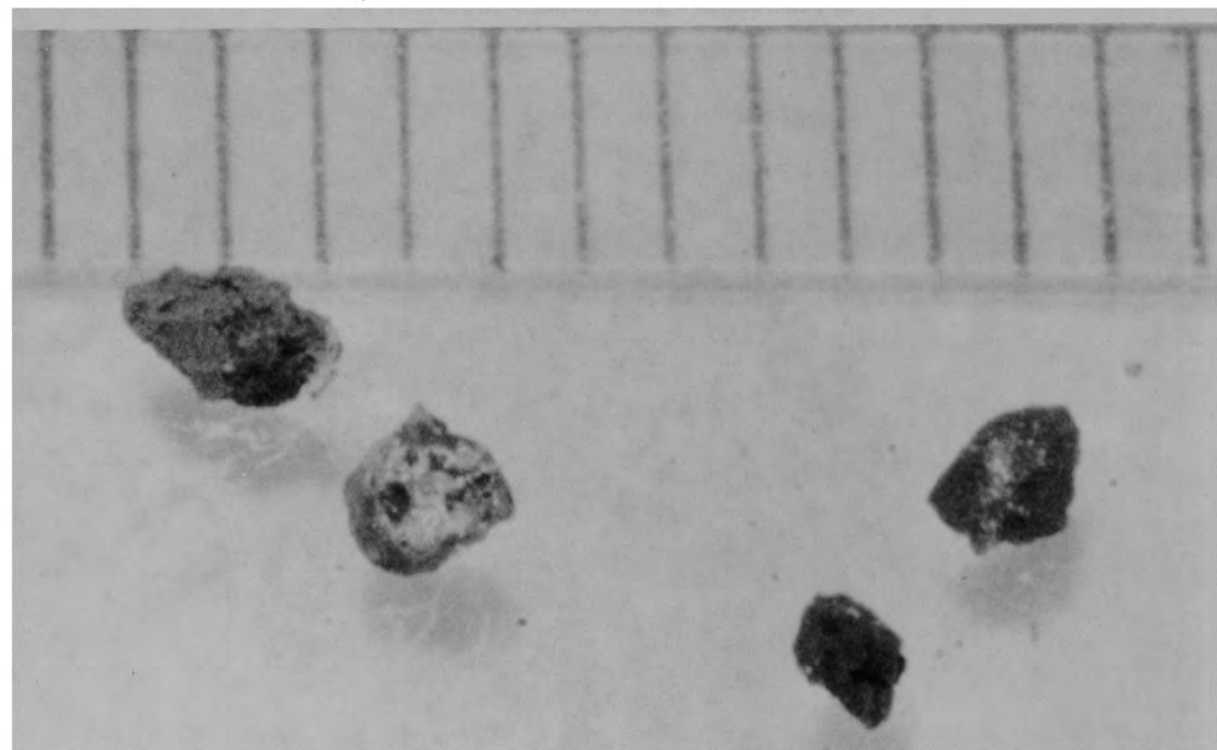
b) Particle 6G (size range: >1680-4000 μm)

Figure B-28. Particles from Sample 6 (E9, 56 cm).



84-199-4-10

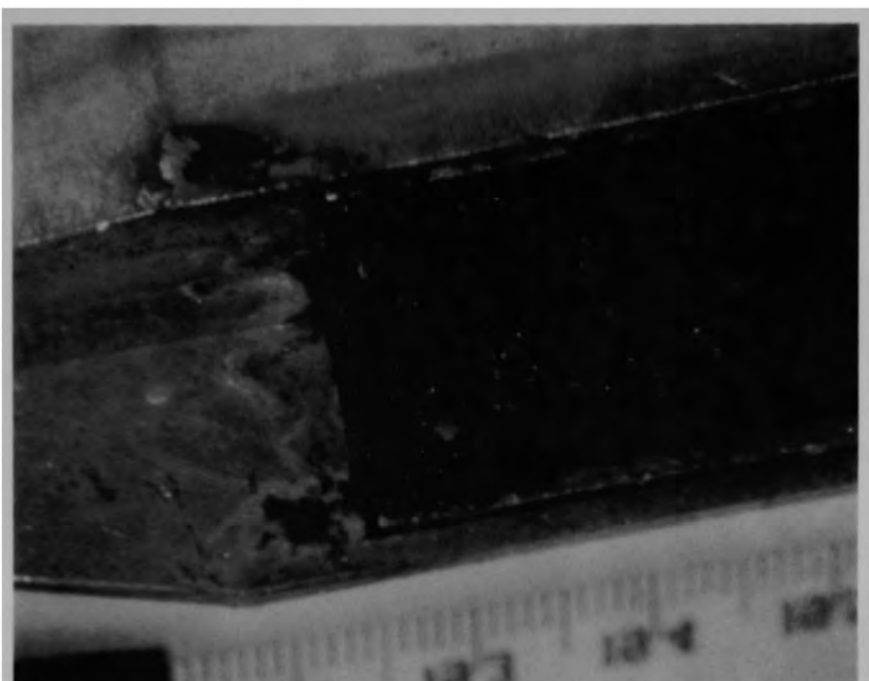
a) Particle 6H (size range: 1680-4000 μm)



84-201-1-5

b) Particle 6I, 6J, and 6K (size range: 1000-1680 μm)

Figure B-29. Particles from Sample 6 (E9, 56 cm).



84-238

a) Material in sampling tool (shows stratification)

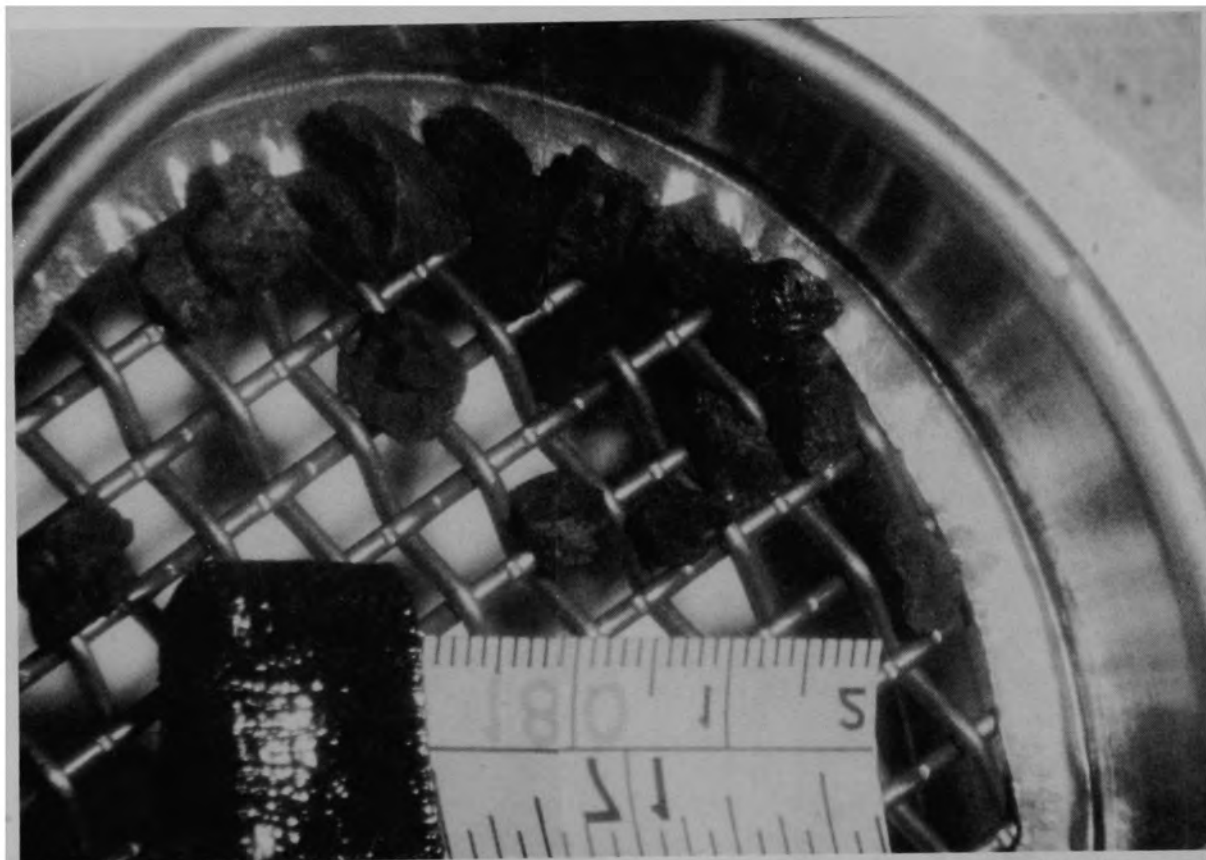


84-240

b) After removing material from sampling tool

Figure B-30. The bulk material for Sample 7, (H8, 36 cm).

B-34



84-394

84-393

Figure B-31. Particles >4000 μm from Sample 7 (H8, 36 cm).

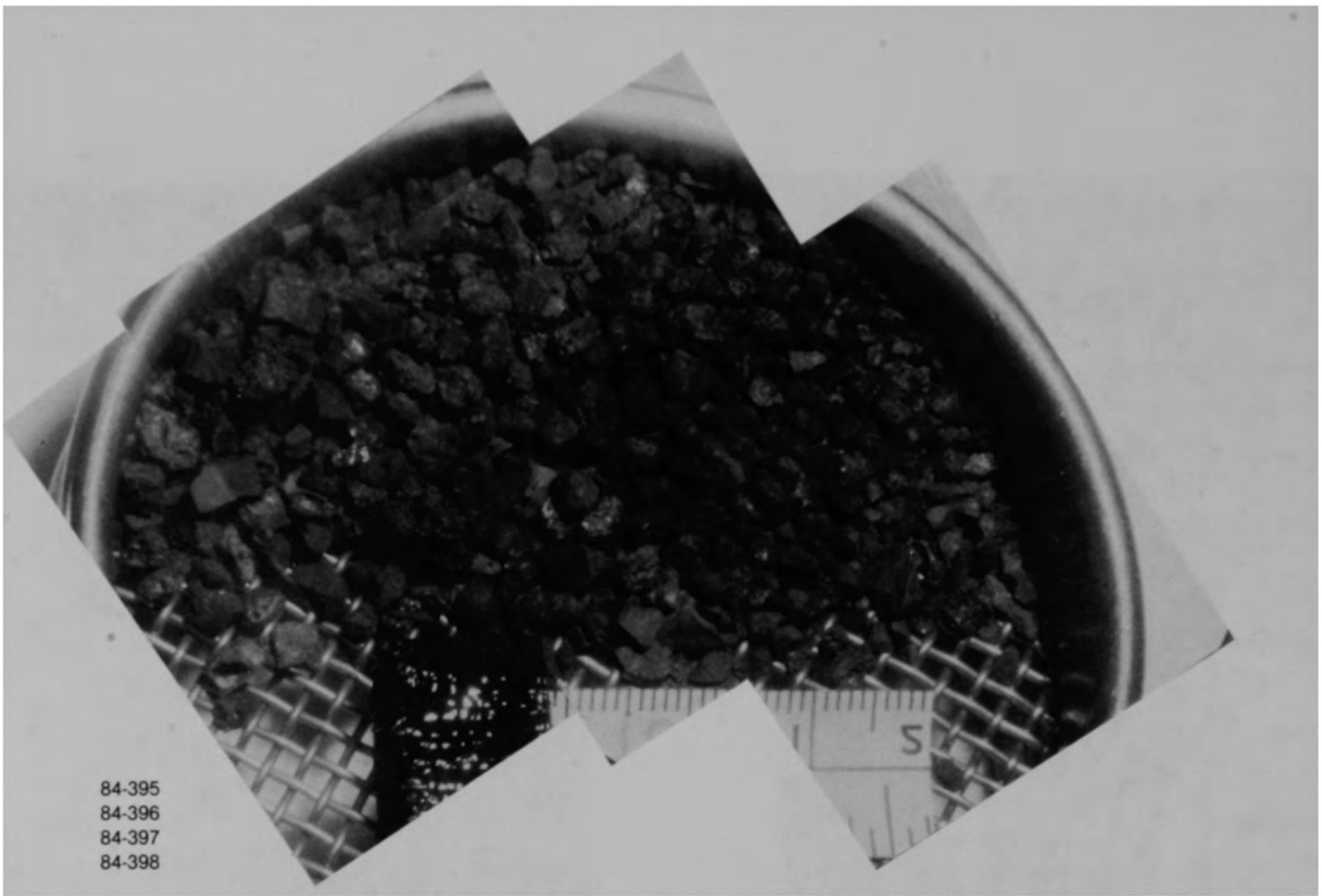
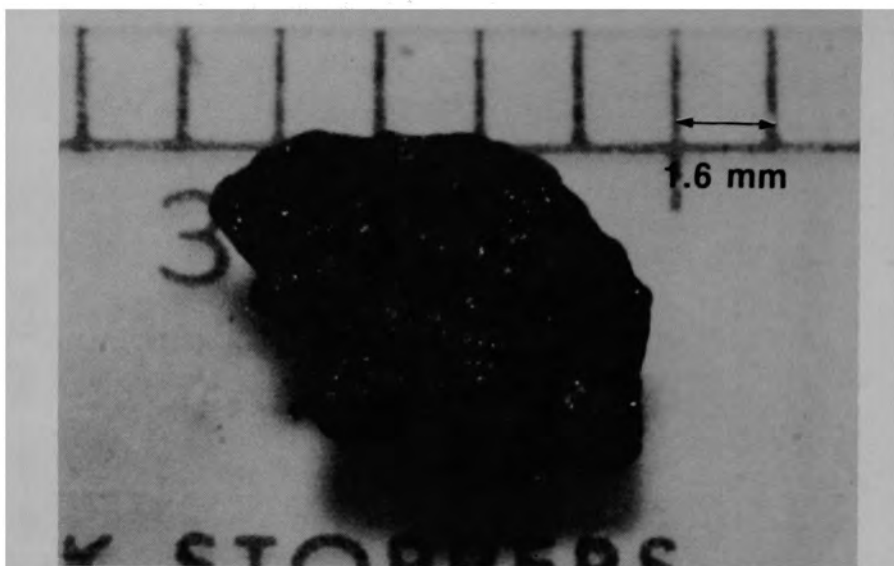
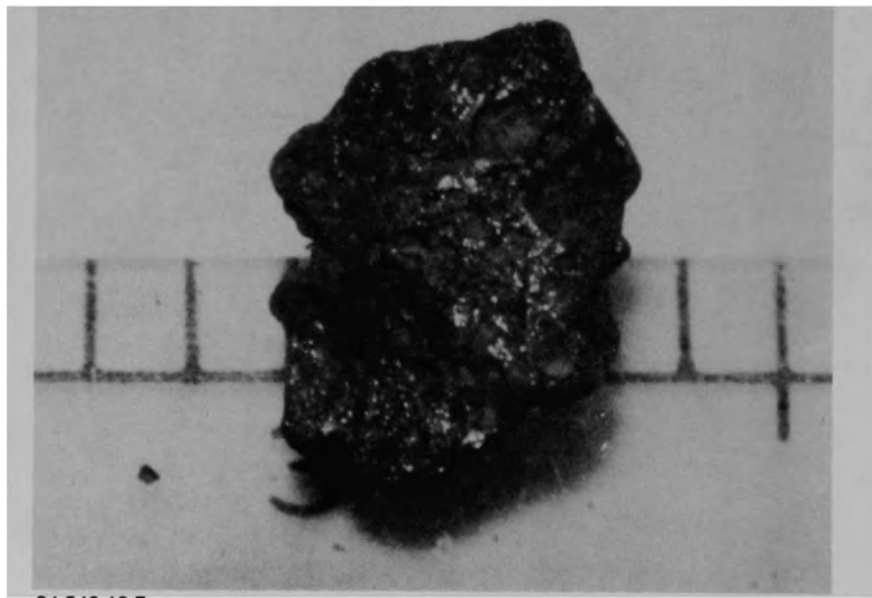


Figure B-32. Particle size fraction (size range 1680-4000 μm) from Sample 7, (H8, 36 cm).



84-546-13-5

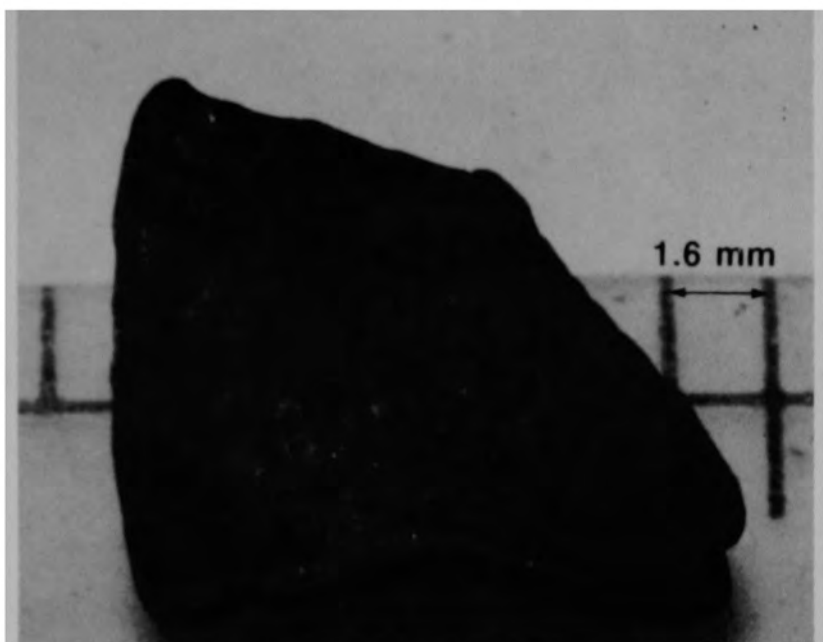
a) Front view of particle



84-546-13-7

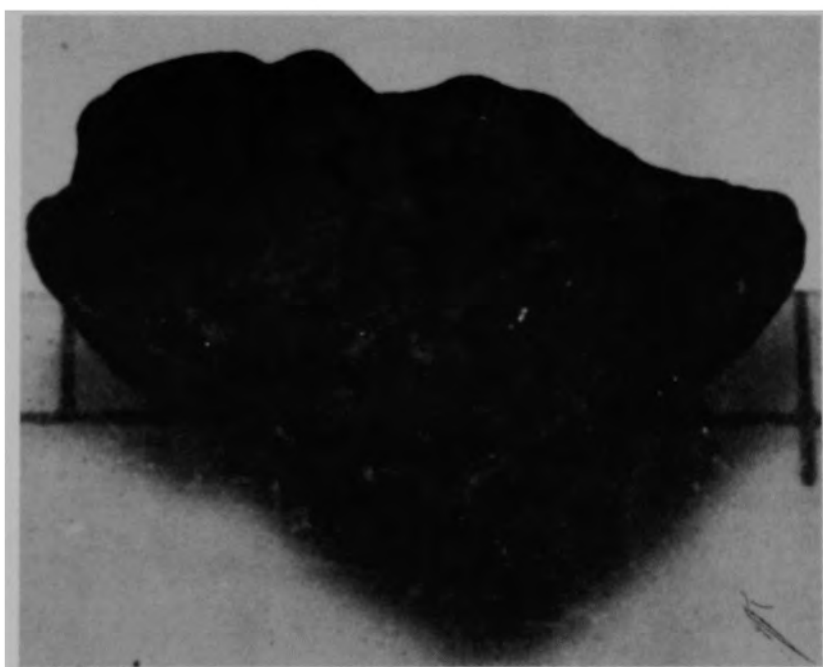
b) Back view of particle

Figure B-33. Particle 7A from Sample 7 (H8, 36 cm), size range:
 $>4000 \mu\text{m}$.



84-546-13-8

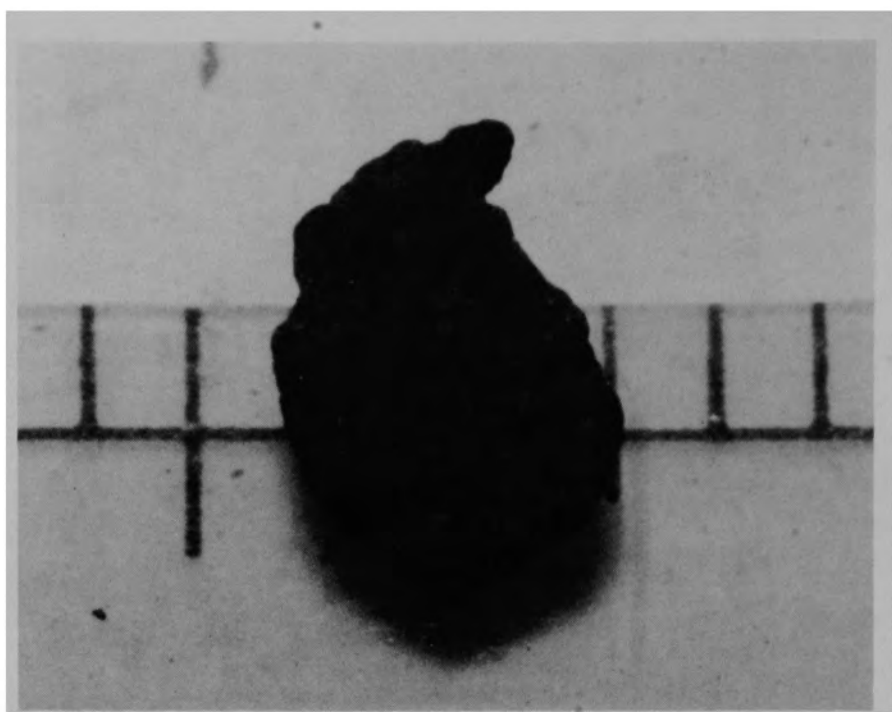
a) Front view of particle



84-546-13-10

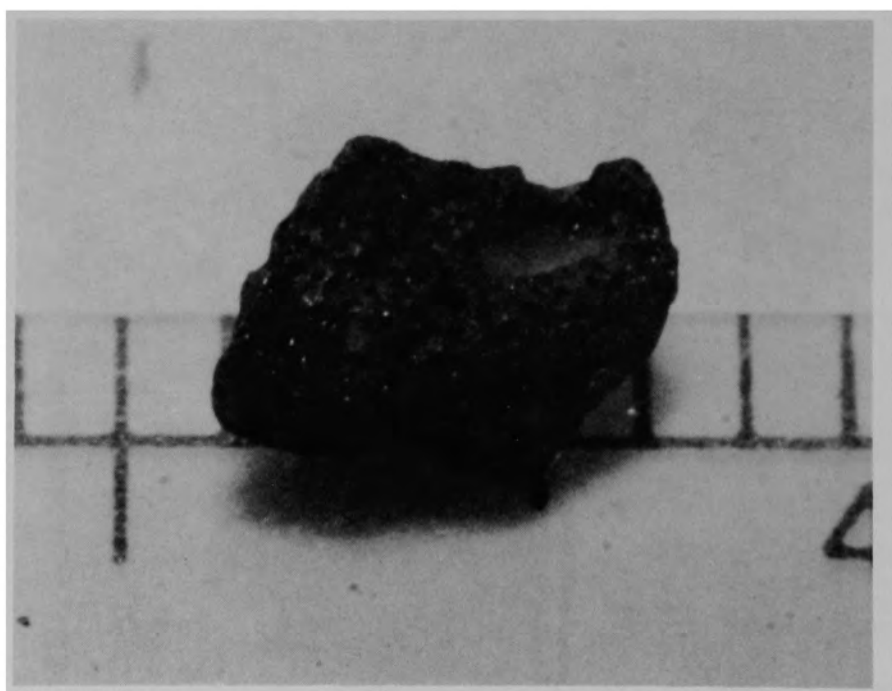
b) Back view of particle

Figure B-34. Particle 7B from Sample 7 (H8, 36 cm), size range:
 $>4000 \mu\text{m}$.



84-546-13-12

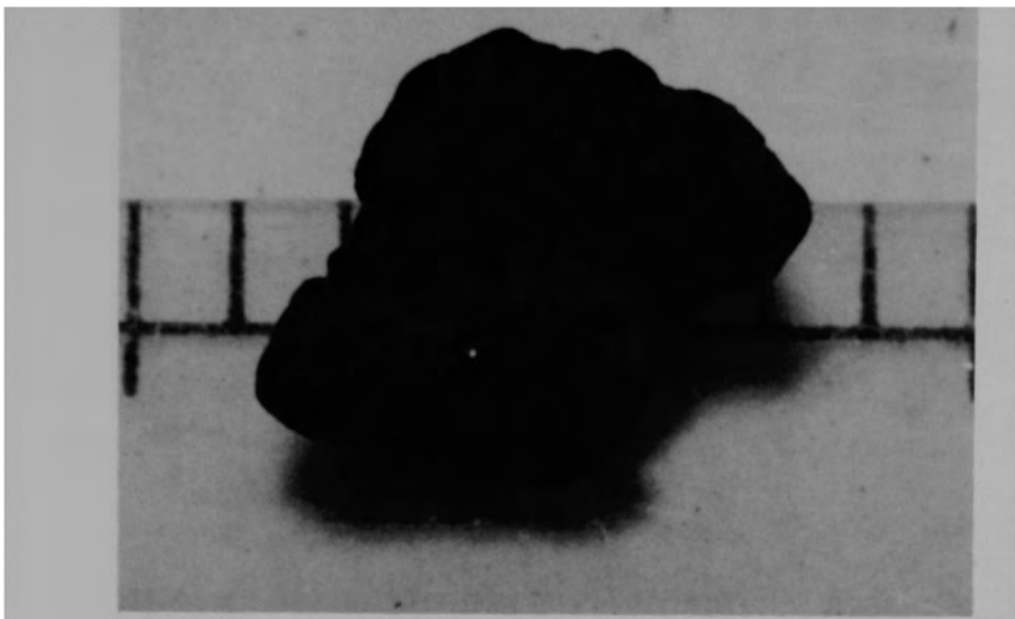
a) Front view of particle



84-546-13-14

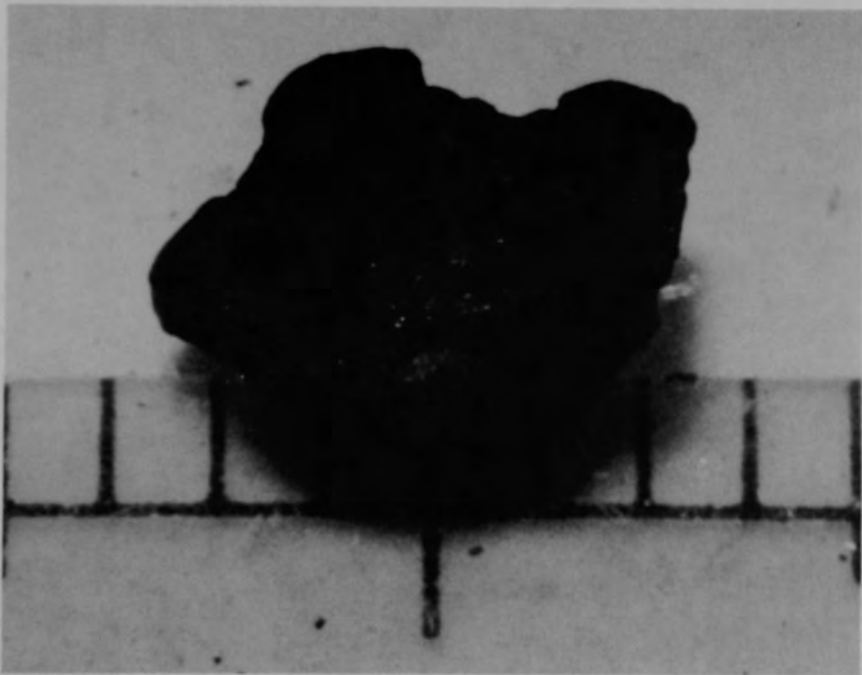
b) Back view of particle

Figure B-35. Particle 7C from Sample 7 (H8, 36 cm), size range: >4000 μm .



84-546-13-16

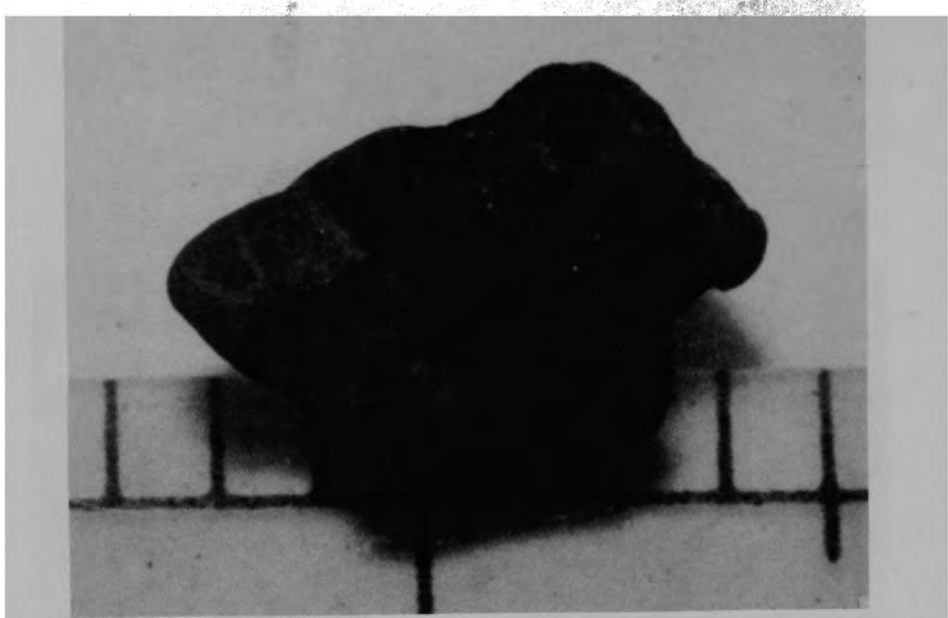
a) Front view of particle



84-546-13-18

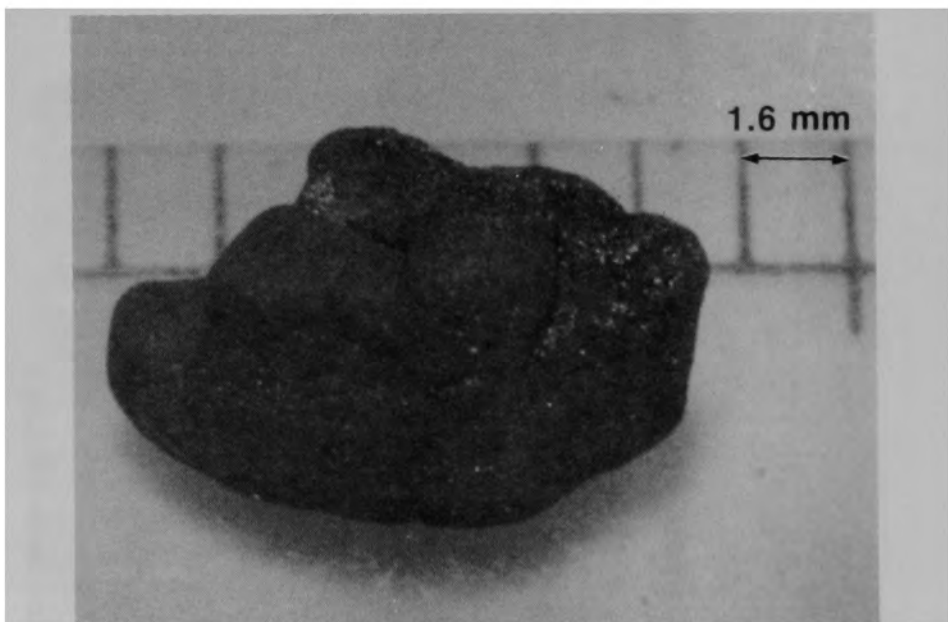
b) Back view of particle

Figure B-36. Particle 7D from Sample 7 (H8, 36 cm), size range: >4000 μm .



84-546-13-20

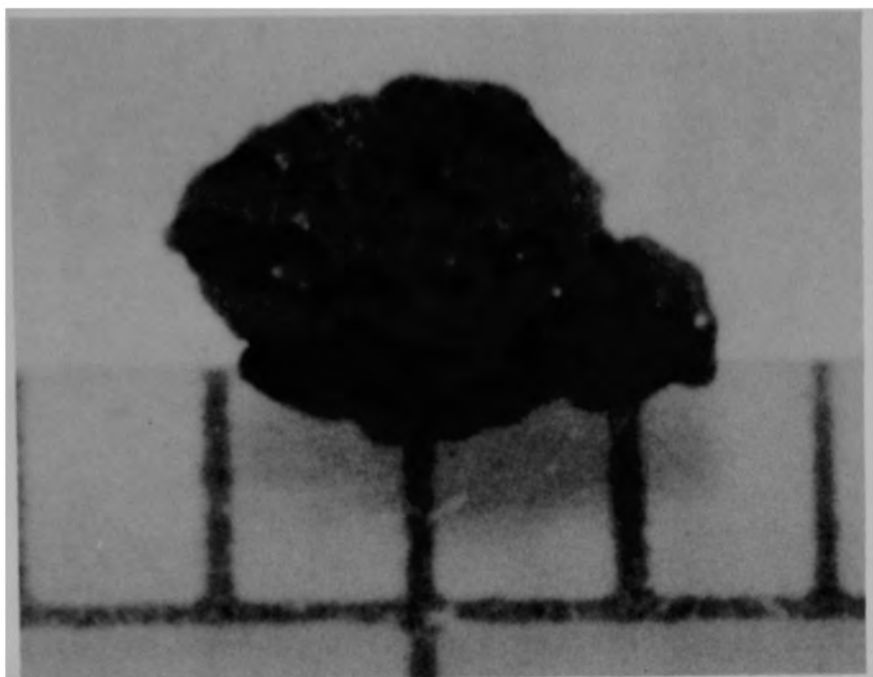
a) Front view of particle



84-546-13-22

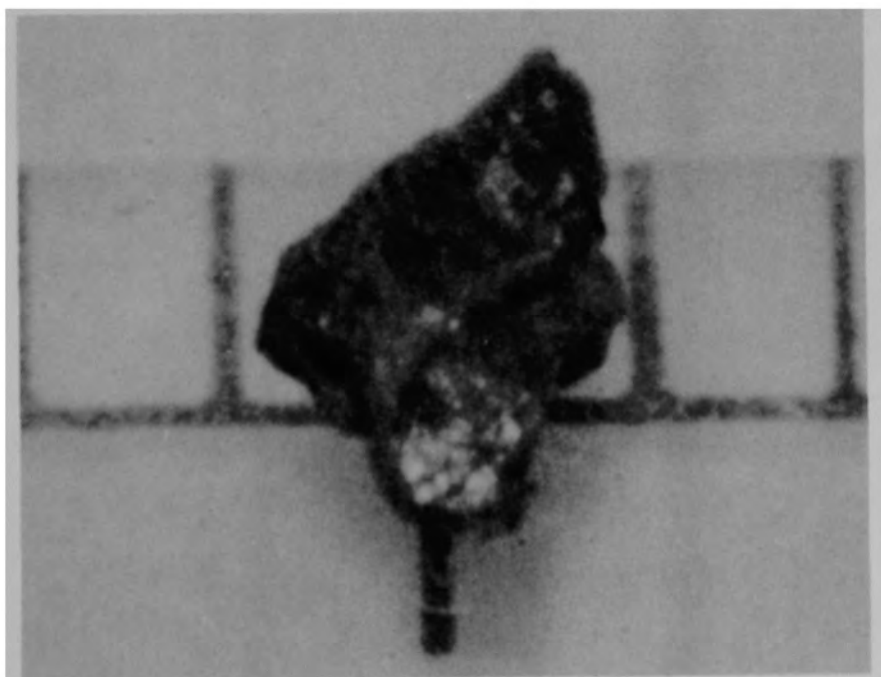
b) Back view of particle

Figure B-37. Particle 7E from Sample 7 (H8, 36 cm), size range:
 $>4000 \mu\text{m}$.



84-546-13-25

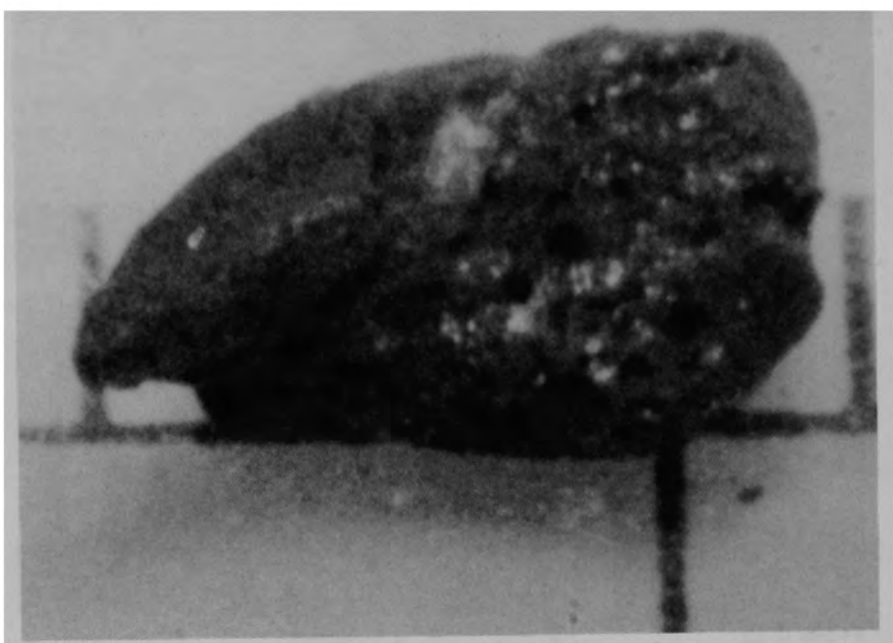
a) Front view of particle



84-546-13-26

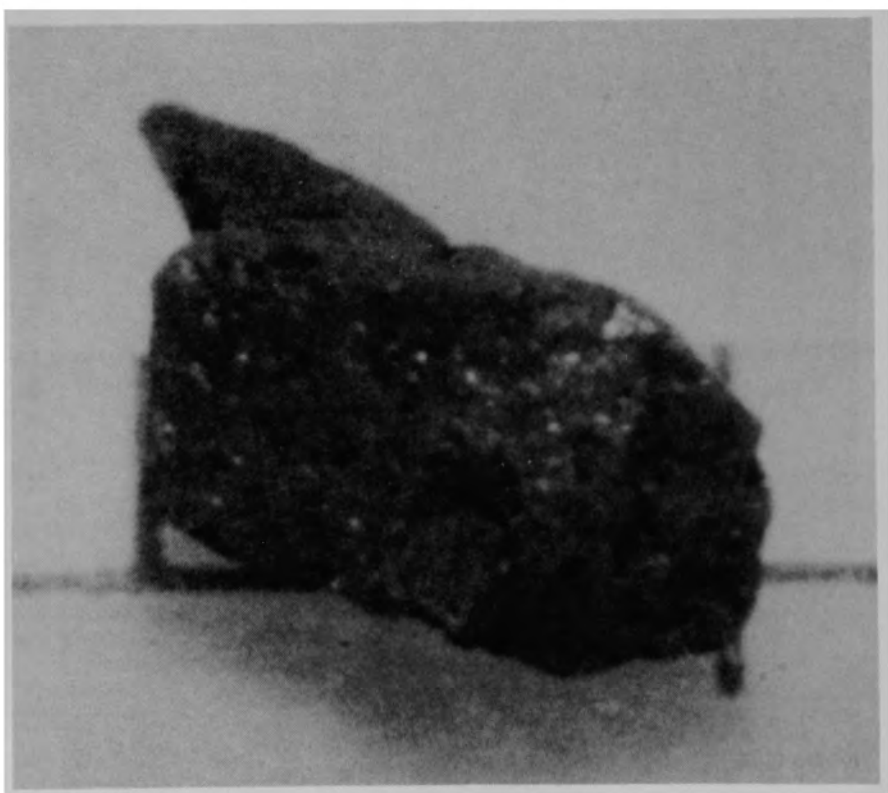
b) Back view of particle

Figure B-38. Particle 7F from Sample 7 (H8, 36 cm), size range: 1680-4000 μm .



884-546-13-29

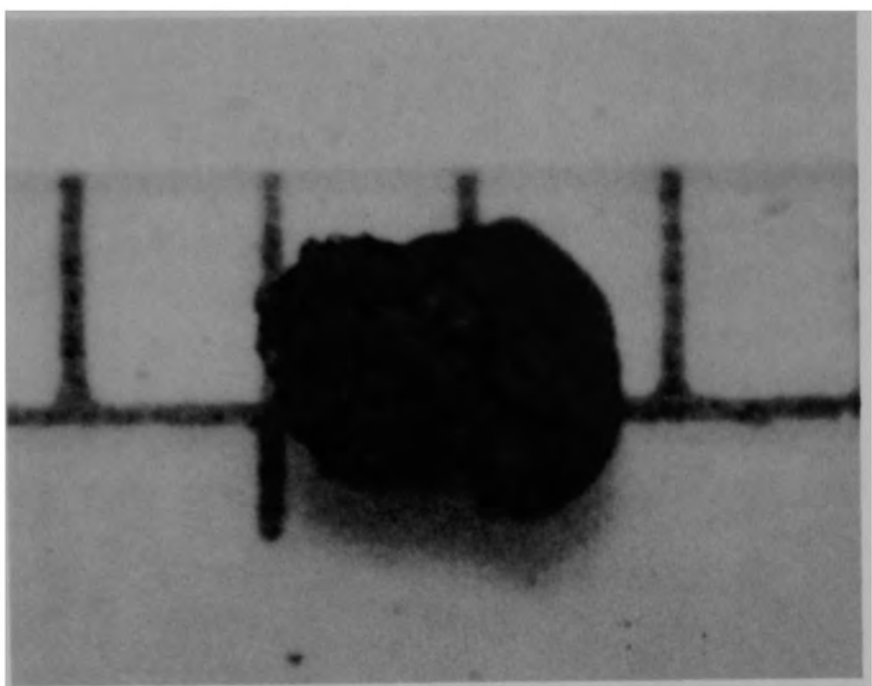
a) Front view of particle



84-546-13-30

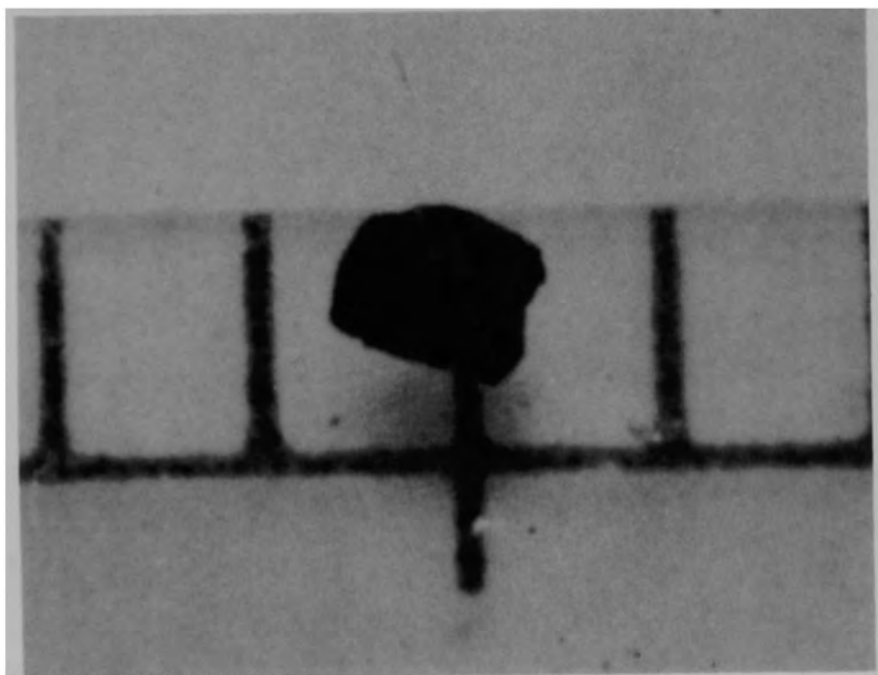
b) Back view of particle

Figure B-39. Particle 7G from Sample 7 (H8, 36 cm), size range: 1680-4000 μm .



84-546-14-7

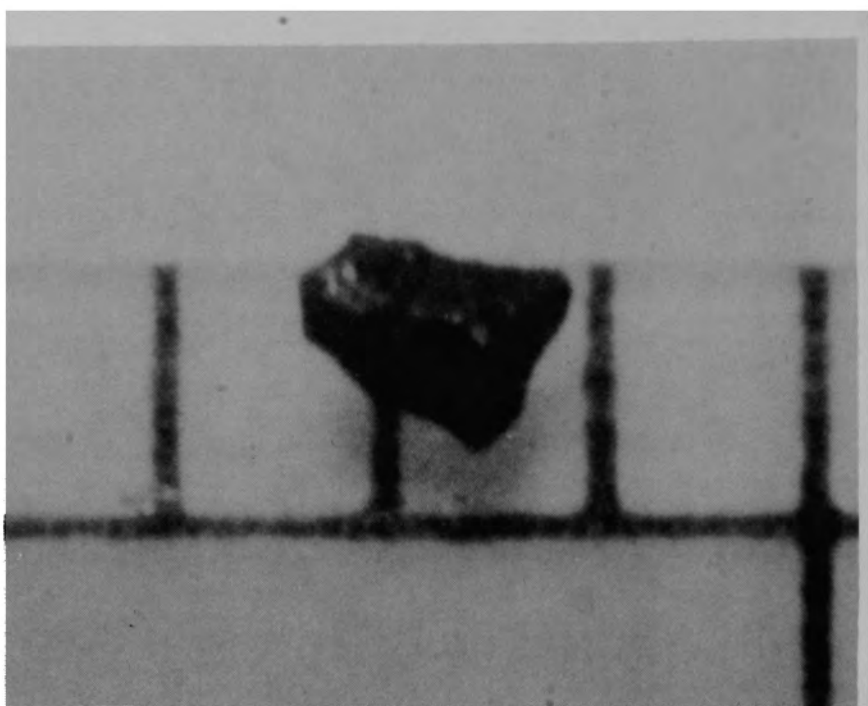
a) Particle 7H (size range: 1680-4000 μm)



84-546-14-9

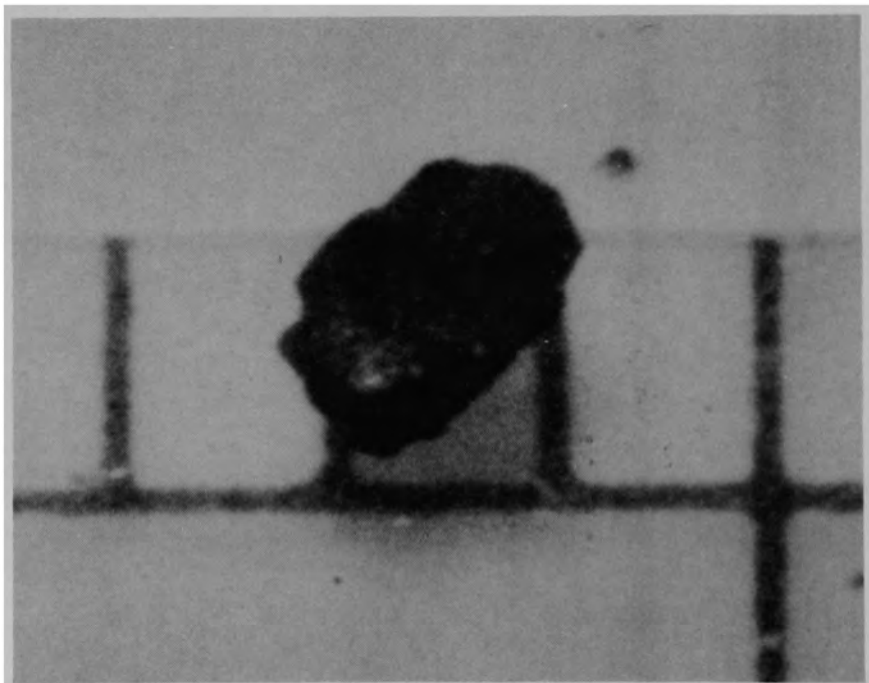
b) Particle 7I (size range: 1000-1680 μm)

Figure B-40. Particles from Sample 7 (H8, 36 cm).



84-546-14-12

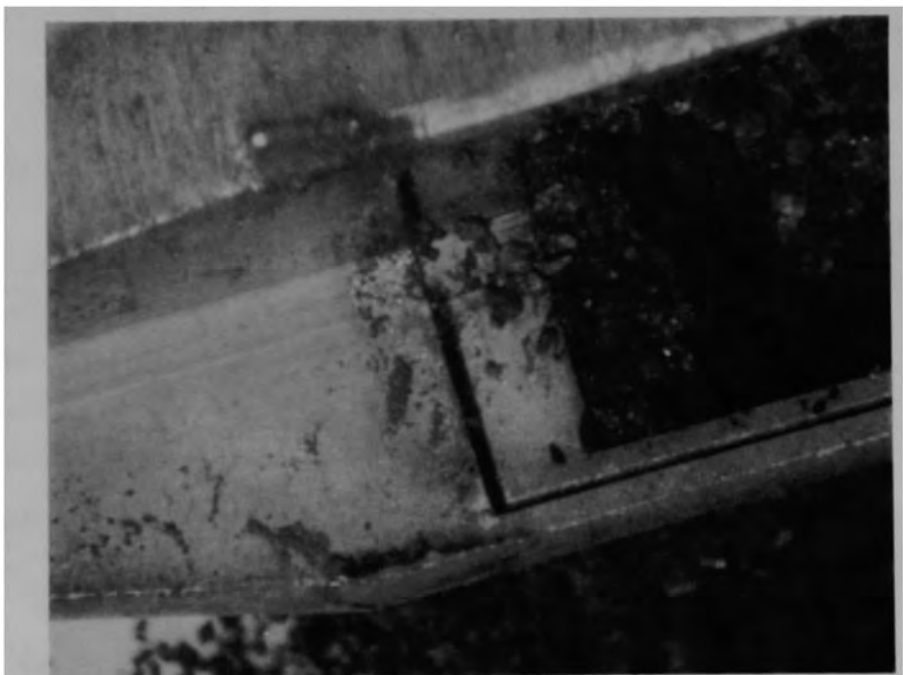
a) Particle 7J (size range: 1000-1680 μm)



84-546-14-13

b) Particle 7K (size range: 1000-1680 μm)

Figure B-41. Particles from Sample 7 (H8, 36 cm).



84-244

Figure B-42. Sample 8 (H8, 70 cm) being removed from sampling tool.

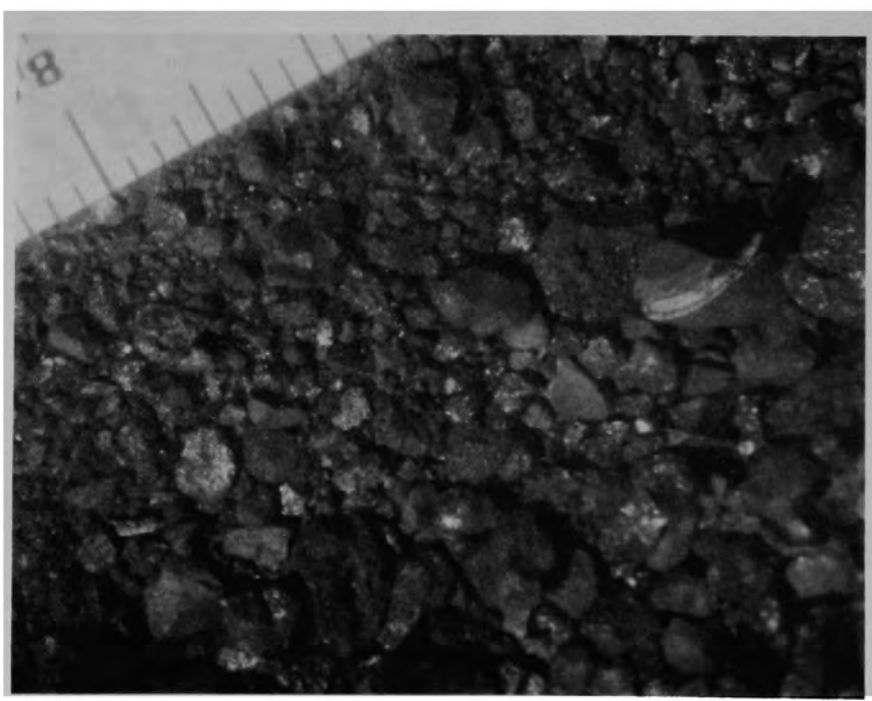
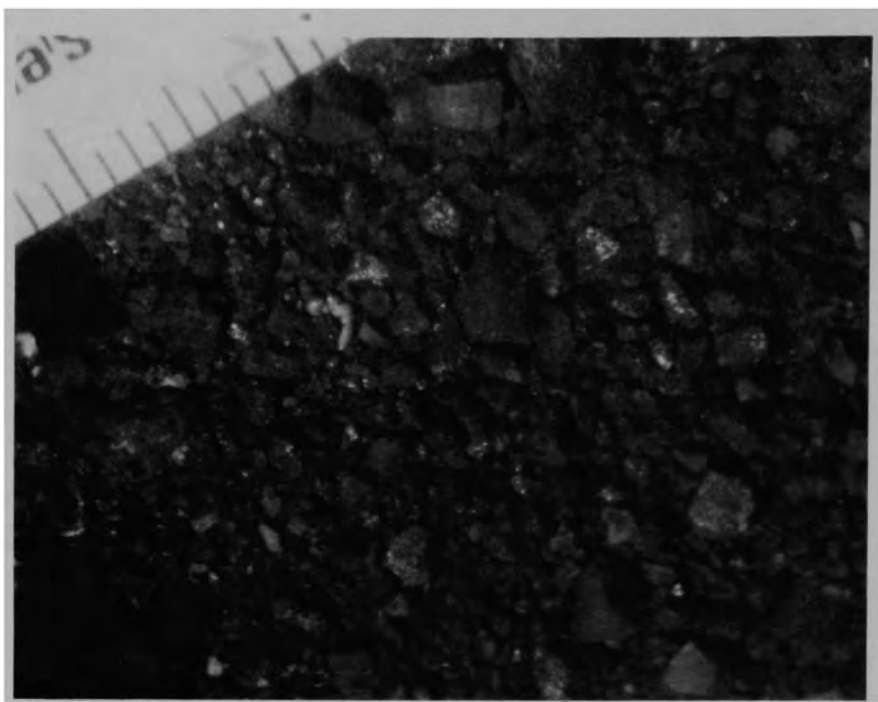


Figure B-43. Views of the bulk material for Sample 8 (H8, 70 cm) after removal from the sampling tool.

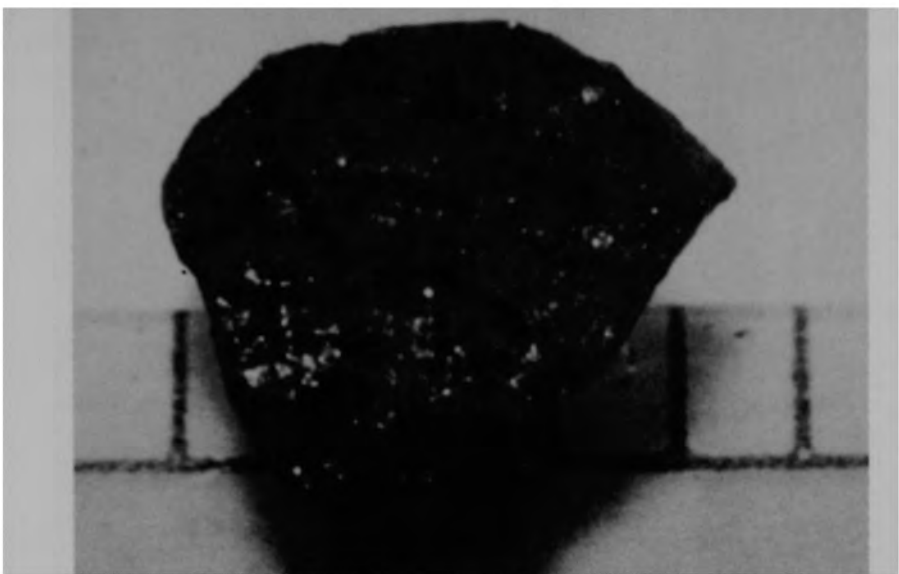


84-365
84-366
84-367
84-368

Figure B-44. Particles >4000 μm from Sample 8 (H8, 70 cm).

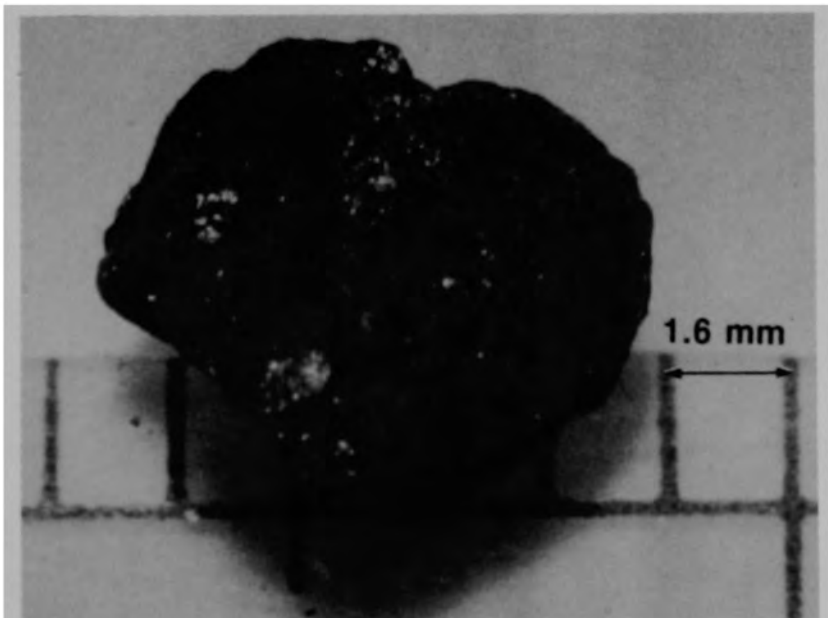


Figure B-45. Particle size fraction (size range: 1680-4000 μm) from Sample 8, (H8, 70 cm).



84-546-10-6

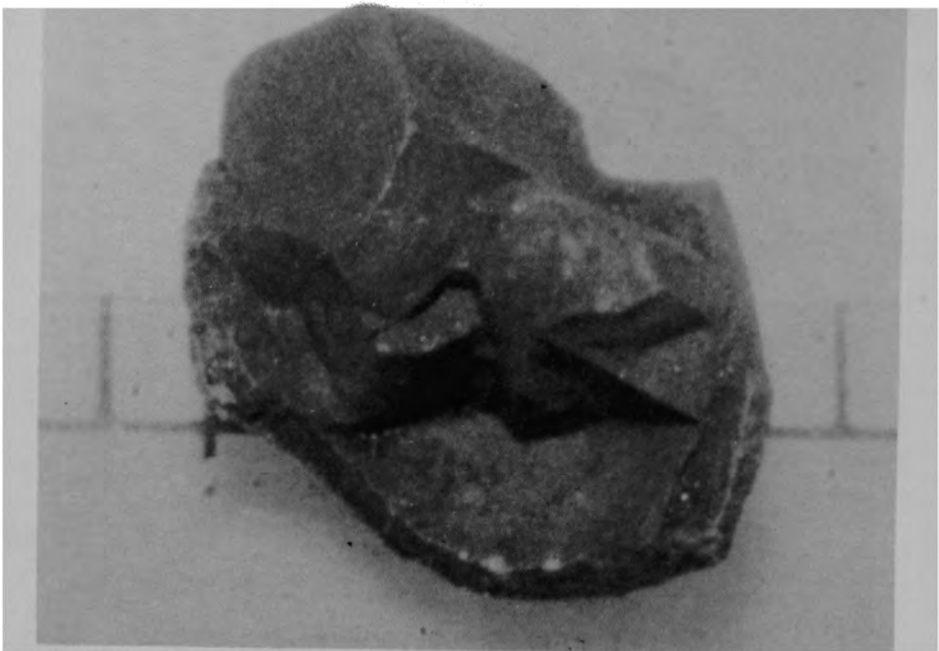
a) Front view of particle



84-546-10-5

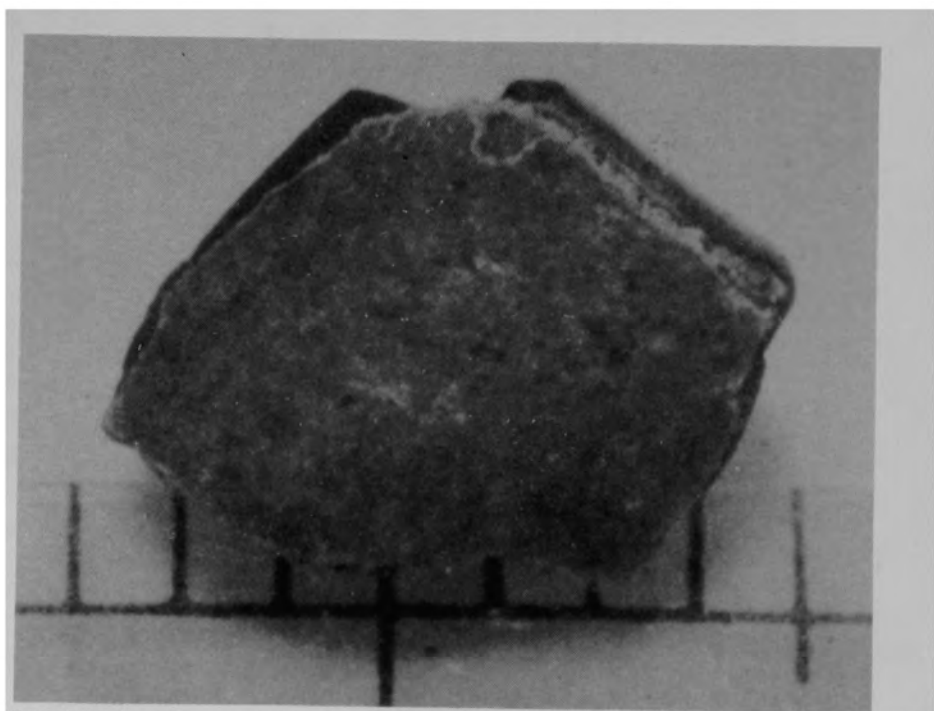
b) Back view of particle

Figure B-46. Particle 8A from Sample 8 (H8, 70 cm), size range:
 $>4000 \mu\text{m}$.



84-546-10-9

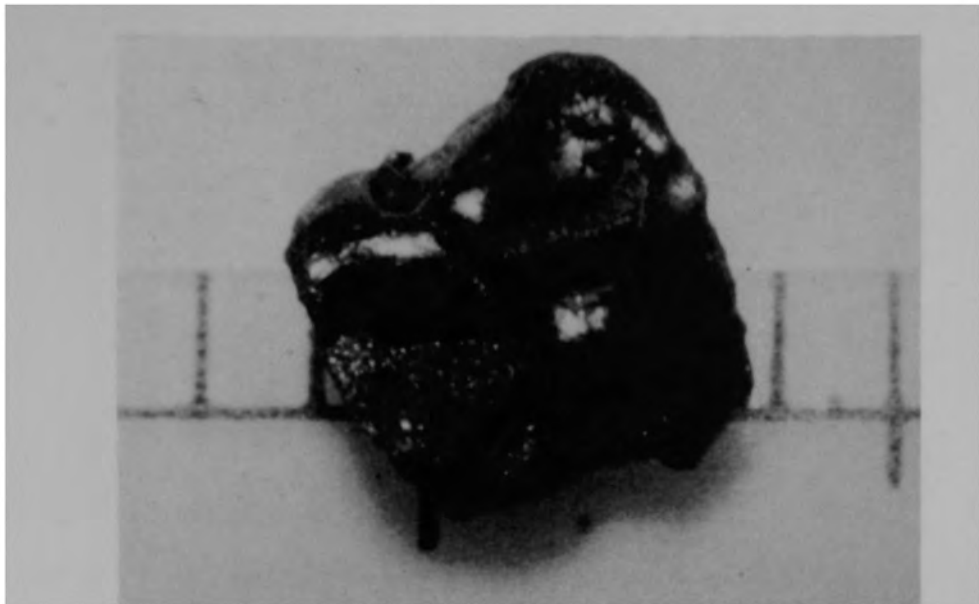
a) Front view of particle



84-546-10-11

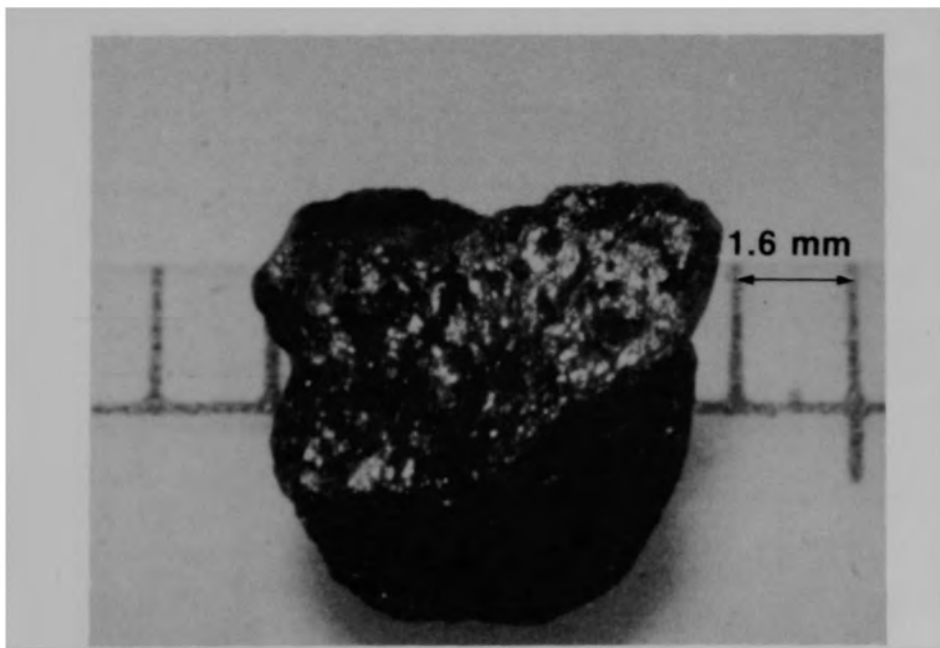
b) Back view of particle

Figure B-47. Particle 8B from Sample 8 (H8, 70 cm), size range:
 $>4000 \mu\text{m}$.



84-546-10-13

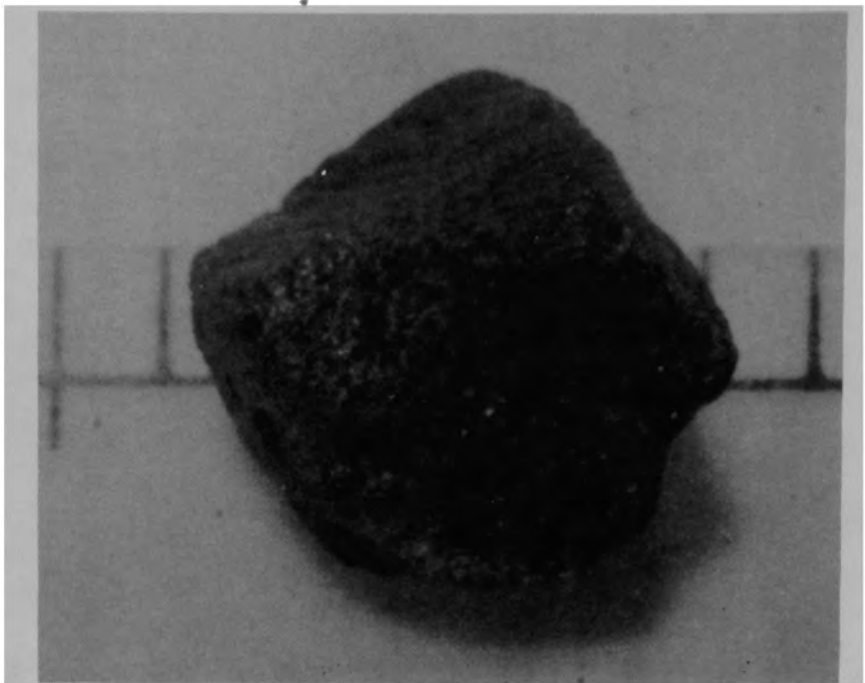
a) Front view of particle



84-546-10-14

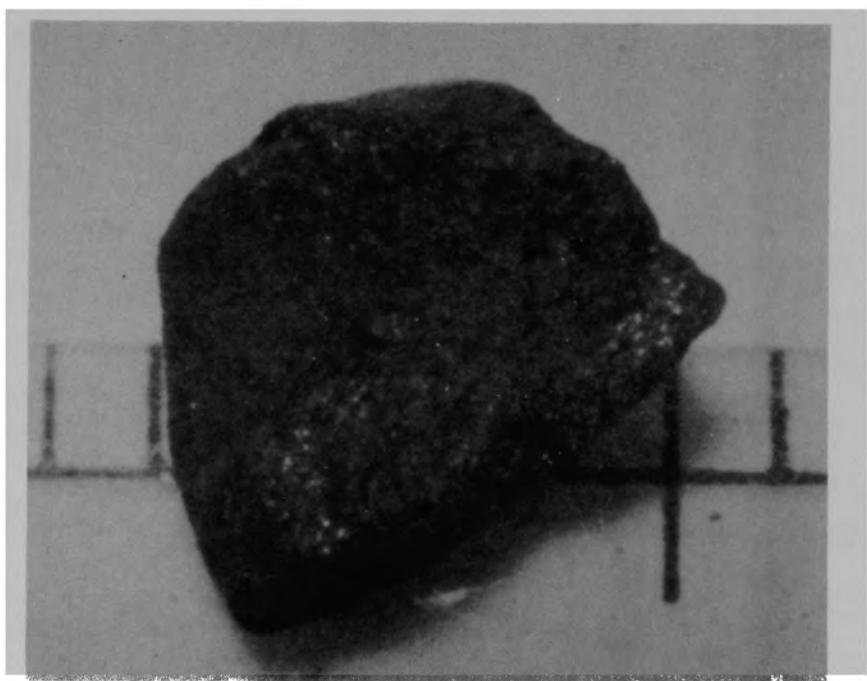
b) Back view of particle

Figure B-48. Particle 8C from Sample 8 (H8, 70 cm), size range:
 $>4000 \mu\text{m}$.



84-546-10-17

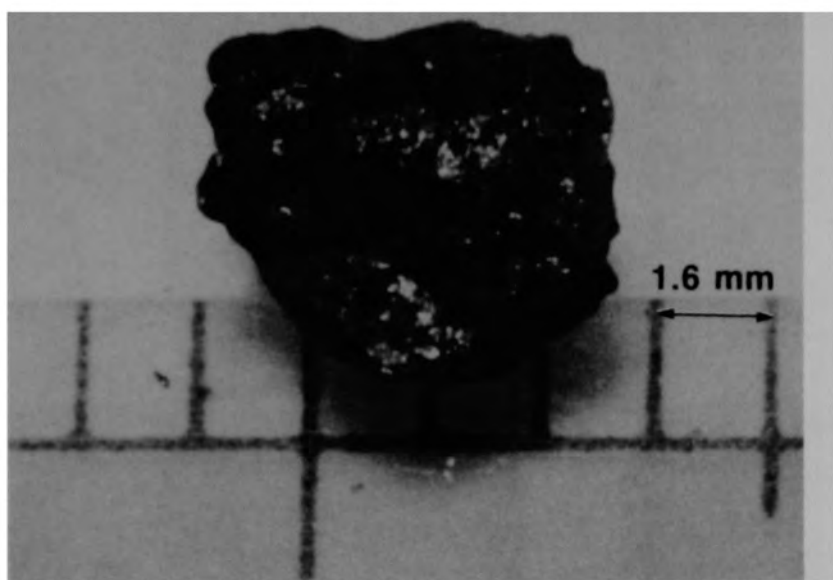
a) Front view of particle



84-546-10-18

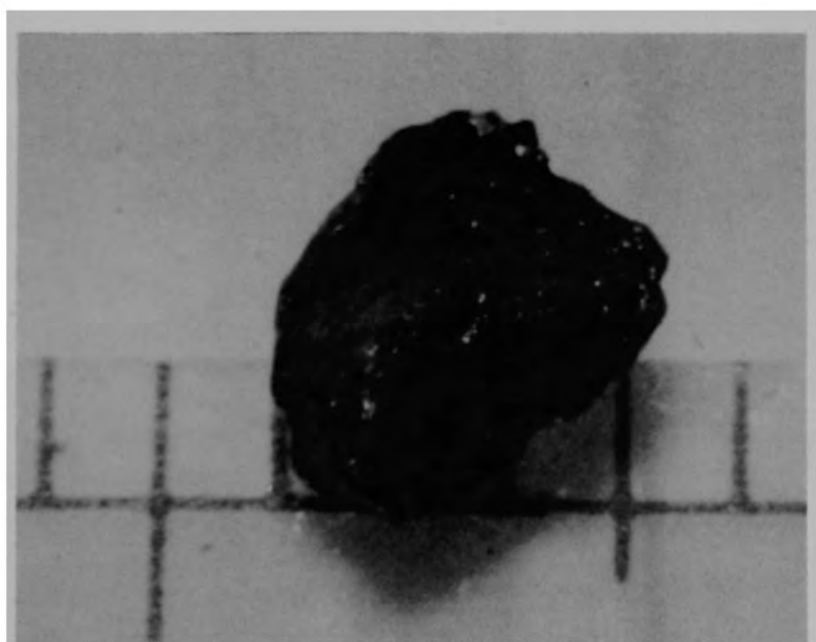
b) Back view of particle

Figure B-49. Particle 8D from Sample 8 (H8, 70 cm), size range:
 $>4000 \mu\text{m}$.



84-546-10-20

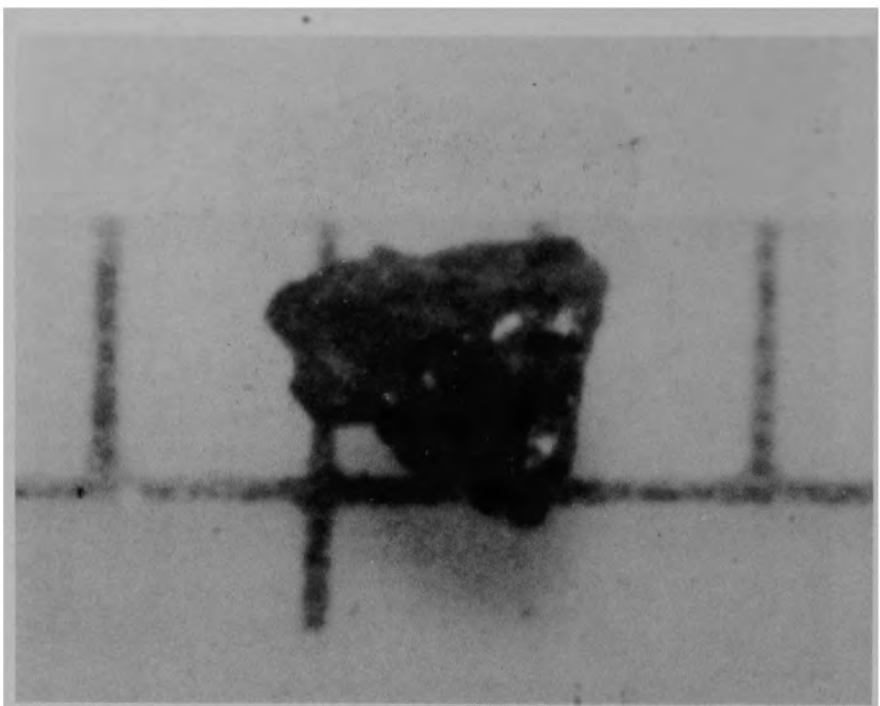
a) Front view of particle



84-546-10-22

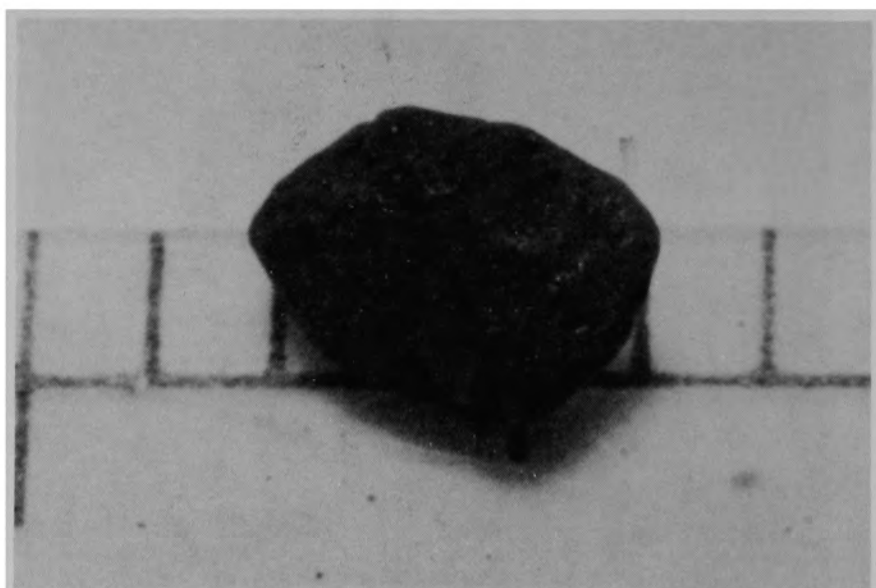
b) Back view of particle

Figure B-50. Particle 8E from Sample 8 (H8, 70 cm), size range:
 $>4000 \mu\text{m}$.



84-546-10-25

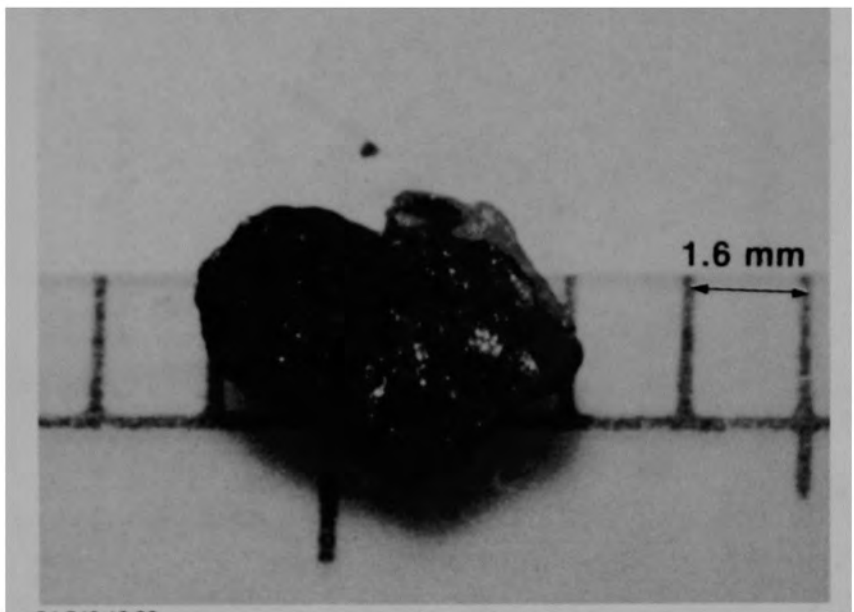
a) Particle 8F (size range: 1680-4000 μm)



84-546-10-26

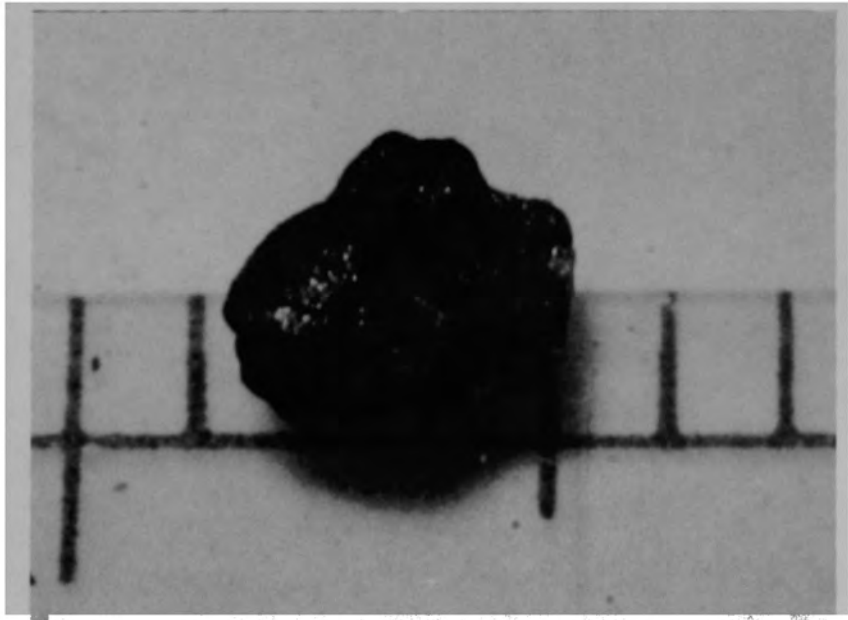
b) Particle 8G (size range: 1680-4000 μm)

Figure B-51. Particles from Sample 8 (H8, 70 cm).



84-546-10-30

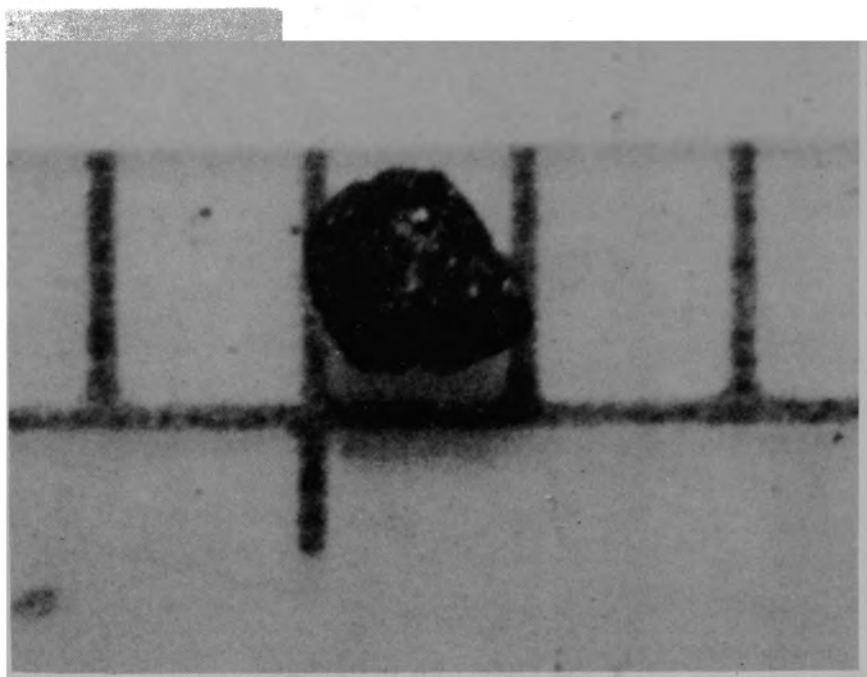
a) Front view of particle



84-546-10-32

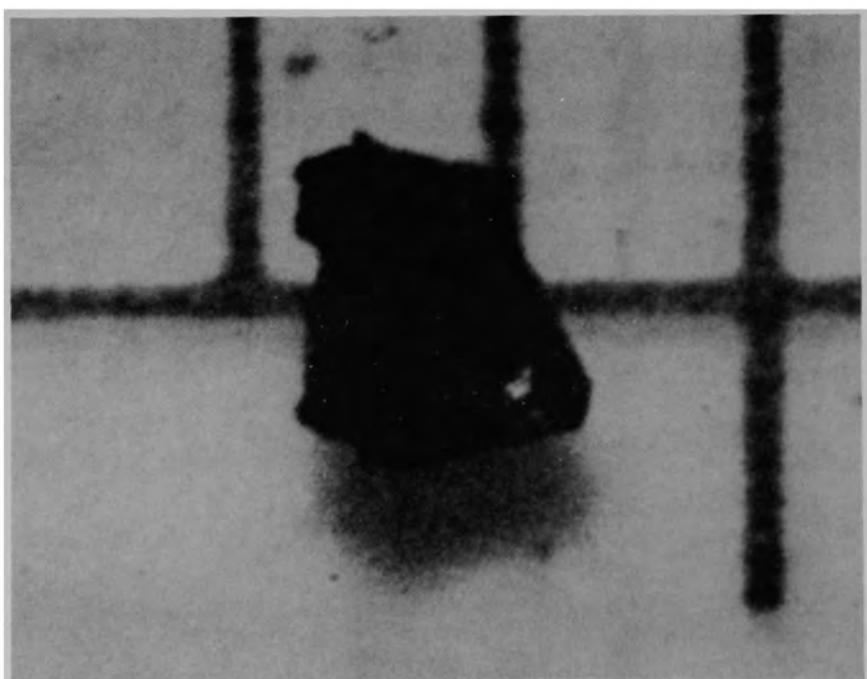
b) Back view of particle

Figure B-52. Particle 8H from Sample 8 (H8, 70 cm), size range:
 $>4000 \mu\text{m}$.



84-546-10-34

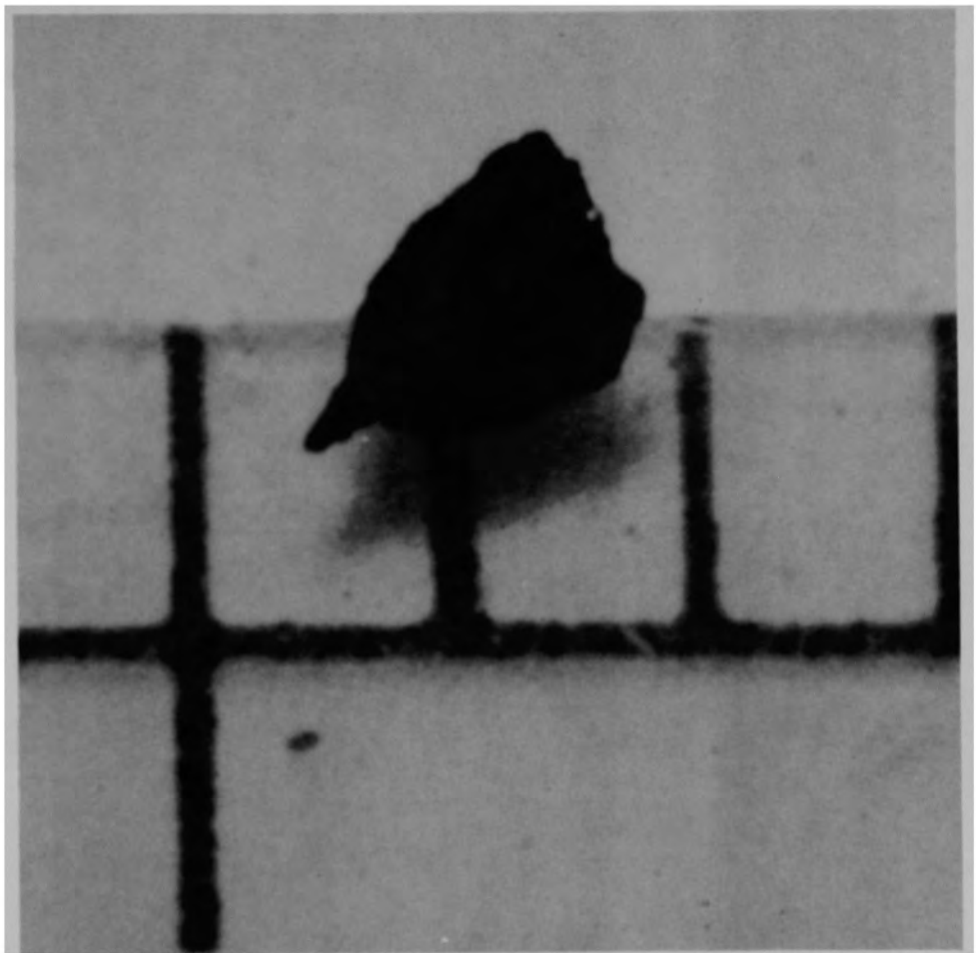
a) Particle 8I (size range: 1000-1680 μm)



84-546-11-6

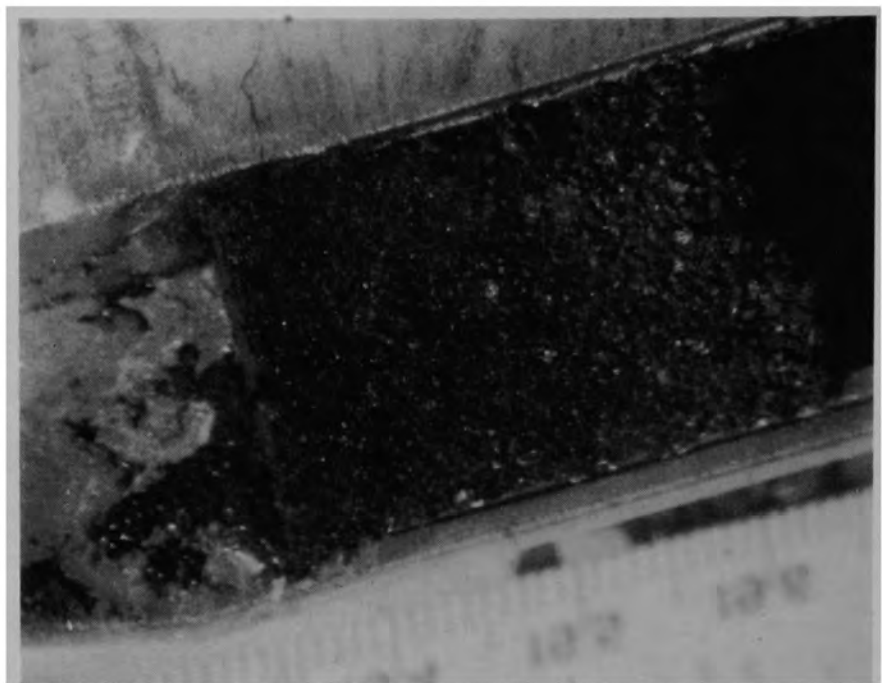
b) Particle 8J (size range: 1000-1680 μm)

Figure B-53. Particles from Sample 8 (H8, 70 cm).



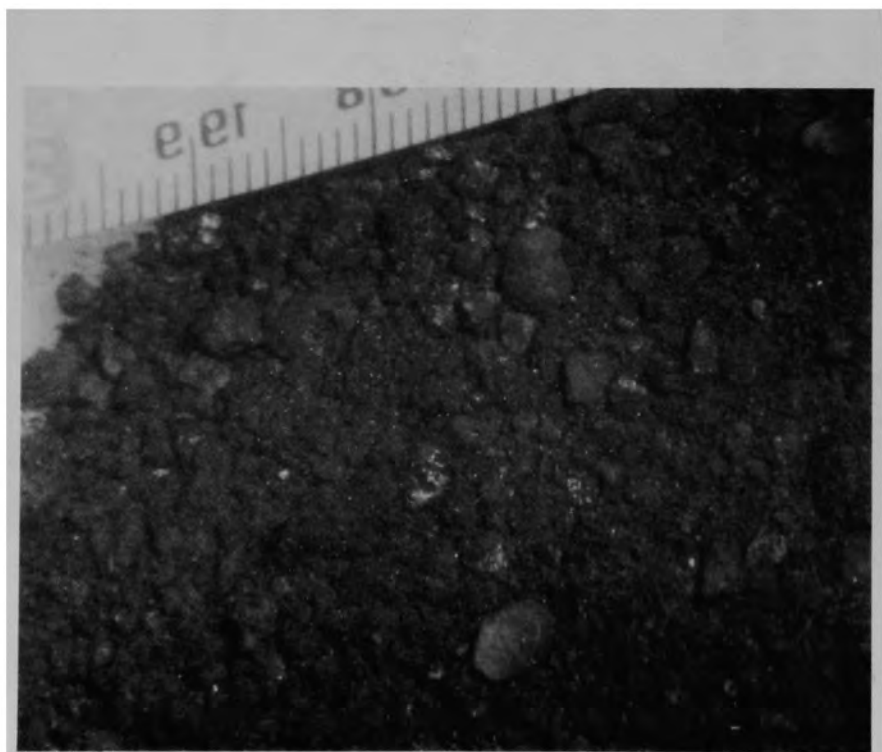
84-546-11-8

Figure B-54. Particle 8K from Sample 8 (H8, 70 cm), size range: 1000-1680 μm .



84-250

a) Material in sampling tool (shows stratification)



84-253

b) After removing material from sampling tool

Figure B-55. The bulk material for Sample 9 (H8, 77 cm).

B-59

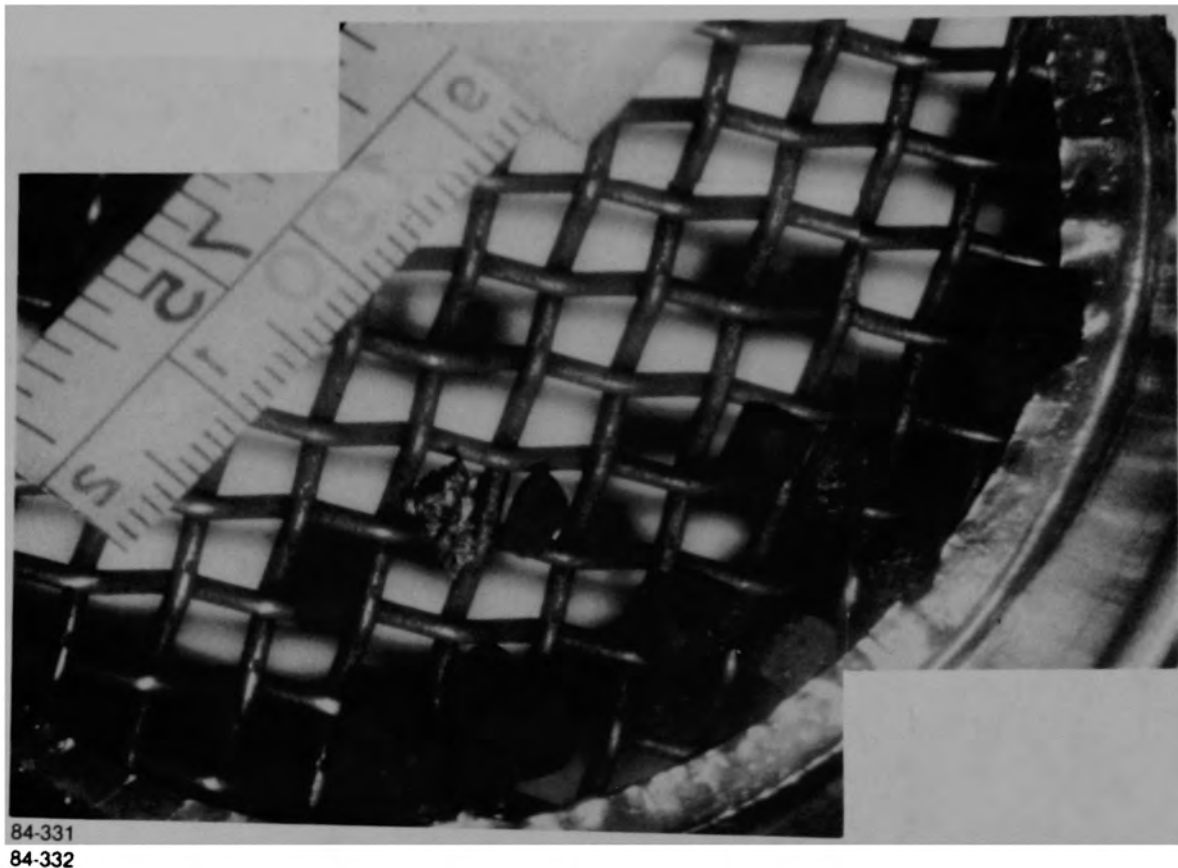


Figure B-56. Particles >4000 μm from Sample 9 (H8, 77 cm).

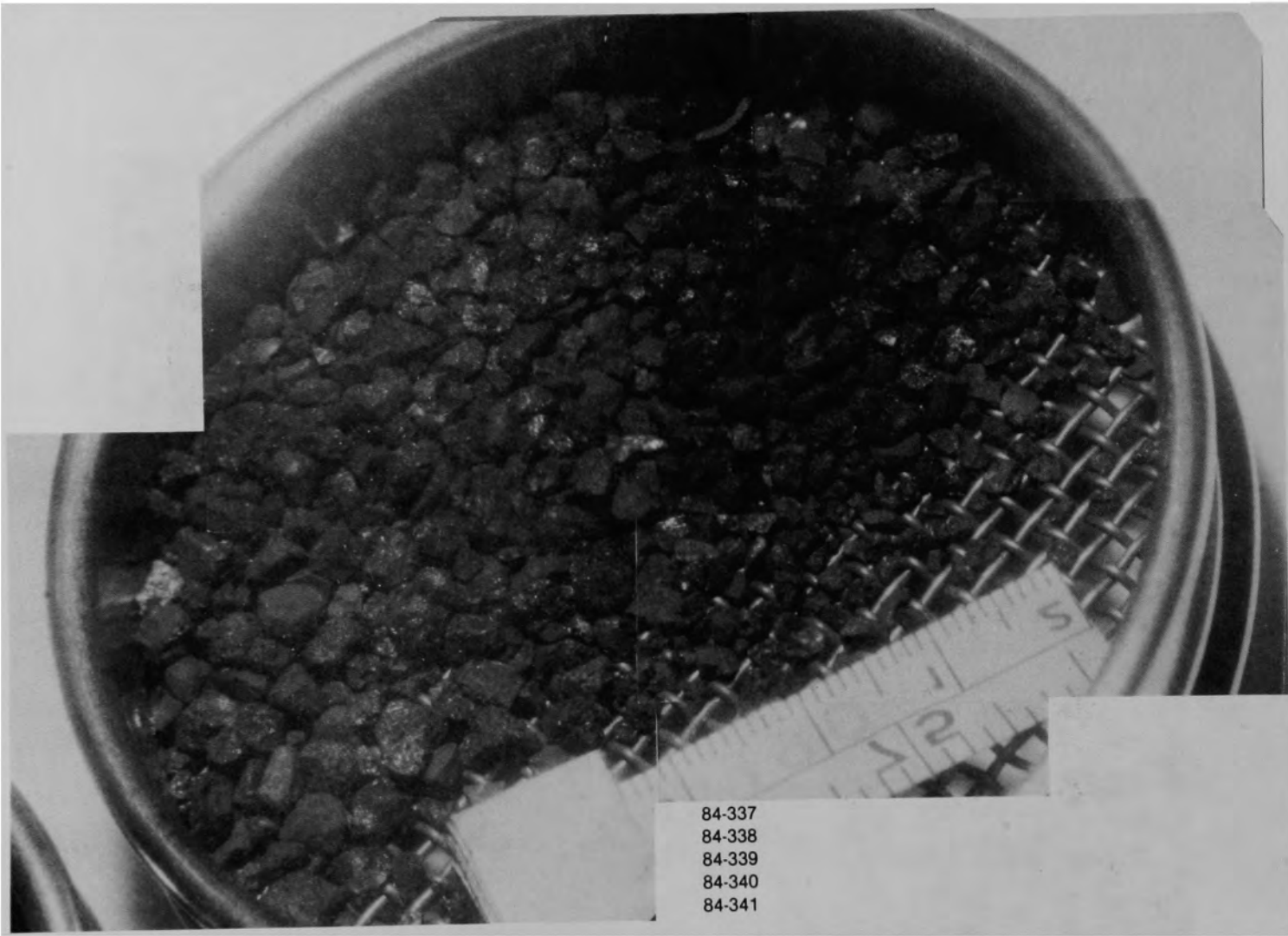
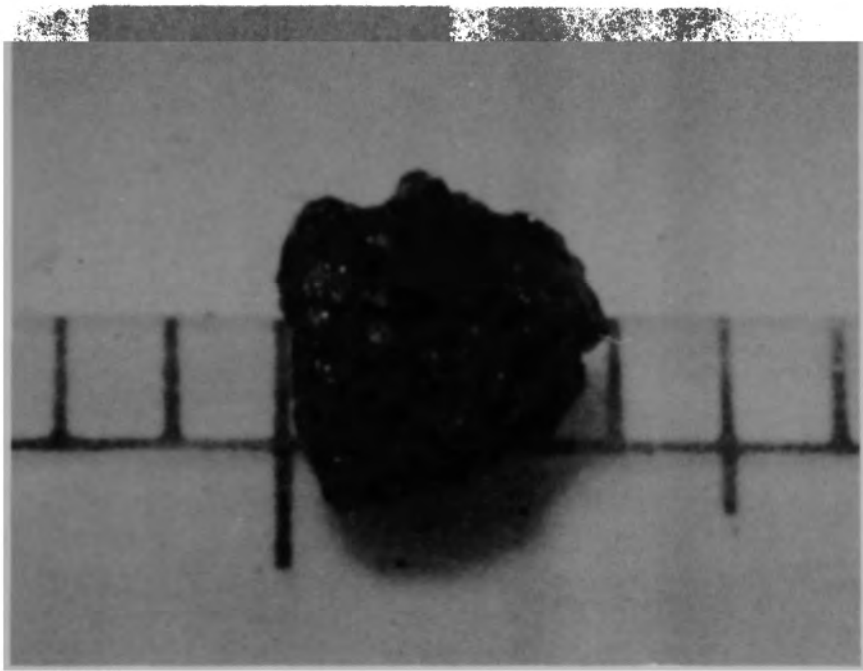


Figure B-57. Particle size fraction (size range: 1680-4000 μm) from Sample 9, (H8, 77 cm).



84-546-5-20

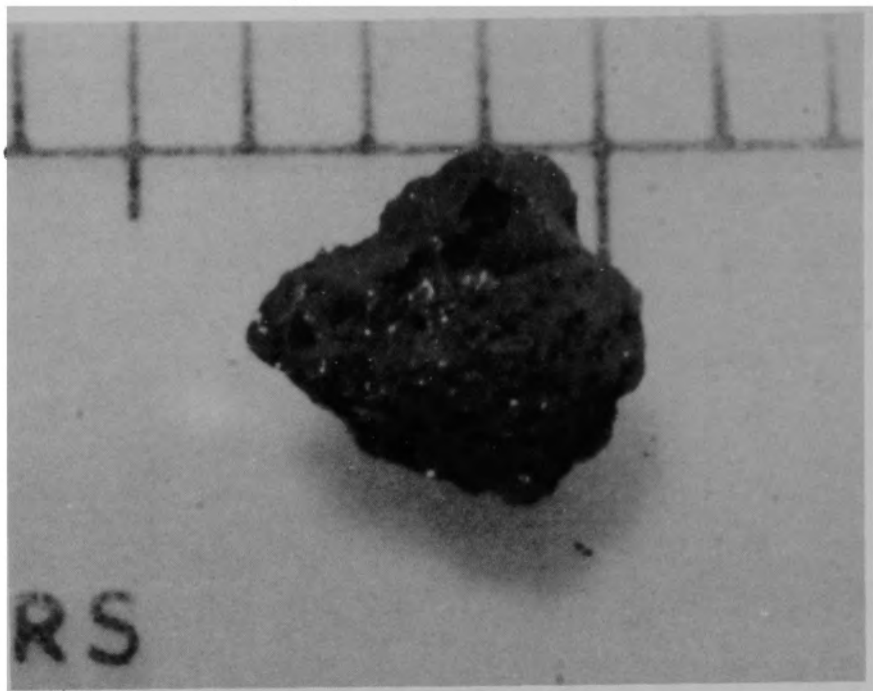
a) Front view of particle



84-546-5-22

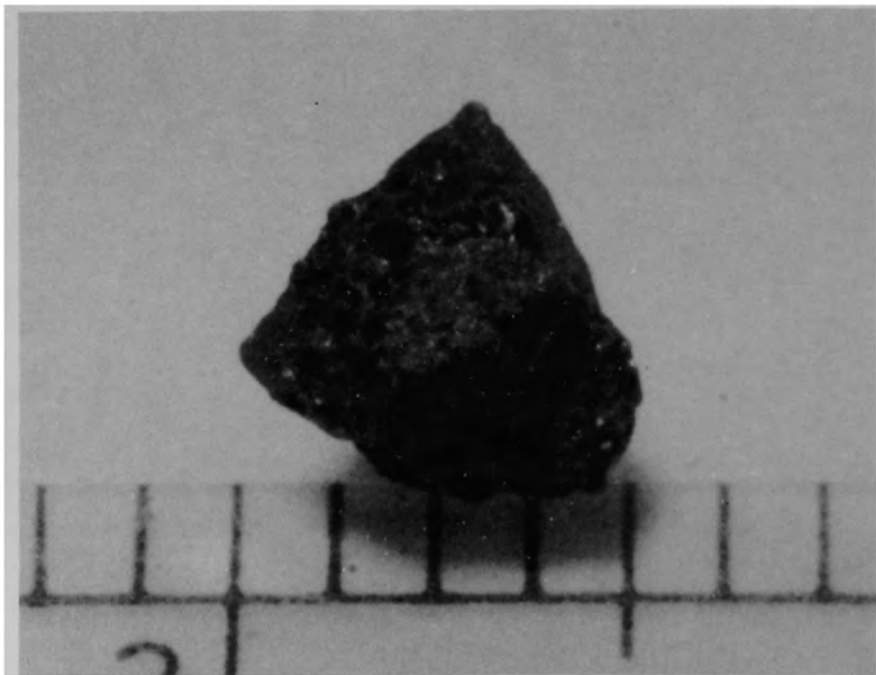
b) Back view of particle

Figure B-58. Particle 9A from Sample 9 (H8, 77 cm), size range: >4000 μm .



84-546-5-24

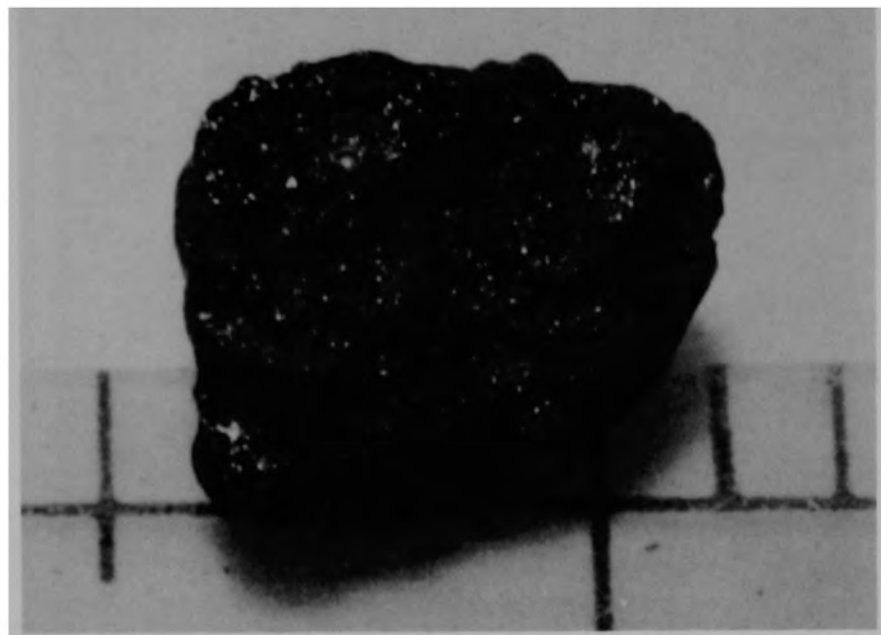
a) Front view of particle



84-546-5-26

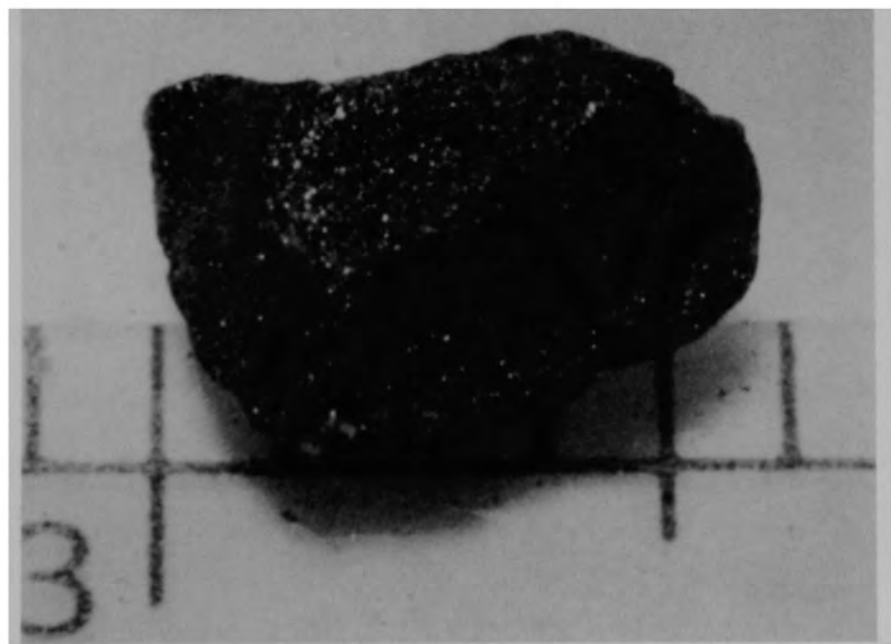
b) Back view of particle

Figure B-59. Particle 9B from Sample 9 (H8, 77 cm), size range: >4000 μm .



84-546-5-27

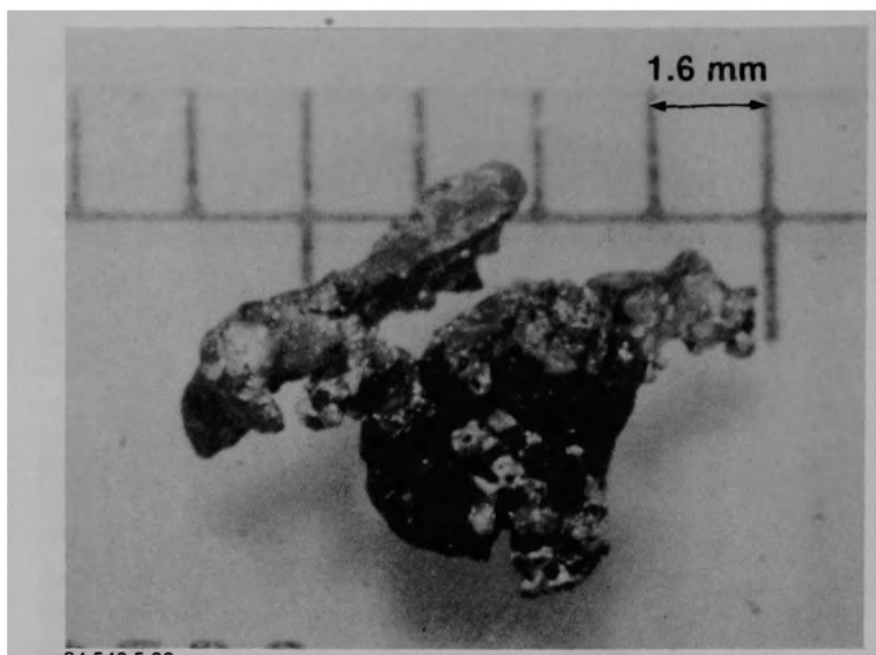
a) Front view of particle



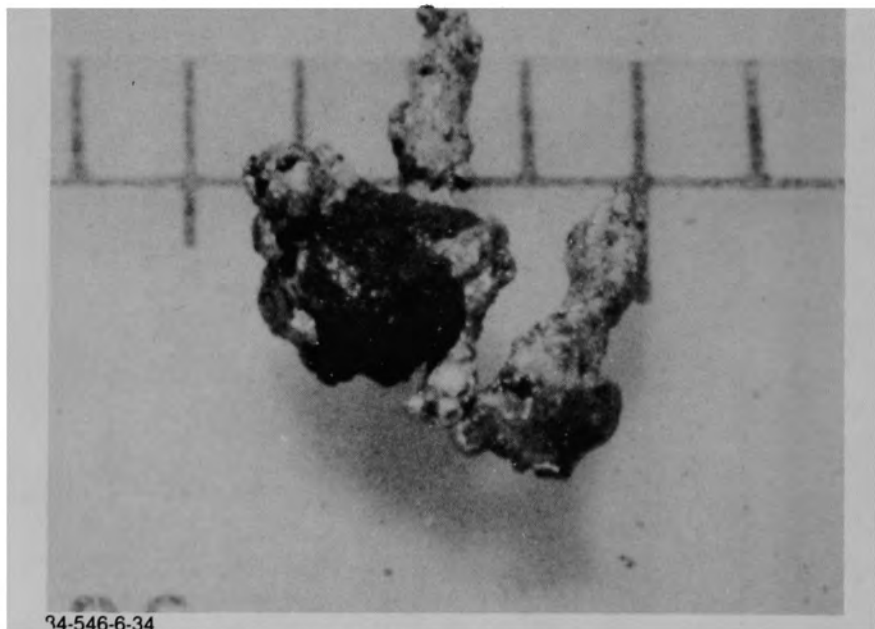
84-546-5-30

b) Back view of particle

Figure B-60. Particle 9C from Sample 9 (H8, 77 cm), size range: >4000 μm .

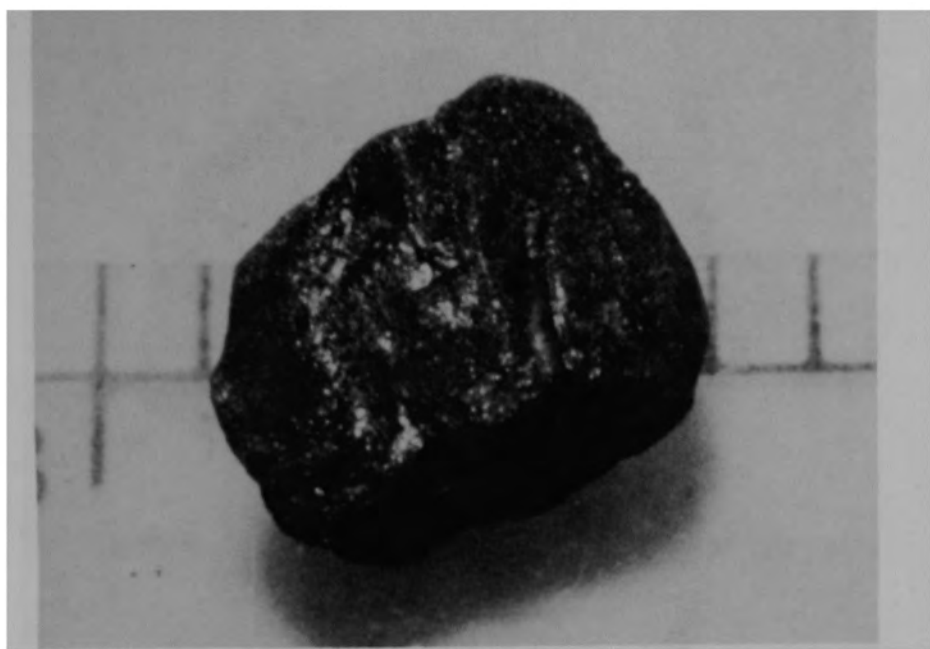


a) Front view of particle



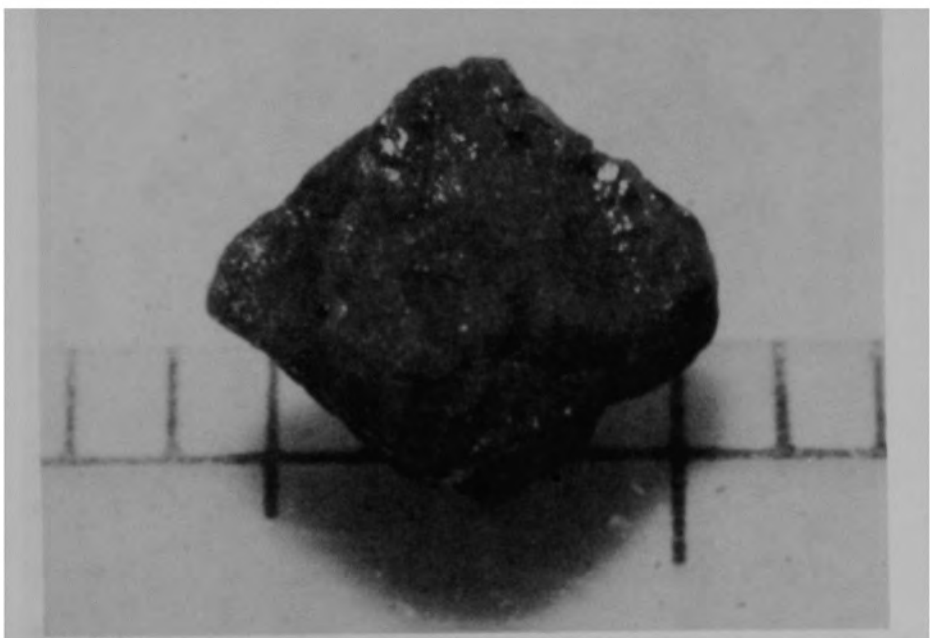
b) Back view of particle

Figure B-61. Particle 9D from Sample 9 (H8, 77 cm), size range:
 $>4000 \mu\text{m}$.



84-546-6-6

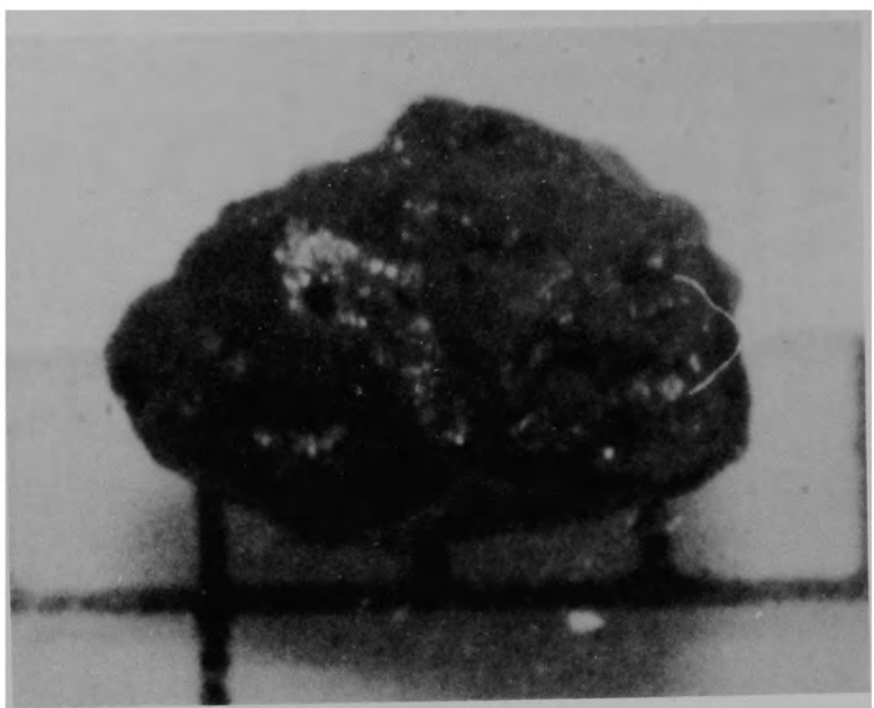
a) Front view of particle



84-546-6-8

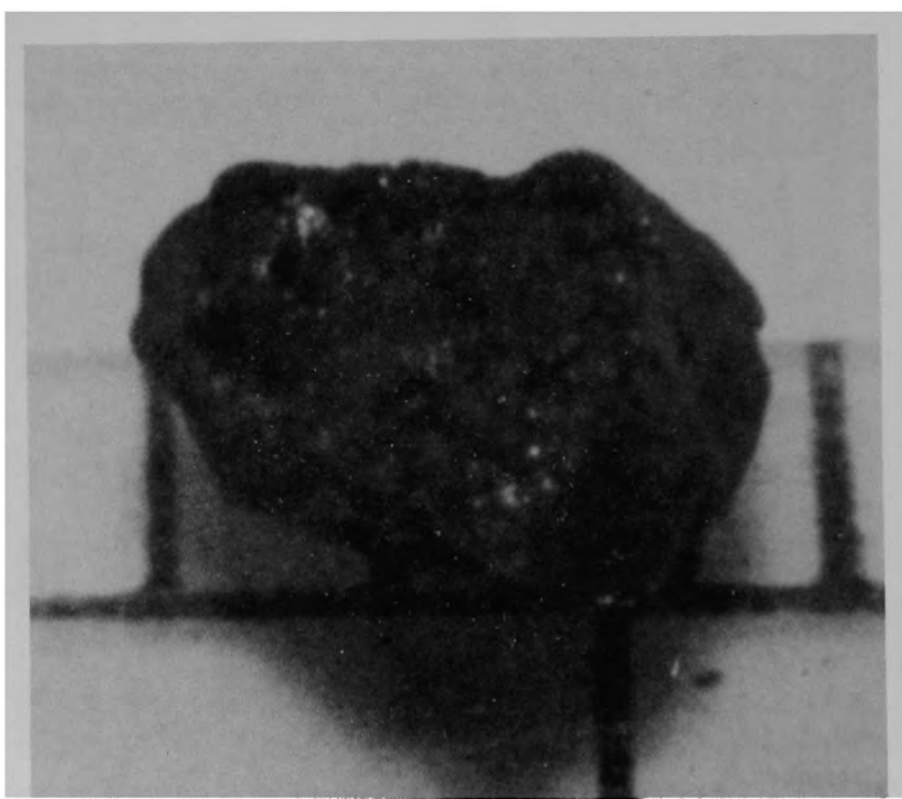
b) Back view of particle

Figure B-62. Particle 9E from Sample 9 (H8, 77 cm), size range: >4000 μm .



84-546-6-10

a) Front view of particle



84-546-6-12

b) Back view of particle

Figure B-63. Particle 9F from Sample 9 (H8, 77 cm), size range: 1680-4000 μm .

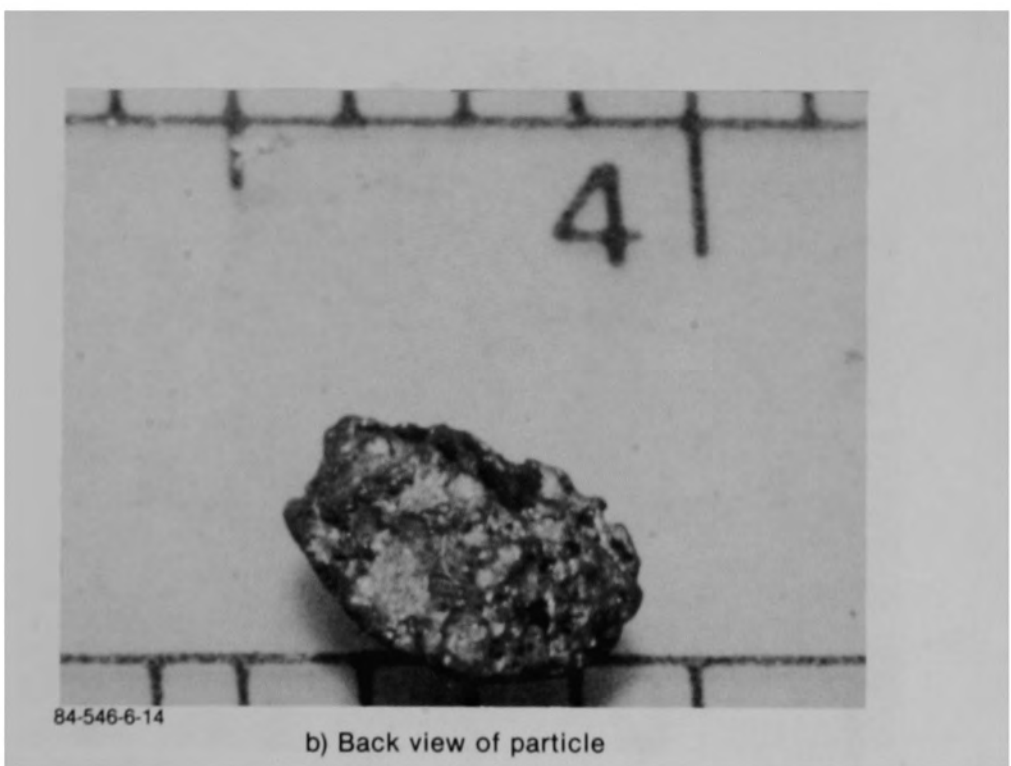
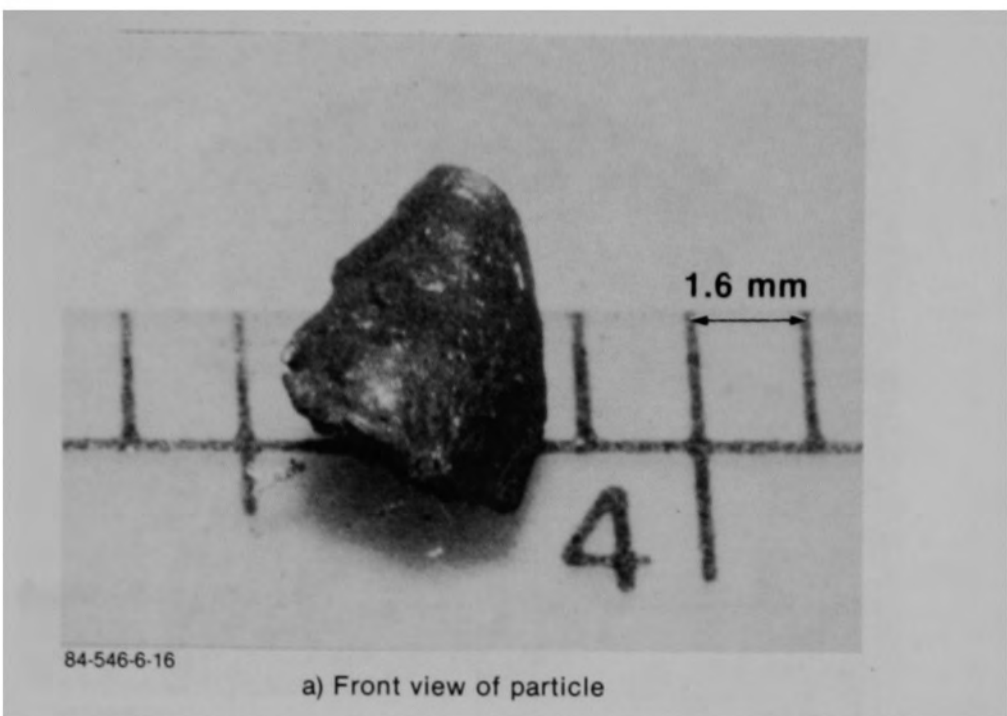
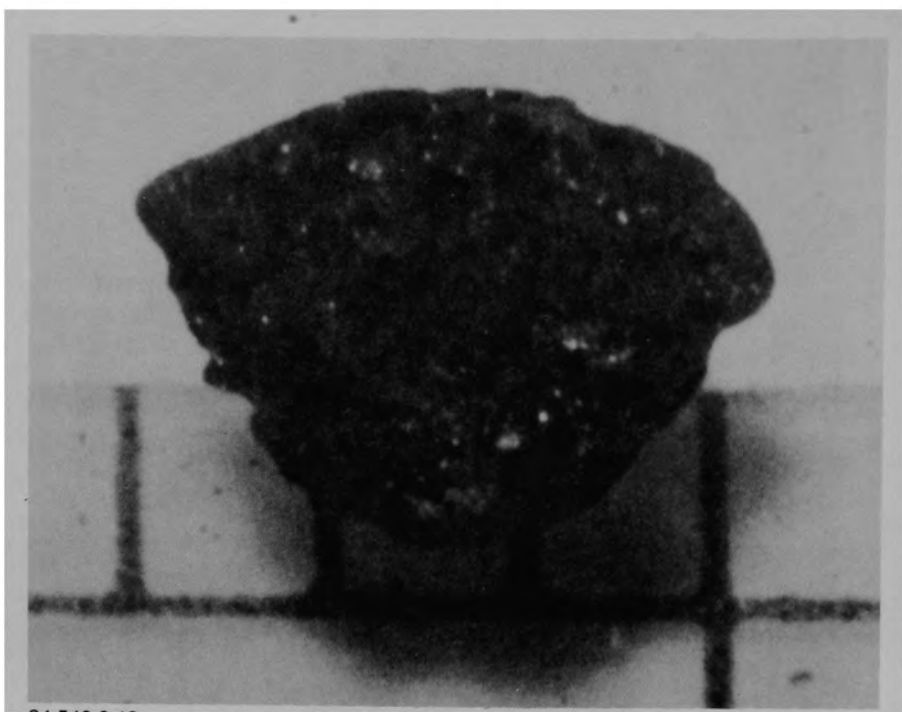
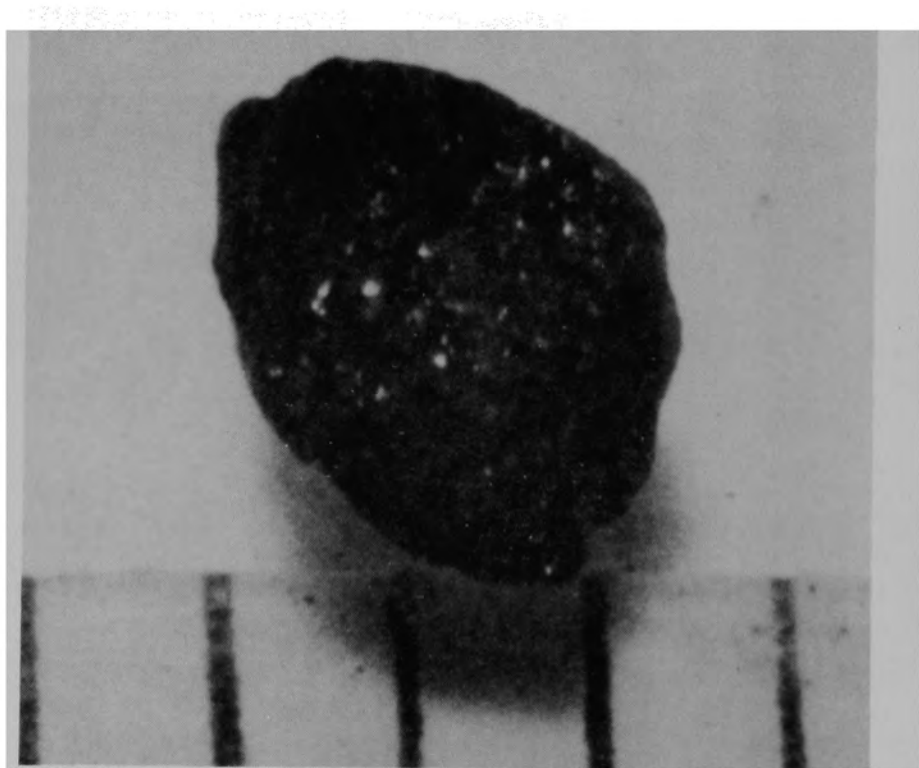


Figure B-64. Particle 9G from Sample 9 (H8, 77 cm), size range: 1680-4000 μm .



84-546-6-18

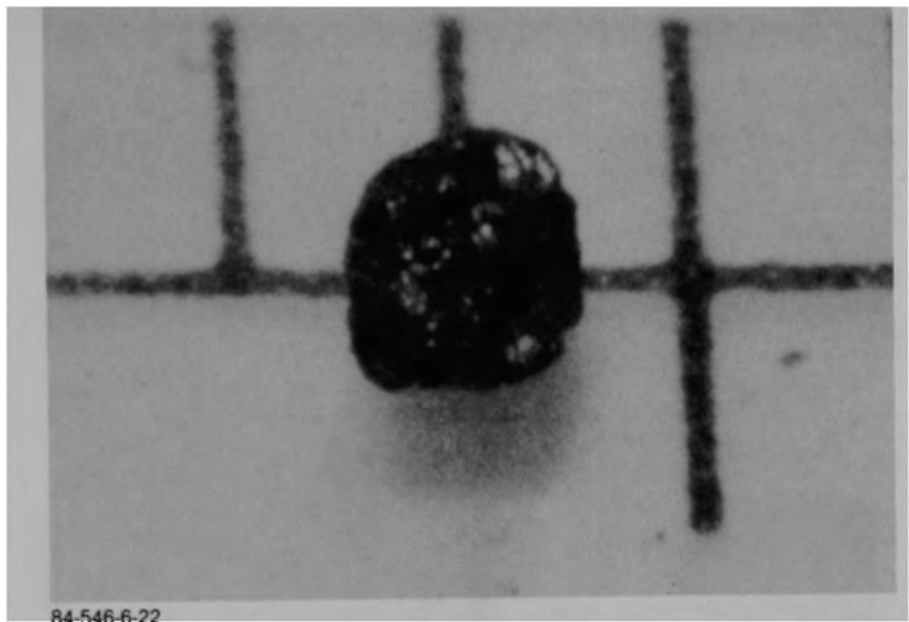
a) Front view of particle



84-546-6-20

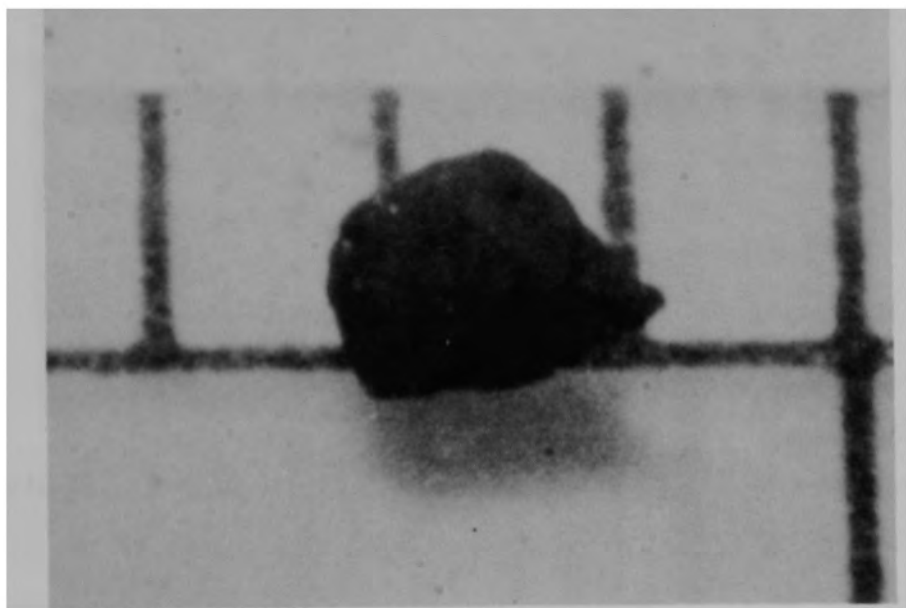
b) Backoview of particle

Figure B-65. Particle 9H from Sample 9 (H8, 77 cm), size range: 1680-4000 μm .



84-546-6-22

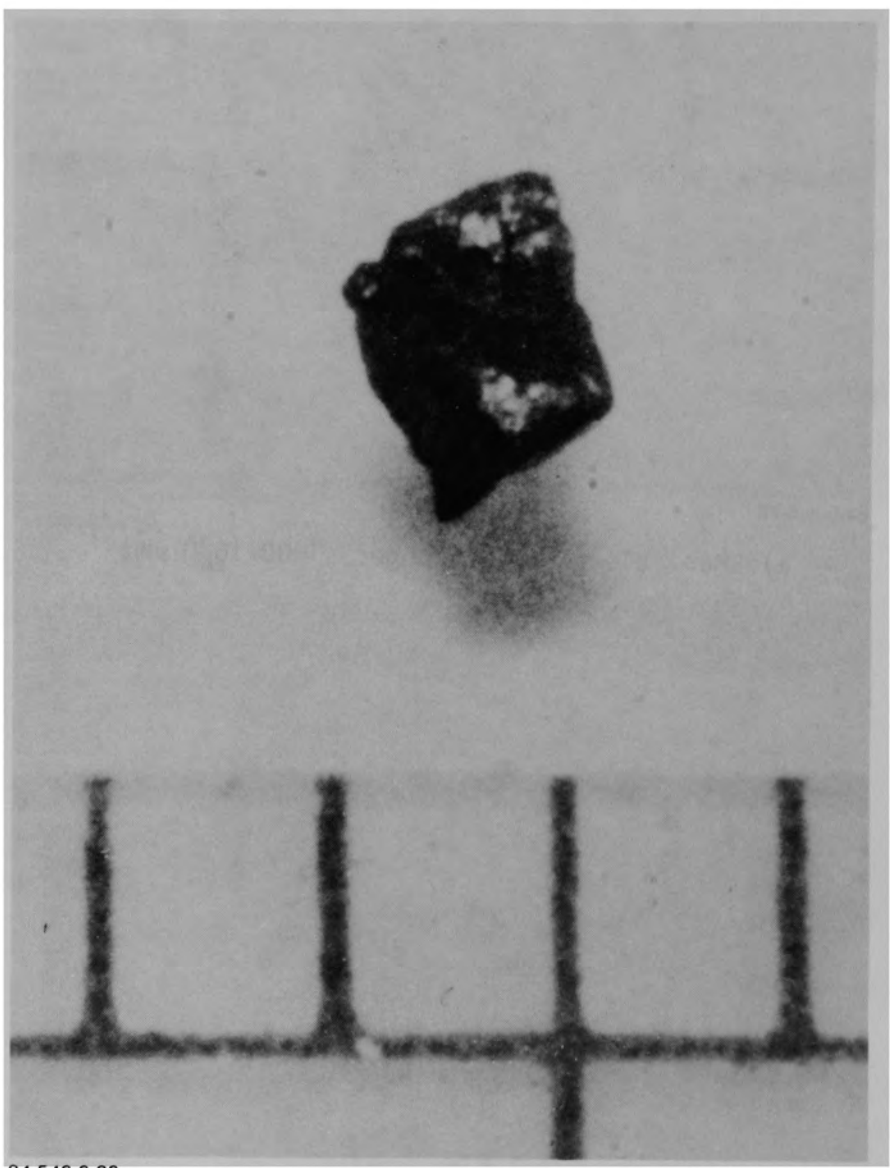
a) Particle 9I (size range: 1000-1680 μm)



84-546-6-24

b) Particle 9J (size range: 1000-1680 μm)

Figure B-66. Particles from Sample 9 (H8, 77 cm).



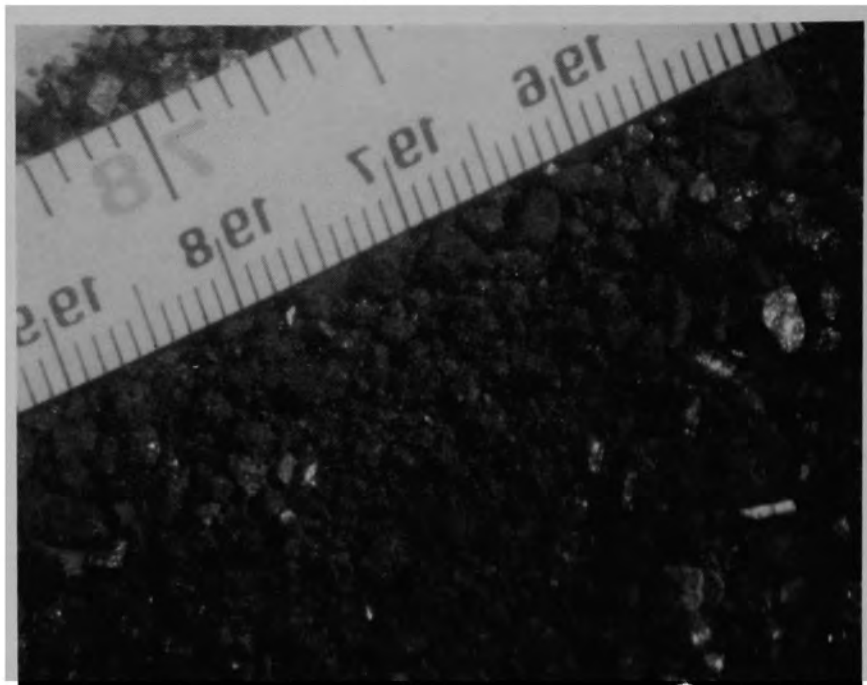
84-546-6-26

Figure B-67. Particle 9K from Sample 9 (H8, 77 cm), size range: 1000-1680 μm .

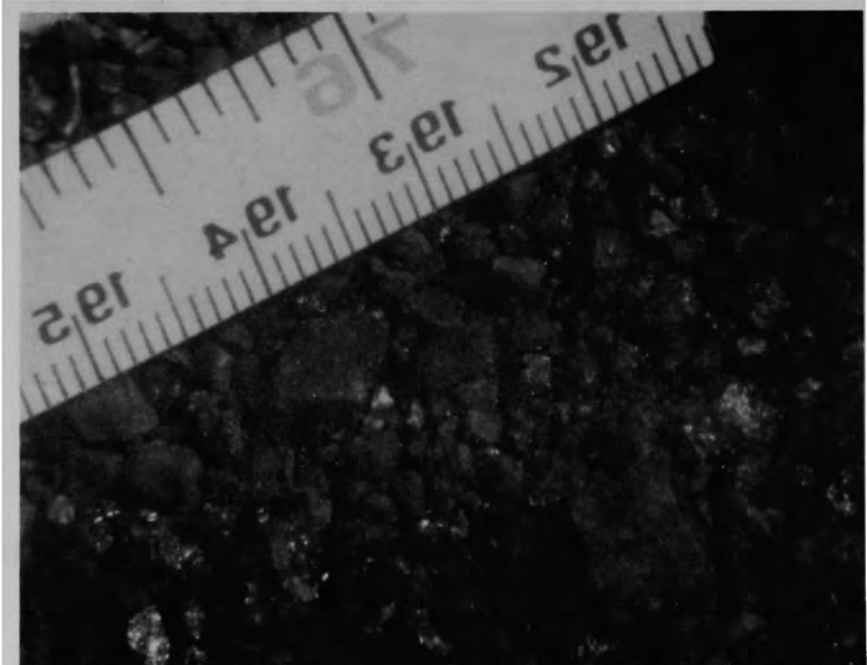


84-228

Figure B-68. Sample 10 (E9, 74 cm) being removed from sampling tool.



84-230



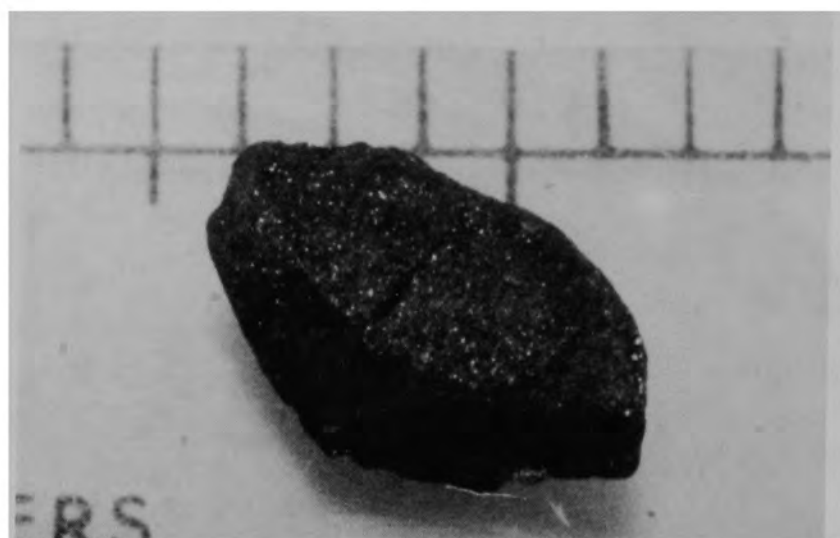
84-231

Figure B-69. Views of the bulk material for Sample 10 (E9, 74 cm) after removal from sampling tool.

8-73

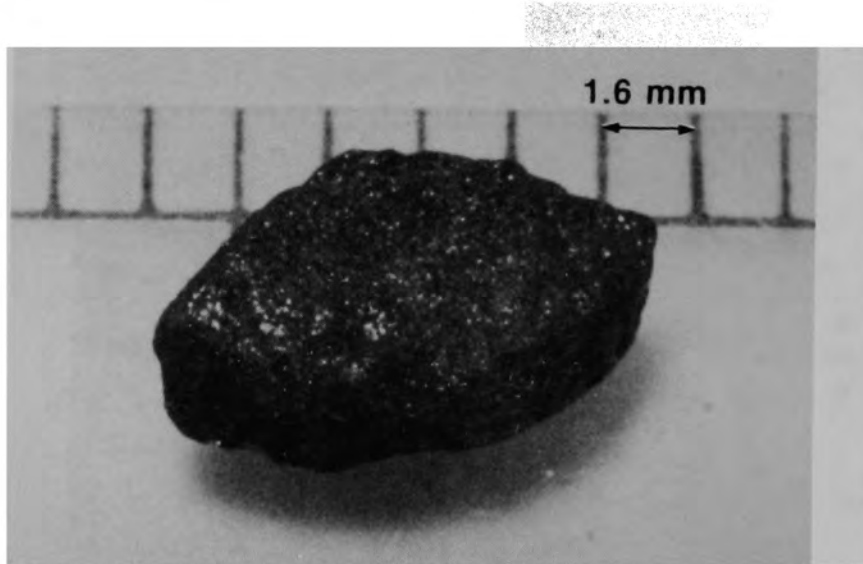


Figure B-70. Particle size fraction (size range: 1680-4000 μm) from Sample 10 (E9, 74 cm).



84-546-4-4

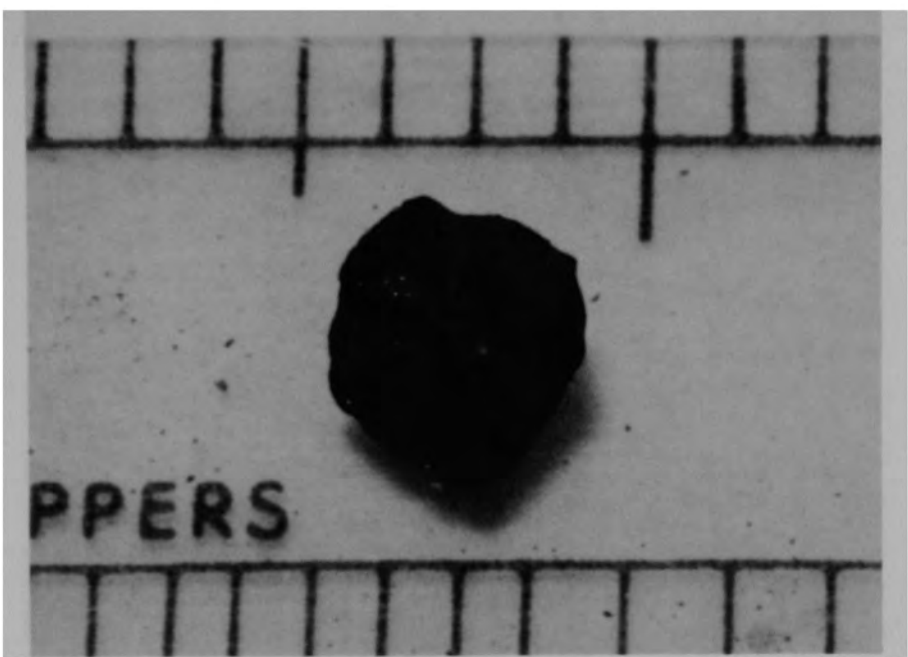
a) Front view of particle



84-546-4-5

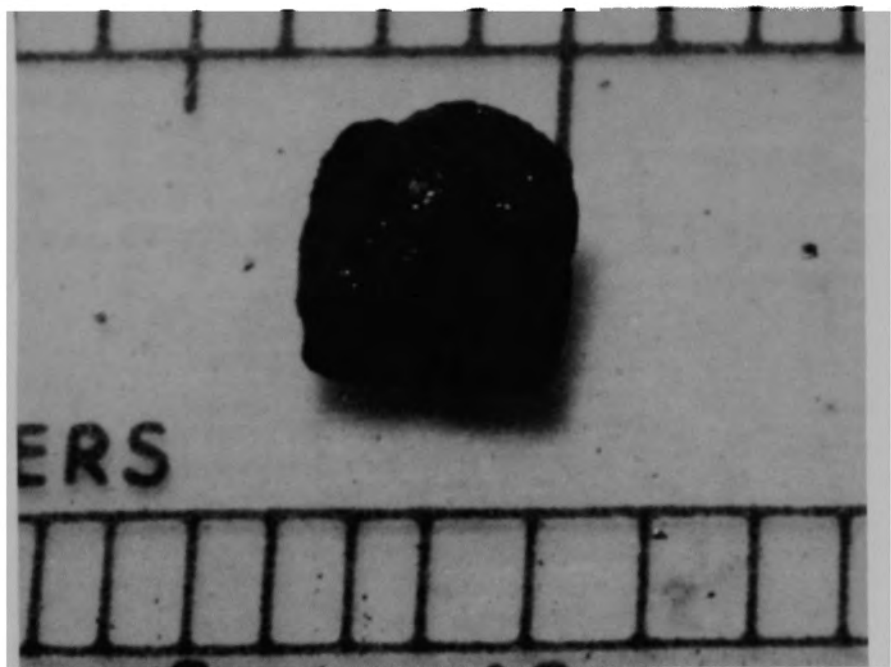
b) Back view of particle

Figure B-71. Particle 10A from Sample 10 (E9, 74 cm), size range:
 $>4000 \mu\text{m}$.



84-546-4-7

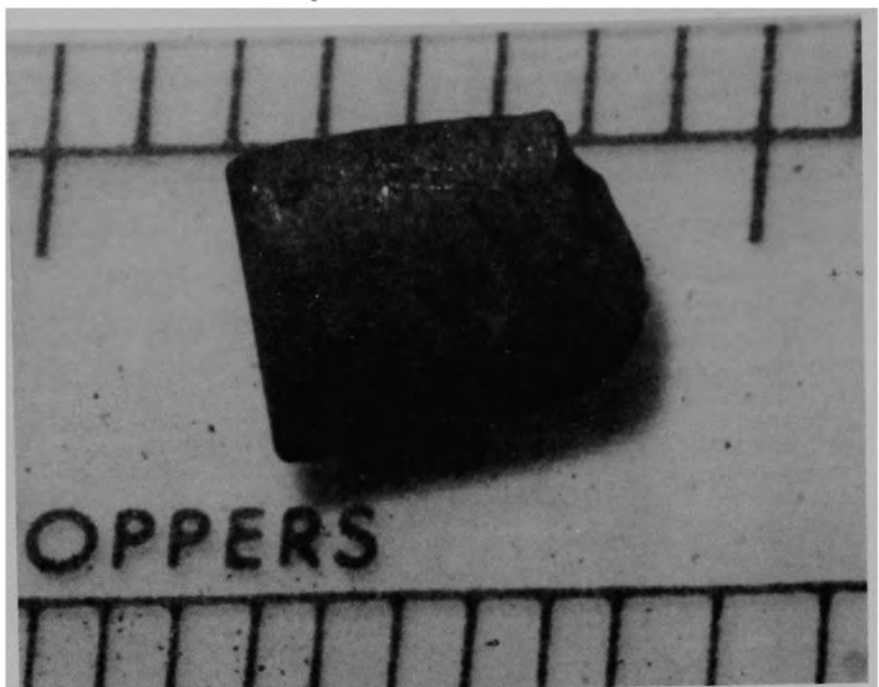
a) Front view of particle



84-546-4-9

b) Back view of particle

Figure B-72. Particle 10B from Sample 10 (E9, 74 cm), size range: >4000 μm .



84-546-4-11

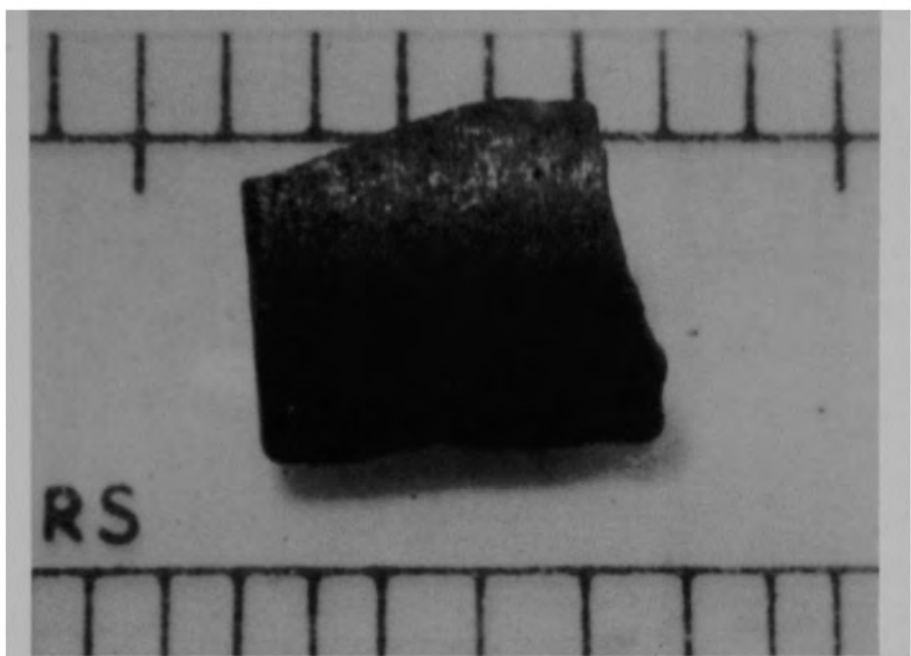
a) Front view of particle



84-546-4-13

b) Back view of particle

Figure B-73. Particle 10C from Sample 10 (E9, 74 cm), size range: >4000 μm .

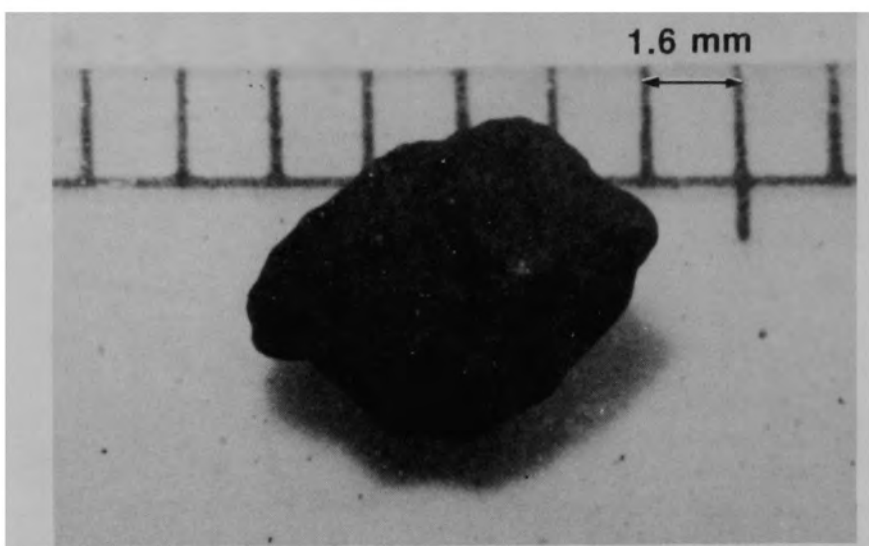


a) Front view of particle



b) Back view of particle

Figure B-74. Particle 10D from Sample 10 (E9, 74 cm), size range: >4000 μm .



84-546-4-20

a) Front view of particle



84-546-4-22

b) Back view of particle

Figure B-75. Particle 10E from Sample 10 (E9, 74 cm), size range:
 $>4000 \mu\text{m}$.

1.6 mm

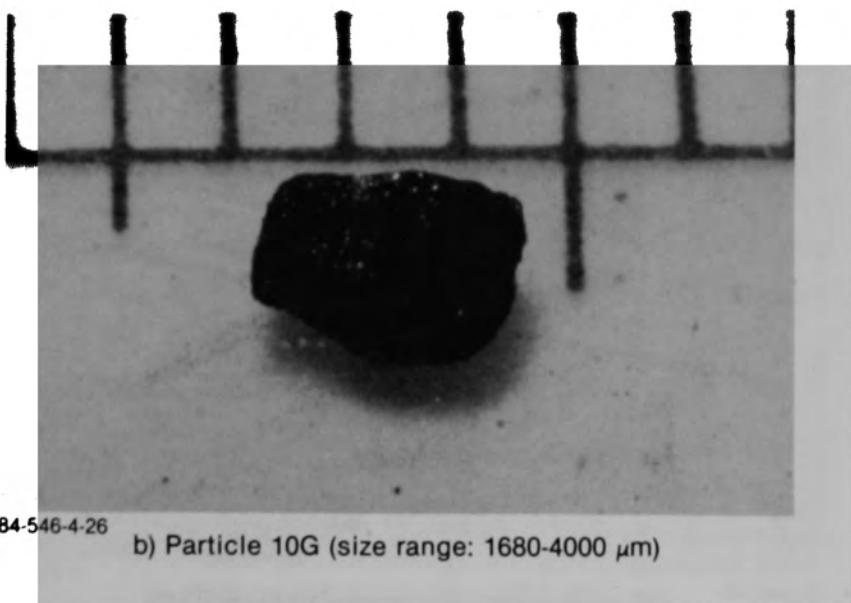
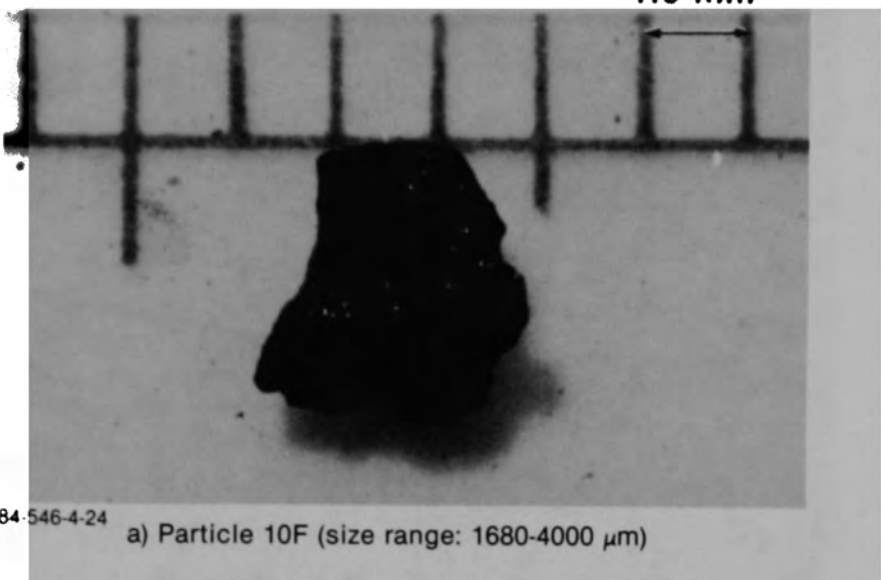
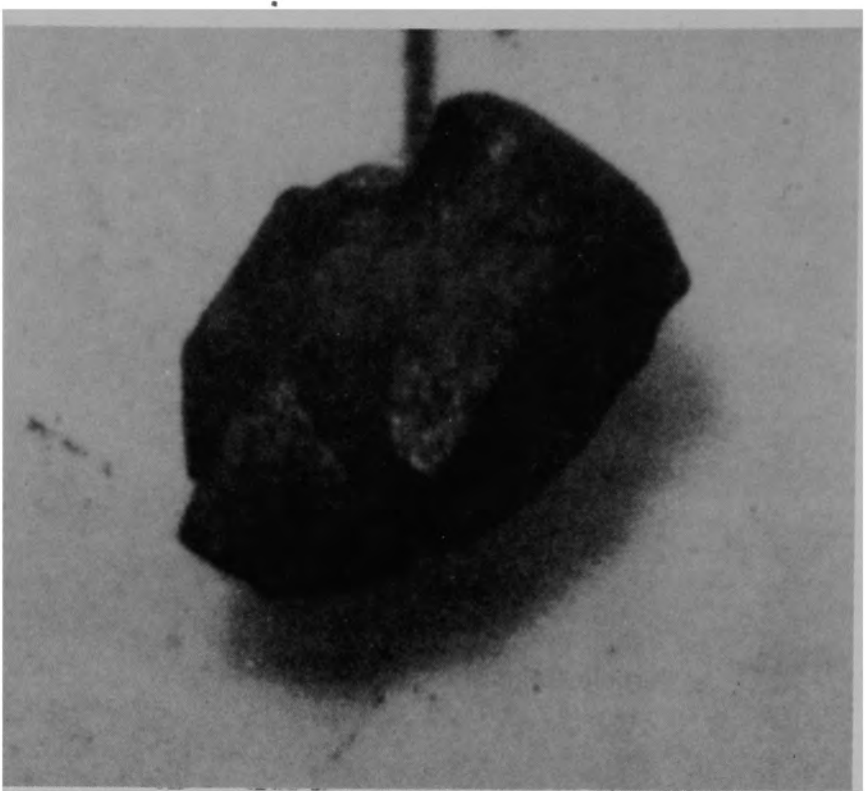
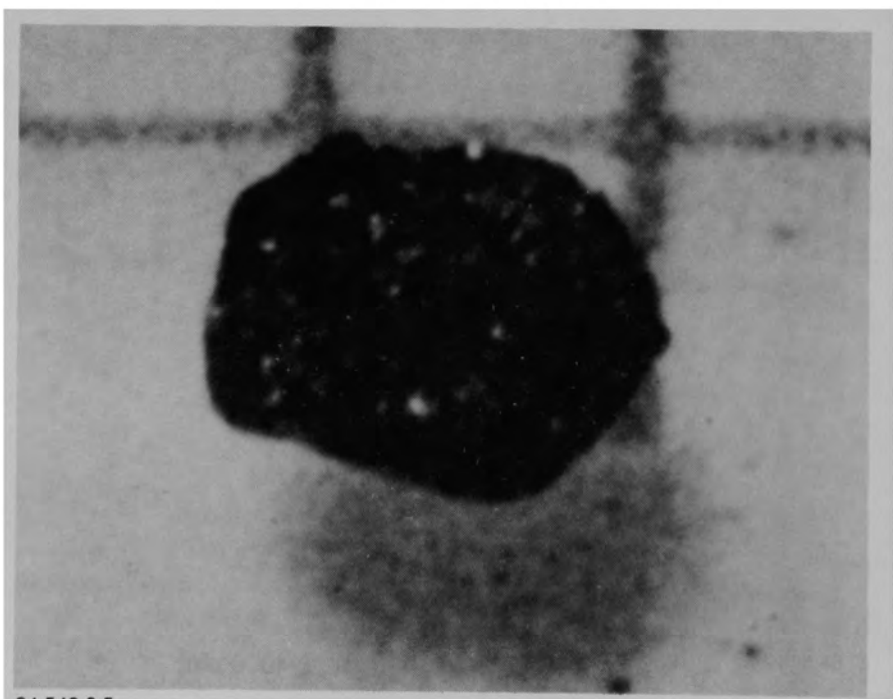


Figure B-76. Particles from Sample 10 (E9, 74 cm).



84-546-4-28

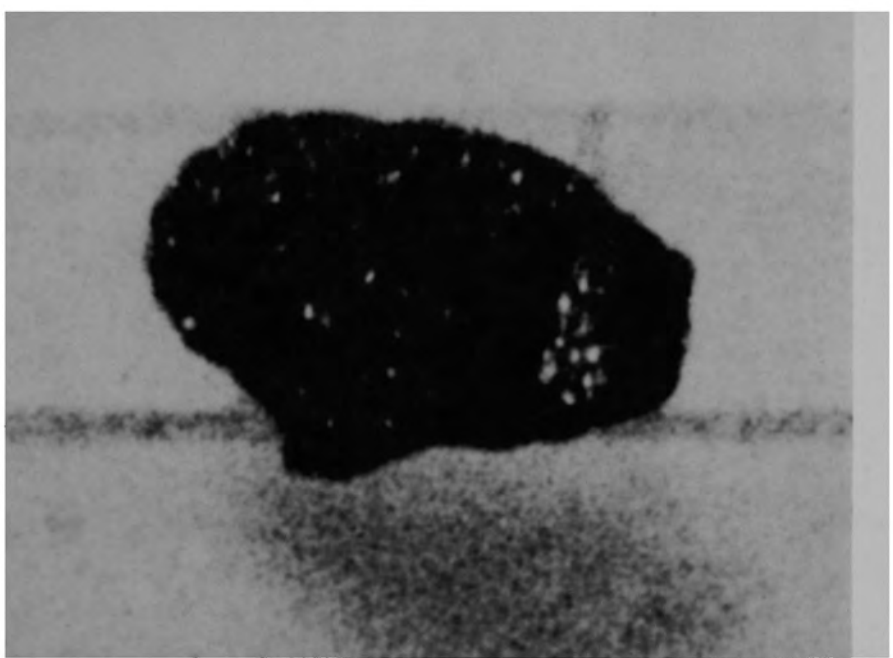
a) Particle 10H (size range: 1680-4000 μm)



84-546-3-5

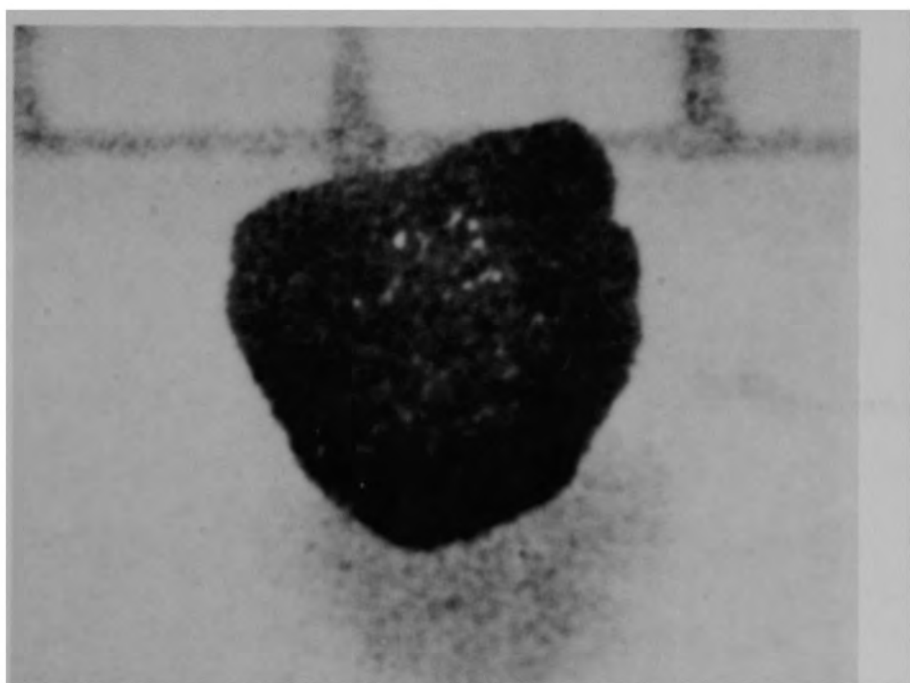
b) Particle 10I (size range: 1000-1680 μm)

Figure B-77. Particles from Sample 10 (E9, 74 cm).



84-546-3-7

a) Particle 10J (size range: 1000-1680 μm)



84-546-3-9

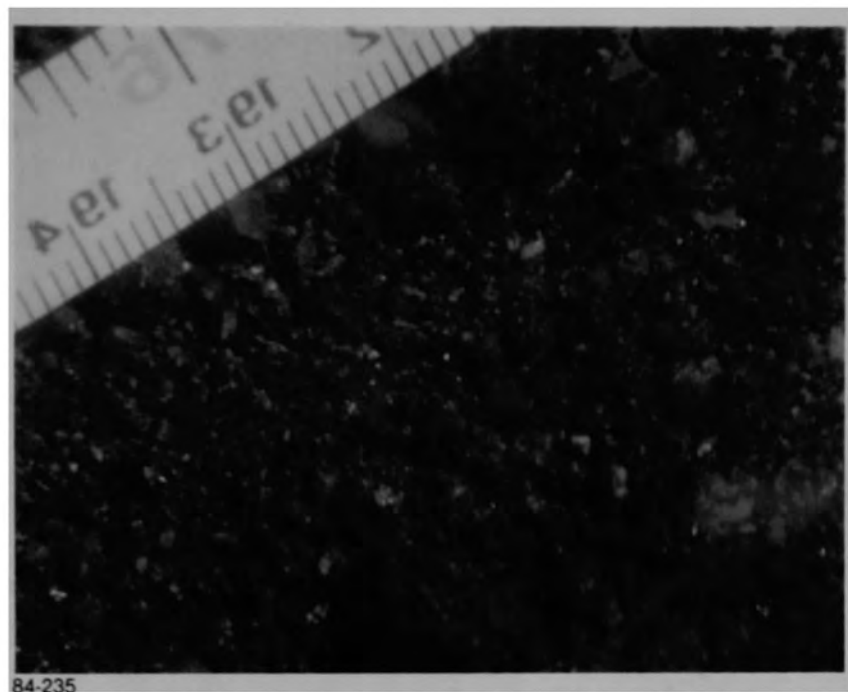
b) Particle 10K (size range: 1000-1680 μm)

Figure B-78. Particles from Sample 10 (E9, 74 cm).

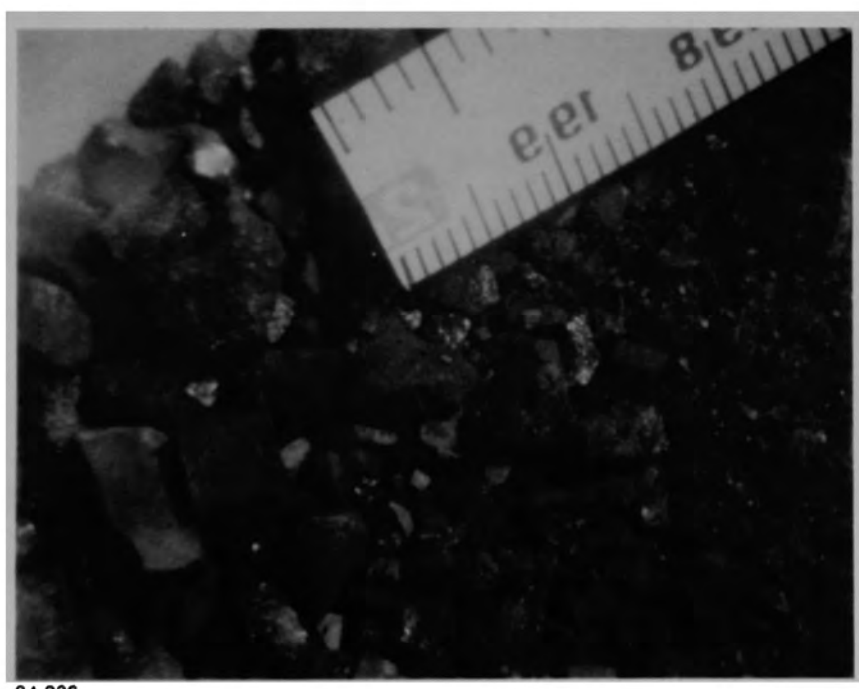


84-233

Figure B-79. Sample 11 (E9, 94 cm) being removed from sampling tool.

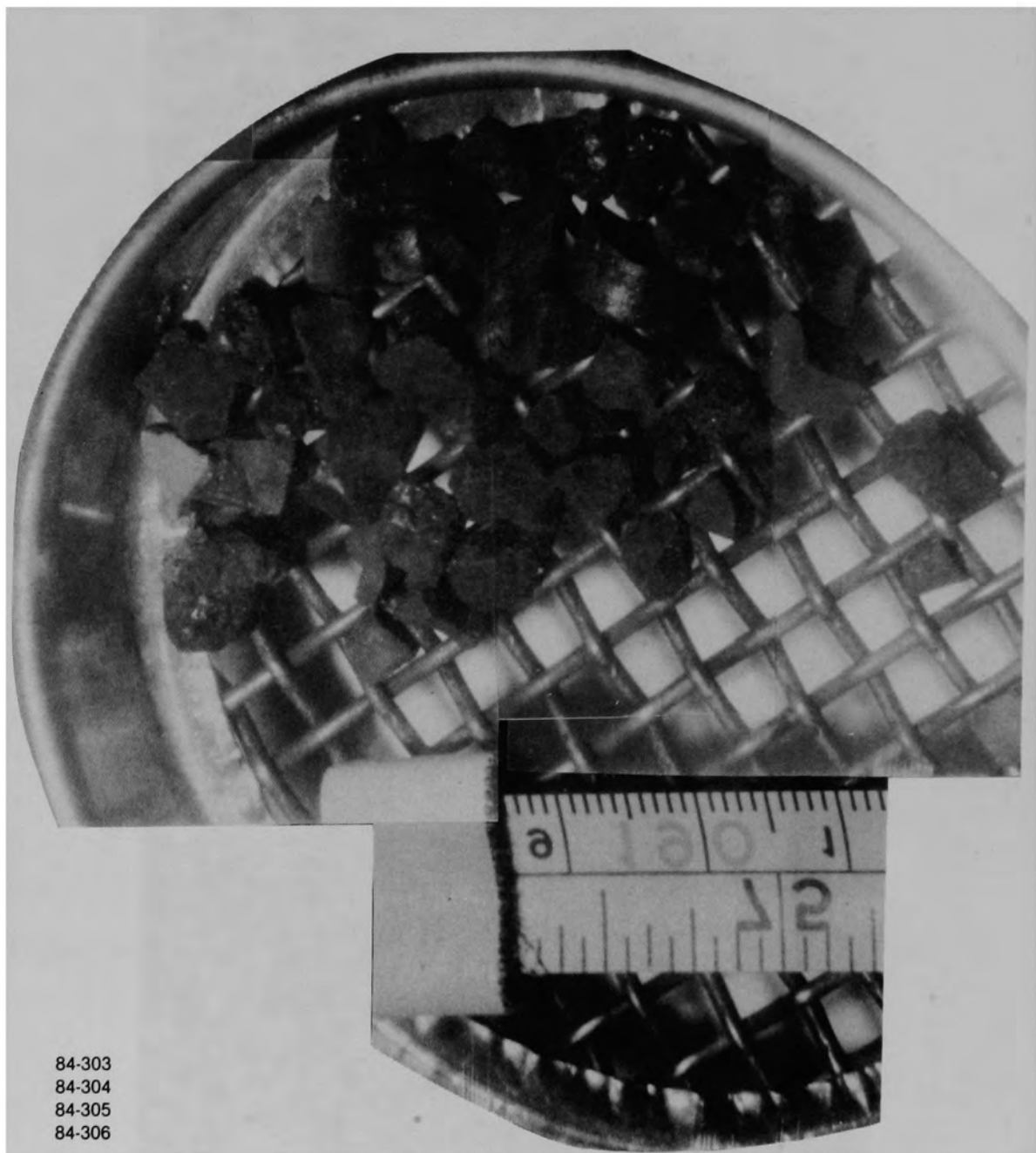


84-235



84-236

Figure B-80. Views of the bulk material for Sample 11 (E9, 94 cm) after removal from the sampling tool.



84-303
84-304
84-305
84-306

Figure B-81. Particles >4000 μm for Sample 11 (E9, 94 cm).

B-85

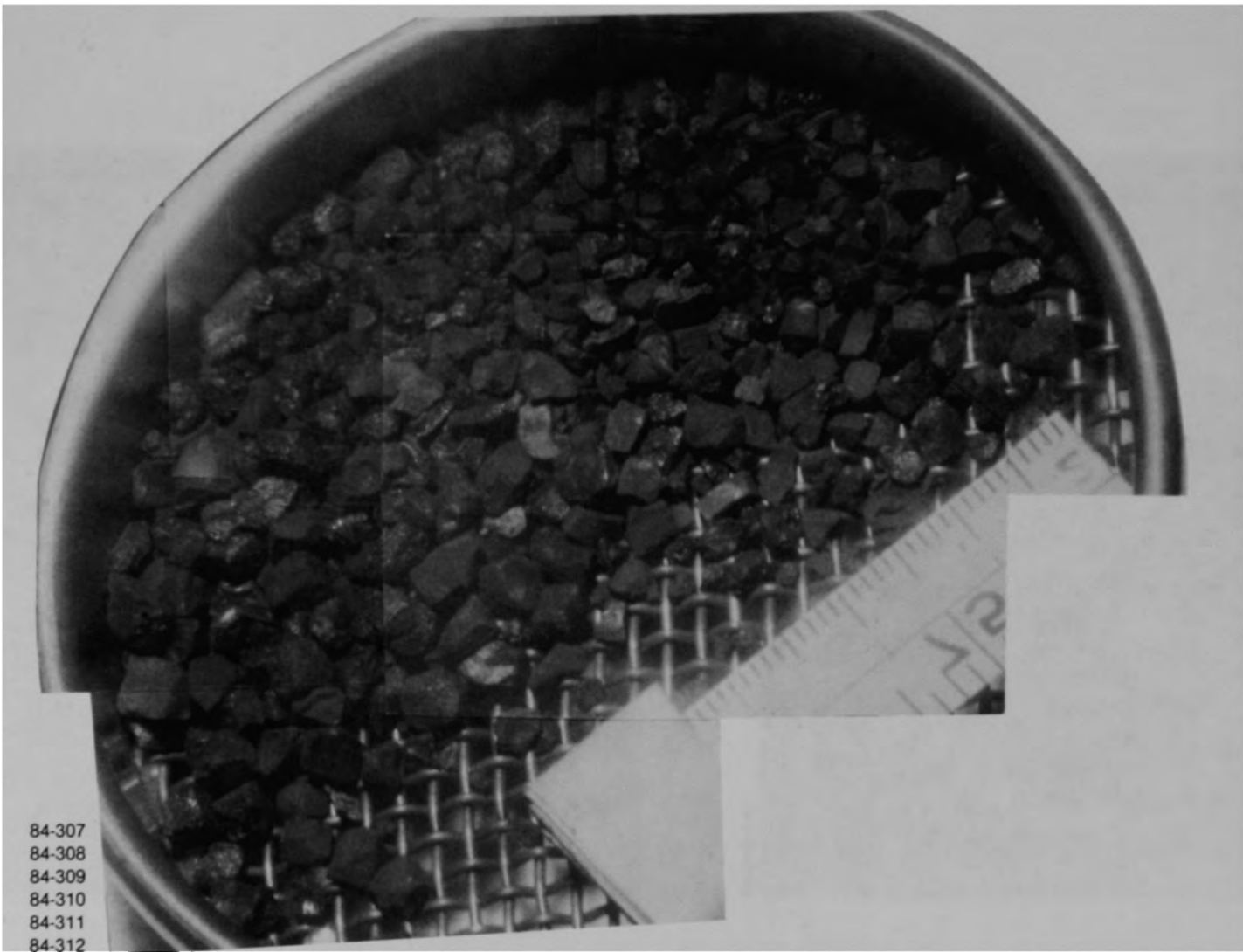
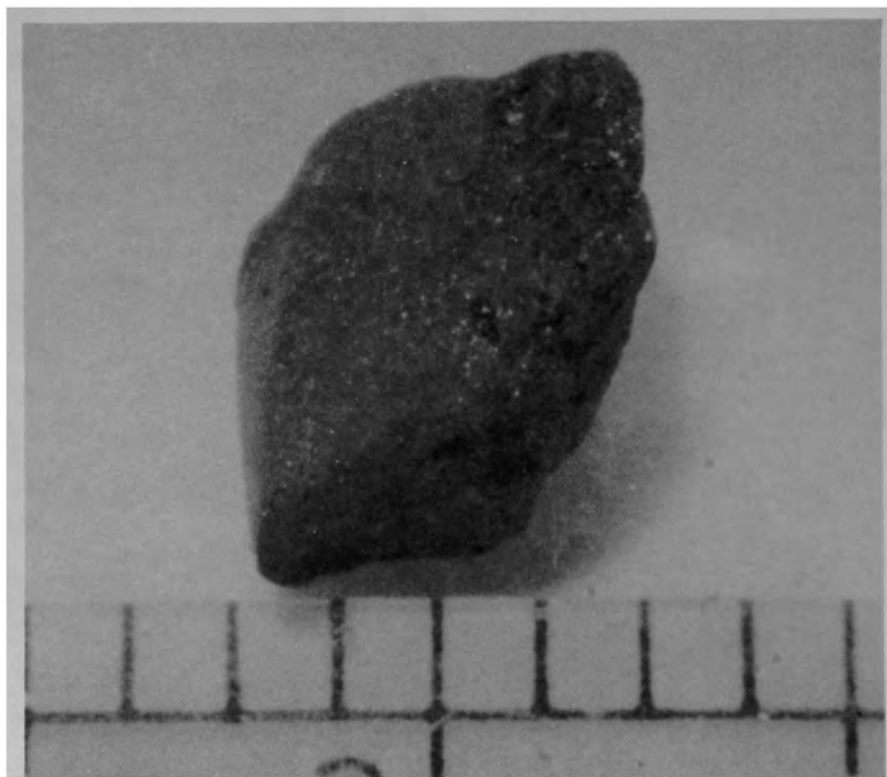


Figure B-82. Particle size fraction (size range: 1680-4000 μm) from Sample 11 (E9, 94 cm).



84-546-7-4

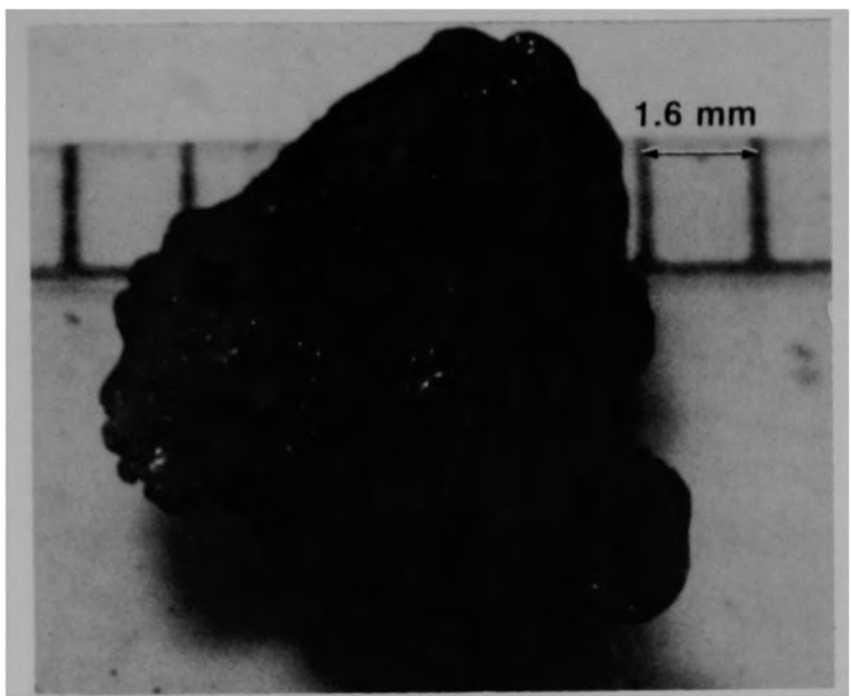
a) Front view of particle



84-546-7-6

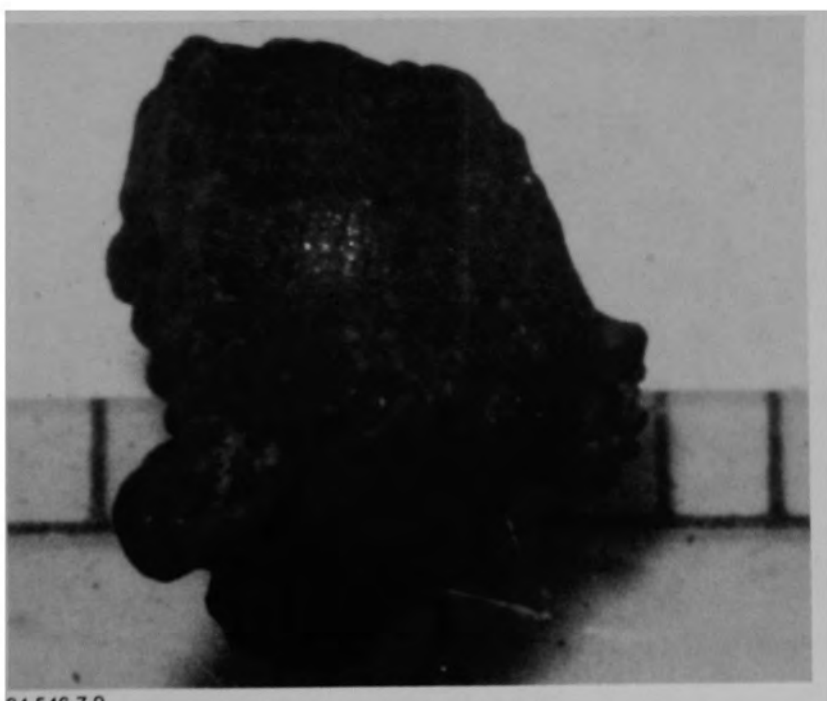
b) Back view of particle

Figure B-83. Particle 11A from Sample 11 (E9, 94 cm), size range:
 $>4000 \mu\text{m}$.



84-546-7-7

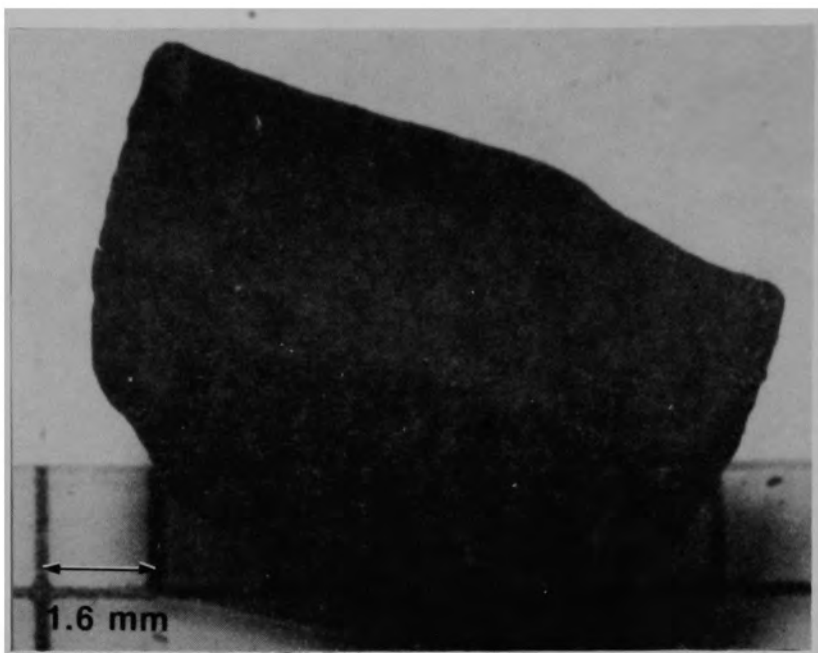
a) Front view of particle



84-546-7-9

b) Back view of particle

Figure B-84. Particle 11B from Sample 11 (E9, 94 cm), size range:
 $>4000 \mu\text{m}$.



84-546-7-11

a) Front view of particle



84-546-7-13

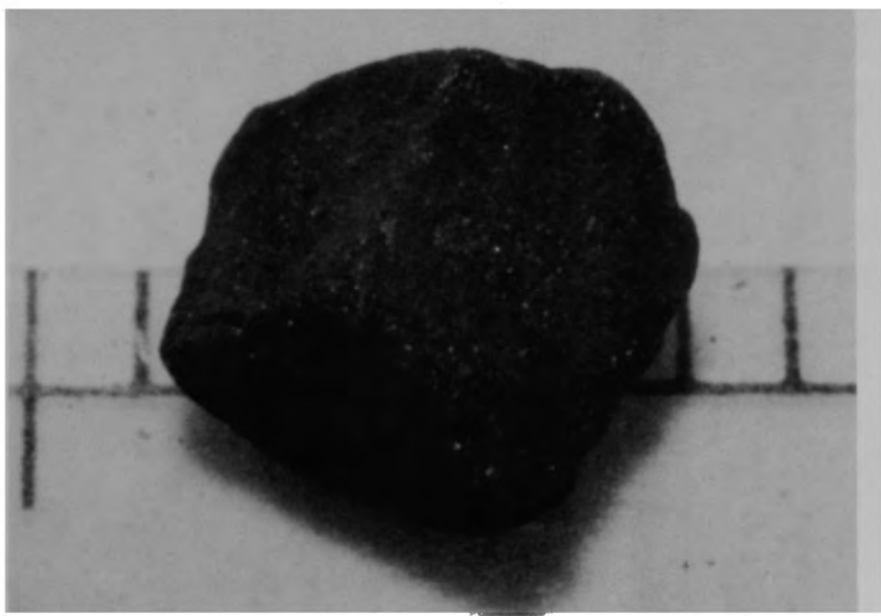
b) Back view of particle

Figure B-85. Particle 11C from Sample 11 (E9, 94 cm), size range:
 $>4000 \mu\text{m}$.



84-546-7-16

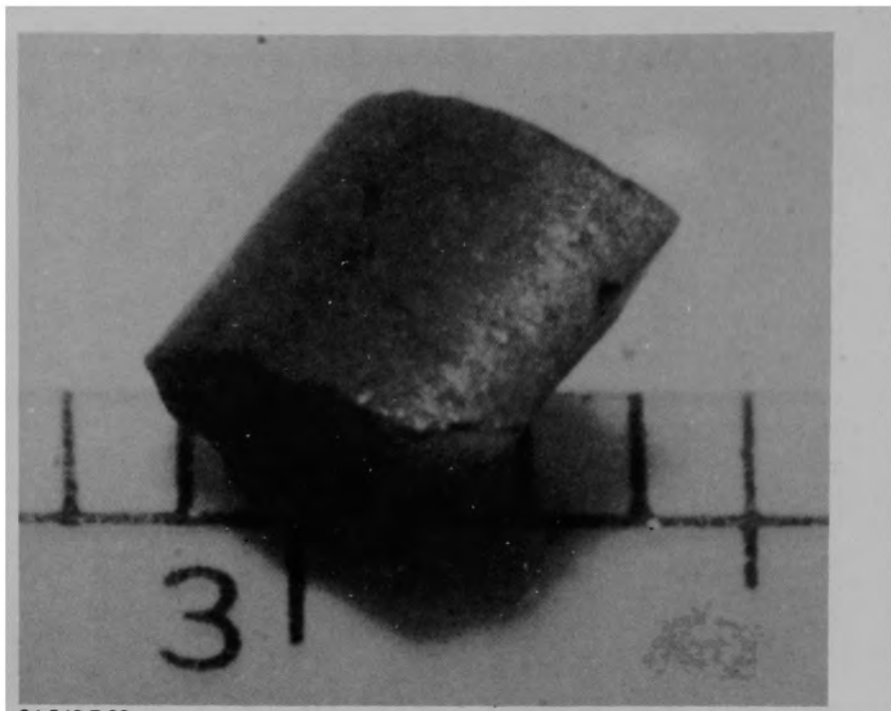
a) Front view of particle



84-546-7-18

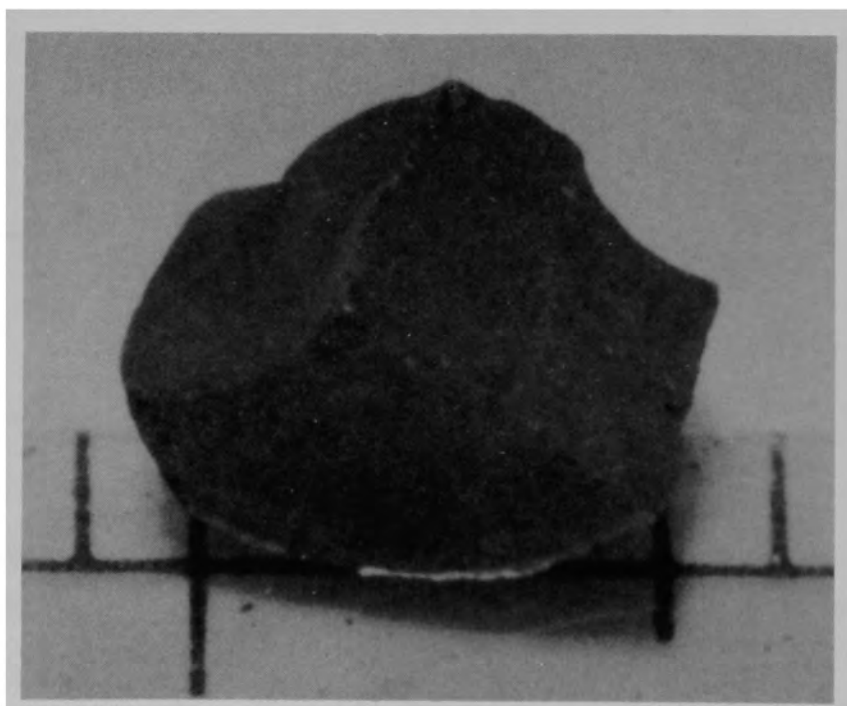
b) Back view of particle

Figure B-86. Particle 11D from Sample 11 (E9, 94 cm), size range:
 $>4000 \mu\text{m}$.



84-546-7-20

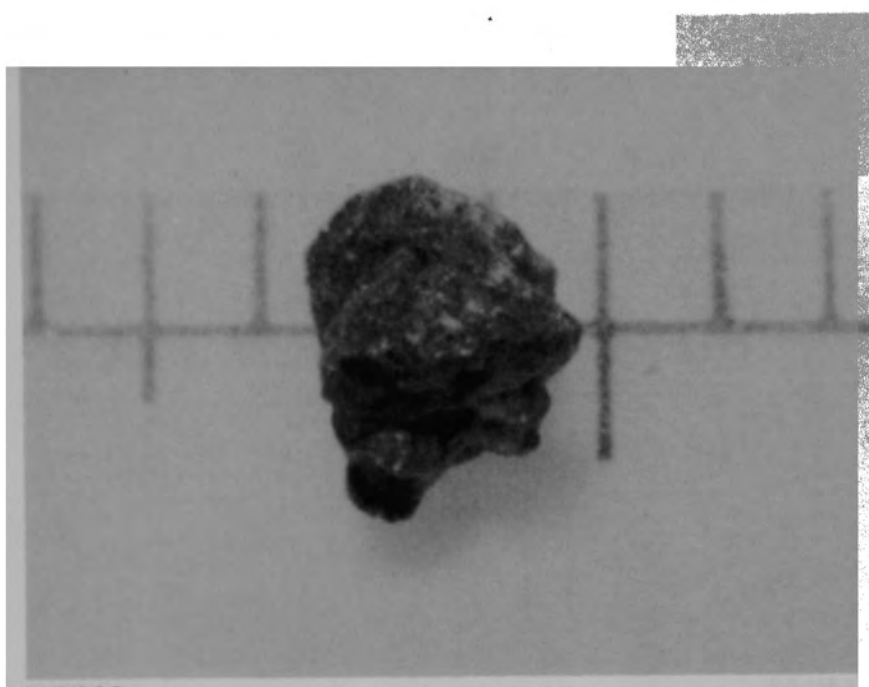
a) Front view of particle



84-546-7-22

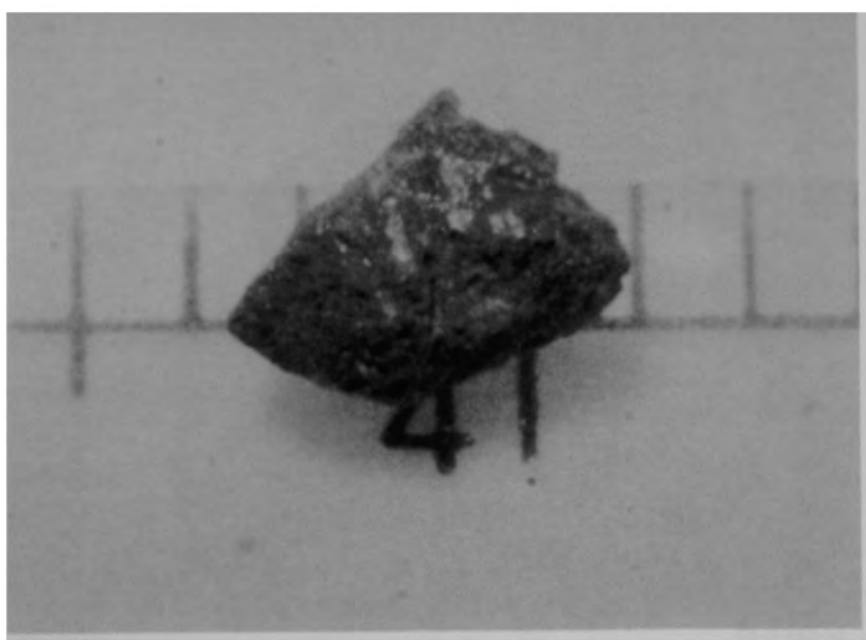
b) Back view of particle

Figure B-87. Particle 11E from Sample 11 (E9, 94 cm), size range:
 $>4000 \mu\text{m}$.



84-546-8-5

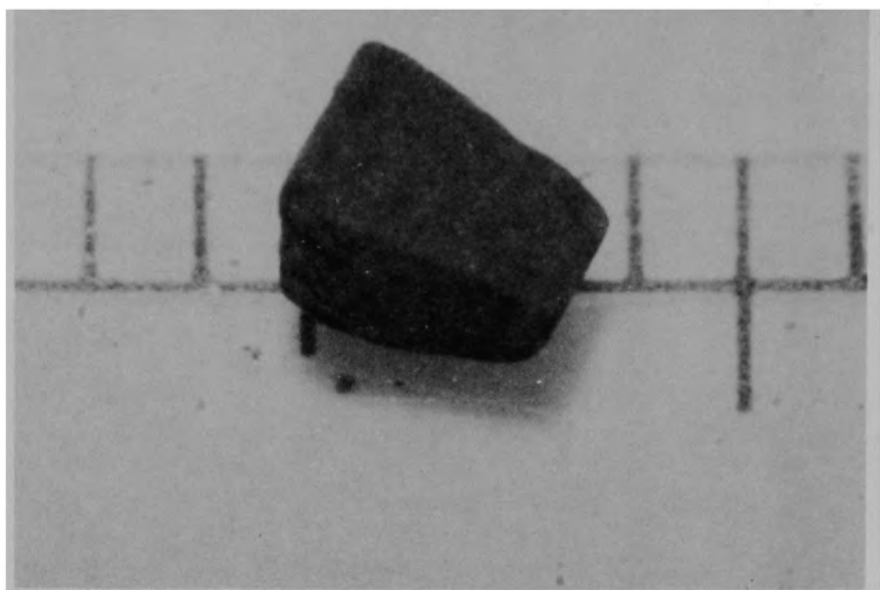
a) Front view of particle



84-546-8-6

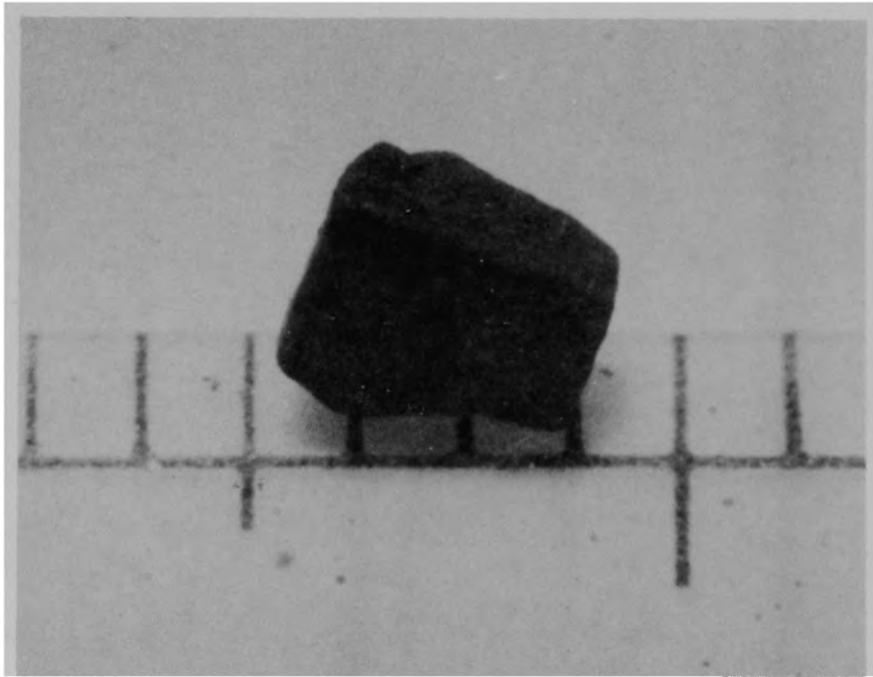
b) Back view of particle

Figure B-88. Particle 11F from Sample 11 (E9, 94 cm), size range: 1680-4000 μm .



84-546-8-9

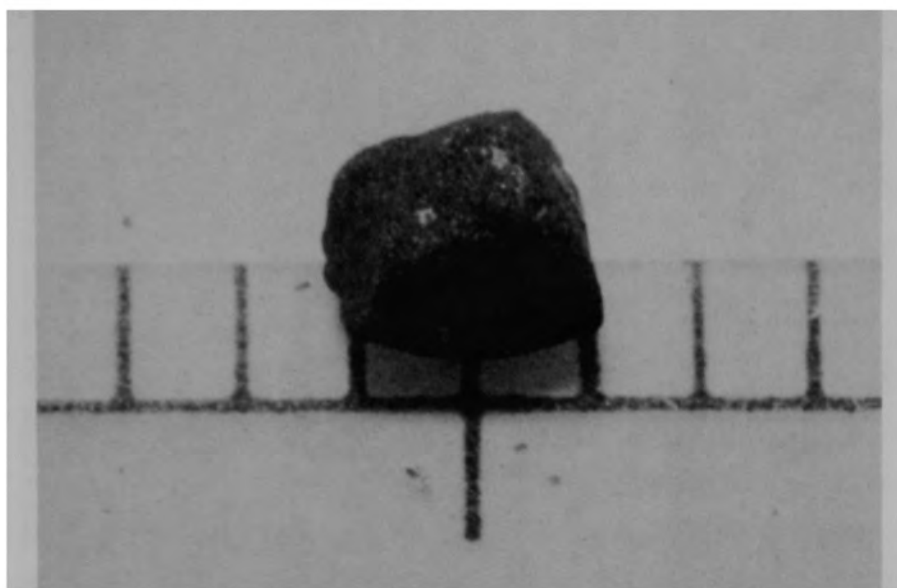
a) Front view of particle



84-546-8-10

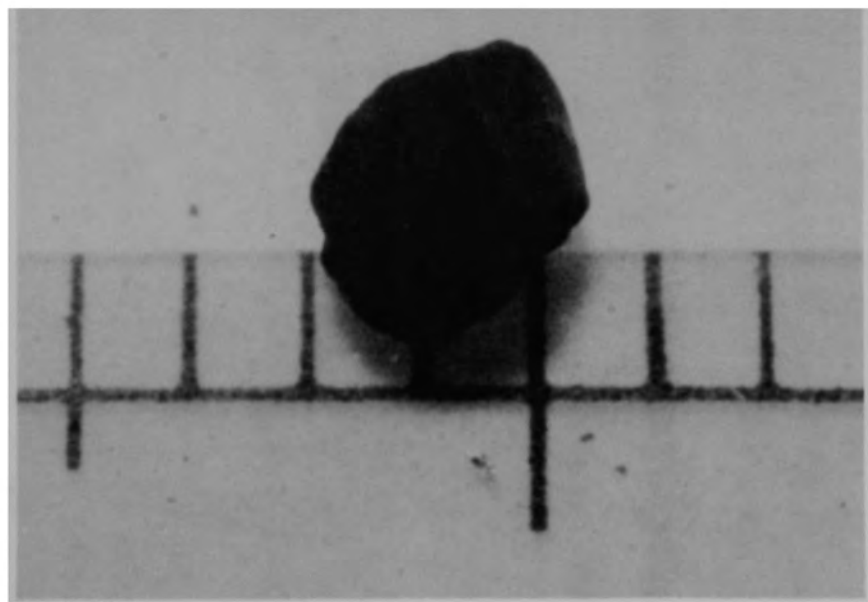
b) Back view of particle

Figure B-89. Particle 11G from Sample 11 (E9, 94 cm), size range: 1680-4000 μm .



84-546-8-13

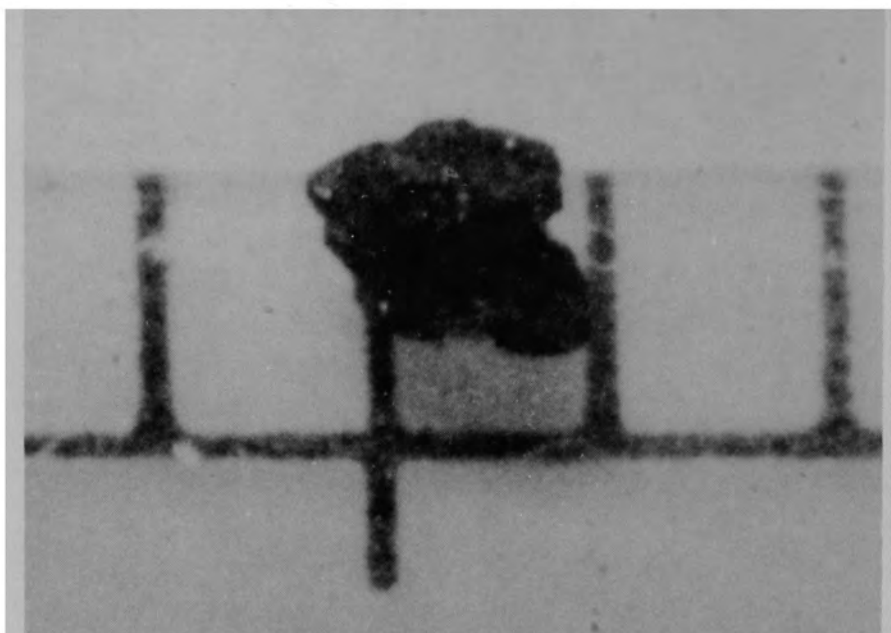
a) Front view of particle



84-546-8-14

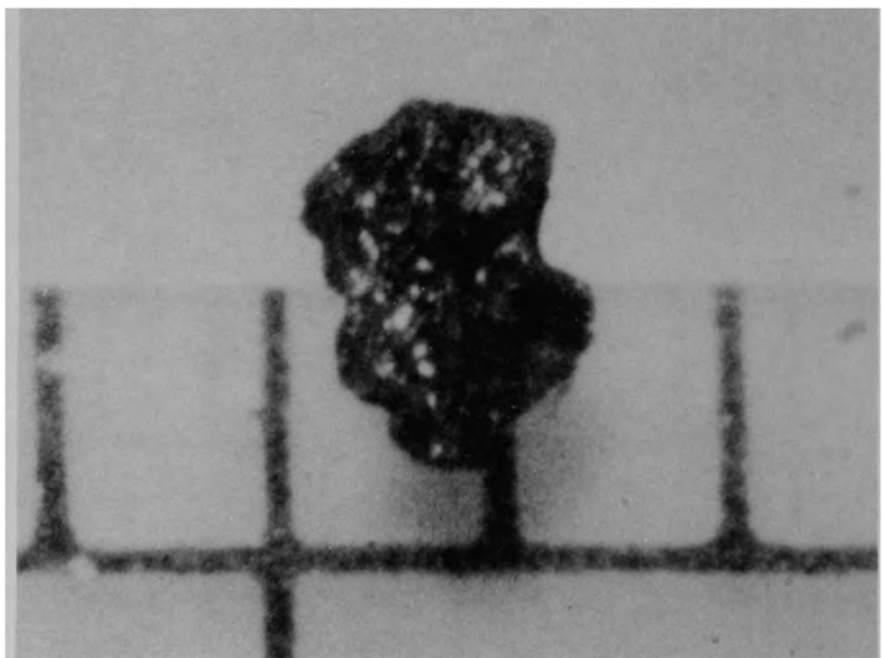
b) Back view of particle

Figure B-90. Particle 11H from Sample 11 (E9, 94 cm), size range:
1680-4000 μm .



84-546-8-17

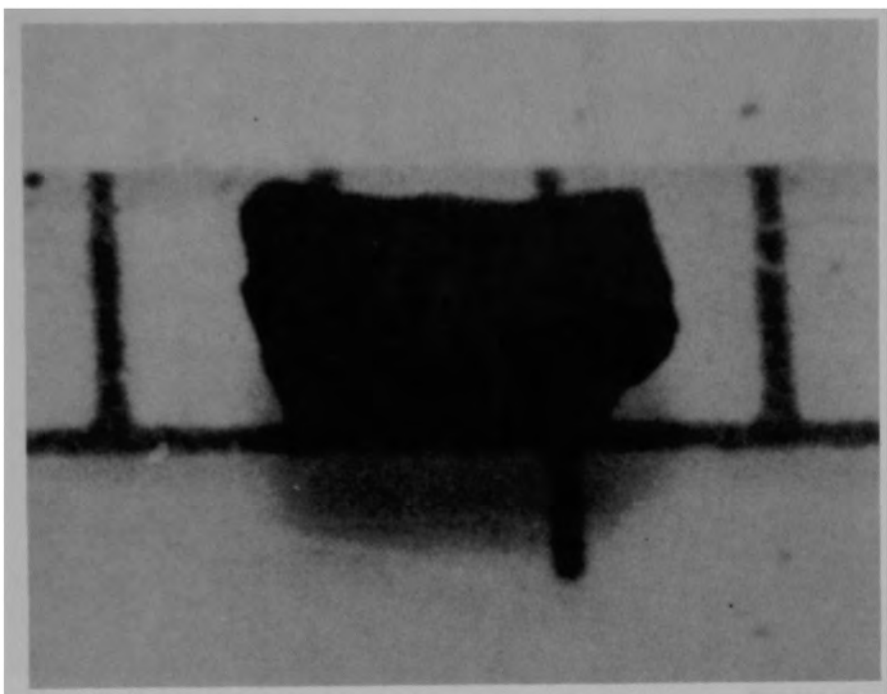
a) Front view of particle



84-546-8-19

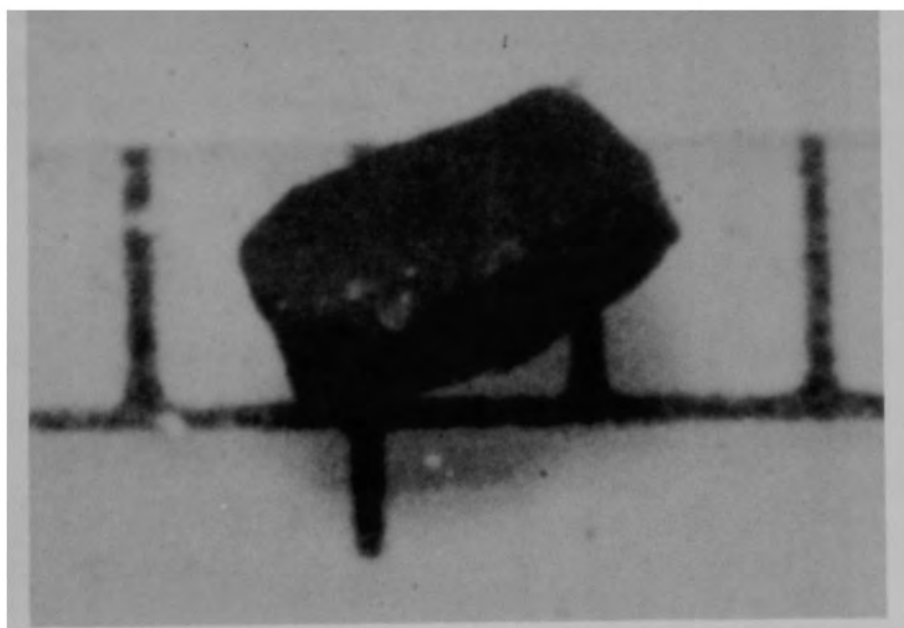
b) Back view of particle

Figure B-91. Particle 11I from Sample 11 (E9, 94 cm), size range: 1000-1680 μm .



84-546-8-21

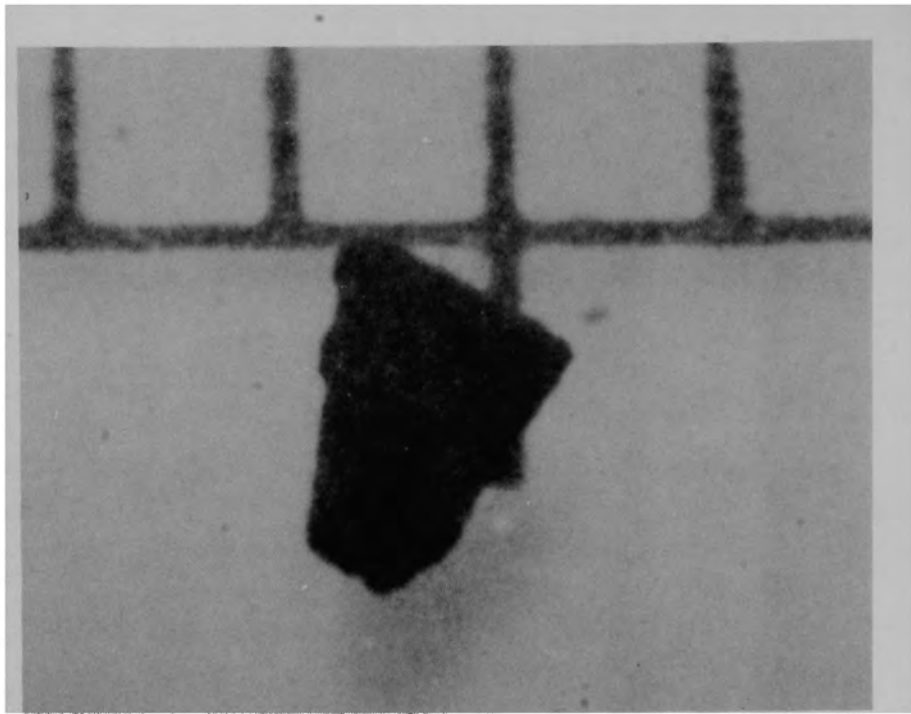
a) Front view of particle



84-546-8-23

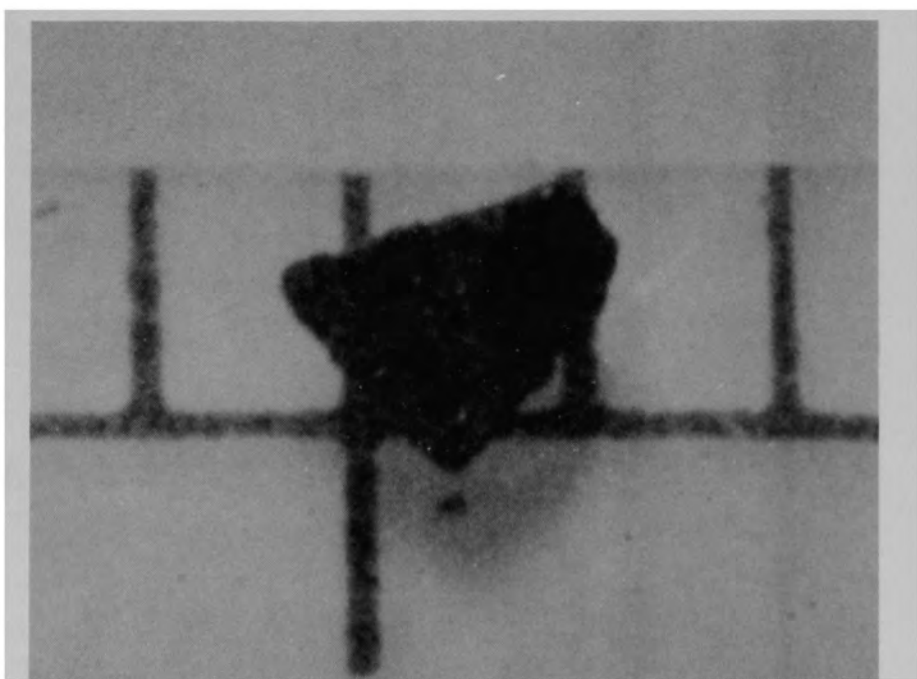
b) Back view of particle

Figure B-92. Particle 11J from Sample 11 (E9, 94 cm), size range:
1000-1680 μm .



84-546-8-25

a) Front view of particle



84-546-8-27

b) Back view of particle

Figure B-93. Particle 11K from Sample 11 (E9, 94 cm), size range: 1000-1680 μm .

APPENDIX C

METALLURGICAL DATA

CROSS REFERENCE INDEX FOR THE PARTICLES AND ASSOCIATED FIGURES AND TABLES

<u>Particle</u>	<u>Figure(s)</u>	<u>Tables</u>
1A ^a	C-1 through C-8	--
1B ^b	C-9 through C-20	C-1
1E ^{a,d}	C-21 through C-26	--
1H ^a	C-27 through C-30	--
3L ^{b,d}	C-31 through C-38	C-2
3M ^b	C-40 through C-49	C-3
4A ^b	C-50 through C-58	C-4
4B ^{b,d}	C-59 through C-69	C-5
4D ^b	C-70 through C-85	C-6
5E ^{b,d}	C-86 through C-95	C-7
6B ^{a,c}	C-96	--
6C ^{b,d}	C-97 through C-109	C-8
6D ^{a,d}	C-110 through C-114	--
6E ^{a,c}	C-115 through C-116	--
6F ^a	C-117 through C-119	--
7A ^b	C-120 through C-130	C-9
7B ^b	C-131 through C-141	C-10
7E ^{b,d}	C-142 through C-152	C-11
8A ^{b,d}	C-153 through C-165	C-12
8C ^{b,d}	C-166 through C-176	C-13
8E ^{b,d}	C-177 through C-189	C-14
8H ^b	C-190 through C-204	C-15
9D ^b	C-205 through C-219	C-16
9G ^b	C-220 through C-232	C-17
10A ^{b,d}	C-233 through C-247	C-18
10E ^{b,d}	C-248 through C-260	C-19
10F ^{b,d}	C-261 through C-270	C-20
11B ^b	C-271 through C-281	C-21
11C ^b	C-282 through C-294	C-22

a. Examination was performed by EG&G Idaho and Westinghouse Idaho Nuclear Co. personnel.

b. Examination was performed by Argonne National Laboratory personnel.

c. SEM examination was not performed.

d. SAS esamination was performed inaddition to SEM examination.

APPENDIX C

METALLURGICAL DATA

The optical metallographic, scanning electron microscope (SEM) and scanning Auger spectroscopy (SAS) analysis of the twenty-nine particles examined from the TMI-2 core debris samples are presented in this appendix. Twenty-two particles were studied jointly by EG&G Idaho and Argonne National Laboratories (East and West), while the remaining seven were characterized by EG&G Idaho and Westinghouse Idaho Nuclear Co. Representative photographs of each sample are presented, along with tables of chemical composition for locations analyzed by electron dispersive x-ray analysis (EDS) in conjunction with the SEM examinations and SAS analysis.^a The first one or two figures in each section are photomacographs of the particle with the locations of the subsequent photographs identified usually by letters. The three digit number identifications refer to chemical analysis locations reported in the tables.

The SEM/EDS data presented here are interpretations of the x-ray spectrums at representative locations. The location of peaks within the spectrum identified elements; the relative peak areas were used to classify the elements as major, minor or trace constituents. In instances where there was difficulty in distinguishing between overlapping peaks or background, the element was classified as questionable. Oxygen concentrations are not included in this data because oxygen can not be measured by this technique.

Quantitative concentrations were determined from the raw SAS data through the use of separate normalization factors (S_x) for each element. These factors relate the peak height of a standard material to the peak height of silver which is the normalizing element. The peak height for normalization factors can be obtained from "handbook" data or, for best accuracy, measured from standard materials which contain the element of

a. Note that not all particles were analyzed by SAS.

interest in the form expected in the unknown material. Using the S_x values, peak heights of different elements are put on a common basis so that relative ratios of measured peak heights become relative compositions.

The Zr and O_2 S_x values used on the initial two particles (6C and 4B) were measured from a piece of ZrO_2 which had been quantitatively analyzed by EDS. The S_x values for the remaining particles were measured from a piece of ZrO_2 which had been quantitatively analyzed by wet chemical techniques. The S_x value for U on the initial two particles was measured using UO_2 test fuel, assuming an S_x value for O_2 from the ZrO_2 standard. This value was updated for the majority of the remaining particles using the corrected S_x value for O_2 . Finally, a direct measurement of the S_x value for U and O_2 from depleted UO_2 (which had not been used in a high temperature test) was used on the final three particles (10E, 10A, and 7E). The S_x values for the remaining elements were obtained from NBS standards (Cr, Fe, and Ni), theoretical interpolations (Tc, Ru, Rh, Pd, and Sn), or "handbook" data (C and Al).

A measure of the accuracy of the SAS system was obtained from 14 readings of the Ag peak. These were taken on pure silver foil, under conditions similar to those of the analysis. From these measurements, a standard deviation of 0.87 and a mean of 63.9 was determined which results in a scatter band of about $\pm 2\%$. This represents the best precision possible. However, most measurements are not this good. The scatter of the data is lowest when the surface being measured is smooth and well polished. Region G of Sample 5E and, to a lesser extent, Region 2 of Sample 10A are examples of rough surfaces with corresponding high scatter.

Particles 1A, 1E, 1H, 6D, and 6F were separately characterized on WINCO instruments in a somewhat different format. Semi-quantitative SEM/EDS data were acquired from all five particles, while quantitative SAS was performed only on Particles 1E and 6D. This was done primarily to verify metallographic inferences on oxygen concentrations and to confirm

related interpretations on peak temperatures. Detailed SEM/metallographic images, comprehensive data listings, and thorough discussions on these five particles are presented in this appendix.

EDS derived composition information is termed "semi-quantitative" for two reasons: (a) oxygen concentrations cannot be measured, which induced significant upward biases in weight percentages for those elements that were detected; and (b) area fractions for x-ray peaks were converted into elemental weight percentages without calibration to standards. The theoretical corrections applied compensate for mass attenuation, self-fluorescence, and atomic number effects. They are more appropriate to metals than oxides. Deficiencies in these correction factors can cause uncertainties of $\pm 5\text{wt}\%$. In addition, bias errors result from the inability to detect oxygen. Consequently, the EDS values reported for Particles 1A, 1E, 1H, 6D, and 6F should be interpreted as relative indications of elemental amounts, rather than absolute determinations.

By comparison, the SAS measurements on Particles 1E and 6D of Zr, U, and O contents were performed with rigorous calibrations and are accurate to within $\pm 2\text{ atom}\%$. A UO_2/Zr interaction standard was graciously donated by the Kernforschungszentrum Karlsruhe (Federal Republic of Germany) where UO_2 , $\alpha\text{-Zr(O)}$, and U,Zr alloy were assessed by both Auger spectroscopy and electron microprobe, each of which had been previously calibrated to numerous standard materials. An extruded ZrO_2 rod (Corning Glass Co.) was also supplied by Babcock & Wilcox Co. to provide a known Zr-O ratio for Auger spectroscopy calibration where the rod composition was precisely determined by inductively coupled plasma spectrometry at INEL. While the $15\text{-}\mu\text{m}$ electron beam diameter prevented analysis of small discrete phases, the relatively large beam also reduced sensitivity to local sample topography, with a beneficial effect on data scatter.

Particle 1A

Particle 1A (Figure B-2) is composed of an outer shell of partially oxidized cladding, an intermediate region of prior-molten U-Zr-O mixture,

and an interior piece of UO_2 fuel. Thickness variations in the prior β -Zr wall, and in the melt layer, indicate that the cladding ballooned asymmetrically (presumably as a consequence of unbalanced heat transfer), with a radial increase of approximately 1 mm at the orientation shown in Figure C-1. Zircaloy in direct contact with fuel pellets above the ballooned region reacted to create a homogeneous U-Zr-O melt that relocated downward to fill the balloon space. The large voids with oxidized surfaces represent two portions of the melt that slumped further downward to be replaced by steam. The extent of oxidation on Figure C-2 suggests that steam flow occurred through these voids between two axially separated cladding breaches. Figure C-2 also demonstrates that the heat of oxidation permitted some segregation of melt constituents along the void surfaces, since the random arrangement of α -Zr(0) grains and U,Zr alloy precipitates in the melt interior has been restructured into parallel bands of dark-gray ZrO_2 and light-gray $(\text{U},\text{Zr})\text{O}_2$ in the oxidized regions.^a

SEM/EDS results from Particle 1A are summarized on Figure C-3 and presented in detail on Figures C-4 through C-8. One noteworthy finding on Figure C-3 is Point 1, an Fe-rich deposit on the exterior surface that indicates post-accident rust accumulation. This explains the reddish-yellow external coloration of many grab sample particles. The melt composition (neglecting oxygen) was measured for area 6 as approximately 87-wt% Zr, 11-wt% U, and 2-wt% Ni, plus traces of Fe and Cr. The Fe and Cr content could be attributed to Zircaloy-4 alloying ingredients, but the Ni originated from another component source.^b As shown in Figure C-4, the melt segregated into three phases upon cooldown: grains of α -Zr(0), irregular patches of (U,Zr) alloy, and a transition metal phase (Ni, Fe, Cr, plus substantial Zr) squeezed between the other two phases. Figure C-4 also demonstrates that very little chemical and diffusional interaction

a. Oxidized areas appear darker on backscattered scanning electron micrographs, due to dilution of the heavy metal scattering centers by large concentrations of oxygen atoms.

b. An Inconel spacer grid, control rod guide tube, fuel assembly end fitting, etc.

occurred across the cladding-melt boundary, despite the melt's tendency to wet both cladding and fuel. This was evident from the oval shape of both voids in Figure C-1. Therefore, melt solidification probably happened shortly after arrival at this fuel rod elevation.

Figure C-5 illustrates the phase make-up of the interior melt region (Area 7), which is very similar to that near the cladding. However, a Sn x-ray peak was partially resolved at this position, so the area distribution of this element was indirectly mapped. As indicated, Sn was found within both the U,Zr alloy and the transition metal phase, but not inside the α -Zr(0) grains to any noticeable extent. Figures C-6 and C-7 display phase structures for Areas 8 and 9, respectively, that are nearly identical to Areas 6 and 7.

Figure C-8 presents the fuel morphology and elemental distributions adjacent to the melt. As shown, some inward diffusion of Zr and Fe has occurred, but no clear signs of fuel liquefaction were found. This suggests prompt melt solidification after contact. Note also that the UO_2 grains in Figure C-8 are typically in the 10- μm range, approximately the as-fabricated size. The lack of equiaxed grain growth, plus the thin ZrO_2 layer thickness on the cladding exterior, confirm that the fuel rod region from which Particle 1A originated stayed relatively cool--within a few hundred degrees of the 1245 K β -zircaloy transition temperature.

Particle 1B

Particle 1B (Figure B-3) appears to be a quarter section of a fuel pellet with a thin layer of prior-molten U-Zr-O as shown in Figure C-9. Initial preparation of this particle was difficult due to severe pullout of individual fuel grains so the particle was backfilled with epoxy to hold the grains in place. Figures C-10 through C-13 are optical photos which show the etched grain structure from pellet center to outside surface. The grain size is consistently about 12 μm across the particle. Figures C-14 and C-15 are optical photos which show the thin U-Zr-O layer at two

locations on the surface. Figures C-16 and C-17 are SEM secondary electron images of the fuel (note the interlinked porosity in C-16) and Figures C-18, C-19, and C-20 are SEM Back Scatter Electron (BSE) images which correspond to Figures C-14, C-15, and C-12, respectively. Note the layers shown in Figure C-18. Table C-1 displays the SEM/EDS elemental analysis indicating the outer surface of this film is pure Zr with U content increasing with position toward the fuel, and with little penetration of Zr into the fuel.

Particle 1E

Particle 1E (Figure B-4) is a partially oxidized cladding section with UO_2 fuel bonded to the interior surface and ZrO_2 on the outer surface. The two parallel, circumferentially oriented cladding bands in Figure C-21 (that are rich in uranium content) provide evidence of high temperature zircaloy- UO_2 interactions. Radially oriented patches of ZrO_2 within the cladding matrix and large metallic stringers along the interior of the ZrO_2 layer indicate that cladding melting occurred. In addition, a small amount of prior-molten $(\text{U}, \text{Zr})\text{O}_2$ ($T > 2810$ K) has solidified on the exterior of the ZrO_2 layer.

Because of prolonged oxidation, the cladding structure at one point during the TMI-2 transient consisted of the following layers (from the outside inward): ZrO_2 , $\alpha\text{-Zr(O)}$, large $\beta\text{-Zr}$ grains at the cladding center, $\alpha\text{-Zr(O)}_b$, $\alpha\text{-U,Zr}$ alloy, $\alpha\text{-Zr(O)}_a$, and the UO_2 . Then this cladding structure melted, which accelerated oxygen uptake from both the UO_2 and external ZrO_2 . For a brief time, UO_2 dissolution by molten cladding must have proceeded rapidly. Upon cooldown, the oxygen-depleted, hypostoichiometric portion of the ZrO_2 decomposed into ZrO_2 and metallic stringers of $\alpha\text{-Zr(O)}$. Meanwhile, the heterogeneous U-Zr-O melt near the fuel interface transformed into $\alpha\text{-Zr(O)}$, $\alpha\text{-U,Zr}$ alloy, and $(\text{U}, \text{Zr})\text{O}_2$. The timing of the molten, single-phase $(\text{U}, \text{Zr})\text{O}_2$ attachment to the exterior ZrO_2 surface cannot be directly inferred from this scenario.

Figures C-22 and C-23 (high magnification) detail the semiquantitative elemental analyses that were performed near the fuel-cladding interface. Only relative weight percentages for U and Zr were measured, because oxygen cannot be detected by EDS. Therefore, the approximate degree of oxidation must be inferred from the gray-level contrast on the backscattered scanning electron images, where brighter regions correspond to higher average atomic numbers. For example, the bands of $(U,Zr)O_2$ are considerably darker than the small patches of U,Zr alloy, due both to lower U concentrations and substantial dilution by oxidation. Point 7 of Figure C-23 demonstrates that microsegregation of an Fe- and Cr-rich phase occurred at isolated portions of this interface. UO_2 grains on the left side of this micrograph are typically 30 μm in diameter, so some grain growth has taken place at this position. This observation is consistent with the determination that the cladding exceeded the α -Zr(0) melting point of 2245 K.

Figure C-24 illustrates how the ZrO_2 layer was reduced by the metallic cladding, creating patches of ZrO_2 in the α -Zr(0) cladding matrix and leaving radially oriented stringers of α -Zr(0) within the ZrO_2 region. However, the sizable separation between these two phases in both instances means that this area was not quenched abruptly from its maximum temperature. As shown by the EDS results from Point 1 and the Al x-ray image, a thin layer of Al-rich material collected at the interface, which suggests an earlier cladding reaction with Al_2O_3 , the dominant Al source within the TMI core. Figure C-25 shows a different view across the ZrO_2 layer, where substantial amounts of an Fe/Cr/Al-rich phase are conspicuous at mid-thickness. Here, the metallic stringers were found to contain significant U concentrations. These (presumably) originated across the cladding in the fuel. Note also that the adherent $(U,Zr)O_2$ at the top of Figure C-25 has not reduced the adjacent ZrO_2 , which confirms the metallurgical interpretation that the $(U,Zr)O_2$ arrived as a molten ceramic ($T > 2810$ K) as opposed to a metallic melt oxidized in place at a lower temperature.

Although the $(U,Zr)O_2$ adhered as a single-phase ceramic melt, the attachment did not necessarily occur at a single time. As shown by the EDS results on the left side of Figure C-26, significant differences were detected in concentrations of transition metals between melt adjacent to and away from the ZrO_2 layer. Some variation in U and Zr composition was also found across the melt during quantitative SAS measurements, according to the right side of Figure C-26. Therefore, the molten ceramic probably arrived at this fuel rod elevation in separate rivulets, solidifying in succession much like candle wax. Nevertheless, the temperature estimation of at least 2810 K is unaffected, because SAS oxygen values are uniformly close to 67 atom%. The exception is Point 9 from the ZrO_2 portion that was reduced by the molten cladding.

Particle 1H

Particle 1H (Figure B-6), as shown in multiple views on Figure C-27, has a very porous (foamy) appearance and is a quench-frozen agglomerate of two distinctly different types of material. Single-phase, large-grained, pore-free fragments have been surrounded by a fine-grained, porous, multi-phase melt. After metallography, it was initially thought that this particle was probably composed of fuel pellet pieces coated by a quenched melt, which would have accounted for the apparent chemical dissolution of the single-phase ceramic blocks. However, very little gray-level contrast is evident between the porous and pore-free regions on the backscattered scanning electron micrograph. This means there is overall similarity in average elemental composition and extent of oxidation.

Metallographic and SEM images are presented on Figure C-28 of area A, one of the regions of Particle 1H where porous melt attack of a solid fragment is especially apparent. The upper photomicrograph shows the grain facets of the pore-free material quite clearly, but grain surfaces along the melt interface are irregular and pitted from dissolution. Melt penetration along grain boundaries is evident from the wide thickness variations of the intergranular material. This eliminates precipitation of a second phase during cooldown of the pore-free solid as a cause for the

presence of this grain boundary substance. As shown in the lower micrograph on Figure C-28, melt-solid interaction was evidently related to pore production, because small pores nucleate near the interface and combine to form larger voids with increasing distance.

Two smaller portions of area A were analyzed by EDS, and are shown at high magnification on Figure C-29. Neglecting oxygen, which cannot be detected by EDS, the melt has an average composition of 68-wt% U, 28-wt% Zr, and 4-wt% Fe, plus traces of Ni, Cr, and Al.^a The Fe content is much higher than the nominal 0.225-wt% in Zircaloy-4 and Ni should not normally be detected, so the melt almost certainly interacted with Inconel or stainless steel early in its evolution. Three phases are apparent in the melt: bright, relatively distinct grains, dark stringers, and mottled patches, with the grains containing the largest U concentrations and the stringers being high in transition metals. However, phase segregation seems incomplete as a consequence of quenching, so the mottled patches may in fact be a multi-phase mixture; the phase compositions might have been different had equilibrium been attained. Note also, that the composition and appearance of the mottled patches are very close to the material between grains of the pore-free solid. This suggests that this phase preferentially wetted the large-grained fragments.

The single-phase, pore-free fragments are almost definitely $(U,Zr)O_2$ solid solutions, although this identification is a metallographic deduction and has not been precisely confirmed by SAS. The $(U,Zr)O_2$ "islands" could represent a ceramic melt ($T > 2810$ K) or a metallic melt oxidized in the liquid state to saturation and solidification ($2175\text{ K} < 2675\text{ K}$). No shrinkage pores, nor other features clearly associated with a prior molten state, were observed, unlike the ceramic melt on Particle 1E. However, mixed ceramic melts that have been superheated and quenched can appear pore-free. But, because the $(U,Zr)O_2$ regions were found to vary from

a. The approximate atomic Zr:U:Fe ratio is 13:12:3.

67-wt% U and 33-wt% Zr to 59-wt% U and 41-wt% Zr^a with no detectable Al, Ni, Fe, and Cr, the pore-free solids did not originate within a single molten region.

Figure C-30 presents micrographs from areas B (upper) and C (lower) of Particle 1H. Area B is quite similar in appearance and average composition to the upper portion of area A, showing the same three-phase melt microstructure. Like area A, area C illustrates how porosity from melt-solid interfaces has coalesced into larger void features. Tiny deposits of Fe, Cr, Al, Ni, and Sn were occasionally detected within the smallest pores during EDS surveys at this position, so the porosity may be nucleated at temperature by minuscule bubbles of metal vapor.^b Nevertheless, area C demonstrates that melt shrinkage during cooldown was equally important in void formation. Note the parallel dendritic freezing features pulled between two $(U,Zr)O_2$ fragments in response to the strong melt tendency to wet the $(U,Zr)O_2$. In addition, area C supplies additional proof that mixed oxide dissolution occurred along all exposed $(U,Zr)O_2$ surfaces and not just within grain boundaries; two regions are indicated where $(U,Zr)O_2$ grains are almost completely dissolved. The rounded, bulbous shape of one of these grain remnants suggests incipient melting, in which case the melt temperature was greater than 2810 K. Note that the melting point of the $(U,Zr)O_2$ would be the same whether the $(U,Zr)O_2$ formed by ceramic melting or by liquid-state oxidation of a metallic melt.

The melt behavior at temperature is difficult to precisely deduce from the phase make-up after quenching. Because the dissolution of the $(U,Zr)O_2$ blocks had progressed quite far, some of the melt represents previously dissolved mixed oxide. Thus, it is not certain whether the melt was initially homogenous or heterogeneous. The melt surrounding the $(U,Zr)O_2$ blocks and along block grain boundaries was nearly identical to the average mottled patch composition. Therefore the patch phase was

a. See Figure C-30.

b. Such deposits might be more common on unetched samples.

likely responsible for attacking the mixed oxide fragments. Because Fe forms a complex eutectic system with U, Zr, and O, the dissolution mechanism was probably eutectic decomposition. However, the melt temperature may also have been higher than 2810 K, as suggested by the bulb shape in area C. In that case $(U,Zr)O_2$ melting would have accelerated the dissolution process. In any event, the melt penetration along grain boundaries confirms that the $(U,Zr)O_2$ had definitely solidified before melt contact concurred.

Particle 3L

From the photomacrograph of Particle 3L in the as-polished condition, shown in Figure C-31, this particle appears to be formed from several different pieces of ceramic material. There are regions of large elongated pores, large round pores, and small pores. Figure C-32 shows closer views of the central section as polished and Figures C-33 and C-34 show typical areas (no visible microstructure) after a very heavy etch with the fuel etchant indicating that it is a glossy phase of the mixed oxides.

Figure C-35 is a BSE overall image, with Figure C-36 showing a very fine dendritic structure from Region A. This type of structure is found throughout the band of the particle identified by large elongated pores. Figure C-37 is from the bottom of Figure C-35. Figures C-38 and C-39 are SEM images of two regions containing large round pores with an Al-Cr-Fe-Ni phase within.

Table C-2 displays the SEM/EDS and SAS analysis. This particle is predominantly $(U,Zr)O_2$ with slight variations in Zr/U ratios between regions ranging from about 2.4 in the top edge, to about 2.2 in the bulk of the sample, to about 1 in a small region seen in Figure C-38. The only occurrence of other elements is in and around a few large pores (see Figures C-37 and C-38).

Particle 3M

Particle 3M appears to be a piece of (UO_2) fuel which has interacted with zircaloy and structural material along one side and in cracks. Figure C-40 shows the two region types that make up Particle 3M. Region Type 1 is UO_2 fuel which has experienced very little grain growth (current grain size $\sim 11 \mu\text{m}$) but has a large void fraction. Region Type 2 is mostly uranium with varying amounts of Zr and a trace of Fe. A Cr, Fe, Ni material fills grain boundaries and occurs in voids in Region 2. Figures C-41 through C-49 are typical optical and SEM images of the particle (see Figure C-40 for locations). Table C-3 displays the SEM/EDS elemental analysis. A gradient in Zr was detected by the SEM/EDS at the interfaces between Regions 1 and 2.

Particle 4A

Figure C-50 shows Particle 4A (Figure B-11) as-polished and after a 5-minute fuel etch. The base material in the over etched region is UO_2 with a trace of Fe in some places. The base material in the region that did not over etch is U with some Zr and Fe; the amount of Zr increases with distance away from the over etched region. There is an Al-Cr-Fe-Ni second phase found throughout the particle but more often in the Zr bearing regions. See Table C-4 for a summary of the chemical composition from the SEM/EDS analysis.

There is a gradient in the pore and grain size across this particle where the minimum grain size (which is on the right side of the particle) is about $18 \mu\text{m}$. Figure C-51 shows three as-polished optical photos of the same magnification from opposite sides of the particle and Figure C-52 shows equivalent SEM images. The grain boundary phase seen in the SEM images in Figure C-53 can be seen in the etched optical images in Figures C-54 and C-55. SEM images showing the Al-Cr-Fe-Ni bearing grain boundary phase in the over etched region are seen in Figure C-56. Figures C-57 and C-58 are representative SEM and optical images of Particles 4A.

Particle 4B

Figure C-59 shows all of Particle 4B (Figure B-12) as-polished and the middle section after being etched for fuel. The center portion of this particle is UO_2 fuel which has experienced some grain growth (to about 18 μm) and void formation. Pullout of individual grains of UO_2 occurred in this region when etched (see Figure C-60). All around the edge of this particle is $(\text{U},\text{Zr})\text{O}_2$ with a small amount of an Al-Cr-Fe-Ni second phase material and a few Ni-Sn inclusions. The amount of Zr in the rim decreases with position from the edge toward the center fuel region. See Table C-5 for composition data and Figures C-61 through C-69 for typical optical and SEM images.

Particle 4D

From the optical as-polished photographs (see Figures C-70 through C-73) Particle 4D appears to be a relatively homogeneous and dense particle. Figure C-74 shows the effect of a two-minute immersion fuel etch which tended to preferentially dissolve material around clusters of small pores. Figures C-75 through C-77 show the effect of a one-minute swab fuel etch which also did not reveal any grain structure. Figures C-78 through C-85 are typical SEM-BSE images of Particle 4D. The different shades of gray indicate that the particle is not homogeneous. In general there was no grain structure or second phase material detected, but there were inclusions of a Cr-Fe-Ni-Al material.^a

Particle 5E

Particle 5E (Figure B-18) can be divided into six regions based on Zr content. Figures C-86 shows the as-polished and etched view of the particle. A map of the regions is shown in Figure C-87; Table C-7 shows the composition in the different regions. Region 5 in the bottom tip of the particle has less than 1 atom% Zr and Region 6 within Region 5 has only

a. See Table C-6 for a summary of chemical compositions.

a trace of Zr and appears to be U_4O_9 from the SAS data. The four regions in the upper areas of the particle vary from 2 to 9 atom% Zr. There is a small amount of Ni-Fe-Cr in some of the grain boundaries and a few Ru-Ni inclusions. Figures C-88 through C-96 are typical optical and SEM images of Particle 5E.

Particle 6B

Particle 6B appears to be a piece of zircaloy; SEM or SAS measurements were not performed on this particle. Figure C-96 is the photomacrograph and Figure B-24 is the particle macro-photograph.

Particle 6C

Particle 6C (Figure B-25) appears to be two pieces of oxidized cladding stuck together with prior molten material as shown in Figure C-97. Assuming the cladding pieces became stuck together while part of an intact fuel bundle, the radius of curvature and relative positions of the cladding pieces indicate about 30% ballooning strains. See Figures C-98 through C-109 for typical optical and SEM magnified images. Table C-8 shows representative compositions. In general, the cladding pieces are ZrO_2 with small amounts of carbon and the prior molten base material is $(Zr,U)O_2$ with a high Zr to U ratio. There is a large amount of second phase materials and inclusions in the prior molten material made up of Al-Ni-Sn-Fe-Cr. There is an inordinate amount of Al and C in this particle, indicating a possible interaction with a $Al_2O_3-B_4C$ poison rod.

Particle 6D

Particle 6D (Figure B-26) is a large fuel pellet fragment with a tiny portion of U-Zr-O melt attached at one end. As shown in Figure C-110, the fracture surfaces appear atypically irregular for UO_2 , while the fuel matrix has a distinctly unusual speckled cast. The external surface of the particle appears "glazed."

The photomicrograph at the upper left of Figure C-111 shows that the fuel experienced elevated temperatures, since considerable porosity has accumulated at grain boundaries. This phenomenon is also observed in fuel operated at standard reactor conditions, but only after burnups of approximately 15 to 20 Gwd/t. The extent of equiaxed grain growth is small, indicating that the peak fuel temperature did not greatly exceed 1900 K over a significant time duration. Figure C-111 also shows the fuel appearance after etching to expose grain boundaries, whereupon a second fuel phase emerged. The existence of a second ceramic fuel phase suggests fuel oxidation, but the U-O phase diagram (see Figure 31 of the main text) shows several possibilities for two-phase mixtures, depending on the average oxygen content. Accordingly, SAS was performed on two representative, widely separated fuel regions, the results of which are listed on the right side of Figure C-111. The average oxygen concentration of approximately 71 atom% (± 2 atom% at worst) converts to $\text{UO}_{2.44}$, which means that the fuel was oxidized beyond the UO_2 crystal structure into a two-phase mixture of U_4O_9 and $\text{UO}_{2.6}$.^a Despite efforts to center the 15- μm SAS beam on grains of each phase, the oxygen concentrations of the major and minor phases could not be separately identified within the resolution and accuracy limitations of the instrument.

The most probable mechanism for fuel oxidation is inward diffusion of oxygen gas or hydroxide radicals. As shown in the U-O phase diagram, this could only have occurred at fuel temperatures above 1900 K, where the two phases segregated during subsequent cooldown. However, temperatures much above 1900 K would presumably have induced more equiaxed grain growth than was observed. Consequently, an approximate temperature of 2000 K is tentatively concluded for the fuel oxidation process. See Section 3.2.2 of Part 1 for further discussion.

Behavior and origin of the adherent melt on Particle 6D were similarly of major interest. EDS derived melt data are summarized on Figure C-112.

a. The crystal structure of $\text{UO}_{2.6}$ is in dispute, with opinions divided between U_5O_{13} and U_8O_{21} .

As shown, the melt composition was uniformly measured as approximately 66-wt% U and 34-wt% Zr, excepting near the melt-fuel interface where the U/Zr ratio increased abruptly. No traces of Fe, Cr, Ni, Sn, nor other alloying impurities were detected. Figure C-112 further demonstrates that melt interactions were not confined to the metallurgical examination plane, because a second Zr-rich area is evident about 100 μm below the conspicuous interface. Therefore, the fuel region near the interface was almost surrounded by melt.

Metallographic examinations of the fuel-melt interaction zone were also quite revealing. As displayed in Figure C-113, the melt is composed of smooth ceramic grains exhibiting only one metallurgical phase at room temperature, which suggests $(\text{U},\text{Zr})\text{O}_2$. The melt evidently absorbed some oxygen from the nearby fuel, because a clearly defined reaction layer was exposed by etching, while only one fuel phase could be perceived adjacent to the melt after etching. This is unlike the two-phase fuel structure elsewhere on Particle 6D. Figure C-133 further illustrates that interfacial fuel experienced somewhat higher temperatures than the rest of Particle 6D, because individual pores collected at grain boundaries have interlinked here to form connected pathways and because grain sizes are somewhat enlarged. These findings infer that the $(\text{U},\text{Zr})\text{O}_2$ was a metallic melt at the time of fuel contact and that it was subsequently oxidized in place until solidified. Moreover, the metallic melt was apparently superheated well above its melting point, because considerable heat was transferred to the adjacent fuel by conduction.

These preliminary deductions were later confirmed by quantitative SAS measurements that are presented in Figure C-114. Oxygen concentration values over the six points are consistently close to 66 atom%, in complete agreement with metallographic indications that this region is composed of UO_2 and $(\text{U},\text{Zr})\text{O}_2$. Because these SAS measurements were taken under identical conditions to those elsewhere on Particle 6D, the SAS agreement with metallography lends additional credence to the 71 atom% oxygen concentration result for regions not reduced by metallic melt contact.

The lower portion of Figure C-114 represents continuous O, U, and Zr information along the band through the middle of the SAS micrograph. These line scans were significantly perturbed by sample porosity. For example, the oxygen profile should appear flat over most of the scan length, but instead falls off noticeably over the porous fuel region. Note also that all three profiles display conspicuous depressions at two particularly porous places. These places are poorly imaged on the SAS micrograph, unfortunately. In any case, the Zr line scan provides an accurate measure of the diffusion bond width (approximately 50 μm), which could be very valuable for time-at-temperature estimates. Consequently, this continuous line scan approach is recommended for further development. This is especially recommended where state-of-the-art SAS devices can be employed to compensate automatically for variations in sample topography, to produce quantitative line scan output, and to provide high quality micrographs.

Particle 6E

Particle 6E appears to be a piece of zircaloy with layers of ZrO_2 on both sides. SEM and SAS measurements were not performed on this particle. Figure C-115 is the photomacrograph and Figure C-116 is a close up of a ZrO_2 layer unetched. See Figure B-27 for the particle macro-photograph.

Particle 6F

Particle 6F (Figure B-28) was originally selected for detailed characterization after it was found to be partially ferromagnetic. Despite the complicated overall appearance in Figure C-117, the source of the ferromagnetic nature of Particle 6F was readily identified as the three large metallic ingots. These ingots were determined by EDS to be 96-wt% Ni and 4-wt% Fe, with a small additional amount of Sn.

The process whereby Inconel-718 (initially 52-wt% Ni) was "refined" to nearly pure Ni is not definitely known but is probably related to higher oxygen affinity for the Fe and Cr constituents. Because of the low extent of oxidation, the Ni rich melt presumably contacted the remainder of

Particle 6F late in its evolution, penetrating along large pores and solidifying from heat losses to a cooler matrix. Thus, the temperature of the oxidized portions of this particle was almost certainly well below 1725 K (the melting point of Ni) when the Ni-rich melt arrived.

In addition to the ingots, Particle 6F consists of roughly equal amounts of porous and solid U-Zr-O materials at the cross-sectional orientation studied. The granular, relatively pore-free structure evidently solidified before contact with the porous melt. The metallographic appearances and etching behavior of both types of U-Zr-O material suggest a high degree of oxidation.

The backscattered electron micrograph at the base of Figure C-118 illustrates major differences in average atomic number of Particle 6F. The composition of the solid-grained structure was determined by EDS to be approximately 32-wt% U and 68-wt% Zr (neglecting oxygen), while the porous heterogeneous melt ranged between 50- and 60-wt% U and 45- to 35-wt% Zr, with the remaining 5-wt% composed of varying amounts of Fe, Cr, Ni, and Al.^a Therefore, most of the gray-level contrast between the solid-grained and porous structures in Figure C-118 is due to a marked difference in U content. However, the porous melt could conceivably be less oxidized, because oxygen concentrations were not measured by SAS.

The large solid grains are almost definitely $(U,Zr)O_2$. The mixed oxide contains no detectable alloying impurities, as with comparable pore-free $(U,Zr)O_2$ in Particles 1H and 6D, and unlike the adherent mixed oxide in Particle 1E. The preponderance of shrinkage pores and the absence of grains in the bright, irregularly shaped melt confirms solidification on cooling.

Figure C-118 also shows several bright regions lacking both shrinkage pores and grain structure. These regions represent diffusion bonding between the solid $(U,Zr)O_2$ and the partially liquid heterogeneous melt.

a. Fe and Cr tend to dominate the impurities, which suggests prior interaction with stainless steel.

Much of this diffusional interaction was caused by melt-solid contact outside the plane of study, because the interfacial area at this orientation is quite small. One such bonding region is shown in closer detail at the right of Figure C-118. Note the absence of diffusional exchange with the Ni ingots, which confirms that the heterogeneous melt had cooled and solidified before the Ni-rich melt arrived. Note also that the heterogeneous melt has not attacked the $(U,Zr)O_2$ grain boundaries.

Figure C-119 provides close-up views of the room-temperature heterogeneous melt microstructure. Metallic ingots present during initial metallography were evidently dislodged or dissolved by etching, so the small inclusions only appear in the upper-left image. Two phases are apparent on the lower backscattered electron micrograph: the U-Zr-O matrix and the dark-gray stringers. The matrix composition at this position is approximately 57-wt% U, 38-wt% Zr, 4-wt% Fe, and 1-wt% Ni (plus a substantial concentration of oxygen), while the stringers here are composed of 34-wt% Cr, 33-wt% Fe, 17-wt% Al, and 16-wt% Ni.

Based on the metallographic appearance and immunity to etchants, the matrix seems to be mostly $(U,Zr)O_2$. Much of this mixed oxide would have been in the form of $(U,Zr)O_{2-x}$ at temperature, so the metallic inclusions could conceivably be U-Zr alloy that emerged as the $(U,Zr)O_{2-x}$ dissociated upon cooling. However, it is more likely that the inclusions were relatively inert metals like Sn or Ni whose low oxygen affinity prevented incorporation within the matrix.

Despite incomplete understanding of the melt structure, the makeup of Particle 6F resembles Particle 1H in that a porous melt has contacted previously solidified $(U,Zr)O_2$. Nevertheless, the melt-solid interactions in these two cases are very different. In Particle 6F the two materials have bonded by diffusion, whereas in Particle 1H the melt has dissolved substantial amounts of the $(U,Zr)O_2$. The heterogeneous melt composition is quite similar in the two particles, although the U content of the mixed oxide is lower in Particle 6F. Therefore, the major distinction between the two situations seems to be the melt temperature. The heterogeneous

melt in Particle 1H was apparently liquefied and superheated above the $(U,Zr)O_2$ melting point, thus accounting for the extensive grain boundary penetration and dissolution of the solid mixed oxide. By comparison, the heterogeneous melt in Particle 6F was evidently a viscous slurry at a temperature well below 2810 K, so only diffusional interactions occurred where the two materials were in contact.

Particle 7A

On a macro scale, Particle 7A (Figure B-33) appears to be a relatively homogeneous particle with many large ($\sim 300 \mu m$) round and irregular shaped pores and small ($\sim 10 \mu m$) irregular shaped pores as shown in Figure C-120. On closer examination a second phase and metallic inclusions appear uniformly throughout the particle. The base material is U and Zr with a trace of Fe. The second phase contains Cr, Fe, Ni and some Al; the metallic inclusions are mostly Ni with a Cr, Fe phase that occurs around the inclusions (see Table C-9 for compositions). See Figures C-121 through C-130 for typical optical and SEM images of Particle 7A.

Particle 7B

In Particle 7B (Figure B-34) as shown in Figure C-131 there is an outside layer of ZrO_2 followed by layers of alpha-zircaloy, prior molten zircaloy mixed with uranium, and a region of UO_2 fuel, respectively. See Table C-10 for elemental identification and Figures C-132 and C-133 for 100x montages of two regions of the particle. The section for this particle appears to be longitudinal rather than a cross section based on the large radius of curvature. The prior molten material seen in Figures C-134 and 135 apparently flowed down from above and filled a 0.35 mm gap. This is four times the radial gap as fabricated; therefore, there was probably ballooning at this point in the fuel rod. It was determined that the prior molten Zr,U material flowed in from another location by the clear interface with the original cladding and from the known dimensions of the original cladding. There is very little Zr

penetration into the fuel at this point, so most of the U in the prior molten U,Zr material came from above. See Figures C-136 through C-141 for typical optical and SEM images.

Particle 7E

All of Particle 7E (Figure B-37) is shown in Figure C-142 and an edge and central region is shown in Figure C-143 after etching. The central portion of this particle is UO_2 fuel which has experienced grain growth (from ~10 to ~28 μm) and void formation. Some loss of individual grains of UO_2 occurred in this region when etched. All around the edge of this particle is $(\text{U},\text{Zr})\text{O}_{2+x}$ with Al-Cr-Fe-Ni second phase material and high Ni/low Sn inclusions. Along one edge there is a cluster of high Ni/low Fe inclusions with Cr and Fe in the base material and Al-Cr-Fe-Ni in a second phase. The amount of Zr in the base material and the amount of second phase material decreases with position toward the central region of this particle. See Table C-11 for more detailed chemical composition and Figures C-144 though C-152 for typical optical and SEM images.

Particle 8A

Particle 8A (Figures B-45 and B-46) is relatively homogeneous with many irregular shaped pores of various sizes as shown in Figure C-153, which shows three regions; region 1 is a horseshoe shaped region of slightly higher Zr content separating regions 2 and 3, which have similar compositions. The surfaces of the pores tend to be rounded. See Figure C-154 for an example of rounded pore surfaces and the slight effect of etching. Note that some of the pores could be caused by pull-out of grains. This particle is predominately $(\text{U},\text{Zr})\text{O}_2$ with slight variations in the U-Zr ratio, and there is an Al-Cr-Fe-Ni material in some of the voids and grain boundaries. See Table C-12 for chemical composition data. See Figures C-155 through C-165 for typical optical and SEM images.

Particle 8C

Particle 8C (Figure B-48) can be divided into three regions based on void morphology and elemental distribution as shown in Figure C-166. In all three regions the base material is $(U,Zr)O_{2-x}$ with an Al-Cr-Fe-Ni material at grain boundaries and in voids. See Table C-13 for composition data. Region 1 contains irregular shaped pores and grains with nonuniform chemical composition. Figures C-167 and C-168 show two different areas within Region 1 at two different contrast settings of the SEM, so that the variation of U and Zr composition within the grain can be separated from the Al-Cr-Fe-Ni grain boundary phase. The effect of etching can be seen in Figure C-169 which seems to be mainly on the grain boundary material. Region 2 contains large round pores and somewhat more uniform grain composition. Region 3 contains elongated grains and fairly uniform grain compositions. See Figures C-170 through C-176 for more SEM and optical images.

Particle 8E

Particle 8E (Figure B-50) can be divided into five regions based on void morphology and chemical composition. The five regions are shown in Figure C-177, and the chemical composition in the five regions is given in Table C-14. Region 4, which is the narrow band of many small voids running across the lower part of the particle, provides a distinct boundary between Regions 3 and 5. The other boundaries are not as visible but can be detected on the SEM. The base material in all five regions is $(U,Zr)O_{2+x}$ with variations in U to Zr ratios from region to region. The grain boundary phase brought out by etching shown in Figures C-178 through C-180 is much higher in Zr than the base material and contains a small amount of Fe with a trace of Cr and Ni. There are also Ni-Sn inclusions and Cr-Fe and Cr-Fe-Ni materials found in and around voids. Figures C-181 through C-189 show typical optical and SEM images.

Particle 8H

Particle 8H (Figure B-52) consists of a ceramic material mechanically bonded to a Ag metallic material. The ceramic material consists of U with some Zr and a trace of Fe. It contains many irregular shaped pores of various sizes and generally rounded surfaces. It can be divided into three regions as shown in Figure C-190 based on the Zr-U ratios. See Table C-15 for elemental identification.

The central region has the lowest Zr content with some increase toward other regions. A Cr, Fe, Ni material occurs in some grain boundaries and voids particularly in Region 3 which has the highest Zr content.

The silver metallic material is pore free with round nickel-low Sn inclusions occurring around the edge. This can be seen in Figure C-191, which shows the results of a spontaneous galvanic etch that occurred in the polisher. See Figures C-192 through C-204 for typical optical and SEM images of Particle 8H.

Particle 9D

Particle 9D (Figure B-61) consists of a Ag metallic material mechanically bonded to several small pieces of U-Zr ceramic material as shown in Figure C-205. The Ag metallic material has round inclusions containing Ni, Sn and traces of Fe (see Figure C-206). The surfaces of the Ag regions are textured with parallel rills which were possibly caused by etching (see Figures C-207 and C-208).

The Zr-U ratios in the ceramic material vary from piece to piece as shown in Table C-16. There are traces of Fe, Ni, and Cr in the ceramic base material, but only the small piece within the large metallic piece contains an Fe-Ni material in grain boundaries and voids. See Figures C-209 through C-219 for typical optical and SEM images.

Particle 9G

Particle 9G (Figure B-64) consists entirely of Ag metallic material with Ni and Sn inclusions. See Figure C-220 for an overall as-polished view, Table C-17 for elemental identification, and Figures C-221 through C-232 for typical optical and SEM images.

Particle 10A

Figure C-233 shows Particle 10A (Figure B-71) before and after a five-minute immersion etch. Rather than reveal a grain structure, the etch tended to preferentially dissolve material around clusters of small pores. This particle was later repolished so the large void seen in Figure C-233 disappeared as shown in the SEM macro in Figure C-234.

This particle is composed entirely of $(\text{U}, \text{Zr})\text{O}_2$ with no grain boundary or other phases and practically no inclusions. There are three different zirconium contents within this particle. The high zirconium content material is about 7 atom% Zr and is generally found around cracks, edges, and voids. This material tends to be almost pore free and contains a trace of iron (Fe). The middle zirconium content material is about 1-1/2 atom% Zr and is found throughout most of the particle. This material contains many small ($< 10 \mu\text{m}$) voids. Figure C-235 shows these two materials. The low zirconium content material is about 0.5 atom% to no zirconium and is found in a small central region (see region Figure C-233). This was the only material in this particle to exhibit a grain structure; the grain size is approximately $28 \mu\text{m}$. Figure C-236 shows this material. See Table C-18 for composition data and Figure C-237 through C-247 for typical optical and SEM images.

Particle 10E

Particle 10E (Figure B-75) appears to be two pieces of fuel stuck together by some prior molten material. Figure C-248 shows the overall mounted particle and a closeup of the upper piece which appears to have

broken off during the mounting process. This figure also shows the severe effect of the etch on the fuel regions and the negligible effect on the prior molten material.

The fuel regions contain UO_2 only, and according to the average of nine SAS readings is slightly hypostoichiometric. See Table C-19 for composition data. The fuel grain size is 10 μm indicating essentially no grain growth from as-fabricated fuel. The adherent prior molten material is composed of $(\text{U}, \text{Zr})\text{O}_{2+x}$ with Ni, Sn, and Ag inclusions. The Zr/U ratio decreases with position moving from the outer edge toward the fuel. See Figures C-249 through C-260 for typical optical and SEM images.

Particle 10F

Particle 10F (Figure B-76) is composed of two distinct regions as shown in Figure C-261. Figure C-262 is a closeup of the region interface before and after etching. Region 1 contains many small irregularly shaped pores and is composed of $(\text{U}, \text{Zr})\text{O}_{2+x}$ with a trace of Fe. There is very little grain boundary or second phase material in this region. Region 2, which cuts across Region 1, contains large round pores and is also composed of $(\text{U}, \text{Zr})\text{O}_{2+x}$ with a trace of Fe. The Zr to U ratio is slightly higher in Region 2 and there is an extensive amount of grain boundary phases containing Cr, Fe, and Ni. There is also a fine grained second phase material found in Region 2 that contains the same constituents as the base material but with more Fe, slightly more Zr, and less oxygen. The second phase material is hypostoichiometric while the base material is hyperstoichiometric as shown in the composition data given in Table C-20. See Figures C-263 through C-270 for typical optical and SEM images of Particle 10F.

Particle 11B

Particle 11B (Figure B-84) is composed of metallic material mechanically bonded to ceramic material as shown in Figure C-271. The metallic material has irregularly shaped interior voids and one complex

rectangular inclusion. See Figure C-272 and Table C-21. The base metallic material is Ni with some Fe and a trace of Sn. The second phase material is also Ni but with substantial amounts of Sn and small amounts of Fe and Ag. There are also Ag inclusions containing small amounts of Mo, Ni, and Fe throughout the metallic material.

The ceramic material is very porous with generally small irregular pores and with rounded surfaces. The base material is U with low Zr, and there is a grain boundary phase containing Cr and Fe, small amounts of U, and a trace of Al and Zr. Throughout the ceramic material there are Ni and Fe inclusions and blisters (see Figure C-273). The inclusions contain some Sn; the blisters contain some Mo and occasionally some Ag, In, and Cd. See Table C-21 for composition data and Figure C-274 through C-281 for typical optical and SEM images.

Particle 11C

Particle 11C (Figure B-85) originally appeared from its dimensions to be a half section of a fuel pellet. Part of this particle was removed for other analysis, so the photomacrographs shown in Figure C-282 are not half sections. This particle was ground down further after initial analysis in an attempt to find the surface layer seen in Figure B-85. Figures C-283 and C-284 are a 100X cross-section of the particle showing the relative uniformity of grain size from pellet center to surface. Figure C-285 is a closeup, as polished view of fuel showing the high porosity at the grain boundaries which makes the grains distinct without etching. The grain size is about 10 μm , indicating virtually no grain growth. The material adhering to the pellet surface is Zr and U with the amount of Zr decreasing with position toward the fuel. There is a small amount of Zr diffused into the surface fuel grains. See Table C-22 for composition data and Figures C-286 through C-290 for typical optical and SEM images.

TABLE C-1. CHEMICAL COMPOSITION OF SELECTED AREAS OF PARTICLE 1B

ID ^a	U	Zr	O	Al	Cr	Fe	Ni	Sn	Miscellaneous	Comments
046	+	--	--	--	--	--	-	--	--	Central fuel region, see figure C-9
054	+	--	--	--	--	--	-	--	--	Central fuel region, see figure C-9
066	+	--	--	--	--	--	-	--	--	Central fuel region, see figure C-9
037	+	--	--	--	?	?	-	--	--	Near large void, see figure C-9
061	+	--	--	--	--	--	-	--	--	Base material, see figure C-9 and C-17
033	+	-	-	--	--	?	-	--	--	Edge of fuel region, see figure C-9
034	+	--	-	--	--	Tr	-	--	--	Edge of fuel region, see figure C-9
045	+	-	-	--	--	Tr	-	--	--	Edge of fuel region, see figure C-9
031	+	--	-	--	--	Tr	-	--	--	Base material, see figure C-16
032	+	--	-	--	--	Tr	-	--	1c(+),Ru(+)	Material in void, see figure C-16
018	+	-	-	--	--	?	-	--	--	See figure C-19
017	+	0	-	--	--	Tr	-	--	--	Gradient across melt-fuel interface
016	0	-	-	--	--	Tr	-	--	--	-
015	0	-	-	--	?	Tr	Tr	-	--	-
019	+	0	-	--	--	?	Tr	--	SM(0) -Pa(+)	Inclusion at melt-fuel interface
022	0	+	--	--	Tr	Tr	Tr	--	--	See figure C-20
023	+	-	--	--	Tr	Tr	-	--	--	Gradient across melt-fuel interface
024	+	0	-	--	--	Tr	-	--	--	-
025	+	--	-	--	--	Tr	-	--	--	-
026	+	0	-	--	--	Tr	Tr	--	Ru(0)	Inclusion at melt-fuel interface
040	--	+	--	--	--	--	-	--	--	See figure C-18
041	--	+	--	--	--	--	-	--	--	Gradient across melt-fuel interface
042	Tr	+	-	--	--	--	-	--	--	-
043	+	+	-	--	--	--	-	--	--	-
044	+	Tr	-	--	--	--	-	--	--	-

a. See figures mentioned in the comments for location of ID numbers.

Quantitative (SAS): Data is in atom percent.

Qualitative (SEM/EDS): ? - uncertain
 Tr - trace
 0 - minor
 + - major

TABLE C-2. CHEMICAL COMPOSITION OF SELECTED AREAS OF PARTICLE 3L

ID ^a	U	Zr	O	Al	Cr	Fe	Ni	Sn	Miscellaneous	Comments
671	+	+	--	--	--	--	--	--	--	Dark phase (low Z) in Figure C-36
676	+	+	--	--	--	--	--	--	--	Light phase (high Z) in Figure C-36
671/ 676	10.0	25.0	65.0	--	--	--	--	--	--	Average of two phases
709	8.0	20.0	72.0	--	--	--	--	--	--	Base material, see Figure C-31 and C-35
710	9.0	22.0	69.0	--	--	--	--	--	--	Base material, see Figure C-31 and C-35
677-1	10.0	23.0	67.0	--	--	--	--	--	--	Base material, see Figure C-37
677-2	10.0	22.0	68.0	--	--	--	--	--	--	--
713	8.0	27.0	65.0	--	--	--	--	--	--	Base material, see Figure C-31
691	9.0	23.0	68.0	--	--	--	--	--	--	Base material, see Figure C-31
688	7.0	23.0	70.0	--	--	--	--	--	--	Base material, see Figure C-31
685	8.0	23.5	68.4	--	--	--	--	--	--	Base material, see Figure C-31
699	7.0	23.0	69.6	--	--	--	--	--	--	Base material, see Figure C-31 and C-38
C-30	697	+	+	--	--	Tr	Tr	?	--	Material in void, see Figure C-38
	689-1	13.5	20.0	66.5	--	--	--	--	--	Base material above void, see Figure C-31 and C-39
	689-2	14.4	15.0	70.4	--	--	--	--	--	Base material below void, see Figure C-31 and C-39
	700	+	+	--	--	+	+	+	--	Material in void, see Figure C-38
	704	+	+	--	+	+	+	+	--	Grain boundary material, see Figure C-39
	706	+	+	--	--	--	Tr	Tr	--	Grain boundary material, see Figure C-39
	714	+	+	--	--	0	0	0	--	Material in void.
	715	+	+	--	+	+	+	+	--	Grain boundary material, see Figure C-39

a. See figures mentioned in the comments for location of ID numbers.

Quantitative (SAS): Data is in atom percent.

Qualitative (SEM/EDS): ? - uncertain

Tr - trace

0 - minor

+- major

TABLE C-3. CHEMICAL COMPOSITION OF SELECTED AREAS OF PARTICLE 3M

ID#	U	Zr	O	Al	Cr	Fe	Ni	Sn	Miscellaneous	Comments
899	+	--	--	--	--	--	--	--	--	Region 1 Base Material, see Figure C-40
886	+	--	--	--	--	--	--	--	--	Region 1 Base Material, see Figure C-40 and C-44
887	+	--	--	--	--	Tr	O	--	Tc(+)--Ru(+)	Bead in Region 1, see Figure C-44
894	+	--	--	--	--	--	--	--	--	--
907	+	--	--	--	--	--	--	--	--	Region 1 base material, see Figure C-40 and C-44
908	+	--	--	--	--	--	--	--	--	--
895	+	+	--	--	Tr	Tr	?	--	--	Region 1 and 2, Figures C-40, C-46
896	+	O	--	--	Tr	Tr	?	--	--	--
897	+	Tr	--	--	--	Tr	--	--	--	--
898	+	--	--	--	--	--	--	--	--	--
902	+	+	--	--	--	O	--	--	--	Region 2 Material, see Figure C-40 and C-49
903	+	O	--	--	--	Tr	--	--	--	--
912	+	O	--	--	Tr	Tr	--	--	--	Region 2 base material, see Figure C-40 and C-48
913	+	Tr	--	--	?	--	?	--	--	--
916	+	O	--	--	Tr	O	Tr	--	--	--
915	+	Tr	--	--	+	+	+	--	Mo(?)	Material in void, see Figure C-48
919	+	O	--	--	--	O	--	--	--	Region 2 base material, see Figure C-40 and C-49
920	Tr	+	--	--	Tr	Tr	--	--	--	--
921	+	Tr	--	--	--	Tr	--	--	--	--
905	O	--	--	--	+	+	+	--	--	Material in void, see Figure C-47
906	+	+	--	--	+	+	+	--	--	--
924	+	Tr	--	--	--	Tr	--	--	--	Base material, see Figure C-40 and C-47
925	Tr	--	--	--	--	Tr	O	?	Tc(+)--Ru(+)	Material in void, see Figure C-47

a. See figures mentioned in the comments for location of ID numbers.

Quantitative (SAS): Data is in atom percent.

Qualitative (SEM/EDS): ? - uncertain
 Tr - trace
 O - minor
 + - major

TABLE C-4. CHEMICAL COMPOSITION OF SELECTED AREAS OF PARTICLE 4A

ID ^a	U	Zr	O	Al	Cr	Fe	Ni	Sn	Miscellaneous	Comments
953	+	0	--	--	--	Tr	--	--	--	Base material, see Figure C-57
954	+	+	--	--	--	+	0	--	Ti(0)	Material in void
957	+	--	--	0	+	+	0	--	--	Material in void
986	+	Tr	--	--	--	Tr	--	--	--	Base material, see Figure C-53
981	Tr	0	--	0	Tr	+	+	0	Ti(0)	Material in void
984	+	+	--	0	0	+	+	+	Ru(+)	Inclusion
985	Tr	--	--	--	--	0	+	0	Ru(+)--Tc(+)	Inclusion
964	+	Tr	--	--	Tr	Tr	--	--	--	Base material, Figures C-52, C-53
967	Tr	--	--	--	--	--	+	+	Ru(Tr) Ag(?)	Inclusion
968	+	0	--	0	+	+	0	--	--	Second phase
963	+	0	--	--	--	Tr	--	--	--	Base material, see Figure C-57
961	Tr	--	--	--	--	--	+	+	Ag(?)	Second phase
C-32	969	+	Tr	--	--	--	Tr	--	--	U-Zr base material, see Figure C-50
	973	+	0	--	--	Tr	Tr	--	--	--
	975	+	0	--	--	Tr	Tr	--	--	--
	976	+	0	--	--	Tr	Tr	--	--	--
	978	+	Tr	--	--	Tr	Tr	--	--	--
	979	+	Tr	--	--	Tr	Tr	--	--	--
	980	+	Tr	--	--	Tr	Tr	--	--	--
	970	+	--	--	--	?	--	--	--	Base material, see Figure C-50
	958	+	--	--	--	--	--	--	--	Base material, see Figure C-52
	974	+	--	--	--	Tr	--	--	--	Base material, see Figure C-58
	988	+	--	--	0	+	+	0	--	Grain boundary material, Fig. C-56
	991	+	0	--	0	0	+	+	--	Grain boundary material, Fig. C-56

a. See figures mentioned in the comments for location of ID numbers.

Quantitative (SAS): Data is in atom percent.

Qualitative (SEM/EDS): ? - uncertain

Tr - trace

0 - minor

+ - major

TABLE C-5. CHEMICAL COMPOSITION OF SELECTED AREAS OF PARTICLE 4B

<u>10^a</u>	<u>U</u>	<u>Zr</u>	<u>O</u>	<u>Al</u>	<u>Cr</u>	<u>Fe</u>	<u>Ni</u>	<u>Sn</u>	<u>Miscellaneous</u>	<u>Comments</u>
725	32.2	--	67.7	--	--	--	--	--	--	Interior base material
	36.4	--	63.5	--	--	--	--	--	--	See Figure C-63
	34.4	--	65.5	--	--	--	--	--	--	--
738	+	--	--	--	--	Tr	--	--	--	Base material, see Figure C-69
743	33.9	2.7 ^b	63.2	--	--	--	--	--	--	--
760	Tr	--	--	--	--	--	+	+	Ru(+)	Bead, see Figure C-61
761	+	--	--	--	--	--	--	--	S(+)	Material in void
762	0	--	--	--	--	0	+	+	Ru(+)	Bead in vicinity of 760
763	0	--	--	--	0	0	0	--	Ru(+)/Tc(+)	Second bead in vicinity of 760
746	32.6	0.9	66.4	--	--	--	--	--	--	Base material, see Figure C-61
748	+	0	--	0	+	+	0	--	--	Material in void
747	31.6	3.0	65.2	--	--	--	--	--	--	Base material
749	27.6	1.8	70.5	--	--	Tr ^c	--	--	--	Base material, see Figure C-66
729	24.1	8.0	67.7	--	--	Tr ^c	--	--	--	--
729-1	11.9	--	61.7	--	3.6	12.7	9.9	--	--	Grain boundary phase near 729
730	+	0	--	--	--	Tr	--	--	--	Material in void
731	+	+	--	Tr	+	+	+	--	--	Base material
732	+	+	--	Tr	+	+	+	--	--	--
733	+	0	--	Tr	0	Tr	--	--	--	--
757	+	Tr	--	--	--	--	--	--	--	Base material, see Figure C-65
753	+	Tr	--	--	--	--	--	--	--	--
752	+	0	--	--	--	--	--	--	--	--
754	--	3.1	--	--	--	--	84.0	1.2	C-11.6	Inclusion
755	9.8	4.9	56.2	--	6.5	11.5	10.7	--	--	Grain boundary material

a. See figures mentioned in the comments for location of IU numbers.

b. Not detected by SEM/EDS.

c. Detected by SEM/EDS and not by SAS.

Quantitative (SAS): Data is in atom percent.

Qualitative (SEM/EDS): ? - uncertain
 Tr - trace element
 0 - minor constituent
 + - major constituent

TABLE C-6. CHEMICAL COMPOSITION OF SELECTED AREAS OF PARTICLE 4D

ID ^a	U	Zr	O	Al	Cr	Fe	Ni	Sn	Miscellaneous	Comments
747	+	Tr	--	--	--	--	--	--	--	High Z material, see Figure 70
748	+	0	--	--	--	--	--	--	--	--
757	+	0	--	--	--	Tr	--	--	--	--
334	+	0	--	--	--	--	--	--	--	High Z material, see Figure C-85
332	+	+	--	--	--	--	--	--	--	Low Z material, see Figure C-85
333	+	0	--	--	--	--	--	--	--	High Z material, see Figure C-85
335	+	0	--	Tr	+	+	+	--	--	Void material, see Figure C-85
752	+	+	--	--	--	Tr	--	--	--	Low Z material, see Figure C-81
753	+	0	--	--	--	?	--	--	--	High Z material, see Figure C-81
749	+	0	--	--	--	Tr	--	--	--	High Z material, see Figure C-81
323	+	+	--	--	--	Tr	--	--	--	Base material, see Figure C-78
324	+	0	--	--	--	--	--	--	--	--
325	+	0	--	?	+	+	+	--	Ti(?)	Dendritic material, see Figure C-78
327	0	0	--	--	0	+	+	0	Ti(Tr)	Other material in void
755	+	+	--	--	--	Tr	--	--	--	Base material, see Figure C-80
756	+	0	--	--	--	--	--	--	--	--
746	+	0	--	--	--	--	--	--	--	Base material, see Figure C-80
729	+	0	--	--	--	--	--	--	--	Base material, see Figure C-82
728	+	+	--	--	--	--	--	--	--	--
734	+	0	--	--	--	Tr	Tr	--	--	Base material near void
731	Tr	Tr	--	?	+	+	+	0	Ti(Tr)	Material in void
732	+	0	--	--	Tr	Tr	Tr	--	--	--
733	+	0	--	?	+	+	+	--	--	--
735	+	0	--	--	--	Tr	Tr	--	--	Bead in void, see Figure C-83
739	0	0	--	Tr	+	+	+	0	Ti(0)	Material in void
740	+	0	--	?	+	0	0	--	--	--
741	Tr	+	--	--	--	Tr	--	--	Ag(0)	Fragment off sample edge, see Figure C-79
744	+	+	--	--	--	--	--	--	--	Base material, see Figure C-79

a. See figures mentioned in the comments for location of ID numbers.

Quantitative (SAS): Data is in atom percent.

Qualitative (SEM/EDS): ? - uncertain
 Tr - trace element
 0 - minor constituent
 + - major constituent

TABLE C-7. CHEMICAL COMPOSITION OF SELECTED AREAS OF PARTICLE 5E

<u>10³</u>	<u>U</u>	<u>Zr</u>	<u>O</u>	<u>Al</u>	<u>Cr</u>	<u>Fe</u>	<u>Ni</u>	<u>Sn</u>	<u>Miscellaneous</u>	<u>Comments</u>
866	32.2	2.0	65.6	--	--	Tr ^b	--	--	--	Region 1 base material, see Figure C-87
846	+	0	--	--	--	--	--	--	--	--
862	+	Tr	--	--	--	Tr	--	--	--	--
852	+	0	--	--	--	Tr	--	--	--	--
873	Tr	Tr	--	--	+	+	+	--	--	Grain boundary phase, see Figure C-89
855	+	Tr	--	--	--	Tr	--	--	--	Base material, see Figure C-87 and C-90
853	Tr ^b	--	--	--	--	--	2.1	5.4	Tc-10.2, Pd-13.8, Ru-52.6, Rh-15.6	Inclusion, see Figure C-90
854	Tr ^b	--	4.5	--	--	--	23.7	5.3	Tc-7.9, Pd-9.8, Ru-34.9, Rh-13.4	Inclusion, see Figure C-90
847	27.5	2.6	69.7	--	--	Tr ^b	--	--	--	Region 2 base material, see Figure C-87
865	+	0	--	--	--	Tr	--	--	--	--
856	Tr	--	--	--	--	Tr	+	--	Ru(+)	Inclusion in region 2, see Figure 93
868	0	--	--	--	+	+	+	--	--	Grain boundary phase, see Figure C-88
860-A	21.0	9.1	69.8	--	--	Tr ^b	--	--	--	Region 3 base material, see Figure C-87
860-B	22.0	8.0	69.8	--	--	--	--	--	--	--
860-C	22.1	8.9	68.8	--	--	--	--	--	--	--
860-D	22.5	9.2	68.1	--	--	--	--	--	--	--
844	25.1	5.9	68.8	--	--	--	--	--	--	--
863	28.3	2.6	69.0	--	--	--	--	--	--	Region 4 base material, see Figure C-87
848	+	0	--	--	--	--	--	--	--	--
861	+	0	--	--	--	?	--	--	--	--
851	+	0	--	--	--	?	--	--	--	--
874	+	0	--	--	+	+	+	--	--	Grain boundary phase, see Figure C-87 and C-95
	3.7	--	40.8	--	2.0	22.5	30.8	--	--	Dark/grain boundary phase similar to 874
	14.7	2.3	54.9	--	--	10.8	17.0	--	--	Light/grain boundary phase similar to 874
850-A	31.0	0.4	68.5	--	--	--	--	--	--	Region 5 base material, see Figure C-87
850-B	30.9	0.6	68.4	--	--	--	--	--	--	--
850-C	30.7	0.9	68.3	--	--	--	--	--	--	--

TABLE C-7. (continued)

<u>ID^a</u>	<u>U</u>	<u>Zr</u>	<u>O</u>	<u>Al</u>	<u>Cr</u>	<u>Fe</u>	<u>Ni</u>	<u>Sn</u>	<u>Miscellaneous</u>	<u>Comments</u>
864-A	32.9	0.6	66.4	--	--	--	--	--	--	Region 6 base material, see Figure C-87
864-B	27.0	0.0	72.9	--	--	--	--	--	--	--
864-C	24.9	1.0	74.0	--	--	--	--	--	--	--
864-D	31.3	0.0	68.6	--	--	--	--	--	--	--
864-E	32.2	0.5	67.3	--	--	--	--	--	--	--
864-1	26.4	0.5	73.0	--	--	--	--	--	--	Region 7 base material, see Figure C-87
864-2	28.1	1.1	70.6	--	--	--	--	--	--	--
864-3	29.2	1.6	69.0	--	--	--	--	--	--	--

a. See figures mentioned in the comments for location of ID numbers.

b. Detected by SEM/EDS and not by SAS.

Quantitative (SAS): Data is in atom percent.

Qualitative (SEM/EDS): ? - uncertain
 Tr - trace element
 0 - minor constituent
 + - major constituent

TABLE C-8. CHEMICAL COMPOSITION OF SELECTED AREAS OF PARTICLE 6C

ID ^a	U	Zr	O	Al	Cr	Fe	Ni	Sn	Miscellaneous	Comments
630	--	Tr	--	0	+	+	--	--	--	Large inclusion, see Figures C-97, C-106 and C-107
625-1	--	4.4	21.6	--	--	--	16.4	18.9	C-38.5	--
627	--	--	--	--	--	--	--	--	--	--
628	--	Tr	--	--	--	--	0	+	Ru(+)	--
629	--	--	--	--	Tr	Tr	+	--	--	--
634	0	+	--	+	--	--	--	--	--	Aluminum bearing phases, see Figure C-108
635	Tr	0	--	+	--	--	--	--	--	--
646	Tr	Tr	--	+	--	--	--	--	--	--
647	0	+	--	+	--	--	--	--	--	--
648	0	+	--	+	--	--	--	--	--	--
637	--	+	--	--	--	--	--	--	--	ZrO ₂ layers, see Figure C-100
638	--	30.4	64.6	--	--	--	--	--	C-4.9	--
639	--	+	--	--	--	--	--	--	--	--
642	--	+	--	--	--	--	--	--	--	ZrO ₂ -(U,Zr)O ₂ interface, see Figure C-101
644	0	+	--	--	--	--	--	--	--	--
643	Tr ^b	28.8	62.5	--	--	--	--	--	C-8.5	--
650	Tr ^b	28.9	65.6	--	--	--	--	--	C-5.3	ZrO ₂ layer, see Figure C-99
651	+	--	--	--	--	--	--	--	--	--
654	--	10.5	25.7	51.3	--	--	--	--	C-12.3	ZrO ₂ interface, see Figure C-109
655	--	Tr	--	+	--	--	--	--	--	--
656	--	+	--	--	--	--	--	--	--	--
658	2.2	27.8	2.1	53.7	3.7	8.6	--	1.5	--	ZrO ₂ interface, see Figure C-99
659	--	+	--	0	0	0	--	0	--	--
660	--	Tr	--	--	--	--	+	--	--	--
661	--	+	--	+	0	0	--	0	--	--
662	3.2	29.6	67.1	--	--	--	--	--	--	--
622-1	0.8	30.3	68.7	--	--	--	--	--	--	Base material sample center, see Figure C-97
666	--	+	--	--	--	--	--	--	--	Base material sample center, see Figure C-104
667	Tr	+	--	+	--	--	--	--	--	--
668	--	0	--	+	--	--	--	--	--	--

a. See figures mentioned in the comments for location of ID numbers.

b. Detected by SEM/EDS and not by SAS.

Quantitative (SAS): Data is in atom percent.

Qualitative (SEM/EDS): ? - uncertain
 Tr - trace element
 0 - minor constituent
 + - major constituent

TABLE C-9. CHEMICAL COMPOSITION OF SELECTED AREAS OF PARTICLE 7A

ID ^a	U	Zr	O	Al	Cr	Fe	Ni	Sn	Miscellaneous	Comments
449	+	0	--	--	Tr	Tr	--	--	--	Base material, see Figure C-124
450	+	0	--	0	+	+	0	--	--	Grain boundary phase
451	+	0	--	--	--	Tr	--	--	--	Second phase
452	+	+	--	--	--	0	--	--	--	Inclusion
465	+	0	--	--	--	--	--	--	--	Base material
466	+	0	--	+	+	+	0	--	--	Grain boundary phase
469	+	0	--	--	--	Tr	--	--	--	Second phase
464	+	0	--	+	+	+	0	--	--	Grain boundary material, see Figure C-130
456	+	0	--	--	--	Tr	--	--	--	Base material
457	+	0	--	--	--	Tr	--	--	--	Second phase
461	0	Tr	--	+	+	+	0	--	--	Complex mixture, see Figure C-129
462	+	+	--	--	0	0	Tr	--	--	--
463	+	+	--	--	Tr	0	Tr	--	--	--
555	--	--	--	--	--	0	+	--	--	Inclusion, see Figure C-127

a. See figures mentioned in the comments for location of ID numbers.

Quantitative (SAS): Data is in atom percent.

Qualitative (SEM/EDS): ? - uncertain
 Tr - trace element
 0 - minor constituent
 + - major constituent

TABLE C-10. CHEMICAL COMPOSITION OF SELECTED AREAS OF PARTICLE 7B

ID	U	Zr	O	Al	Cr	Fe	Ni	Sn	Miscellaneous	Comments
975	+	+	--	--	--	Tr	--	--	--	Complex layering, see Figure C-134
976	Tr	+	--	--	--	--	--	--	--	--
977	Tr	+	--	--	--	--	--	Tr	--	--
978	--	+	--	--	--	--	--	--	--	--
980	D	+	--	--	--	--	--	--	--	--
989	--	+	--	--	--	--	--	--	--	--
994	--	+	--	--	--	--	--	--	--	--
998	--	+	--	--	--	--	--	--	--	--
000	--	+	--	--	--	--	--	?	--	--
001	--	+	--	--	--	--	--	--	--	--
002	Tr	+	--	--	Tr	Tr	--	--	--	--
003	Tr	+	--	--	0	0	Tr	--	--	--
004	+	Tr	--	--	--	--	--	--	--	--
981	+	+	--	--	--	--	--	--	--	--
982	--	+	--	--	Tr	0	0	0	--	--
983	--	+	--	--	--	--	--	--	--	--
984	0	+	--	--	Tr	0	0	--	--	--
985	Tr	+	--	--	0	0	0	0	--	--
996	Tr	+	--	--	--	Tr	--	--	--	--
997	--	+	--	--	Tr	0	0	0	--	--
999	--	+	--	--	--	--	--	--	--	--
988	Tr	+	--	--	--	--	--	Tr	--	Complex mixture, see Figure C-135
990	--	+	--	--	--	--	--	--	--	--
991	Tr	+	--	--	Tr	0	0	--	--	--
992	Tr	+	--	--	--	Tr	Tr	--	--	--
993	Tr	+	--	--	--	--	--	--	--	--
006	+	+	--	--	--	--	--	--	--	Base material in crack, see Figure C-138
007	?	+	--	--	--	?	--	--	--	--
964	+	0	--	--	--	--	--	--	--	Material at interface, see Figure C-136
965	+	+	--	--	--	--	--	--	--	--
969	+	+	--	--	Tr	Tr	Tr	--	--	--
966	--	+	--	--	--	?	--	--	--	--
967	--	+	--	--	--	--	?	Tr	--	--
959	?	+	--	--	--	--	--	?	--	Prior molten (U,Zr,U), see Figure C-141
957	?	+	--	--	--	--	--	--	--	--
958	+	+	--	--	Tr	Tr	--	--	--	--
955	+	+	--	--	?	Tr	--	--	--	--
971	--	+	--	--	--	--	--	?	--	Base material, see Figure C-137
972	--	+	--	--	Tr	Tr	--	--	--	Second phase
973	0	+	--	--	--	--	--	--	--	Second phase

TABLE C-10. (continued)

ID ^a	U	Zr	O	Al	Cr	Fe	Ni	Sn	Miscellaneous	Comments
008	--	+	--	--	--	--	--	--	--	Base material, see Figure C-131
935	--	+	--	--	--	--	--	--	--	--
009	Tr	+	--	--	Tr	Tr	--	--	--	--
934	?	+	--	--	--	--	--	?	--	--
010	+	?	--	--	--	--	--	--	--	--
933	+	--	--	--	--	--	--	--	--	--
936	+	--	--	--	--	--	--	--	--	--

a. See figures mentioned in the comments for location of ID numbers.

Quantitative (SAS): Data is in atom percent.

Qualitative (SEM/EDS): ? - uncertain
 Tr - trace element
 O - minor constituent
 + - major constituent

TABLE C-11. CHEMICAL COMPOSITION OF SELECTED AREAS OF PARTICLE 7E

<u>ID^a</u>	<u>U</u>	<u>Zr</u>	<u>O</u>	<u>Al</u>	<u>Cr</u>	<u>Fe</u>	<u>Ni</u>	<u>Sn</u>	<u>Miscellaneous</u>	<u>Comments</u>
478-A	34.4	--	65.6	--	--	--	--	--	--	Base material in sample center, see Figure C-145
478-B	34.5	--	65.4	--	--	--	--	--	--	--
478-C	35.7	--	64.2	--	--	--	--	--	--	--
507-A	--	--	--	--	--	3.8	92.7	--	C-3.4 ^b	Metallic base material, see Figure C-149
507-B	--	--	--	--	--	0.7	84.3	0.4 ^b	C-14.5	--
507-C	--	0.4	--	--	--	--	95.9	0.3 ^b	C-3.2	--
508-A	35.9	4.6	69.4	--	Tr ^c	Tr ^c	--	--	--	Ceramic base material
508-B	37.4	4.4	68.0	--	Tr ^c	Tr ^c	--	--	--	--
508-C	26.8	3.7	69.3	--	Tr ^c	Tr ^c	--	--	--	--
509 ^d	+ ^c	Tr ^c	33.8	40.6	9.2	10.4	5.7	--	--	Low Z second phase
511 ^d	10.2	4.9	57.8	? ^b	9.6	9.0	8.2	--	--	High Z second phase
534-A	13.8	6.9	79.1	--	--	--	--	--	--	Base material, see Figure C-142
534-B	22.7	5.3	71.8	--	--	--	--	--	--	--
534-C	30.2	--	65.5	--	--	--	--	--	C-4.2	--
535	+	0	--	--	--	--	--	--	--	--
536	+	--	--	--	--	--	--	--	--	--
537	--	--	--	--	--	+	0	--	Inclusion, see Figure C-152	
538	+	0	--	--	--	--	--	--	Base material	
545	+	0	--	--	--	--	--	--	Base material, see Figure C-152	
546	Tr	--	--	0	--	+	--	--	Cd(0), Mo(0), Si-Tr	Void material
550	--	--	--	0	--	+	--	--	Mo(0), Ag(0), Si-Tr	Particle near location 546
552	Tr	--	--	--	--	+	--	--	Cd(0), Mo(0)	Second particle near location 546

a. See figures mentioned in the comments for location of ID numbers.

b. Not detected by SEM/EDS.

c. Detected by SEM/EDS only.

d. SAS examination not coincident with SEM/EDS.

Quantitative (SAS): Data is in atom percent.

Qualitative (SEM/EDS): ? - uncertain
 Tr - trace element
 0 - minor constituent
 + - major constituent

TABLE C-12. CHEMICAL COMPOSITION OF SELECTED AREAS OF PARTICLE 8A

ID ^a	U	Zr	O	Al	Cr	Fe	Ni	Sn	Miscellaneous	Comments
003-1	24.8	3.6	71.4	--	--	? ^b	--	--	--	Region 1 base material see Figure C-153
003-2	26.9	3.5	69.5	--	--	--	--	--	--	--
003-3	25.8	4.6	69.4	--	--	--	--	--	--	--
003-4	26.6	4.5	68.7	--	--	--	--	--	--	--
003-5	27.4	3.7	68.8	--	--	--	--	--	--	12 consecutive SAS readings with continuous sputter reveals a depth profile of about 1 μm ; Avg: 27.9 U, 4.2 Zr, 67.8% O
003-6	26.8	4.6	68.4	--	--	--	--	--	--	--
003-7	30.5	4.1	65.3	--	--	--	--	--	--	--
003-8	27.6	4.5	67.7	--	--	--	--	--	--	--
003-9	27.6	4.2	68.0	--	--	--	--	--	--	--
003-10	30.2	4.0	65.7	--	--	--	--	--	--	--
003-11	29.1	4.3	66.5	--	--	--	--	--	--	--
003-12	28.7	4.9	66.3	--	--	--	--	--	--	--
020	27.6	3.7	68.5	--	--	--	--	--	--	Region 2 base material, see Figure C-153
044	28.4	4.0	67.5	--	--	--	--	--	--	Region 3 base material, see Figure C-153
007	+	0	--	--	--	--	--	--	--	--
999	+	+	--	+	+	+	+	--	--	Second phase, see Figure C-161
998	+	+	--	--	0	0	0	--	--	Second phase, see Figure C-161
002	+	0	--	--	Tr	Tr	Tr	--	--	Base material, see Figure C-161
15	17.5	7.9	68.1	? ^b	--	3.1	3.1	--	--	Second phase, see Figure C-162
16	21.9	10.9	65.8	--	--	0.7	0.4	--	--	Base material
17	20.2	6.1	73.5	--	--	--	--	--	--	Base material
18	5.7	2.9	30.9	47.4	--	4.2	8.6	--	--	Grain boundary phase
012	+	0	--	--	--	?	--	--	--	Base material, see Figure C-158
014	+	+	--	+	0	0	0	--	--	Second phase, see Figure C-158
018	+	0	--	--	--	--	--	--	--	Base material, see Figure C-158
016	0	+	--	--	0	0	0	--	--	Surface material, see Figure C-158
025	+	0	--	--	--	?	--	--	--	Base material, see Figure C-165
022	+	--	--	--	0	0	0	+	Mo(+)	Inclusion, see Figure C-165
030	+	+	--	+	+	+	+	--	--	Grain boundary phase see Figure C-163
031	+	+	--	--	--	Tr	--	--	--	Base material, see Figure C-163
034	Tr	+	--	--	0	0	0	--	--	Surface material, see Figure C-163
038	+	0	--	--	--	--	--	--	--	Base material, see Figure C-164
039	+	+	--	+	+	+	+	--	--	Void material, see Figure C-164
042	+	0	--	+	+	+	+	--	--	Void material, see Figure C-164

a. See figures mentioned in the comments for location of ID numbers.

b. Detected by SEM/EDS only.

Quantitative (SAS): Data is in atom percent.

Qualitative (SEM/EDS): ? - uncertain

Tr - trace element

U - minor constituent

+ - major constituent

TABLE C-13. CHEMICAL COMPOSITION OF SELECTED AREAS OF PARTICLE 8C

ID ^a	U	Zr	O	Al	Cr	Fe	Ni	Sn	Miscellaneous	Comments
175	25.3	10.1	64.4	--	Tr ^b	Tr ^b	--	--	--	Base material Region 1, see Figure C-167
176	+	+	--	+	+	+	0	--	--	Grain boundary material Region 1
177	3.7	4.1	33.3	46.2	3.9	7.0	1.4	--	--	Dark phase Region 1
180	3.4	2.5	36.1	45.0	4.0	8.0	Tr ^b	--	--	Average eutectic Region 1
181	+	+	--	--	--	Tr	--	--	--	Second phase Region 1
182	26.6	6.7	66.6	--	--	--	--	--	--	Base material Region 1
183	Tr	Tr	--	--	--	--	--	--	Ag(+) S(0)	Bead in void Region 1
231A	+	0	--	--	--	--	--	--	--	High contrast Region 1 material, see Figure C-168
232	+	+	--	--	--	Tr	--	--	--	Medium contrast Region 1 material
233	+	+	--	--	Tr	Tr	--	--	--	Low contrast Region 1 material
201	+	0	--	--	--	?	--	--	--	Base material Region 2, see Figure C-172
224	0	0	--	+	+	+	0	--	--	Dark phase Region 2, see Figure C-172
225	+	+	--	+	+	+	0	--	--	Dendritic material Region 2, see Figure C-172
226	+	+	--	--	Tr	Tr	--	--	--	Light phase Region 2, see Figure C-172
227-1	25.1	11.4	63.3	--	--	--	--	--	--	Region 2 base material, see Figure C-172
227-2	27.9	11.2	60.8	--	--	--	--	--	--	--
227-3	27.0	10.3	62.5	--	--	--	--	--	--	Nine consecutive SAS readings with continue sputter reveals a depth profile of about 1 μm
227-4	30.0	7.0	62.8	--	--	--	--	--	--	--
227-5	29.9	8.5	61.4	--	--	--	--	--	--	--
227-6	30.3	7.4	62.2	--	--	--	--	--	--	--
227-7	31.8	7.6	60.4	--	--	--	--	--	--	--
227-8	31.4	6.8	61.6	--	--	--	--	--	--	--
227-9	30.8	7.3	61.7	--	--	--	--	--	--	--
227-10	27.3	7.4	65.1	--	--	--	--	--	--	Edge of 227 grain
227-11	28.7	7.3	63.9	--	--	--	--	--	--	--
227-12	21.9	10.6	67.4	--	--	--	--	--	--	Dark grain near 227
227-13	24.0	7.7	68.2	--	--	--	--	--	--	Light grain near 227
195	+	0	--	--	--	Tr	--	--	--	Region 2 base material, see Figure C-171
229	+	0	--	--	--	--	--	--	--	Region 2 base material, see Figure C-174
235	+	0	--	--	--	--	--	--	--	Region 2 base material, see Figure C-171
238	+	0	--	--	--	Tr	--	--	--	Region 2 base material, see Figure C-174
185	+	+	--	+	+	+	0	--	--	Second phase Region 3 material, see Figure C-176
186-1	24.4	7.9	67.5	--	--	Tr ^b	--	--	--	Base material Region 3 material
186-2	26.5	8.3	65.1	--	--	--	--	--	--	Base material near 186 Region 3
187	+	+	--	0	0	0	--	--	--	gb material Region 3
189	Tr	+	--	--	Tr	0	0	--	Ag(+) Ag(0)	Surface material Region 3
191	Tr	+	--	--	0	0	0	--	--	Surface material Region 3

TABLE C-13. (continued)

<u>ID^a</u>	<u>U</u>	<u>Zr</u>	<u>U</u>	<u>Al</u>	<u>Cr</u>	<u>Fe</u>	<u>Ni</u>	<u>Sn</u>	<u>Miscellaneous</u>	<u>Comments</u>
192	+	+	--	--	Tr	--	--	--	--	Region 3 base material, see Figure C-175

a. See figures mentioned in the comments for location of ID numbers.

b. Detected by SEM/EDS only.

Quantitative (SAS): Data is in atom percent.

Qualitative (SEM/EDS): ? - uncertain
 Tr - trace element
 *0 - minor constituent
 + - major constituent

TABLE C-14. CHEMICAL COMPOSITION OF SELECTED AREAS OF PARTICLE 8E

<u>10⁴</u>	<u>U</u>	<u>Ir</u>	<u>O</u>	<u>Al</u>	<u>Cr</u>	<u>Fe</u>	<u>Ni</u>	<u>Sn</u>	<u>Miscellaneous</u>	<u>Comments</u>
830	16.6	13.3	70.0	--	--	--	--	--	--	Region 1 base material, see Figure C-177
812	17.6	10.7	71.5	--	--	Tr ^b	--	--	--	Region 2 base material
834	15.6	13.7	70.6	--	--	Tr ^b	--	--	--	Region 3 base material
784	12.2	17.3	70.3	--	--	Tr ^b	--	--	--	Region 4 base material
835	14.9	15.3	69.7	--	--	Tr ^b	--	--	--	Region 5 base material
803	+	+	--	--	--	--	--	--	--	Base Region 1 material, see Figure C-179
804	+	+	--	--	--	Tr	--	--	--	Grain boundary Region 1 material
807	12.8	26.6	60.5	--	--	Tr ^b	--	--	--	Grain boundary Region 1 material
808	6.7	25.0	63.8	--	Tr ^b	4.0	Tr ^b	--	--	Grain boundary Region 1 material
832	+	+	--	--	--	0	--	--	--	Grain boundary Region 1 material, see Figure C-180
810	+	+	--	--	--	Tr	--	--	--	Base Region 1 material, see Figure C-182
770	+	+	--	--	0	0	--	--	--	Light phase Region 3 material, see Figure C-184
771	0	0	--	--	*	+	--	--	--	Dark phase Region 3 material
774	--	--	--	--	--	Tr ^b	76.6	19.3	C-4.0	Inclusion Region 3 material
769-A	5.9	6.7	51.6	--	12.5	23.0	--	--	--	Dark phase Region 3 material, see Figure C-183
769-B	4.3	22.4	60.4	--	--	12.6	--	--	--	Light phase Region 3 material
769-C	--	3.4	44.7	--	3.7	14.2	--	--	C-33.8	Average of A and B Region 3 material
768-A	12.6	19.4	67.8	--	--	--	--	--	--	gb material Region 3 material
779	--	--	--	--	--	0	+	+	Ru(0)	Inclusion Region 3 material, see Figure C-187
782	+	+	--	--	--	0	--	--	--	Second phase Region 3 material
783	+	+	--	--	--	?	--	--	--	Base Region 3 material
778	--	--	--	--	--	--	--	--	Si(+)	Particle in void
789	Tr	--	--	--	*	*	0	--	--	Dark phase Region 3 material, see Figure C-185
793	Tr	0	--	--	0	*	0	--	Tl(?)	Dark strip Region 3 material
794	+	+	--	--	*	*	Tr	--	--	Light strip Region 3 material
795	+	+	--	--	Tr	--	--	--	--	Base Region 3 material
796	+	+	--	--	--	Tr	--	--	--	Base in void Region 3 material, see Figure C-189
798	--	--	--	--	--	Tr	*	*	Ru(?)	Base in inclusion Region 3 material
799	--	--	--	--	--	--	*	*	Ru(?)	Other phase Region 3 material
801	Tr	Tr	--	--	--	Tr	*	--	Tc(+)/Ru(+)	Other phase Region 3 material

a. See figures mentioned in the comments for location of ID numbers.

b. Detected by SEM/EOS only.

Quantitative (SAS): Data is in atom percent.

Qualitative (SEM/EOS): ? - uncertain
 Tr - trace element
 0 - minor constituent
 + - major constituent

TABLE C-15. CHEMICAL COMPOSITION OF SELECTED AREAS OF PARTICLE 8H

<u>ID^a</u>	<u>U</u>	<u>Zr</u>	<u>O</u>	<u>Al</u>	<u>Cr</u>	<u>Fe</u>	<u>Ni</u>	<u>Sn</u>	<u>Miscellaneous</u>	<u>Comments</u>
147	+	0	--	--	--	Tr	--	--	--	Region 1 base material, see Figure C-190
161	+	0	--	--	--	Tr	--	--	--	Region 2 base material
120	+	0	--	--	--	Tr	--	--	--	Region 2 base material
127	+	+	--	--	--	0	--	--	--	Region 3 base material
117	+	0	--	--	--	Tr	--	--	--	Region 1 base material, see Figure C-196
118	+	Tr	--	--	--	Tr	--	--	--	Region 1 base material
168	+	0	--	--	--	Tr	--	--	--	Region 1 base material, see Figure C-201
143	+	0	--	--	--	Tr	--	--	--	Base Region 1 material, see Figure C-195
144	+	0	--	--	--	0	--	--	--	High Z crystals Region 1 material
135	+	0	--	--	--	Tr	--	--	--	Region 1 base, see Figure C-200
137	+	+	--	--	Tr	0	--	--	--	Region 3 base
138			--	--	+	0	--	--	--	Dark grain boundary material
140	+	+	--	--	--	+	0	--	--	Inclusion
141	+	+	--	--	--	0	--	--	--	Light grain boundary material
166	+	+	--	--	--	Tr	--	--	--	Base Region 3 material, see Figure C-203
165	Tr	--	--	--	+	+	0	--	--	Grain boundary Region 3 material
167	0	+	--	--	--	0	0	--	--	Surface material Region 3 material
123	--	--	--	--	--	+	Tr	--	--	Second phase metallic material
124	--	--	--	--	--	--	--	--	Ag(+)	Base metallic material
125	+	0	--	--	--	Tr	--	--	--	High Z bead metallic material

a. See figures mentioned in the comments for location of ID numbers.

Quantitative (SAS): Data is in atom percent.

Qualitative (SEM/EDS): ? - uncertain
 Tr - trace element
 0 - minor constituent
 + - major constituent

TABLE C-16. CHEMICAL COMPOSITION OF SELECTED AREAS OF PARTICLE 90

<u>ID^a</u>	<u>U</u>	<u>Zr</u>	<u>O</u>	<u>Al</u>	<u>Cr</u>	<u>Fe</u>	<u>Ni</u>	<u>Sn</u>	<u>Miscellaneous</u>	<u>Comments</u>
766	--	--	--	--	--	--	--	--	Ag(+)	Base metallic material, see Figure C-207
765	--	--	--	--	Tr	+	0		Ag(Tr), Ru(Tr)	Inclusion metallic material
764	+	0	--	--	Tr	Tr	Tr	--	--	Ceramic piece number 1 base material
777	+	+	--	--	?	Tr	Tr	--	--	Ceramic piece number 1 base material
768	--	--	--	--	--	Tr	+	+	Ag(Tr), Ru(Tr)	High Z material in round two-phase inclusions in metallic material
769	--	--	--	--	--	Tr	+	0	Ag(Tr), Ru(Tr)	Low Z material, see Figure C-206
801	--	--	--	--	--	Tr	+	0	Ru(Tr)	Low Z material
802	--	--	--	--	--	Tr	+	+	Ru(Tr)	High Z material
783	+	+	--	--	Tr	Tr	Tr	--	--	Ceramic piece number 2 base material, see Figure C-208
784	+	+	--	--	Tr	Tr	Tr	--	--	Ceramic piece number 2 base material
778	Tr	--	--	--	--	Tr	+	0	Ru(+)	Void material in piece number 1, see Figure C-213
785	+	+	--	--	--	Tr	Tr	--	--	Second phase piece number 2
787	--	--	--	--	--	Tr	+	0	Ag(Tr)	Void material piece number 2
791	+	+	0	--	Tr	Tr	Tr	--	--	Base piece number 3, see Figure C-210
792	+	0	--	--	Tr	Tr	--	--	--	Base piece number 3
793	Tr	--	--	--	--	Tr	+	0	Ru(0)	Void material piece number 3
794	Tr	--	--	--	--	Tr	+	0	Ru(+)	Void material piece number 3
798	+	+	--	--	Tr	Tr	Tr	--	--	Ceramic piece number 4 base material, see Figure C-215
799	+	+	--	--	Tr	Tr	Tr	--	--	Ceramic piece number 4 base material

a. See figures mentioned in the comments for location of ID numbers.

Quantitative (SAS): Data is in atom percent.

Qualitative (SEM/EDS): ? - uncertain
 Tr - trace element
 0 - minor constituent
 + - major constituent

TABLE C-17. CHEMICAL COMPOSITION OF SELECTED AREAS OF PARTICLE 9G

ID ^a	U	Zr	O	Al	Cr	Fe	Ni	Sn	Miscellaneous	Comments
809	--	--	--	--	--	Tr	+	O	Ru(Tr), Ag(Tr)	Inclusion Area D, see Figure 224
810	--	--	--	--	--	--	--	--	Ag(+)	Base Area D, see Figure 224
811	--	--	--	--	Tr	Tr	Tr	--	Ag(+), Cu(Tr), Mo(0)	Surface bead Area D, see Figure 232
832	--	--	--	--	--	--	--	--	Ag(+), S(Tr)	Surface lump Area D
833	--	--	--	Tr	--	Tr	Tr	--	Ag(+), Cu(Tr), S(Tr)	Void material Area D
836	--	--	--	O	--	Tr	O	--	Ag(+), S(Tr)	Void material Area D
837	--	--	--	--	--	--	+	?	Ag(+)	Inclusion second phase Area D, see Figure 227
841	--	--	--	--	--	--	0	--	Ag(+)	Base Area D
842	--	--	--	--	--	--	+	O	--	Inclusion Area D
846	--	--	--	--	--	Tr	+	O	Ag(+), S(O)	Surface bead Area A, see Figure C-221
847	--	--	--	--	--	Tr	+	O	Ag(Tr)	Inclusion Area A
848	--	--	--	--	--	--	--	--	Ag(+)	Base Area A
862	--	--	--	O	Tr	Tr	Tr	--	Ti(+), S(O), Ag(+), Cu(Tr)	Void material Area A, see Figure C-223
864	--	--	--	--	--	--	--	--	Ag(+)	Base Area A
852	--	--	--	--	--	Tr	+	O	Ag(?)	Inclusion Area A, see Figure C-222
853	--	--	--	--	--	Tr	+	+	Ag(O)	Inclusion second phase Area A
854	--	--	--	--	--	Tr	+	+	Ag(+)	Inclusion phase Area A
855	--	--	--	--	--	Tr	+	Tr	Ag(+)	Inclusion phase Area A
856	--	--	--	--	Tr	Tr	Tr	--	Ag(+), Cu(Tr)	Inclusion phase Area A
868	--	--	--	--	--	Tr	+	O	Ag(Tr)	Inclusion Area B, see Figure C-229
867	--	--	--	--	--	--	--	--	Ag(+)	Base Area B
870	--	--	--	O	--	Tr	Tr	--	Ag(+), S(O)	Surface bead Area B
									Cu(Tr)	
871	--	--	--	--	--	--	--	--	Ag(+)	Sample center base material, see Figure C-220 and 230
874	--	--	--	--	--	--	--	--	Ag(+)	Base Area F, see Figure C-226
875	--	--	--	--	--	Tr	+	O	Ag(Tr), Ru(Tr)	Inclusion Area F

a. See figures mentioned in the comments for location of ID numbers.

Quantitative (SAS): Data is in atom percent.

Qualitative (SEM/EDS): ? - uncertain
 Tr - trace element
 O - minor constituent
 + - major constituent

TABLE C-18. CHEMICAL COMPOSITION OF SELECTED AREAS OF PARTICLE 10A

ID ^a	U	Zr	O	Al	Cr	Fe	Mn	Sn	Miscellaneous	Comments
272-A	25.8	6.3	67.8	--	--	--	--	--	--	Low Z Region 1 base material, see Figure C-235
272-B	23.2	7.0	69.6	--	--	--	--	--	--	Low Z Region 1 base material
272-C	24.0	7.6	68.2	--	--	--	--	--	--	Low Z Region 1 base material
273-A	32.7	1.2	65.9	--	--	--	--	--	--	High Z Region 1 base material
273-B	32.5	1.5	65.8	--	--	--	--	--	--	High Z Region 1 base material
273-C	32.2	1.8	65.9	--	--	--	--	--	--	High Z Region 1 base material
291-A	31.9	1.9	66.0	--	--	--	--	--	--	Region 2 base material, see Figure C-236
291-B	34.2	0.0	65.7	--	--	--	--	--	--	Region 2 base material
291-C	32.5	0.7	66.6	--	--	--	--	--	--	Region 2 base material
291-D	30.4	0.3	69.2	--	--	--	--	--	--	Region 2 base material
291-E	34.6	0.3	65.0	--	--	--	--	--	--	Region 2 base material
291-F	35.2	0.0	64.7	--	--	--	--	--	--	Region 2 base material
274	Ir	Ir	--	--	--	--	Ir	--	1c(+), Ru(+)	Material in voids, see Figure C-247
290	*	*	--	--	--	--	Ir	--	1c(0), Ru(0)	Material in voids, see Figure C-236
302	0	*	--	Ir	0	0	*	0	11(0)	Material in voids, see Figure C-237
313	*	*	--	--	--	--	0	--	1c(+), Ru(+)	Material in voids, see Figure C-238
286	*	0	--	--	--	Ir	--	--	--	Low Z Region 1 base material, see Figure C-242
287	*	Ir	--	--	--	?	--	--	--	High Z Region 1 base material
309	*	Ir	--	*	--	--	--	--	--	High Z Region 1 base material

a. See figures mentioned in the comments for location of ID numbers.

Quantitative (SAS): Data is in atom percent.

Qualitative (SEM/EDS): ? - uncertain
 Ir - trace element
 0 - minor constituent
 * - major constituent

TABLE C-19. CHEMICAL COMPOSITION OF SELECTED AREAS OF PARTICLE 10E

ID ^a	U	Zr	O	Al	Cr	Fe	Ni	Sn	Miscellaneous	Comments
062-A	16.5	15.1	68.2	--	--	--	--	--	--	Three scans at location 062, see Figure C-258
062-B	16.0	13.3	70.6	--	--	--	--	--	--	--
062-C	16.2	14.7	69.0	--	--	--	--	--	--	--
063-A	33.1	--	66.8	--	--	--	--	--	--	Four separate fuel grains near 063, see Figure C-258
063-B	35.4	--	64.5	--	--	--	--	--	--	--
063-C	35.9	--	64.0	--	--	--	--	--	--	--
--	--	--	--	--	--	--	--	--	--	--
063-E	37.2	--	62.7	--	--	--	--	--	--	--
064-A	37.6	--	62.3	--	--	--	--	--	--	Three separate fuel grains near 064, see Figure C-258
064-B	33.5	--	66.4	--	--	--	--	--	--	--
064-C	34.3	--	65.6	--	--	--	--	--	--	--
061	Tr	--	--	--	--	?	+	+	--	Inclusion, see Figure C-258
097	Tr	Tr	--	--	--	0	--	--	Ag(+), Mo(0)	Material in void, see Figure C-258
101	Tr	--	--	--	--	Tr	0	+	Ag(+), Mo(0)	--
102	Tr	--	--	--	--	--	+	+	Ag(+), Mo(0)	--
078-A	35.0	--	65.0	--	--	--	--	--	--	Three separate grains near 078 (sample center), see Figure 250
078-B	37.0	--	63.0	--	--	--	--	--	--	--
078-C	36.0	--	64.0	--	--	--	--	--	--	--
075-A	23.7	6.7	69.4	--	--	Tr ^b	--	--	--	On Zr band, see Figure C-251
075-B	33.2	--	66.7	--	--	--	--	--	--	Off Zr band
075-C	34.7	--	65.2	--	--	--	--	--	--	Off Zr band
073	+	--	--	--	--	--	--	--	--	Base material, see Figure C-257
088	Tr	Tr	--	--	0	0	Tr	--	Ag(+), Mo(0)	Particle in void, see Figure C-256
092	+	+	--	--	+	+	--	--	--	Base material
081	Tr	Tr	--	--	Tr	Tr	+	+	Ag(0), Ru(Tr)	Inclusion, see Figure C-255
083	Tr	Tr	--	--	Tr	Tr	--	--	Ag(+), Mo(0)	Inclusion
086	+	+	--	--	Tr	Tr	--	--	--	Base material
084-A	12.4	16.1	71.3	--	--	Tr ^b	--	--	--	Two locations, near 084
084-B	11.8	15.6	72.4	--	--	--	--	--	--	Two locations, near 084
085-A	32.1	3.5	64.2	--	--	Tr ^b	--	--	--	10 μ in from interface
085-B	32.2	1.9	65.7	--	--	--	--	--	--	60 μ in from interface

a. See figures mentioned in the comments for location of ID numbers.

b. Detected by SEM/EDS only.

Quantitative (SAS): Data is in atom percent.

Qualitative (SEM/EDS): ? - uncertain
 Tr - trace element
 0 - minor constituent
 + - major constituent

TABLE C-20. CHEMICAL COMPOSITION OF SELECTED AREAS OF PARTICLE 10F

<u>10^b</u>	<u>U</u>	<u>Zr</u>	<u>U</u>	<u>Al</u>	<u>Cr</u>	<u>Fe</u>	<u>Ni</u>	<u>Sn</u>	<u>Miscellaneous</u>	<u>Comments</u>
411	23.9	3.3	70.8	--	--	Tr ^b	2.0 ^c	--	--	Region 1, base material, see Figure C-261
894	23.6	5.9	70.4	--	--	Tr ^b	--	--	--	Region 1, base material
908	25.9	4.7	69.2	--	--	Tr ^b	--	--	--	Region 1, base material
901	19.2	7.7	71.3	--	--	1.6	--	--	--	Region 2, base material
882	26.4	5.8	67.6	--	--	Tr ^b	--	--	--	Base material, see Figure C-264
883	+	0	--	--	--	Tr	--	--	--	Base material
884	+	+	--	--	Tr	0	Tr	--	--	Grain boundary material
885	Tr ^b	--	5.7	--	--	Tr ^b	12.6	--	Tc-5.0 ^c , Pd-3.4 ^c , Ru-60.5, Rh-12.5 ^c	Inclusion
890	+	0	--	--	--	Tr	--	--	--	Base material, see Figure C-269
891	+	0	--	--	+	+	+	--	--	Grain boundary material
896	+	0	--	--	--	Tr	--	--	--	Base material, see Figure C-270
897	+	0	--	?	+	+	+	--	--	Grain boundary material
898	+	+	--	--	?	0	Tr	--	--	Fine grain material
897-A	4.7	1.4	51.6	--	13.0	17.6	11.4	--	--	Grain boundary material, material similar to point 897 (see Figure C-270) in center of Region 2
897-B	2.6	0.9	53.4	--	15.8	15.5	11.5	--	--	Grain boundary material
898-A	25.1	9.7	63.7	--	--	3.3	--	--	--	Fine grain material, material similar to point 898 (see Figure C-270) in center of Region 2
898-B	23.0	10.8	62.1	--	--	3.9	--	--	--	Fine grain material
905	+	0	--	--	--	Tr	--	--	--	Base, see Figure C-270
906	0	Tr	--	?	+	+	0	--	--	Grain boundary material
907	10.9	3.6	59.5	--	7.7	10.8	7.1	--	--	Average of two eutectic phases
912	--	--	--	--	--	+	--	--	--	Inclusion in void

a. See figures mentioned in the comments for location of 10 numbers.

b. Detected by SEM/EDS only.

c. Not detected by SEM/EDS.

Quantitative (SAS): Data is in atom percent.

Qualitative (SEM/EDS): ? - uncertain
 Tr - trace element
 0 - minor constituent
 + - major constituent

TABLE C-21. CHEMICAL COMPOSITION OF SELECTED AREAS OF PARTICLE 11B

ID ^a	U	Zr	O	Al	Cr	Fe	Ni	Sn	Miscellaneous	Comments
566	--	--	--	--	--	+	+	Tr	--	Base, metallic region, see Figure 277
567	--	--	--	--	--	0	+	0	Ag(+)	Second phase, metallic region
568	--	--	--	--	--	0	0	--	Ag(+), Mo(0)	Inclusion, metallic region
574	+	0	--	--	--	0	Tr	--	--	Rectangular inclusion in metallic region, see Figure C-272
575	--	--	--	--	+	+	0	--	--	--
576	--	--	--	--	+	+	0	--	Mo(+)	--
577	--	--	--	--	+	+	0	--	Mo(0)	--
578	--	--	--	--	0	+	0	--	Mo(0)	--
579	--	--	--	--	Tr	0	--	--	Ag(+)	--
584	0	Tr	--	Tr	+	+	--	--	--	Other phases, see Figure C-273
585	0	--	--	0	+	+	--	--	--	--
586	+	+	--	0	+	+	--	--	--	--
587	+	+	--	--	+	+	--	--	--	--
588	+	0	--	--	--	--	--	--	--	--
589	+	+	--	--	--	0	--	--	--	--
593	Tr	--	--	--	--	+	+	0	S/Mo(+), In(0) Ag(0), Cd(0)	Material in blister, see Figure C-274
594	0	--	--	--	--	--	+	--	Mo(+)	Material in blister
599	0	0	--	0	+	+	--	--	--	Other phases, see Figure C-281
600	+	+	--	--	+	+	--	--	--	Other phases
601	--	--	--	--	--	+	+	0	--	Inclusion
602	+	+	--	--	--	0	--	--	--	Other phase

a. See figures mentioned in the comments for location of ID numbers.

Quantitative (SAS): Data is in atom percent.

Qualitative (SEM/EDS): ? - uncertain
 Tr - trace element
 0 - minor constituent
 + - major constituent

TABLE C-22. CHEMICAL COMPOSITION OF SELECTED AREAS OF PARTICLE 11C

<u>10⁴</u>	<u>U</u>	<u>Zr</u>	<u>O</u>	<u>Al</u>	<u>Cr</u>	<u>Fe</u>	<u>Ni</u>	<u>Sn</u>	<u>Miscellaneous</u>	<u>Comments</u>
930	+	--	--	--	--	--	--	--	--	Center region (G) base material, see Figure C-290
934	0	+	--	--	--	Tr	--	--	--	Surface, adherent melt, see Figure C-287
933	0	+	--	--	--	--	--	--	--	Interior, adherent melt
931	0	+	--	--	--	--	--	--	--	Interior, adherent melt
935	+	+	--	--	--	--	--	--	--	Interface, adherent melt
936	+	--	--	--	--	--	--	--	--	Base, adherent melt
938	0	+	--	--	Tr	Tr	--	--	--	Surface base material, see Figure C-289
940	+	+	--	--	+	+	--	?	--	Beads and inclusions, surface reaction layer
942	+	0	--	--	--	Tr	--	--	--	Beads and inclusions, surface reaction layer
943	0	+	--	--	+	+	--	0	--	Beads and inclusions, surface reaction layer
944	+	0	--	--	--	Tr	--	--	--	Interior, surface reaction layer
950	--	--	--	--	--	--	--	--	Ag(+)	Inclusion, surface reaction layer

a. See figures mentioned in the comments for location of ID numbers.

Quantitative (SAS): Data is in atom percent.

*

Qualitative (SEM/EDS): ? - uncertain
 Tr - trace element
 0 - minor constituent
 + - major constituent

C-54



Figure C-1. Photomacrograph of Particle 1A, (H8, surface).

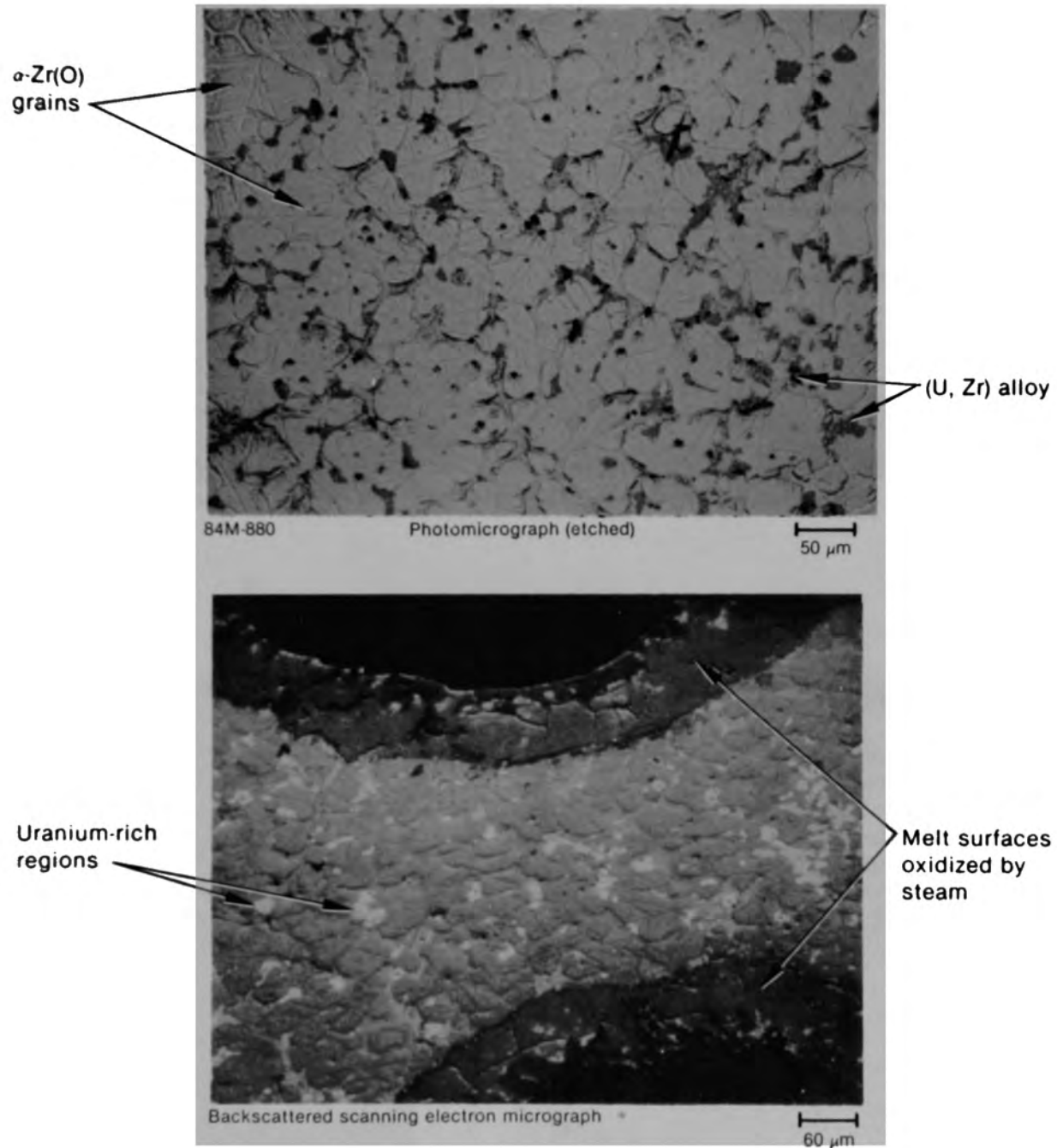
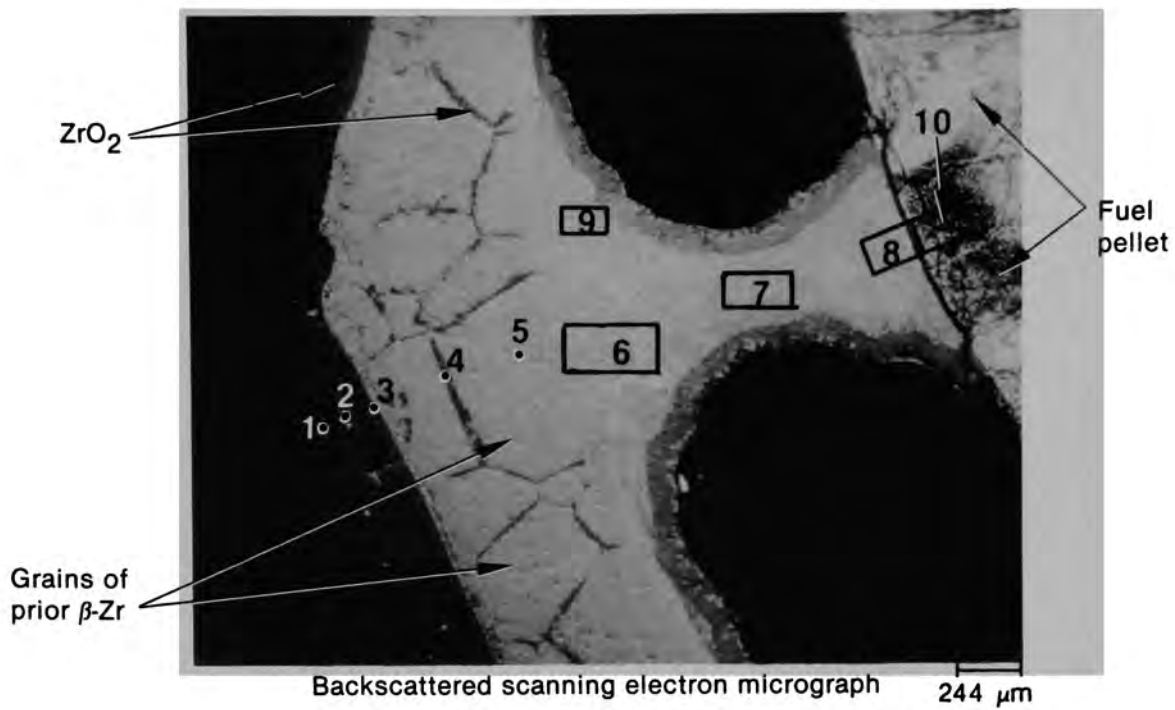


Figure C-2. Metallographic (top) and SEM (bottom) images of liquefied material structures in Particle 1A (H8, surface).



Summary of Particle 1A Composition Data

Point 1: 96.0 weight % Fe, 4.1 weight % Si, trace of Ca

Point 2: 100.0 weight % Zr

Point 3: 100.0 weight % Zr

Point 4: 100.0 weight % Zr

Point 5: 100.0 weight % Zr

Area 6: 86.7 weight % Zr, 11.5 weight % U, 1.9 weight % Ni, plus traces of Fe and Cr

Areas 7, 8, 9, and 10 were not quantitatively analyzed, but appear similar to Area 6

(see Figures C-4 through C-8).

Figure C-3. Regions of Particle 1A investigated by energy-dispersive X-ray spectroscopy.

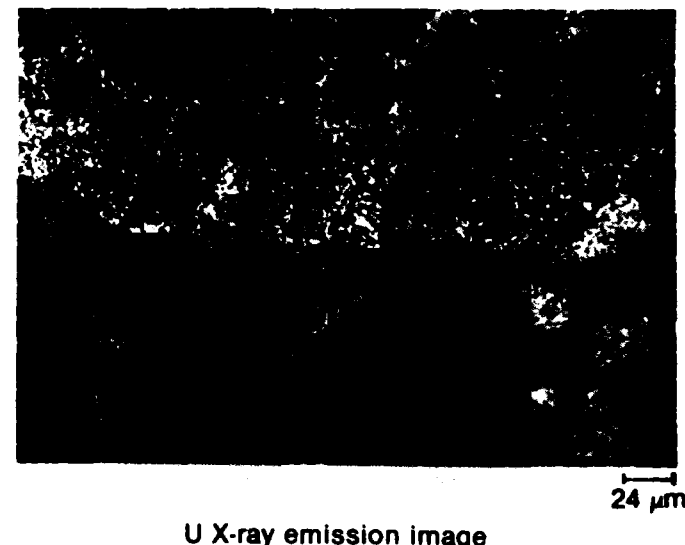
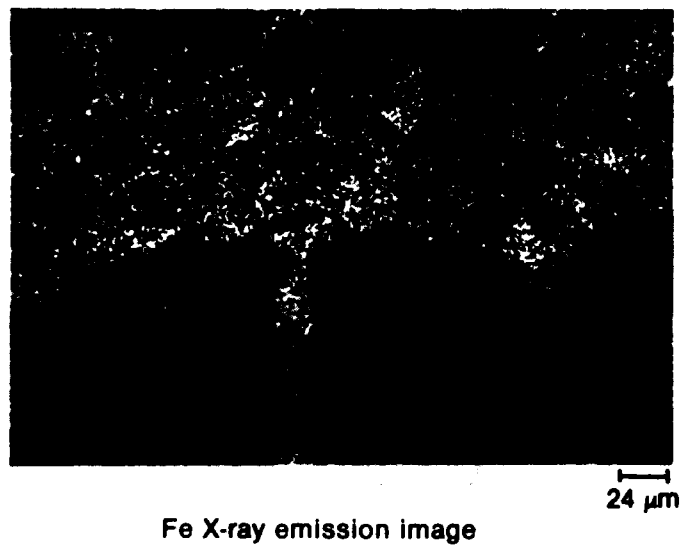
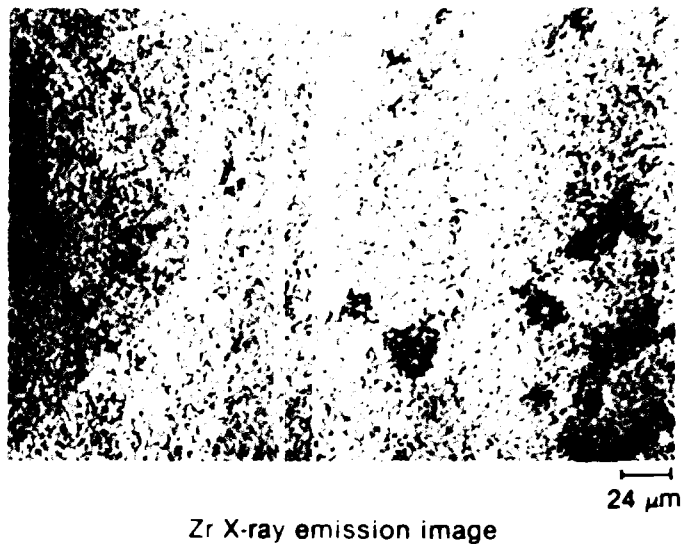
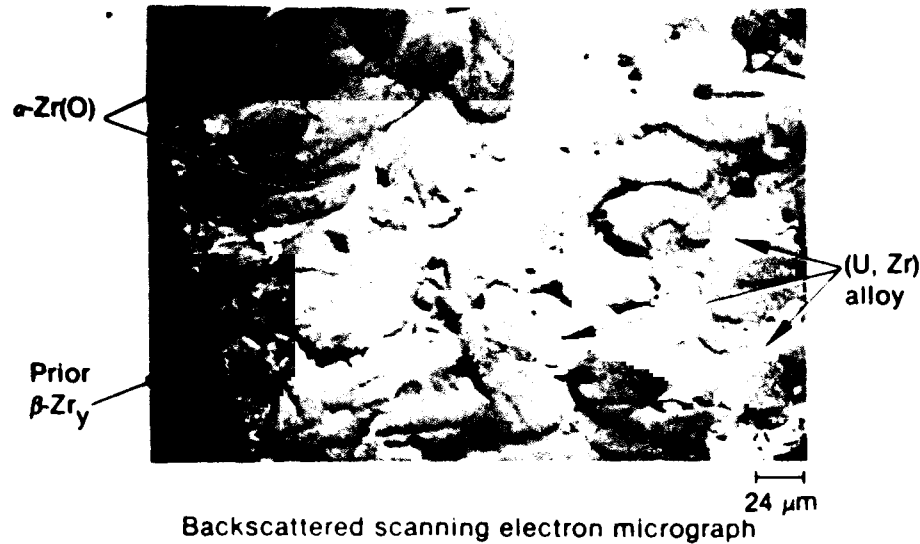
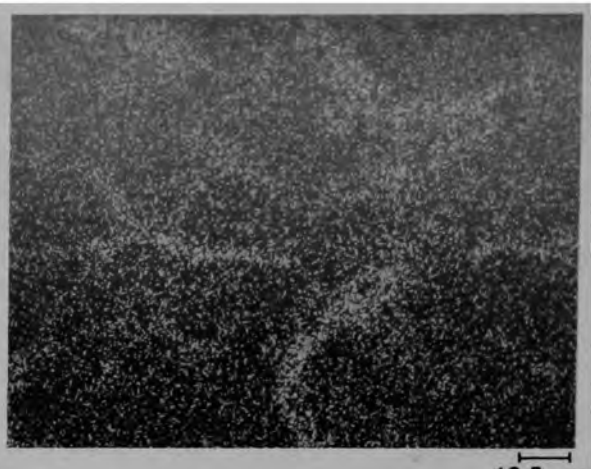


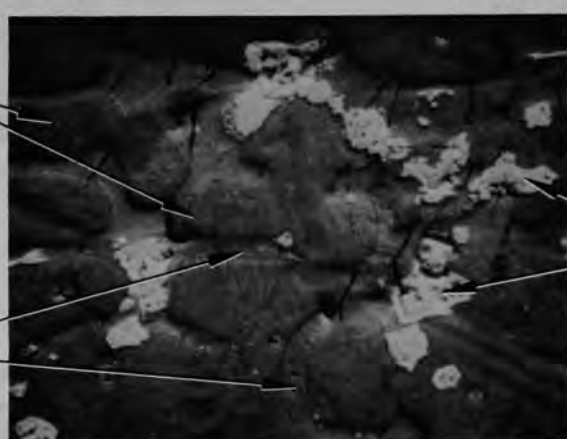
Figure C-4. Area 6 of Particle 1A, elemental distributions in melt phases adjacent to zircaloy cladding.



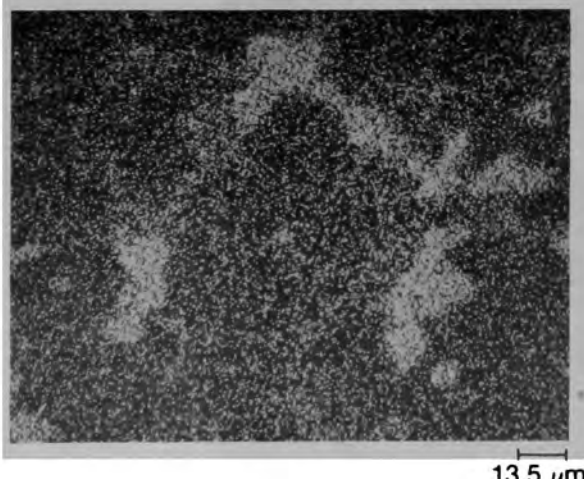
Zr X-ray emission image



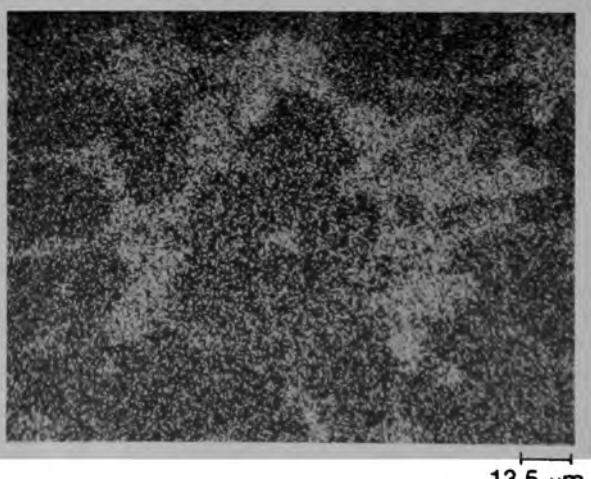
Fe X-ray emission image



Backscattered scanning electron micrograph



U X-ray emission image



U plus Sn X-ray emission image

Figure C-5. Area 7 of Particle 1A, phase make-up of interior melt region.

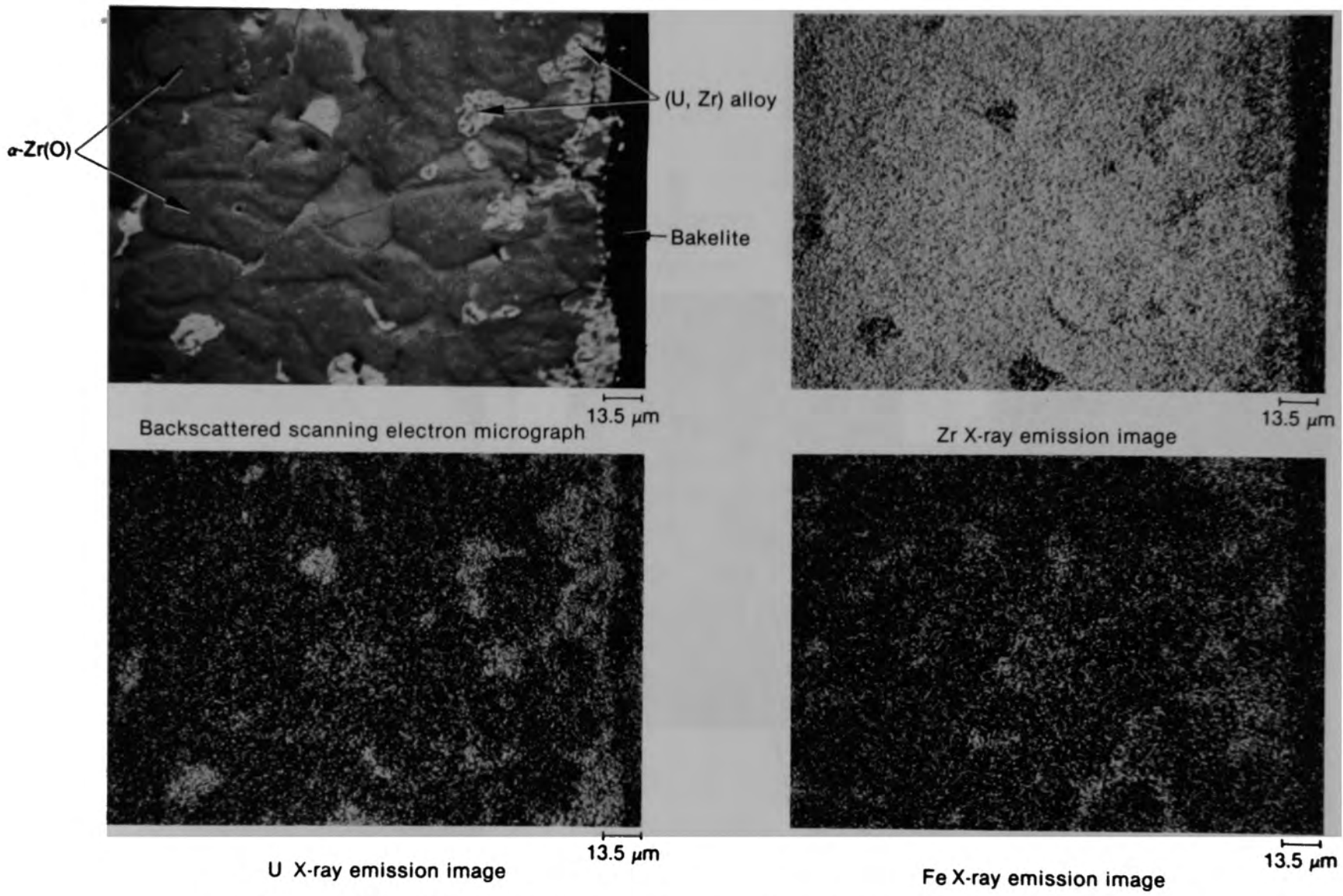
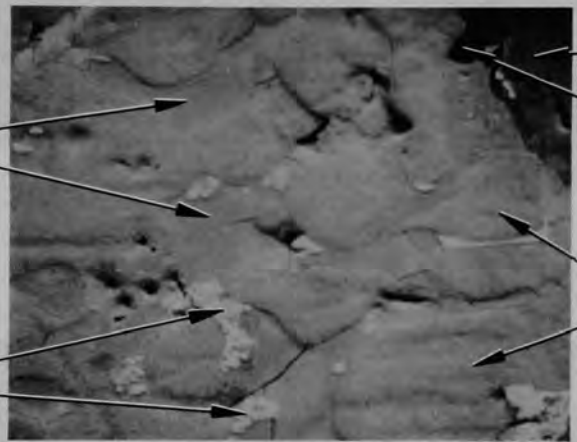
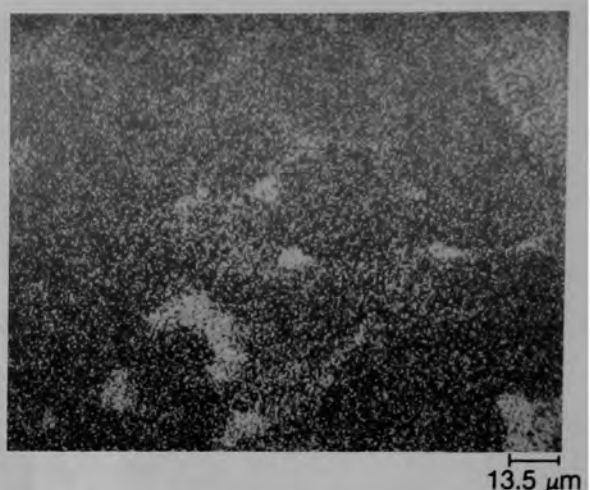
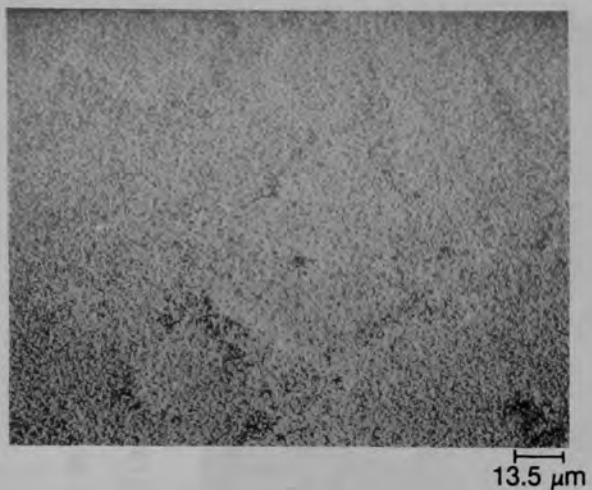


Figure C-6. Area 8 of Particle 1A, elemental distributions in melt phases near fuel pellet.



Backscattered scanning electron micrograph

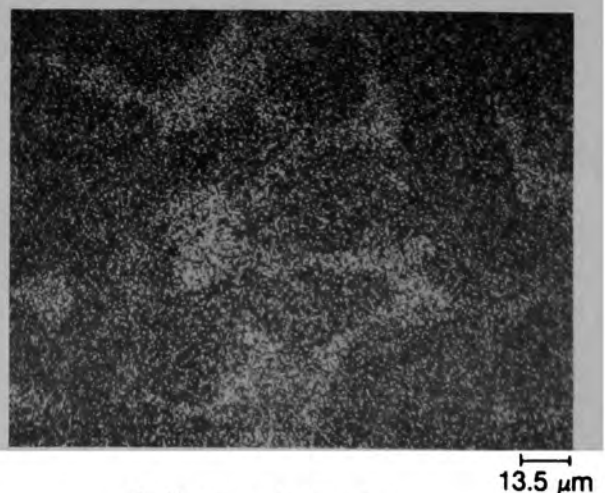
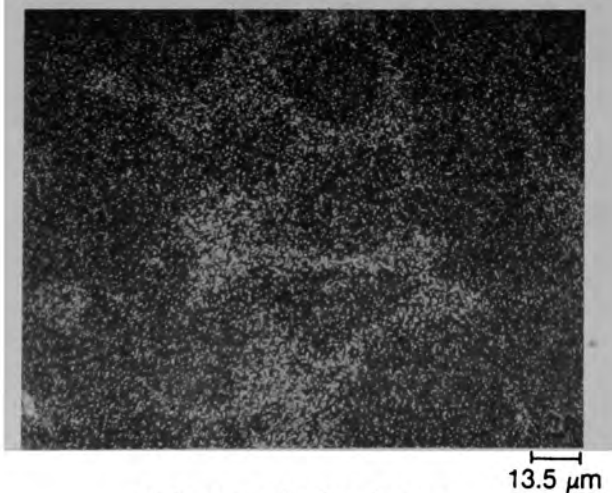


Figure C-7. Area 9 of Particle 1A, phase compositions in melt near oxidized pore surface.

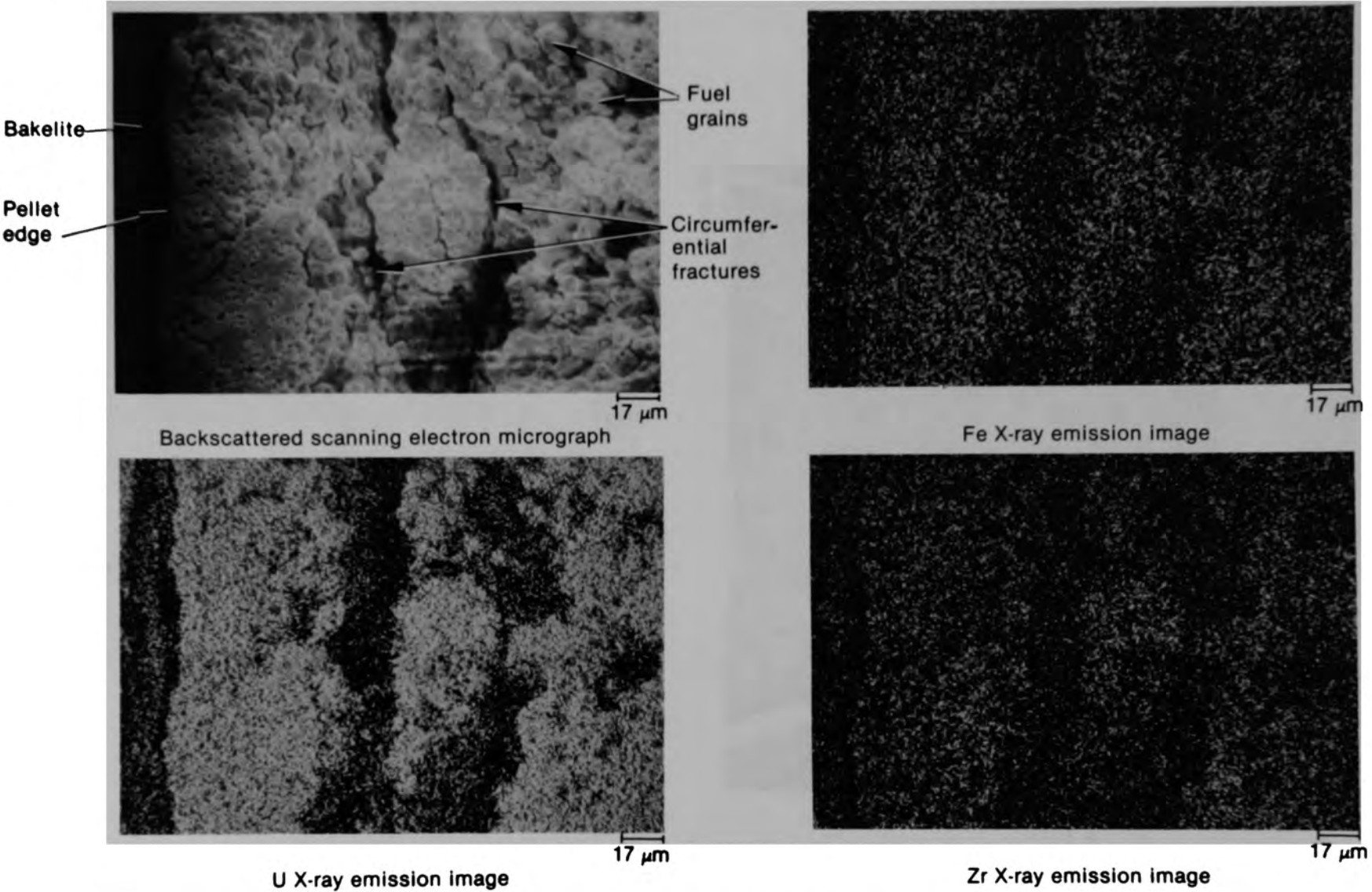


Figure C-8. Area 10 of Particle 1A, periphery of fuel pellet adjacent to homogeneous melt.

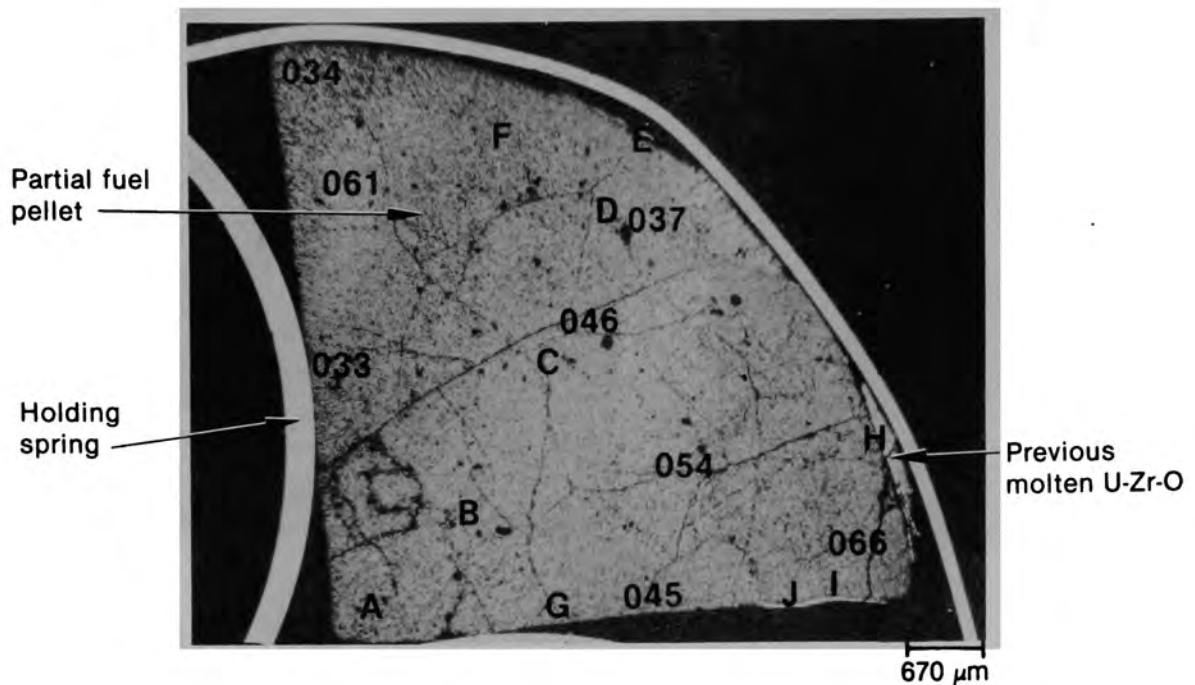
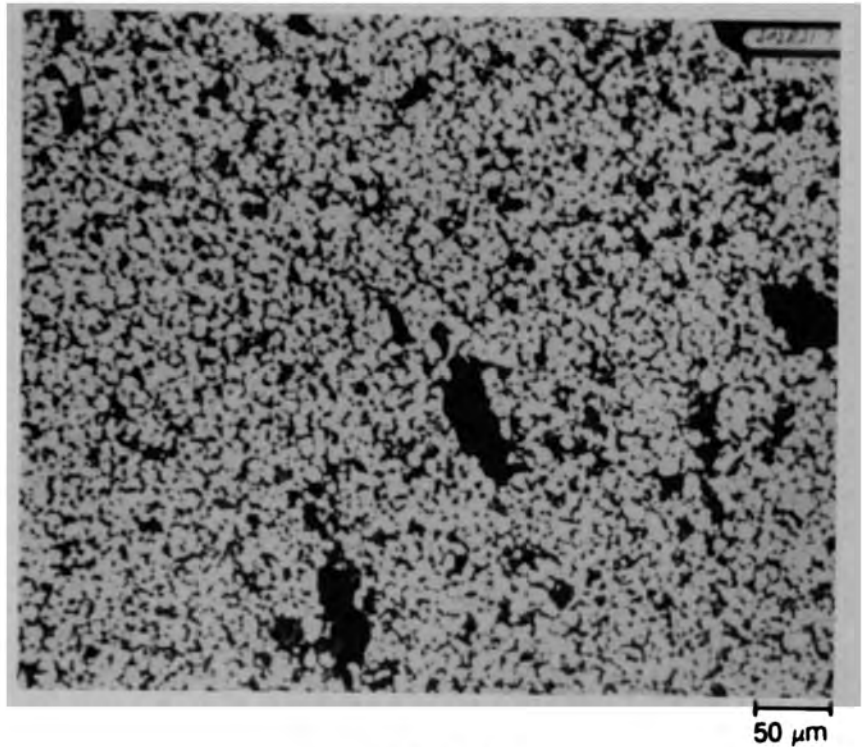
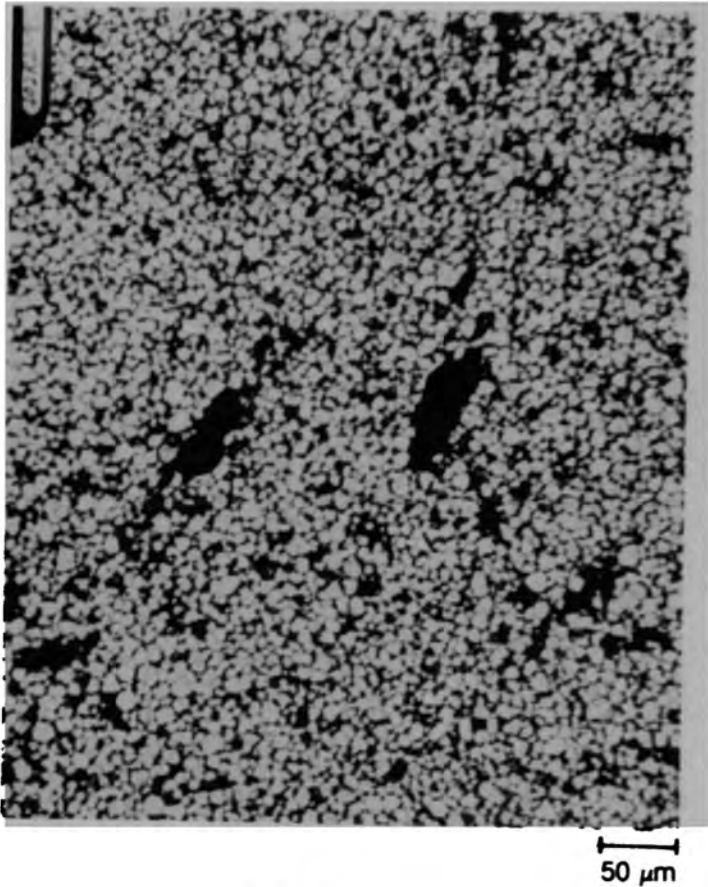


Figure C-9. Photomacrograph of Particle 1B (H8, surface).

C-63



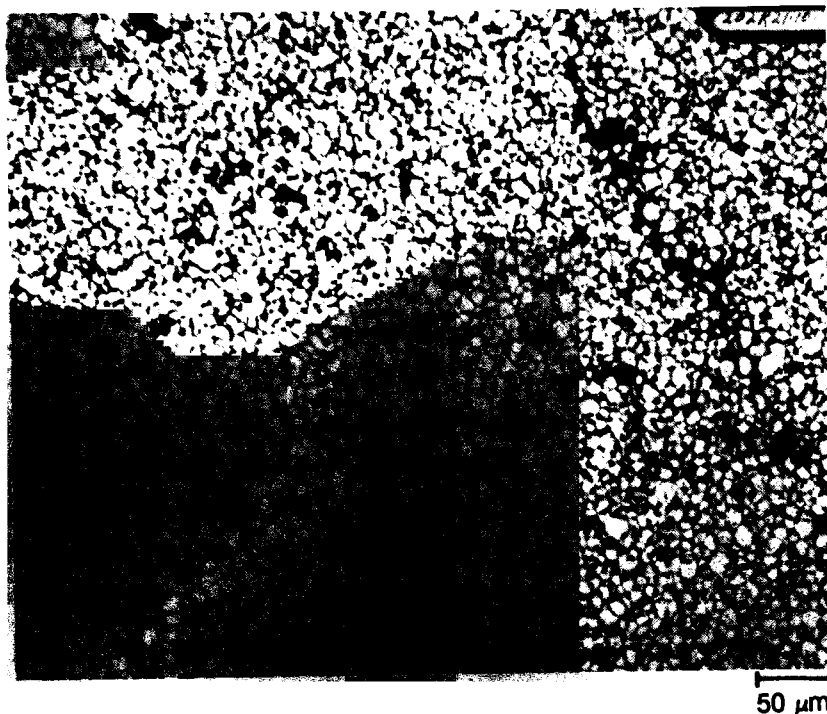
(a) As polished



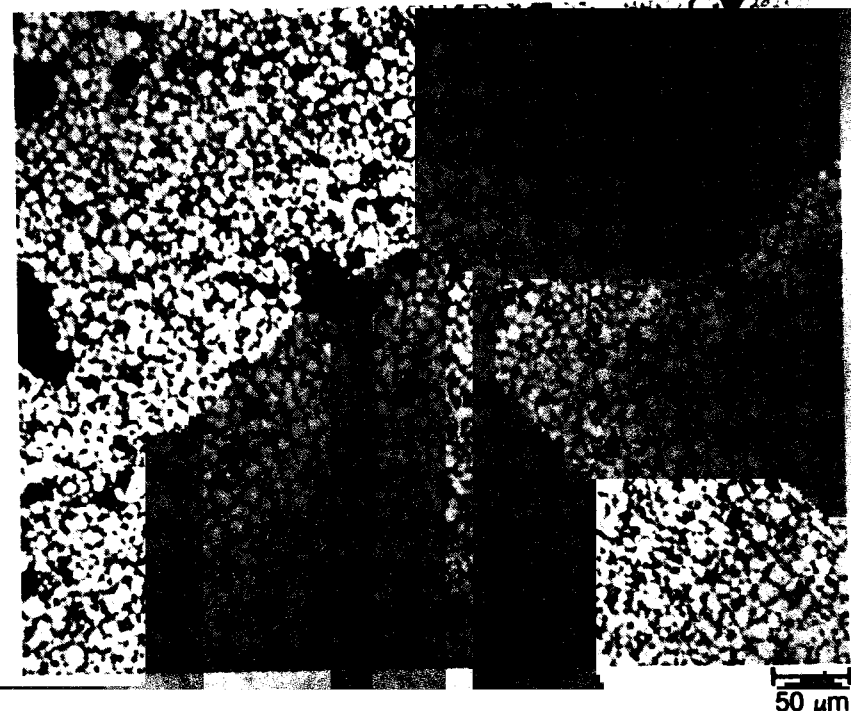
(b) Etched

Figure C-10. Photomicrographs of Particle 1B (H8, surface) showing fuel grain structure at Location A.

C-64

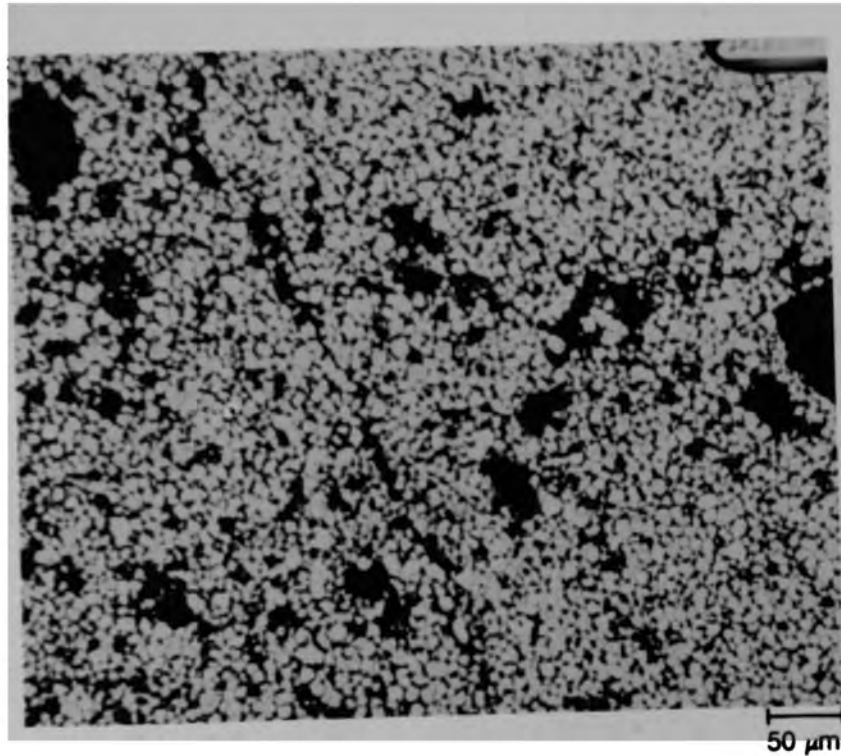


(a) Location B

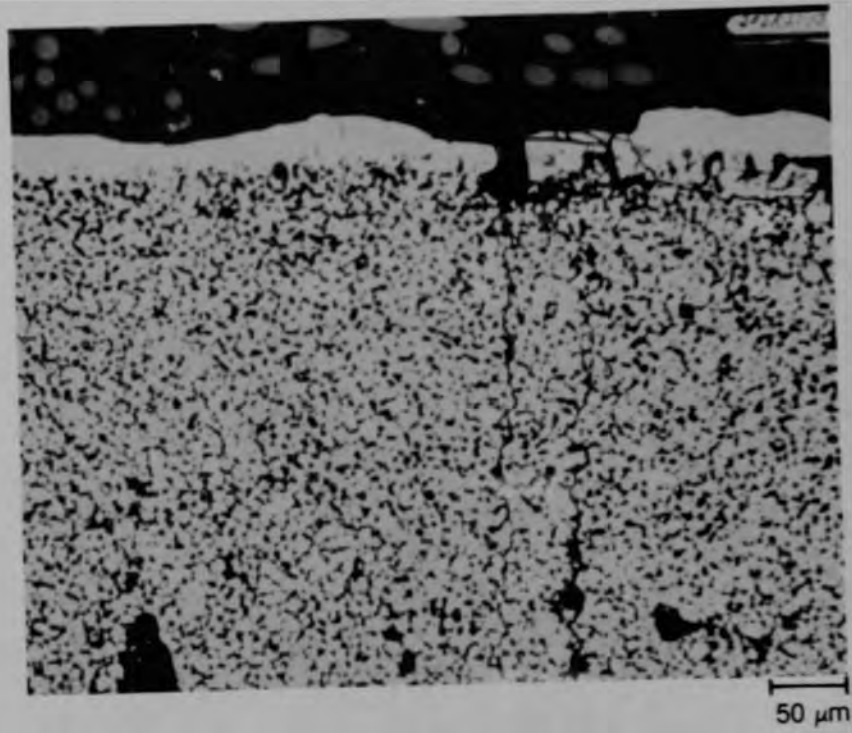


(b) Location C

Figure C-11. Photomicrographs of Particle 1B (H8, surface) showing etched fuel grain structure.



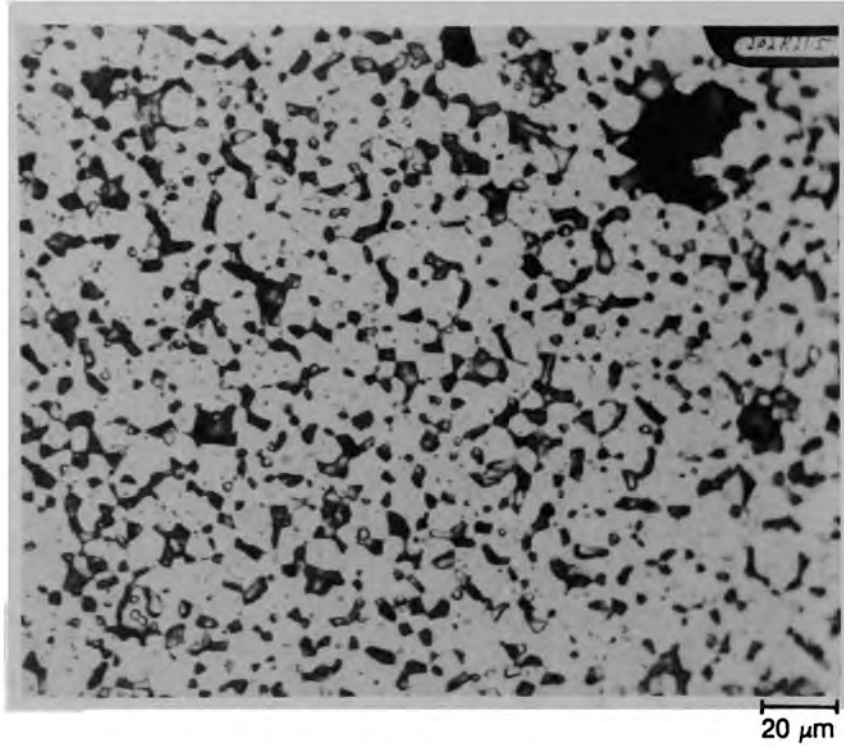
(a) Location D



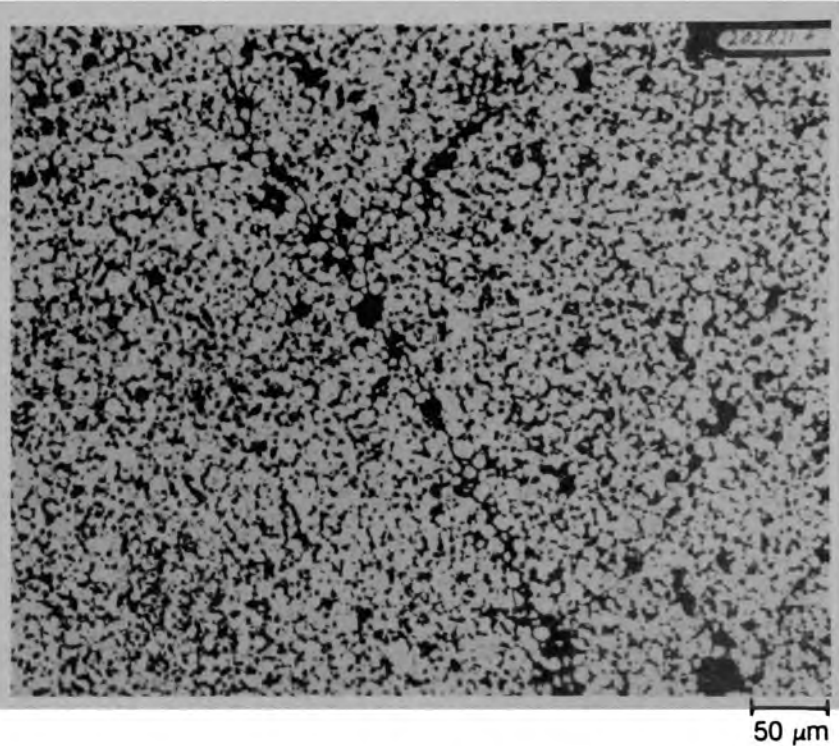
(b) Location E

Figure C-12. Photomicrographs of Particle 1B (H8, surface) showing etched fuel grain structure.

C-66



(a) Location F



(b) Location G

Figure C-13. Photomicrographs of Particle 1B (H8, surface) showing etched fuel grain structure.

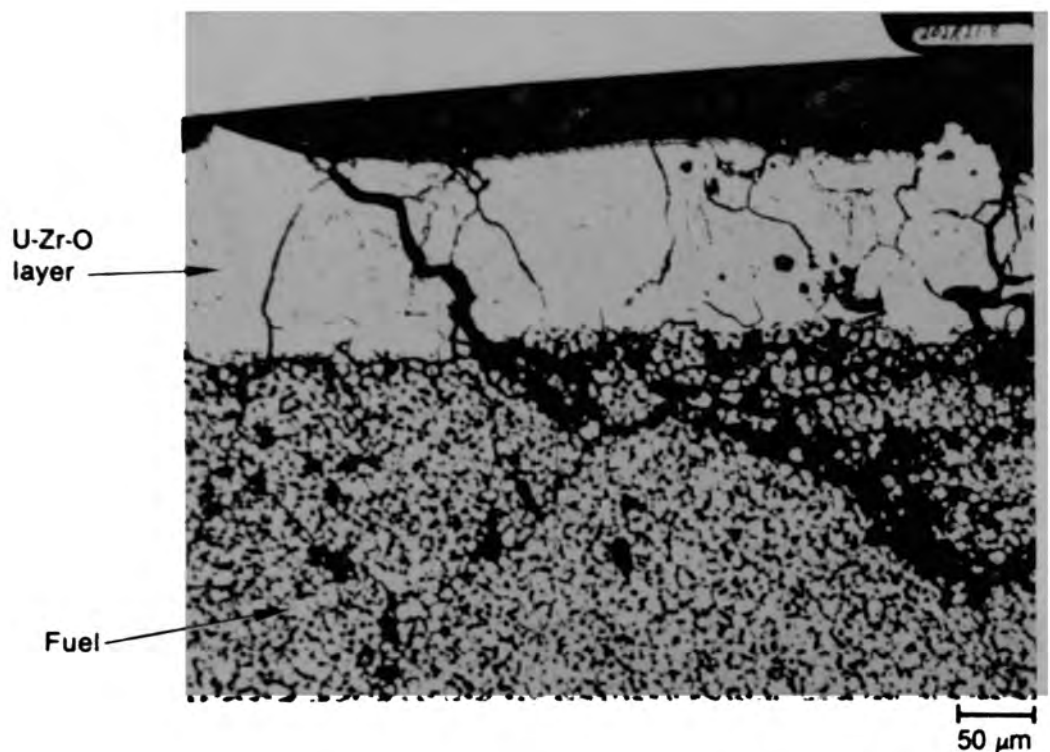
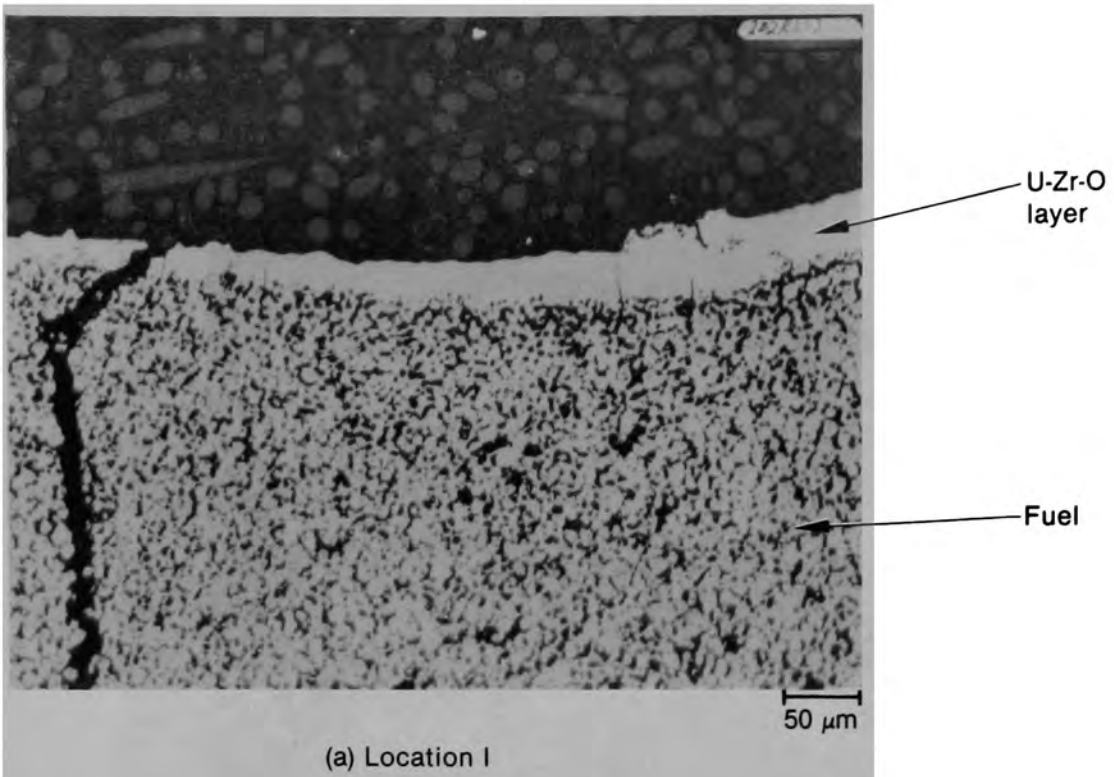
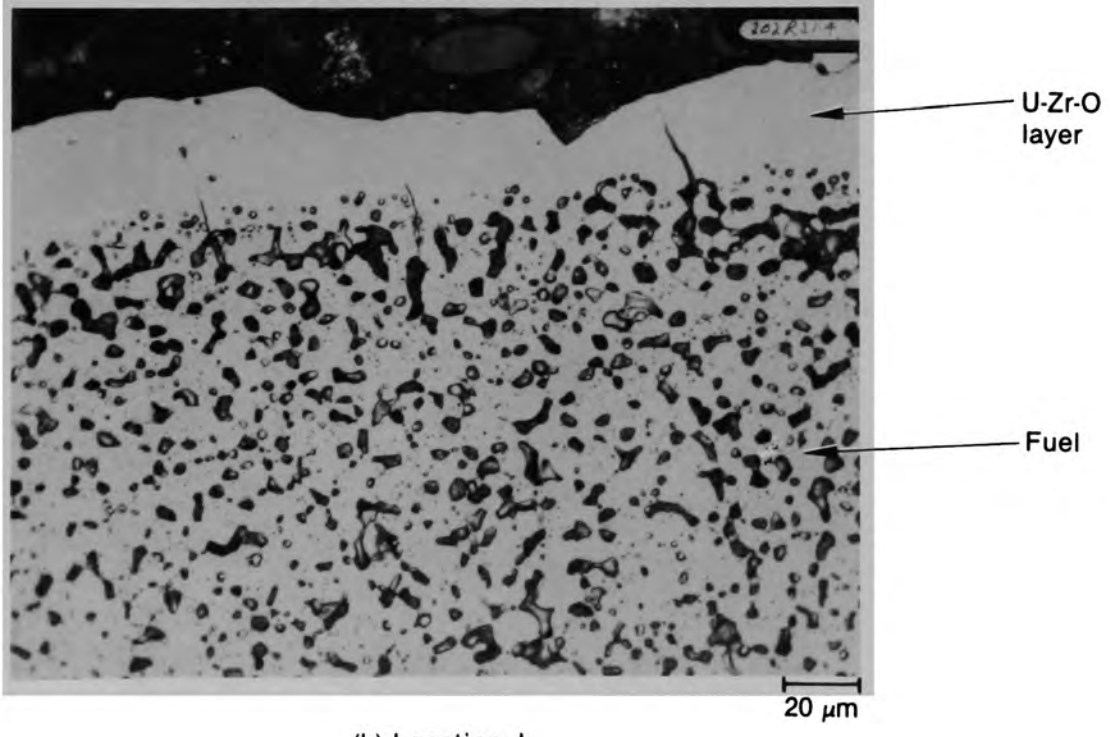


Figure C-14. Photomicrograph of Particle 1B (H8, surface) at Location H.



(a) Location I



(b) Location J

Figure C-15. Photomicrograph of Particle 1B (H8, surface) showing etched fuel grain structure.

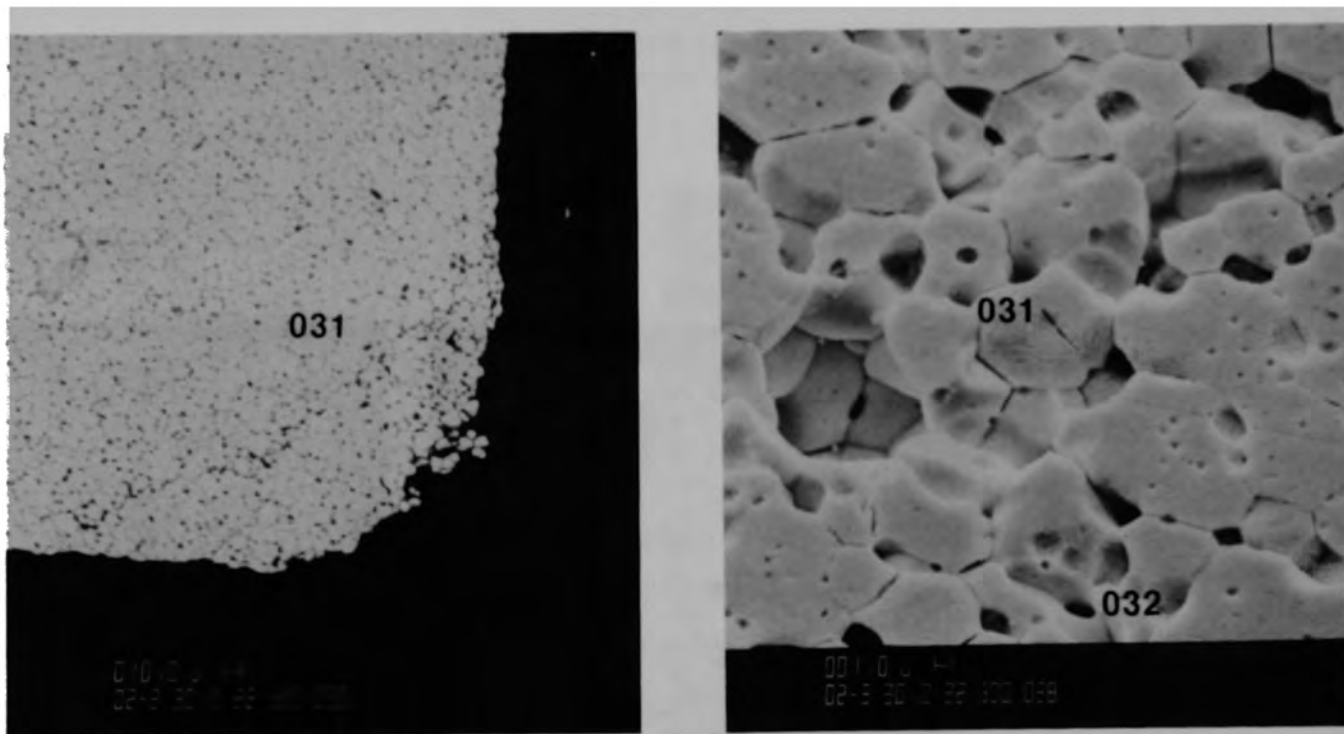


Figure C-16. SEM secondary electron image of fuel from Particle 1B (H8, surface) showing interlinked porosity.

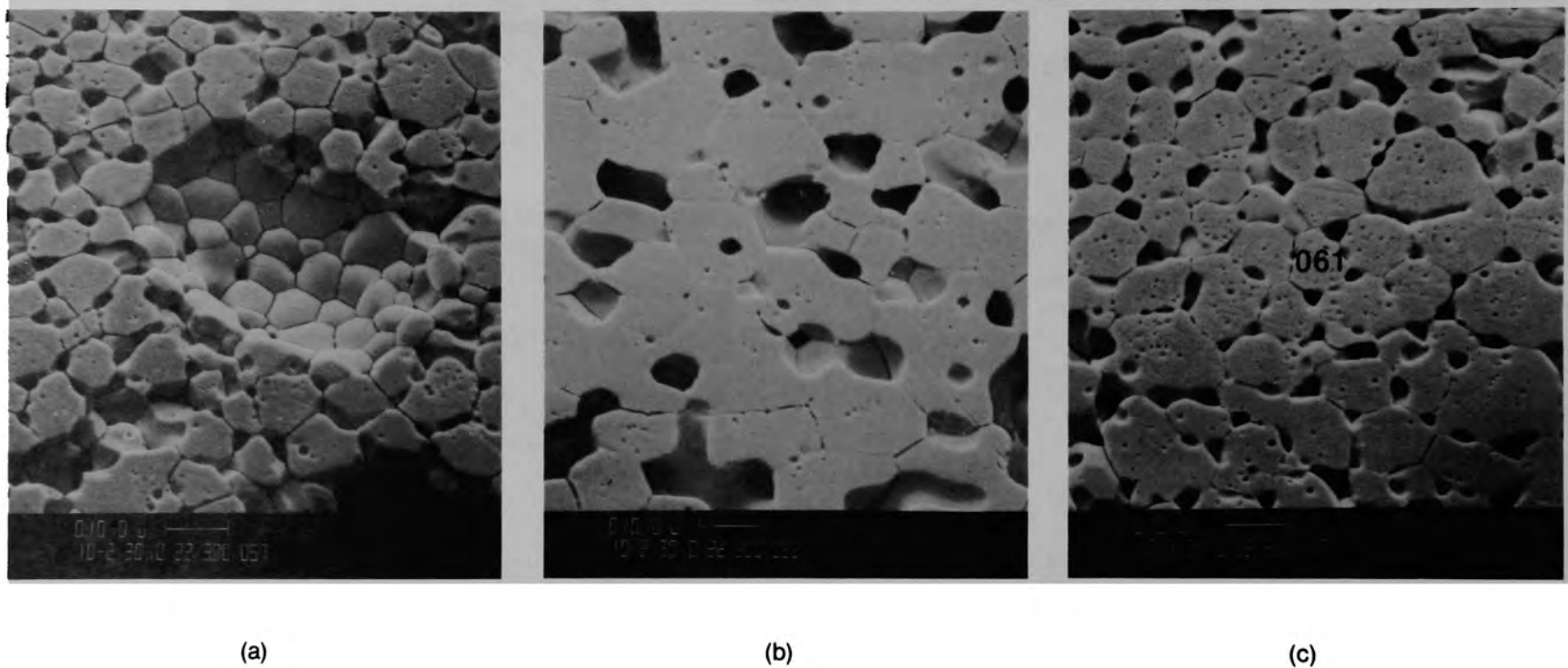


Figure C-17. SEM secondary electron image of fuel from Particle 1B (H8, surface) showing interlinked porosity.

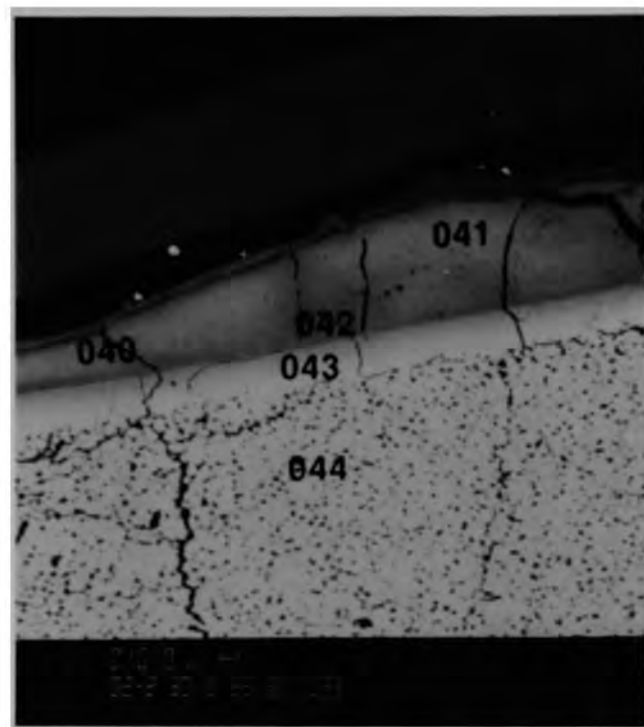


Figure C-18. SEM backscattered electron image of fuel from Particle 1B (H8, surface), corresponding to Figure C-14.

C-72

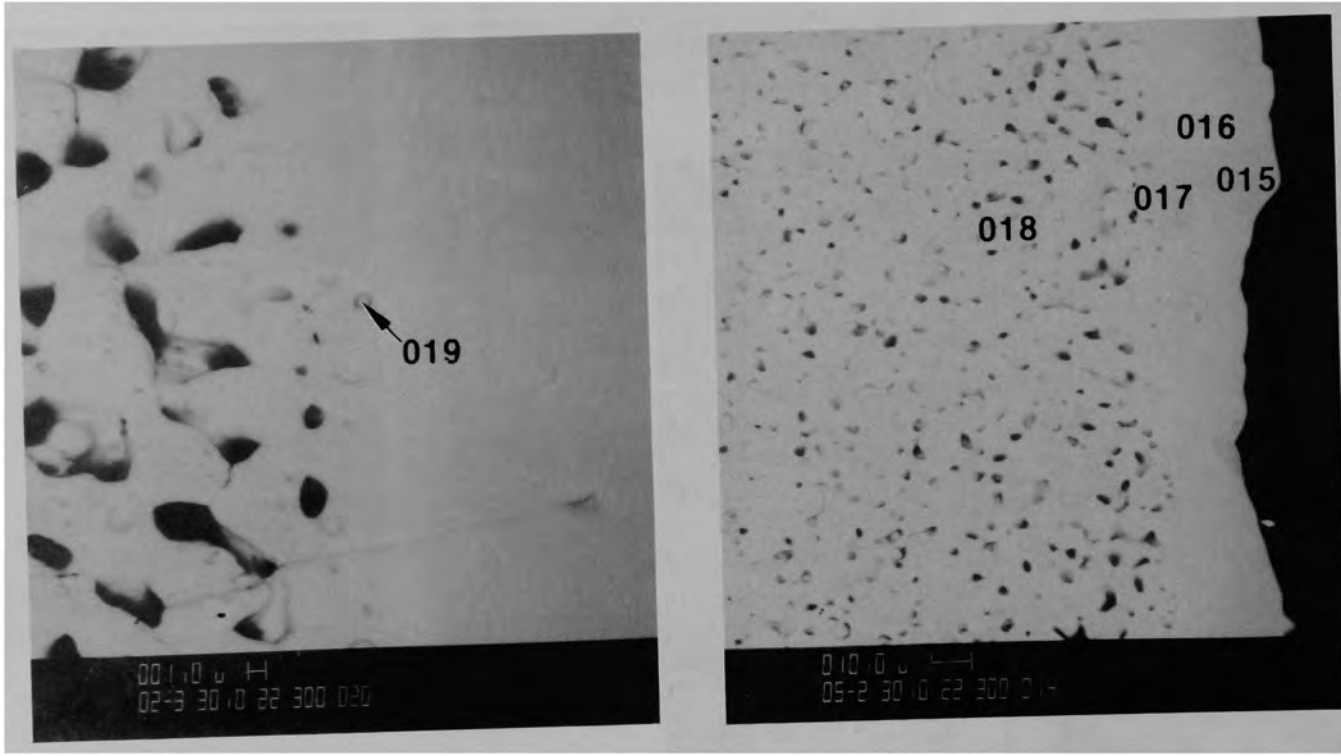


Figure C-19. SEM backscattered electron image of fuel from Particle 1B (H8, surface), corresponding to Figure C-15.

C-73

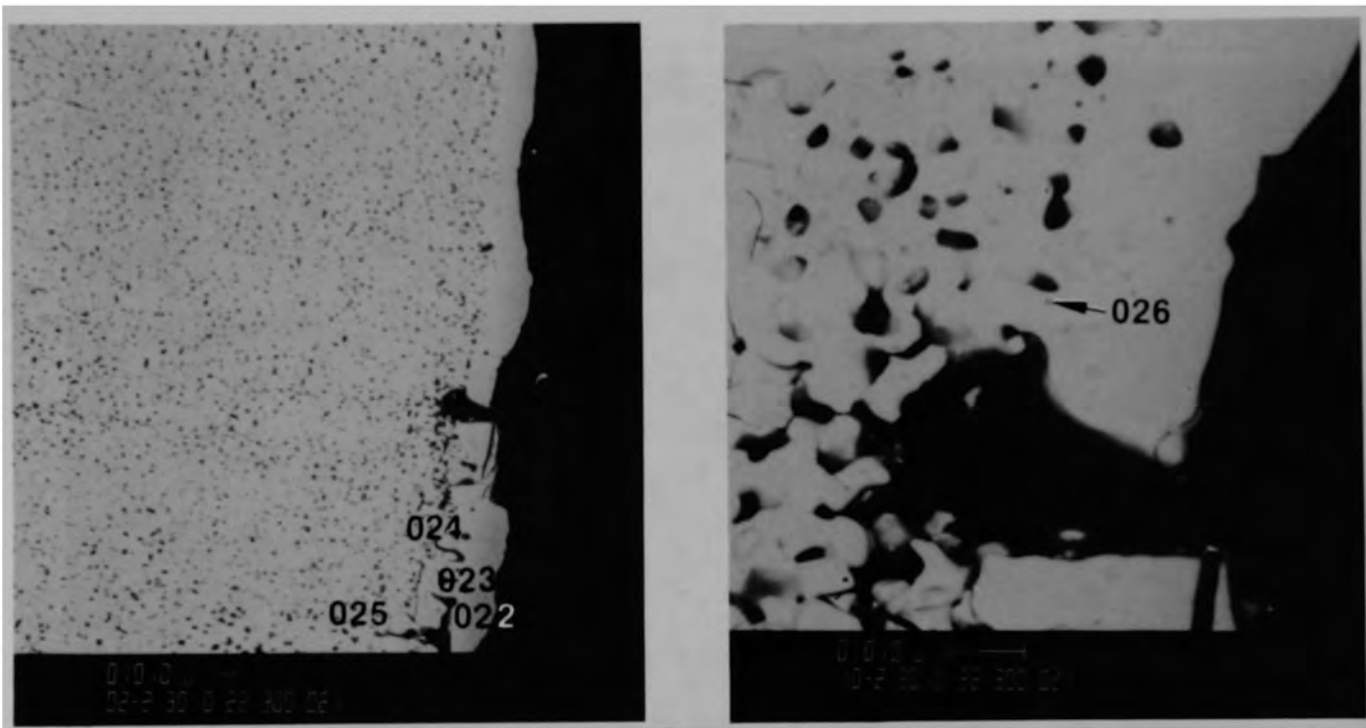


Figure C-20. SEM backscattered electron image of fuel from Particle 1B (H8, surface), corresponding to Figure C-12.

C-74

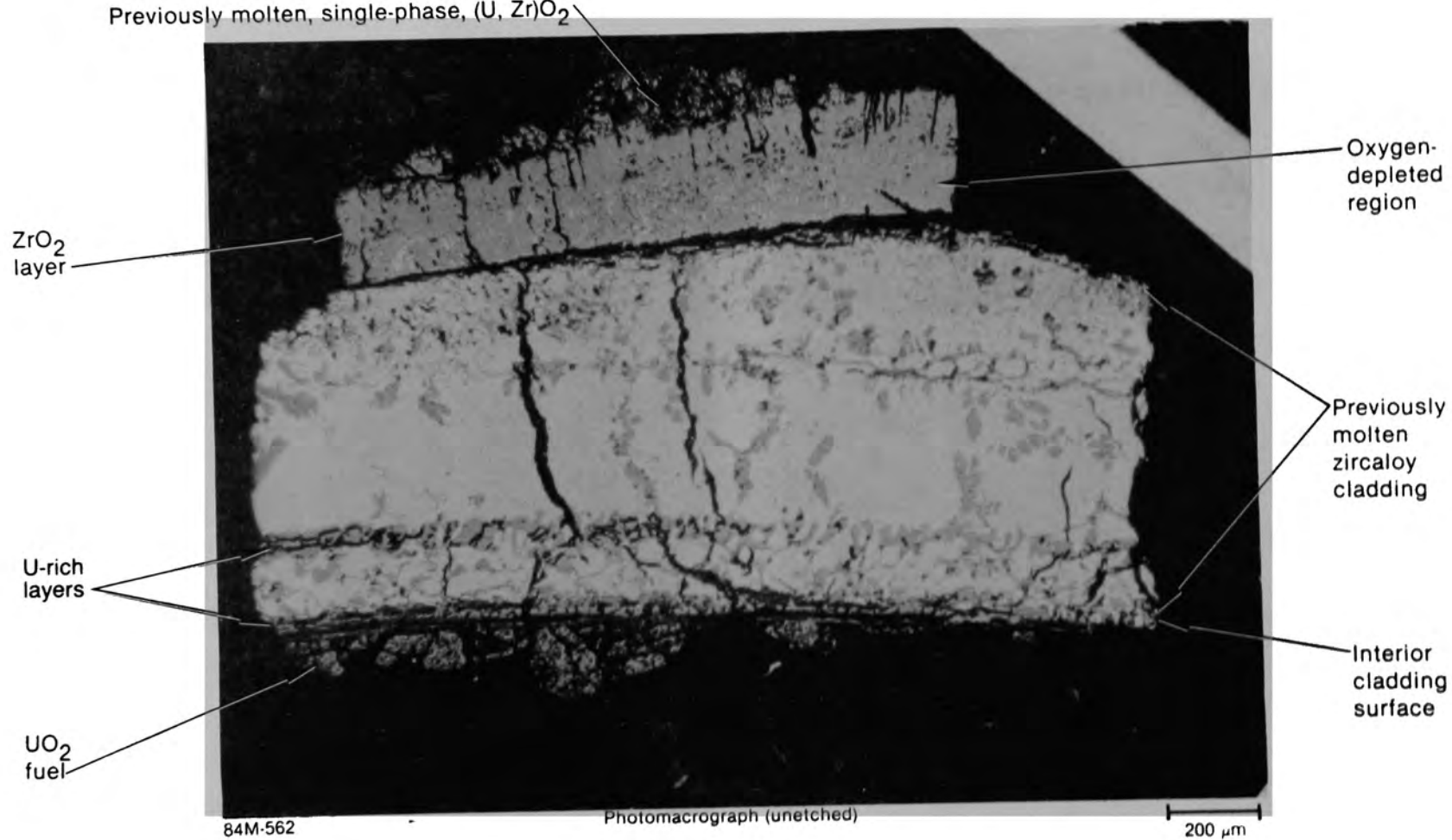
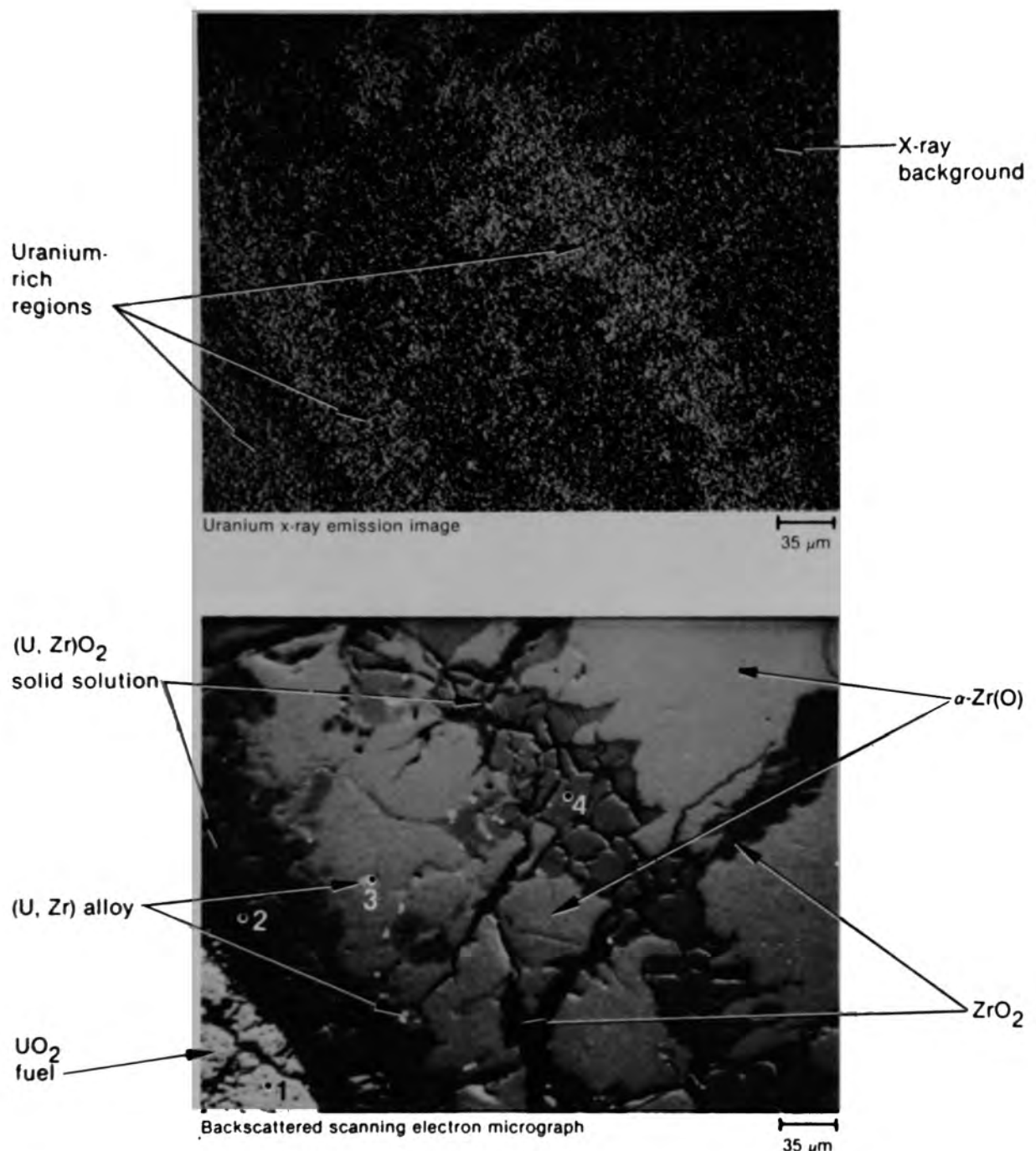
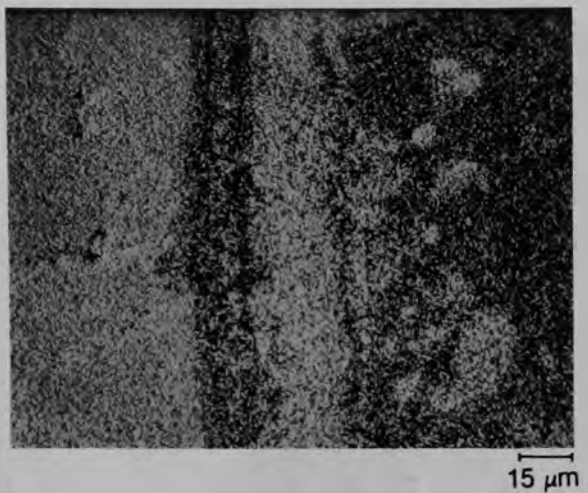


Figure C-21. Photomicrograph of Particle 1E (H8, surface) showing cladding fragment with adherent fuel and once-molten mixed ceramic.

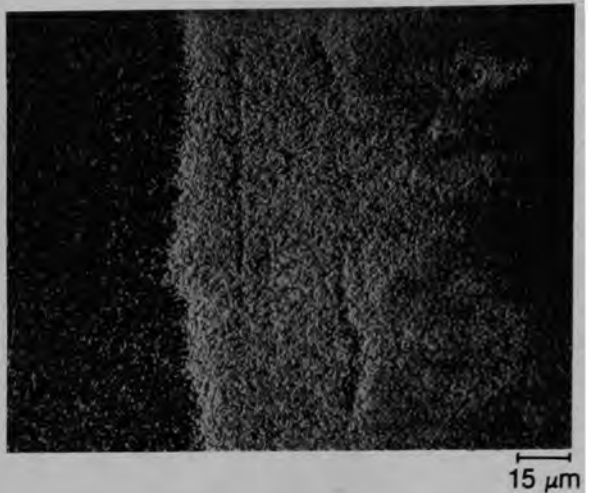


- Point 1: 100.0 weight % U
- Point 2: 33.0 weight % U, 67.0 weight % Zr
- Point 3: 83.0 weight % U, 17.0 weight % Zr
- Point 4: 32.1 weight % U, 67.9 weight % Zr

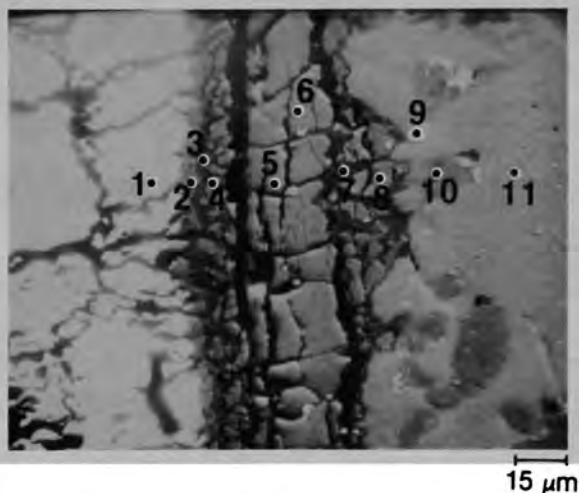
Figure C-22. Uranium and zirconium segregation near the fuel-cladding interface on Particle 1E.



Uranium X-ray emission image



Zirconium X-ray emission image

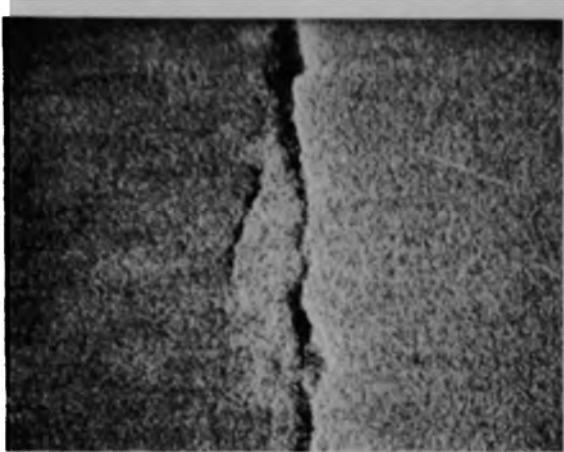


Backscattered scanning electron micrograph

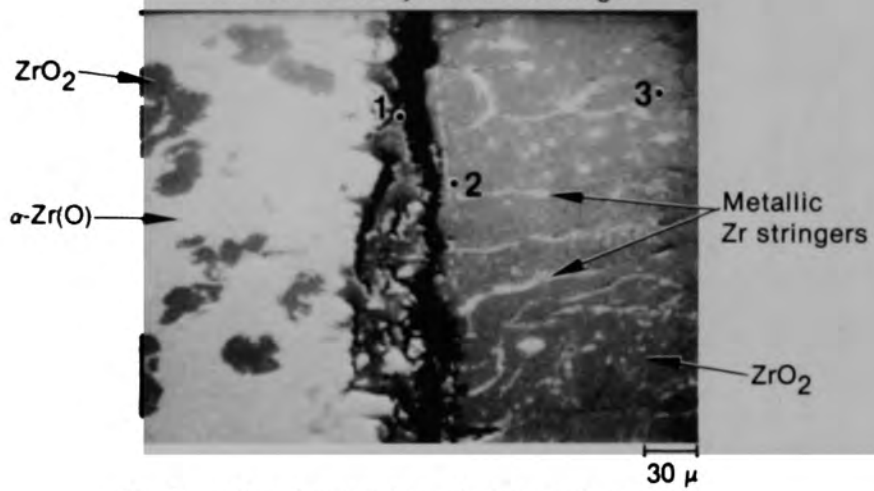
- Point 1: 100.0 weight % U
- Point 2: 25.8 weight % U, 74.2 weight % Zr
- Point 3: 100.0 weight % Zr
- Point 4: 19.6 weight % U, 80.5 weight % Zr
- Point 5: 37.0 weight % U, 63.1 weight % Zr
- Point 6: 67.4 weight % U, 32.7 weight % Zr
- Point 7: 3.8 weight % U, 10.6 weight % Cr, 14.0 weight % Fe, 71.7 weight % Zr
- Point 8: 32.0 weight % U, 68.1 weight % Zr
- Point 9: 84.6 weight % U, 15.5 weight % Zr
- Point 10: 32.3 weight % U, 67.8 weight % Zr
- Point 11: 7.8 weight % U, 92.3 weight % Zr, plus trace of Fe and Cr

Figure C-23. High magnification elemental composition finding at the pellet-cladding interface on Particle 1E.

C-77



Zirconium X-ray emission image

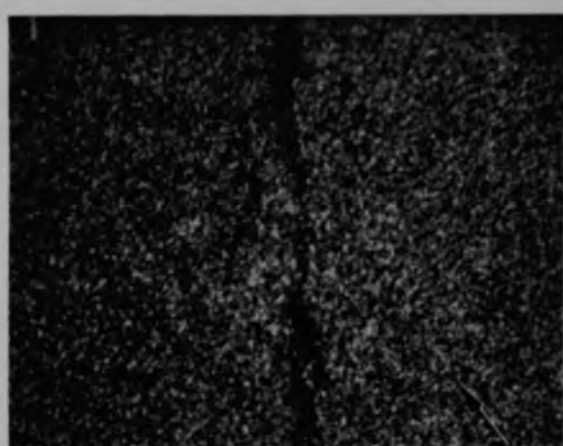


Backscattered scanning electron micrograph

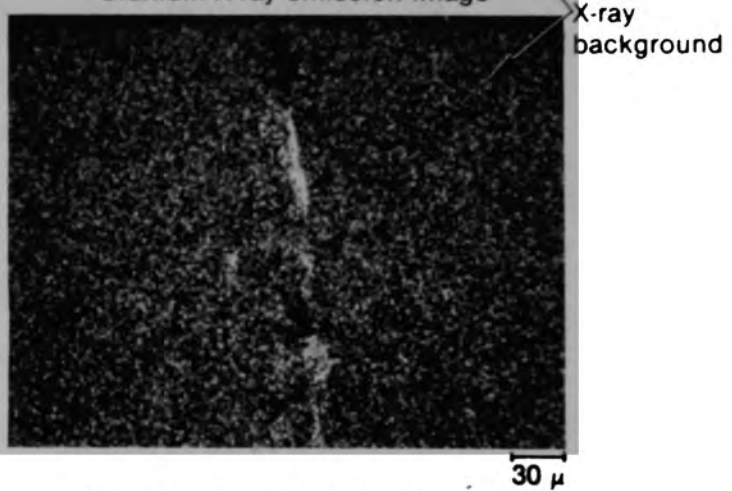
Point 1: 67.0 weight % Al, 27.2 weight % Zr, 3.0 weight % Fe, 2.8 weight % Cr

Point 2: 100.0 weight % Zr

Point 3: 100.0 weight % Zr

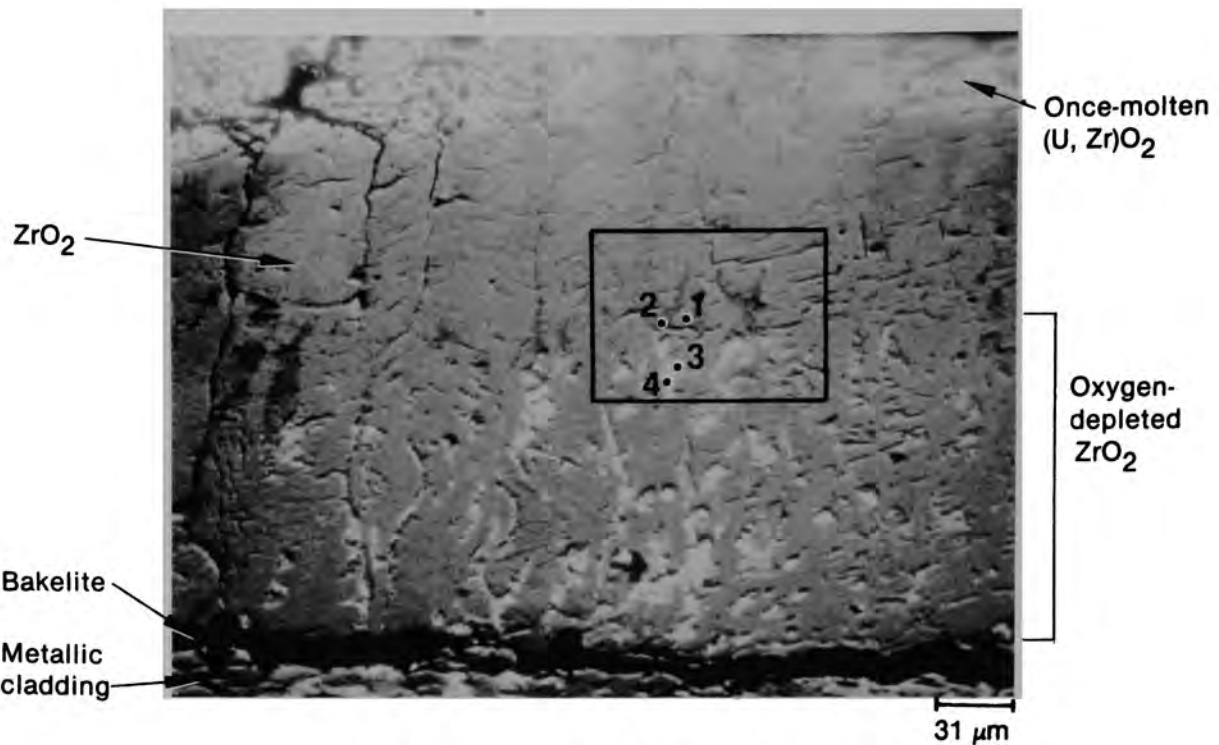


Uranium X-ray emission image



Aluminum X-ray emission image

Figure C-24. Phase distributions surrounding the Zr-ZrO₂ interface on Particle 1E.



Backscattered scanning electron micrograph

Point 1: 11.1 weight % U, 89.0 weight % Zr

Point 2: 71.3 weight % Zr, 11.4 weight % Cr, 13.6 weight % Fe, 3.8 weight % Al

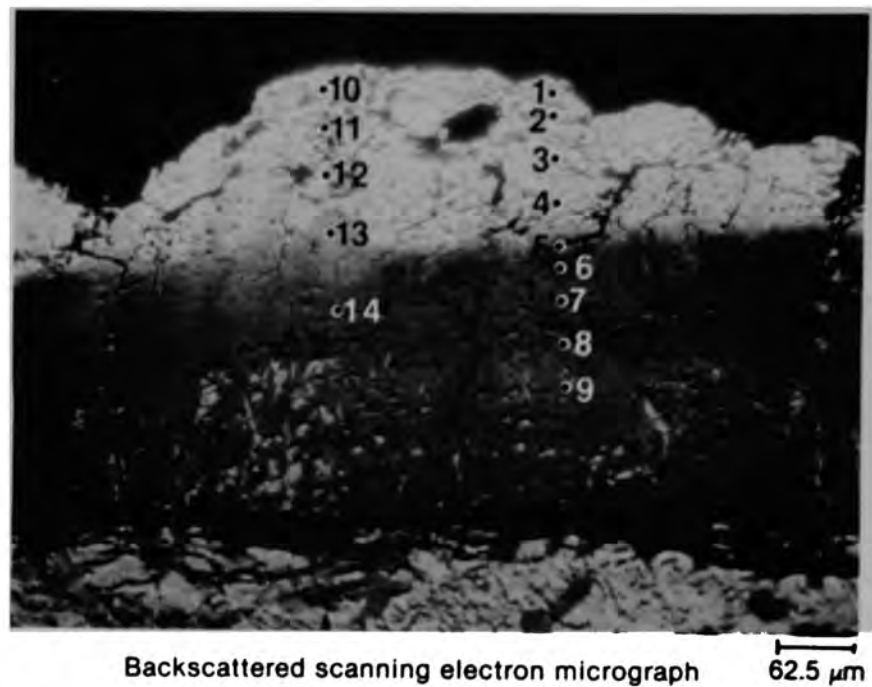
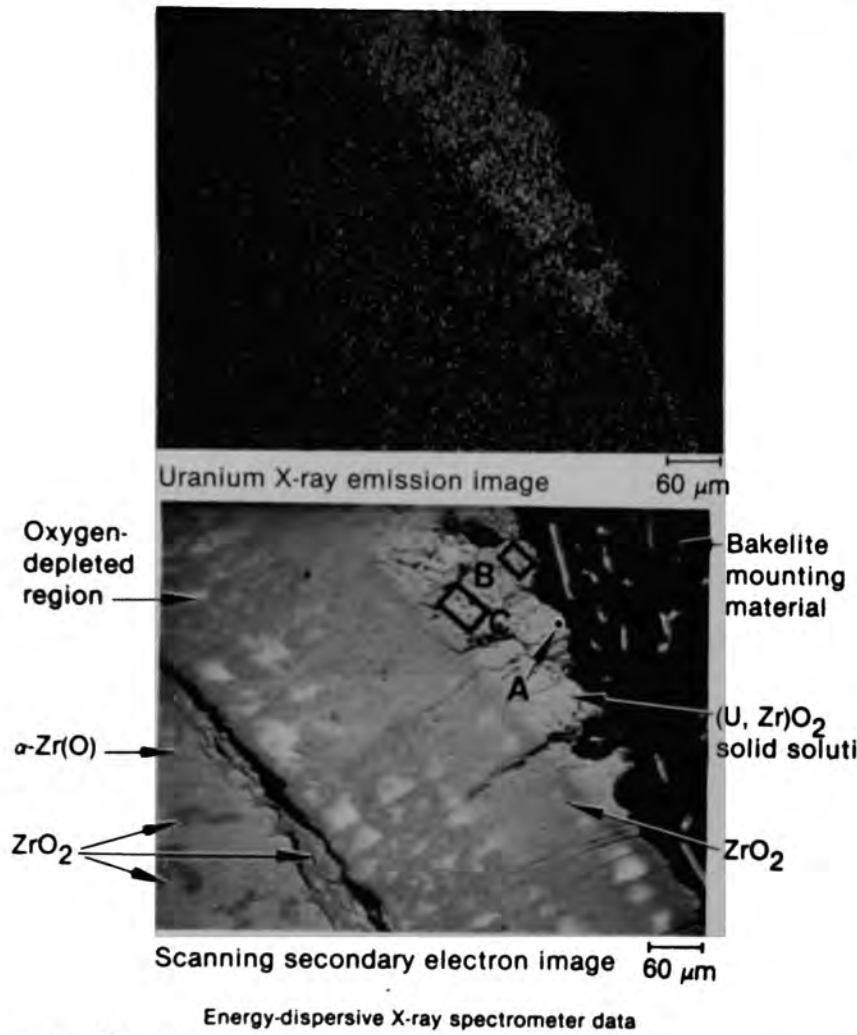
Point 3: 80.9 weight % Zr, 10.3 weight % Sn, 4.2 weight % Al, 4.0 weight % Fe,
0.6 weight % Cr

Point 4: 39.9 weight % U, 60.2 weight % Zr

Area average: 10.6 weight % U, 86.0 weight % Zr, 2.0 weight % Fe,
1.1 weight % Cr, 0.4 weight % Al, plus trace of Sn

Figure C-25. Energy-dispersive x-ray spectroscopy measurements within the ZrO₂ layer on Particle 1E.

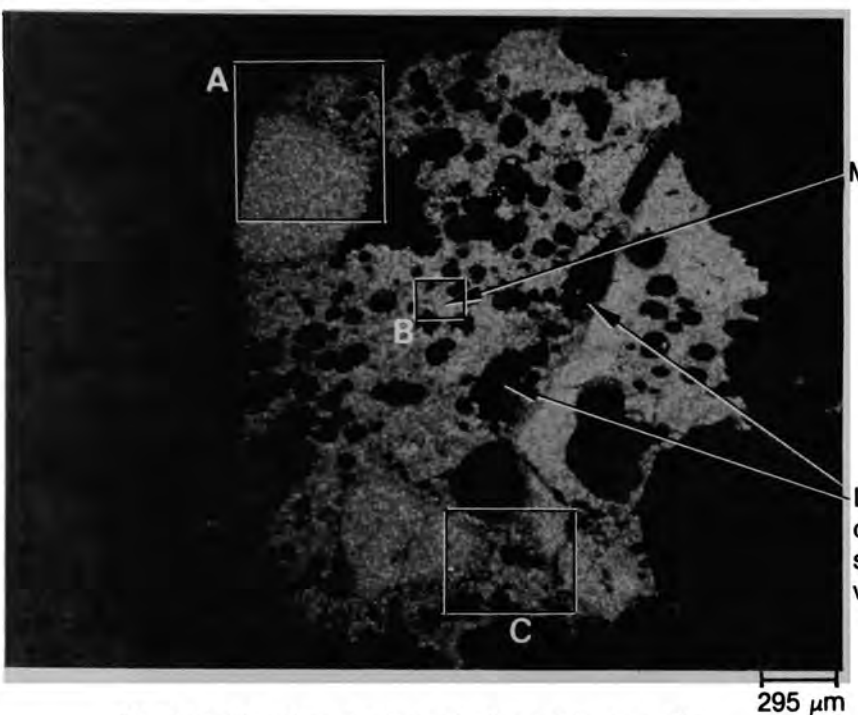
C-79



Auger electron spectroscopy data (15-μm beam size)

Point	U (atom %)	Zr (atom %)	O (atom %)	Trace elements
1	16.7	12.6	70.7	C, Cs
2	18.0	13.8	68.2	Sb, Fe
3	21.0	12.9	66.1	
4	20.9	12.8	66.3	Cr, Al
5	7.1	28.0	64.9	C
6	10.9	23.8	65.3	C, Cr
7	3.2	33.0	63.8	C
8	2.8	33.0	64.2	Fe
9	2.9	35.3	61.8	Fe, C
10	20.2	13.0	66.8	Cr
11	19.0	14.3	66.7	Cr, Fe, C
12	14.1	19.5	66.4	Cr, Fe, C
13	6.7	27.3	66.0	Pr
14	4.7	29.3	66.0	C

Figure C-26. Summary of elemental determinations on and near the adherent, once-molten mixed oxide on Particle 1E.



Backscattered scanning electron micrograph

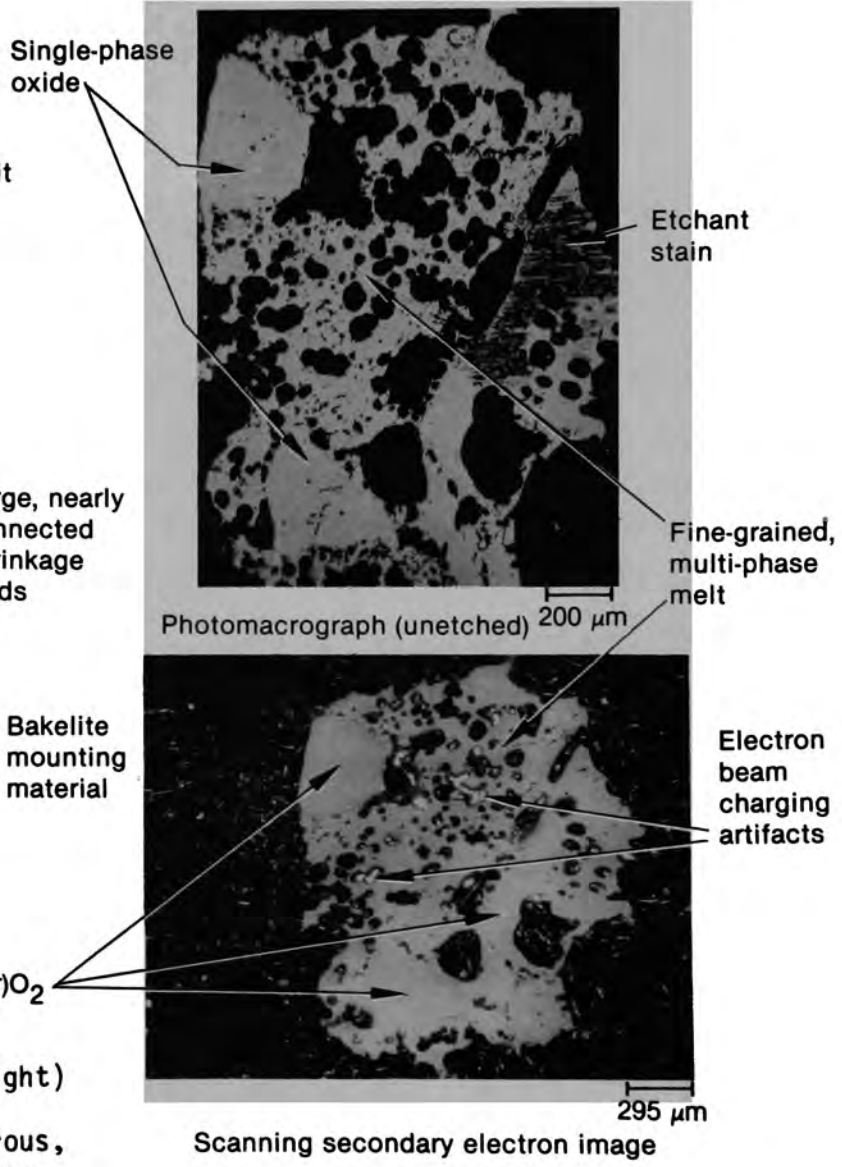


Figure C-27.

Metallographic (upper right) secondary electron (lower right) and backscattered electron images of Particle 1H, an agglomerate of single phase mixed oxide fragments and porous, multiphase (U, Zr, O) melt. Areas of Particle 1H that were investigated in detail are shown on the left.

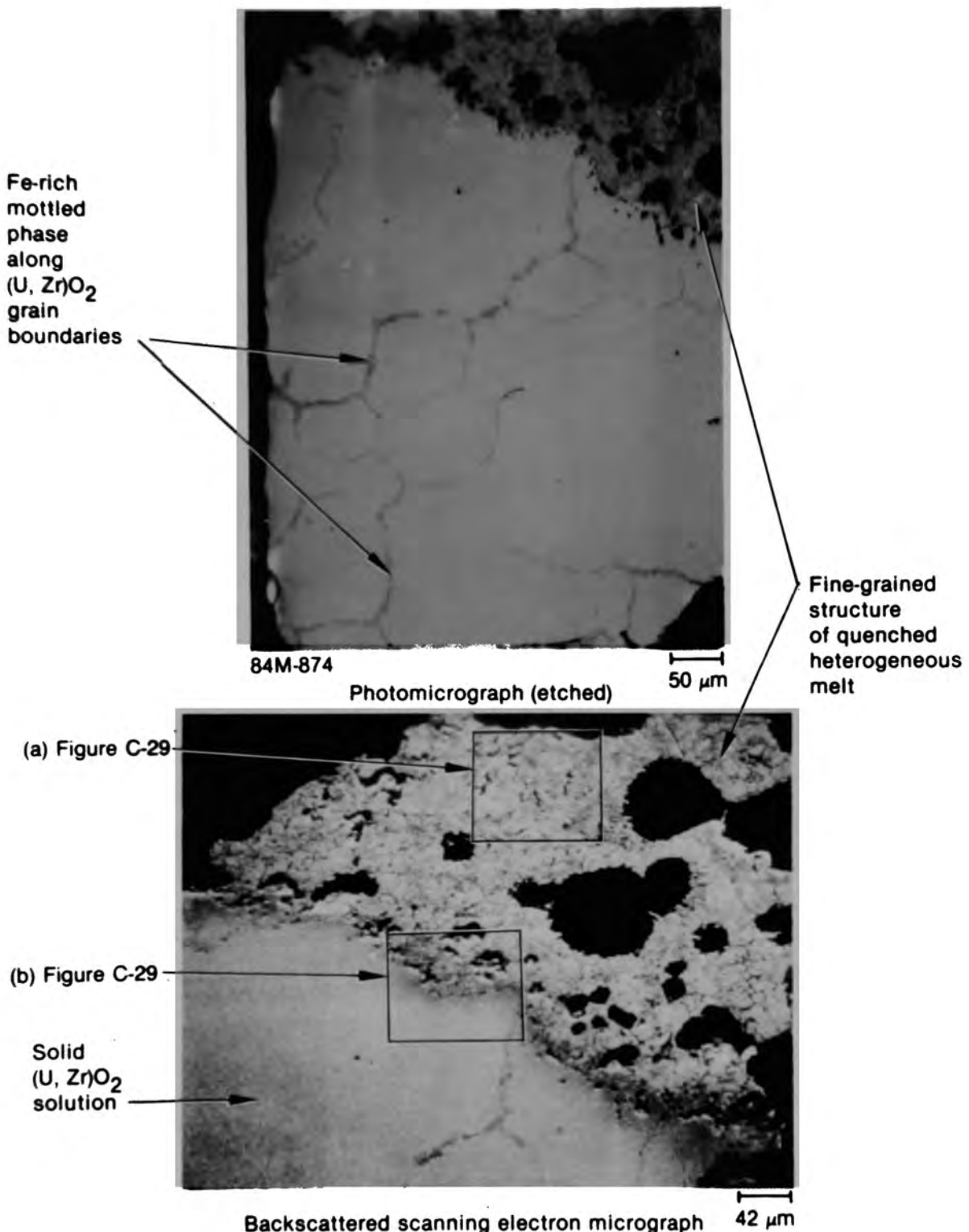
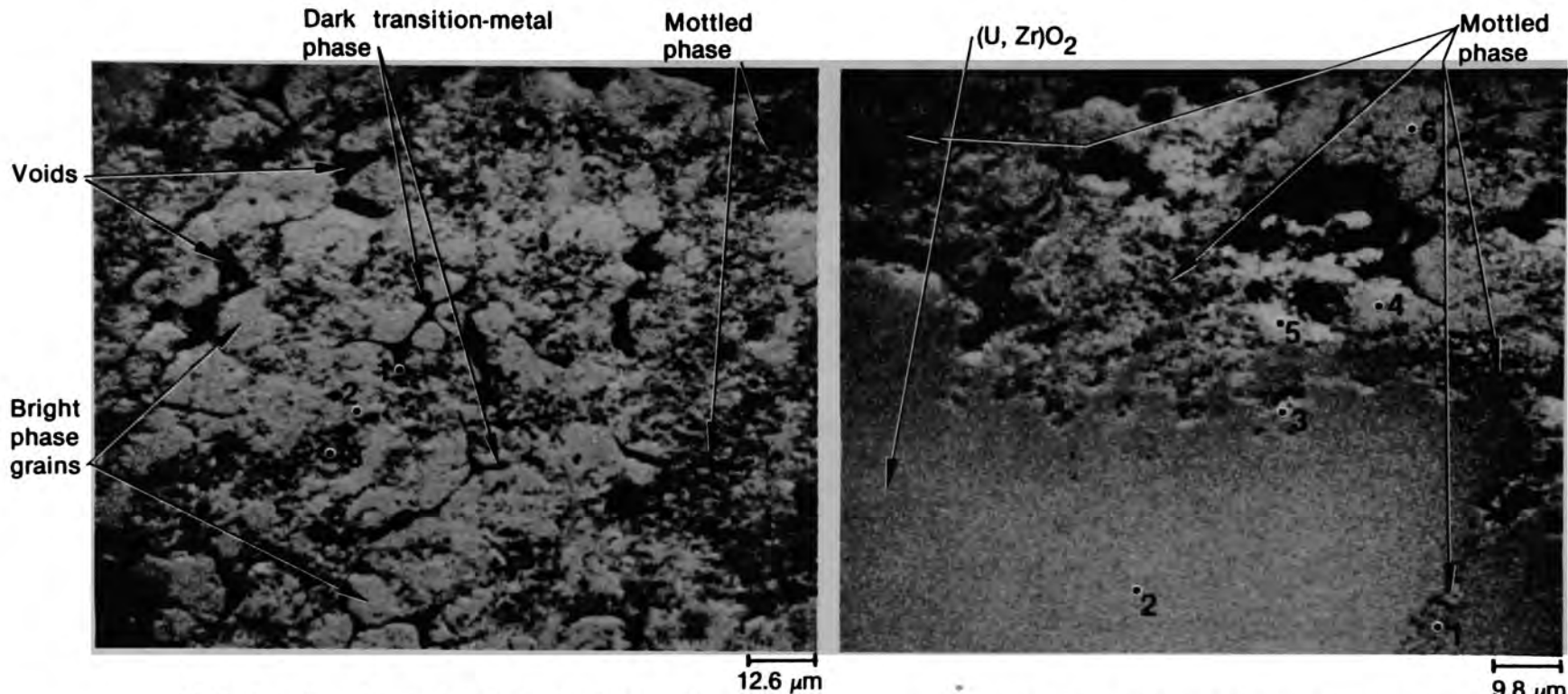


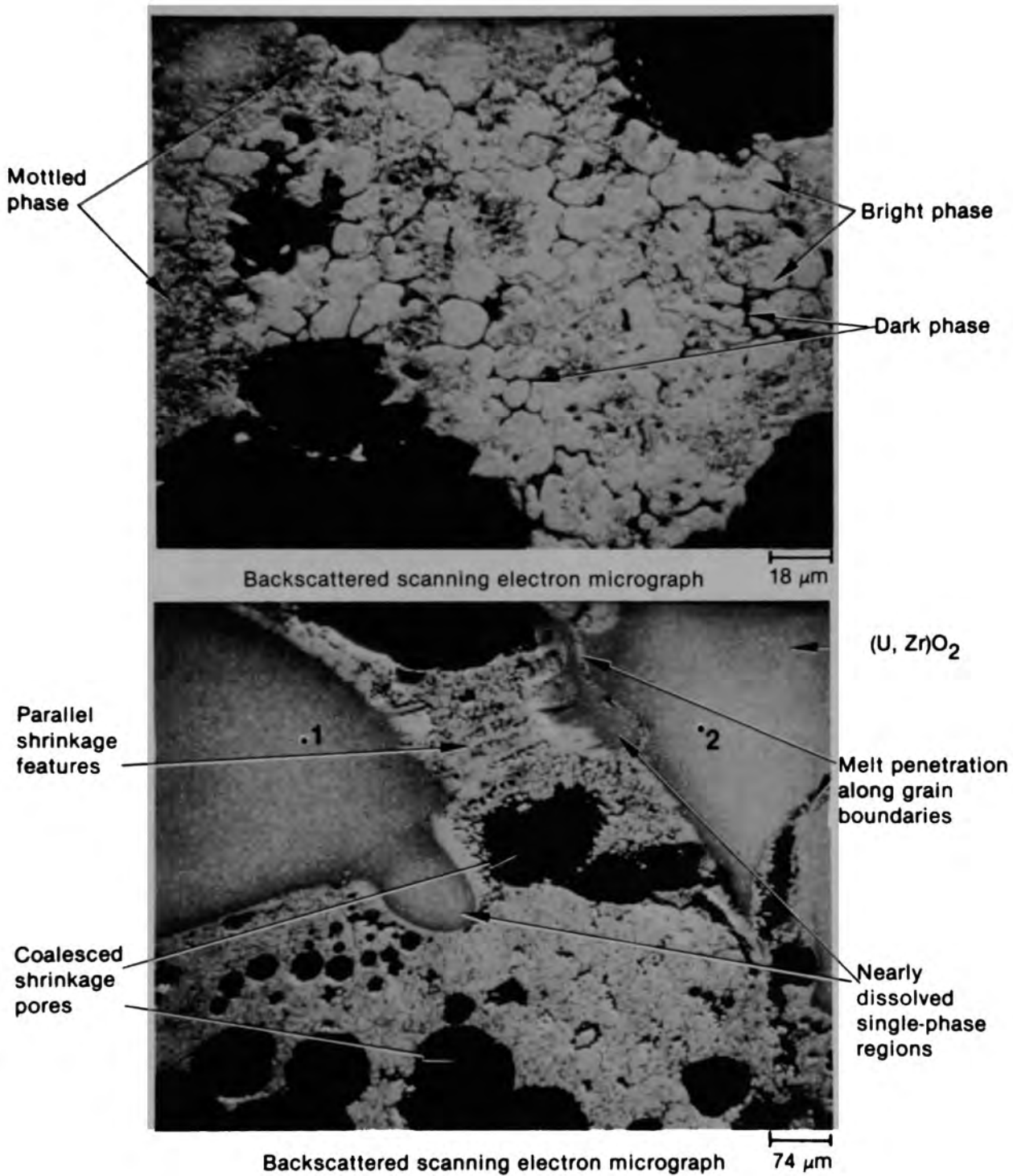
Figure C-28. Metallographic (top) and SEM appearances of (U, Zr) O₂ attack along grain boundaries by an iron rich melt phase, within area A of Particle 1H. Lower image shows locations in which primary composition measurements were made.



Point 1: 24.6 weight % U, 11.1 weight % Zr, 25.7 weight % Fe,
12.5 weight % Ni, 17.4 weight % Cr, 8.7 weight % Al
Point 2: 70.1 weight % U, 26.0 weight % Zr, 3.9 weight % Fe,
Point 3: 53.6 weight % U, 40.5 weight % Zr, 5.9 weight % Fe,
Area Average (approx.): 68 weight % U, 28 weight % Zr, 4 weight % Fe,
plus traces of Ni, Cr, and Al

Point 1: 53.6 weight % U, 42.2 weight % Zr, 4.2 weight % Fe,
Point 2: 58.7 weight % U, 41.3 weight % Zr
Point 3: 43.6 weight % U, 18.4 weight % Zr, 22.4 weight % Fe,
7.3 weight % Ni, 4.4 weight % Al, 3.9 weight % Cr
Point 4: 64.8 weight % U, 31.1 weight % Zr, 4.1 weight % Fe,
Point 5: 50.9 weight % U, 38.4 weight % Zr, 8.0 weight % Fe,
1.7 weight % Ni, 1.0 weight % Cr
Point 6: 66.1 weight % U, 29.5 weight % Zr, 4.4 weight % Fe,

Figure C-29. Melt phase structures away from (left) and adjacent to (U,Zr) O_2 fragment in region A of Particle 1H.



Area B Average (approx.): 68 weight % U, 28 weight % Zr, 4 weight % Fe, plus traces of Ni, Cr, and Al

Point 1 (approx.): 67 weight % U, 33 weight % Zr

Point 2: 67.3 weight % U, 32.7 weight % Zr

Figure C-30. Regions B (upper) and C (lower) of Particle 1H. Note similarities in heterogeneous melt appearance and in wetting of (U, Zr) O_2 fragments to Region A (Figure C-29).

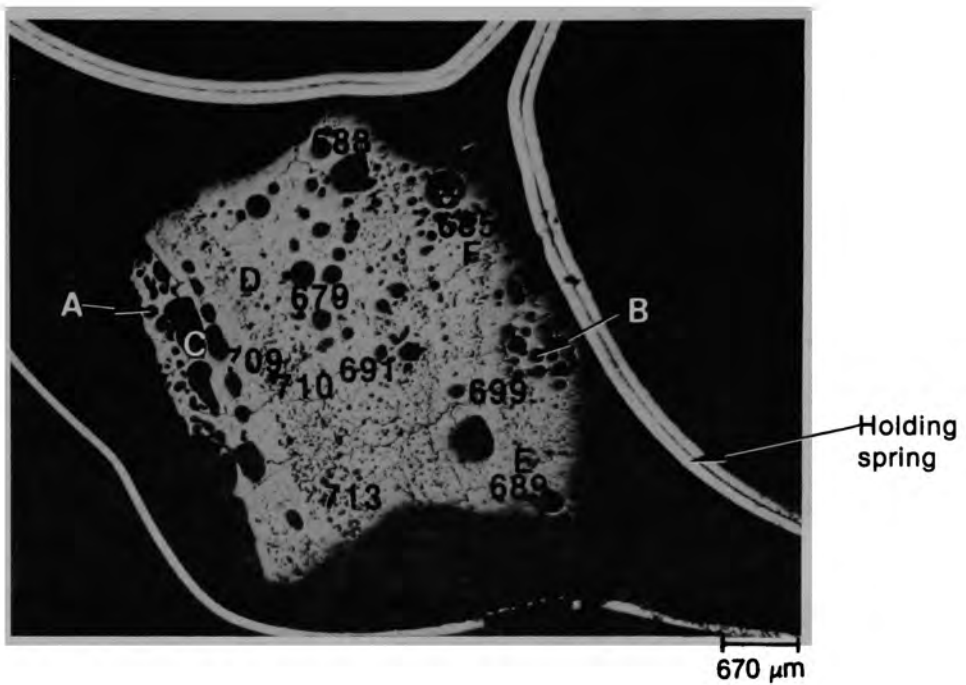
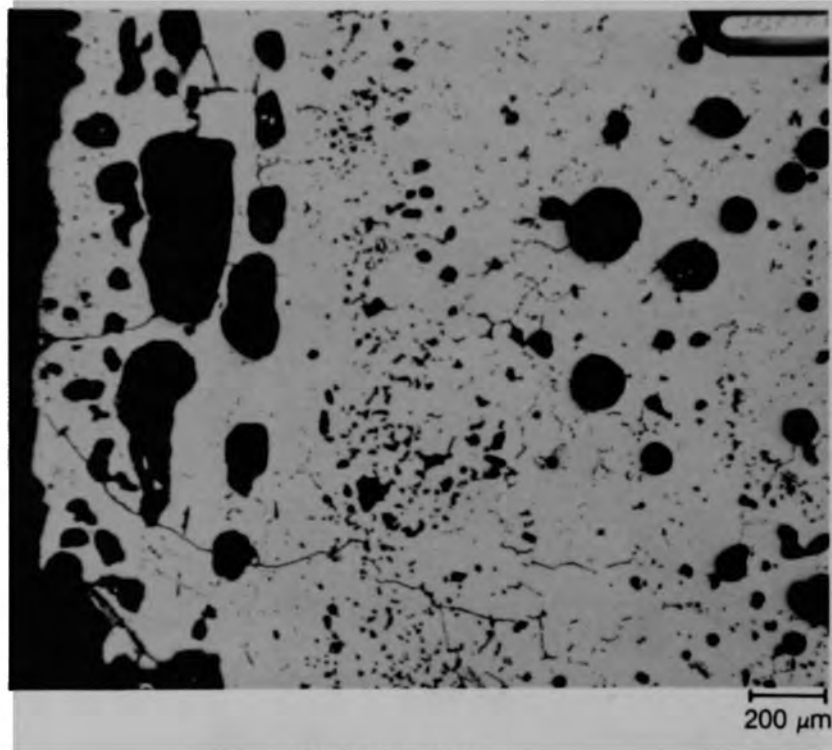
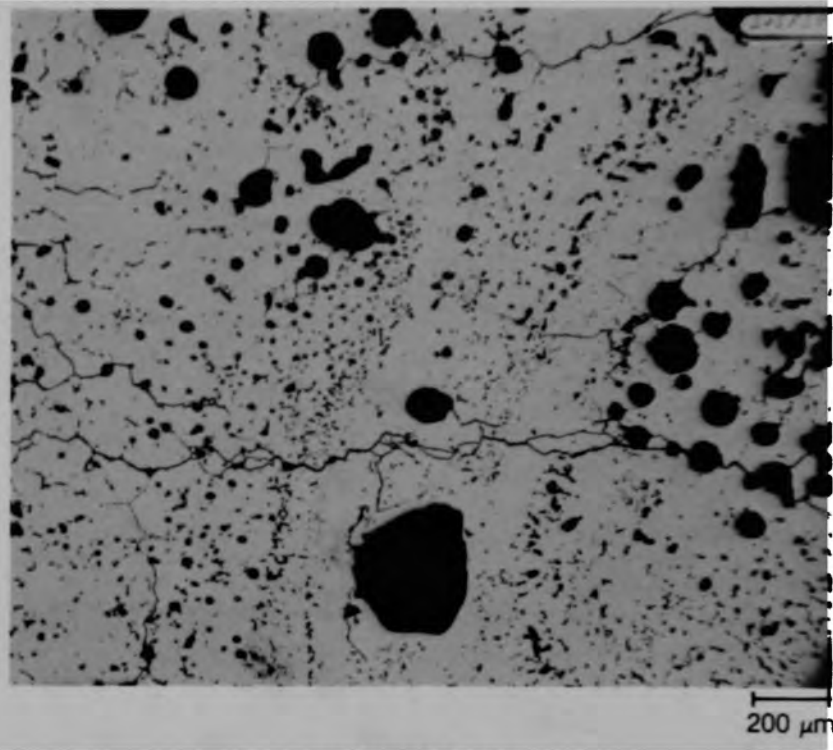


Figure C-31. Photomacrograph of Particle 3L (H8, 56 cm).



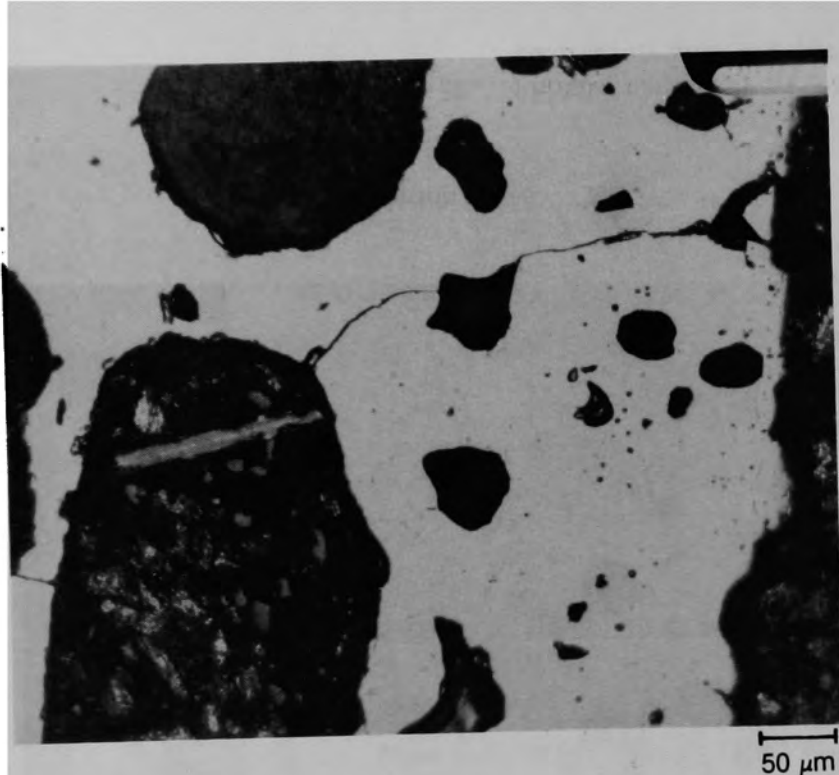
(a) Location A



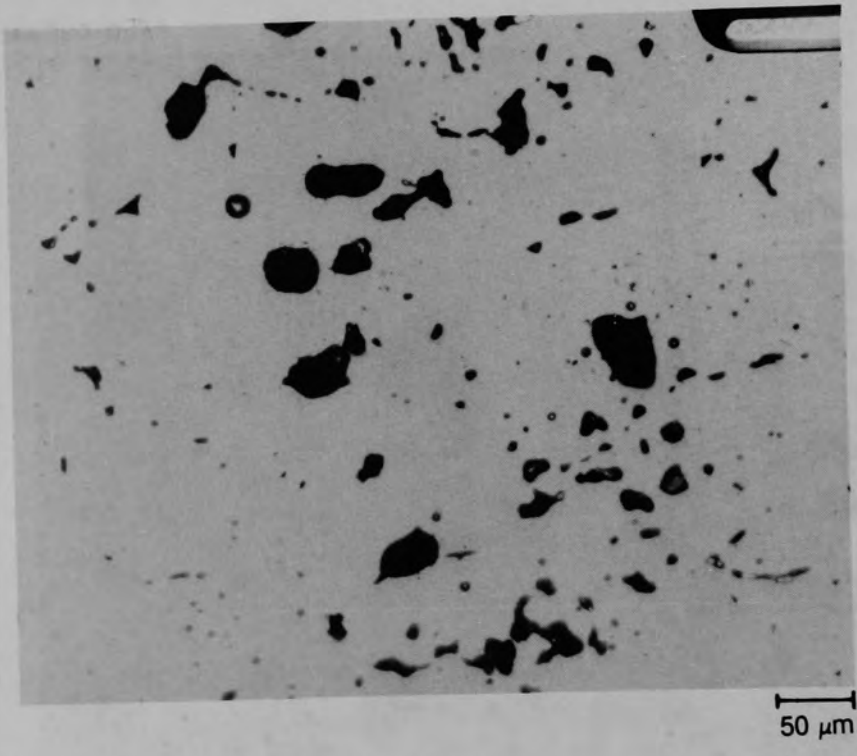
(b) Location B

Figure C-32. Photomicrograph of Particle 3L (H8, 56 cm) in the unetched condition showing pore morphology.

C-986



(a) Location C



(b) Location D

Figure C-33. Photomicrograph of Particle 3L (H8, 56 cm) in the etched condition showing pore morphology.

C-87



(a) Location E



(b) Location F

Figure C-34. Photomicrograph of Particle 3L (H8, 56 cm) in the etched condition showing pore morphology.

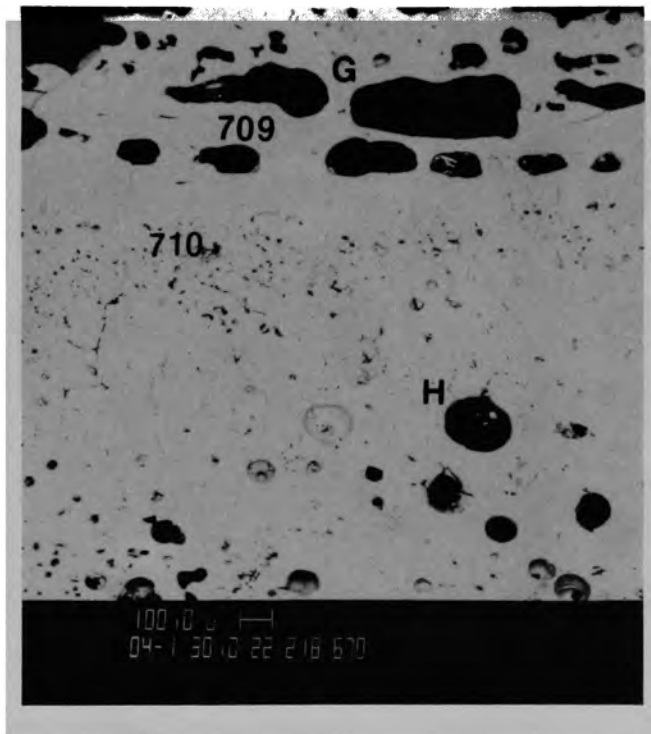


Figure C-35. SEM backscattered electron image at Location C of Particle 3L (H8, 56 cm).

C-89

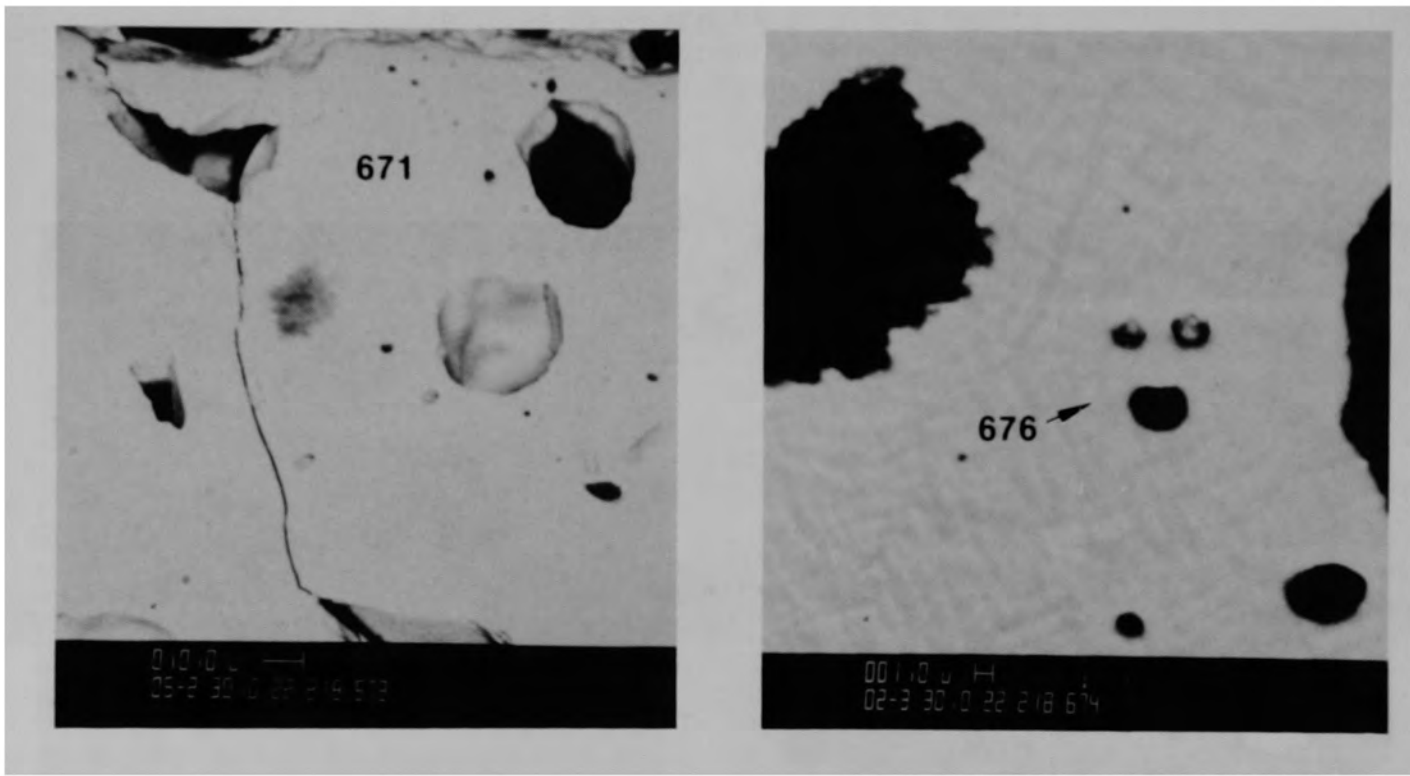


Figure C-36. SEM backscattered electron images of Particle 3L (H8, 56 cm) showing fine grain structure, corresponding to location G on Figure C-35.

C-90

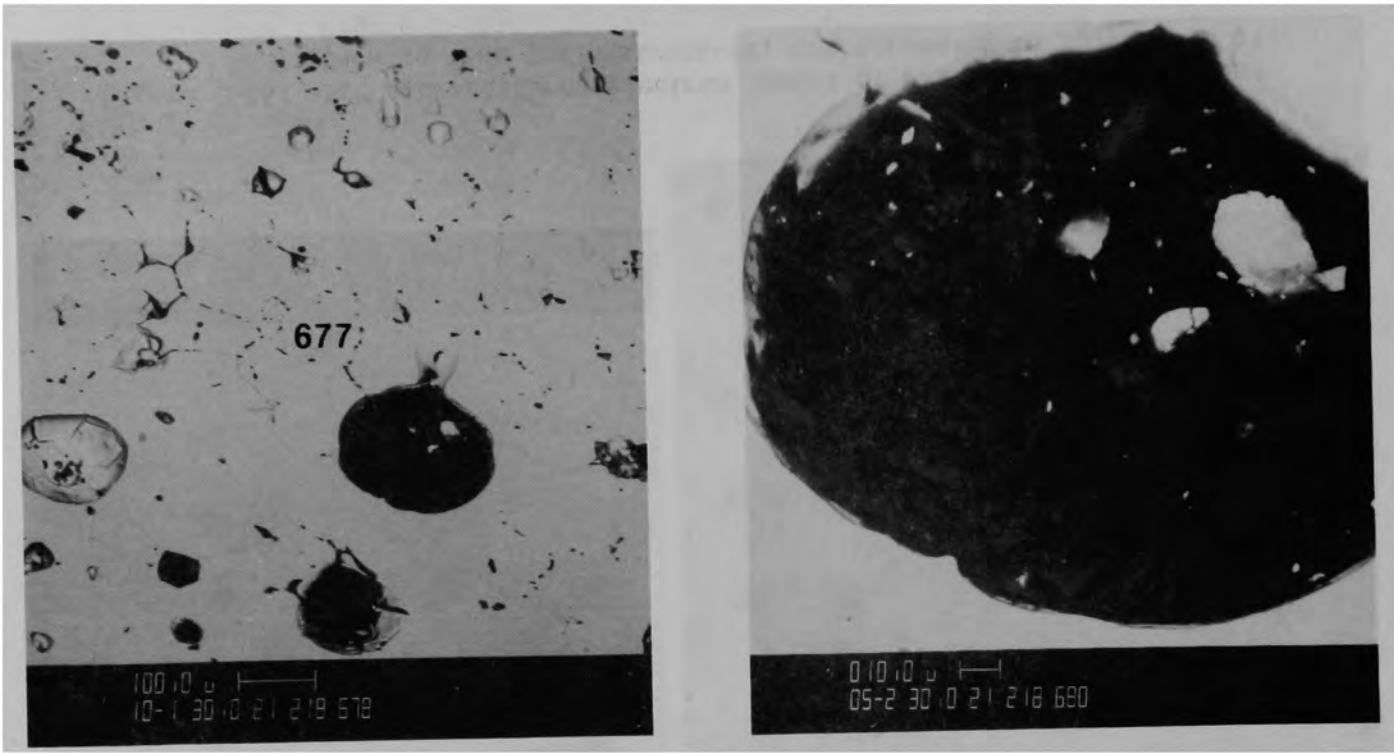


Figure C-37. SEM backscattered electron images of Particle 3L (H8, 56 cm)
corresponding to location H on Figure C-35.

C-91

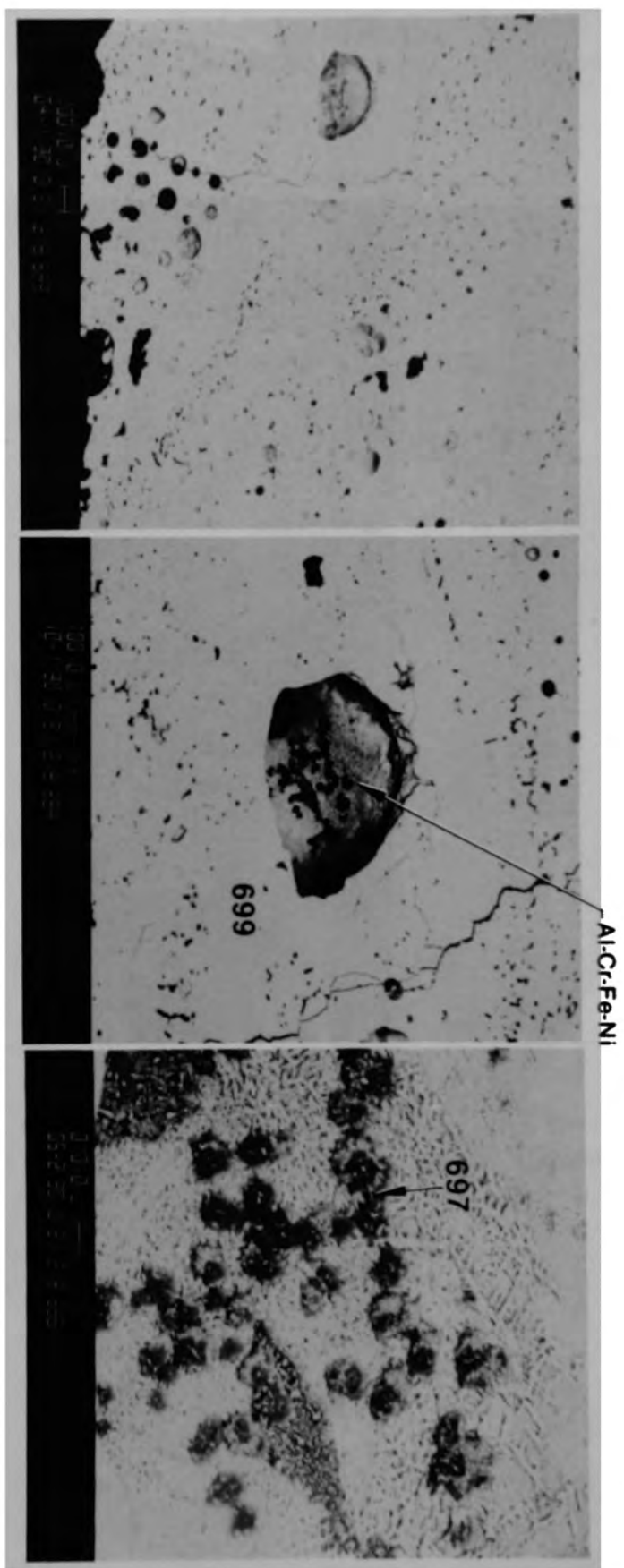


Figure C-38. SEM backscattered electron image of Particle 3L (H8, 56 cm) showing Al-Cr-Fe-Ni phase in large pores.

C-92

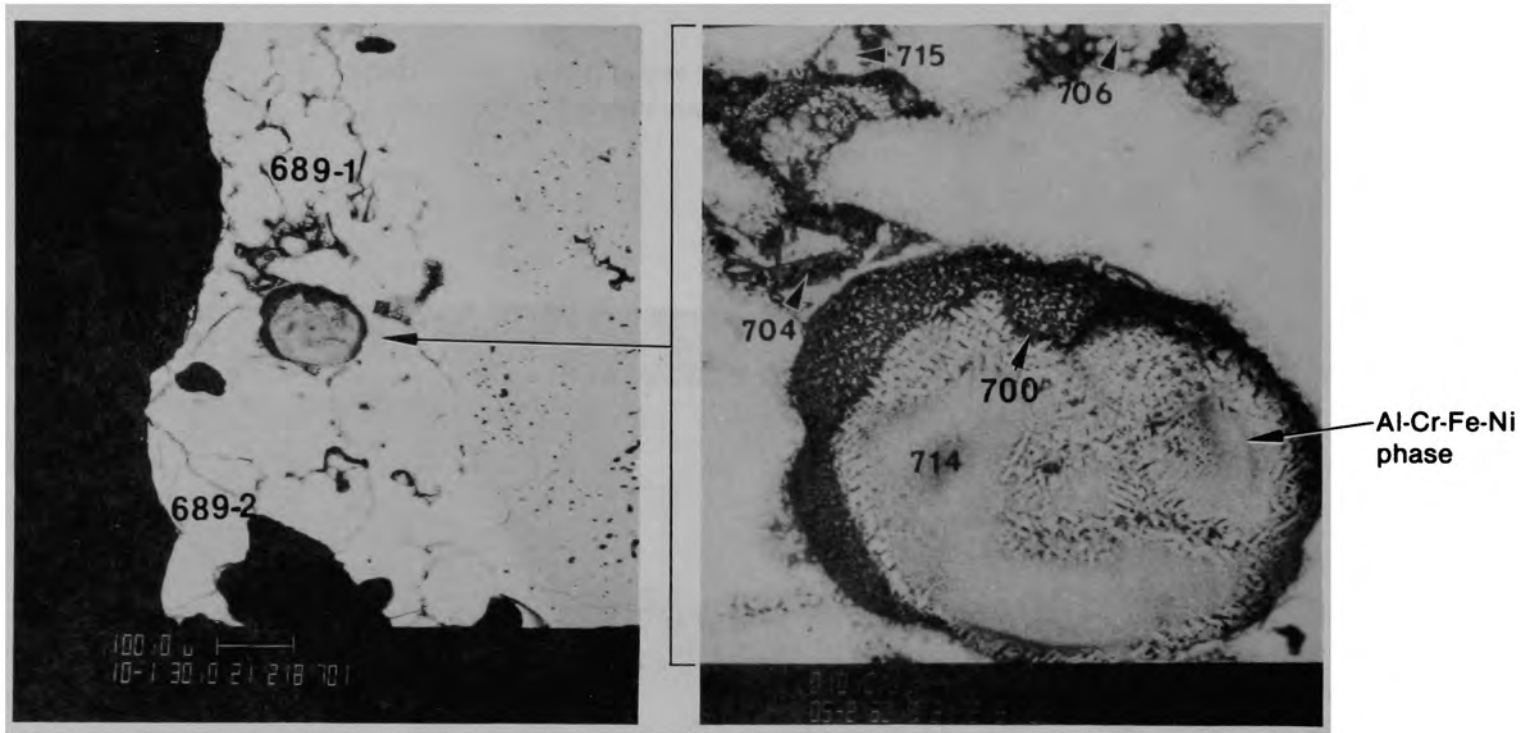


Figure C-39. SEM backscattered electron images of Particle 3L (H8, 56 cm) showing Al-Cr-Fe-Ni phase in large pores.

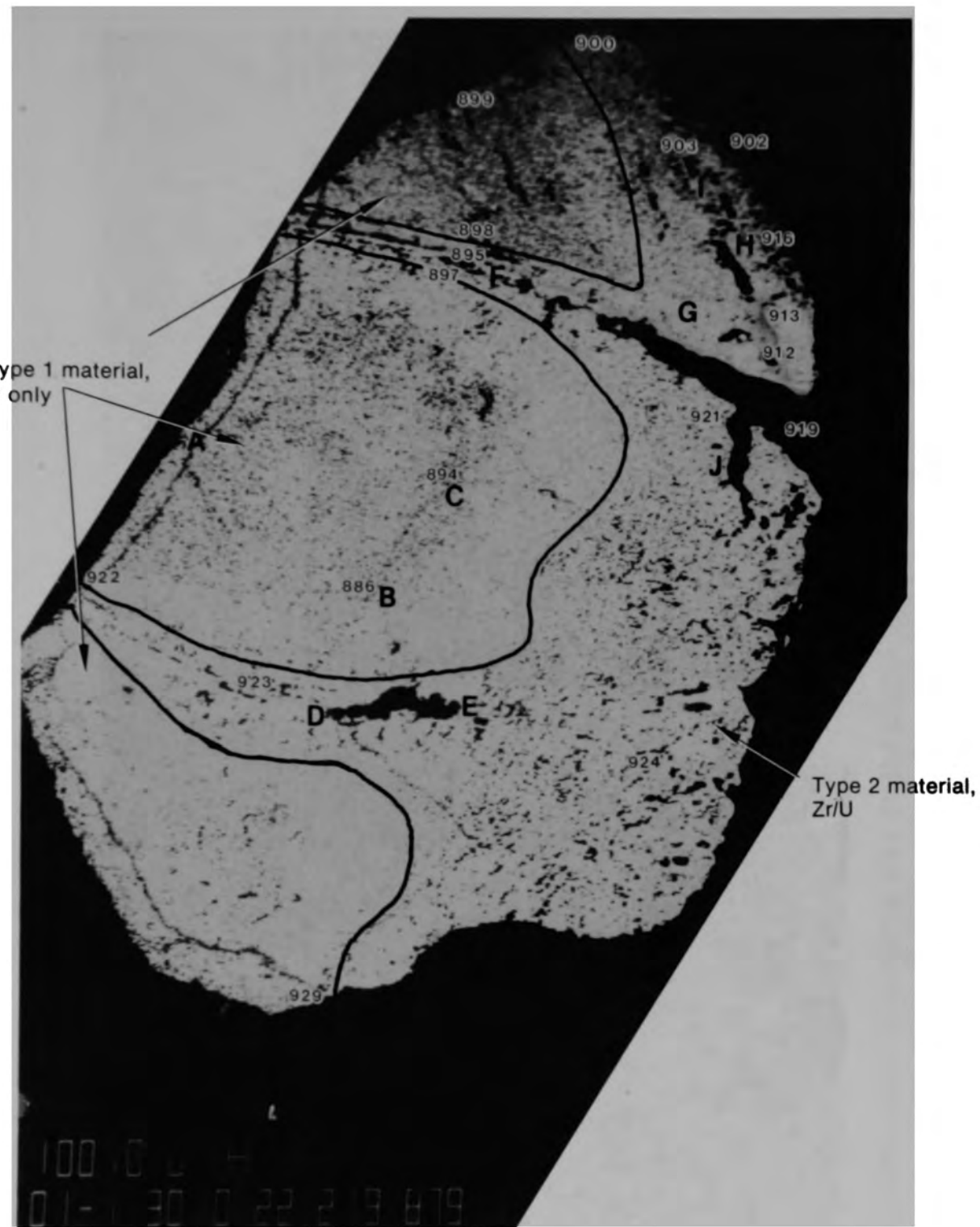
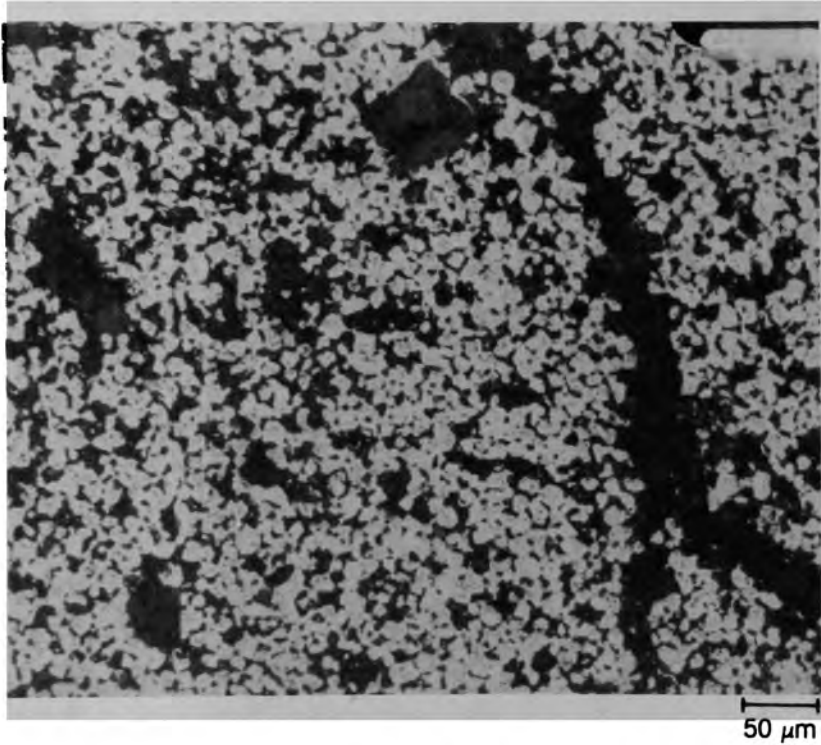
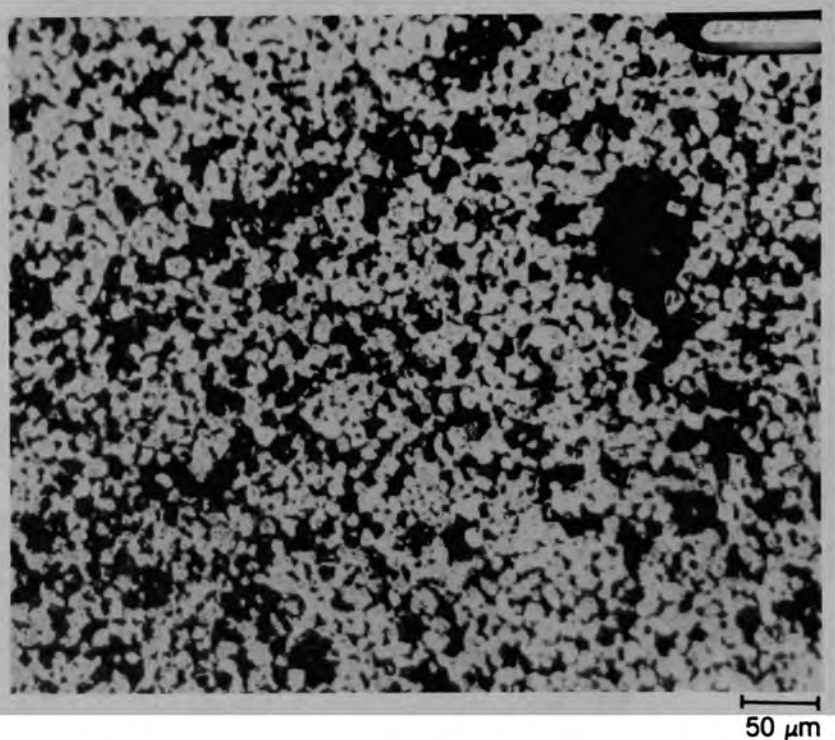


Figure C-40. Photomacrograph of Particle 3M (H8, 56 cm) showing two regions, Type 1 and 2.



(a) Fuel etch



(b) Unetched

Figure C-41. Photomicrographs of fuel in lower Type 1 region of Particle 3M (H8, 56 cm).

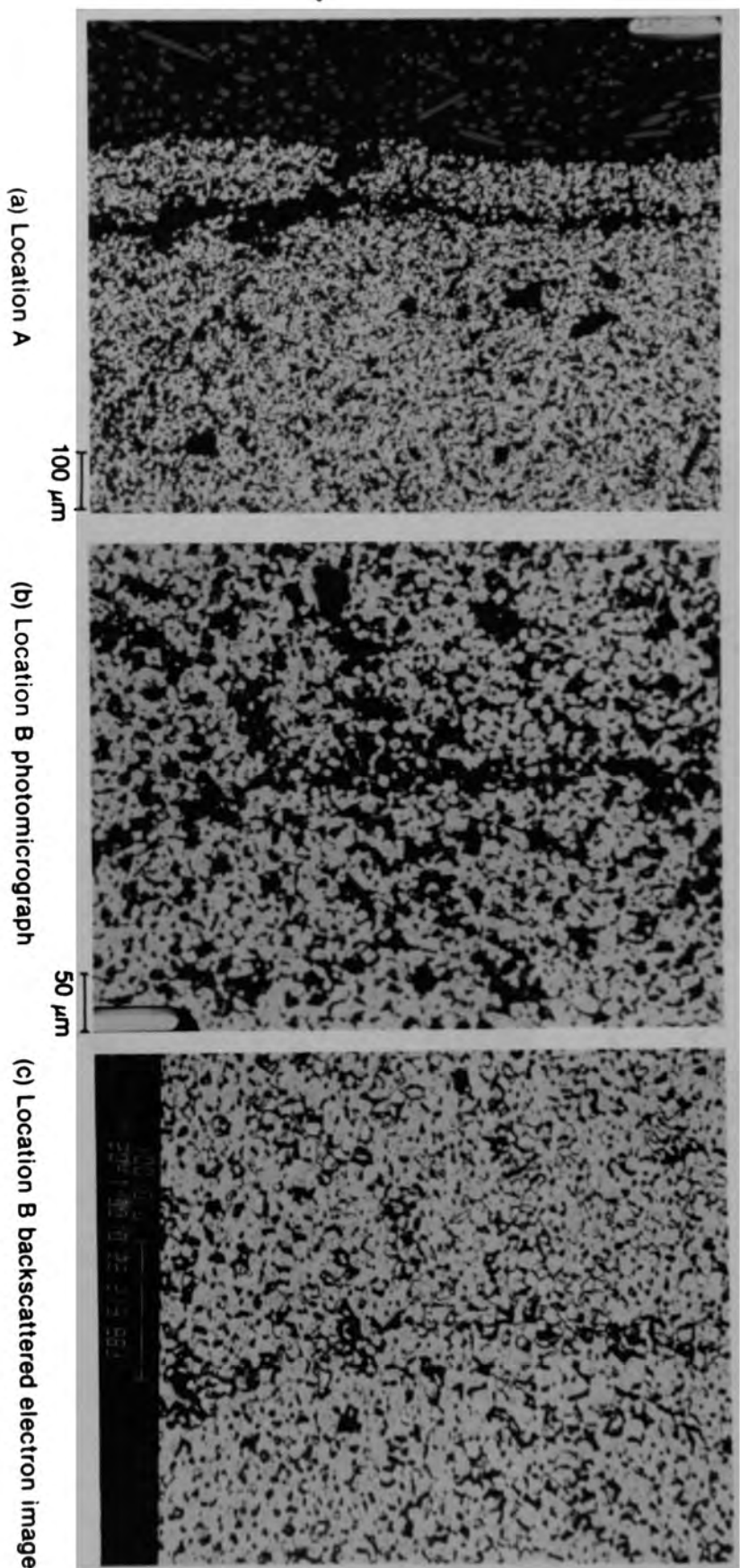
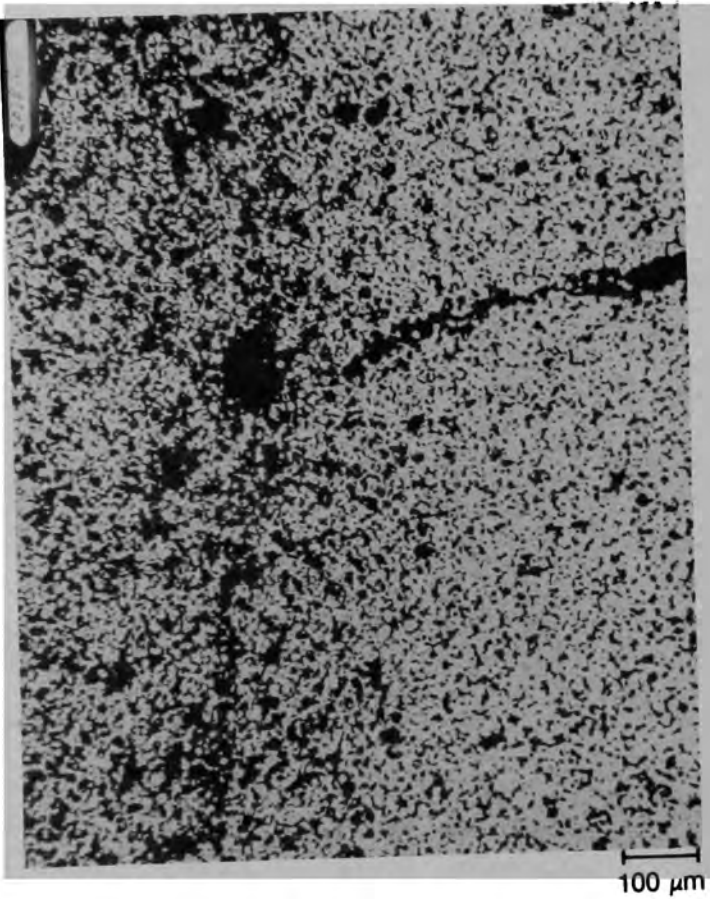
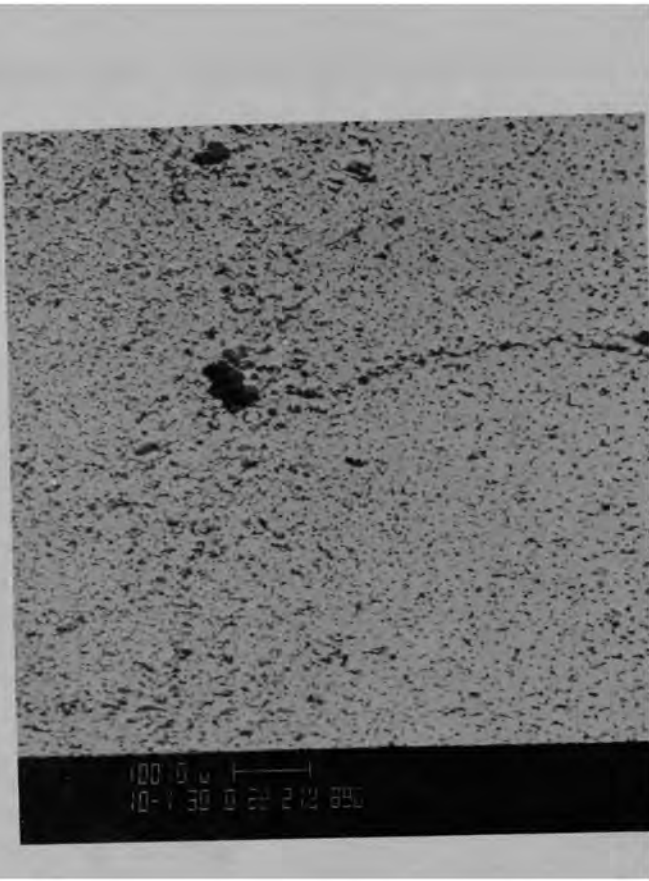


Figure C-42. Photomicrographs of the middle type 1 region of Particle 3M (H8, 56 cm).

C-96



(a) Photomicrograph



(b) Backscattered electron image

Figure C-43. Fuel at location C of Particle 3M (H8, 56 cm).

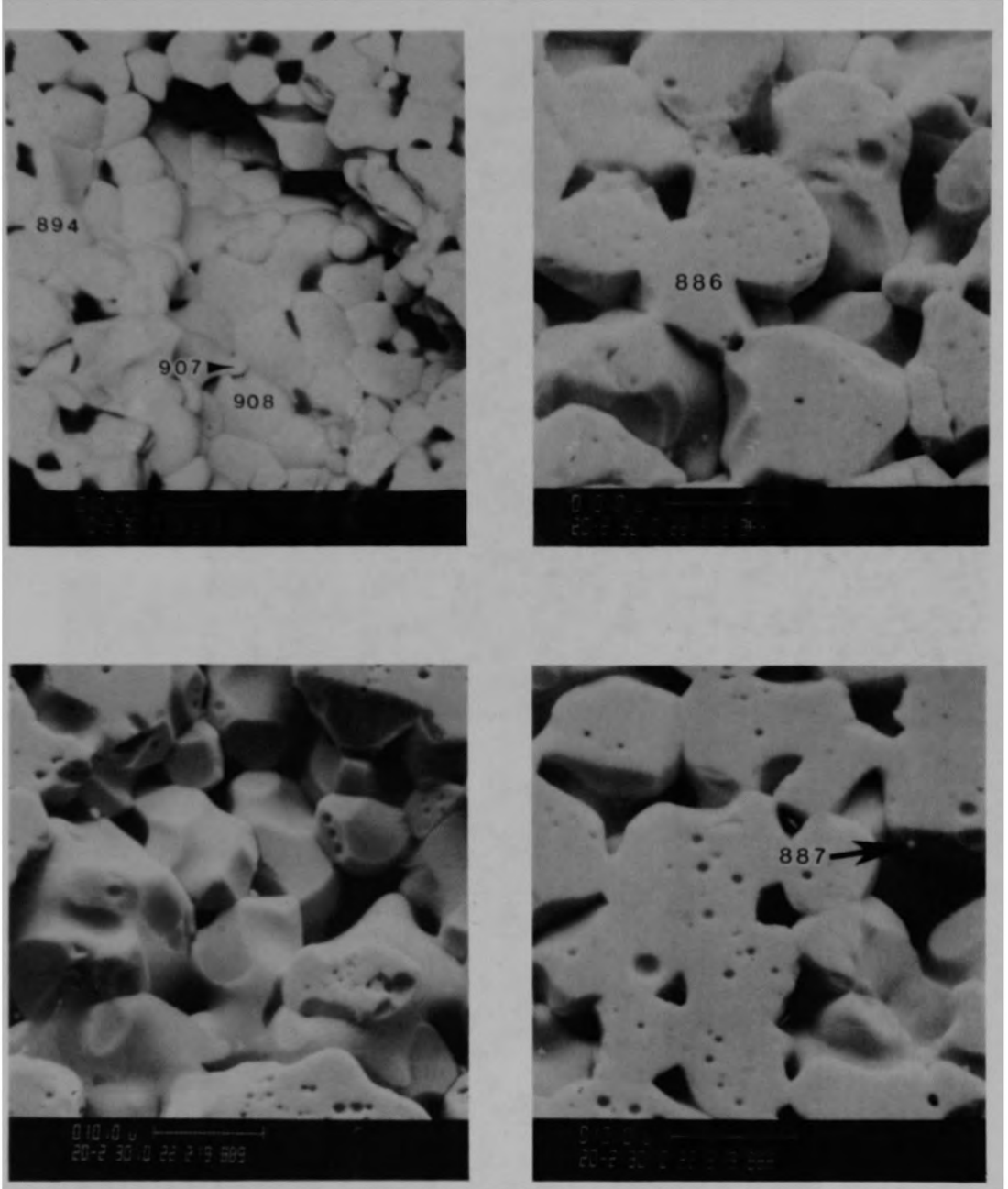
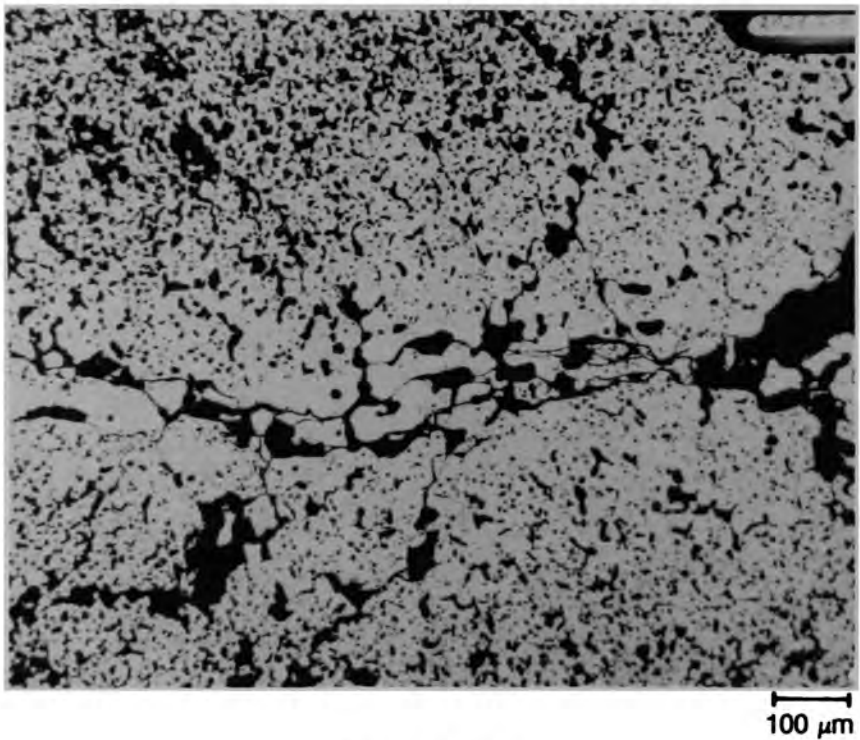
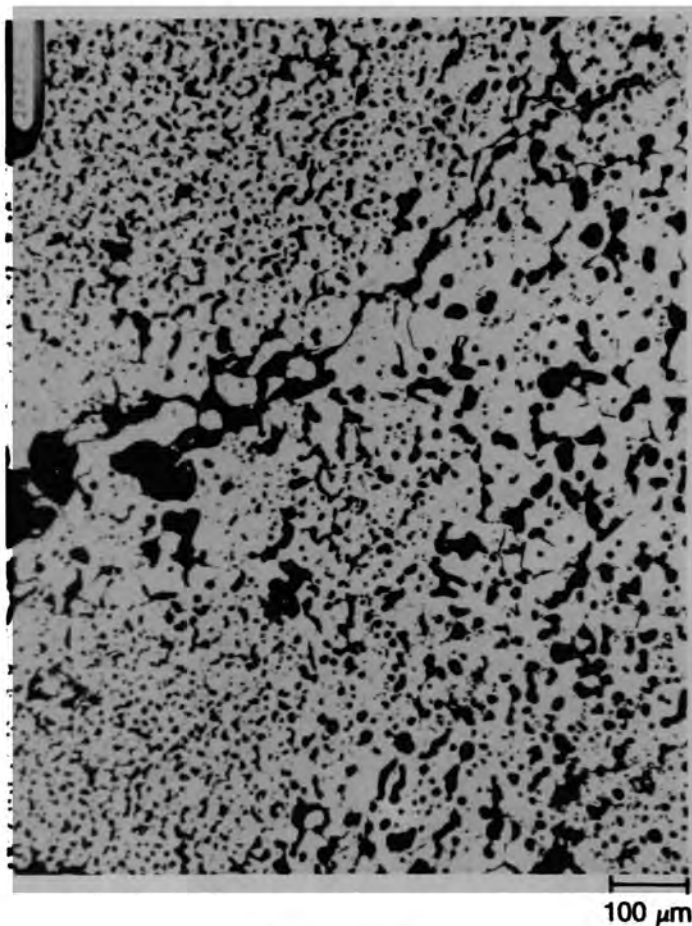


Figure C-44. Backscattered electron images of fuel in Type 1 region of Particle 3M (H8, 56 cm).

C-98



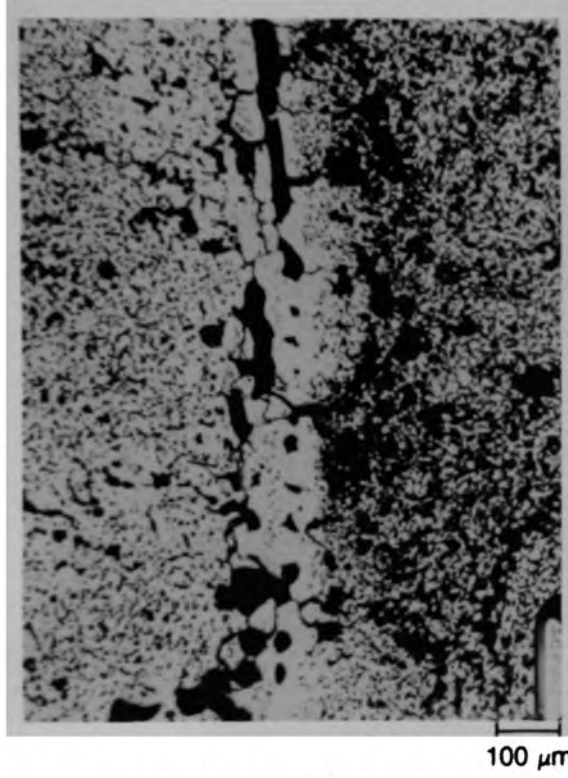
(a) Location D



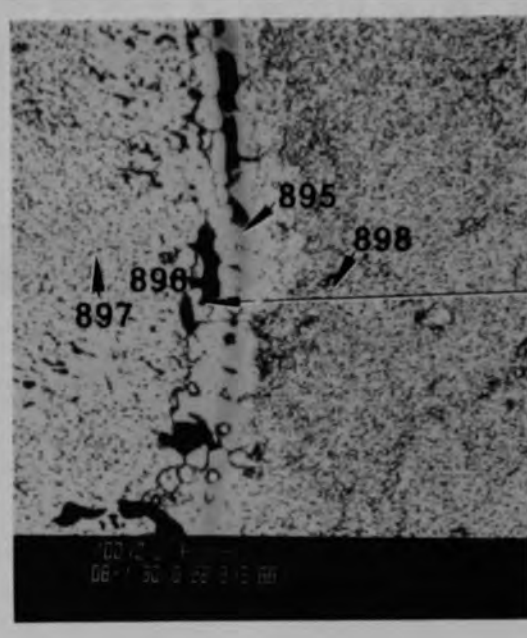
(b) Location E

Figure C-45. Photomicrographs of material in Type 2 region of Particle 3M
(H8, 56 cm).

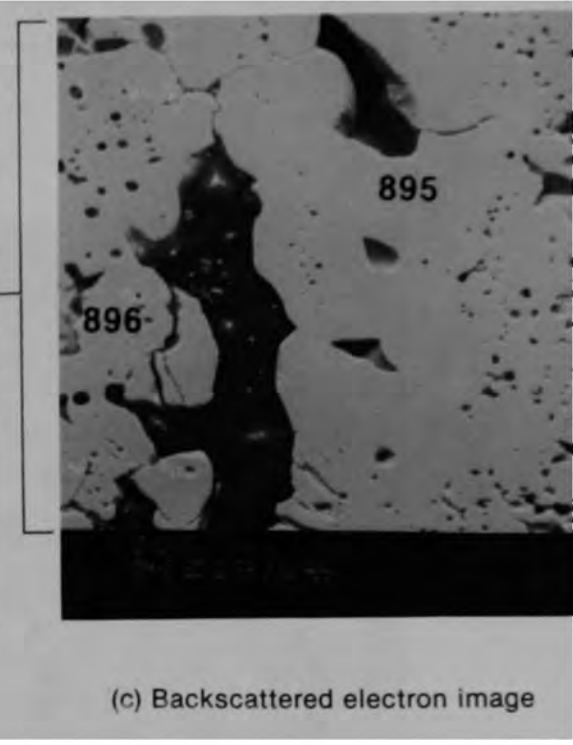
C-99



(a) Photomicrograph



(b) Backscattered electron image



(c) Backscattered electron image

Figure C-46. Material structure from location F in Type 2 region of Particle 3M (H8, 56 cm).

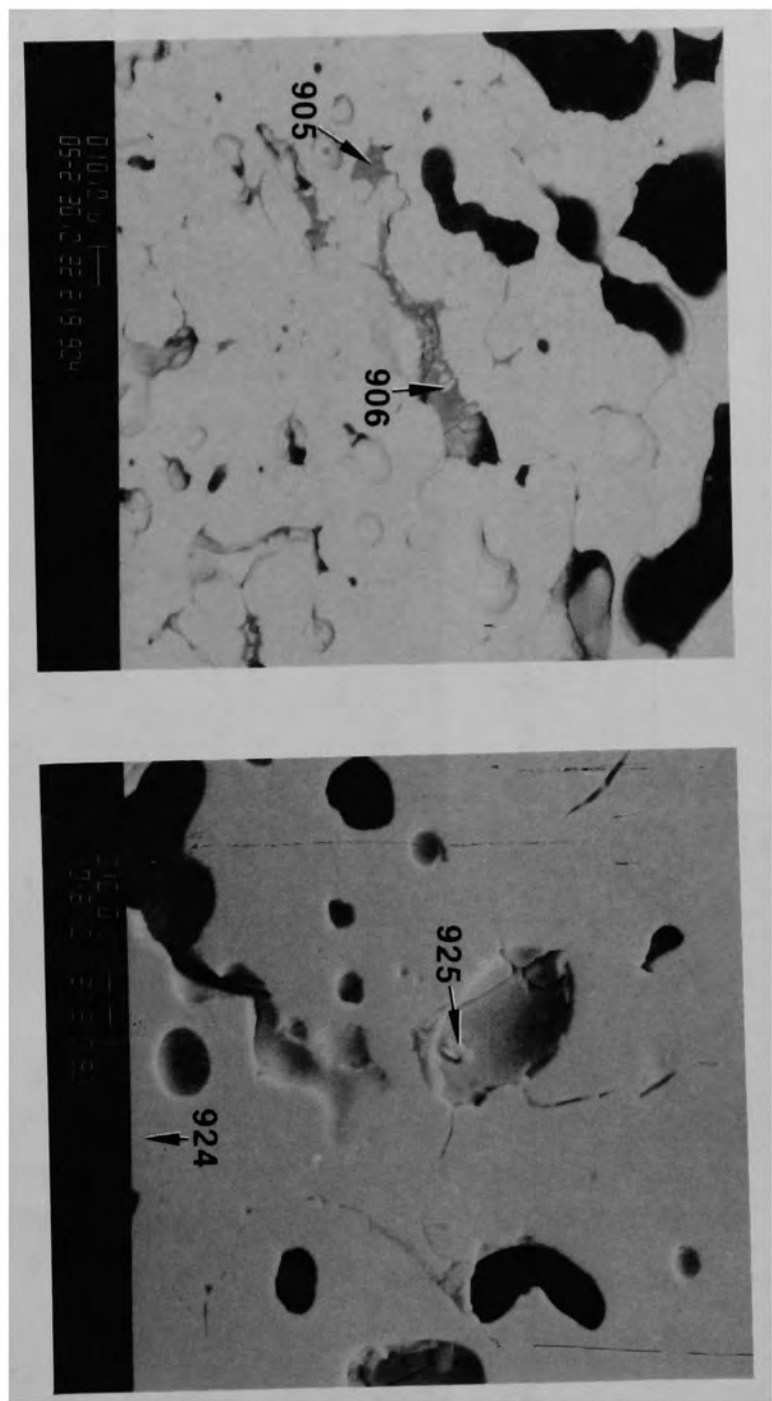
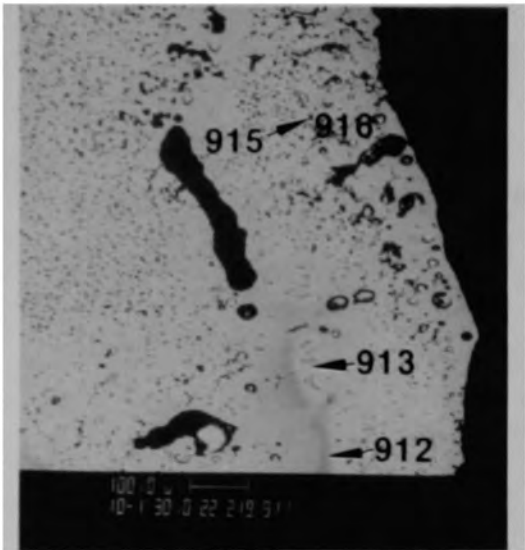
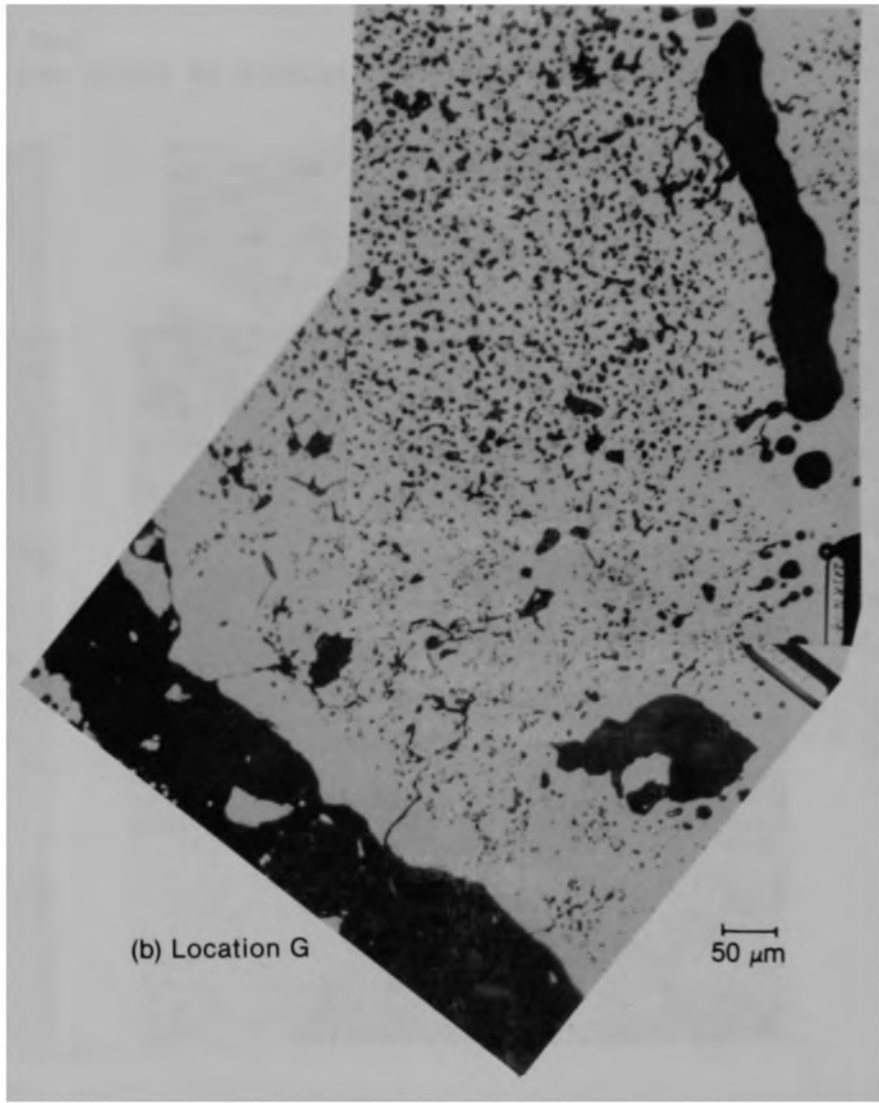


Figure C-47. Backscattered electron images of pore morphology in Type 2 region material of Particle 3M (H8, 56 cm).

C-101



(a) Location H



(b) Location G

Figure C-48. Material in Type 2 region of Particle 3M (H8, 56 cm).

(a) Location J



(b) Location I

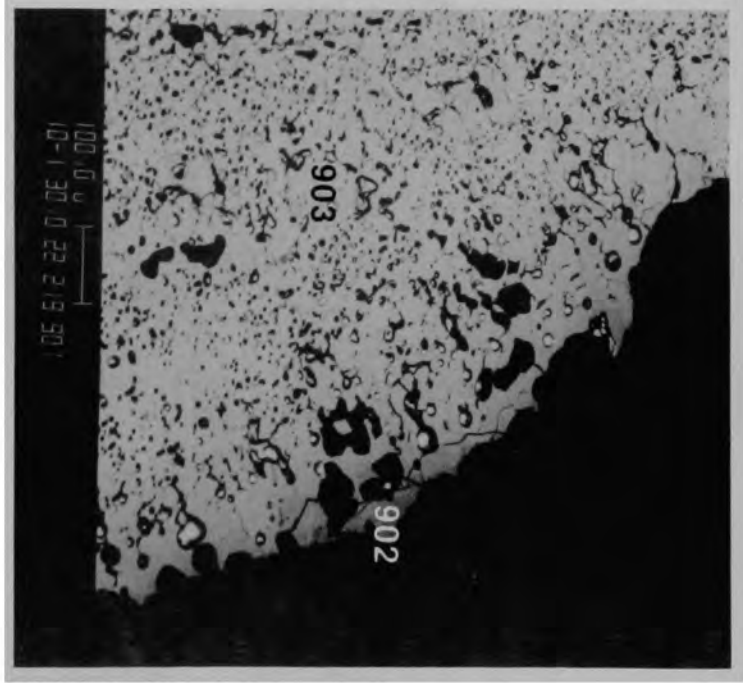
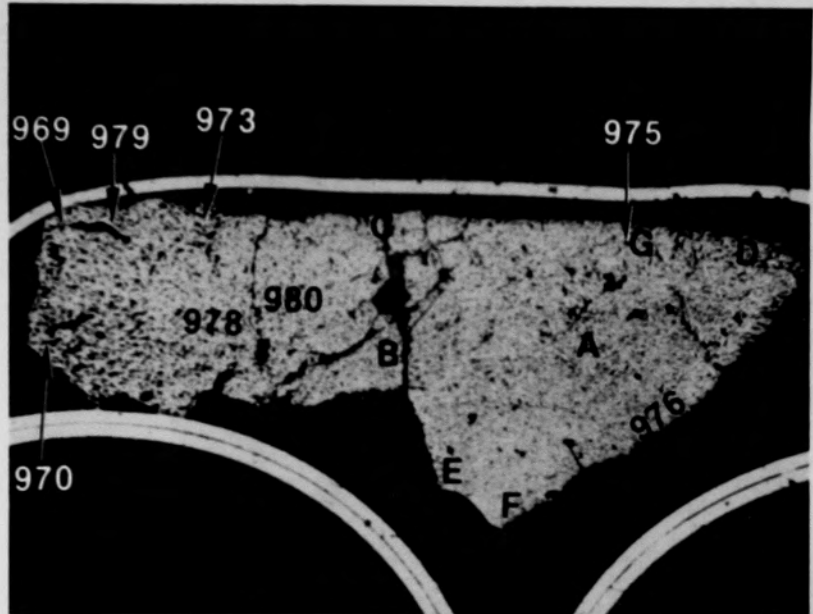
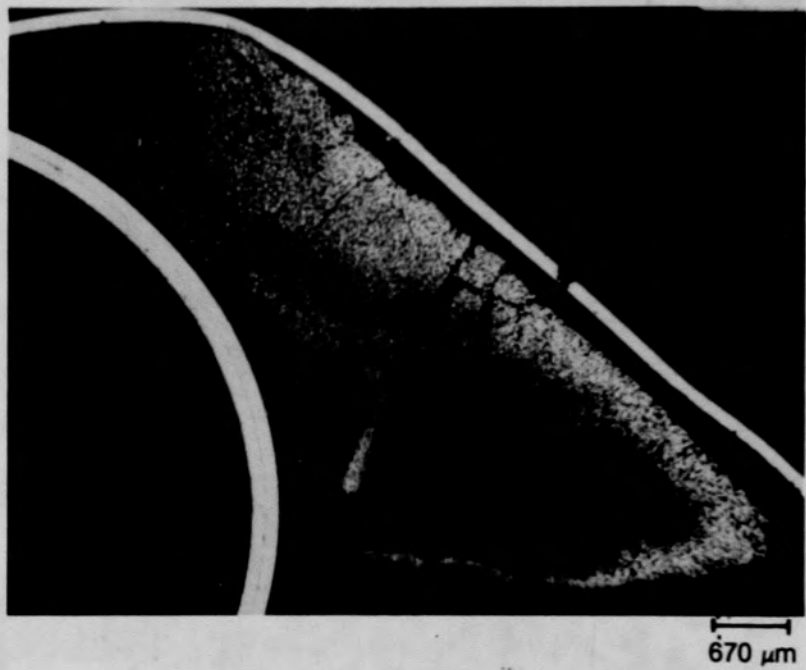


Figure C-49. Backscattered electron images of material in Type 2 region of particle 3M (H8, 56 cm).

C-103

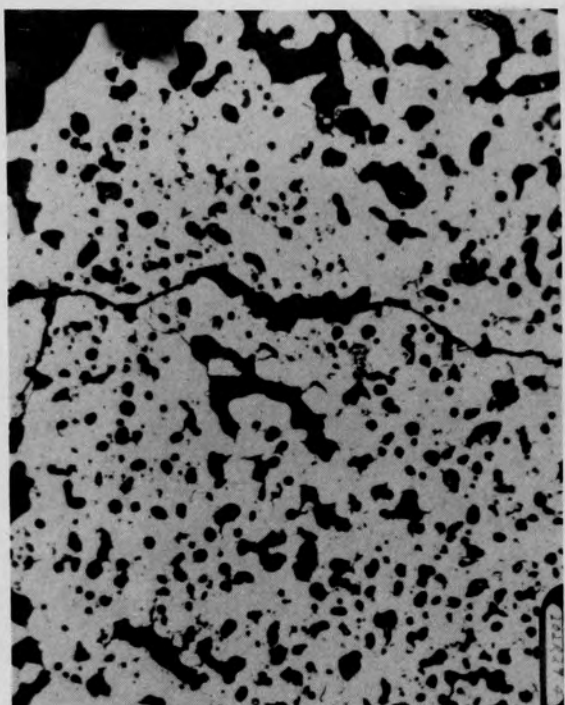


(a) Unetched

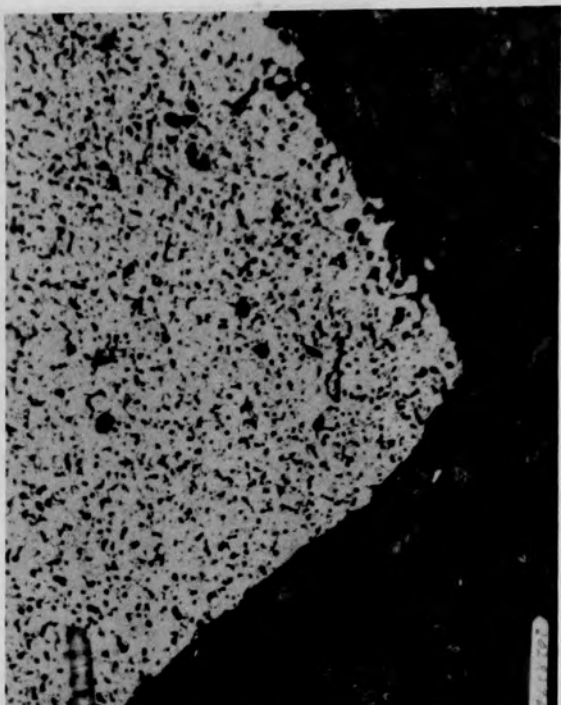


(b) Fuel etch

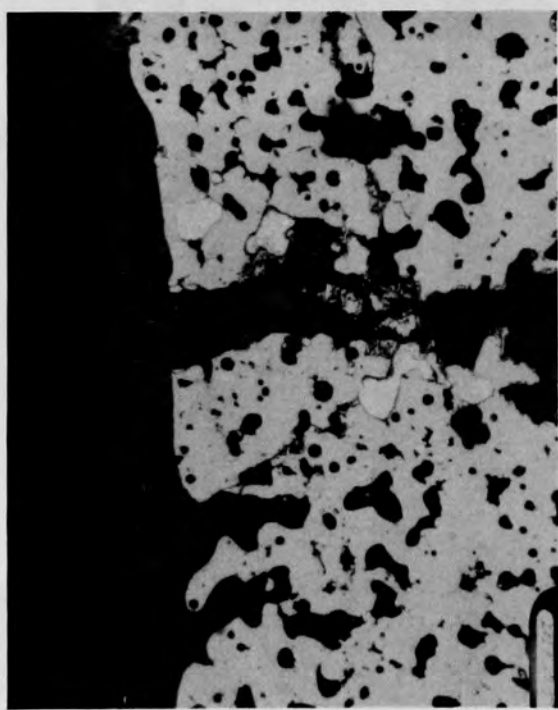
Figure C-50. Photomacrographs of Particle 4A (E9, surface).



(a) Location G



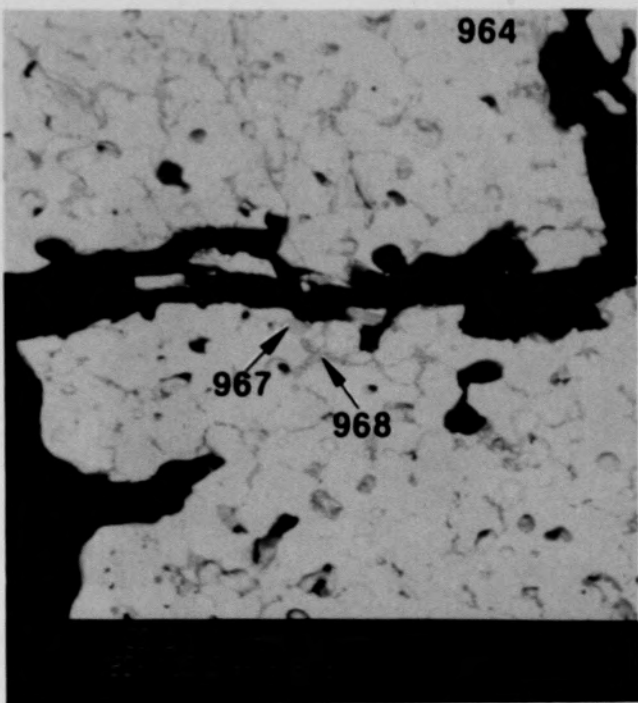
(b) Location F



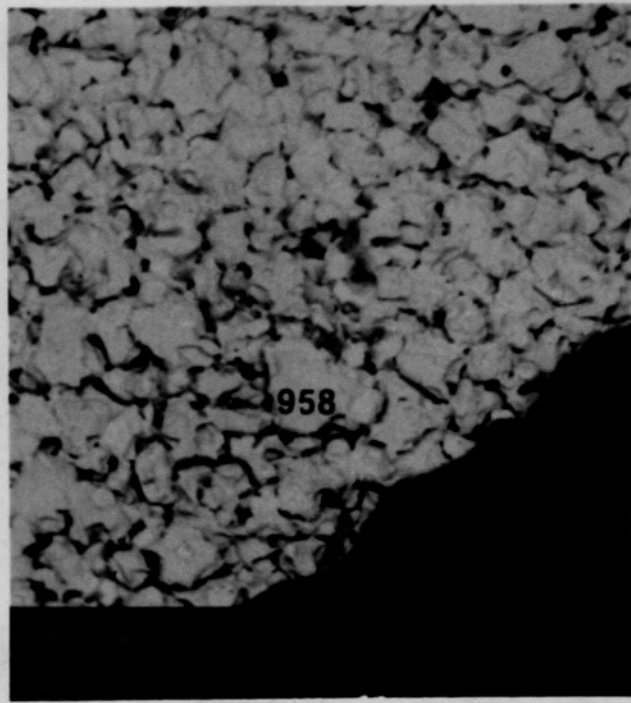
(c) Location C

50 μm

Figure C-51. Photomicrographs of Particle 4A (E9, surface).



(a) Location C



(b) Location F

Figure C-52. SEM backscattered electron images of Particle 4A (E9, surface).

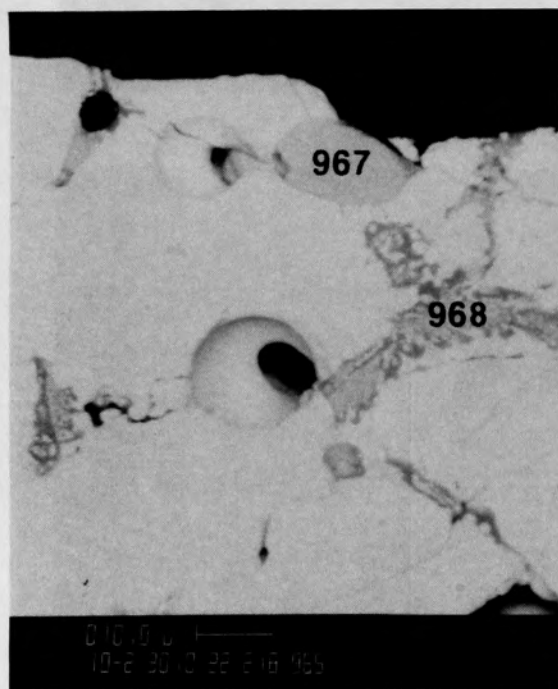
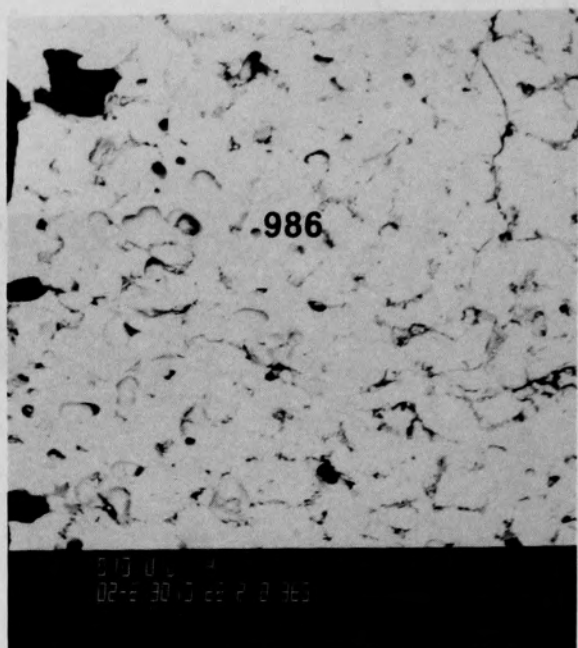
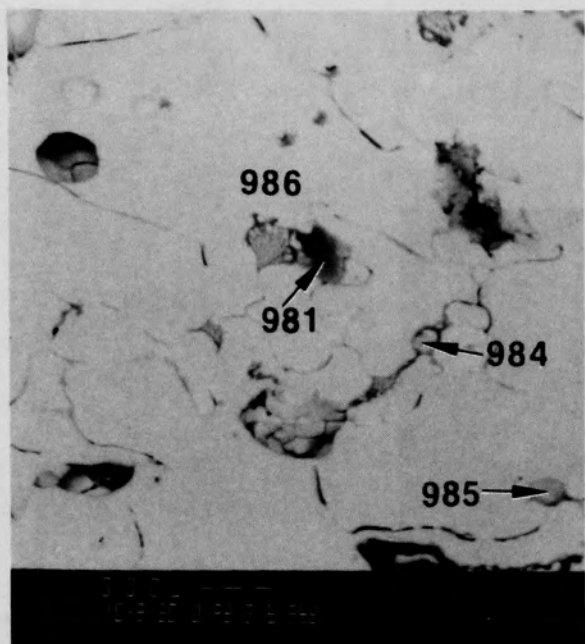


Figure C-53. SEM backscattered electron images showing the grain boundary phase in Particle 4A (E9, surface).

C-107

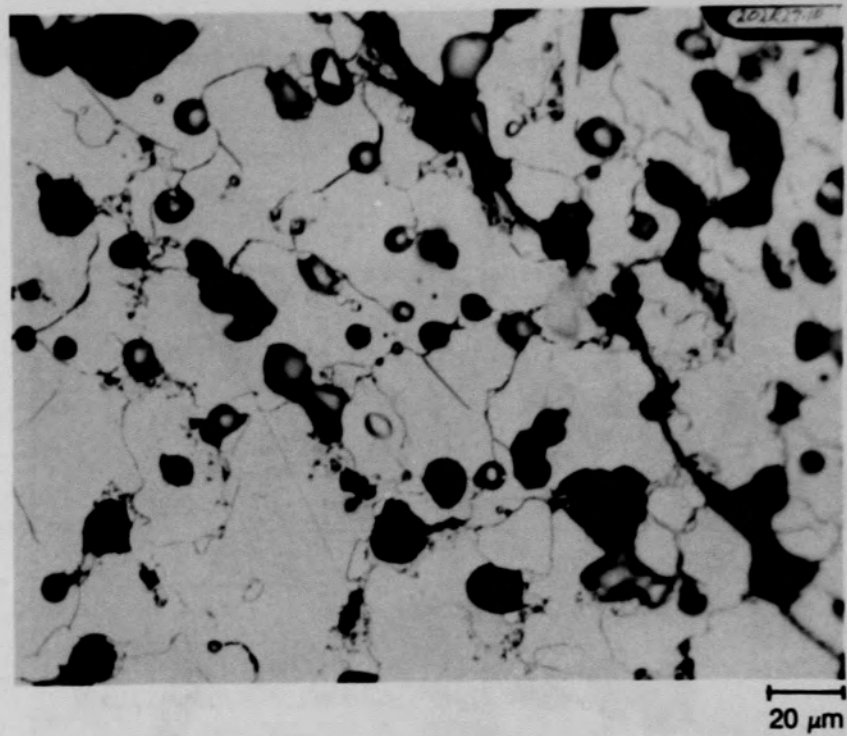
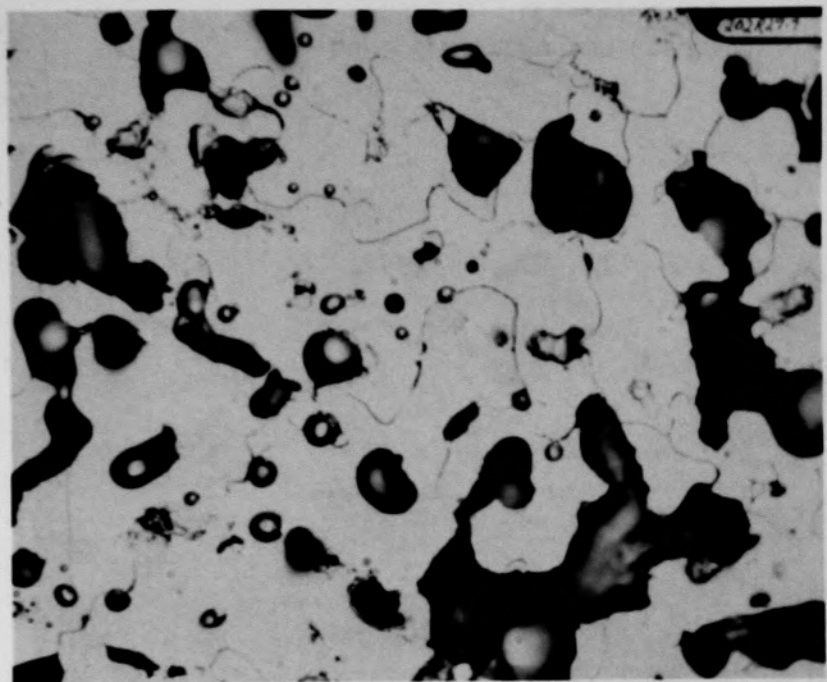


Figure C-54. Photomicrographs of the grain boundary phase in Particle 4A (E9, surface).

C-108

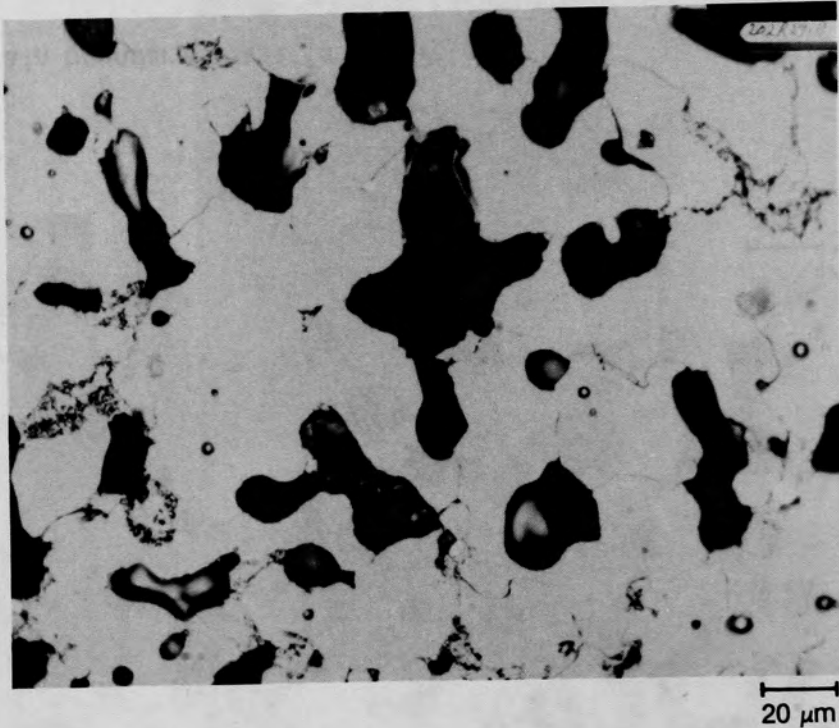
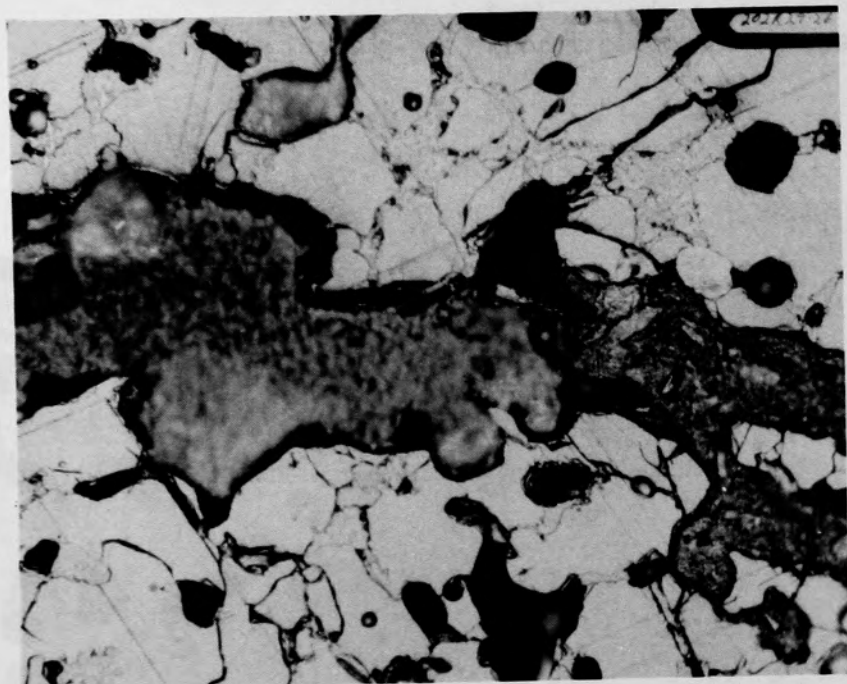


Figure C-55. Photomicrographs of the grain boundary phase in Particle 4A (E9, surface).

C-109

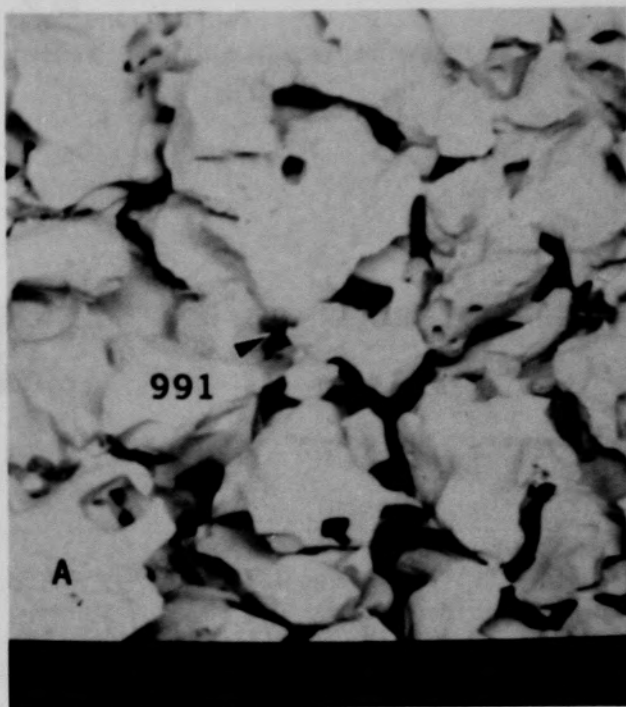
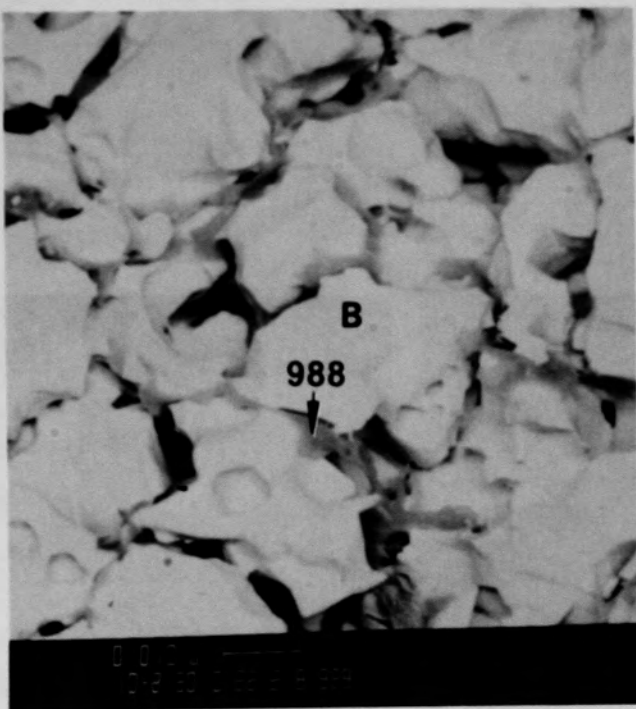
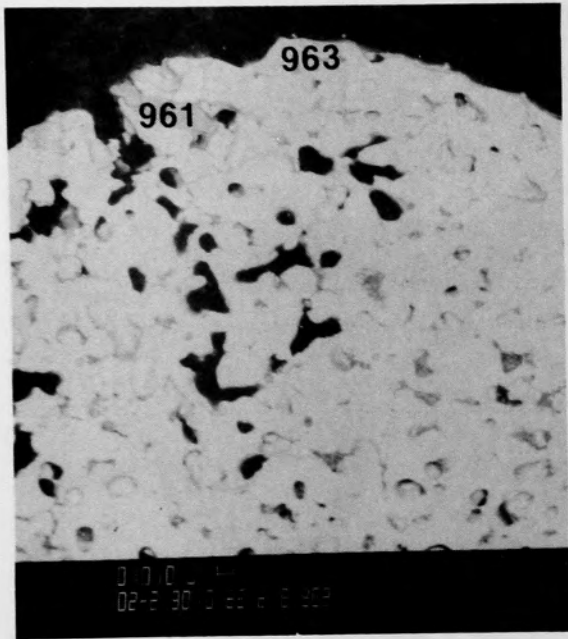
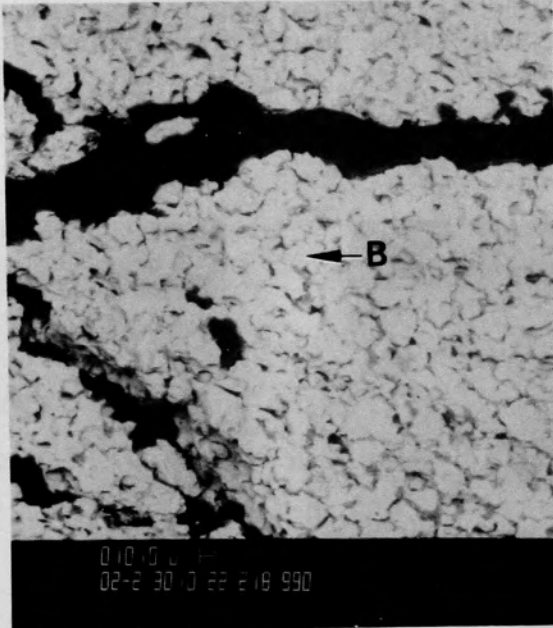


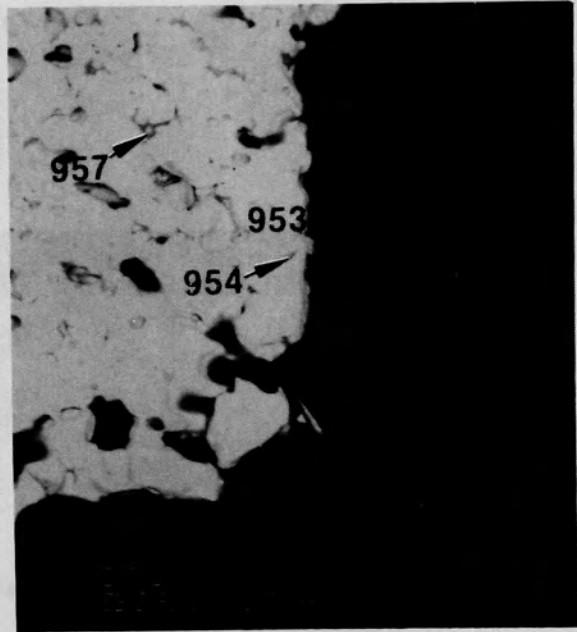
Figure C-56. SEM backscattered electron images showing Al-Cr-Fe-Ni grain boundary phase of Particle 4A (E9, surface).



(a) Location D



(b) Location B



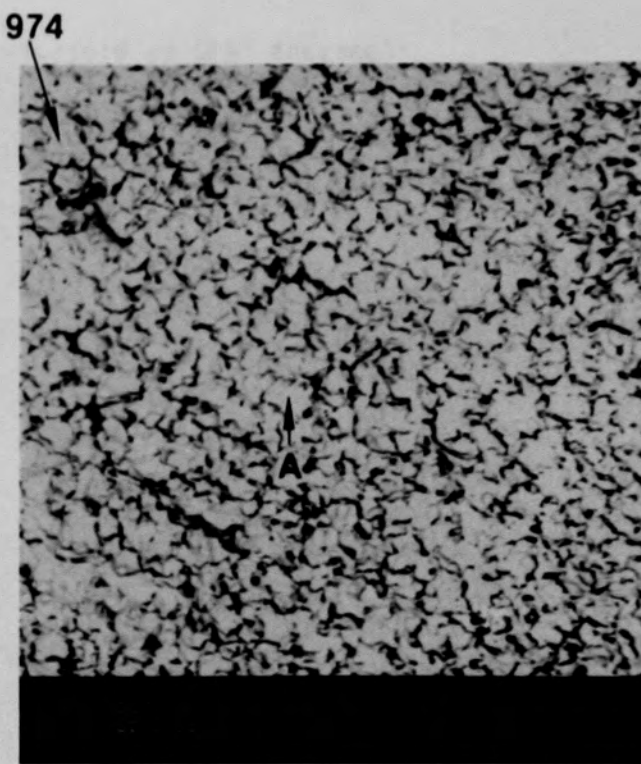
(c) Location E

Figure C-57. SEM backscattered electron images of representative material structures for Particle 4A (E9, surface).

C-111



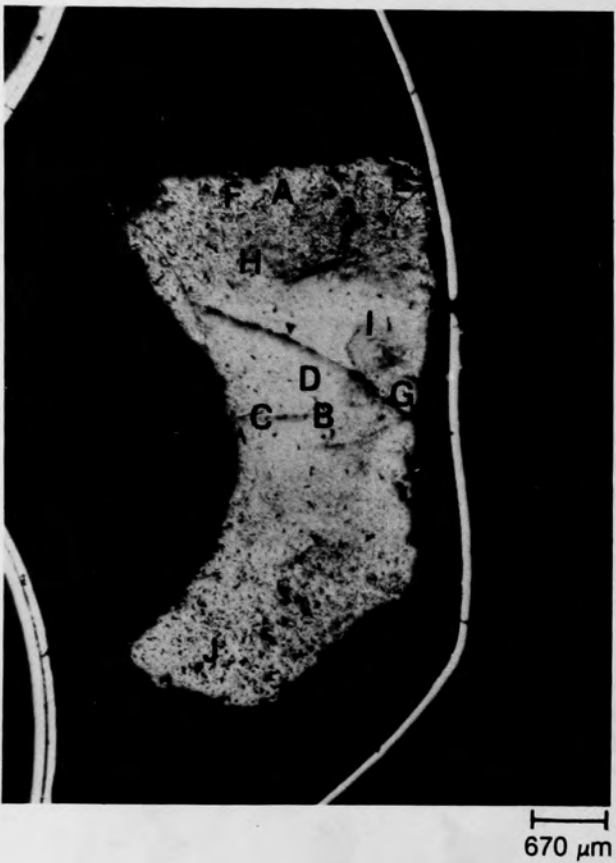
(a) Photomicrograph



(b) SEM backscattered electron image

Figure C-58. Representative material from Particle 4A (E9, surface).

C-112



(a) Unetched



(b) Fuel etch

Figure C-59. Photomacrograph of Particle 4B (E9, surface).

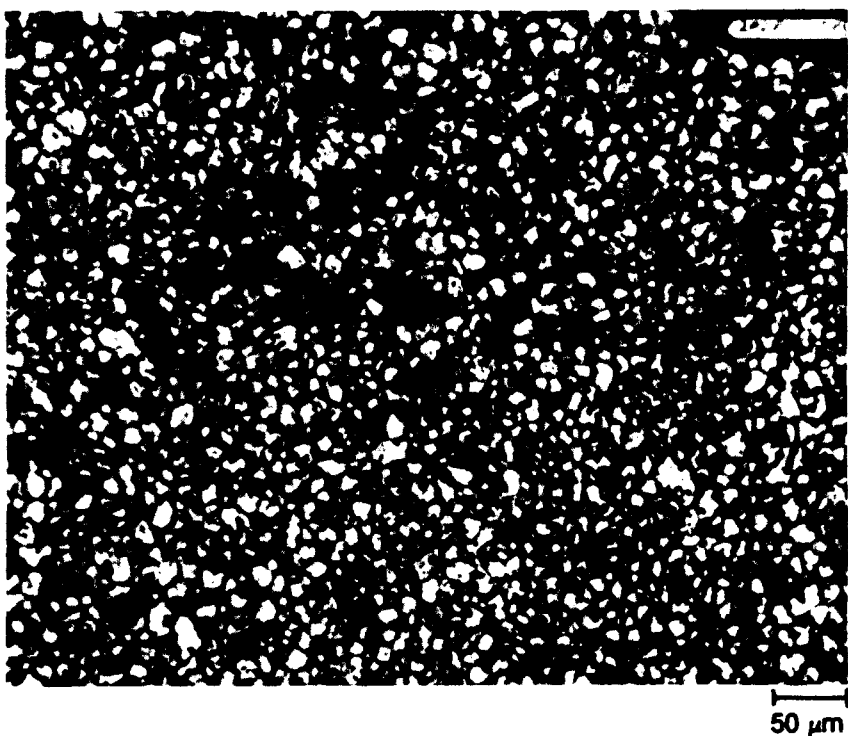
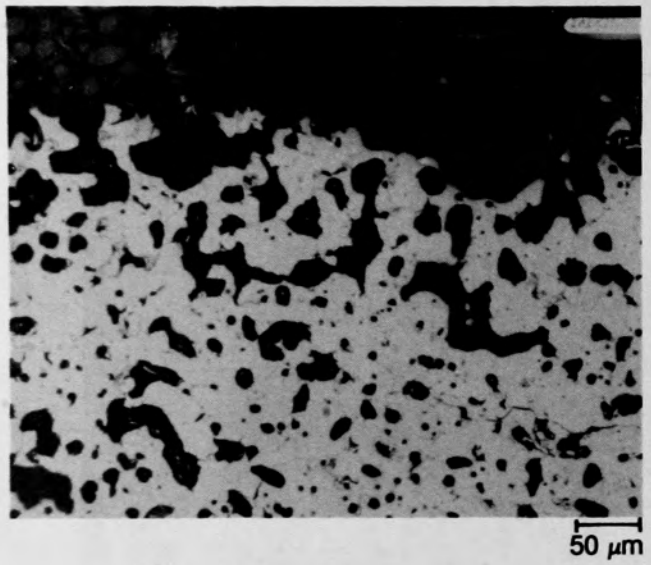
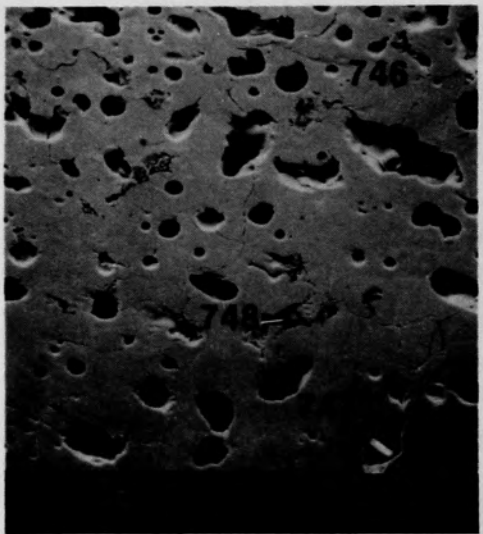


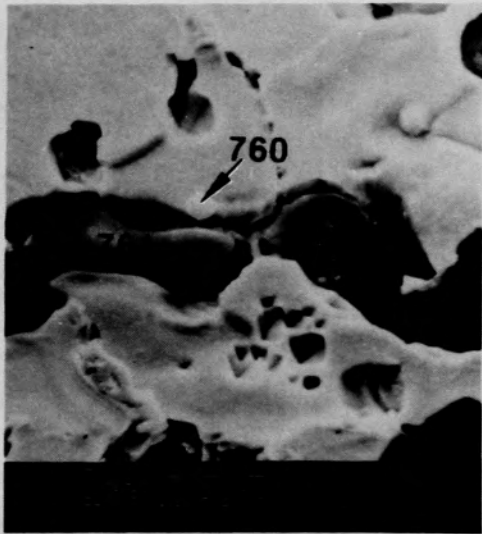
Figure C-60. Photomicrograph of center of Particle 4B (E9, surface) showing fuel pullout.



(a) Photomicrograph



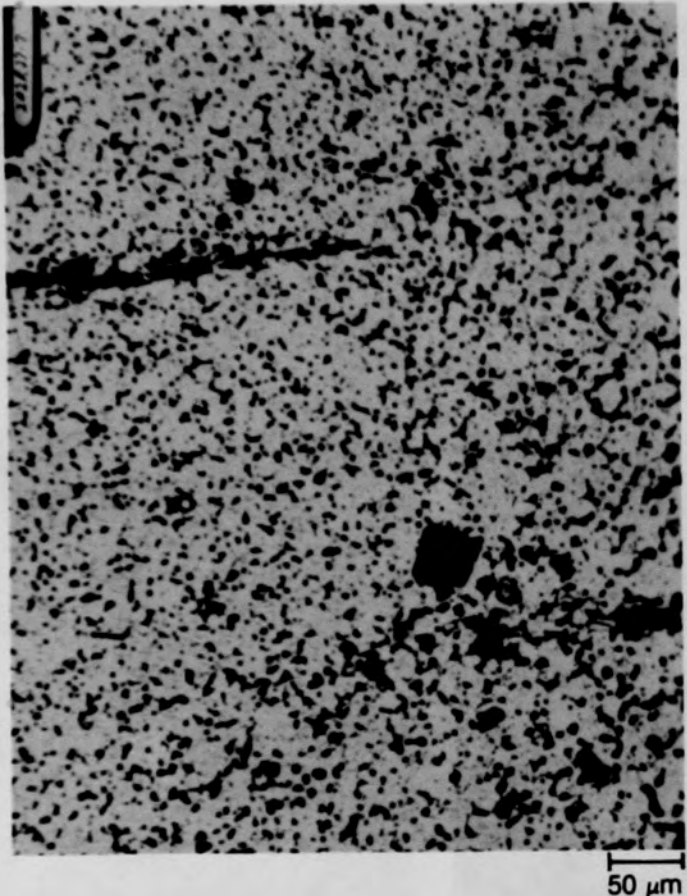
(b) SEM backscattered electron image



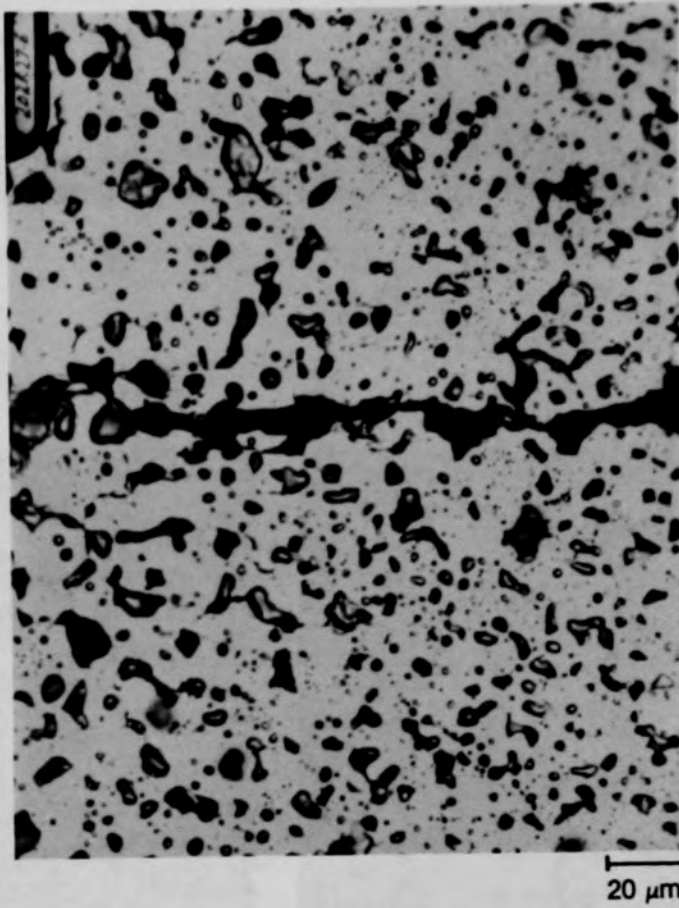
(c) SEM backscattered electron image

Figure C-61. Photographs of material from location A (U, low Zr) of Particle 4B (E9, surface).

C-115



(a) Location B



(b) Location C

Figure C-62. Photomicrographs of material near center of Particle 4B (E9, surface).

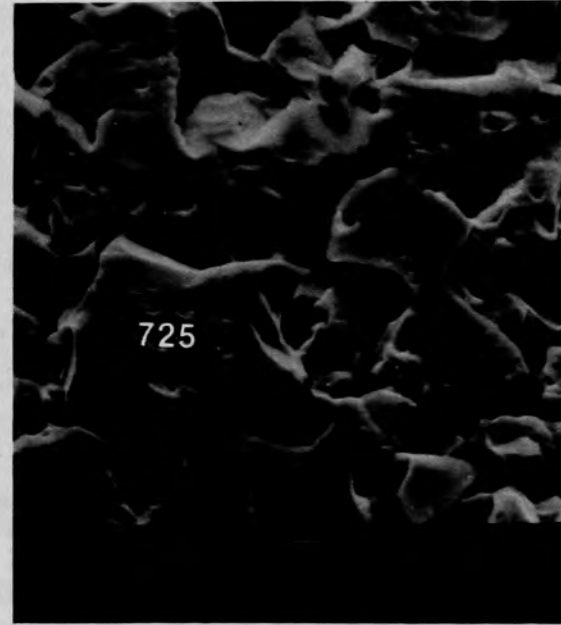
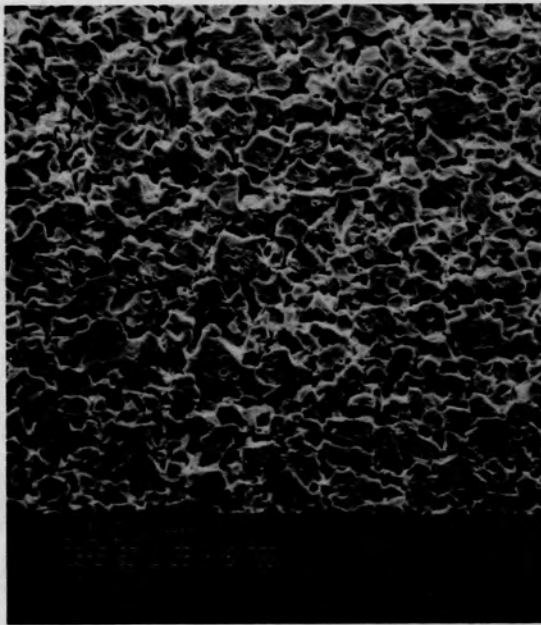
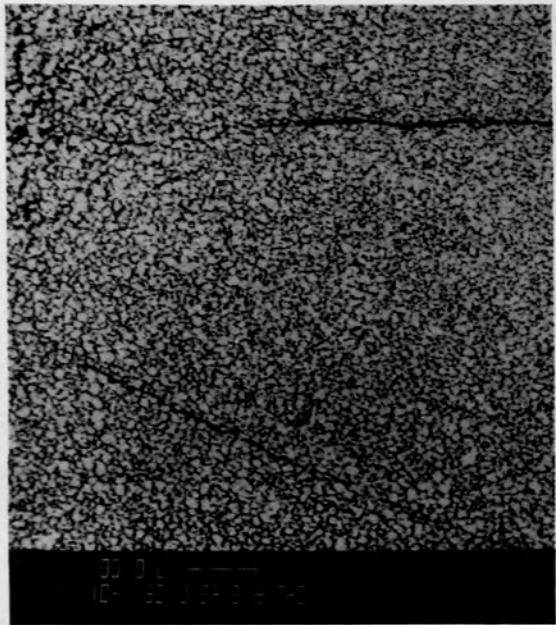
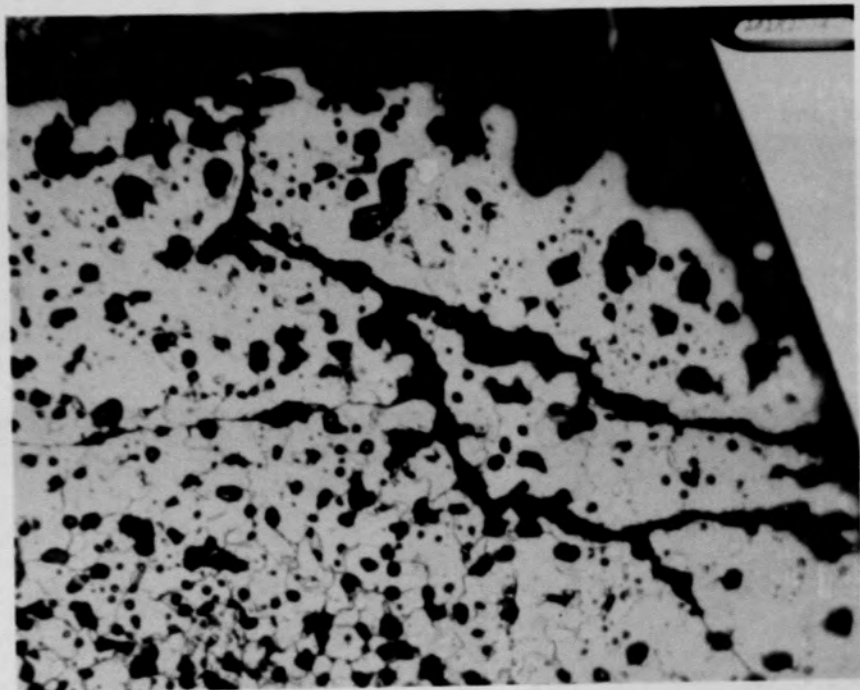
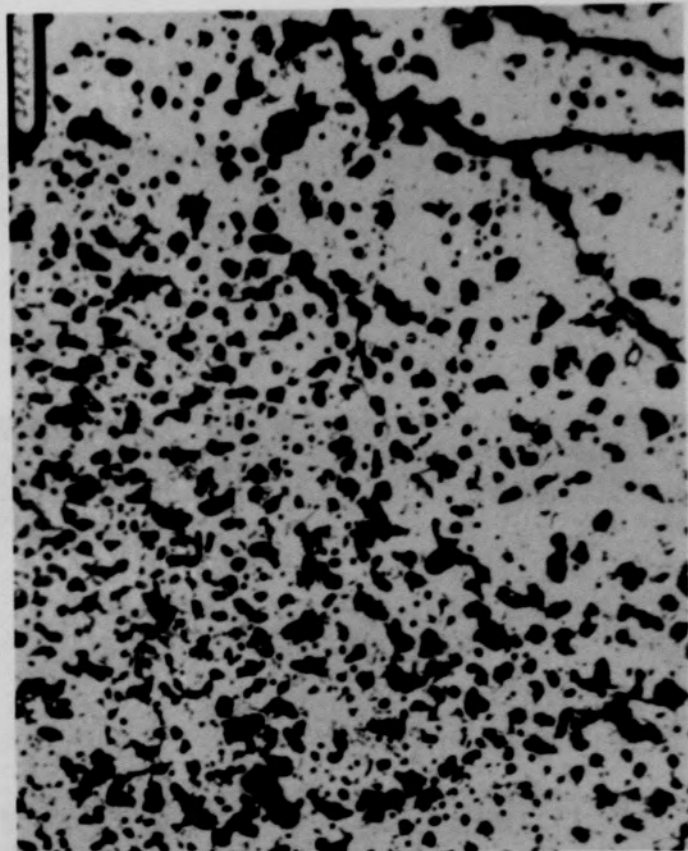


Figure C-63. SEM backscattered electron images from location D of fuel at center of Particle 4B (E9, surface).



(a) Etched



(b) Unetched

50 μm

Figure C-64. Photomicrographs of U, low Zr material at location E of Particle 4B (E9, surface).

C-118

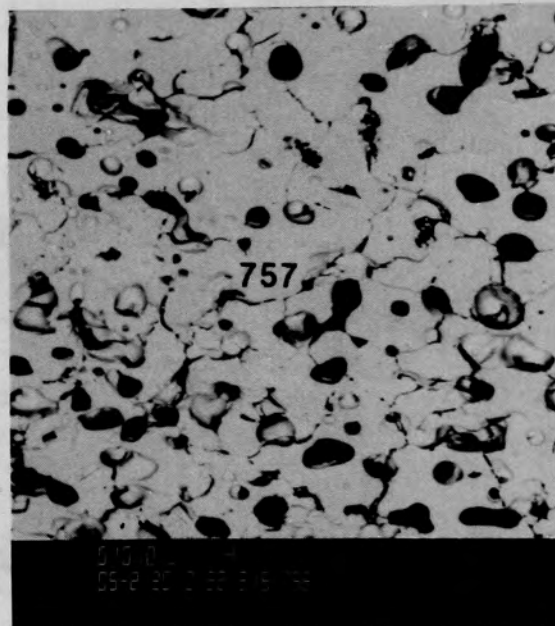
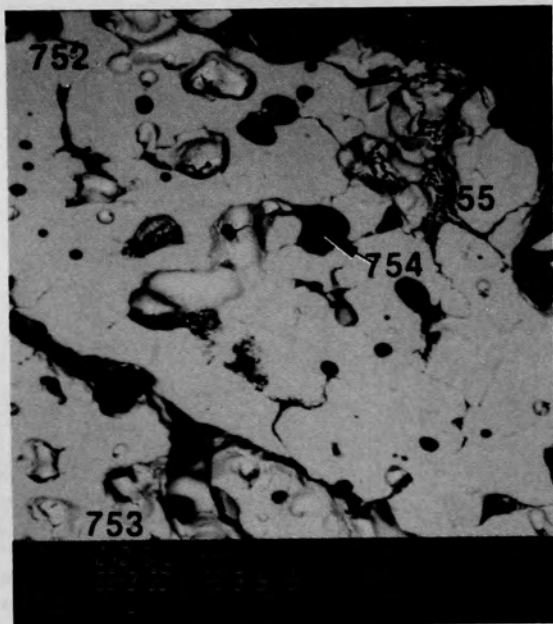
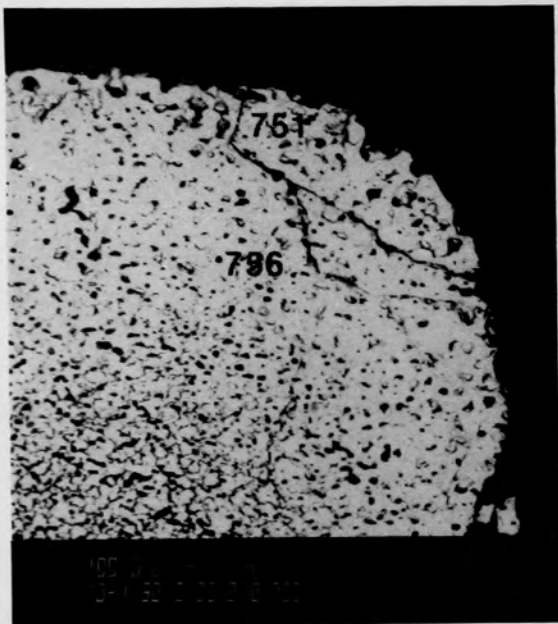


Figure C-65. SEM backscattered electron images of material at location E of Particle 4B (E9, surface).

C-119

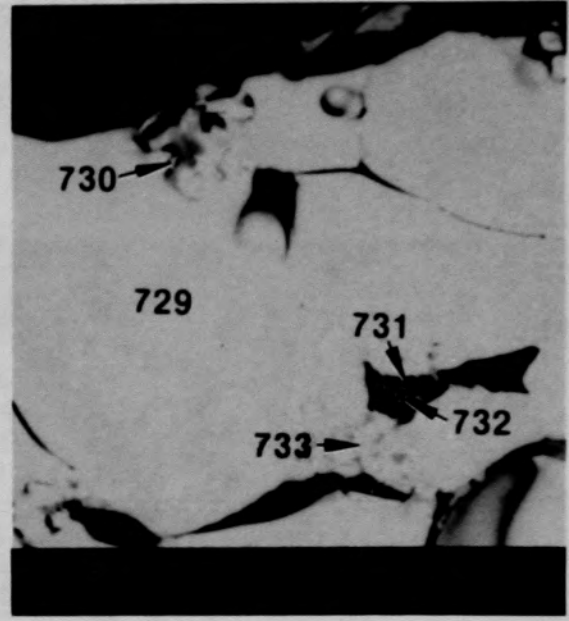
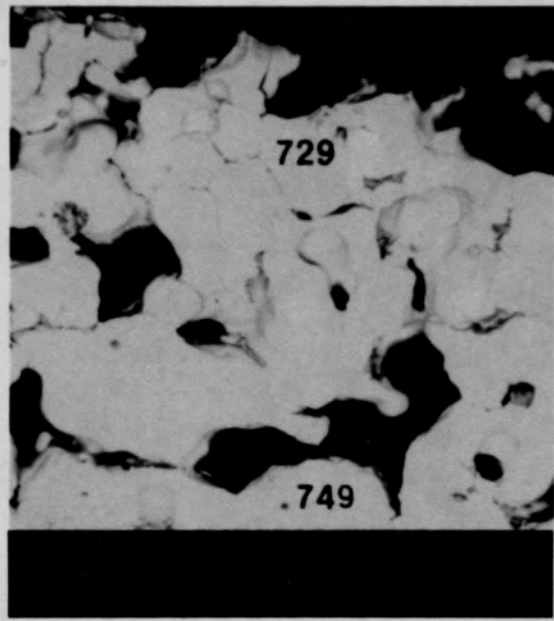
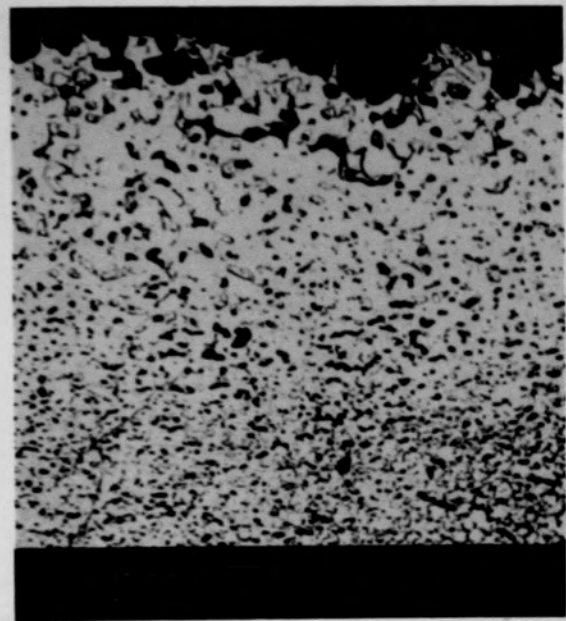
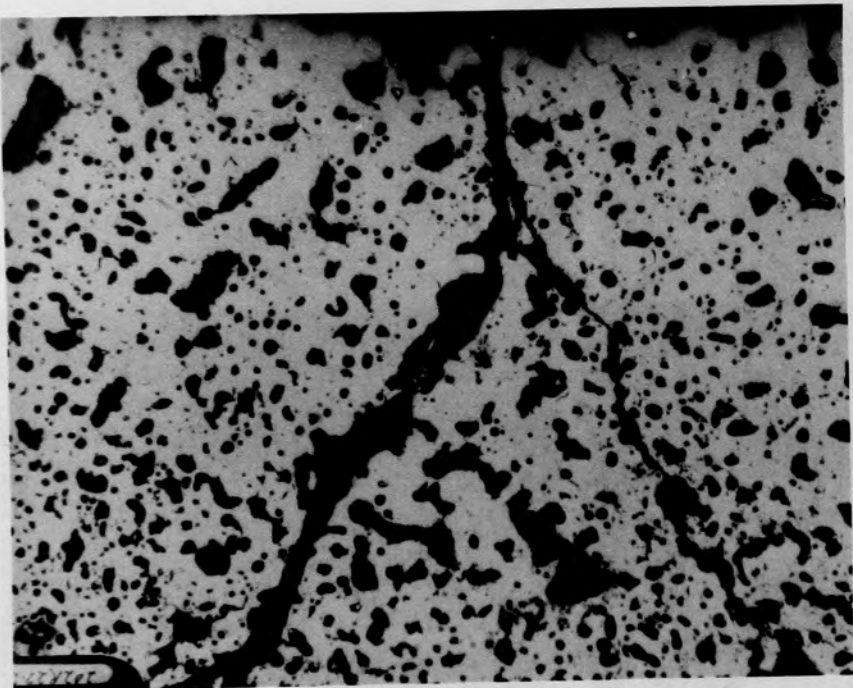
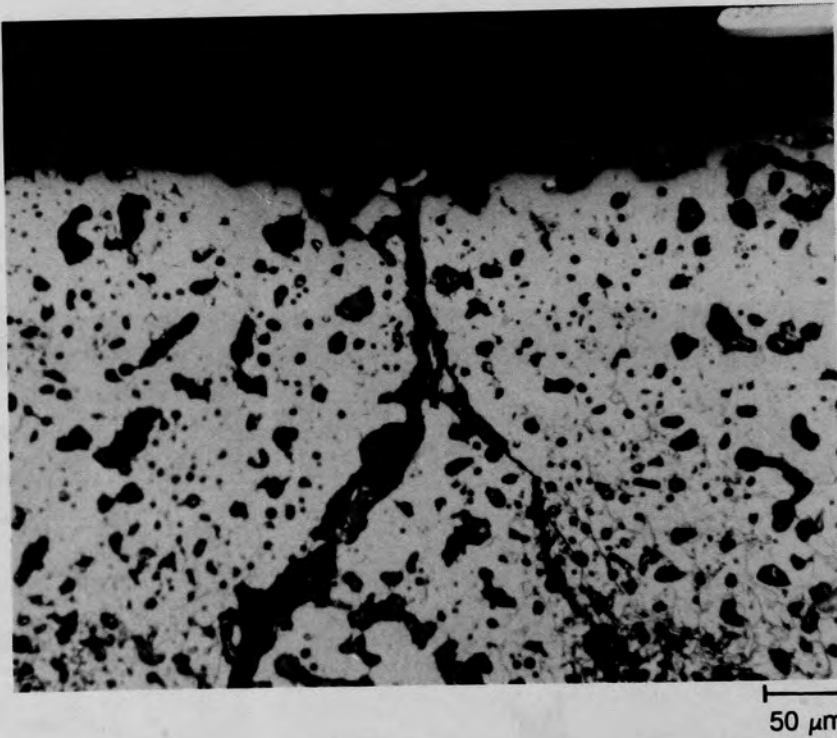


Figure C-66. SEM backscattered electron images from location F of Particle 4B (E9, surface).

C-120



(a) Unetched

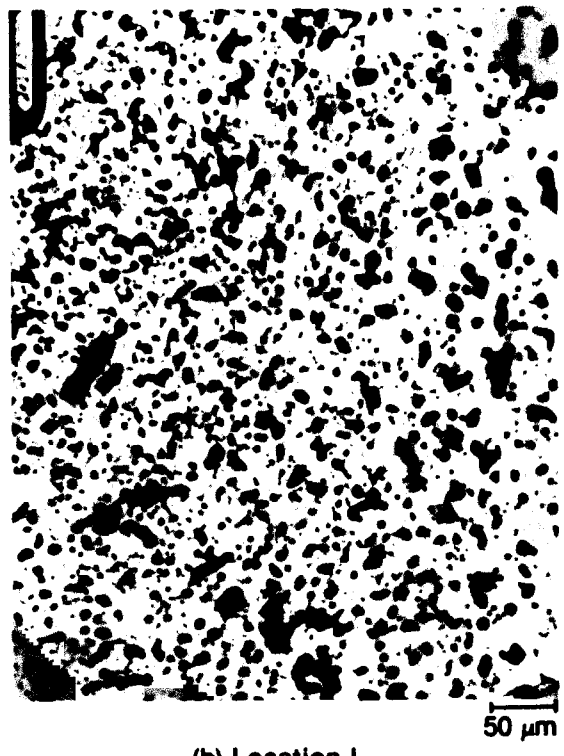


(b) Etched

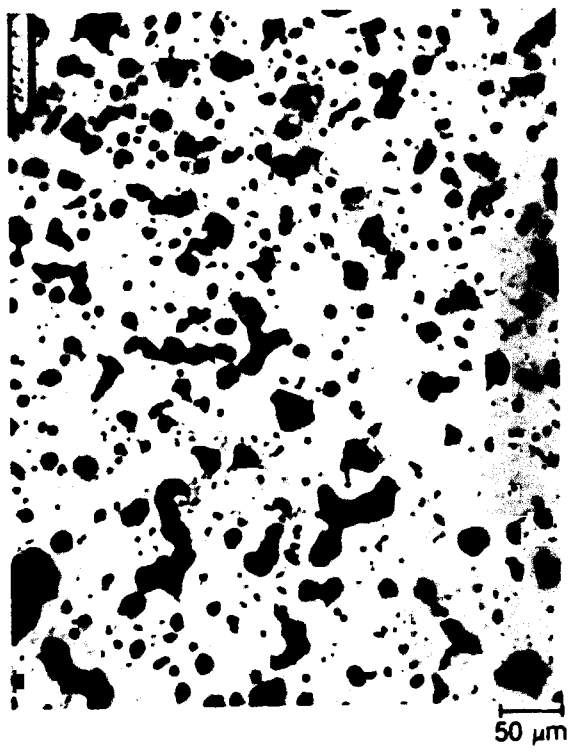
Figure C-67. Photomicrographs from location G of Particle 4B (E9, surface).



(a) Location H



(b) Location I



(c) Location J

Figure C-68. Typical structures of material from Particle 4B (E9, surface).

C-122

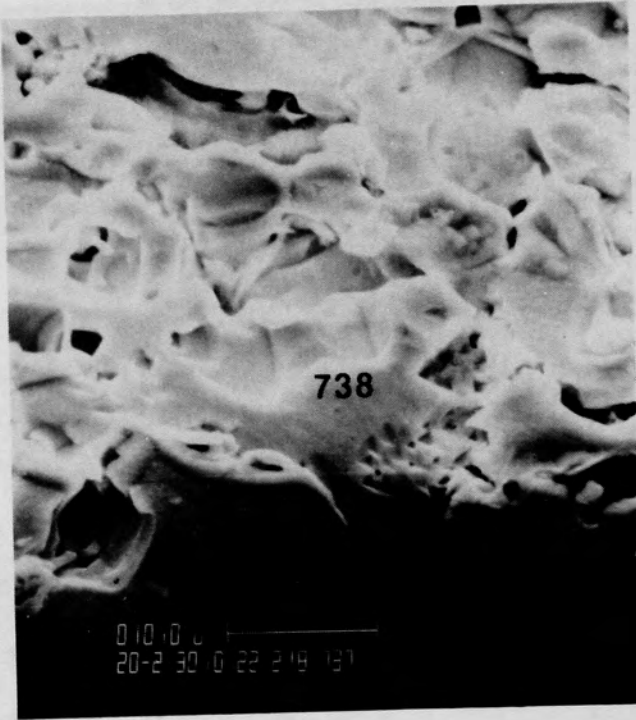
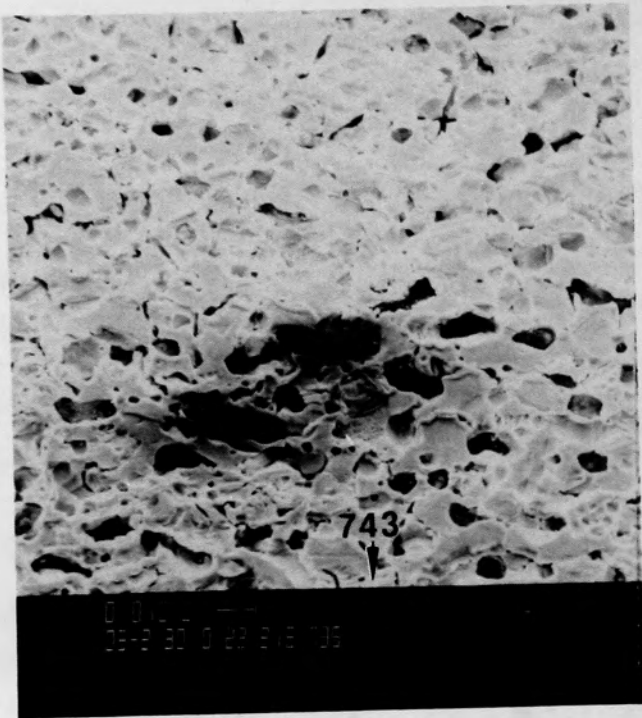


Figure C-69. SEM backscattered electron images of material in outer rim of Particle 4B (E9, surface).

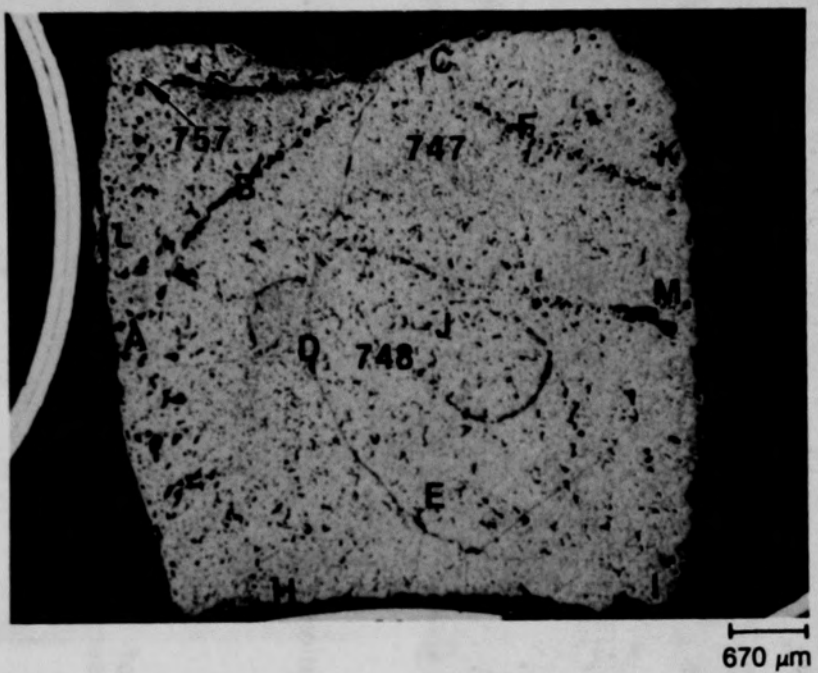


Figure C-70. Photomacrograph of Particle 4D (E9, surface).

C-124

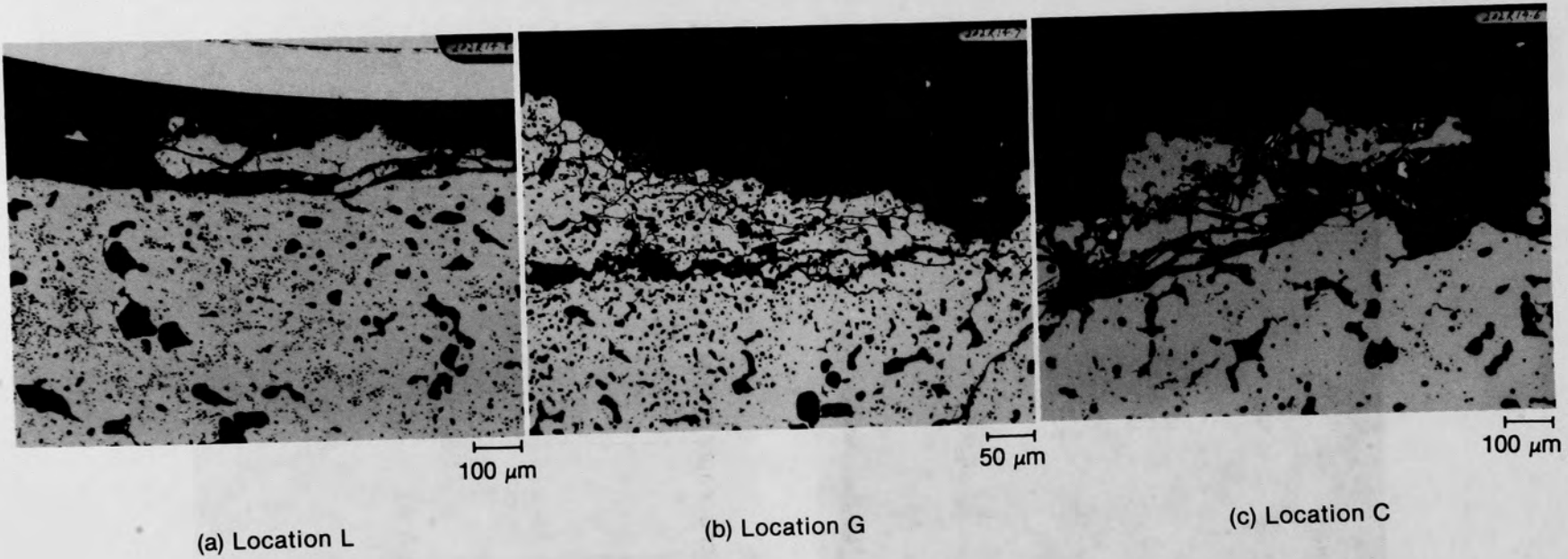
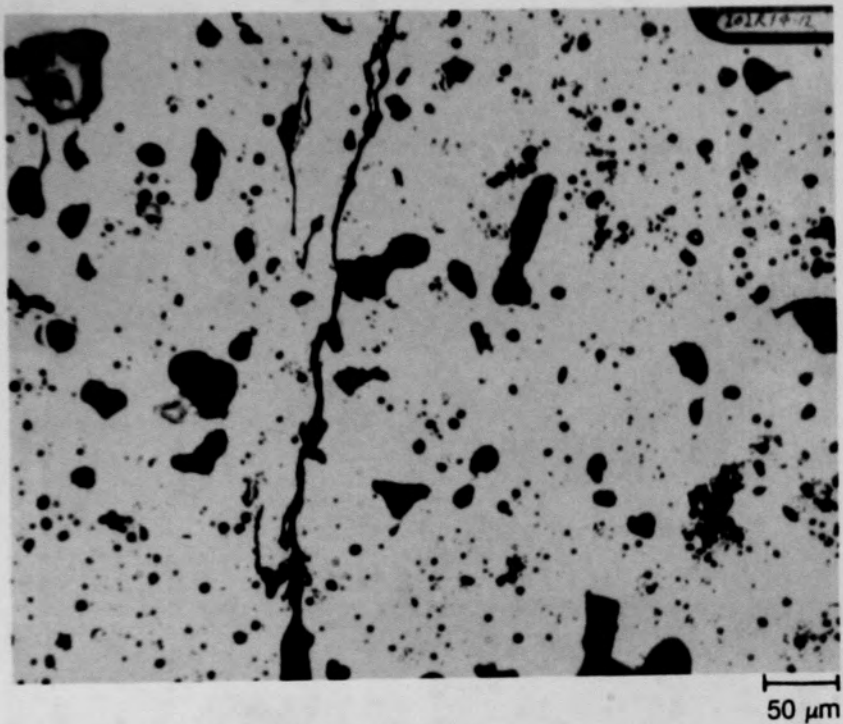
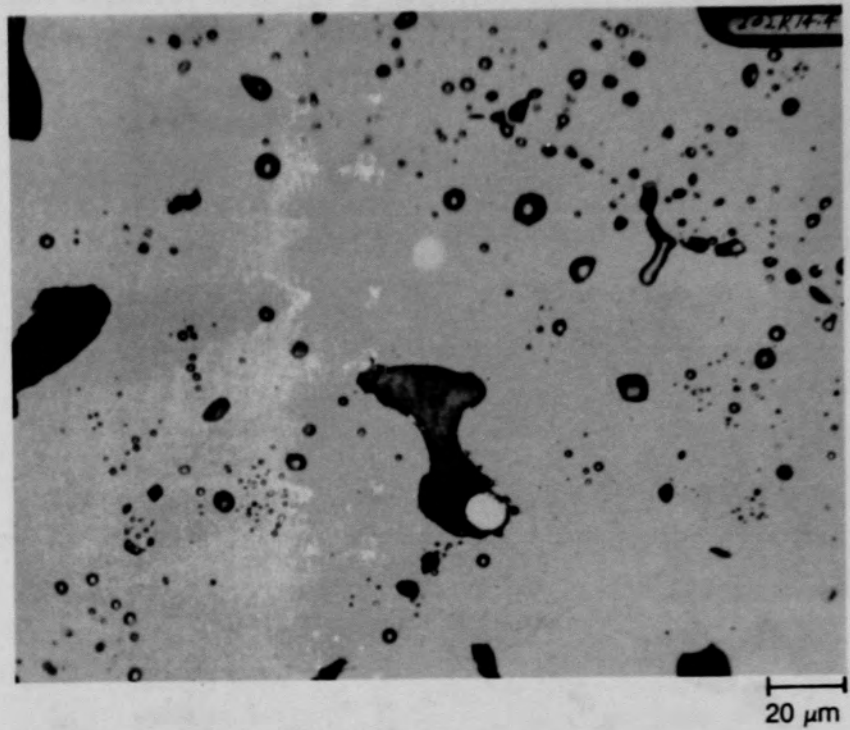


Figure C-71. Photomicrographs of unetched material near the edge of Particle 4D (E9, surface).

C-125



(a) Location D



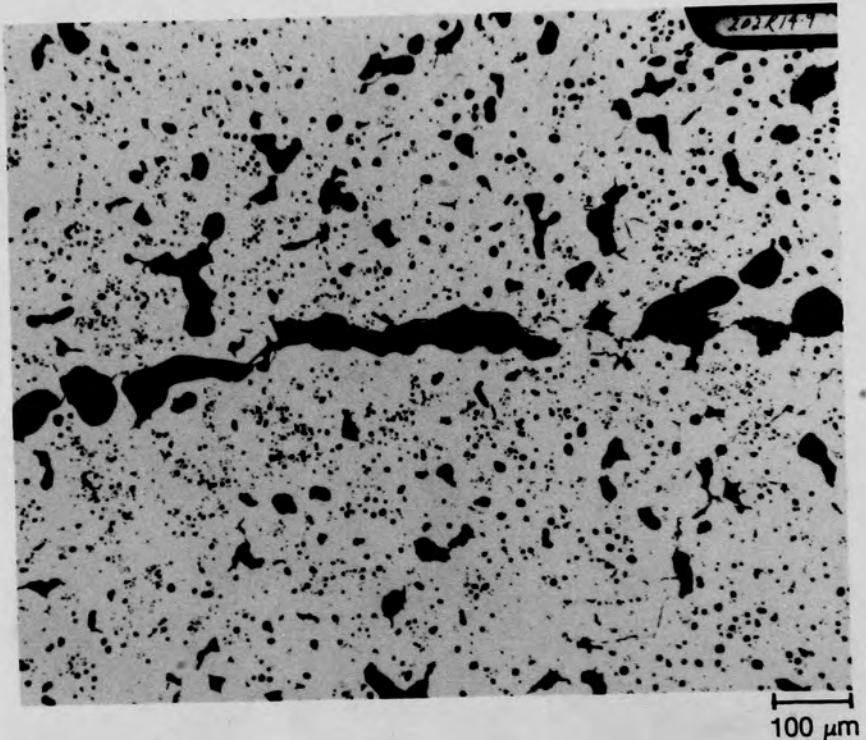
(b) Location E

Figure C-72. Photomicrographs of unetched material near the center of Particle 4D (E9, surface).

C-126



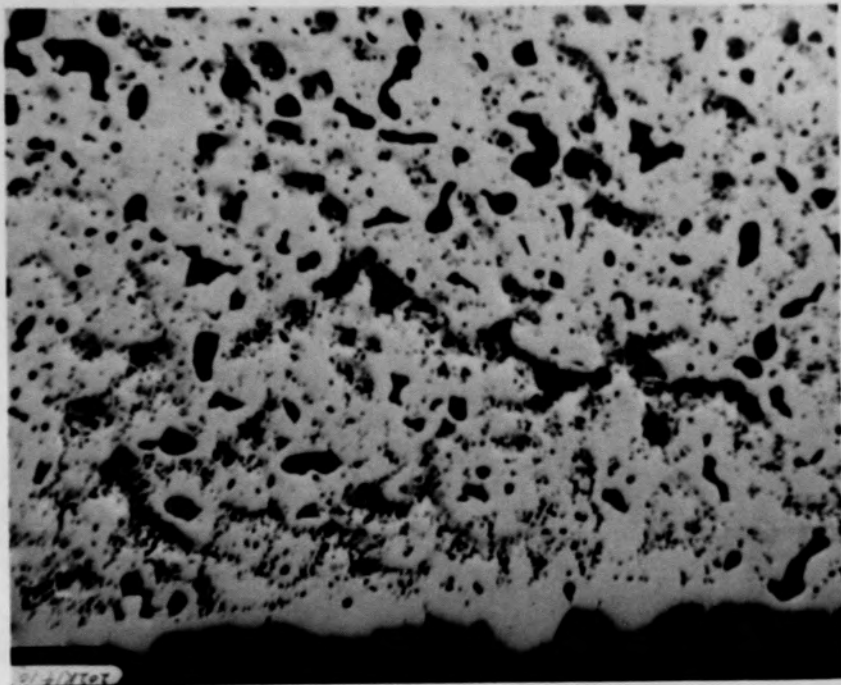
(a) Location F



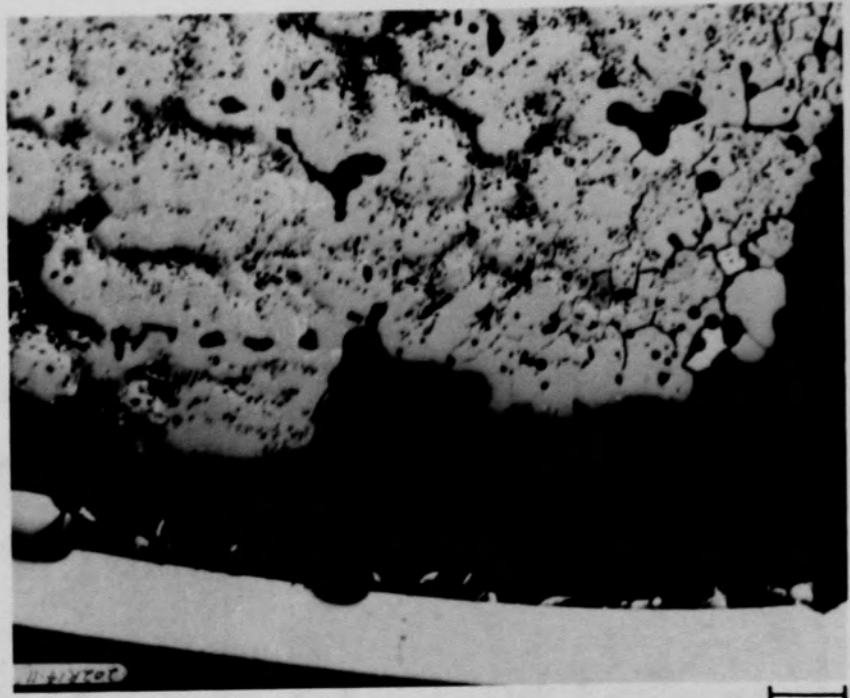
(b) Location B

Figure C-73. Photomicrographs of unetched material near the mid-radius of Particle 4D (E9, surface).

C-127



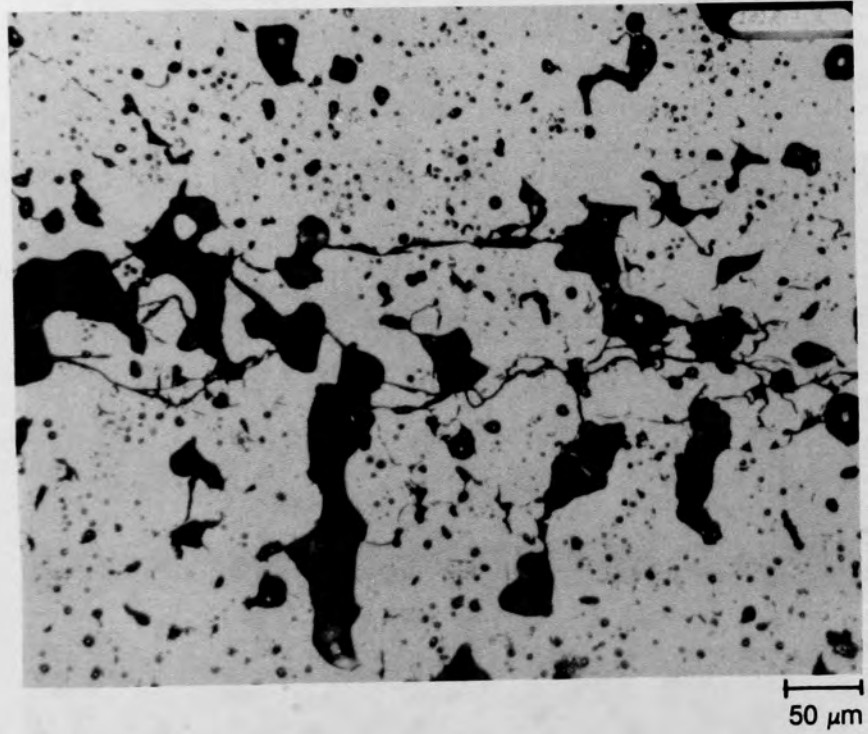
(a) Location H



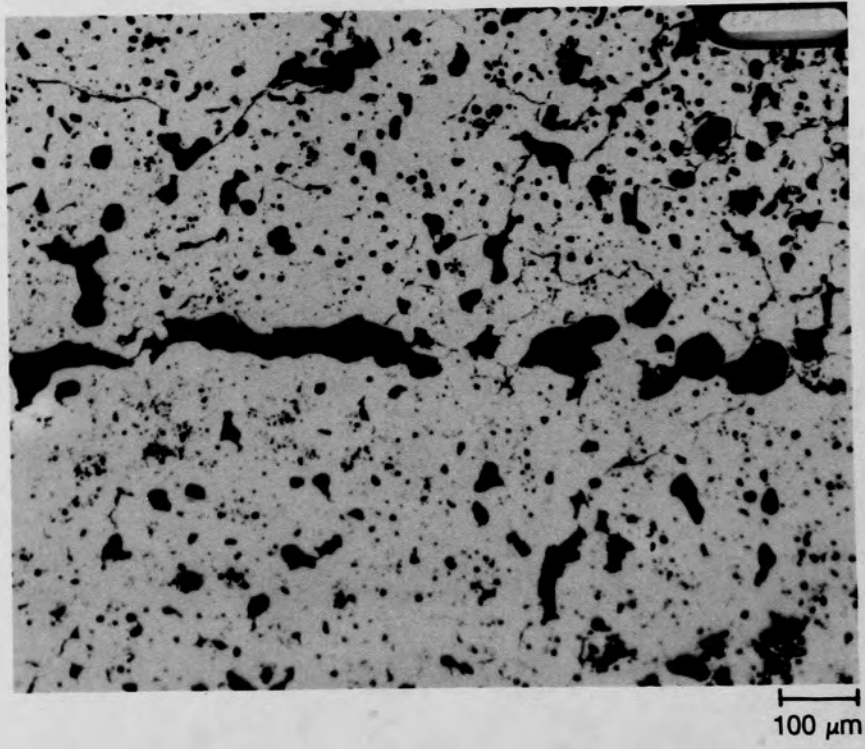
(b) Location I

Figure C-74. Photomicrographs of etched material near the edge of Particle 4D (E9, surface).

C-128



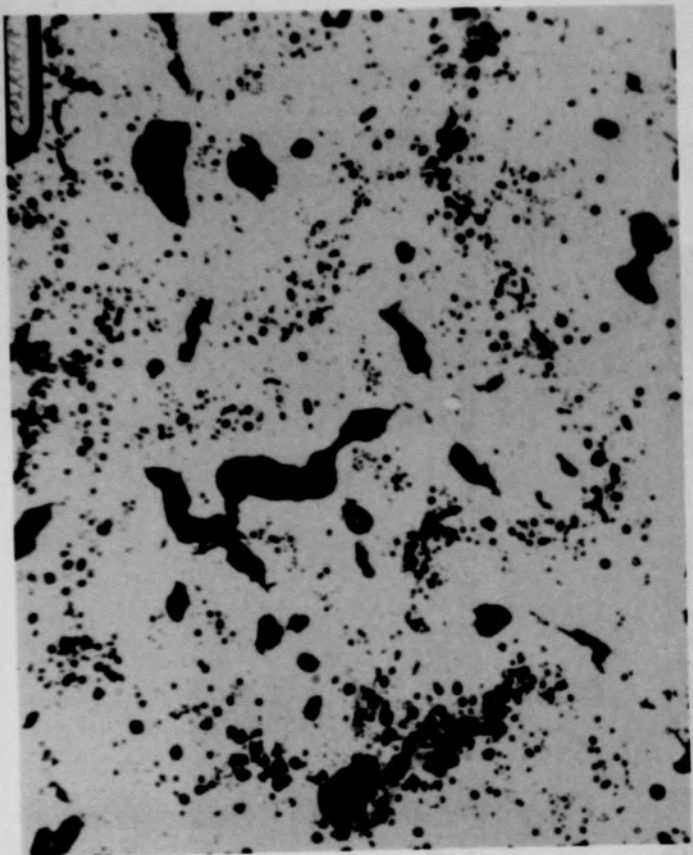
(a) Location F



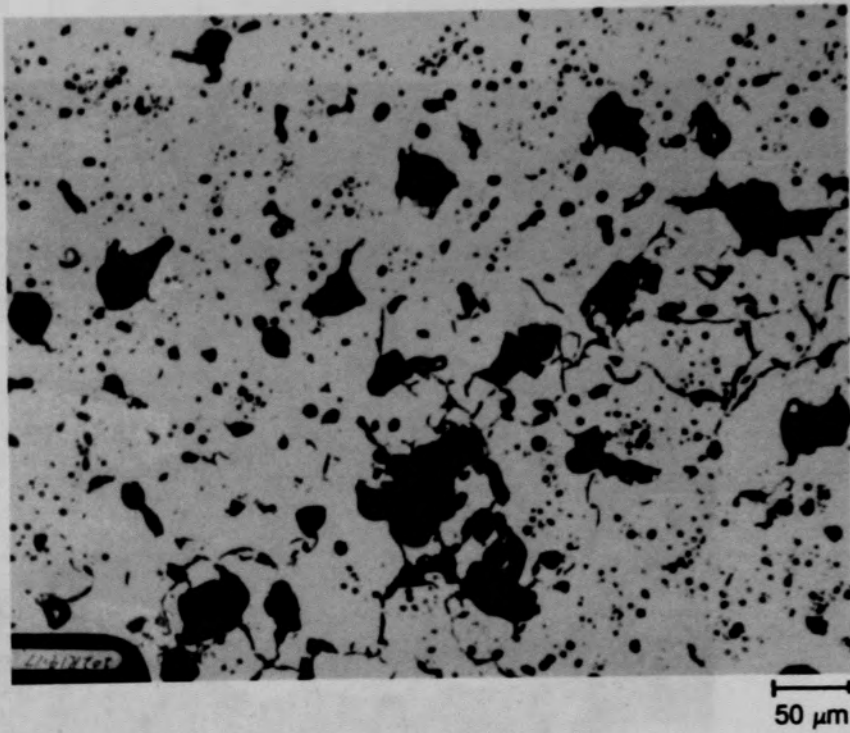
(b) Location B

Figure C-75. Photomicrographs of etched material near the mid-radius of Particle 4D (E9, surface).

C-129



(a) Location E



(b) Location J

Figure C-76. Photomicrographs of etched material near the center of Particle 4D (E9, surface).

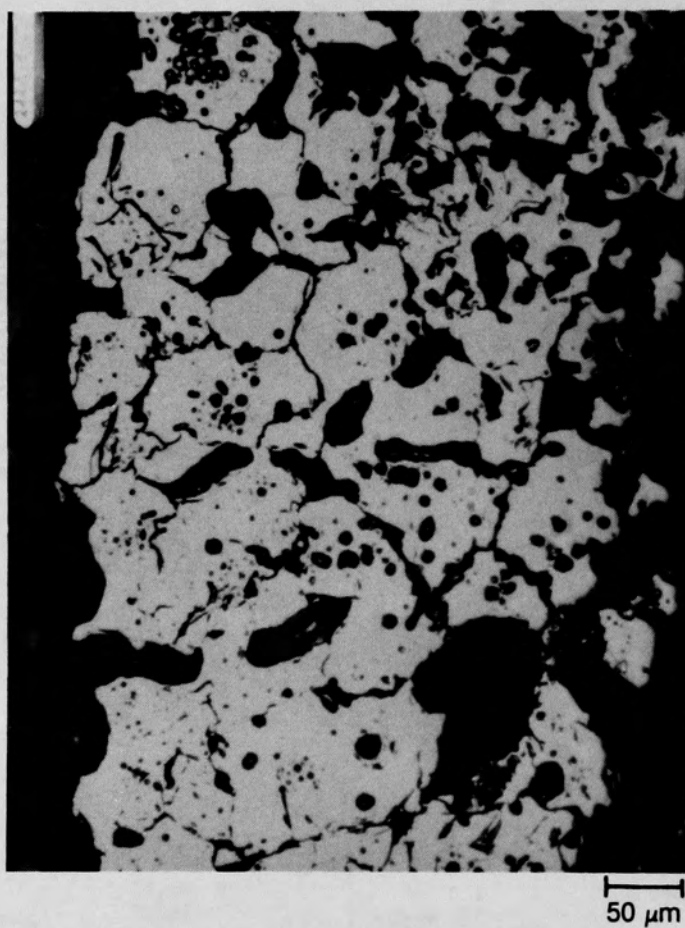


Figure C-77. Photomicrographs of etched material at location G of Particle 4D (E9, surface).

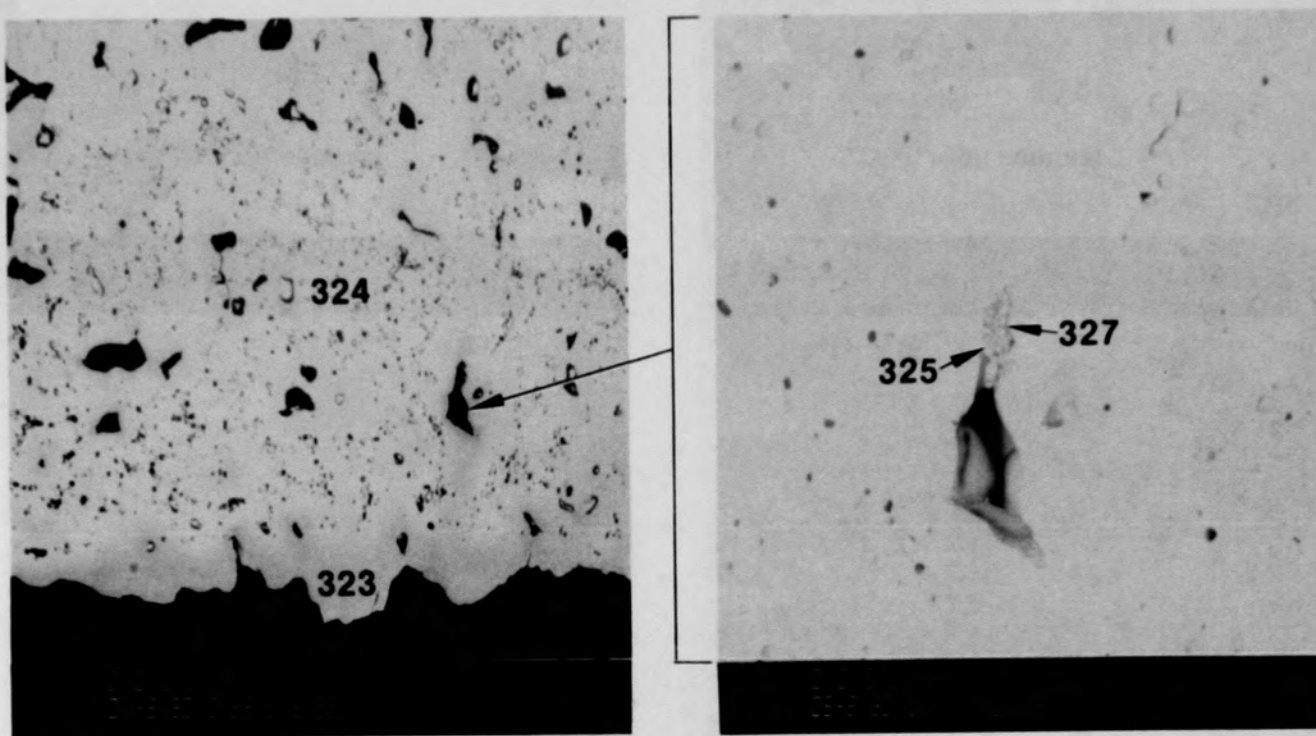
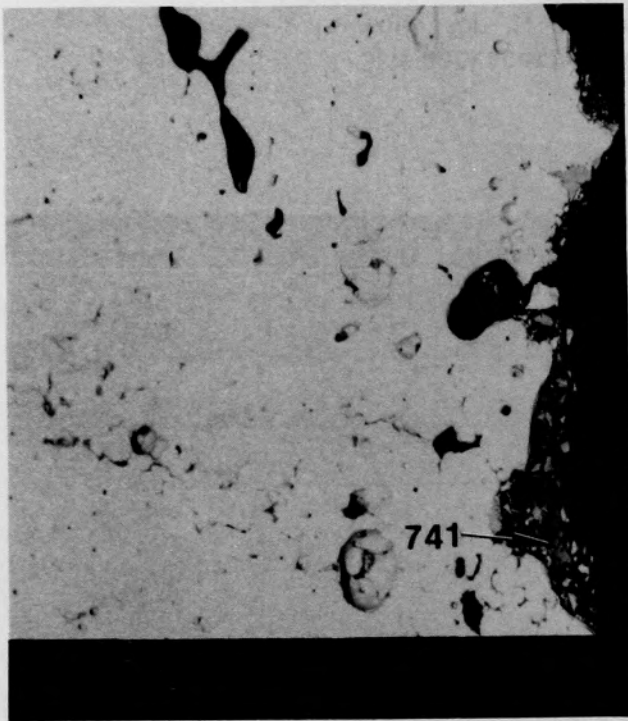


Figure C-78. SEM backscattered electron images of material at edge, location H, of Particle 4D (E9, surface).

C-132



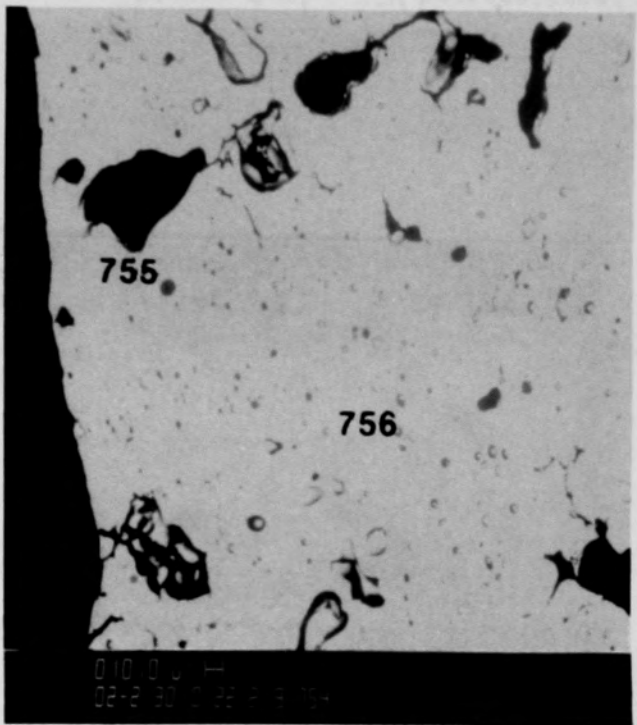
(a) Low contrast



(b) High contrast

Figure C-79. SEM backscattered electron images of location K of Particle 4D (E9, surface).

C-133

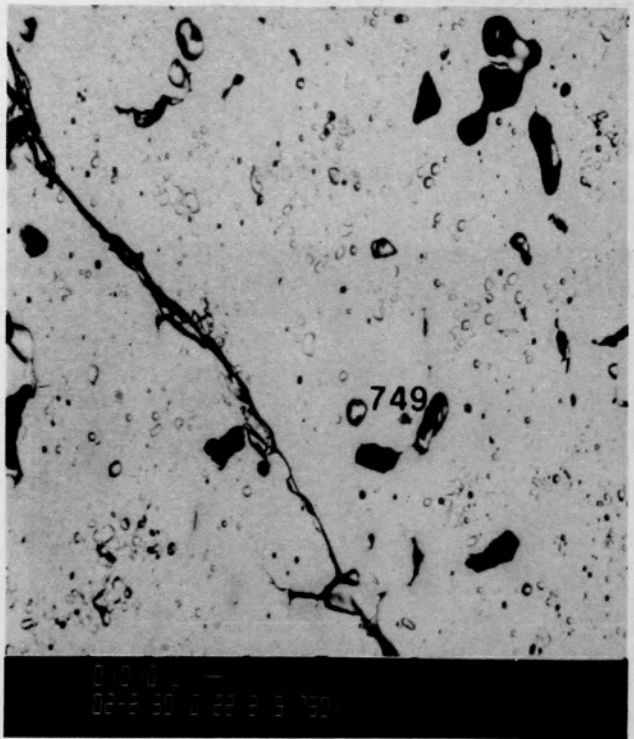


(a) Location A

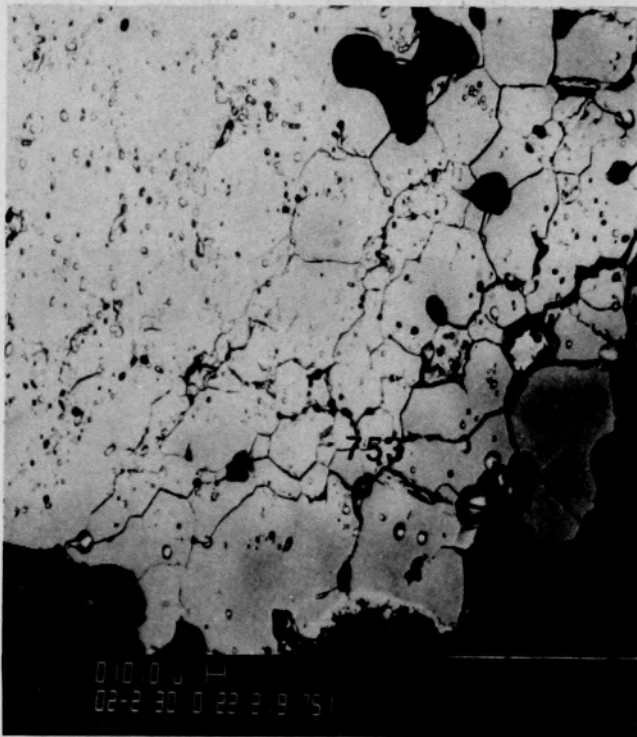


(b) Location C

Figure C-80. SEM backscattered electron images of material from Particle 4D (E9, surface).



(a) Location E



(b) Location I

Figure C-81. SEM backscattered electron images of material from Particle 4D (E9, surface).

C-135

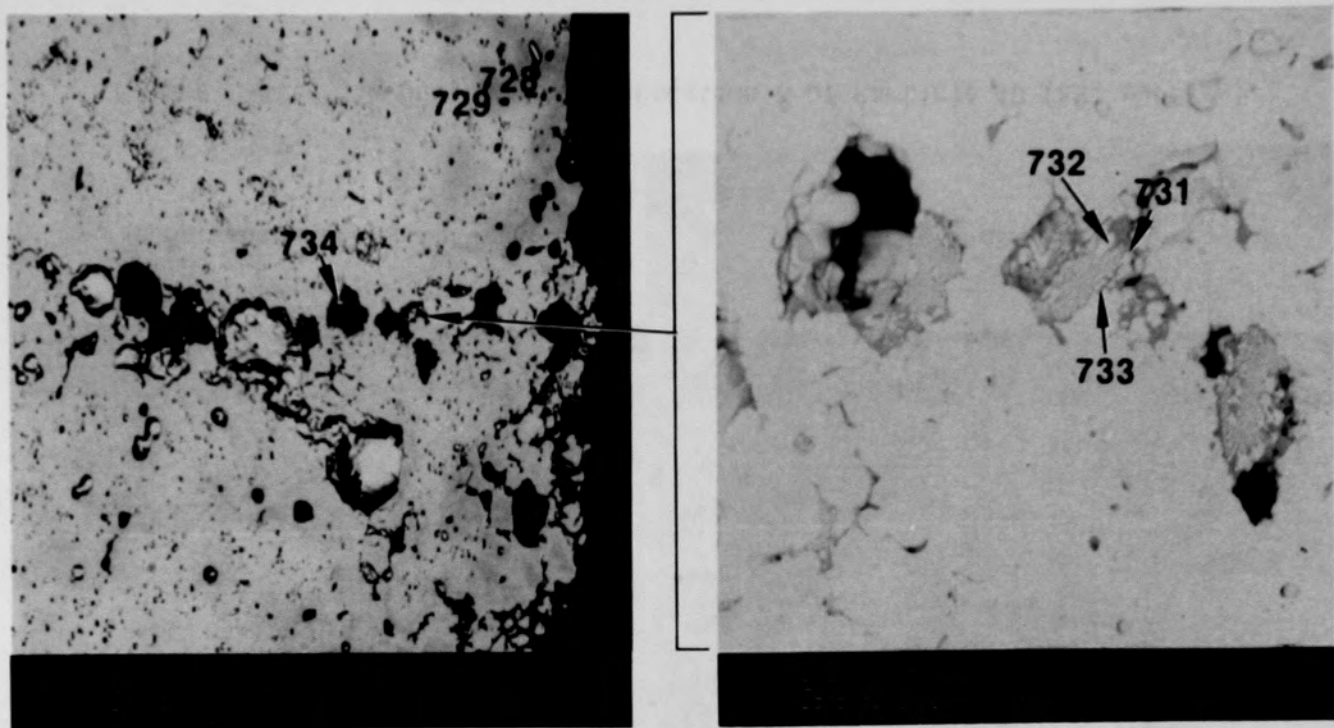
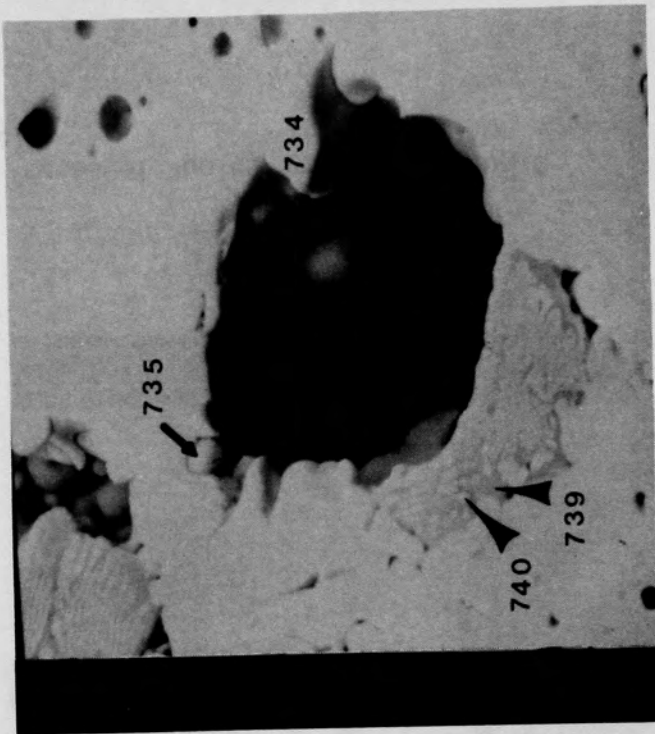


Figure C-82. SEM backscattered electron images of inclusions at location M of Particle 4D (E9, surface).

C-136



(a) Backscattered electron image



(b) Secondary electron image

Figure C-83. SEM photographs of Location M of Particle 4D (E9, surface).

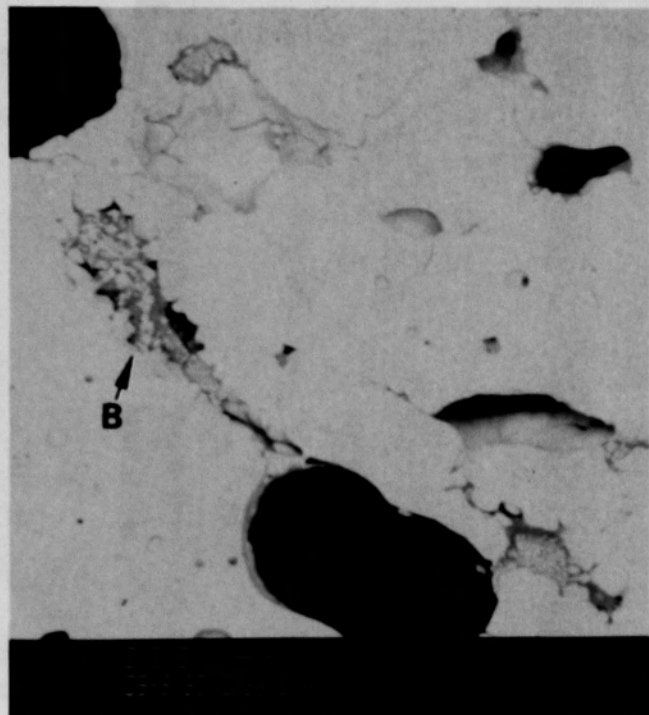


Figure C-84. SEM backscattered electron image of material in location B from Particle 4D (E9, surface).

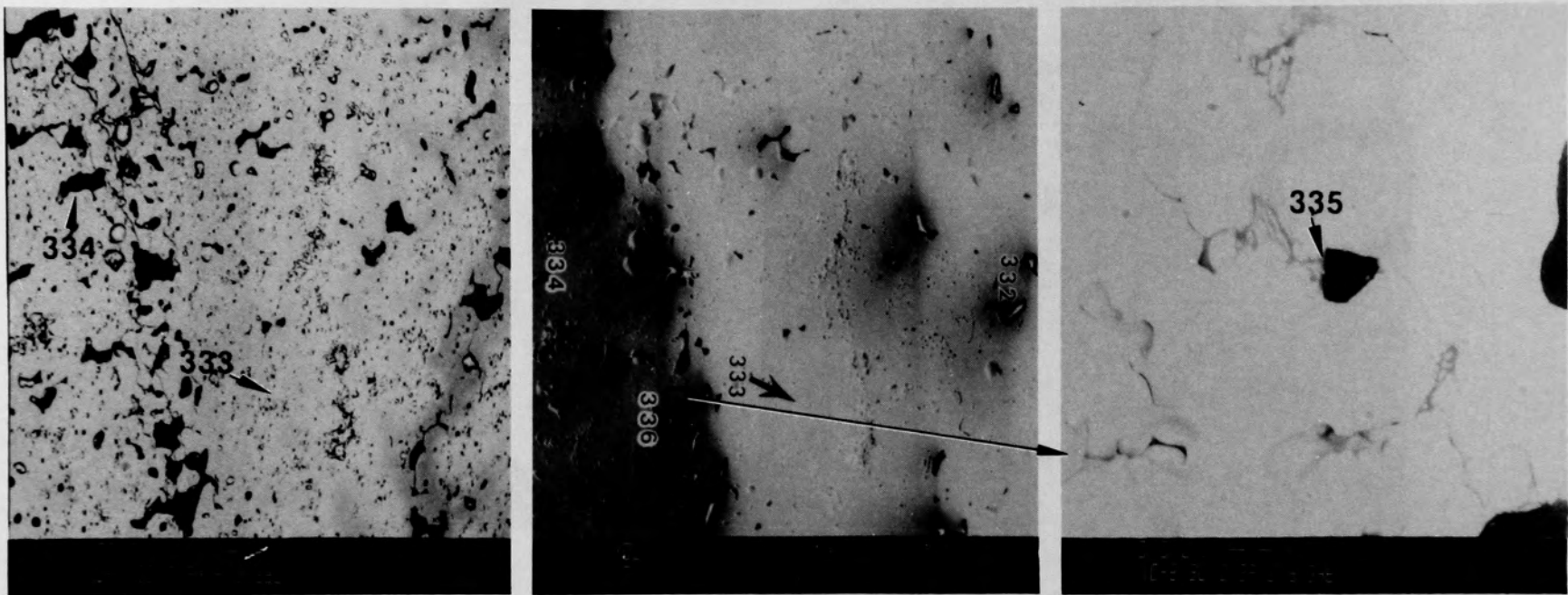
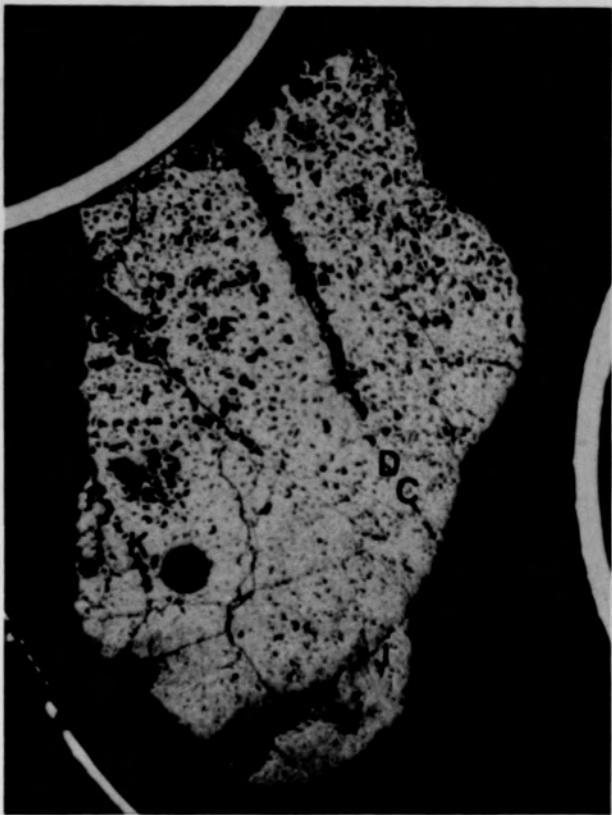
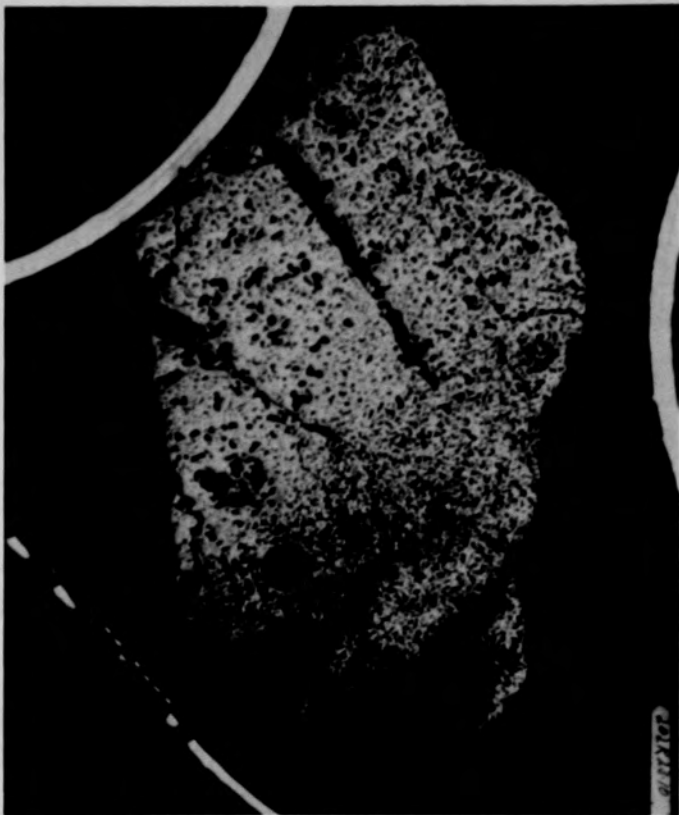


Figure C-85. SEM backscattered electron images of material at location F from Particle 4D (E9, surface).

C-139



(a) Unetched



(b) Etched

670 μm

Figure C-86. Photomacrographs of Particle 5E (E9, 8 cm).

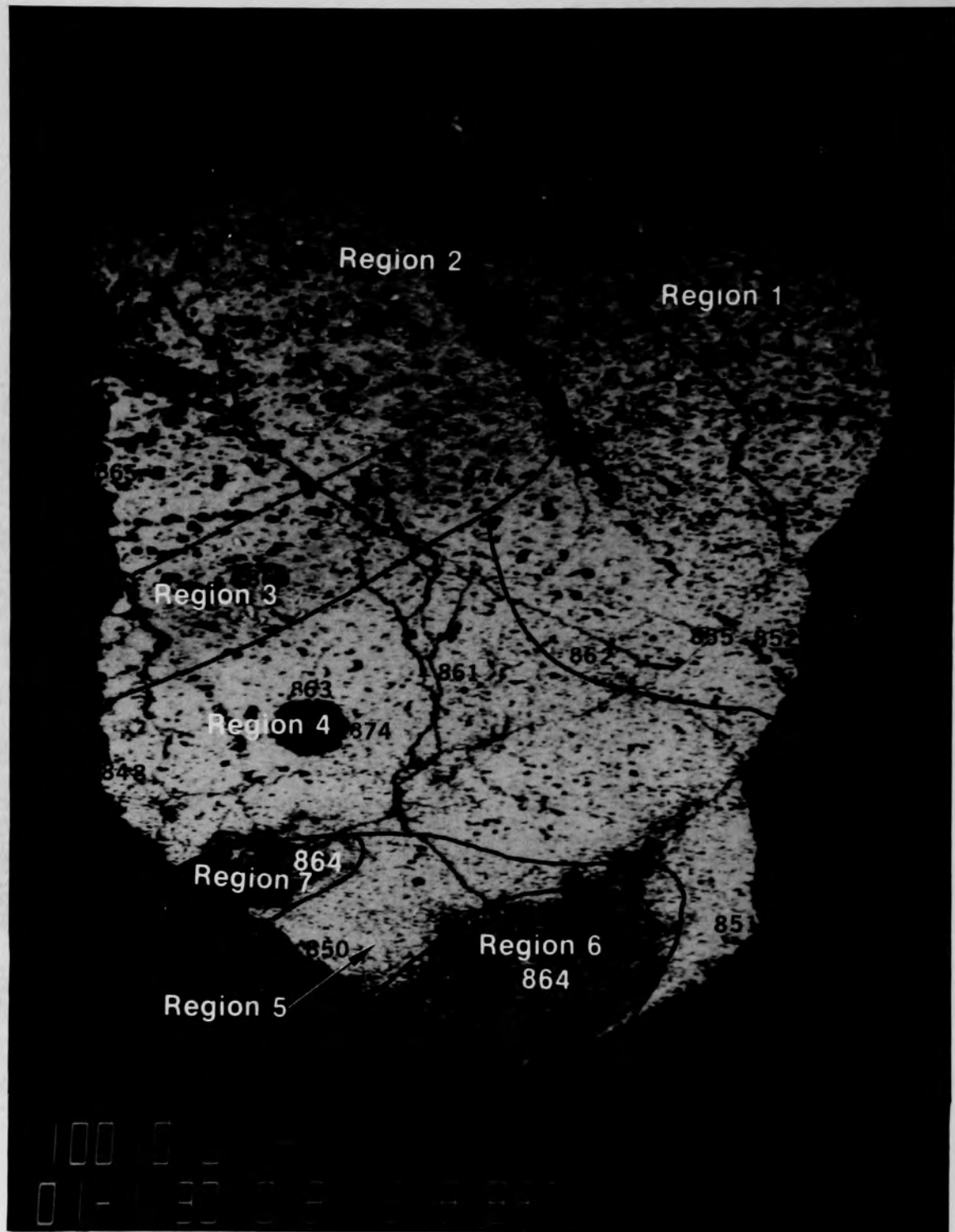
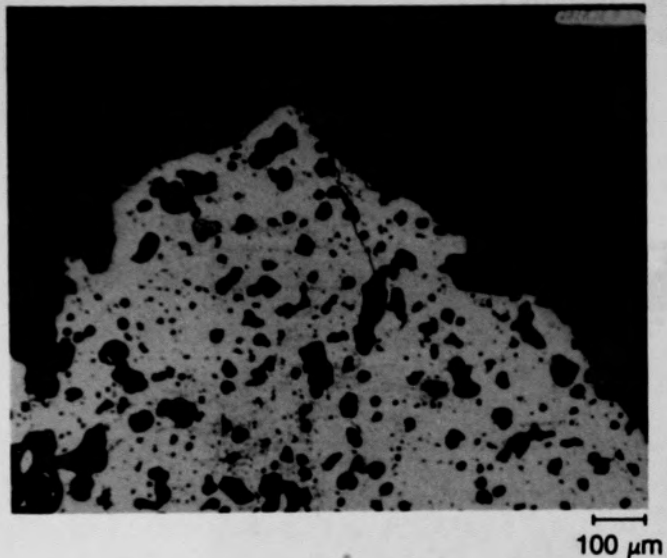
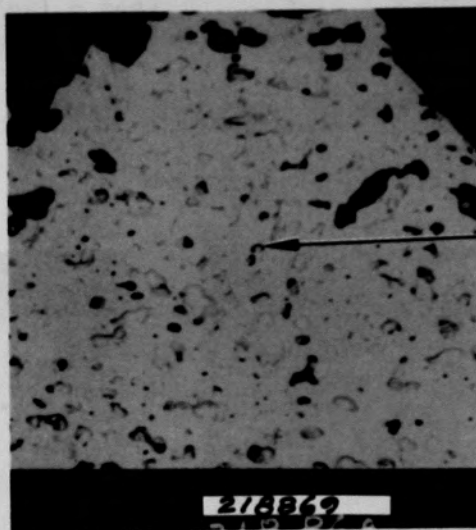


Figure C-87. SEM backscattered electron images showing 7 regions of Particle 5E (E9, 8 cm).

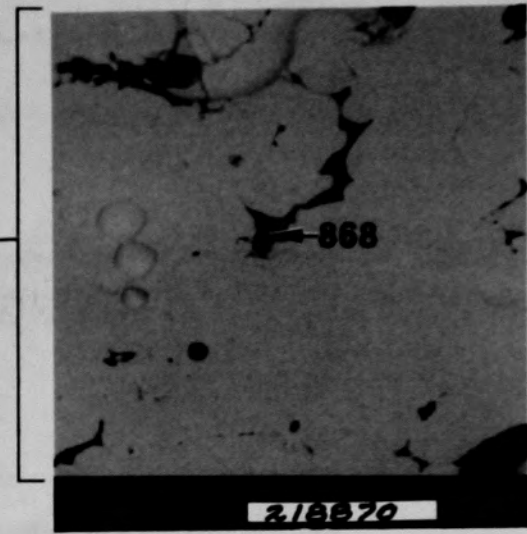
C-141



(a) Photomicrograph



(b) SEM backscattered electron image



(c) SEM backscattered electron image

Figure C-88. Photographs of material in Region 1, location A, of Particle 5E (E9, 8 cm).

C-142

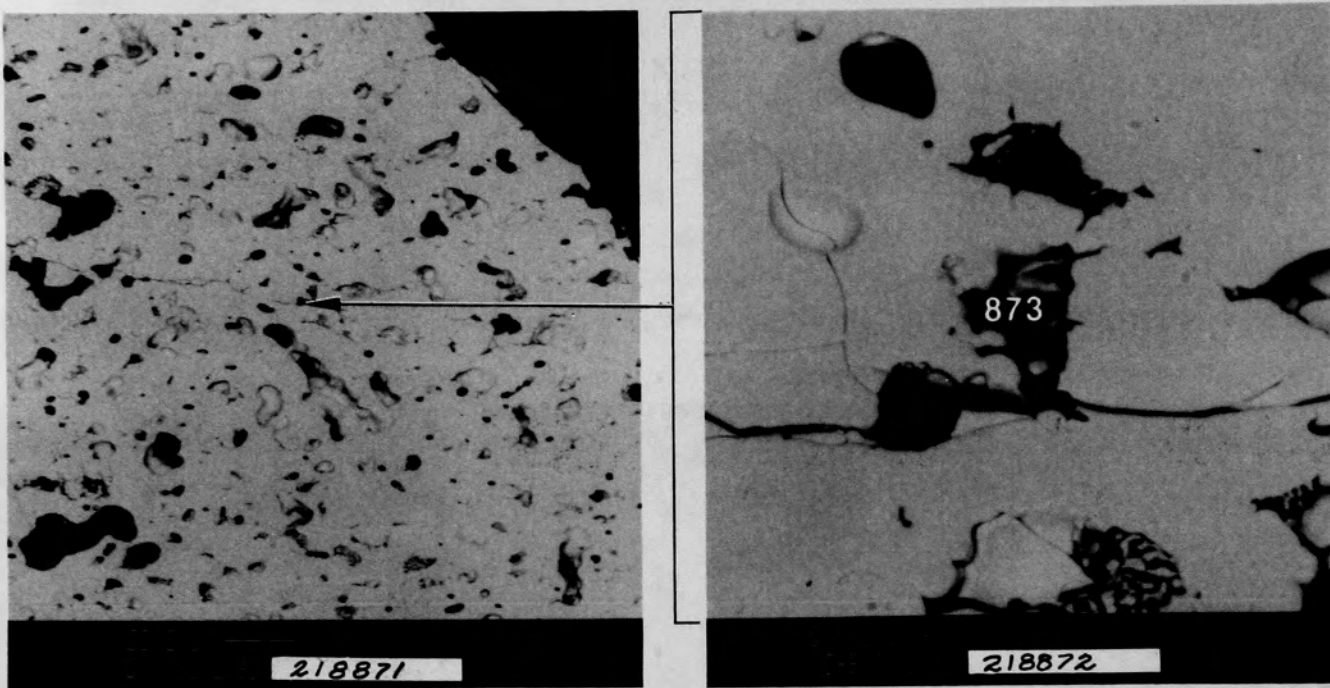
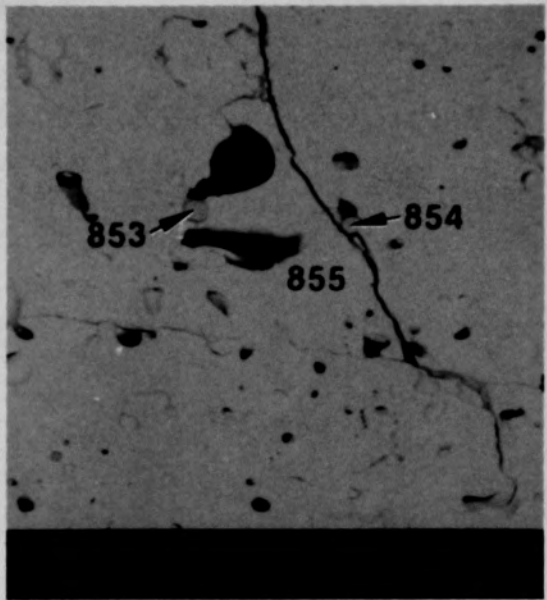


Figure C-89. SEM backscattered electron images of Region 1, location B, of Particle 5E (E9, 8 cm).

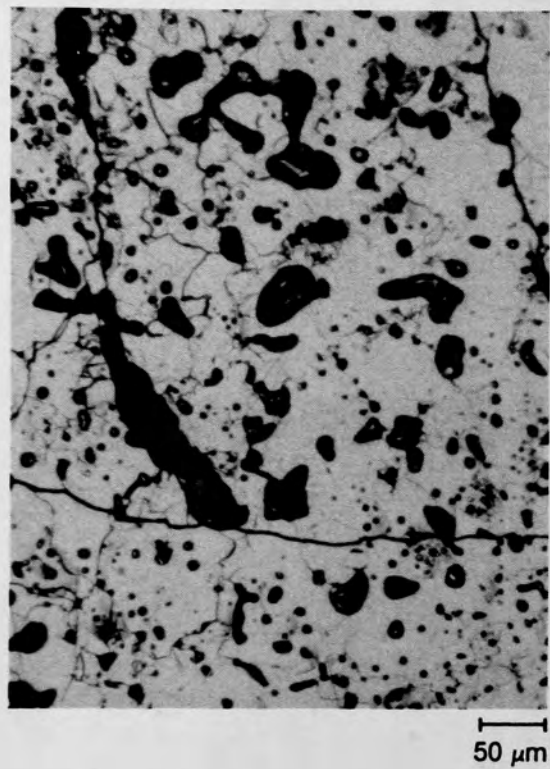


(a) Photomicrograph

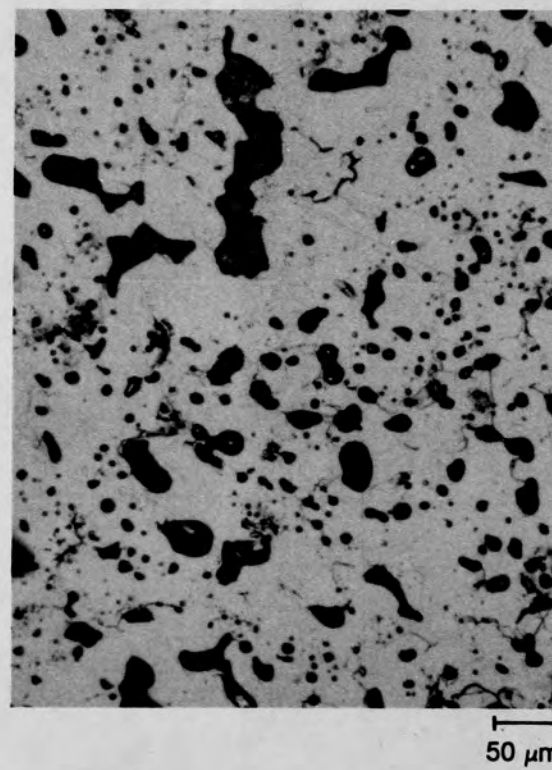


(b) SEM backscattered electron image

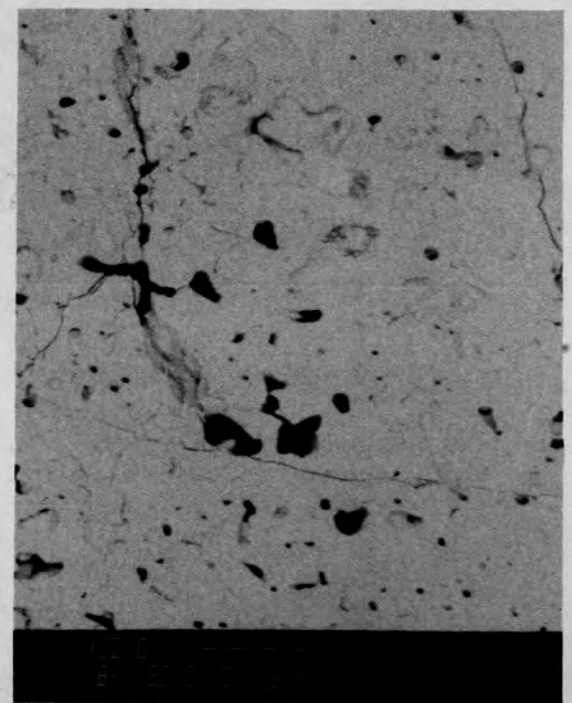
Figure C-90. Photographs of material from Region 1, Location C of Particle 5E (E9, 8 cm).



(a) Photomicrograph



(b) Photomicrograph



(c) SEM backscattered electron image

Figure C-91. Photographs of material from Region 1, Location D, of Particle 5E (E9, 8 cm).

C-145

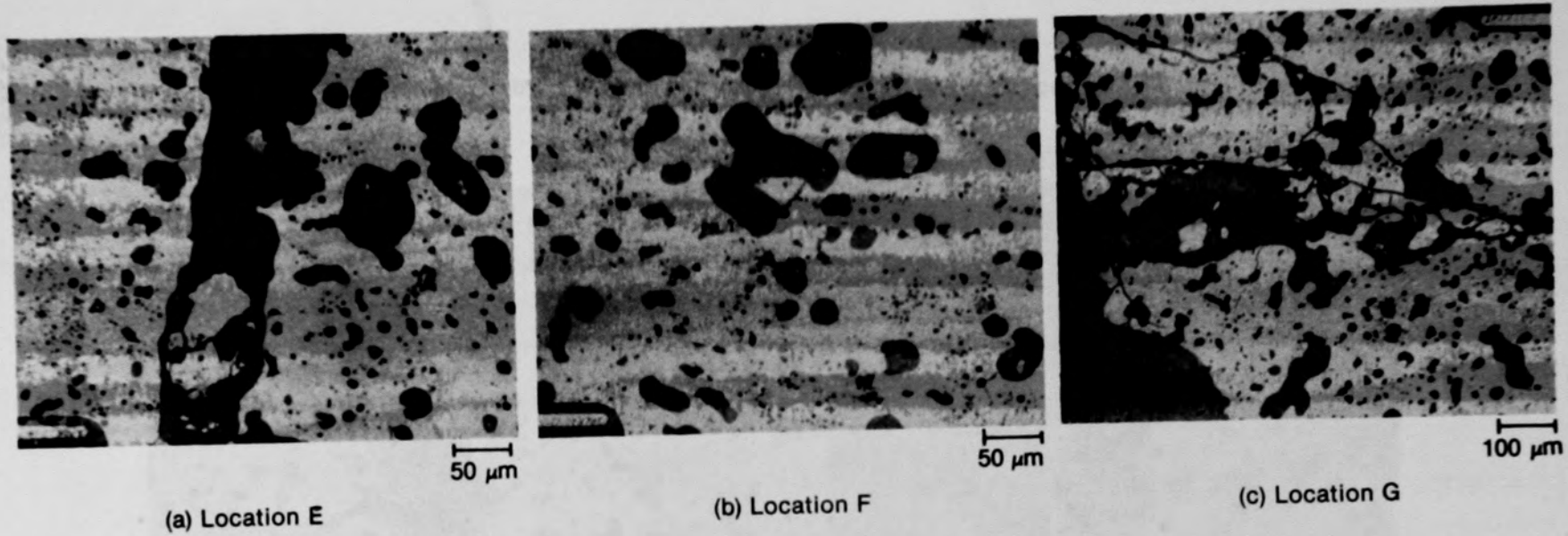
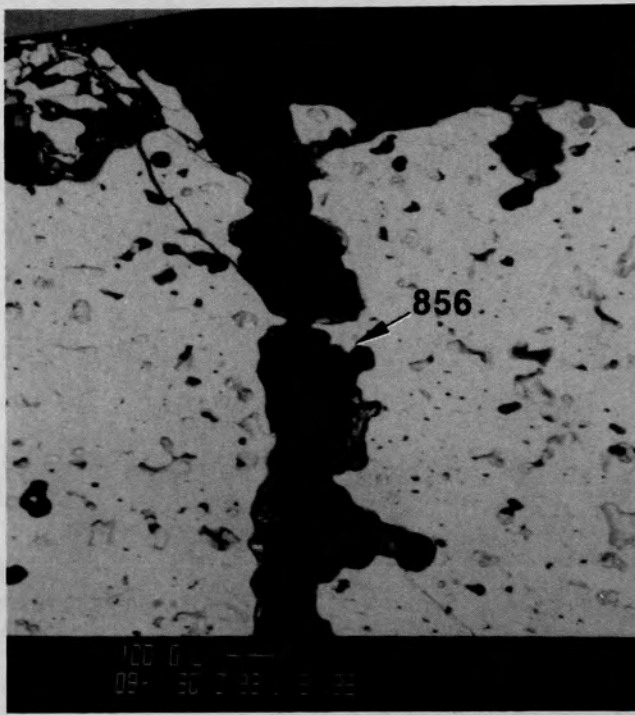


Figure C-92. Photomicrographs of material from Region 2 of Particle 5E
(E9, 8 cm).

C-146



(a) Photomicrograph



(b) SEM backscattered electron image

Figure C-93. Photographs of material from Region 2, Location H, of Particle 5E (E9, 8 cm).



Figure C-94. Photomicrograph of material from Region 3 of Particle 5E (E9, 8 cm).

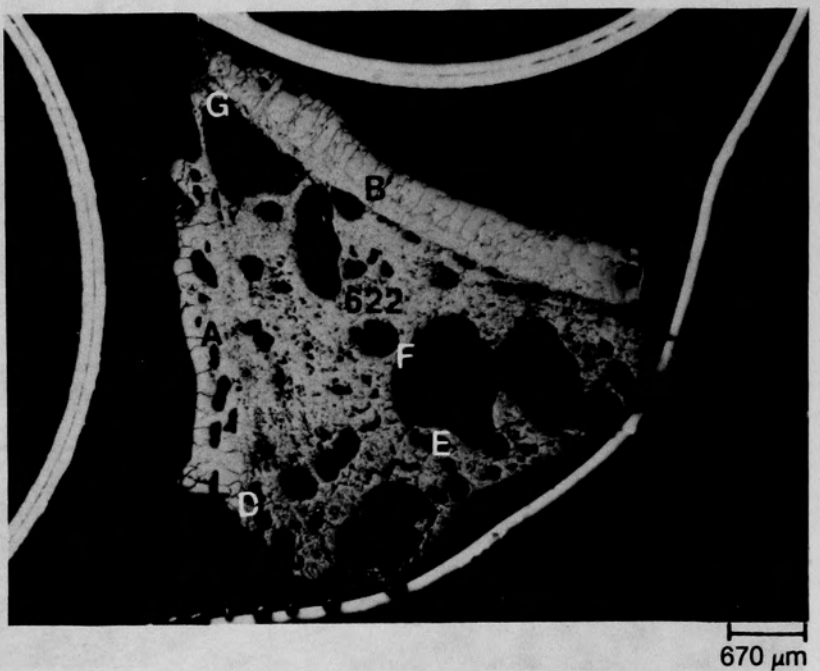


Figure C-97. Photomacrograph of Particle 6C (E9, 56 cm).

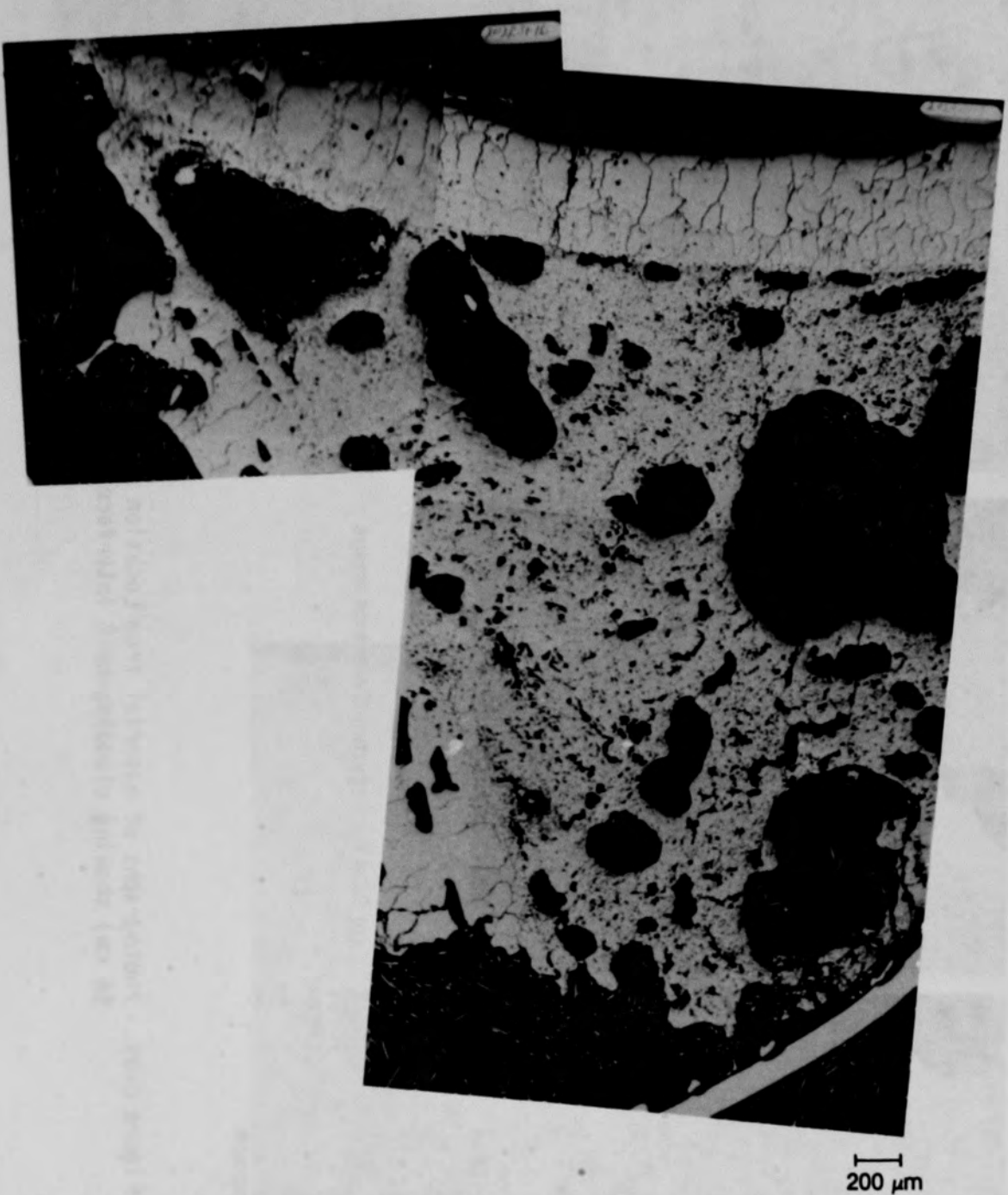
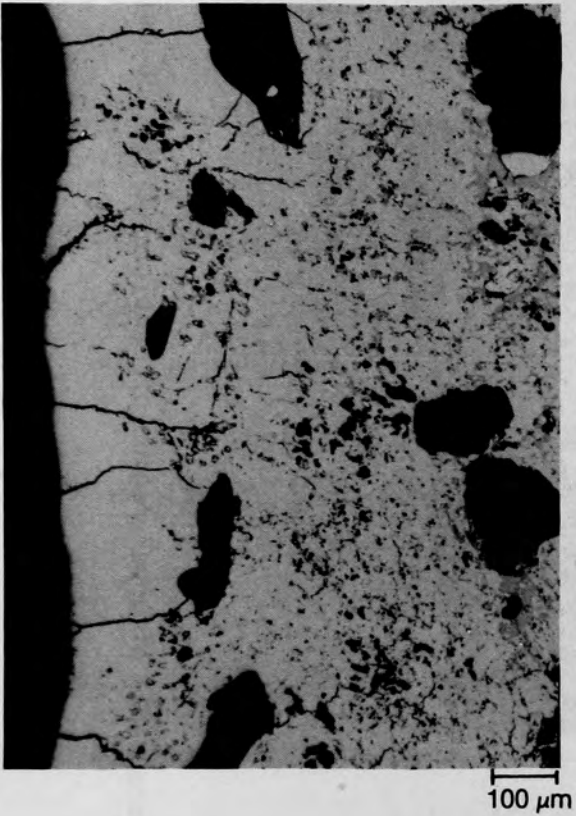
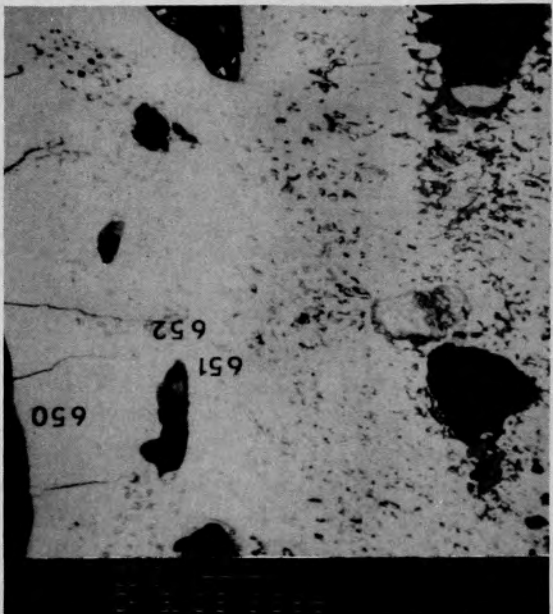


Figure C-98. Photomacrographs of upper region of Particle 6C (E9, 56 cm).

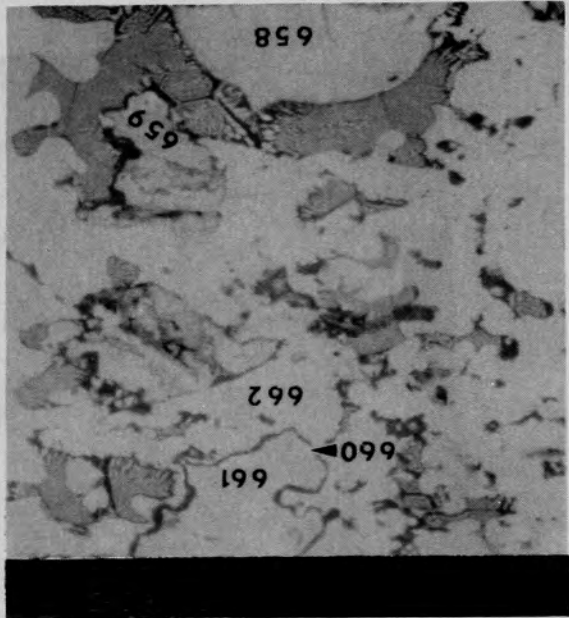
C-152



(a) Photomicrograph

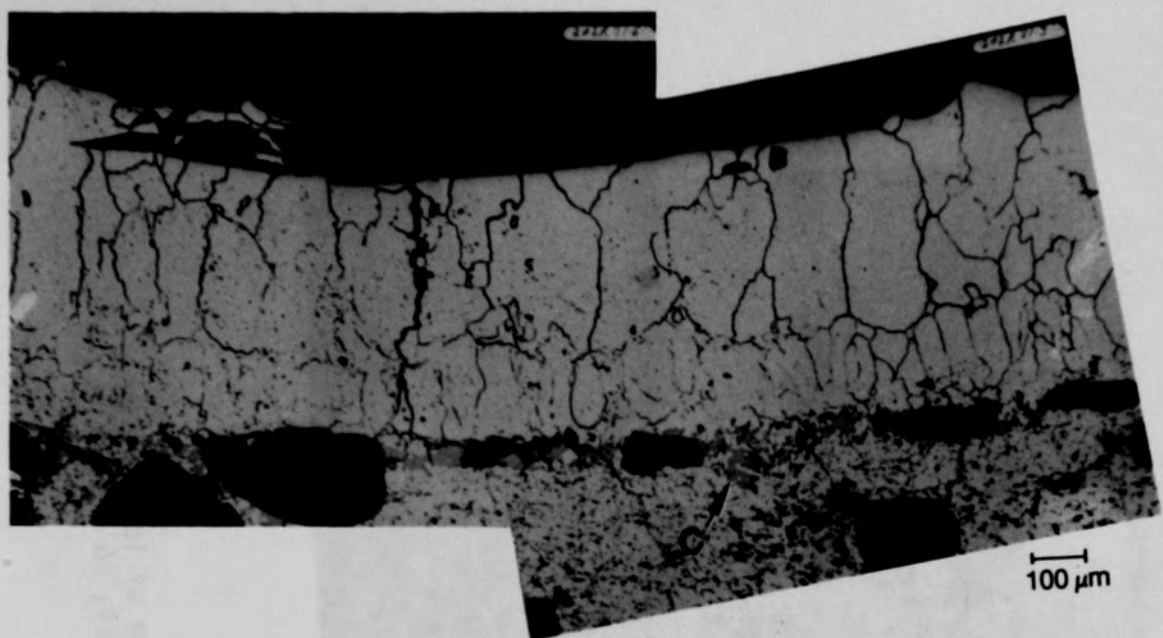


(b) SEM backscattered electron image

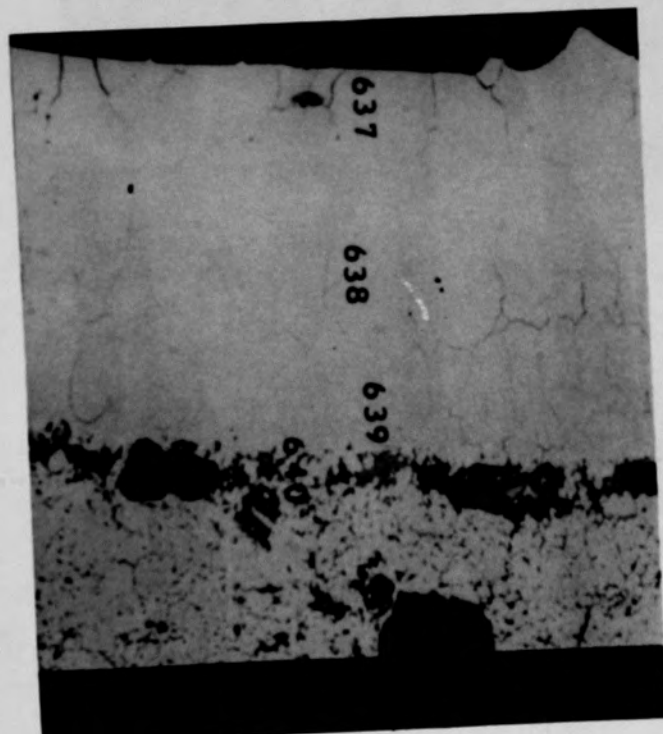


(c) SEM backscattered electron image

Figure C-99. Photographs of material from Location A of Particle 6C (E9, 56 cm) showing cladding-melt interface.



(a) Photomicrograph



(b) SEM backscattered electron image

Figure C-100. Photographs of material from location B of Particle 6C (E9, 56 cm).

C-154

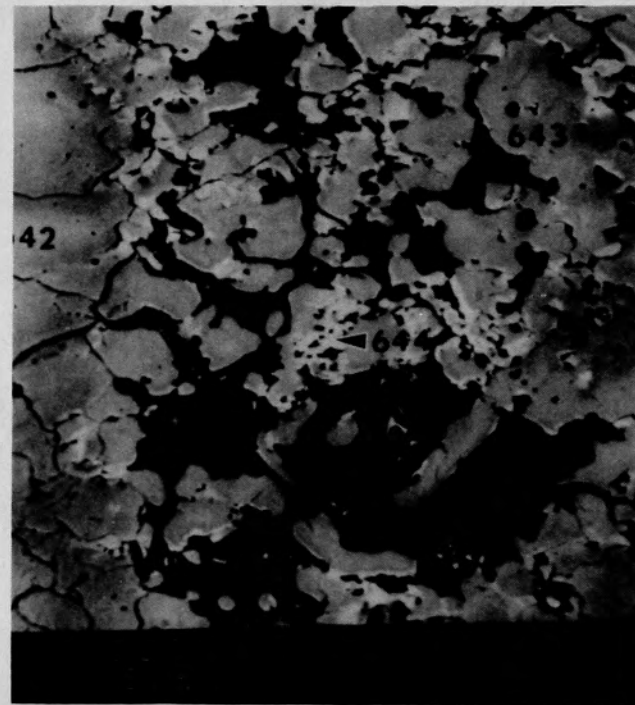
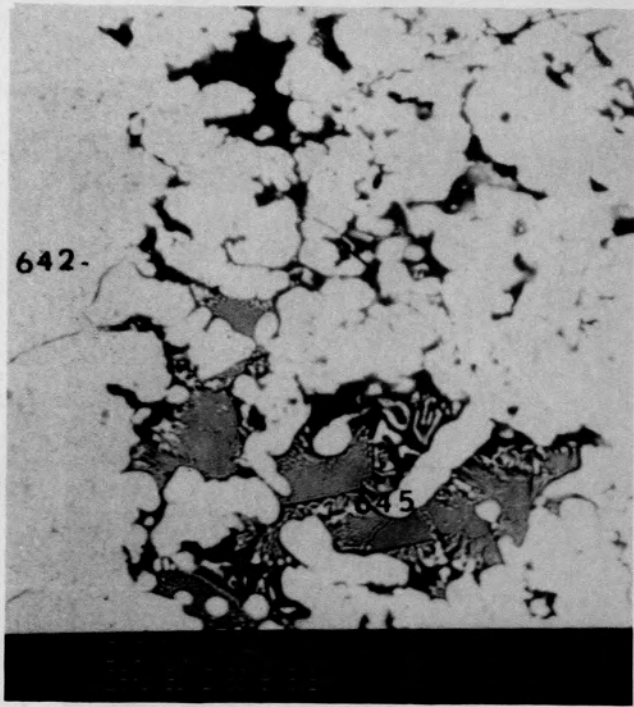


Figure C-101. SEM backscattered electron image of location C
(Figure C-100) of Particle 6C (E9, 56 cm).

C-155

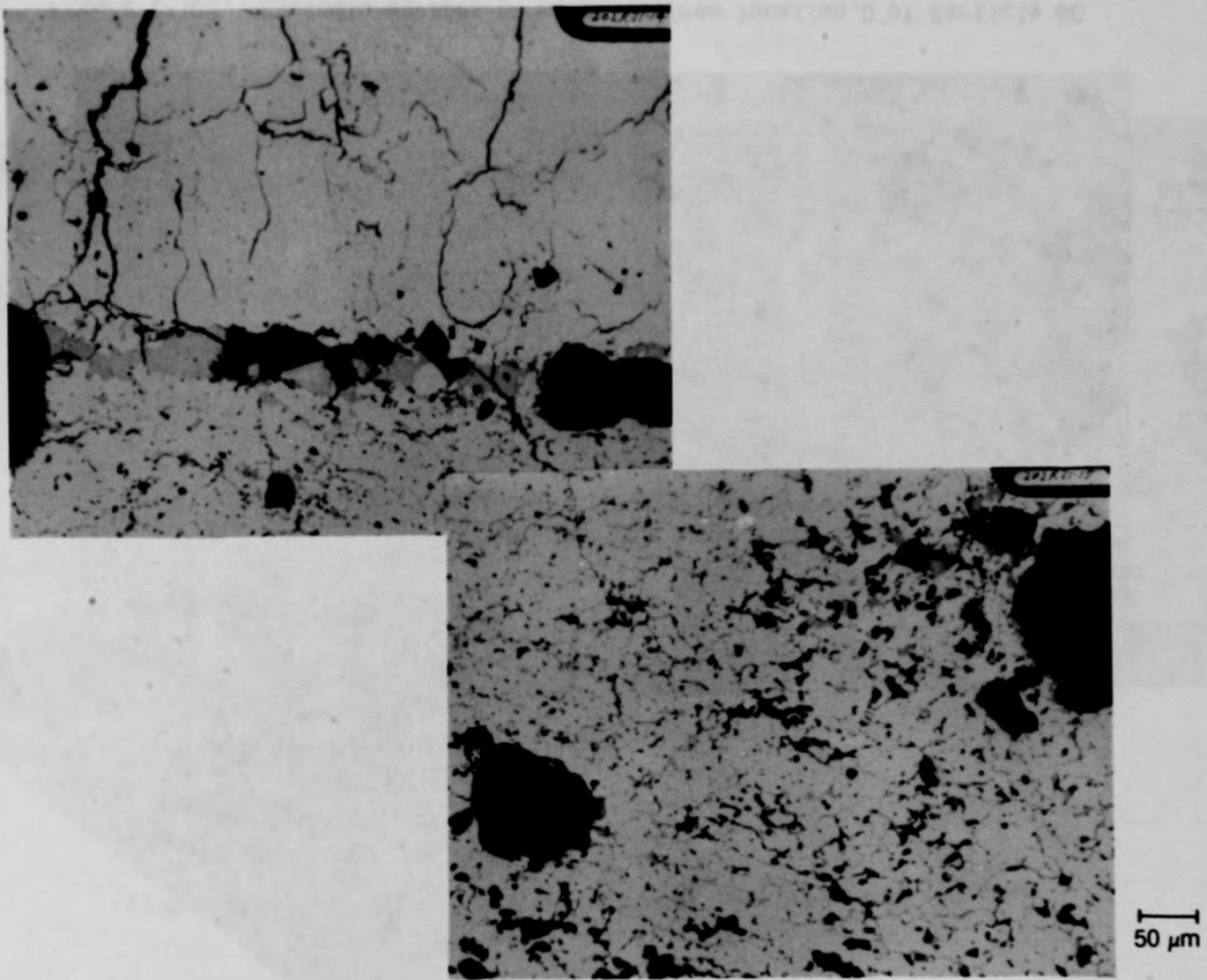


Figure C-102. Photomicrographs of material from location B of Particle 6C (E9, 56 cm).

C-156

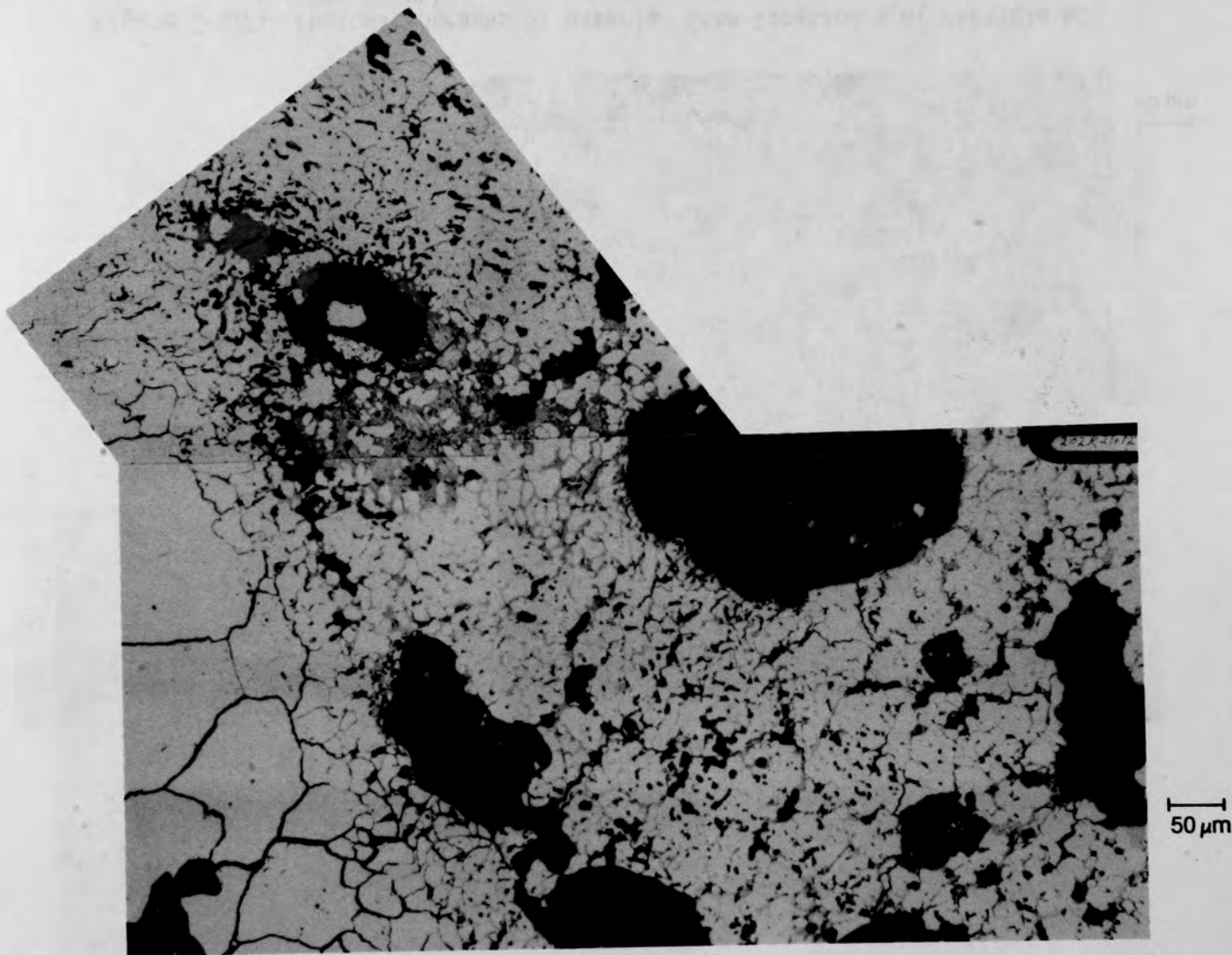


Figure C-103. Photomicrographs of material from location D of Particle 6C
(E9, 56 cm).

C-157

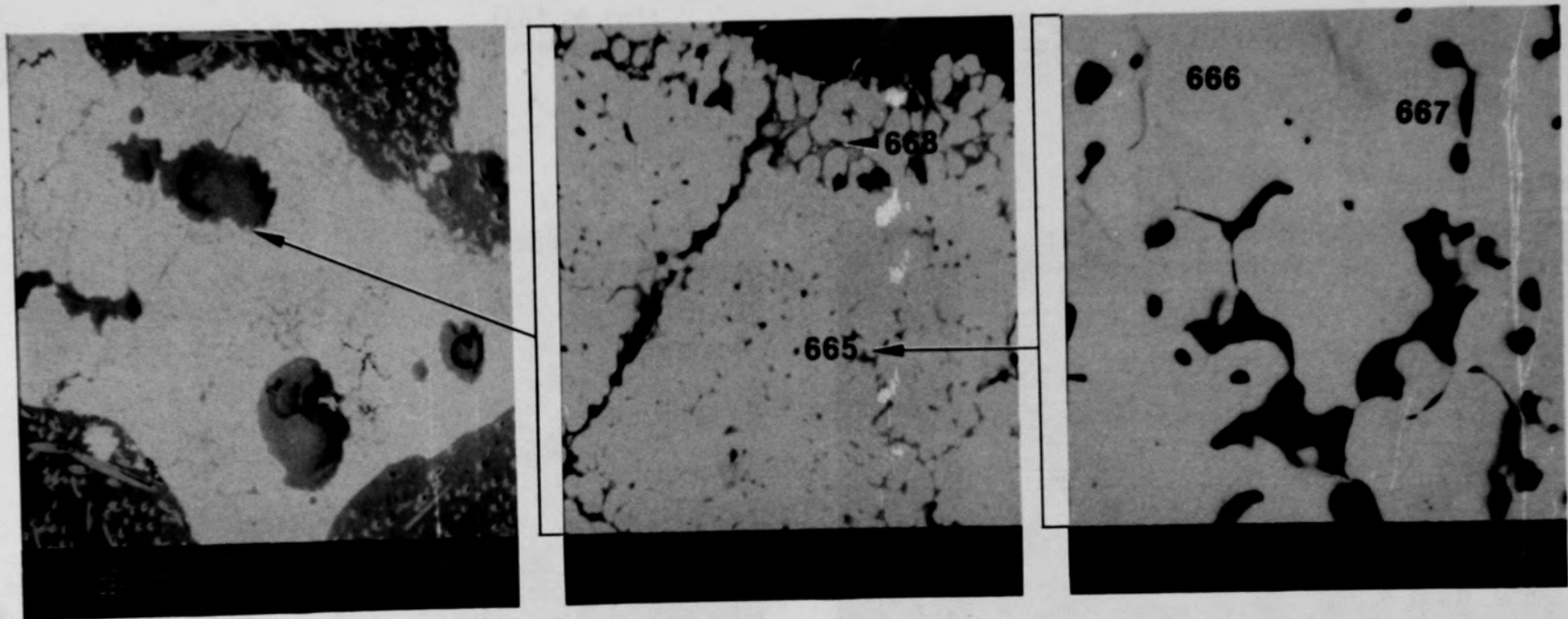


Figure C-104. SEM backscattered electron images of material from location E of Particle 6C (E9, 56 cm).

C-158

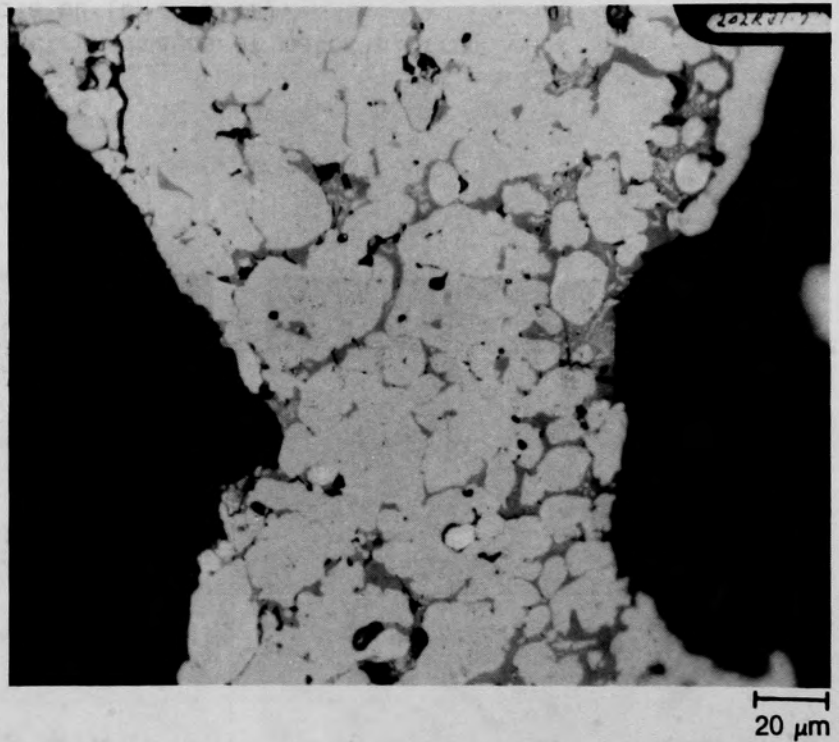
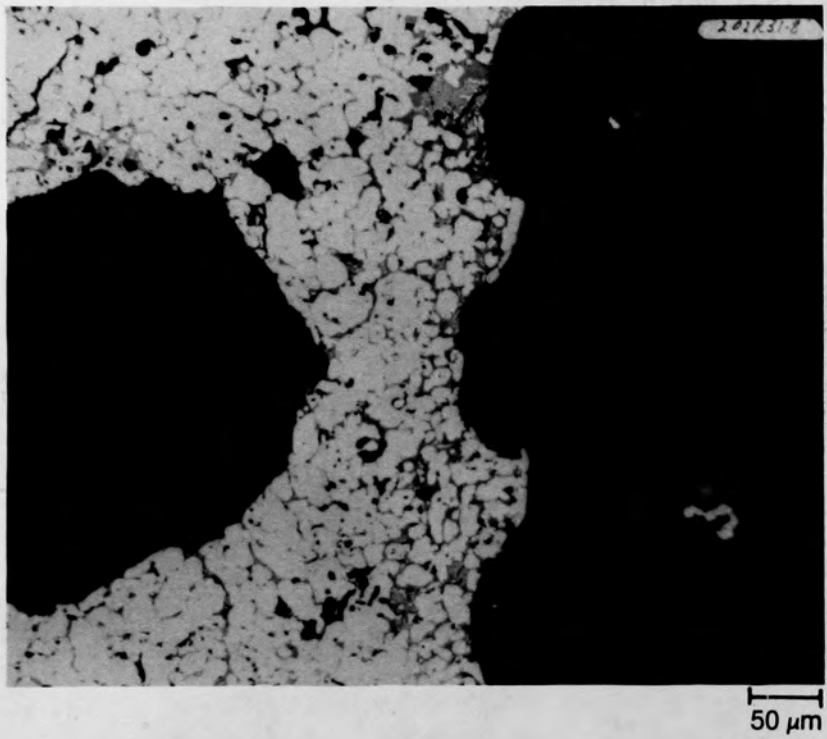
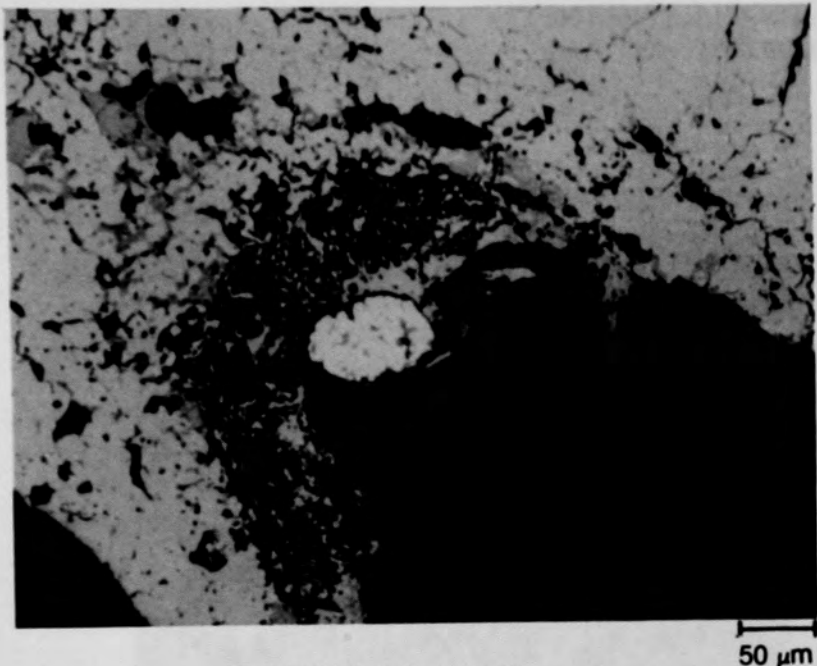
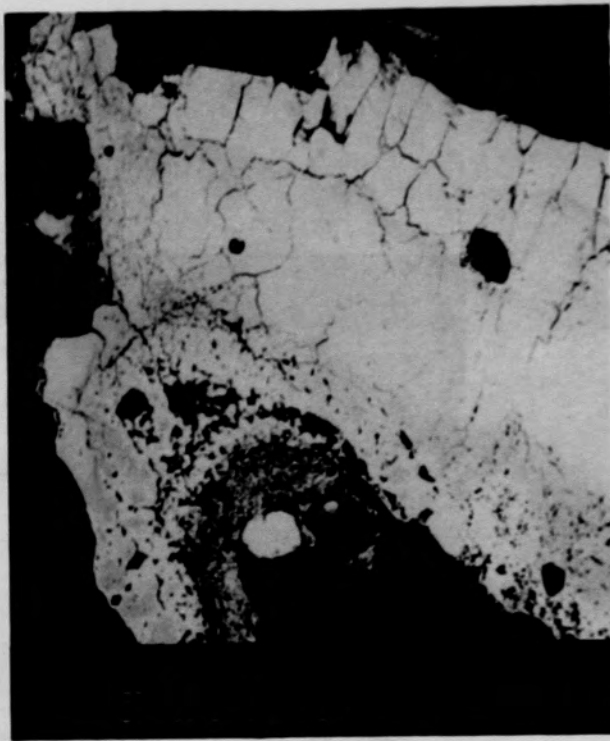


Figure C-105. Photomicrographs of material from location F of Particle 6C (E9, 56 cm).

C-159



(a) Photomicrograph



(b) SEM backscattered electron image

Figure C-106. Photographs of material from location G of Particle 6C (E9, 56 cm).

C-160

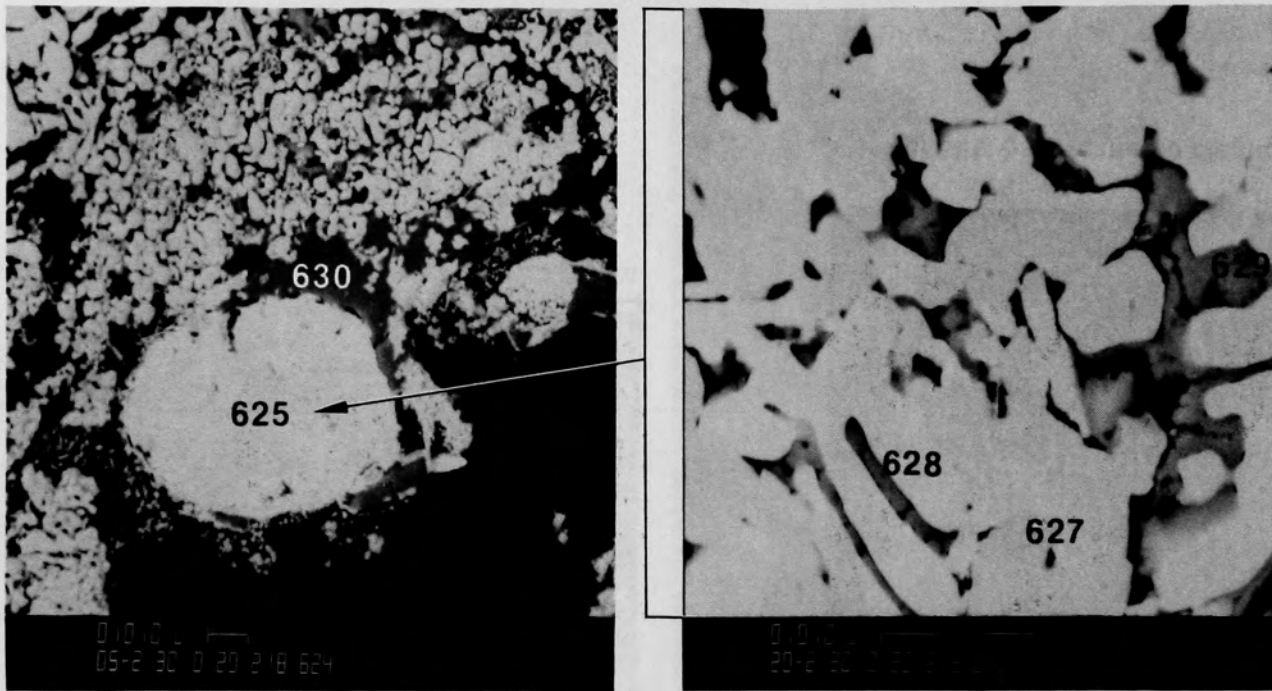


Figure C-107. SEM backscattered electron images of material from location D of Particle 6C (E9, 56 cm).

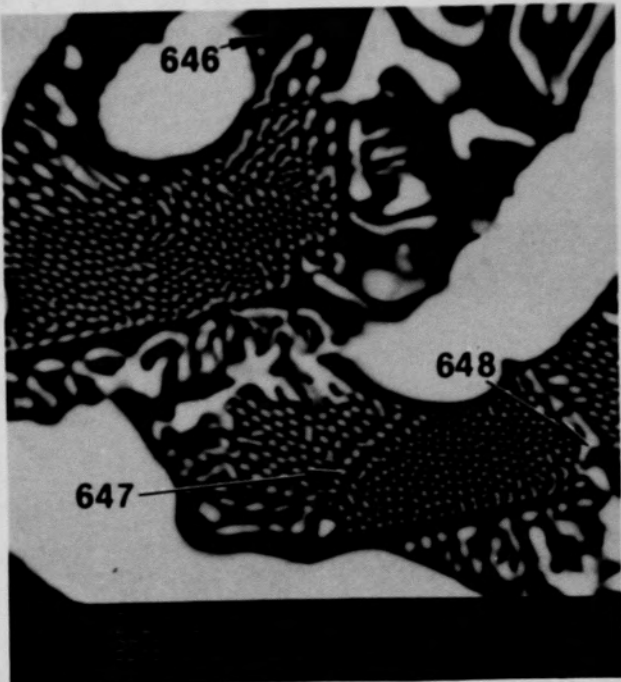
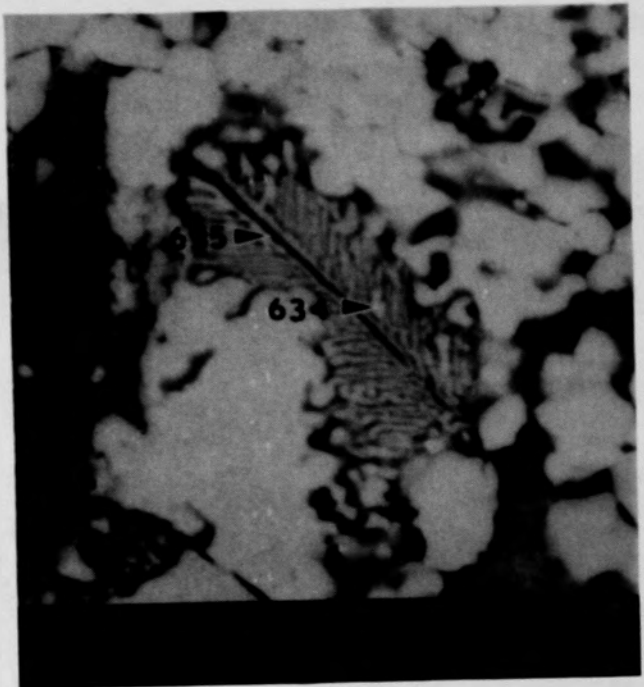


Figure C-108. SEM backscattered electron images of material from location D of Particle 6C (E9, 56 cm) showing two phase structure.

C-162

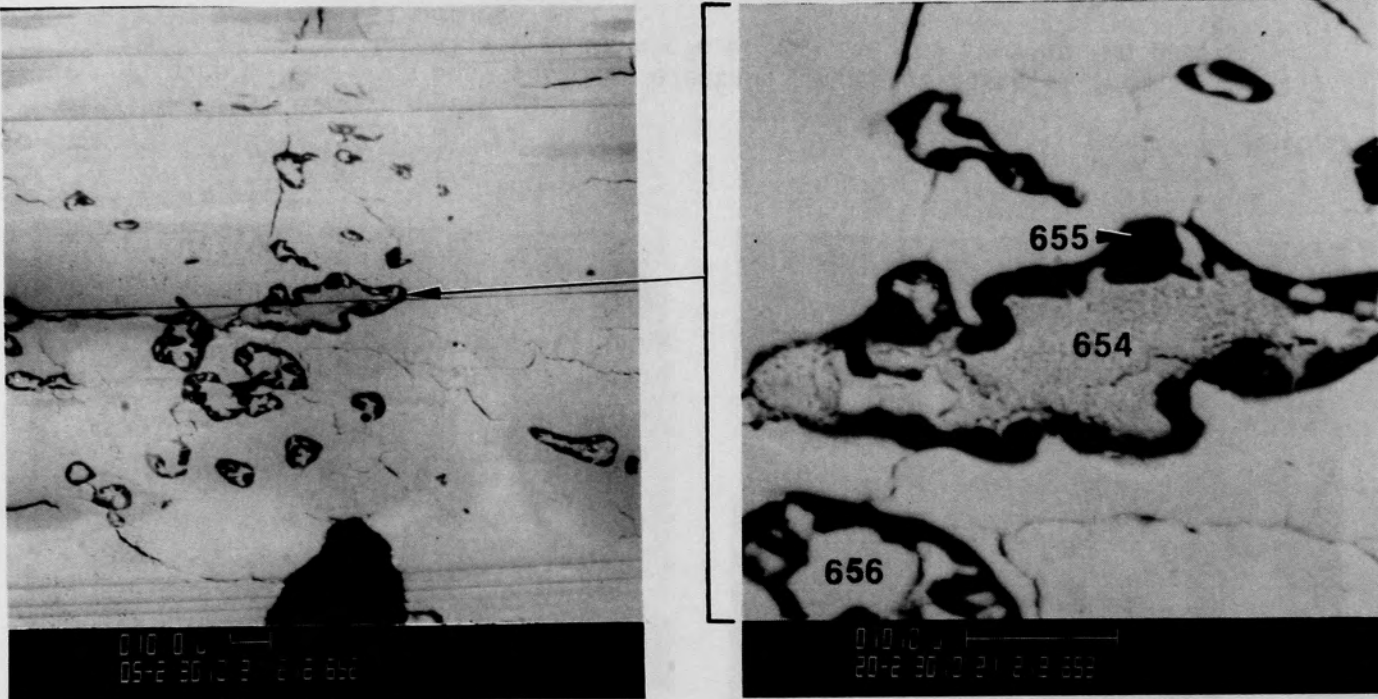
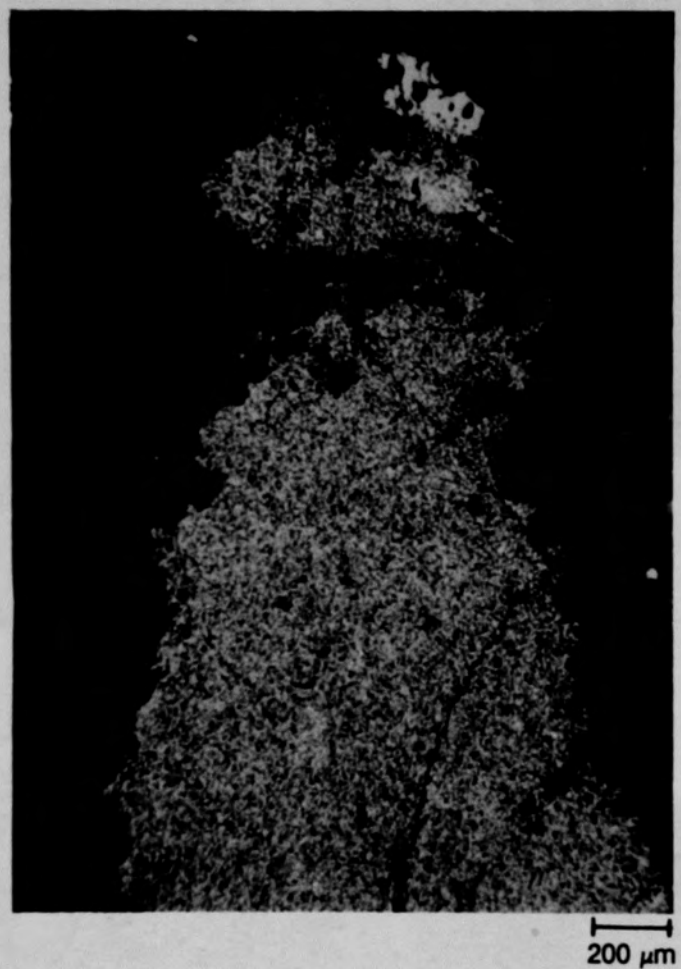
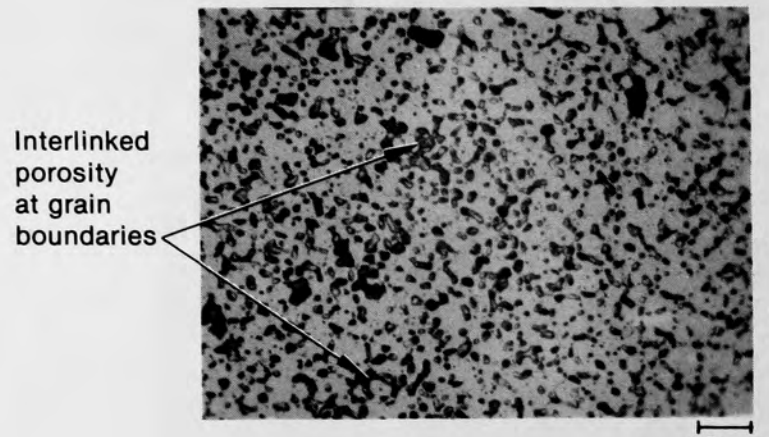


Figure C-109. SEM backscattered electron images of material from location A of Particle 6C (E9, 56 cm).

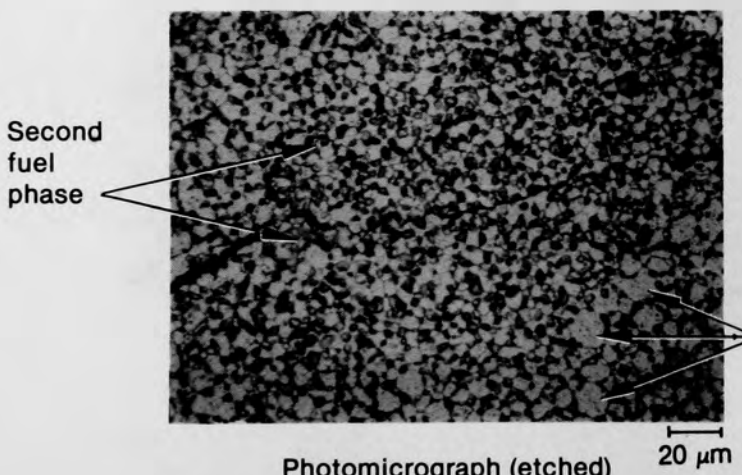


Photomacrograph (unetched)

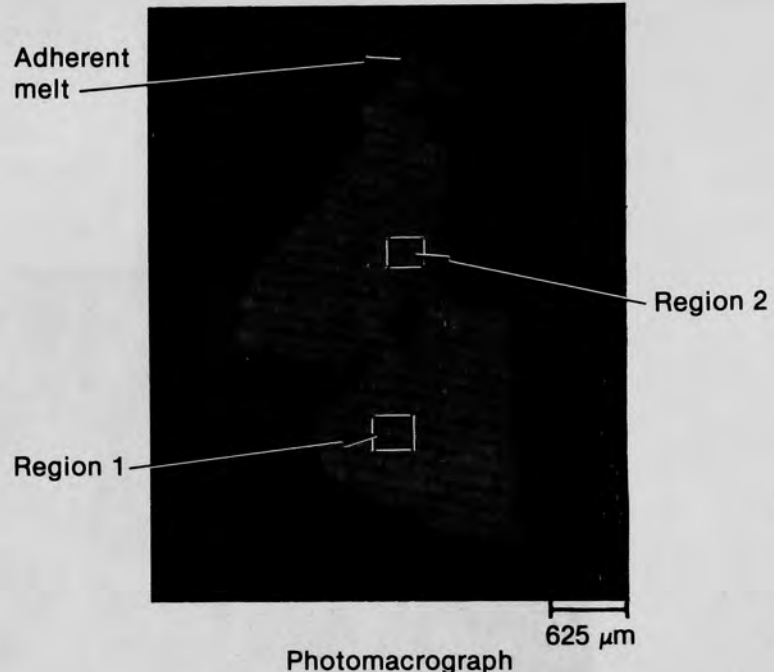
Figure C-110. Upper portion of Particle 6D (E9, 56 cm) showing oxidized fuel with adherent (U, Zr, O) melt.



Photomicrograph (unetched)



Photomicrograph (etched)



Photomacrograph

Auger electron spectroscopy data (15-μm beam)

Region 1: Point 1: U = 28.8 atom %, O = 71.2 atom %
 Point 2: U = 29.7 atom %, O = 70.3 atom %
 Point 3: U = 27.5 atom %, O = 72.5 atom %
 Average: U = 28.7 atom %, O = 71.3 atom % ($\text{UO}_{2.48}$)

Region 2: Point 1: U = 29.1 atom %, O = 70.9 atom %
 Point 2: U = 30.9 atom %, O = 69.1 atom %
 Point 3: U = 28.6 atom %, O = 71.4 atom %
 Average: U = 29.5 atom %, O = 70.5 atom % ($\text{UO}_{2.39}$)

Figure C-111. Typical fuel grain structure of Particle 6D before and after etching (left), plus Auger spectroscopy measurements of elemental composition.

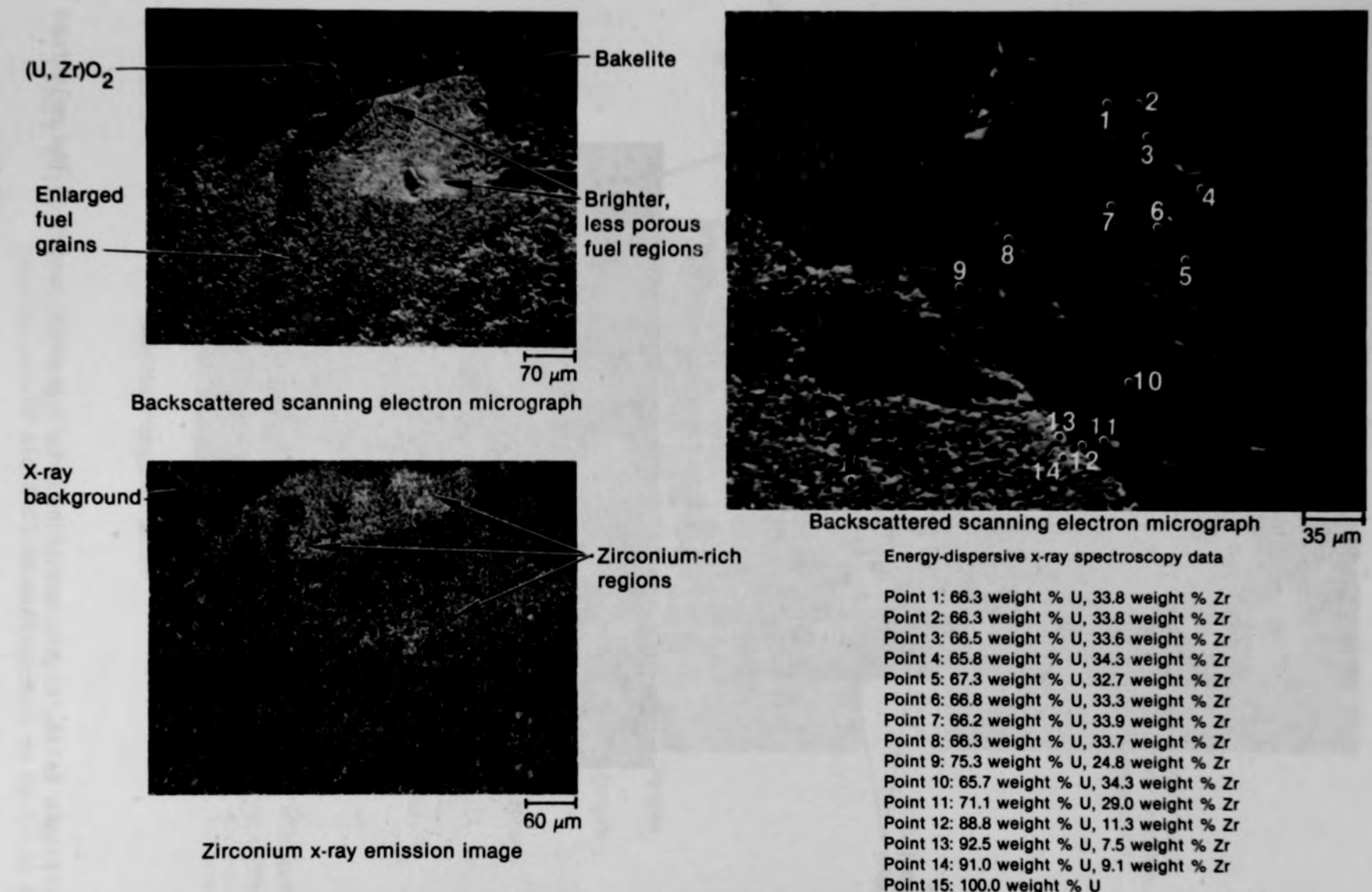


Figure C-112. Energy dispersive x-ray spectroscopy studies of melt-fuel interactions on Particle 6D.

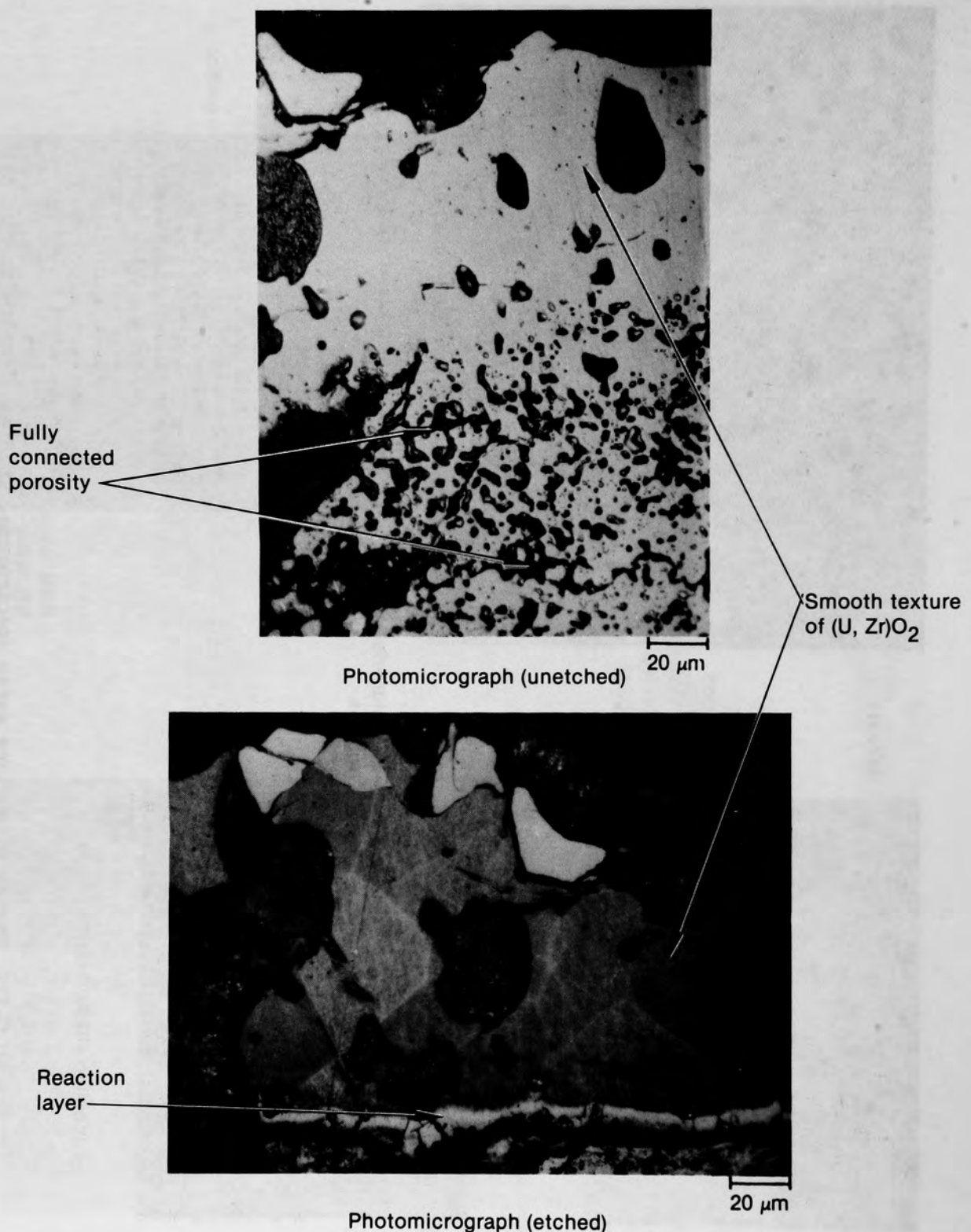
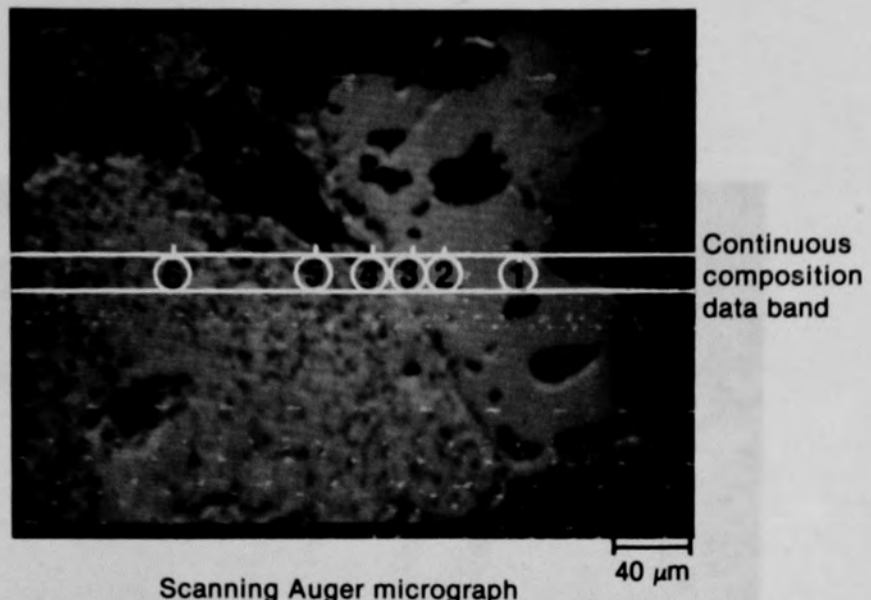
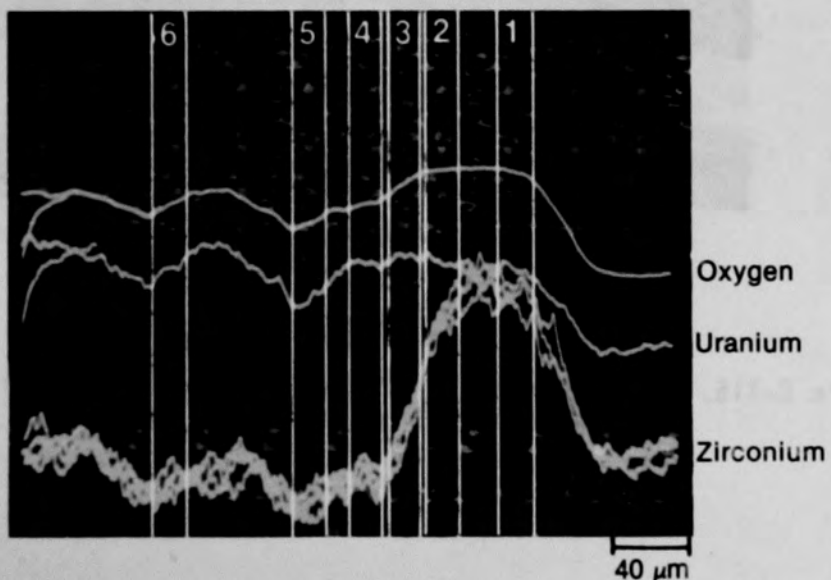


Figure C-113. Highly magnified metallographic images of the melt-fuel interface on Particle 6D.



Scanning Auger micrograph



Superimposed oscilloscope traces

Point 6	Point 5	Point 4	Point 3	Point 2	Point 1
65.9 atom % O	63.8 atom % O	67.2 atom % O	65.6 atom % O	64.6 atom % O	66.5 atom % O
31.1 atom % U	32.1 atom % U	27.6 atom % U	18.9 atom % U	16.0 atom % U	15.4 atom % U
3.0 atom % Zr	4.1 atom % Zr	5.3 atom % Zr	15.5 atom % Zr	19.4 atom % Zr	18.0 atom % Zr

Figure C-114. Scanning Auger microprobe investigations of diffusion bonding across the melt-fuel interface on Particle 6D.

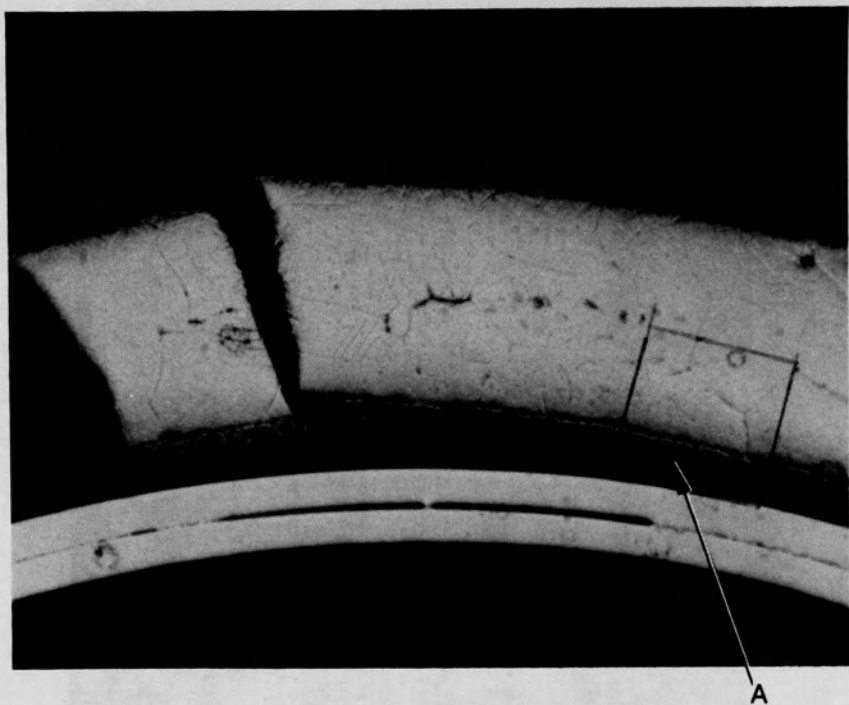


Figure C-115. Photomacrograph of Particle 6E (E9, 56 cm); area A is shown in Figure C-116.

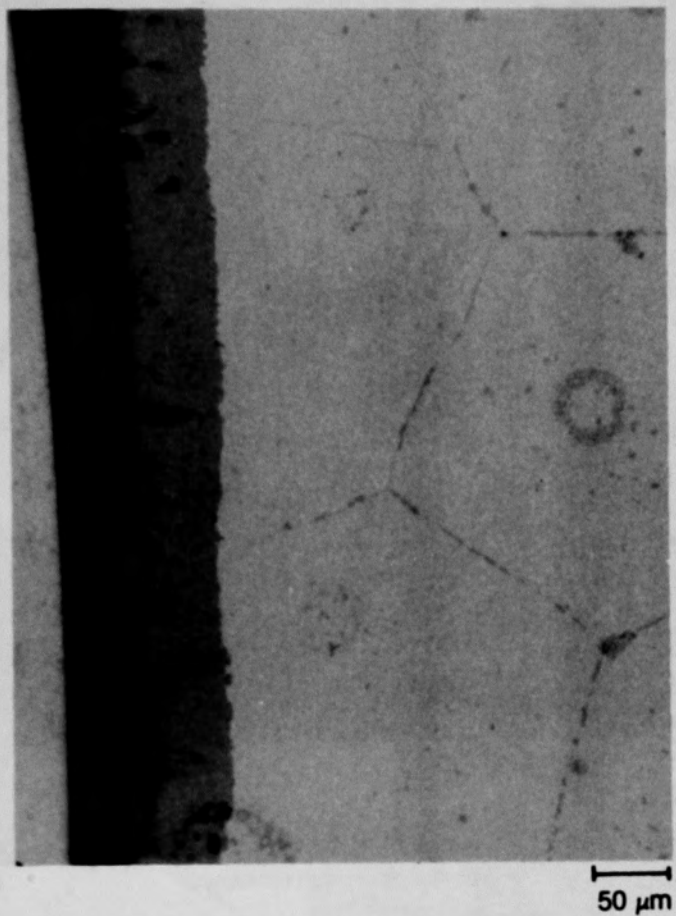


Figure C-116. Photomicrograph of material from area A (Figure C-115) of Particle 6E (E9, 56 cm).

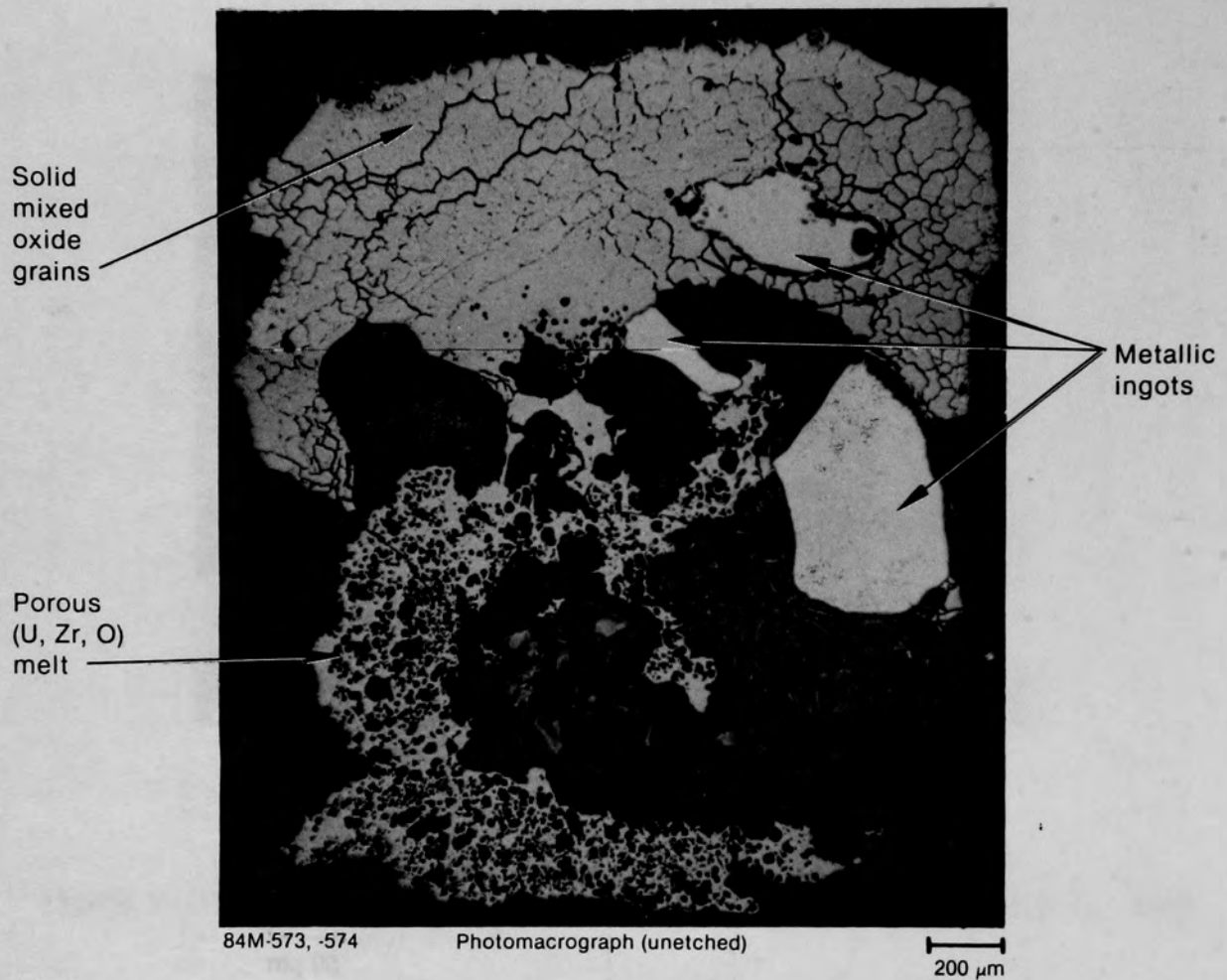
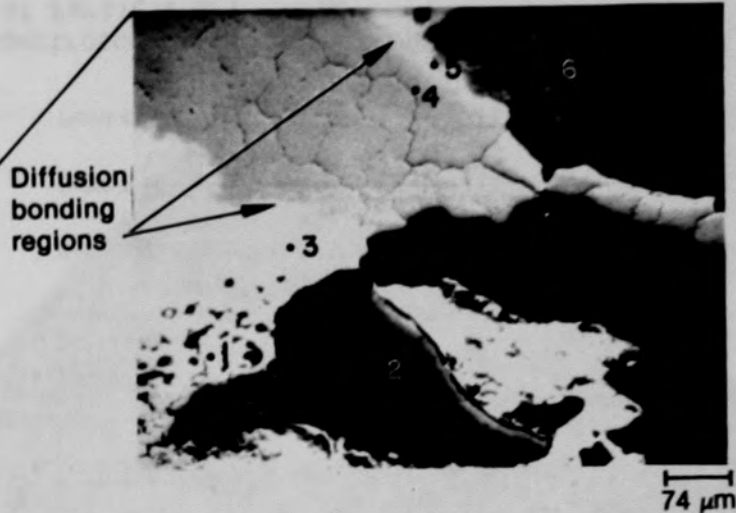
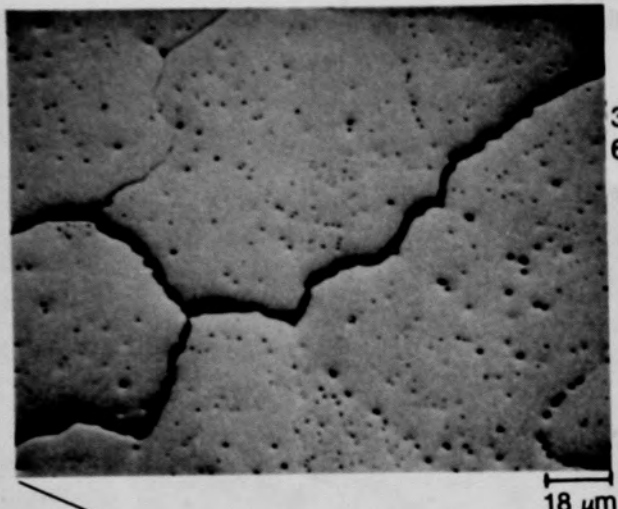
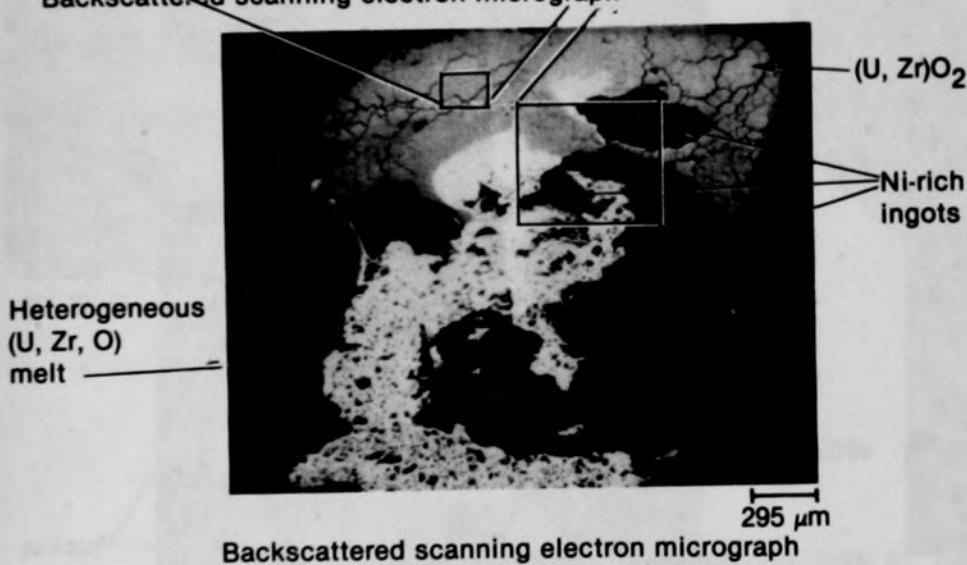


Figure C-117. Particle 6F from 56 cm of E9 position. An agglomerate of porous and solid (U, Zr, O) melts, both highly oxidized and metallic, ferromagnetic ingots.

C-1171



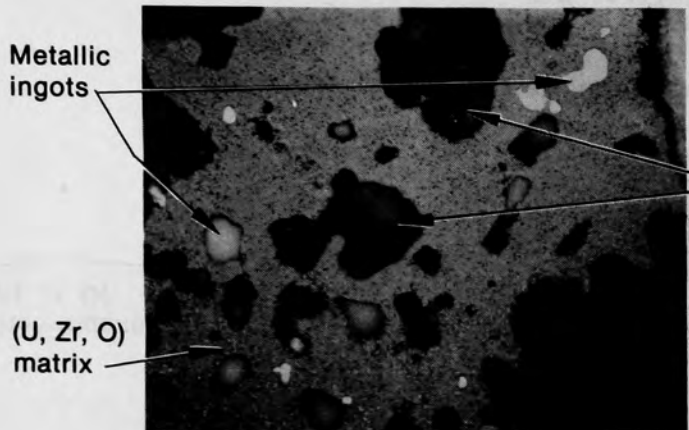
Backscattered scanning electron micrograph



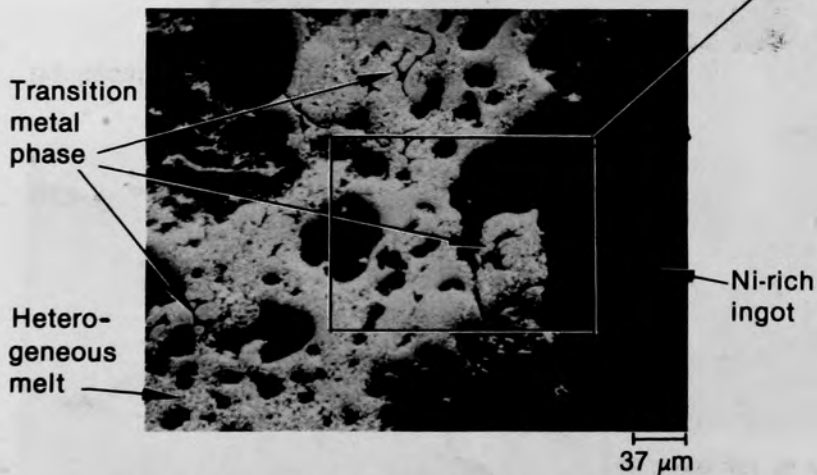
- Point 1: 62.4 weight % U, 34.7 weight % Zr, 2.9 weight % Fe,
- Point 2: 95.7 weight % Ni, 3.0 weight % Fe, 1.2 weight % Sn
- Point 3: 61.1 weight % U, 35.4 weight % Zr, 2.7 weight % Fe,
0.9 weight % Ni
- Point 4: 72.4 weight % Zr, 27.7 weight % U
- Point 5: 49.2 weight % Zr, 43.1 weight % U, 4.5 weight % Ni,
3.2 weight % Fe
- Point 6: 96.4 weight % Ni, 3.5 weight % Fe

Figure C-118. Energy dispersive x-ray spectroscopy results on upper portion
of Particle 6F.

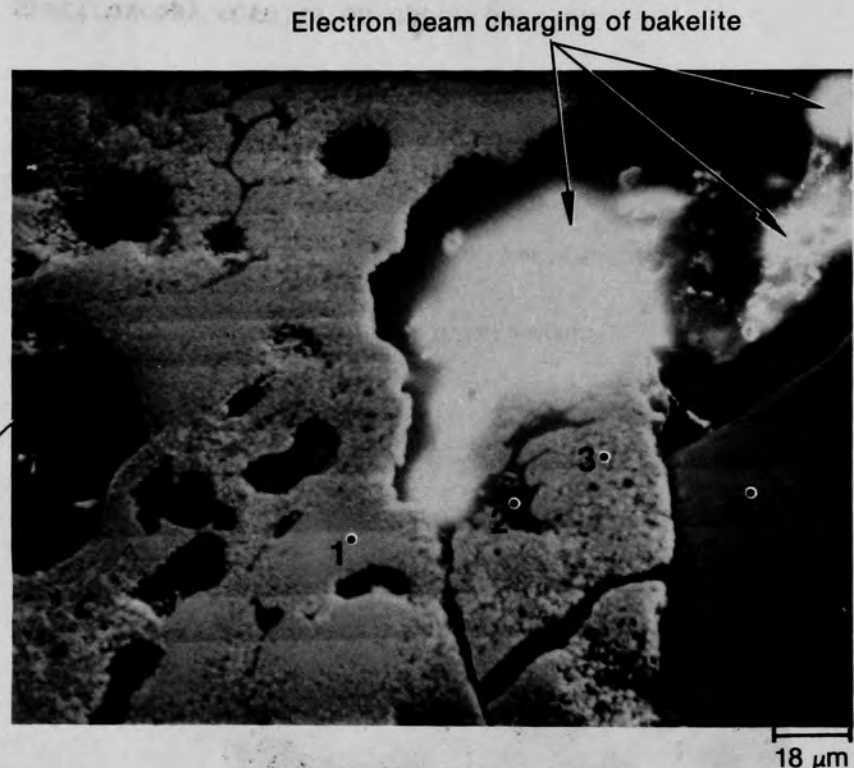
C-172



Photomicrograph (unetched)



Backscattered scanning electron micrograph



Scanning secondary electron image

Point 1: 56.9 weight % U, 38.1 weight % Zr, 4.2 weight % Fe,
0.9 weight % Ni

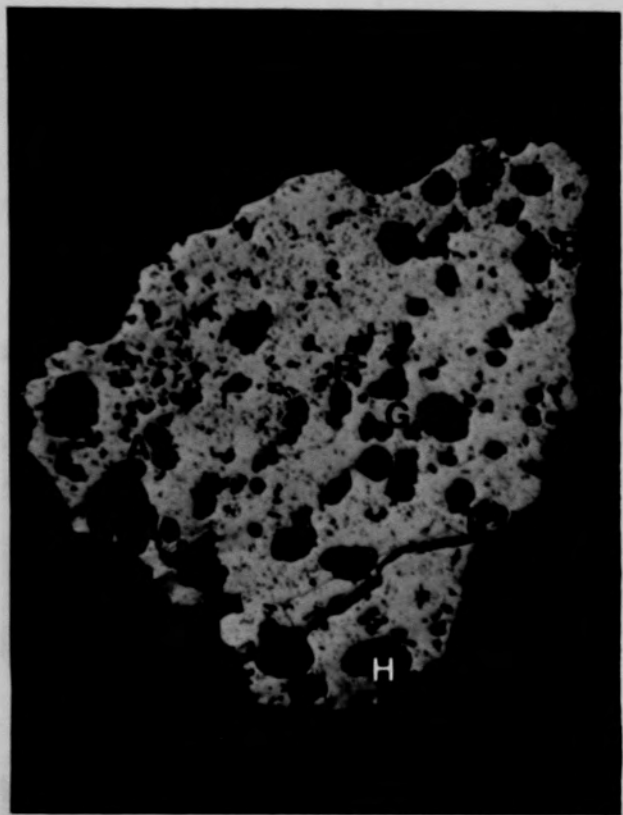
Point 2: 33.8 weight % U, 32.8 weight % Fe, 17.3 weight % Al,
16.2 weight % Ni

Point 3: 50.7 weight % U, 45.4 weight % Zr, 2.7 weight % Fe,
1.2 weight % Ni

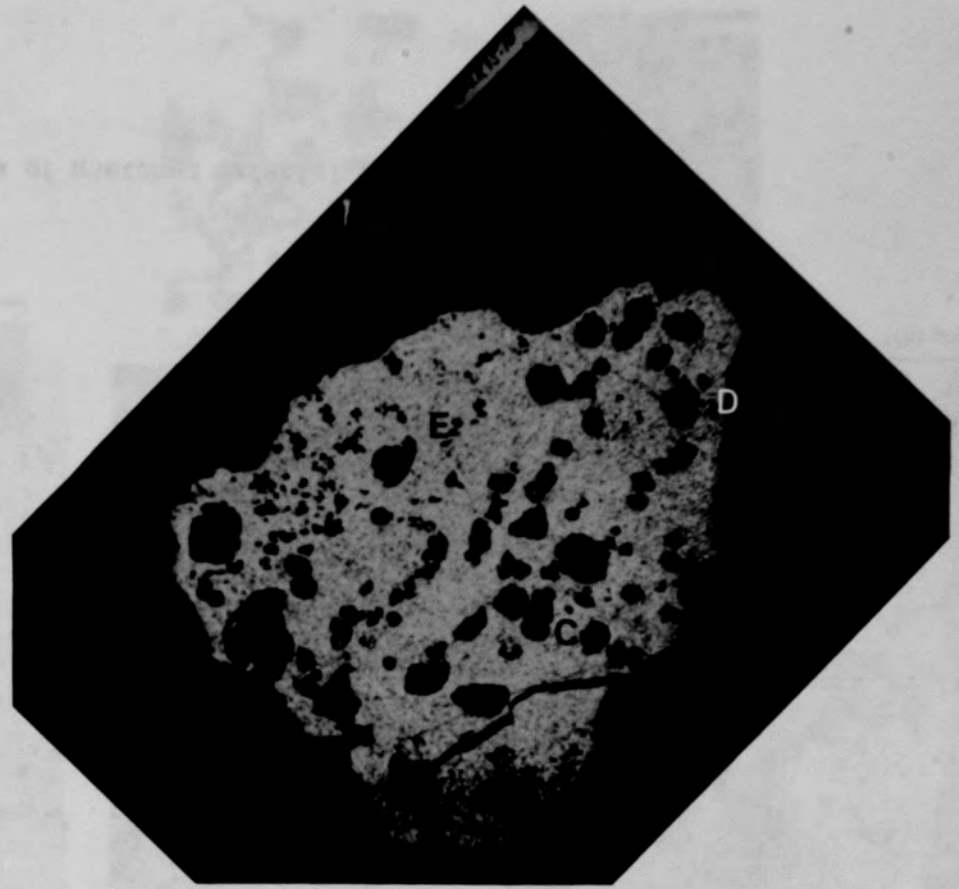
Point 4: 96.2 weight % Ni, 3.7 weight % Fe

Figure C-119. Energy dispersive x-ray spectroscopy findings on the lower, heterogeneous melt region of Particle 6F.

C-173



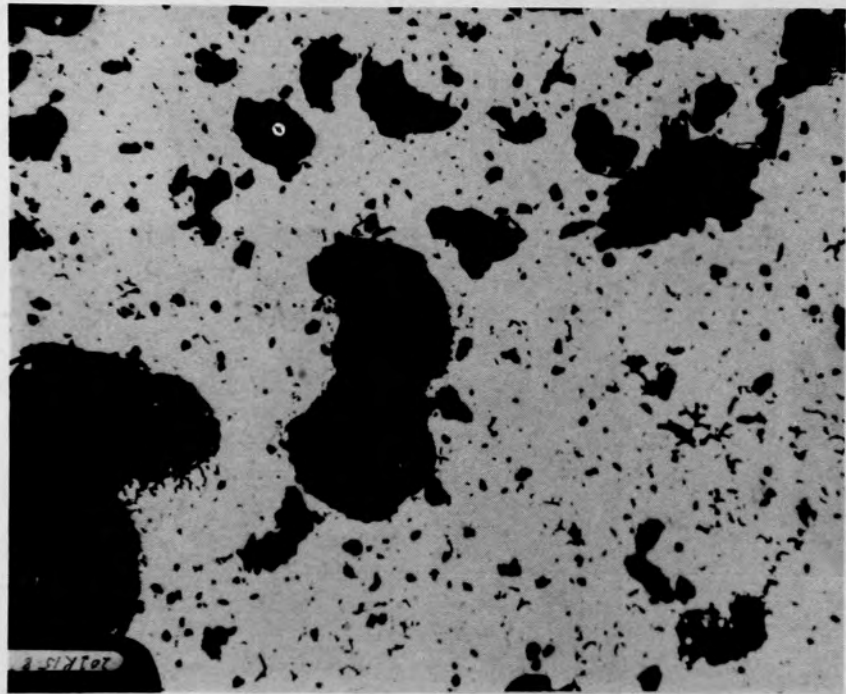
(a) Unetched



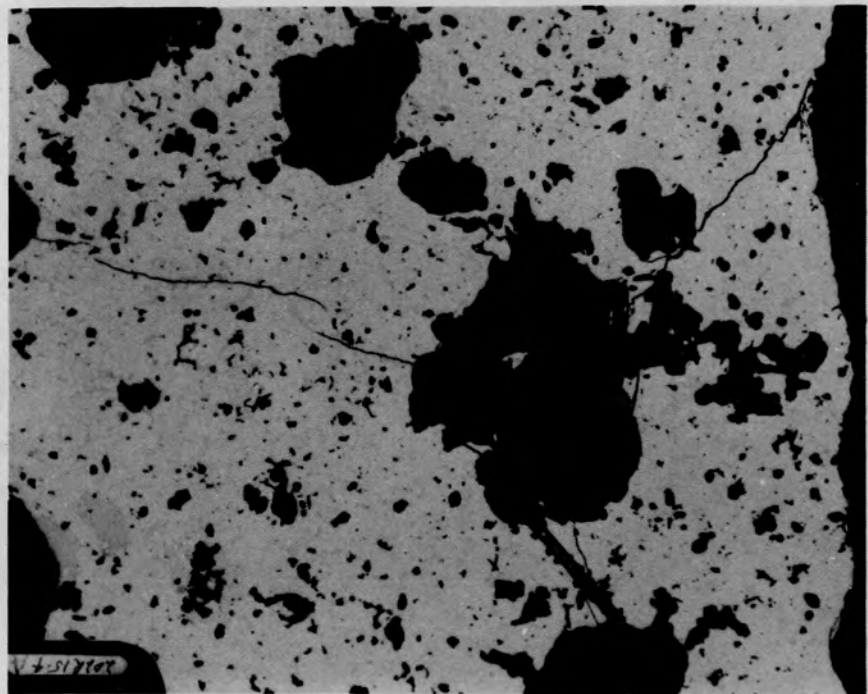
(b) Fuel etch

Figure C-120. Photomicrographs of Particle 7A (H8, 36 cm).

C-174

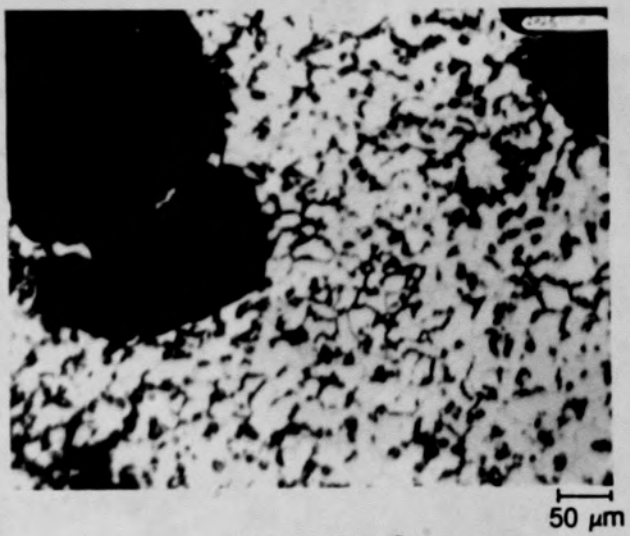


(a) Location A

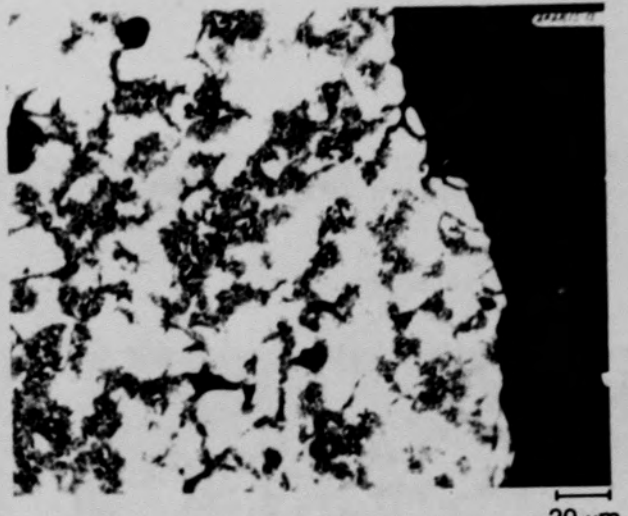


(b) Location B

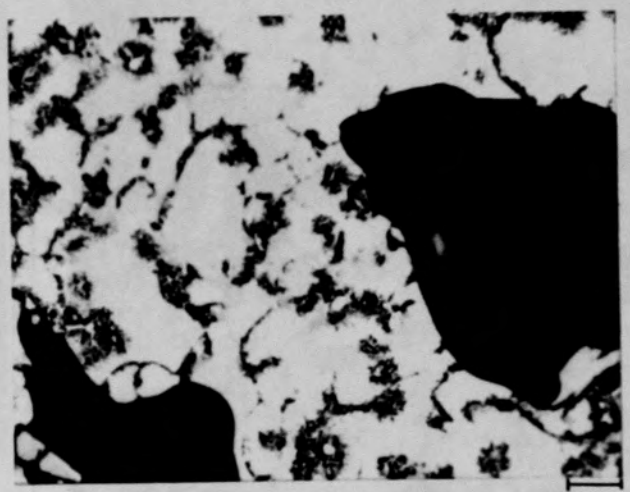
Figure C-121. Photomicrographs of unetched material from Particle 7A (H8, 36 cm).



(a) Location C



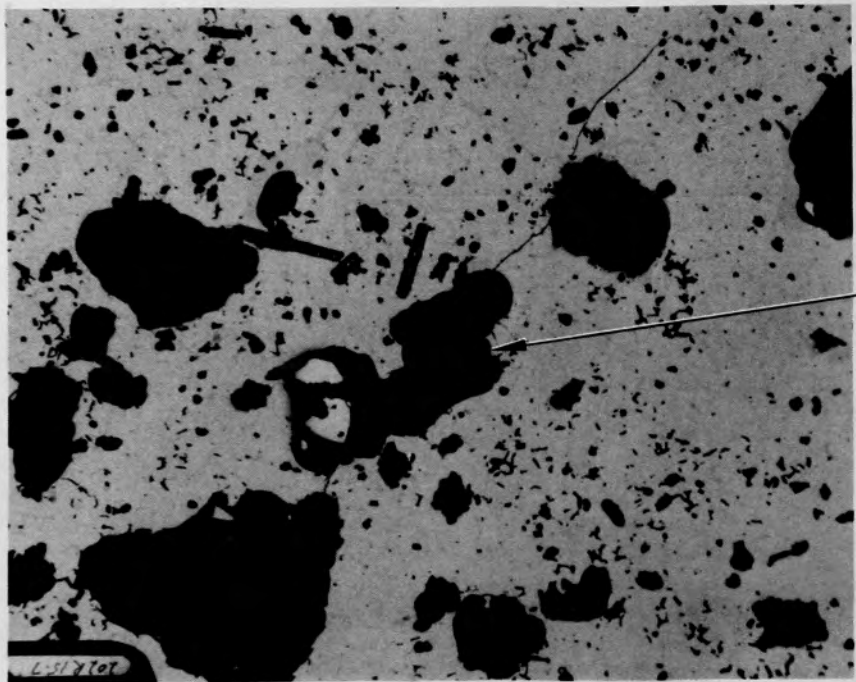
(b) Location D



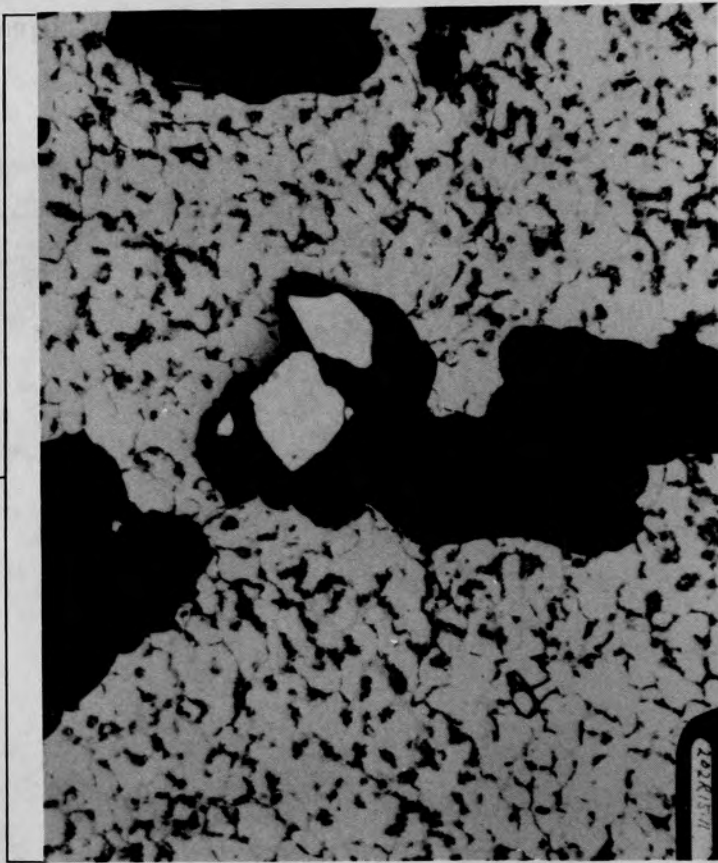
(c) Location E

Figure C-122. Photomicrographs of etched material from Particle 7A (H8,
36 cm).

C-176



(a) Unetched



(b) Etched

Figure C-123. Photomicrographs of material from Location F of Particle 7A
(H8, 36 cm).

C-177

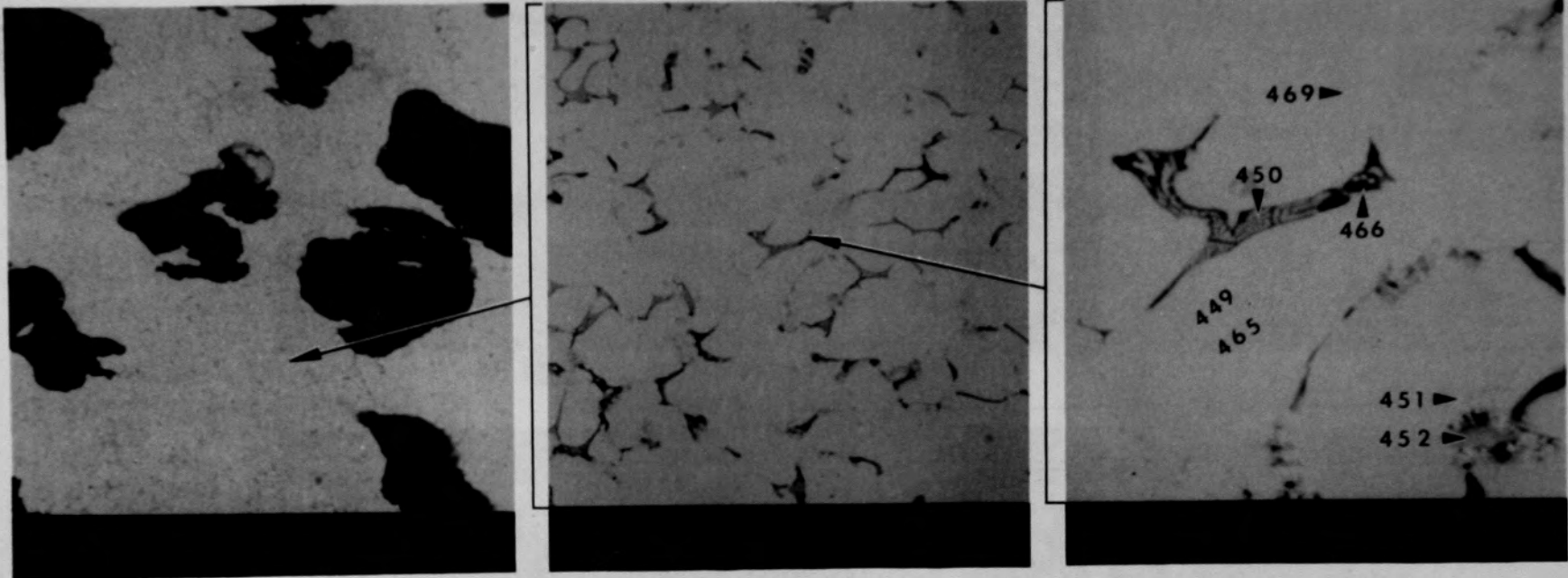


Figure C-124. SEM backscattered electron images of material from location G of Particle 7A (H8, 36 cm).



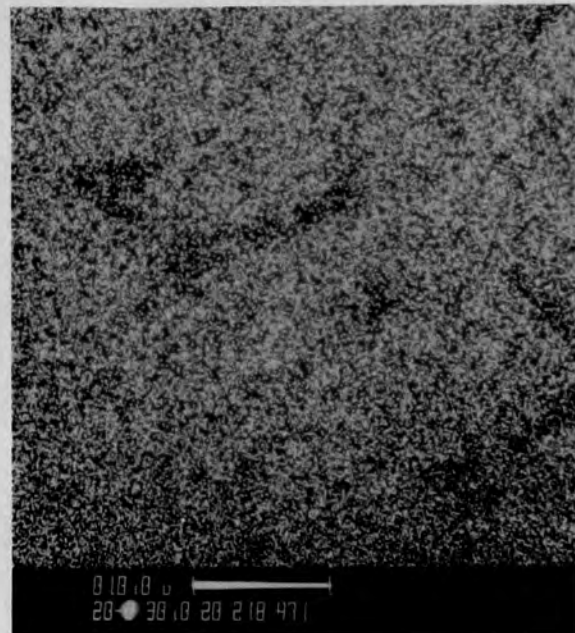
(a) Cr



(b) Fe

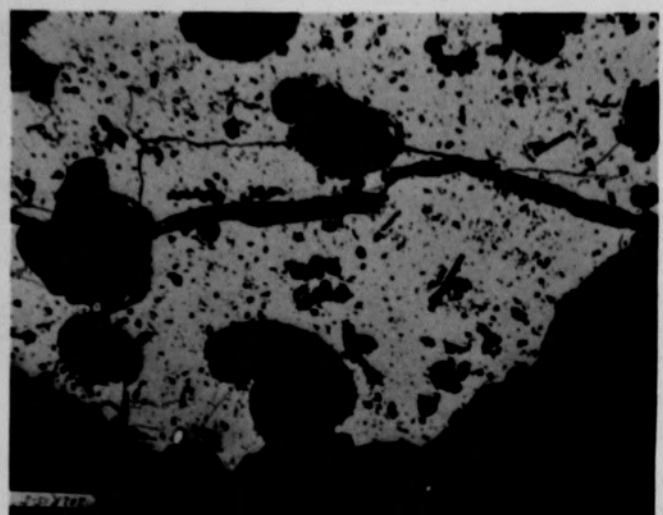


(c) Zr

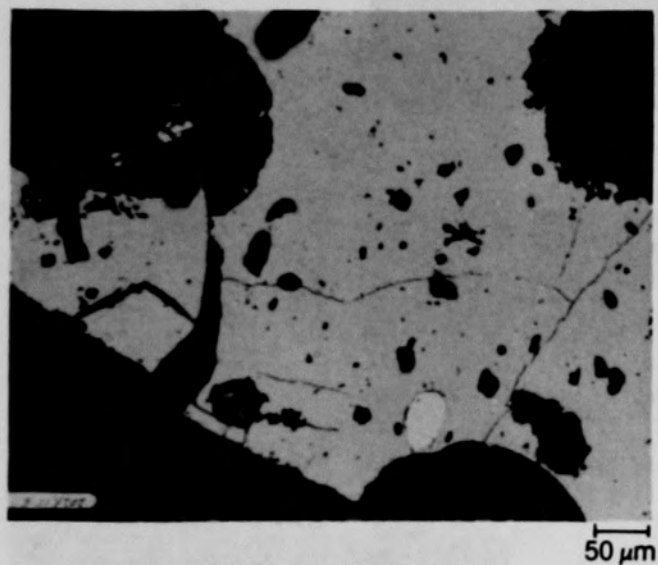


(d) U

Figure C-125. X-ray dot maps of second phase material in location G of Particle 7A (H8, 36 cm).



(a) Photomicrograph



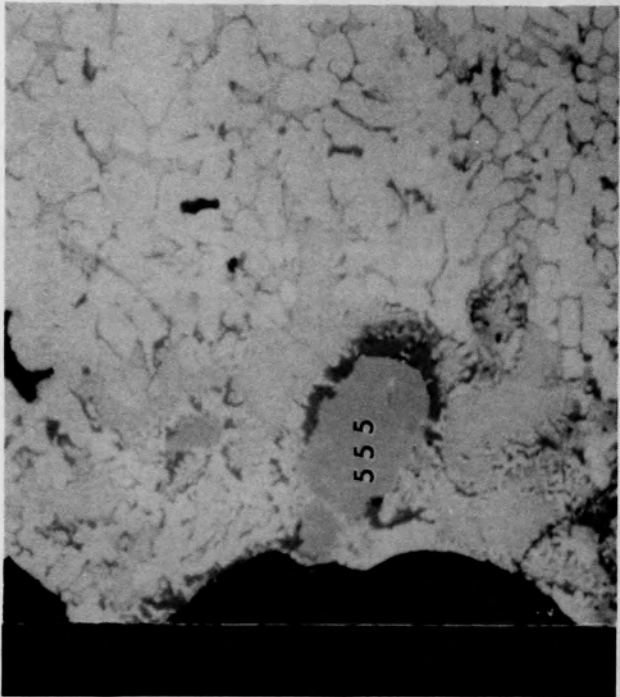
(b) Photomicrograph



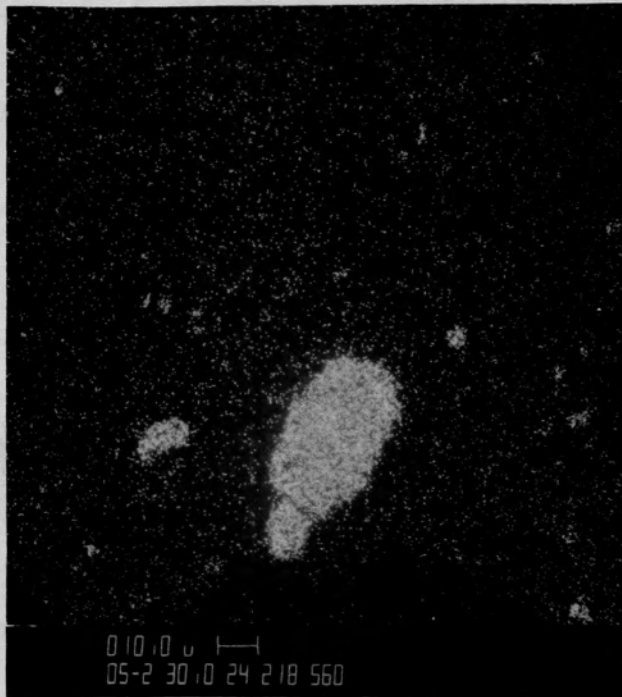
(c) SEM backscattered electron image

Figure C-126. Photographs of material from location H of Particle 7A (H8, 36 cm).

C-180



(a) SEM backscattered electron image

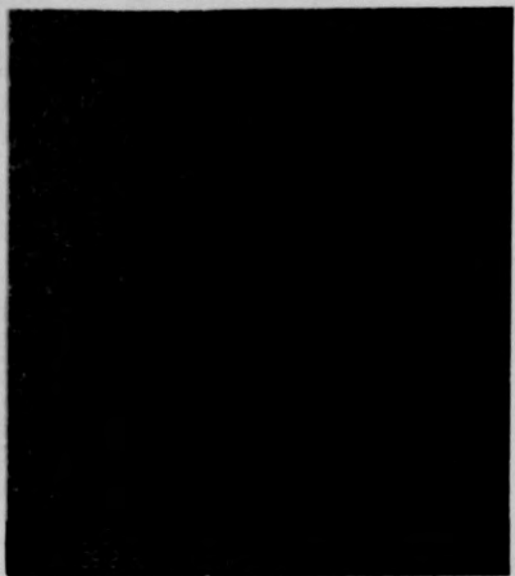


(b) X-ray dot map of Ni

Figure C-127. Photographs of material from location H of Particle 7A (H8, 36 cm).



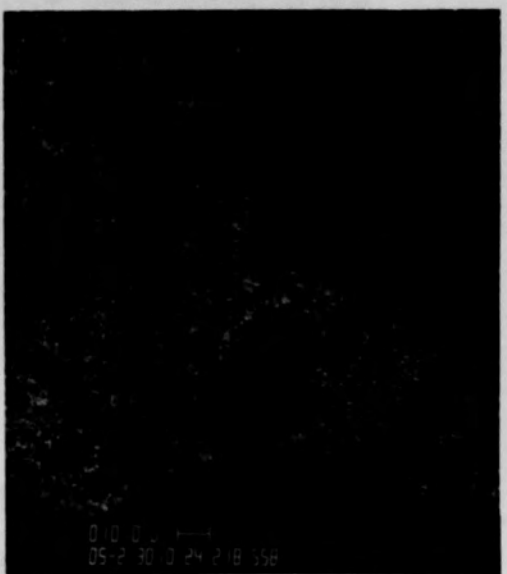
(a) U



(b) Zr



(c) Fe



(d) Cr

Figure C-128. X-ray dot map of second phase material from location H,
Figure C-127a, of Particle 7A (H8, 36 cm).

C-182

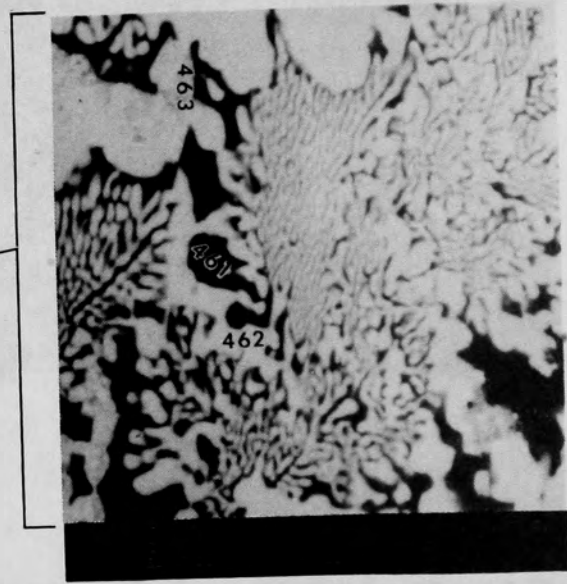
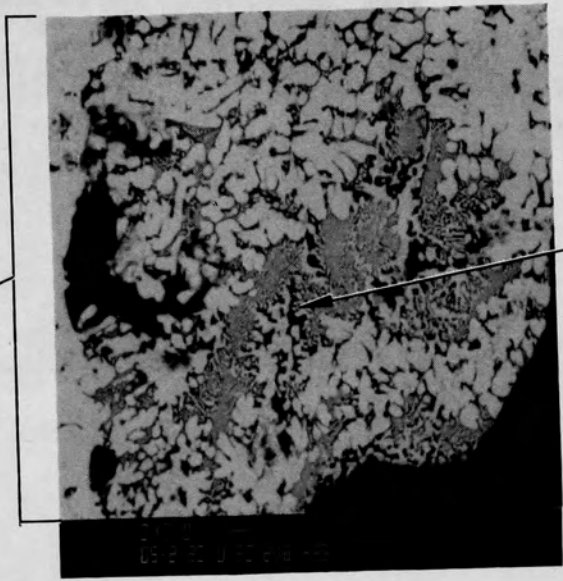


Figure C-129. SEM backscattered electron images of material from location I of Particle 7A (H8, 36 cm).

C-183

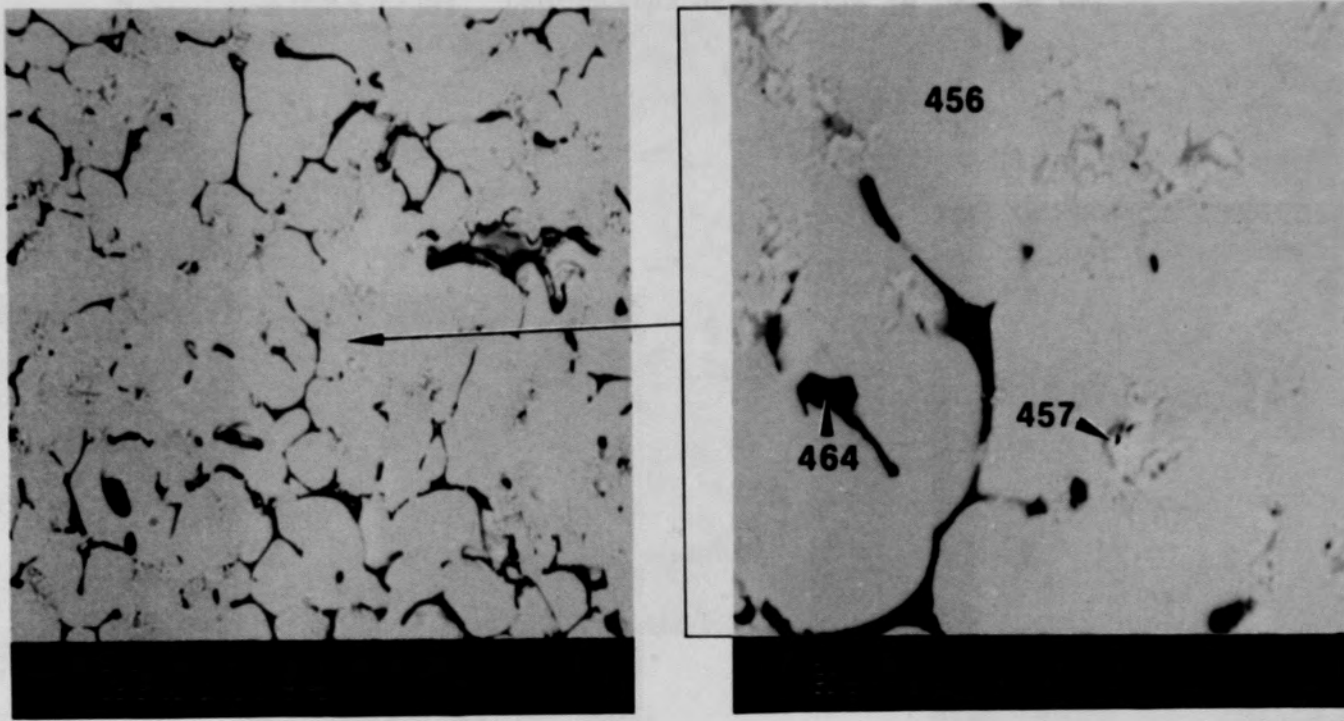
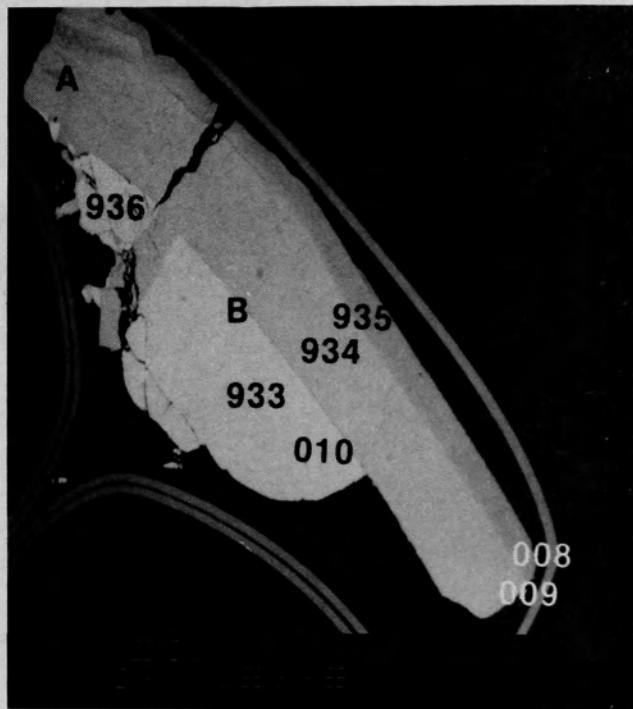


Figure C-130. SEM backscattered electron images of material from location J, Figure C-129, of Particle 7A (H8, 36 cm).



(a) Photomicrograph



(b) SEM backscattered electron image

Figure C-131. Photographs of Particle 7B (H8, 36 cm).

C-185

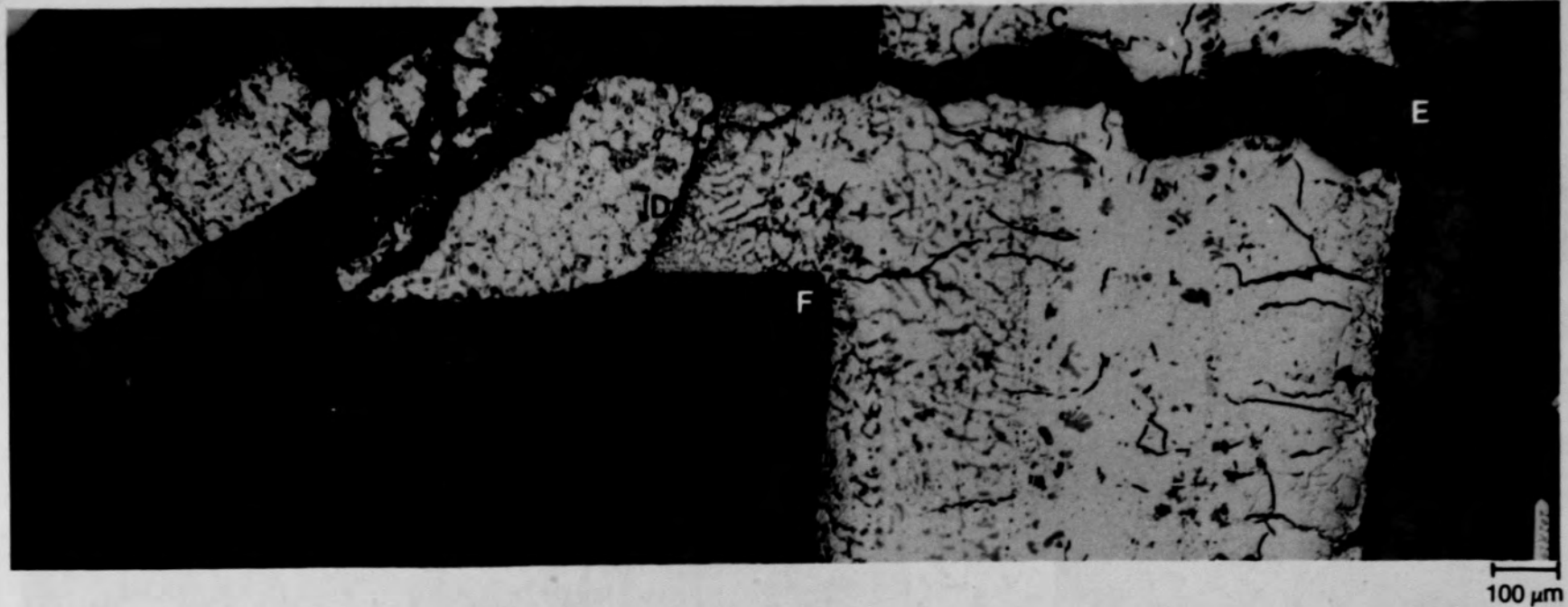


Figure C-132. Photomicrographs of prior molten material in cladding gap and fuel crack of Particle 7B (H8, 36 cm).

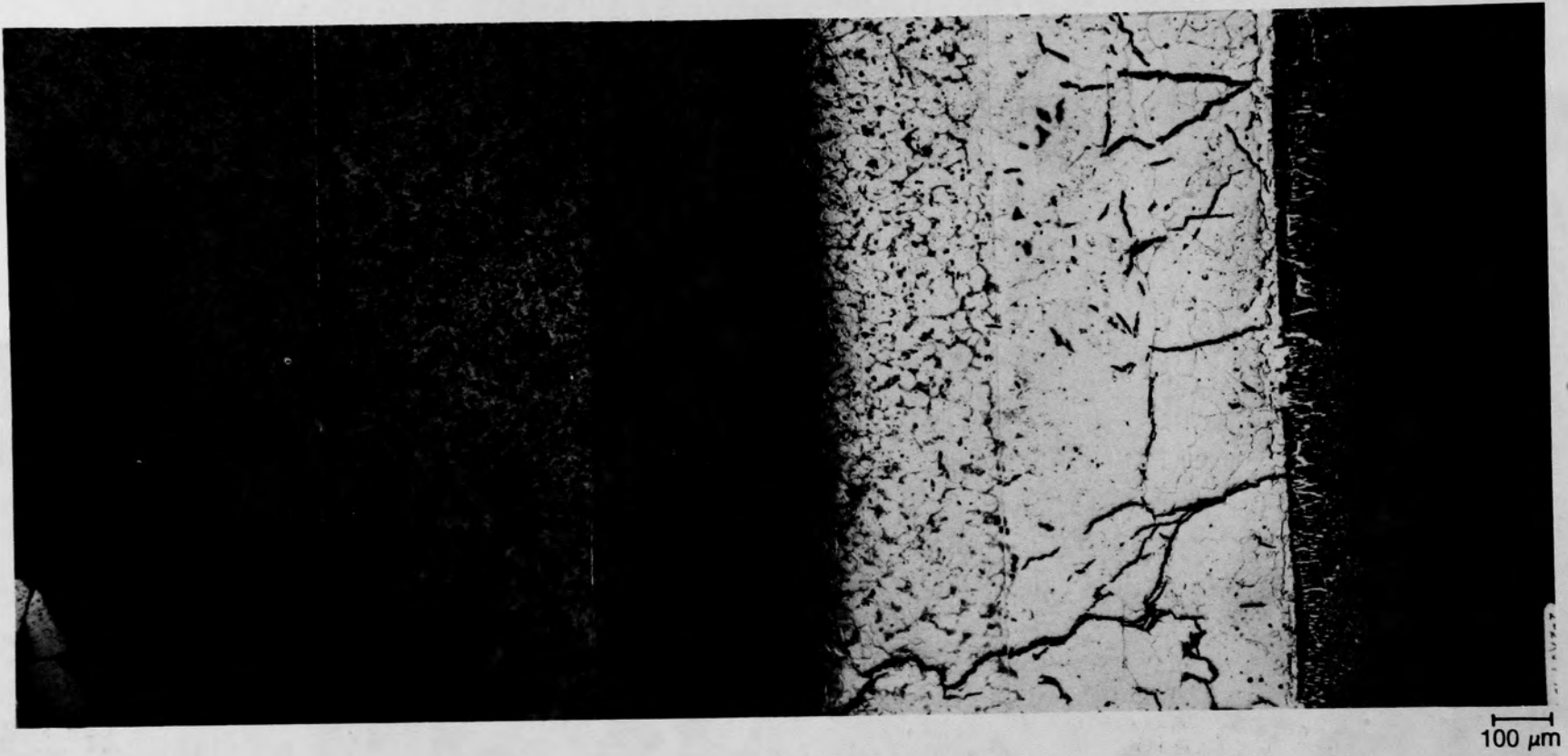


Figure C-133. Photomicrographs of cladding in Particle 7B (H8, 36 cm).

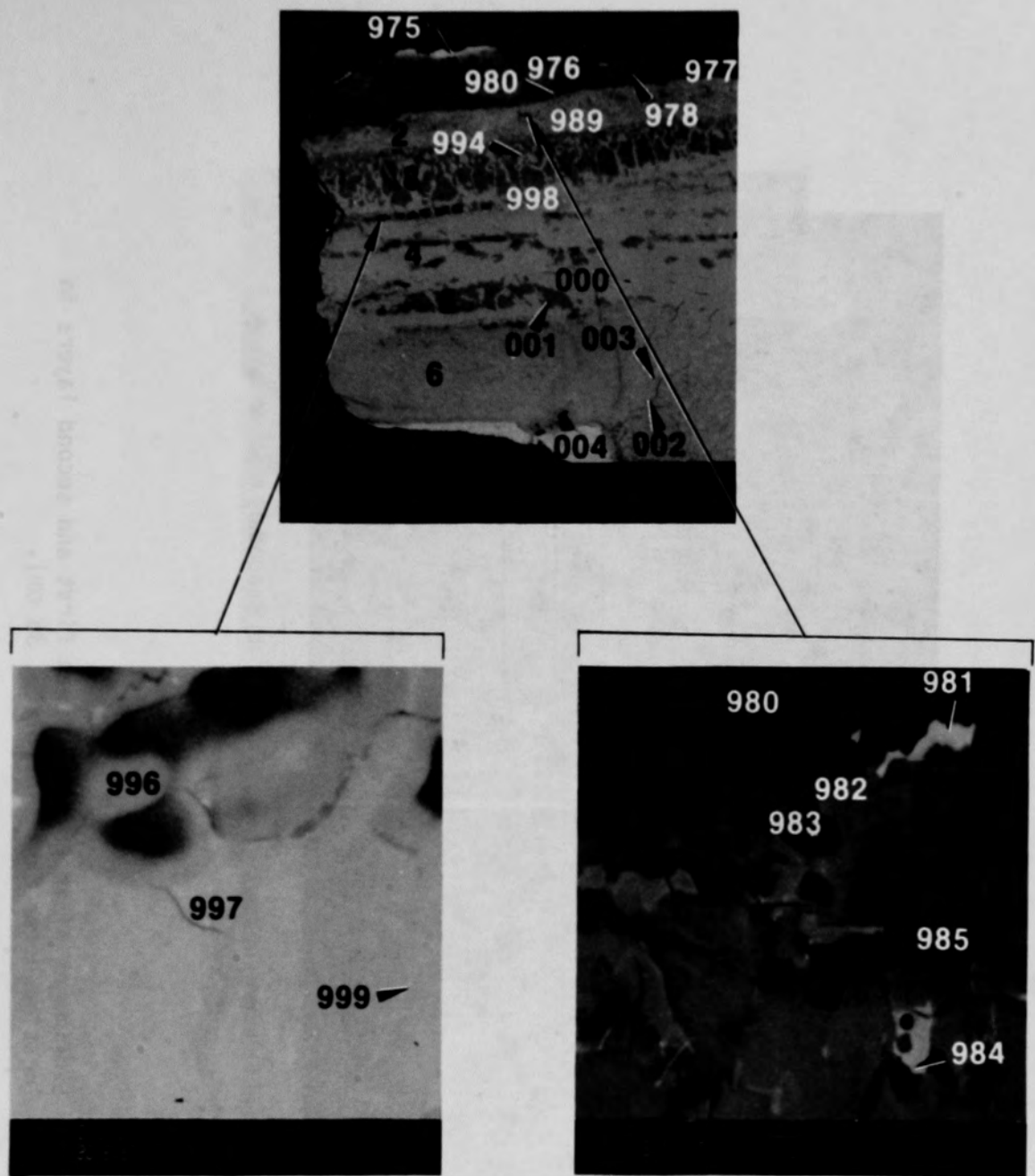
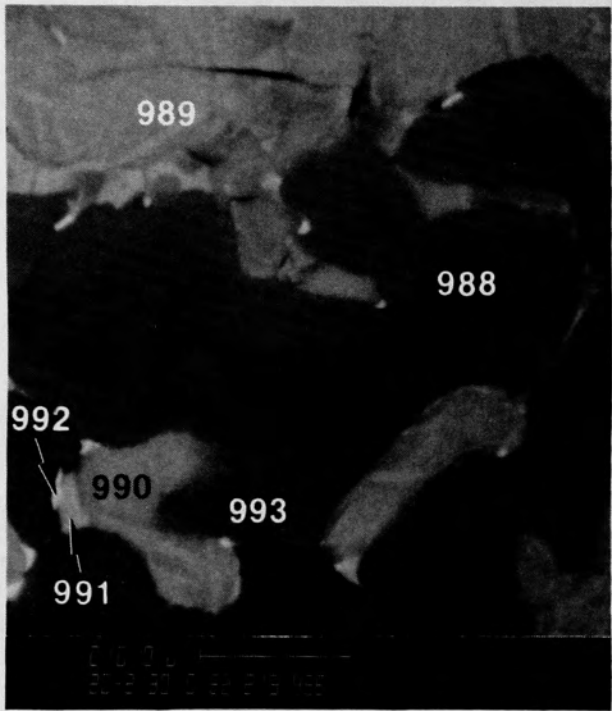
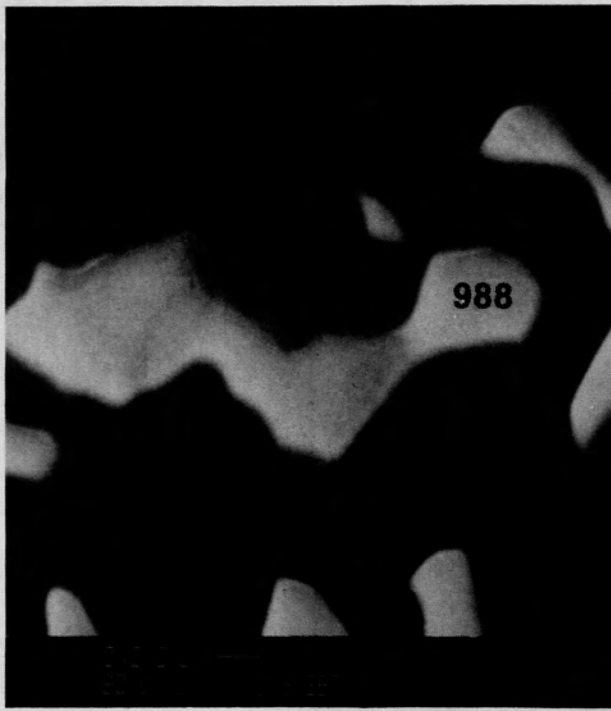


Figure C-134. SEM backscattered electron images of material from location A of Particle 7B (H8, 36 cm).



(a) Backscattered electron image



(b) Secondary electron image

Figure C-135. SEM images of interface between first and second layers in location A for Particle 7B (H8, 36 cm).

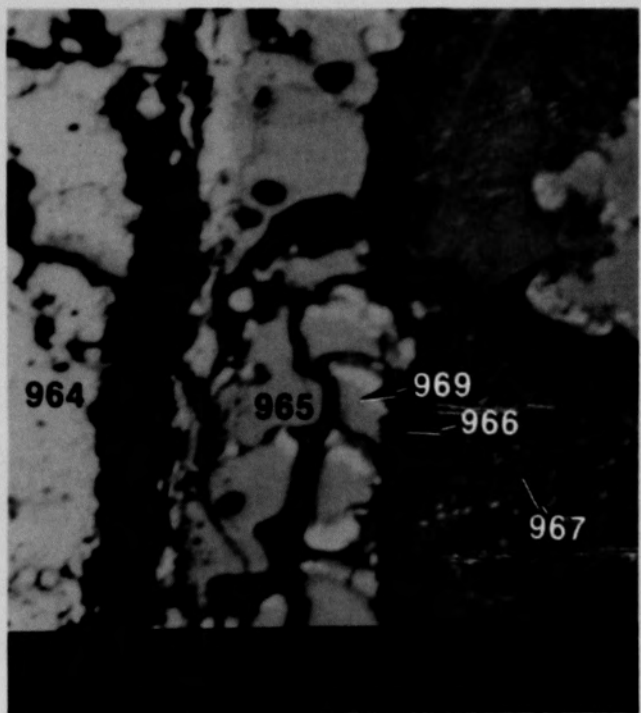
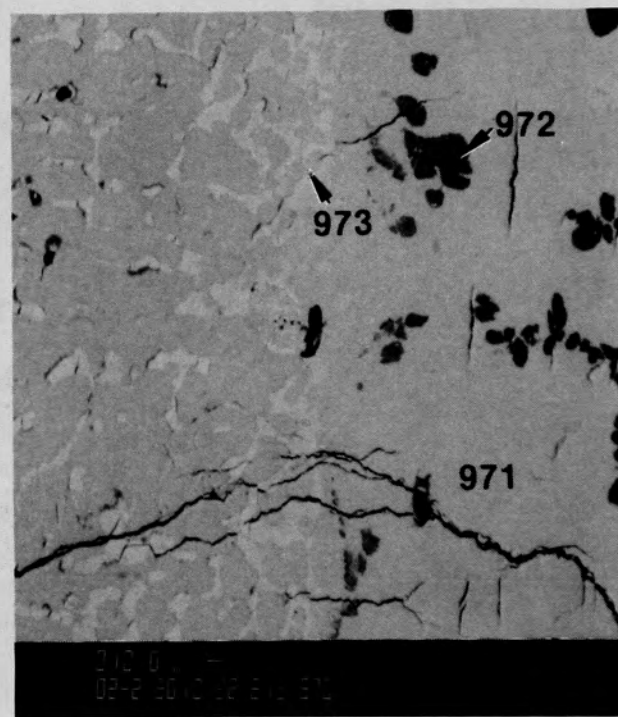


Figure C-136. SEM backscattered electron image of material from location B of Particle 7B (H8, 36 cm).

C-190



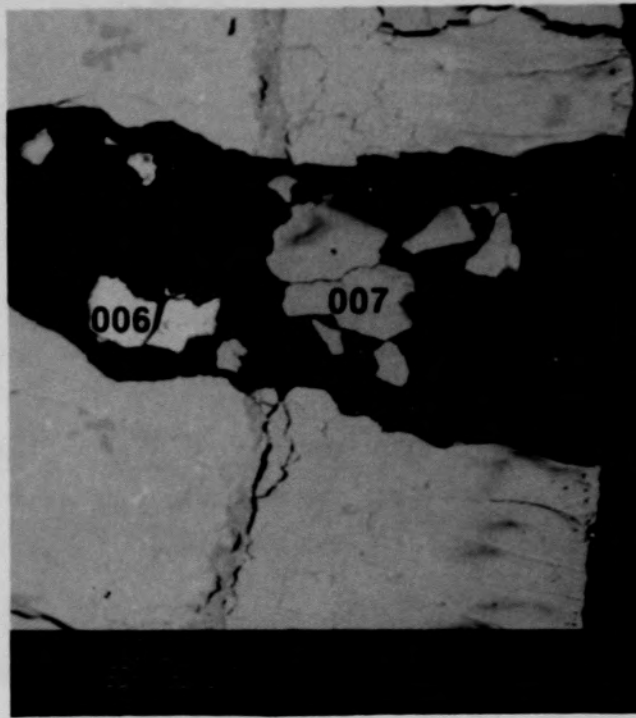
(b) SEM backscattered electron image

Figure C-137. Photographs of material from location C, Figure C-132, of Particle 7B (H8, 36 cm).

C-191



(a) Photomicrograph of location D



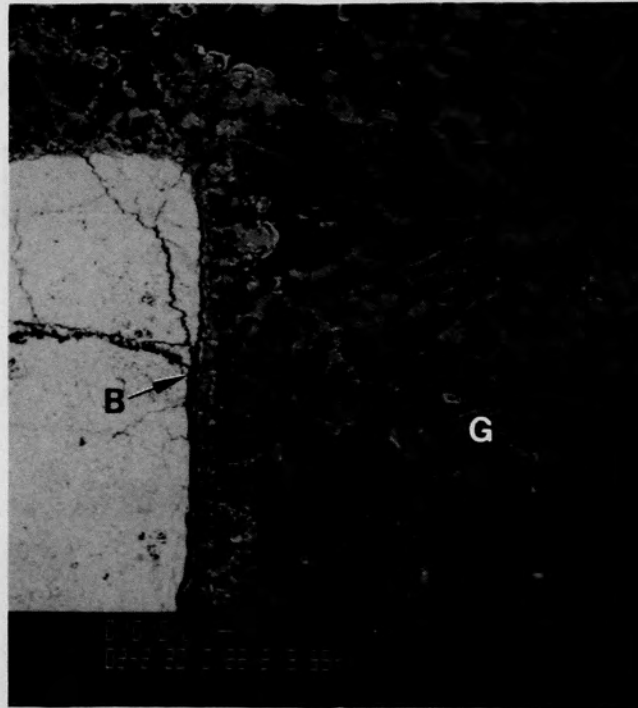
(b) SEM backscattered electron image of location E

Figure C-138. Photographs of material in crack shown in Figure C-132 of Particle 7B (H8, 36 cm).

C-192



(a) Photomicrograph



(b) SEM backscattered electron image

Figure C-139. Photographs of material from location F, Figure C-132, of Particle 7B (H8, 36 cm).

C-193

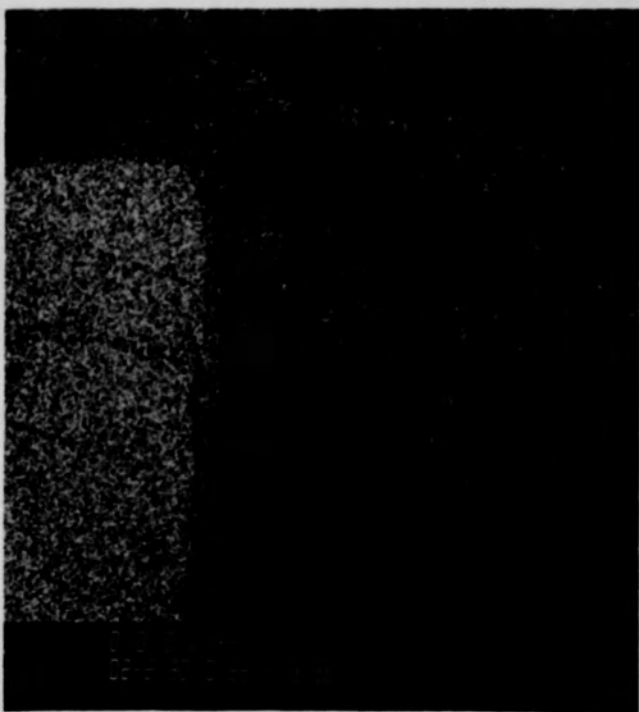
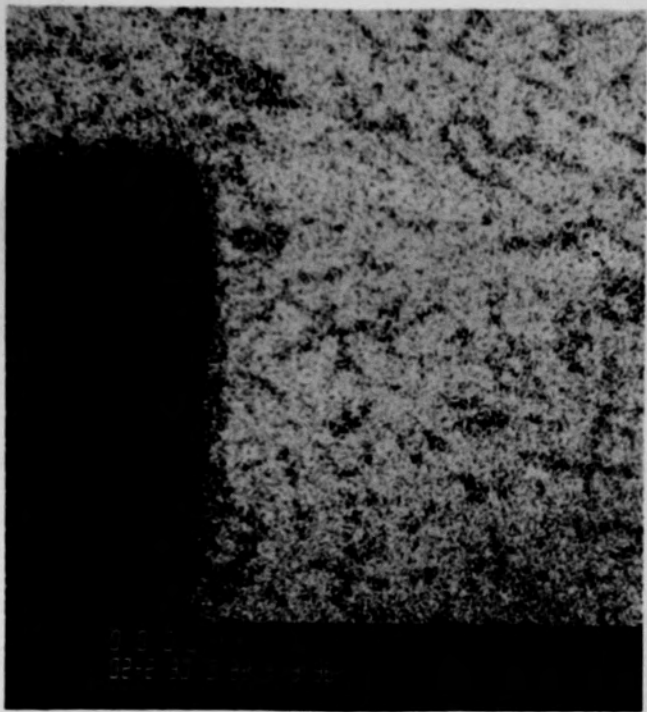
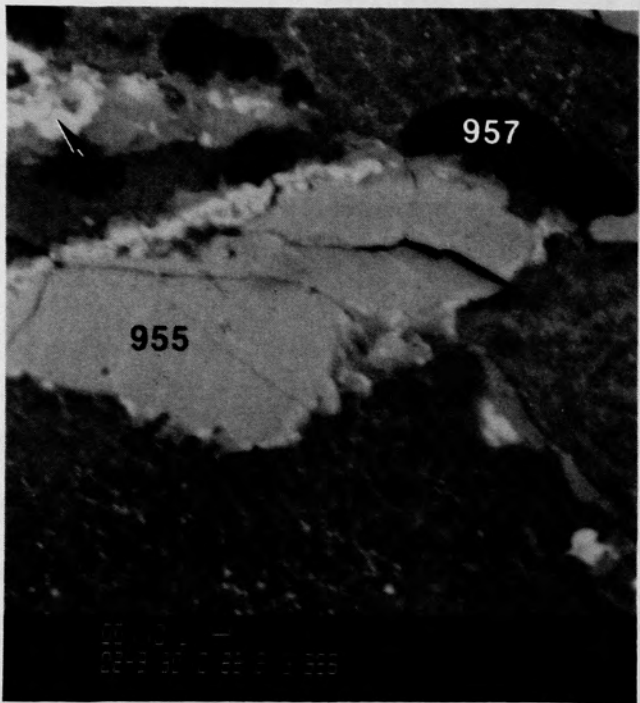
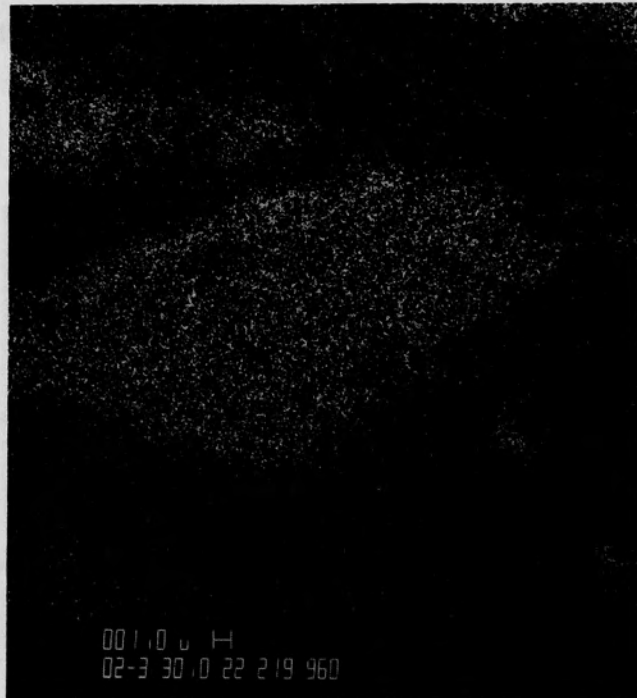


Figure C-140. X-ray dot map of material from location F, Figure C-132, of Particle 7B (H8, 36 cm).

C-194



(a) SEM backscattered electron image



(b) X-ray dot map of U

Figure C-141. Photographs of material from location G, Figure C-139, of Particle 7B (H8, 36 cm).

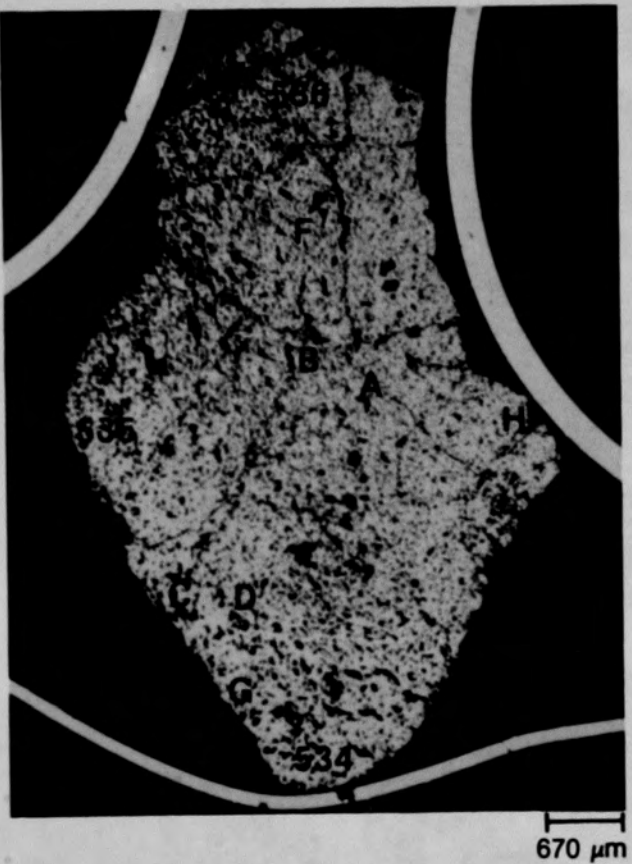
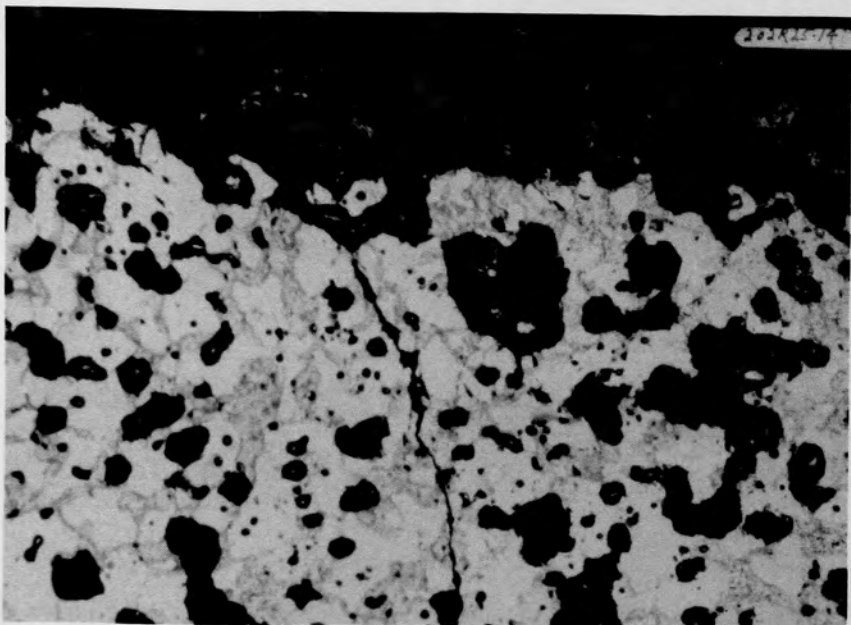
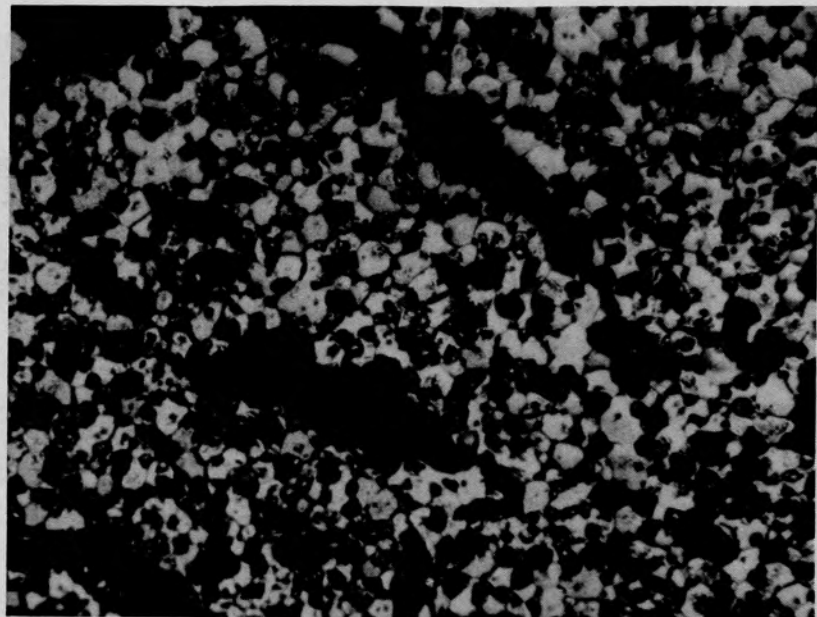


Figure C-142. Photomacrograph of Particle 7E (H8, 36 cm).

C-196



(a) Edge

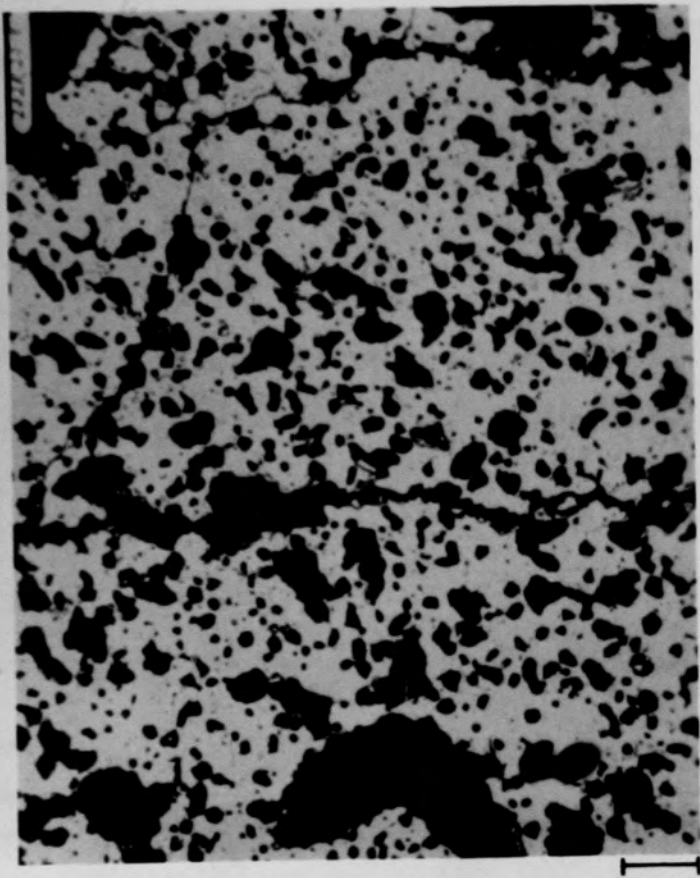


(b) Central

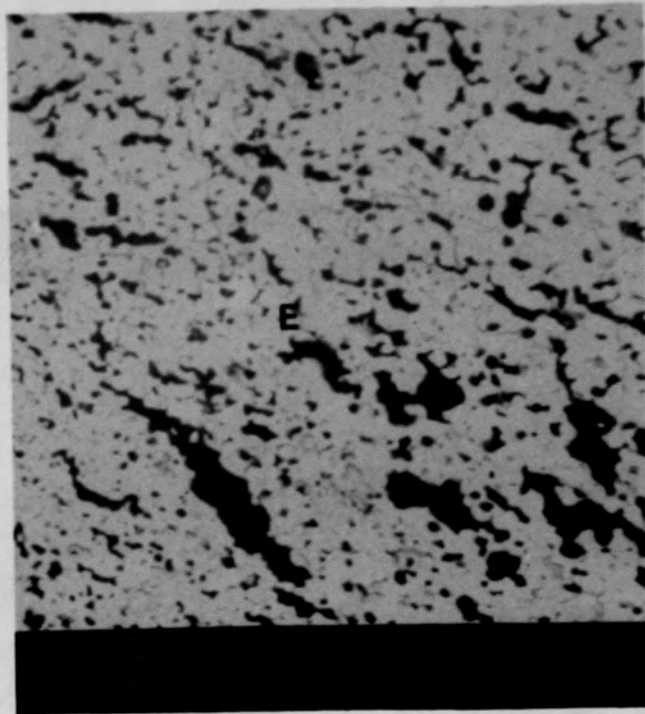
50 μm

Figure C-143. Photomicrograph of etched material from Particle 7E (H8, 36 cm).

C-197



(a) Photomicrograph of location A



(b) SEM backscattered electron image of location B

Figure C-144. Photographs of material near center of Particle 7E (H8, 36 cm).

C-198

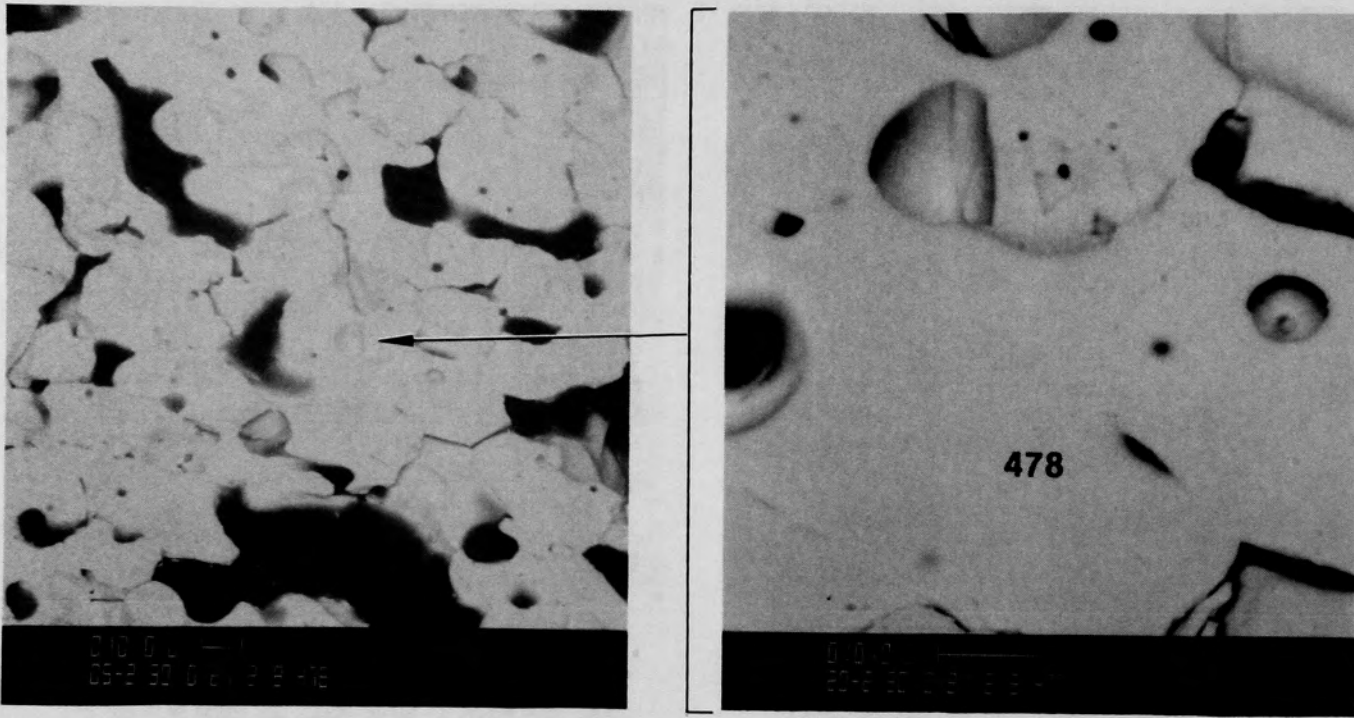
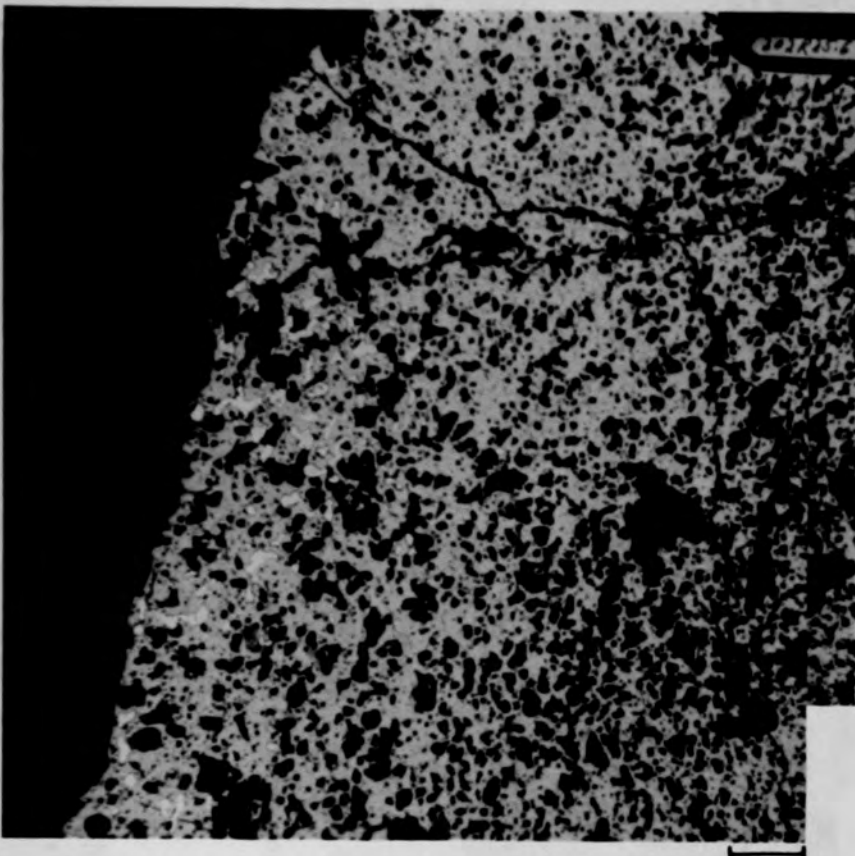
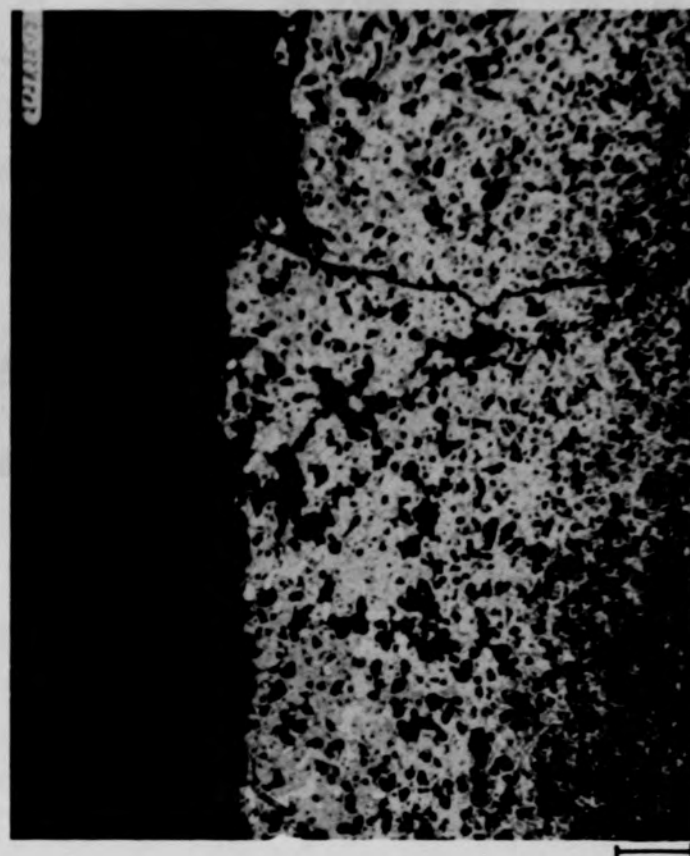


Figure C-145. SEM backscattered electron images of material from location E, Figure C-144, of Particle 7E (H8, 36 cm).

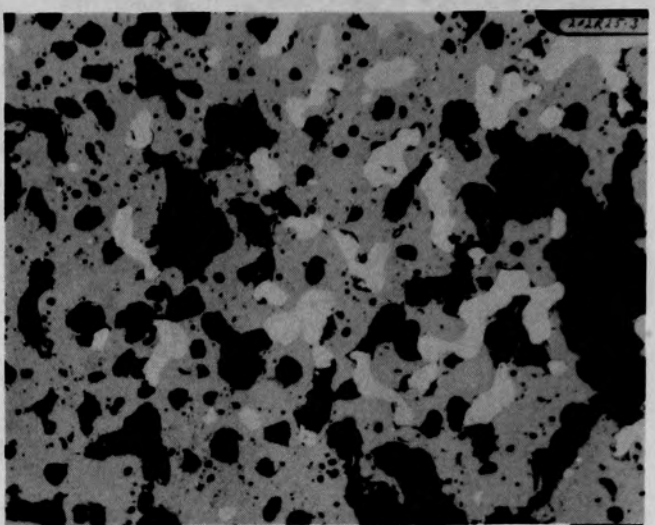


(a) Unetched

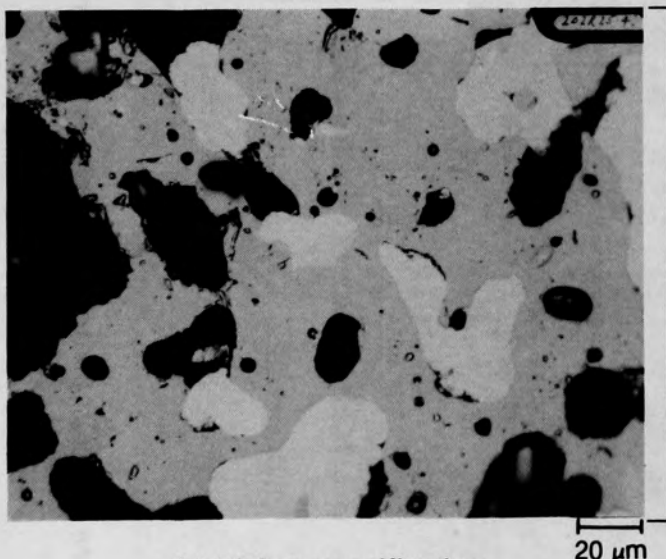


(b) Etched

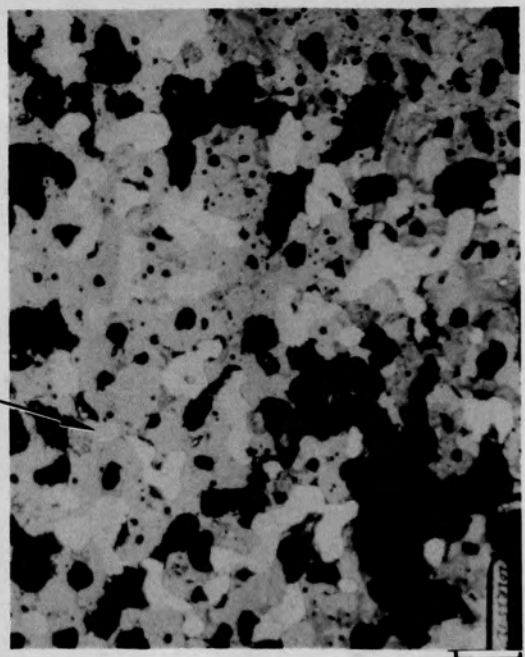
Figure C-146. Photomicrographs of material from location C of Particle 7E
(H8, 36 cm).



(a) Unetched



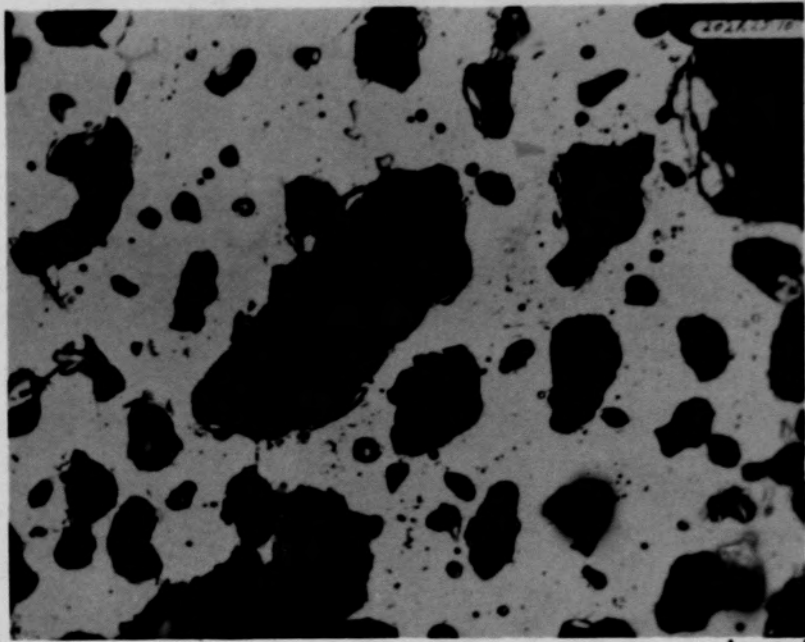
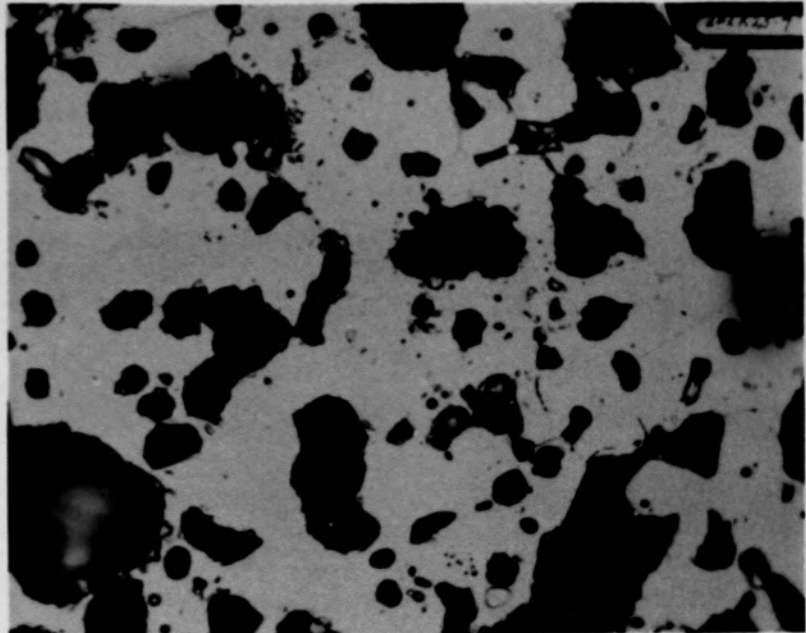
(c) Higher magnification



(b) Etched

Figure C-147. Photomicrographs of material from location D of Particle 7E (H8, 36 cm).

C-201



20 μm

Figure C-148. Photomicrographs of unetched material from location F of Particle 7E (H8, 36 cm).

C-202

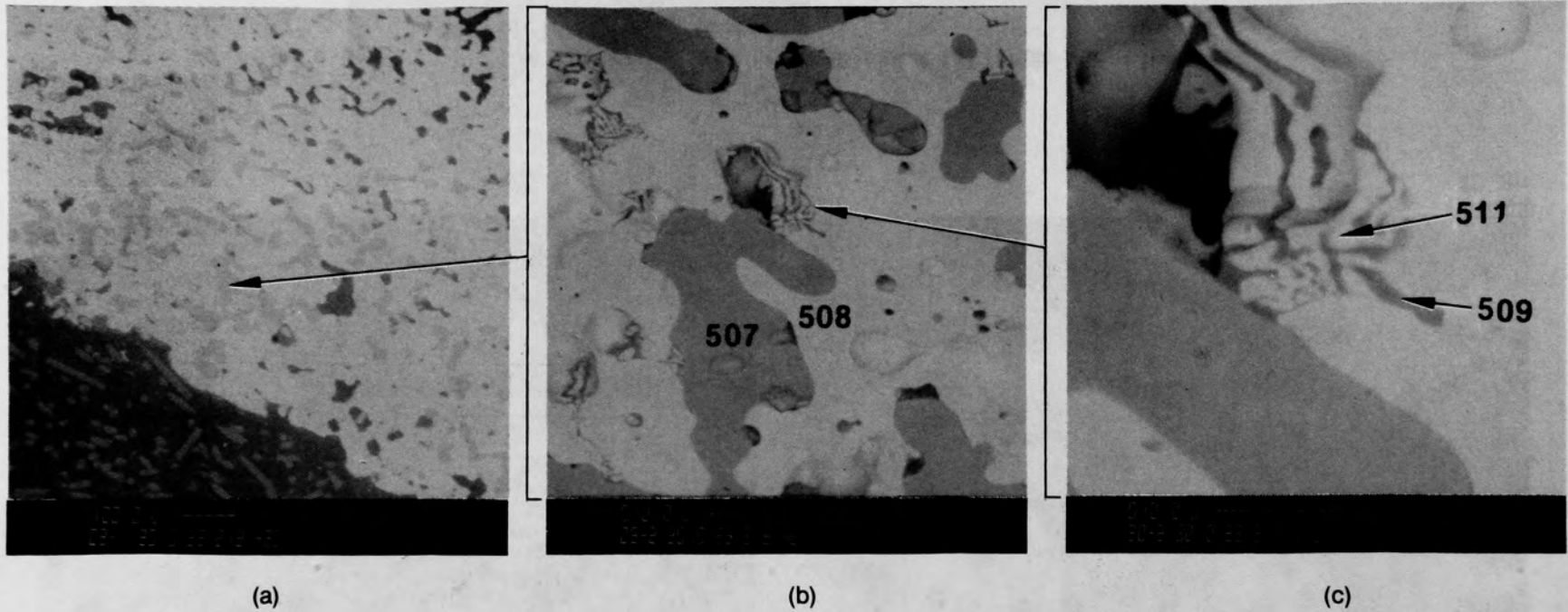
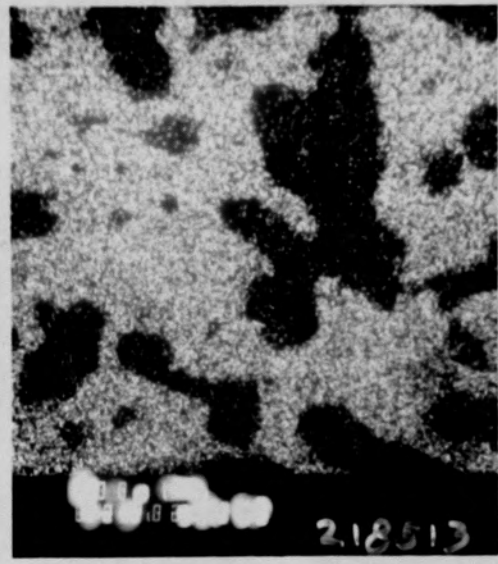


Figure C-149. SEM backscattered electron images of material from location G of Particle 7E (H8, 36 cm).

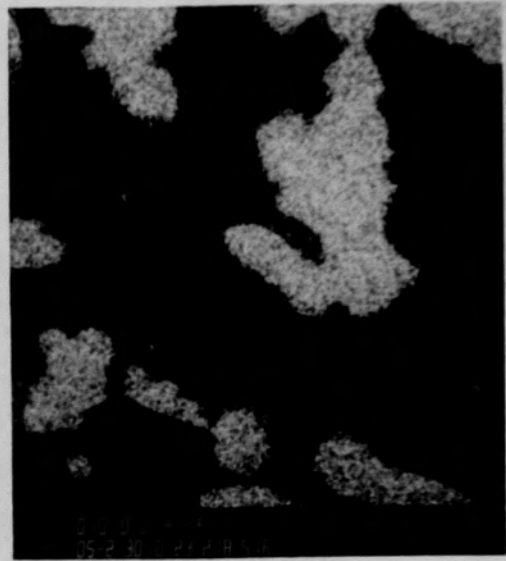
C-203



Zr



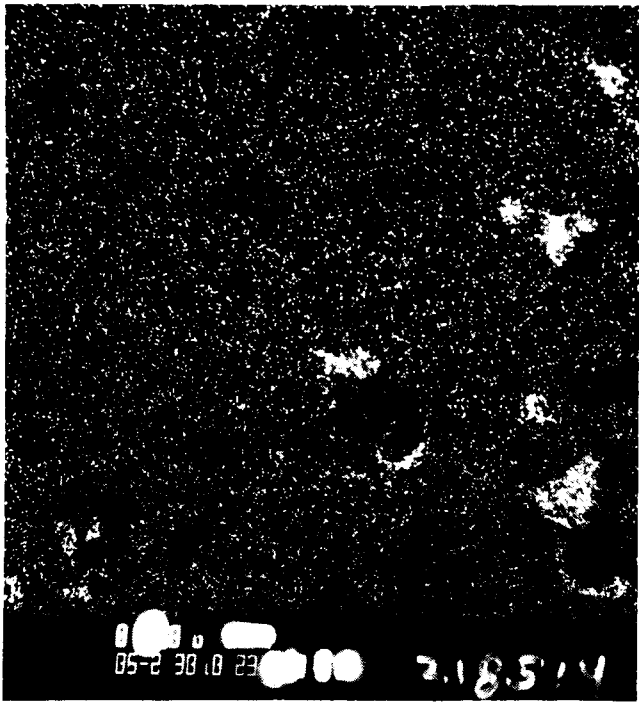
U



Ni

Figure C-150. X-ray dot map of material shown in Figure C-149b of Particle 7E (H8, 36 cm).

C-204

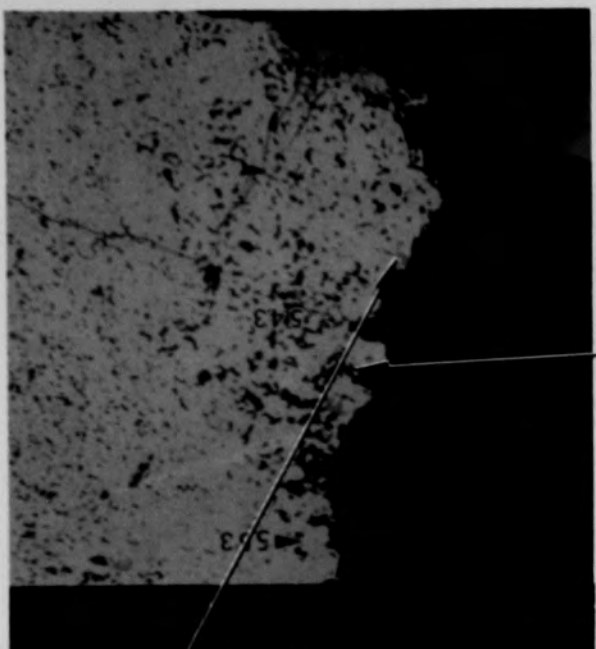


(a) Cr

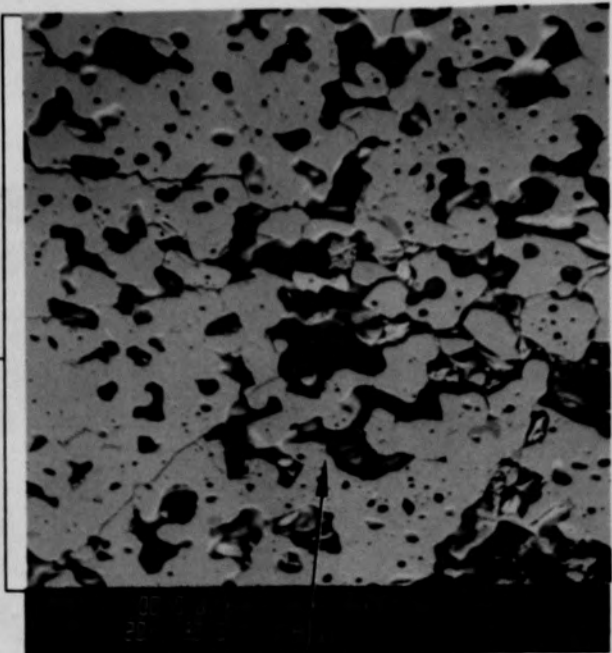


(b) Fe

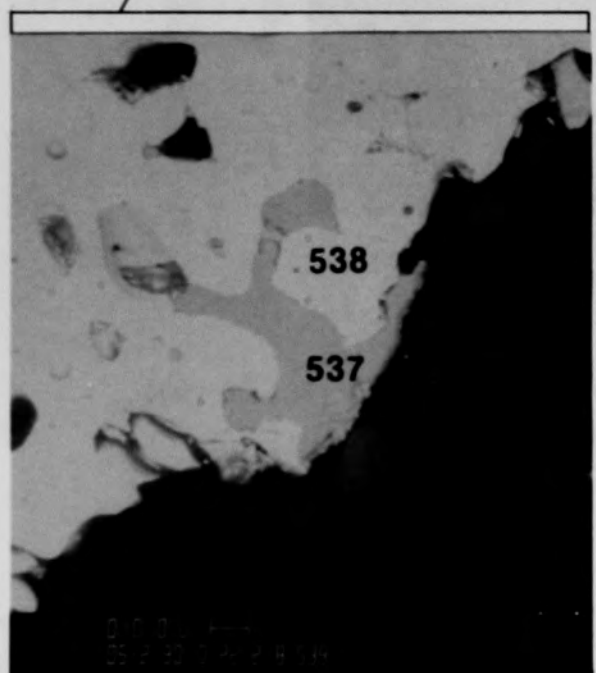
Figure C-151. X-ray dot map of material shown in Figure C-149c of Particle 7E (H8, 36 cm).



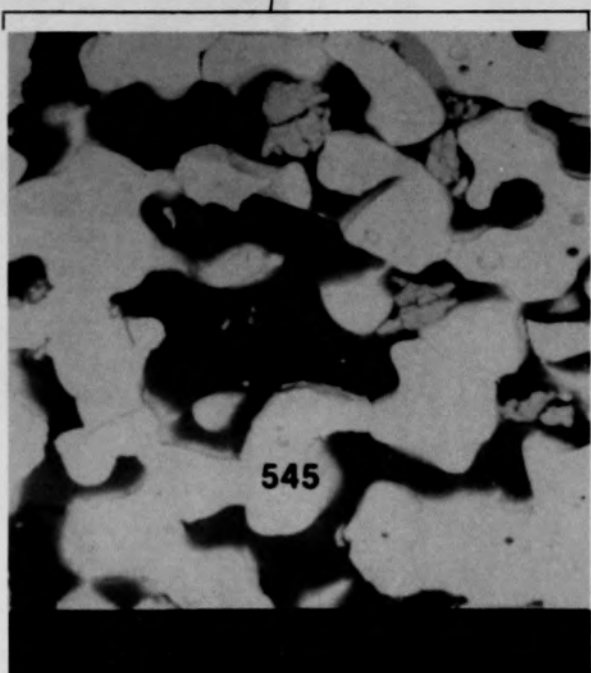
(a) SEM backscattered electron image



(b) SEM secondary electron image



(c) SEM backscattered electron image



(d) SEM backscattered electron image

Figure C-152. SEM images of material from location H of Particle 7E (H8, 36 cm).

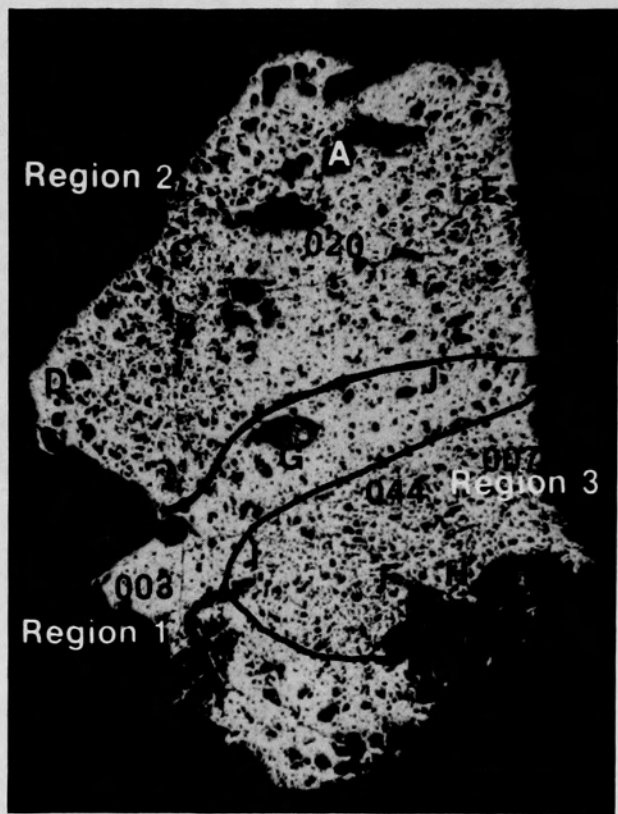
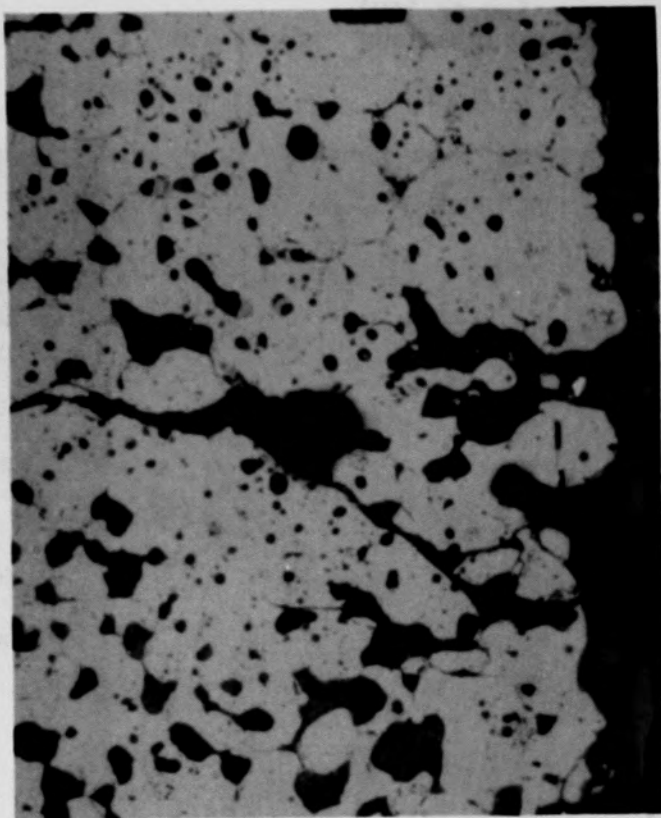
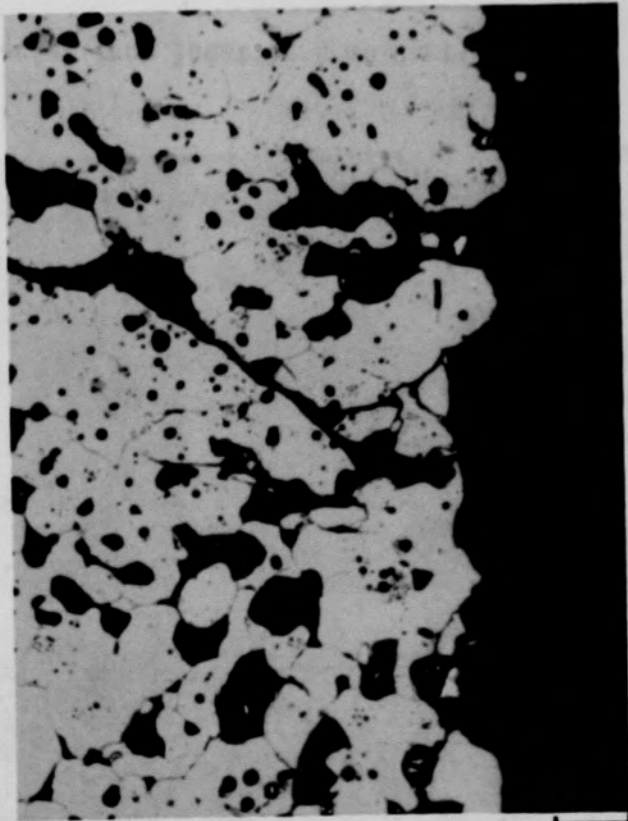


Figure C-153. Photomacrograph of Particle 8A (H8, 70 cm).



(a) Unetched



(b) Etched

50 μm

Figure C-154. Photomicrographs of material from location E of Particle 8A (H8, 70 cm) showing rounded pore surfaces and the effect of etching.

C-208

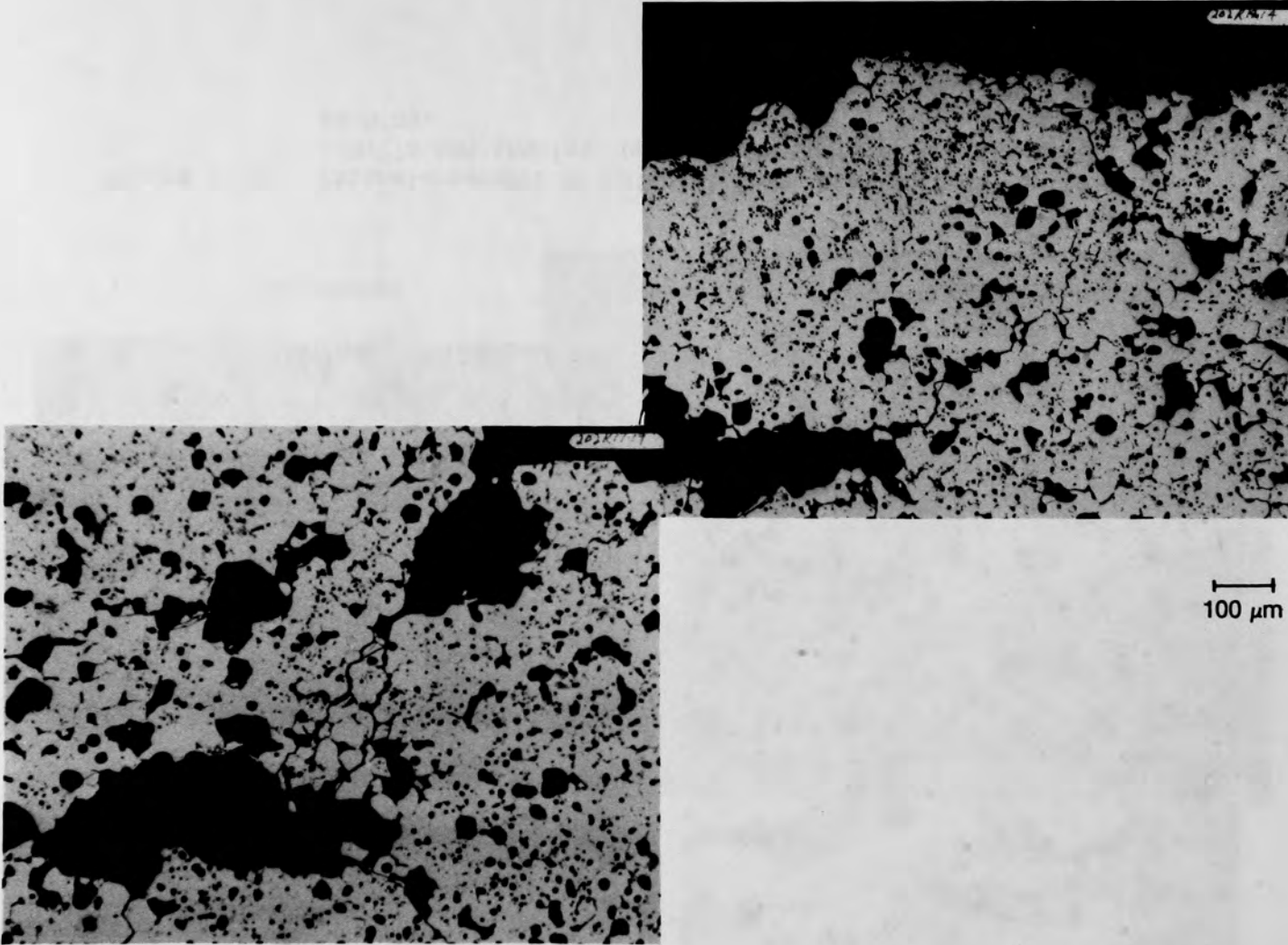


Figure C-155. Photomicrographs of material from location A of Particle 8A
(H8, 70 cm).

C-209

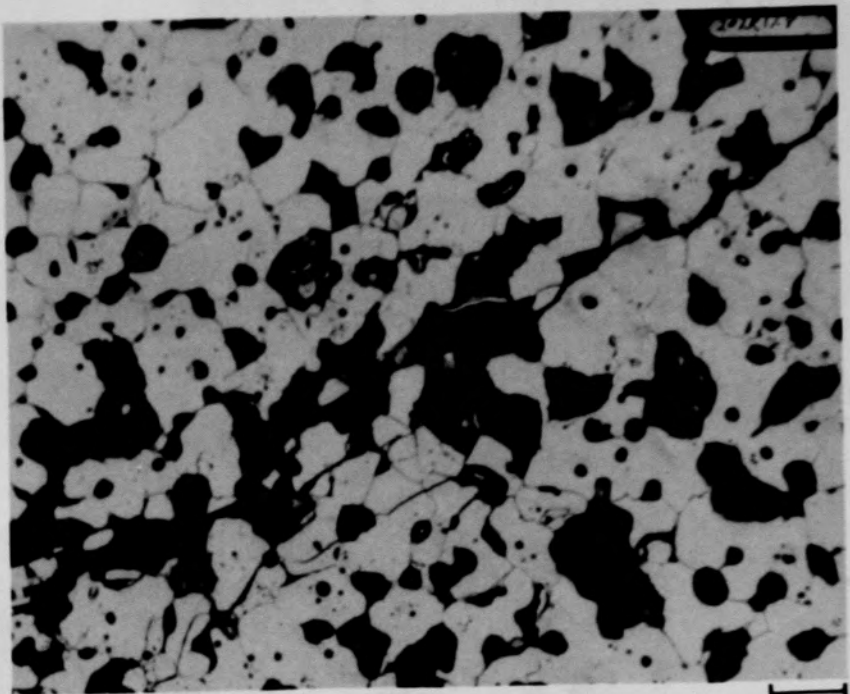
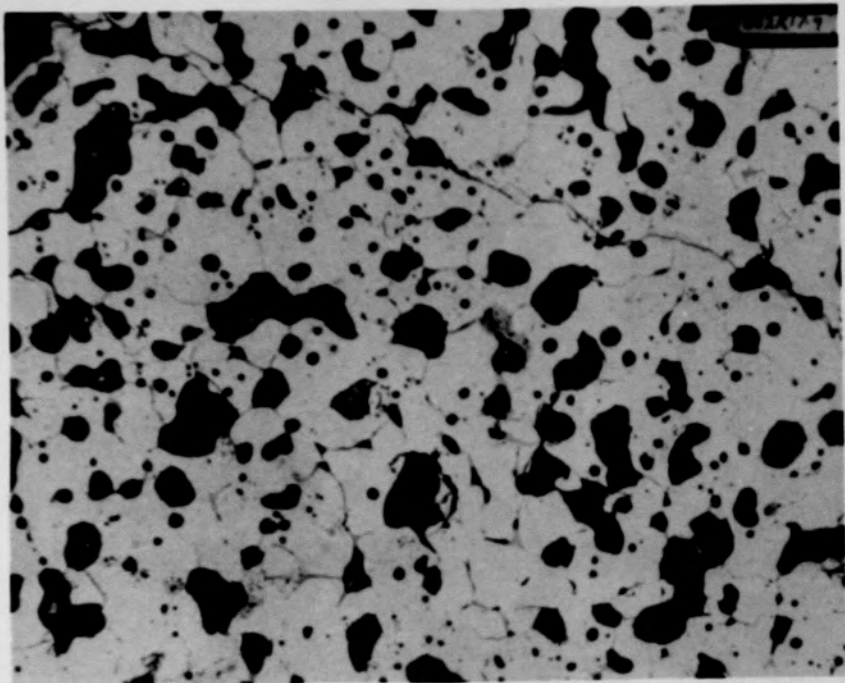
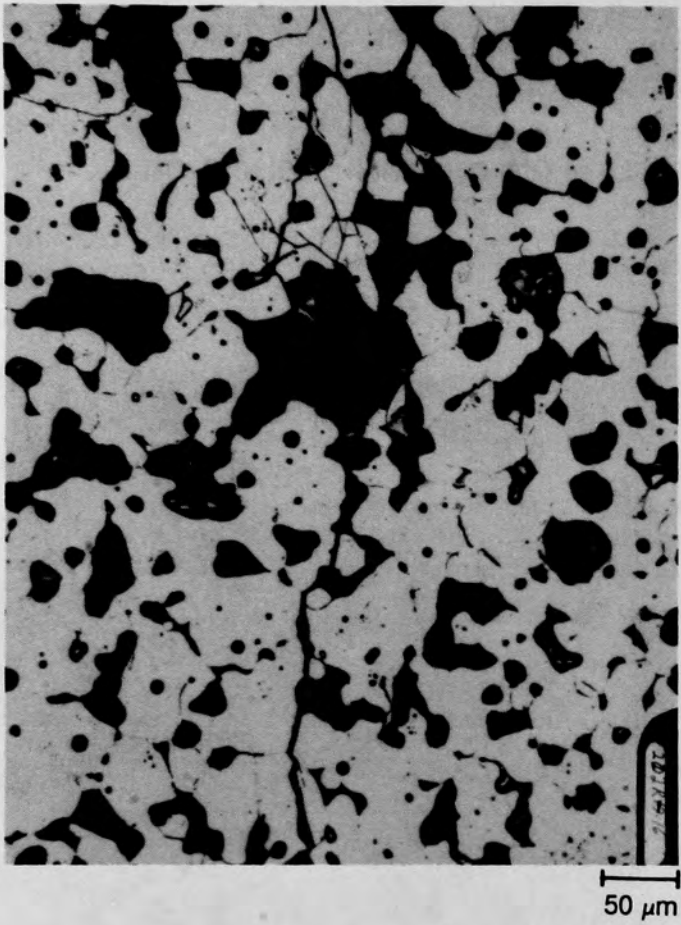
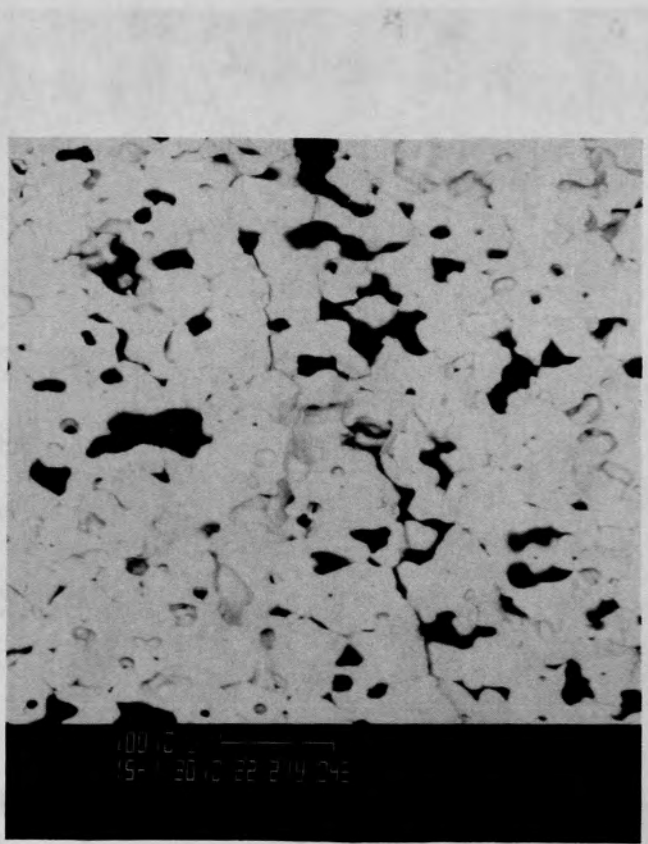


Figure C-156. Photomicrographs of material from location B of Particle 8A
(H8, 70 cm).

C-210

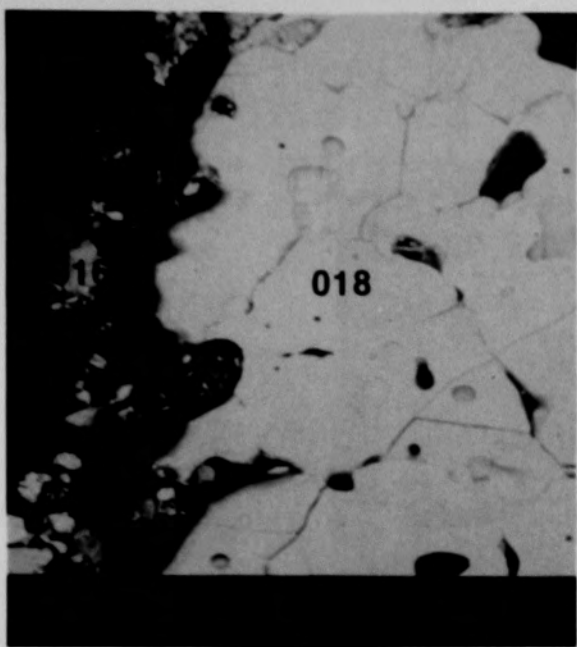


(a) Photomicrograph

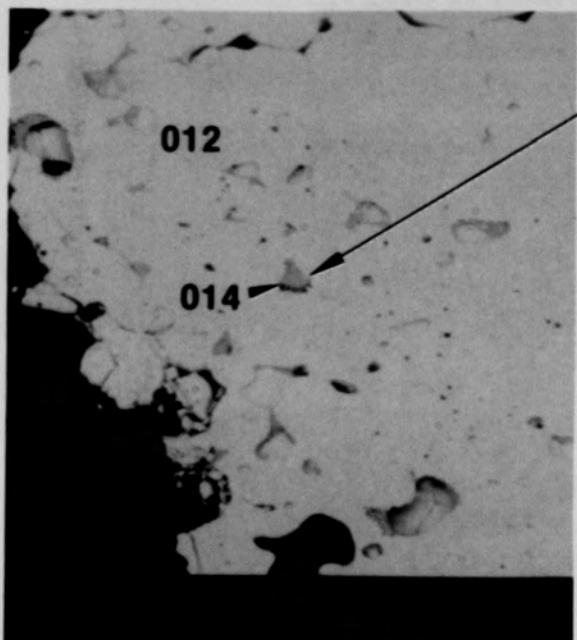


(b) SEM backscattered electron image

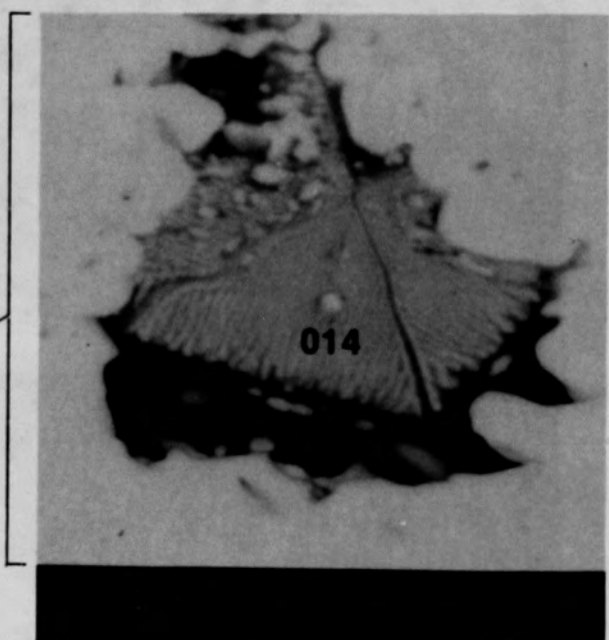
Figure C-157. Photographs of material from location B of Particle 8A (H8, 70 cm).



(a) Location C



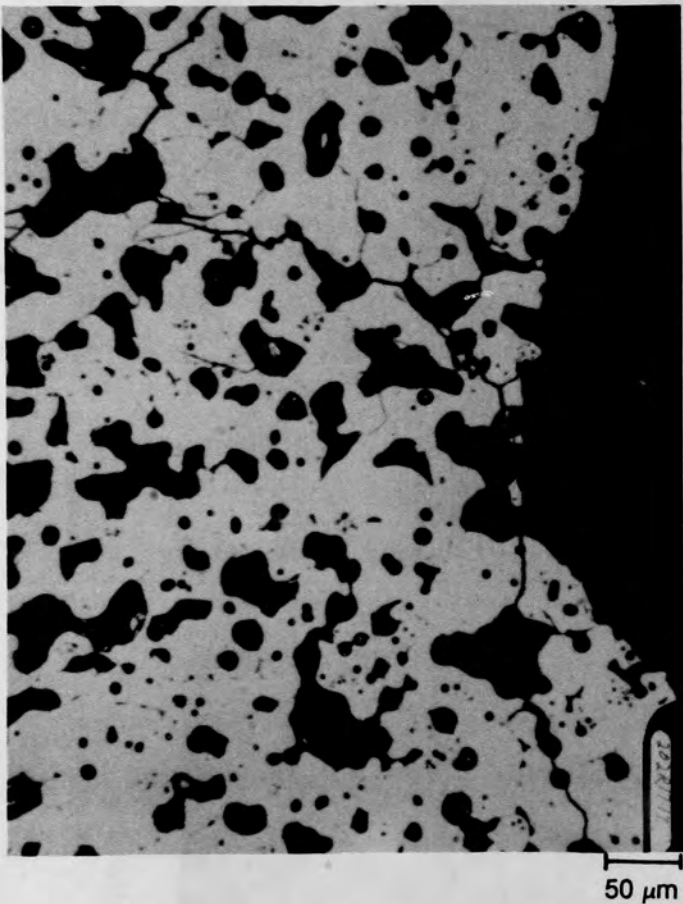
(b) Location D



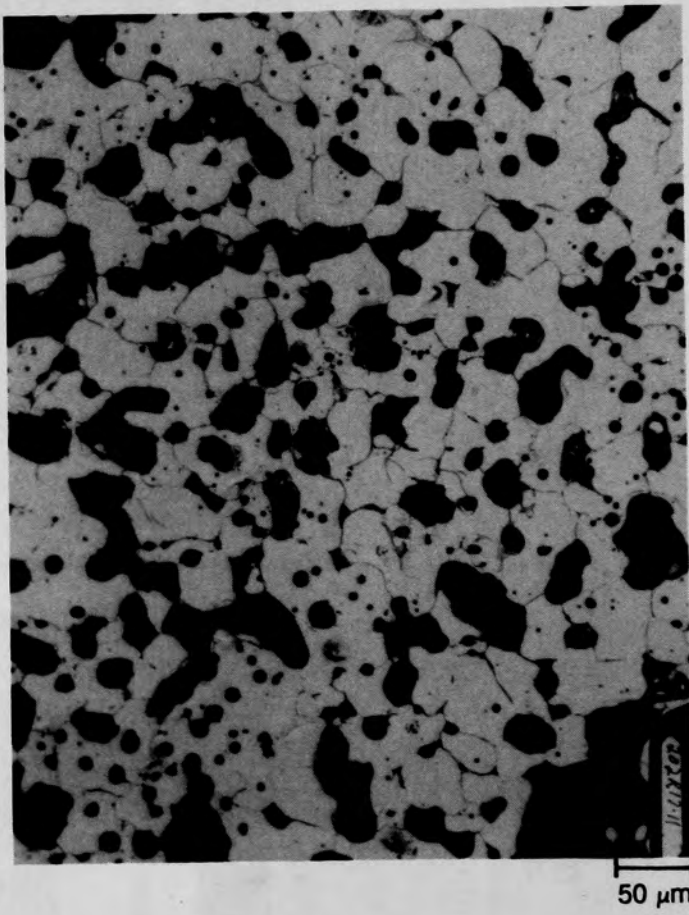
(c)

Figure C-158. SEM backscattered electron images of Particle 8A (H8, 70 cm).

C-212



(a) Unetched



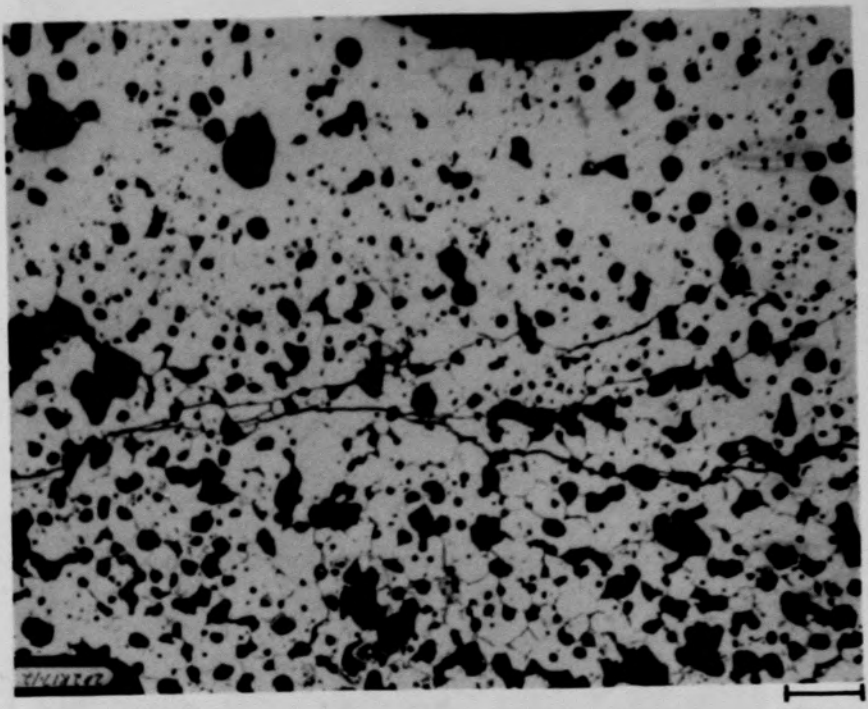
(b) Etched

Figure C-159. Photomicrographs of material from location F of Particle 8A
(H8, 70 cm).

C-213



(a) Unetched



(b) Etched

Figure C-160. Photomicrographs of material from location G of Particle 8A
(H8, 70 cm).

C-214

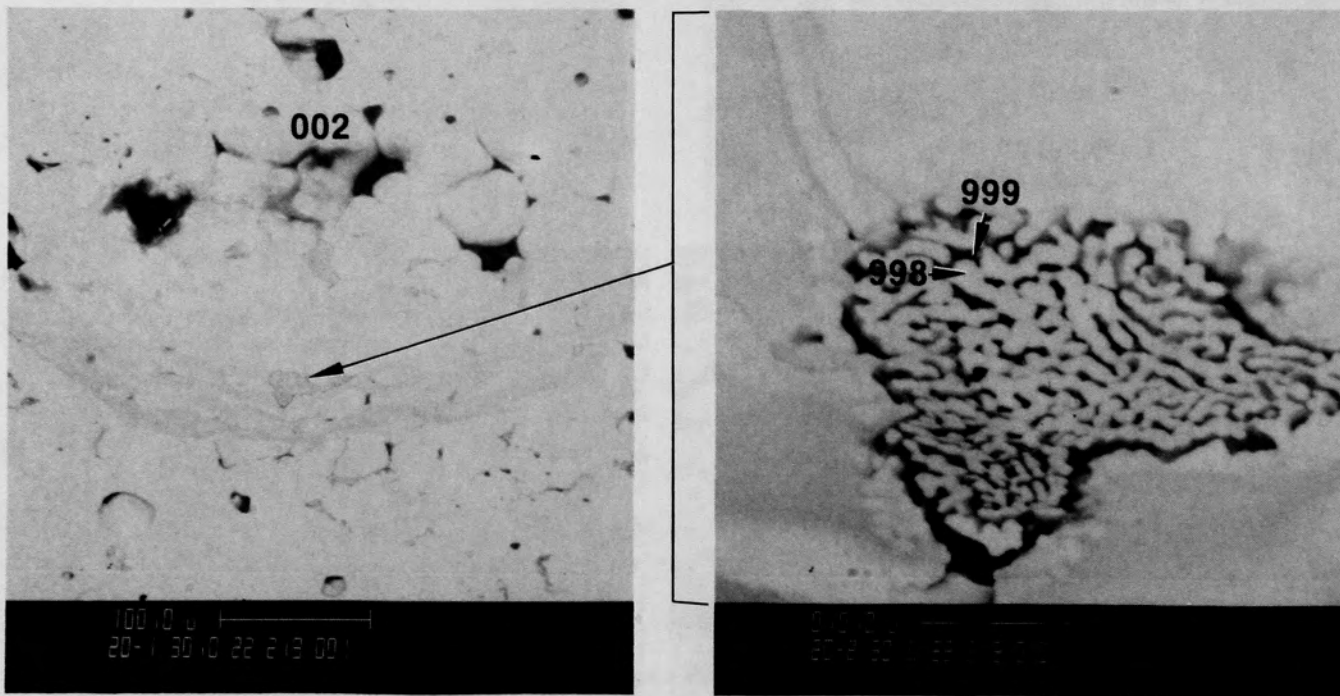


Figure C-161. SEM backscattered electron images of material from location G of Particle 8A (H8, 70 cm).

C-215

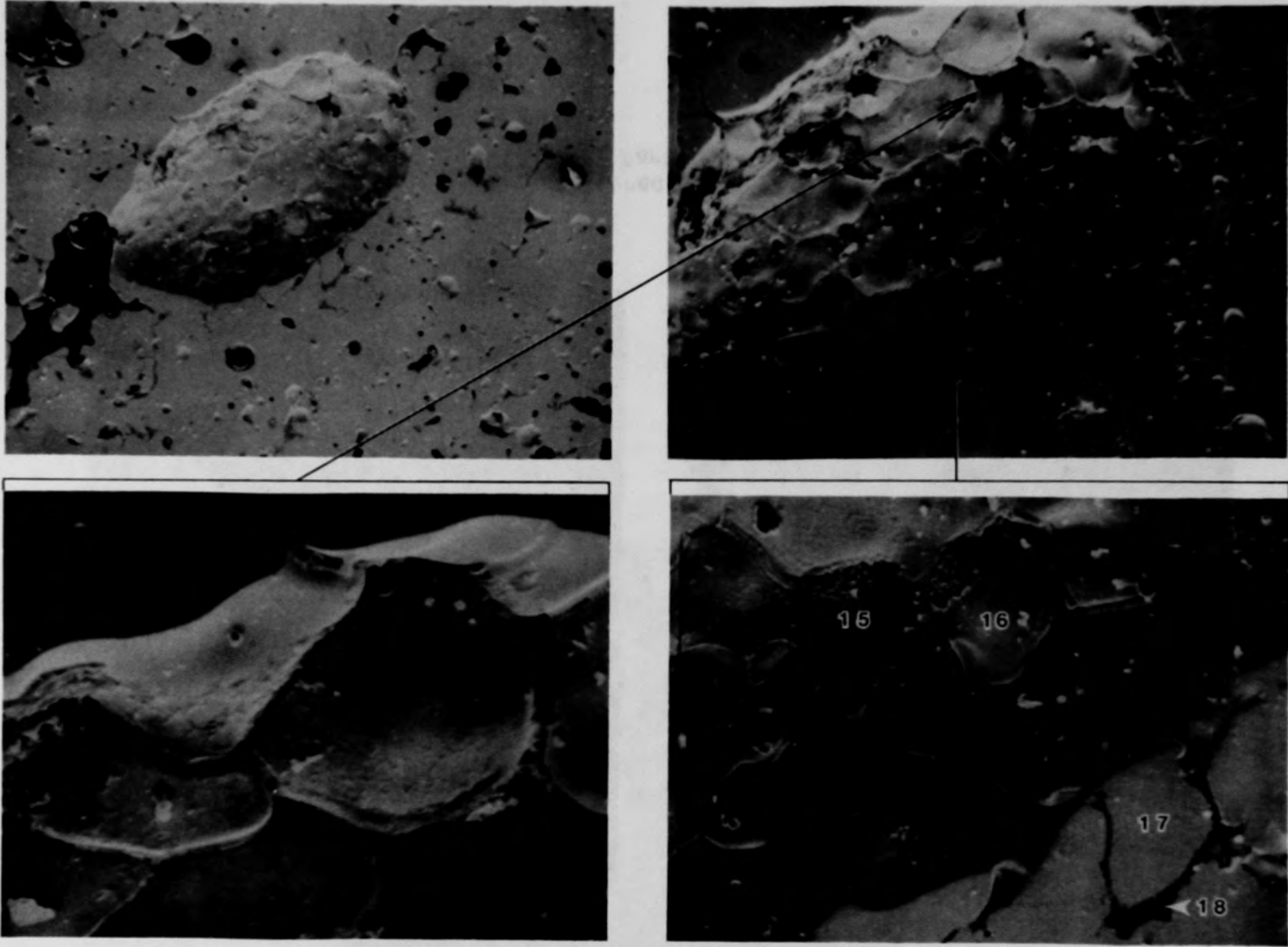


Figure C-162. Auger images of material from location G of Particle 8A (H8, 70 cm).

C-216

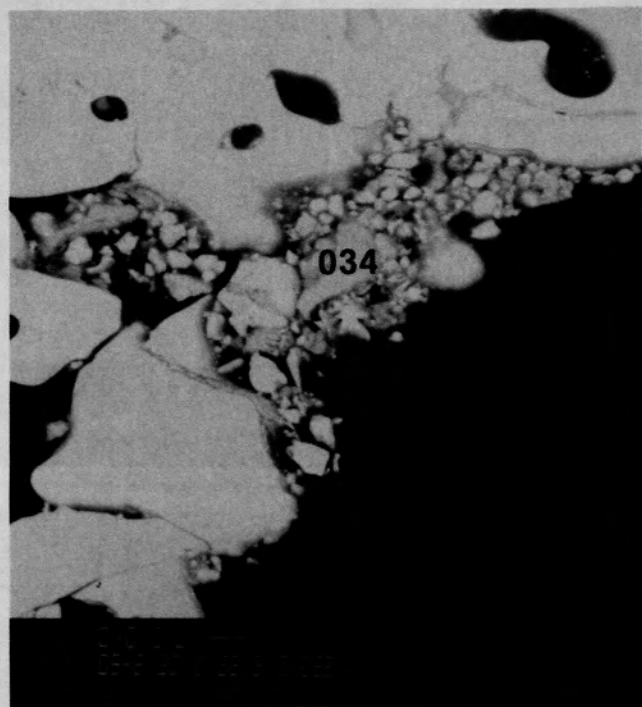
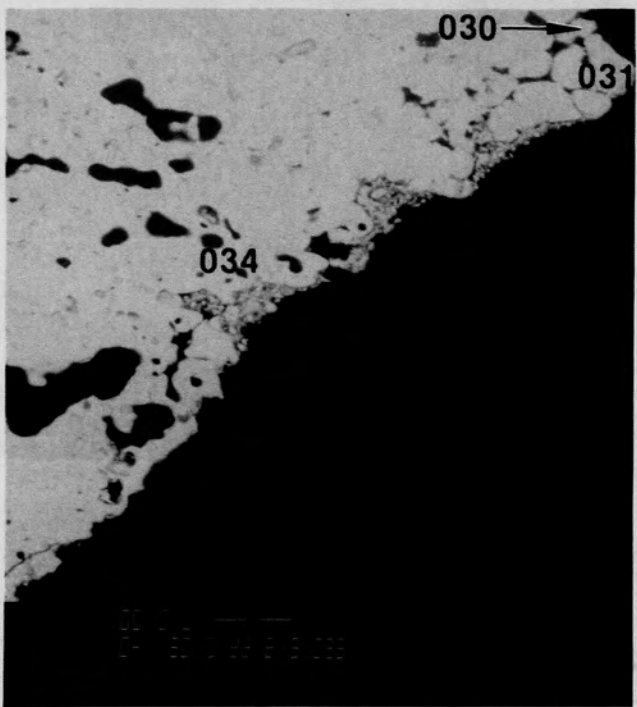


Figure C-163. SEM backscattered electron images of material from location H of Particle 8A (H8, 70 cm).

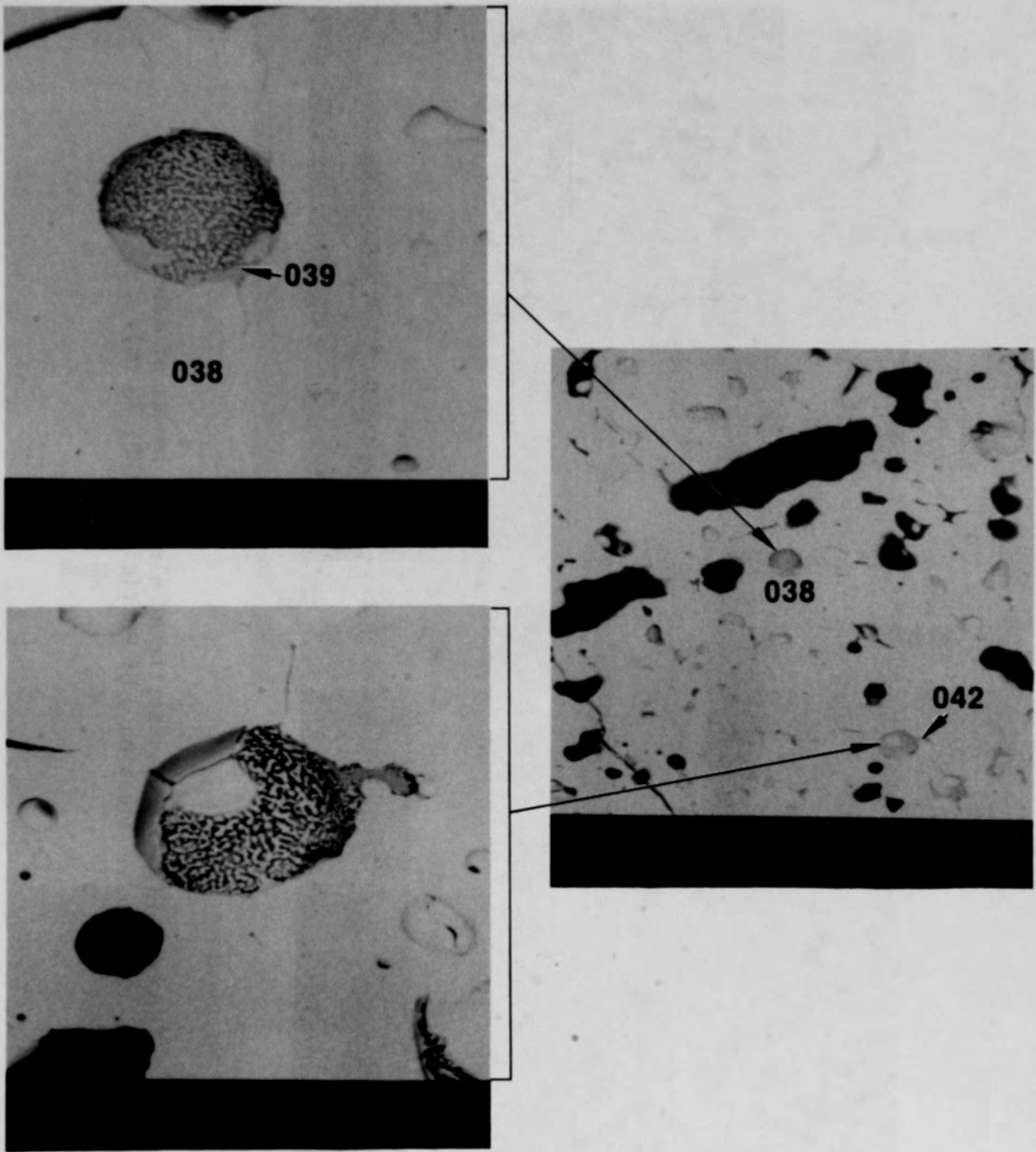


Figure C-164. SEM backscattered electron images of material from location I of Particle 8A (H8, 70 cm).

C-218

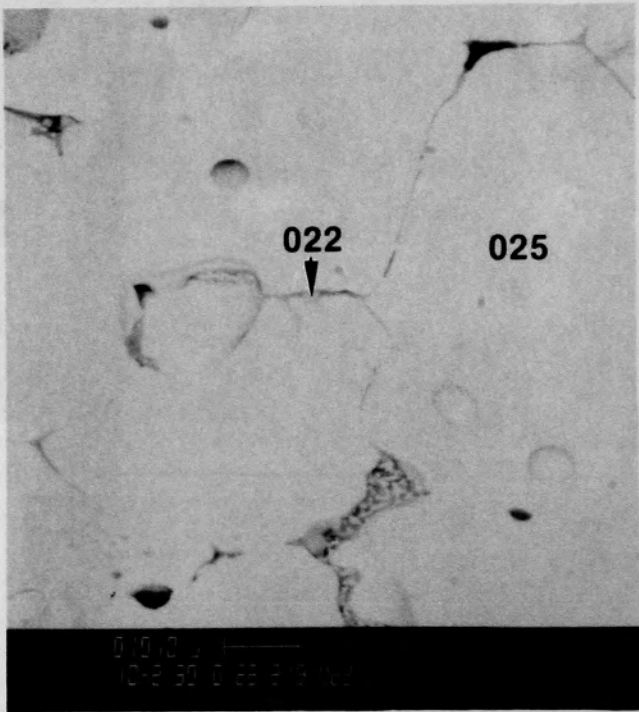
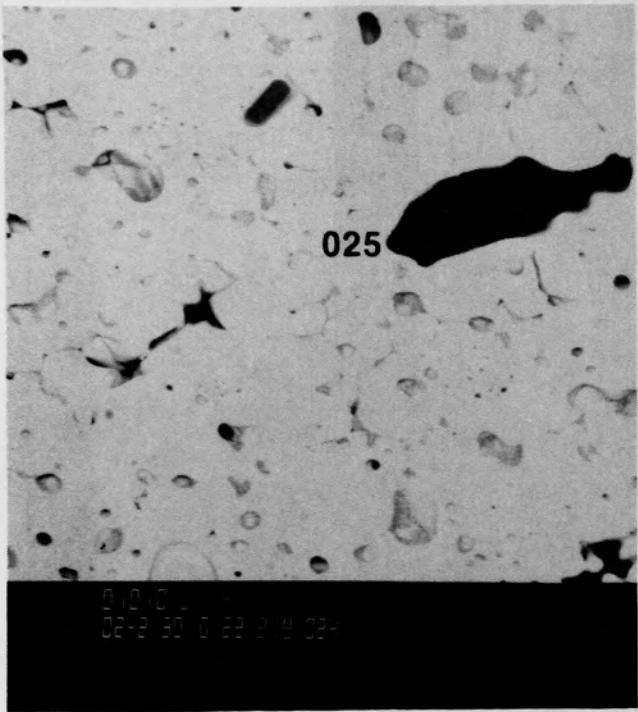


Figure C-165. SEM backscattered electron images of material from location J of Particle 8A (H8, 70 cm).

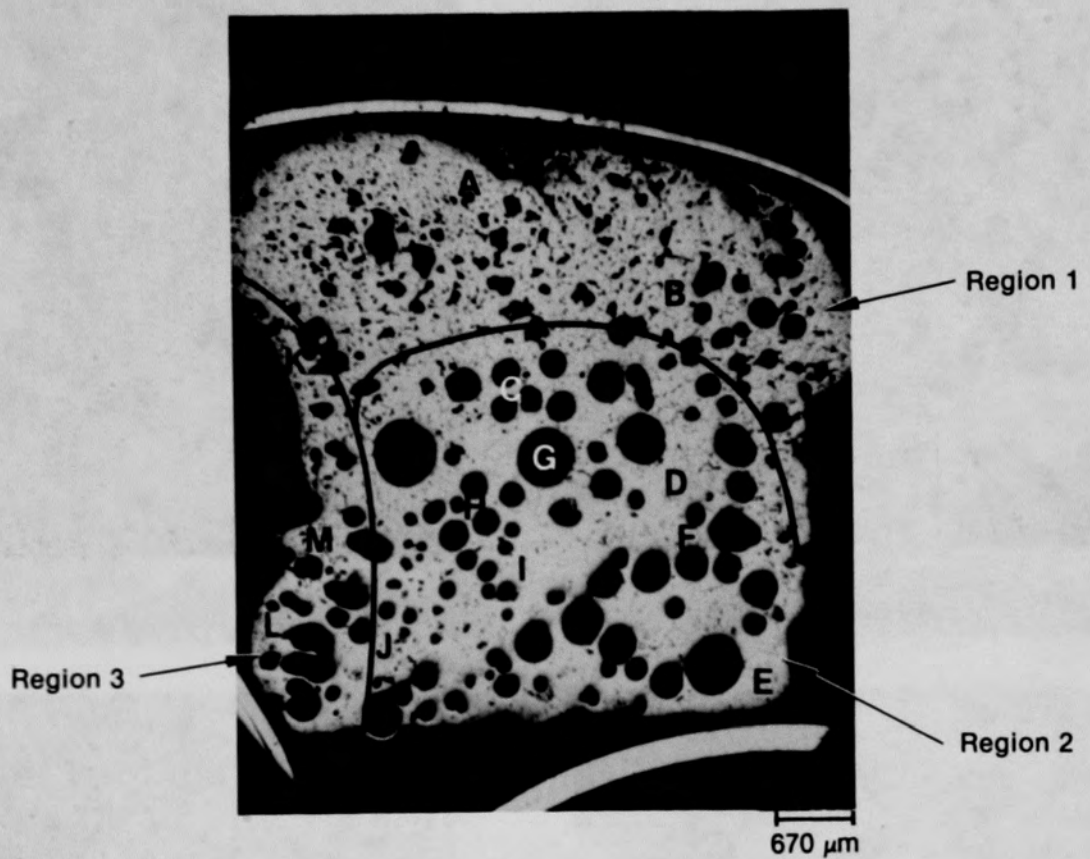
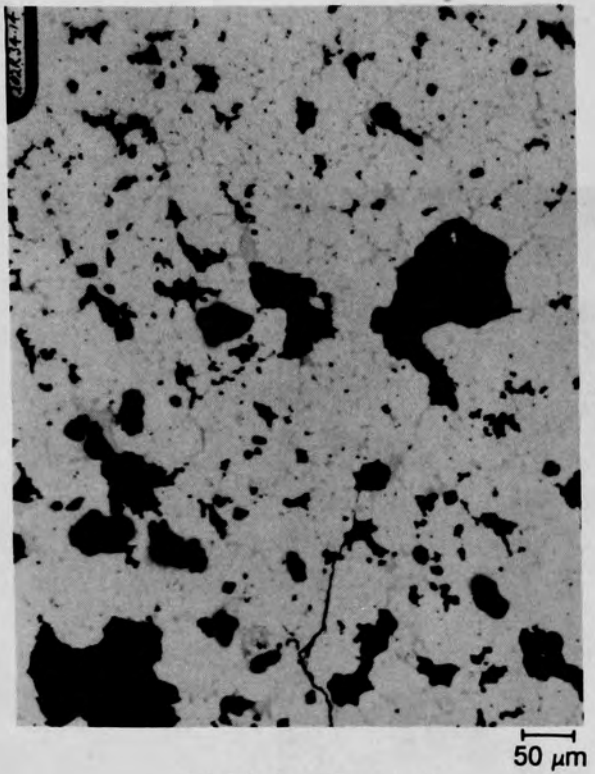
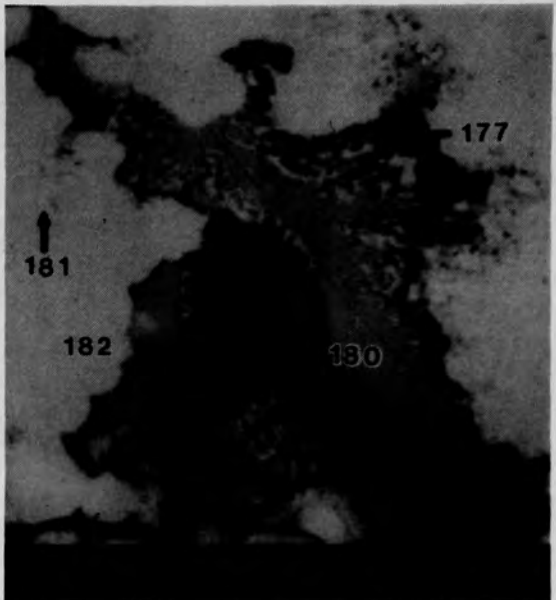


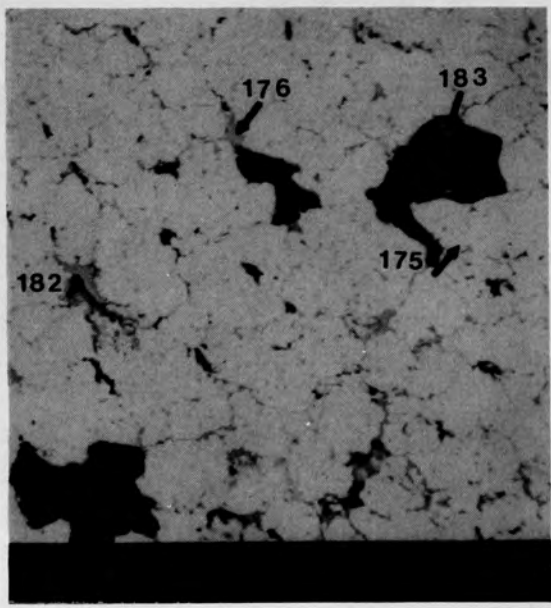
Figure C-166. Photomacrograph of Particle 8C (H8, 70 cm).



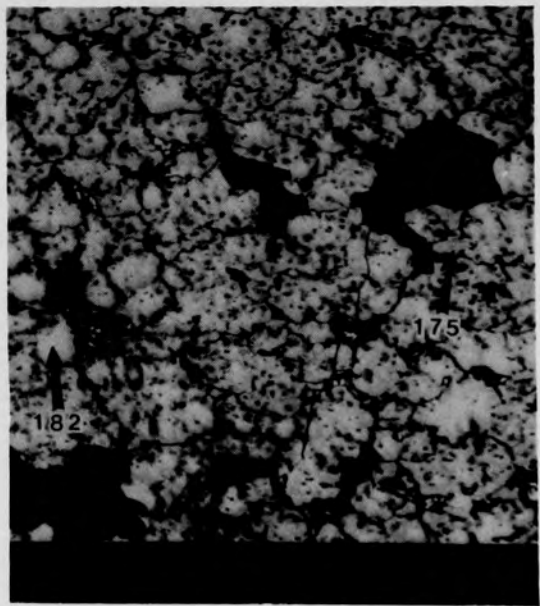
(a) Photomicrograph



(b) SEM backscattered electron image



(c) SEM backscattered electron image



(d) Higher contrast of (c)

Figure C-167. Photographs of material from Region 1, location A of Particle 8C (H8, 70 cm).

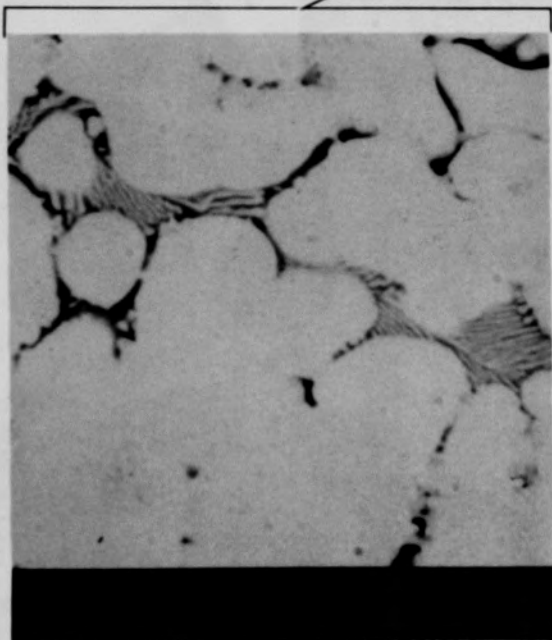
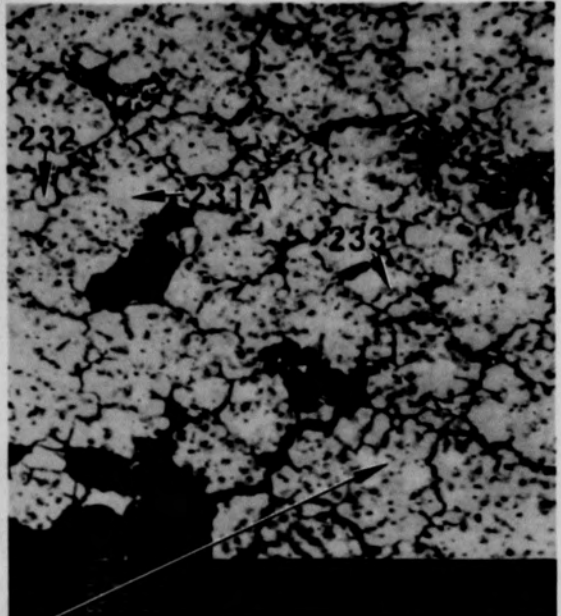
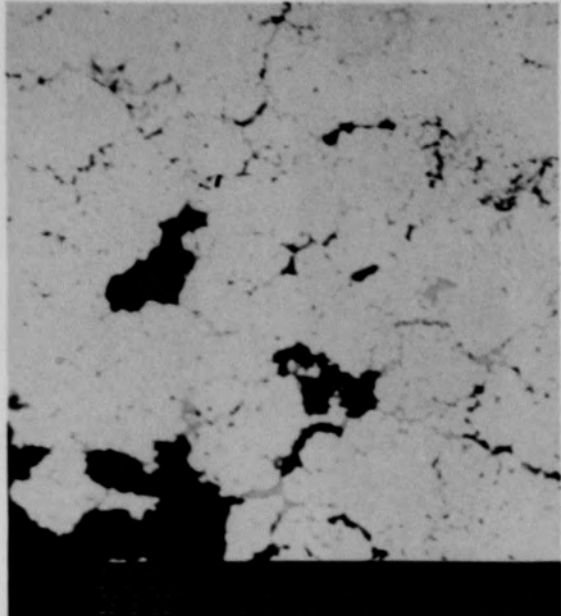


Figure C-168. SEM backscattered electron images of material from Region 1, location B of Particle 8C (H8, 70 cm).

C-222

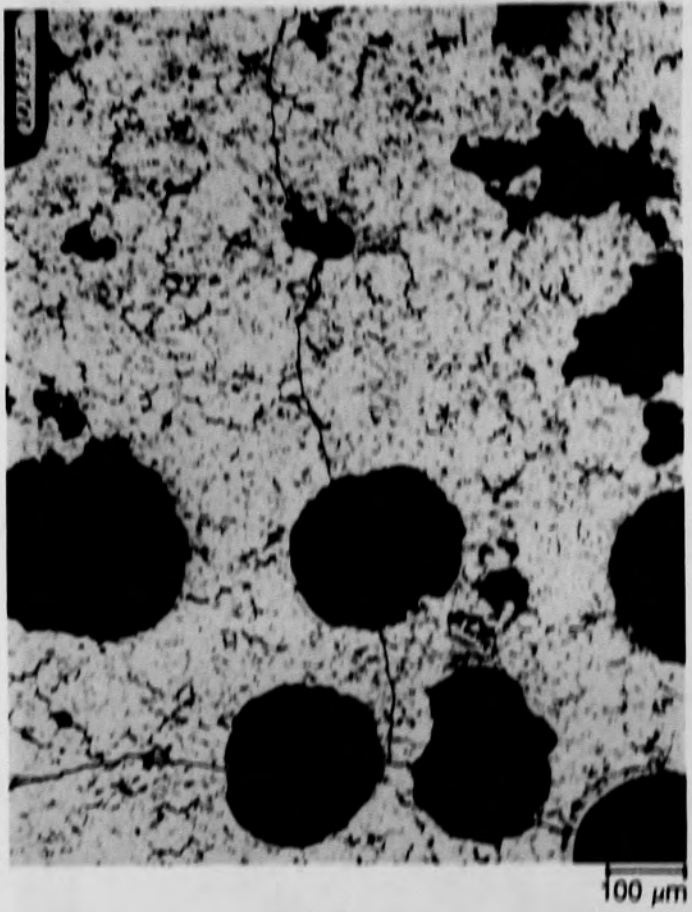
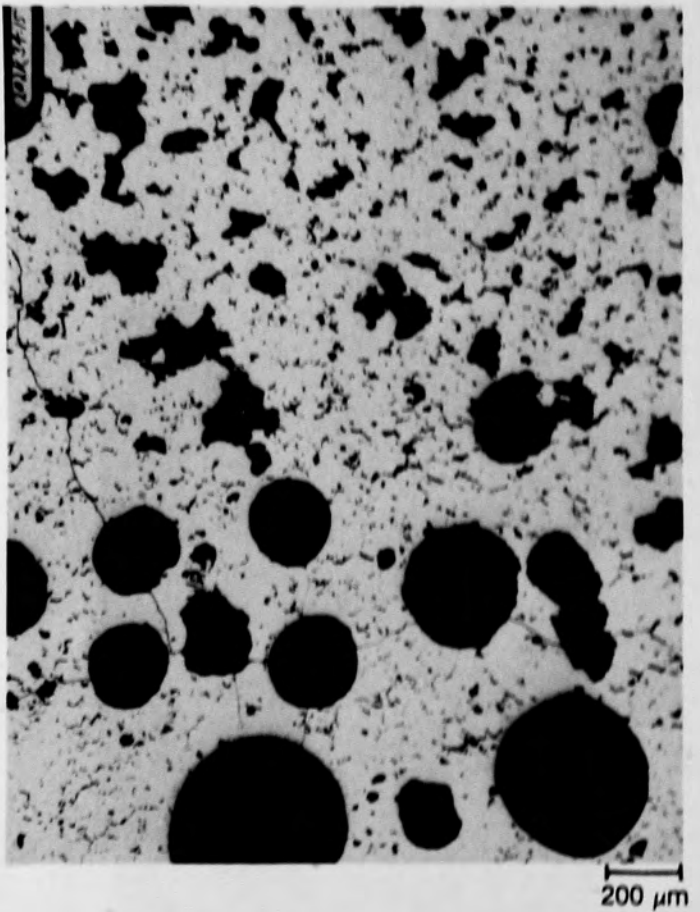


Figure C-169. Photomicrographs of material from Region 2, location F of Particle 8C (H8, 70 cm).

C-223

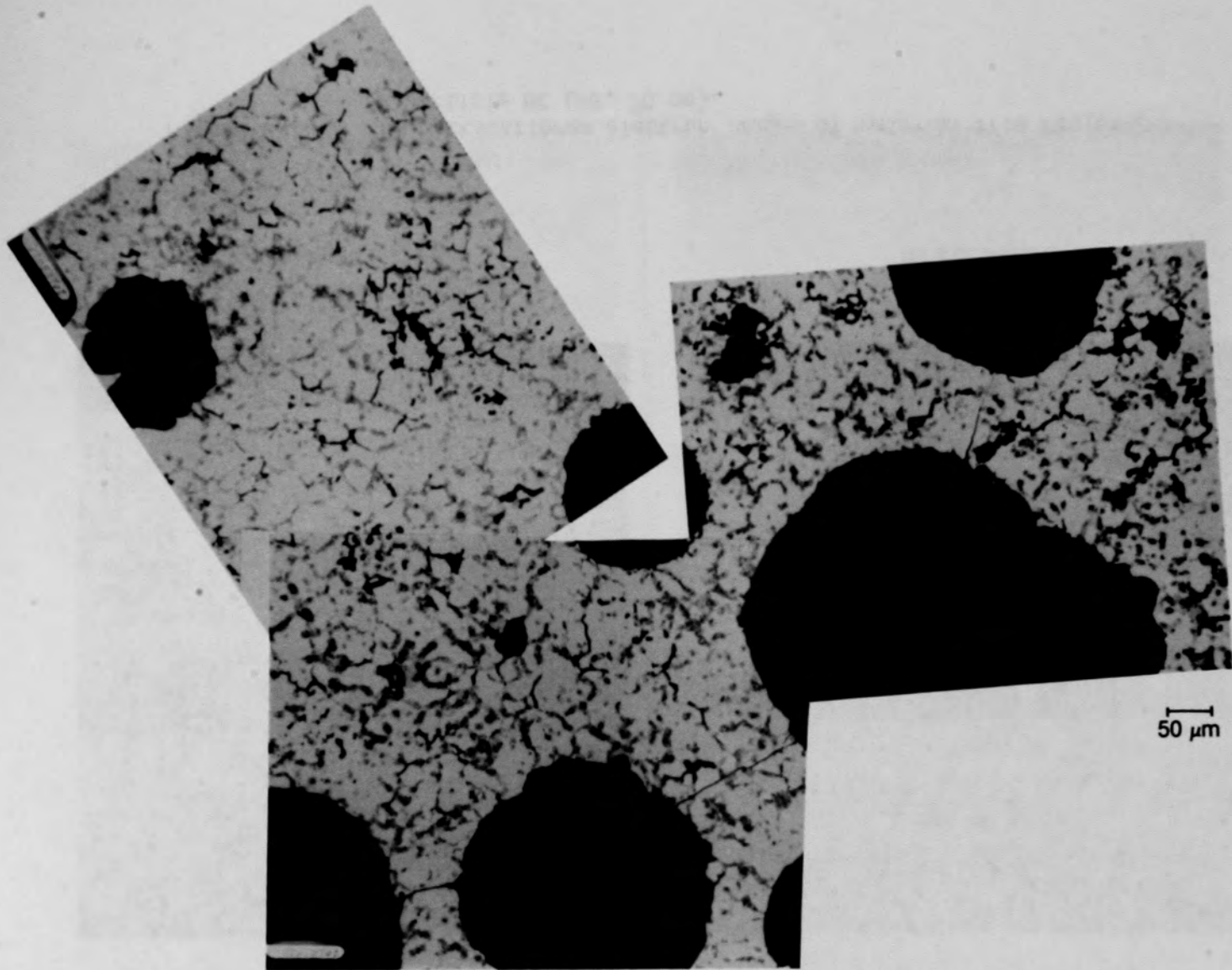
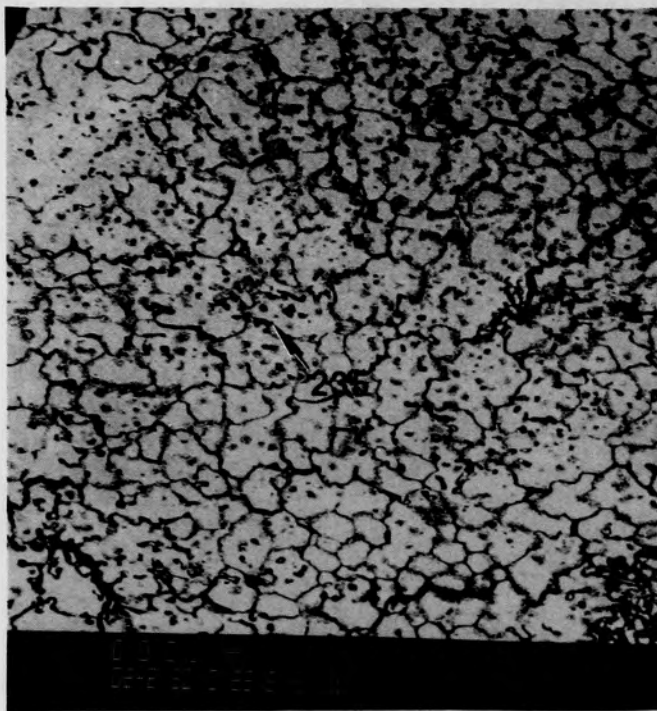


Figure C-170. Etched photomicrographs of material from Region 2,
location F of Particle 8C (H8, 70 cm).

C-224



(a) Location D



(b) Location E

Figure C-171. SEM backscattered electron images of material from Region 2 of Particle 8C (H8, 70 cm).

C-225

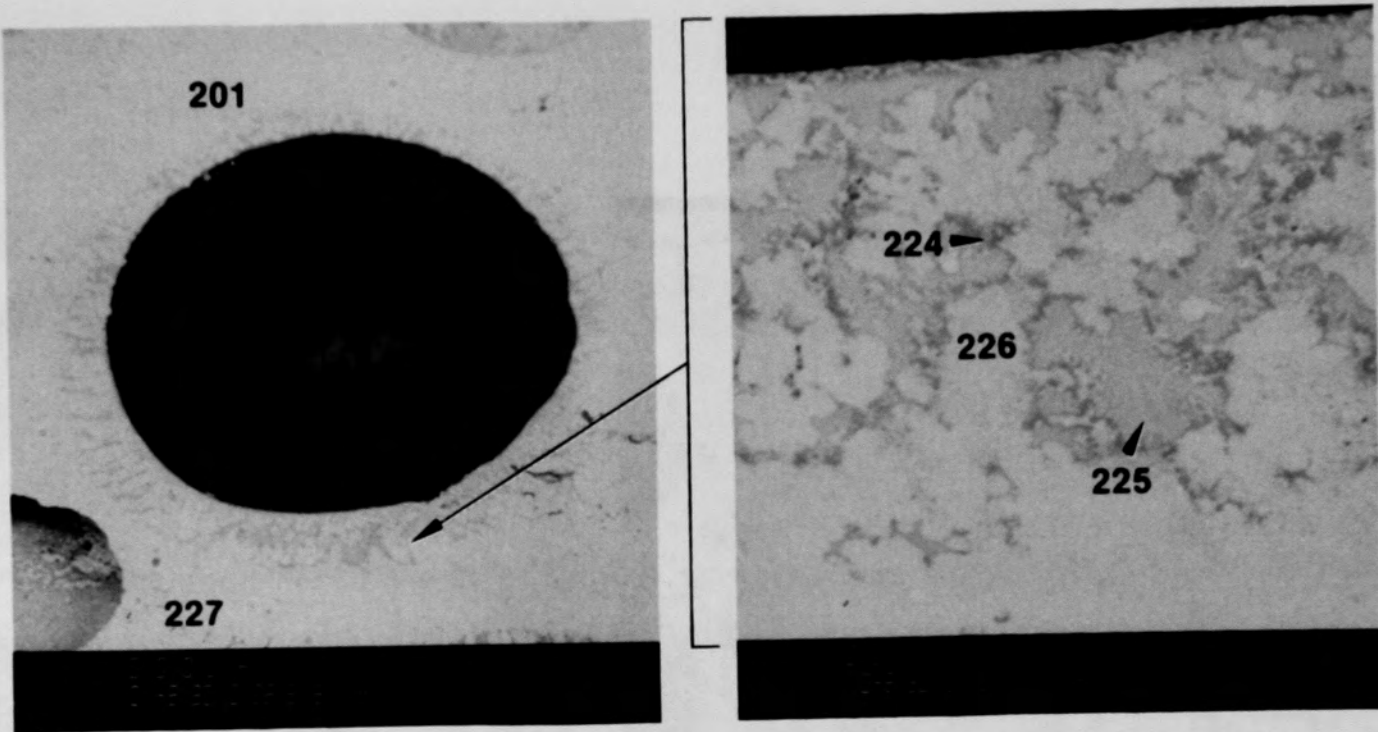
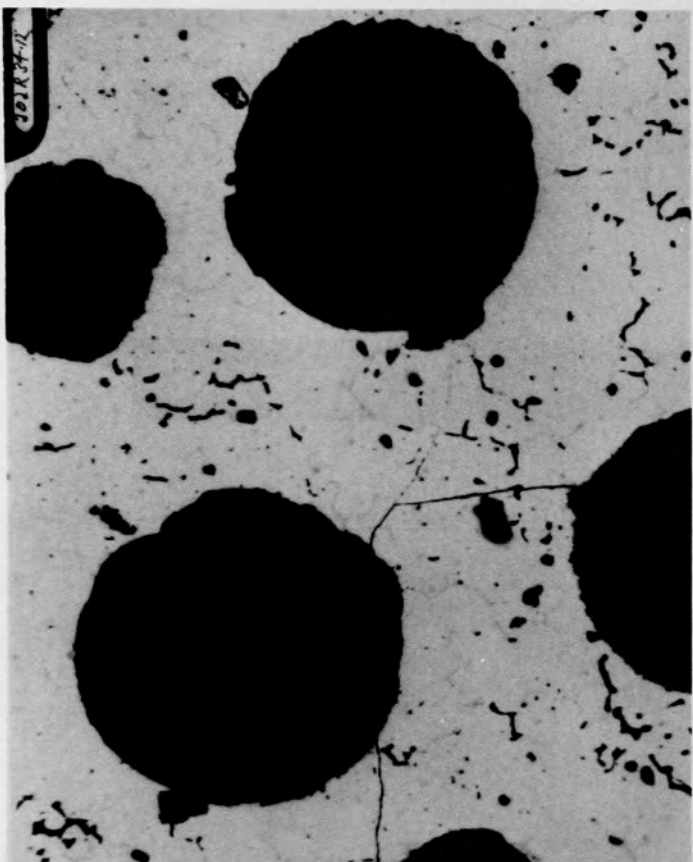
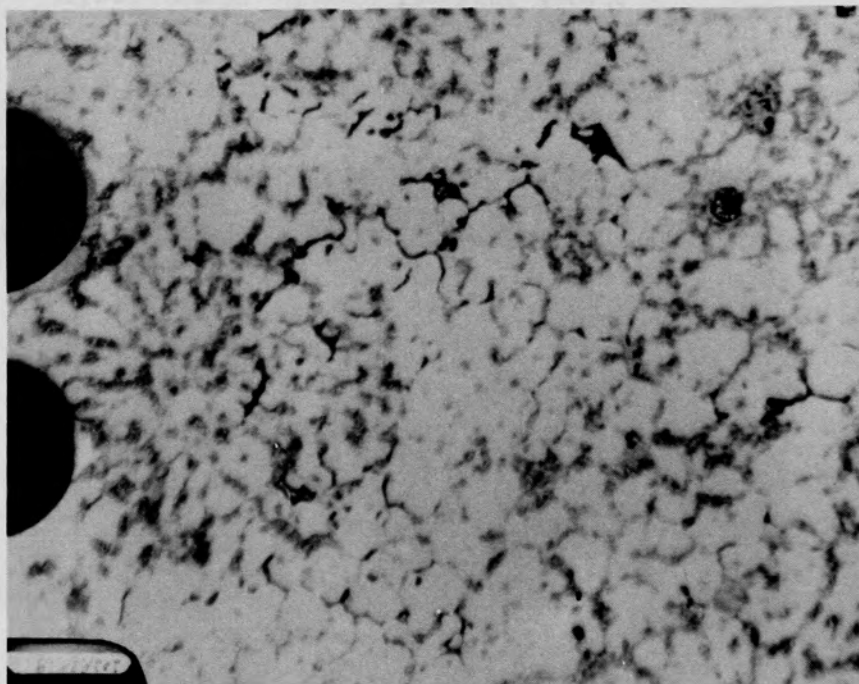


Figure C-172. SEM backscattered electron images of material from Region 2
location G of Particle 8C (H8, 70 cm).

C-226



(a) Location H



(b) Location I

Figure C-173. Photomicrographs of material from Region 2 of Particle 8C
(H8, 70 cm).

C-227

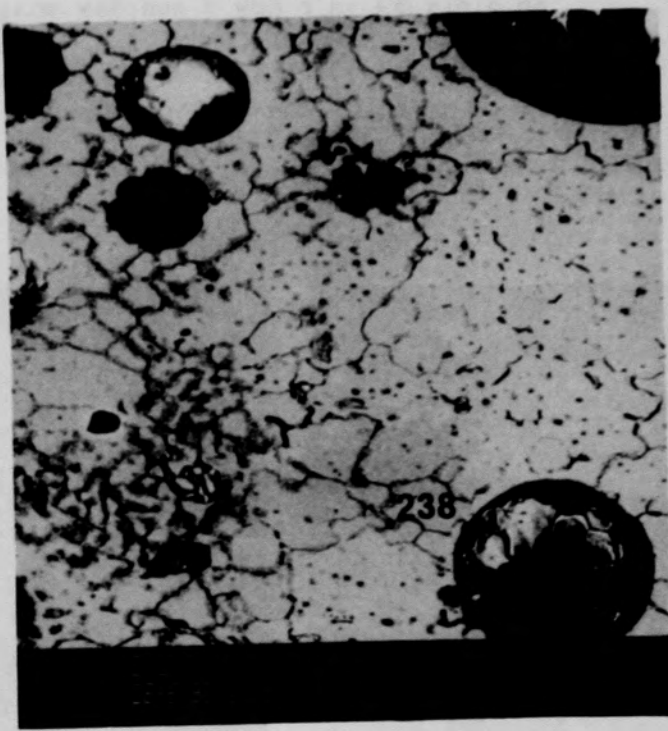
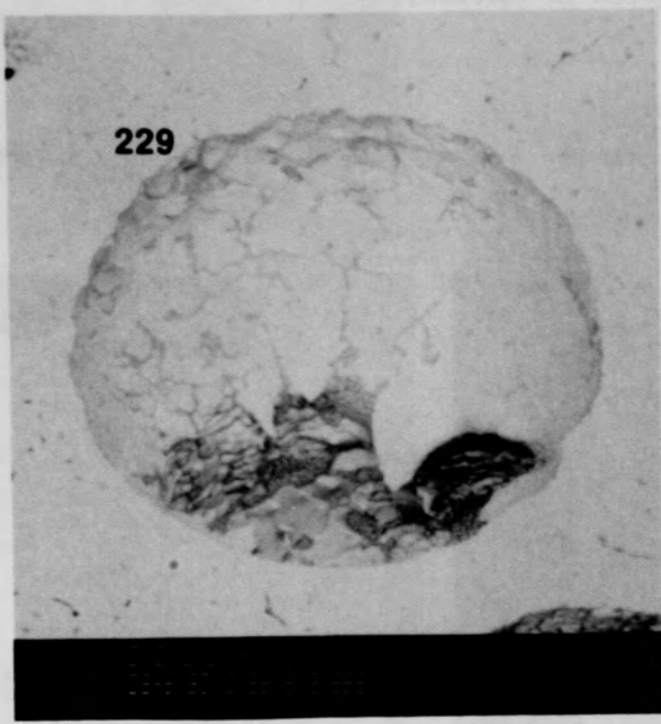
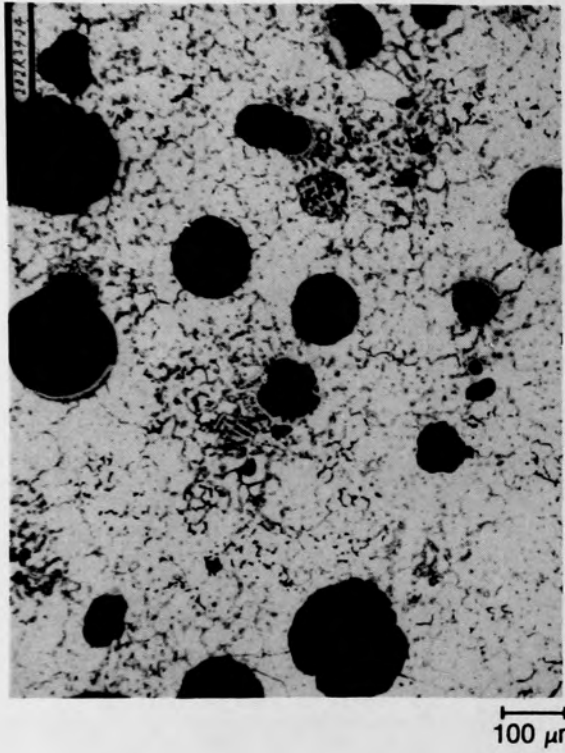
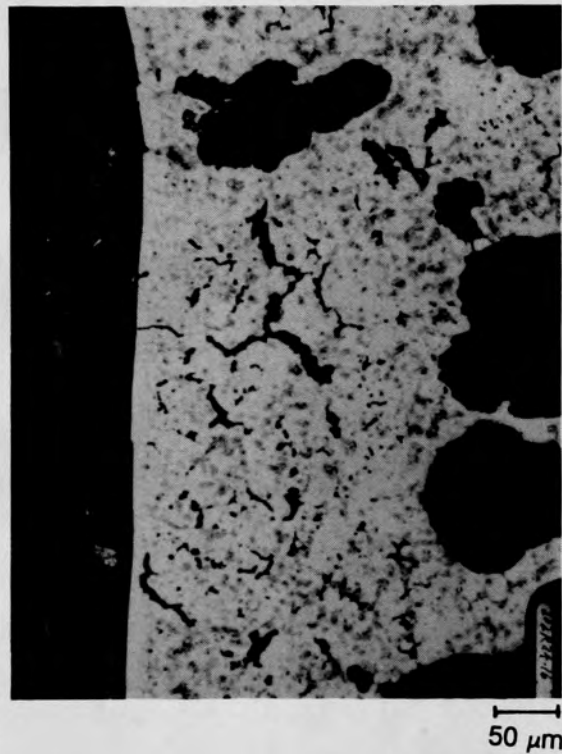


Figure C-174. SEM backscattered electron images of material from Region 2,
location H of Particle 8C (H8, 70 cm).

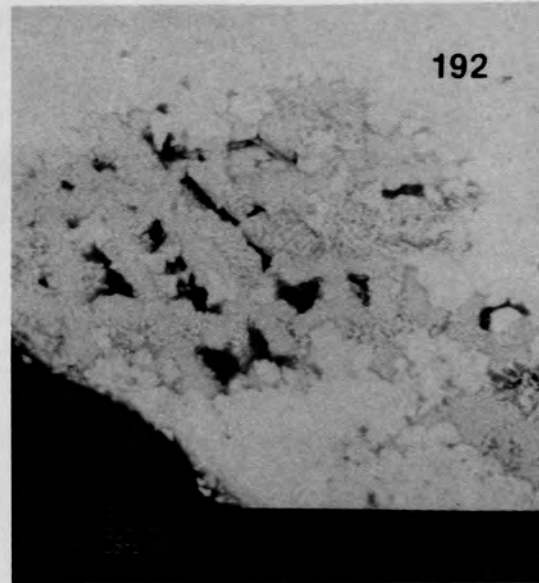
C-228



(a) Region 2/Region 3, location J



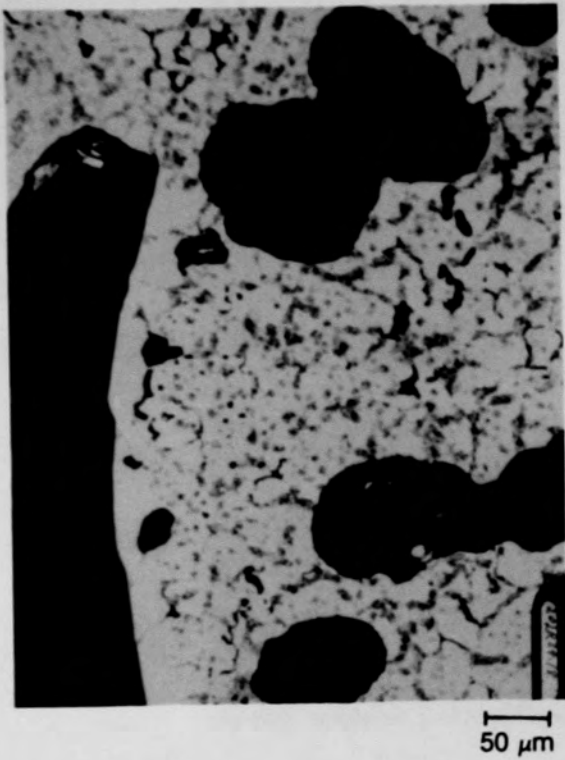
(b) Region 3, location K



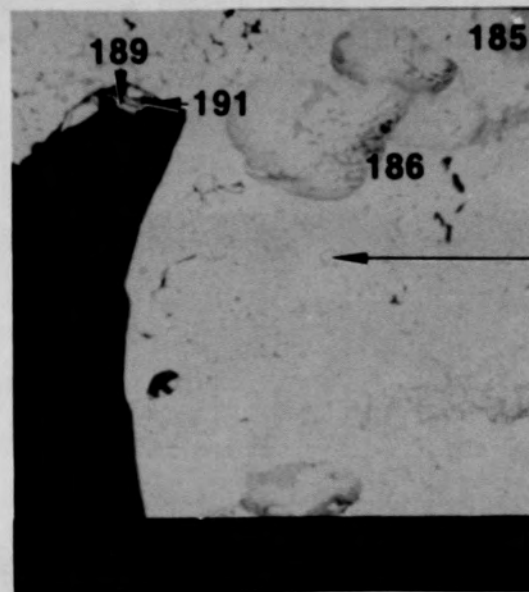
(c) Region 3, location L

Figure C-175. Photographs of material from Regions 2 and 3 of Particle 8C
(H8, 70 cm).

C-229



(a) Photomicrograph



(b) SEM backscattered electron image



(c) SEM backscattered electron image

Figure C-176. Photographs of material from Region 3, location M of Particle 8C (H8, 70 cm).

C-230

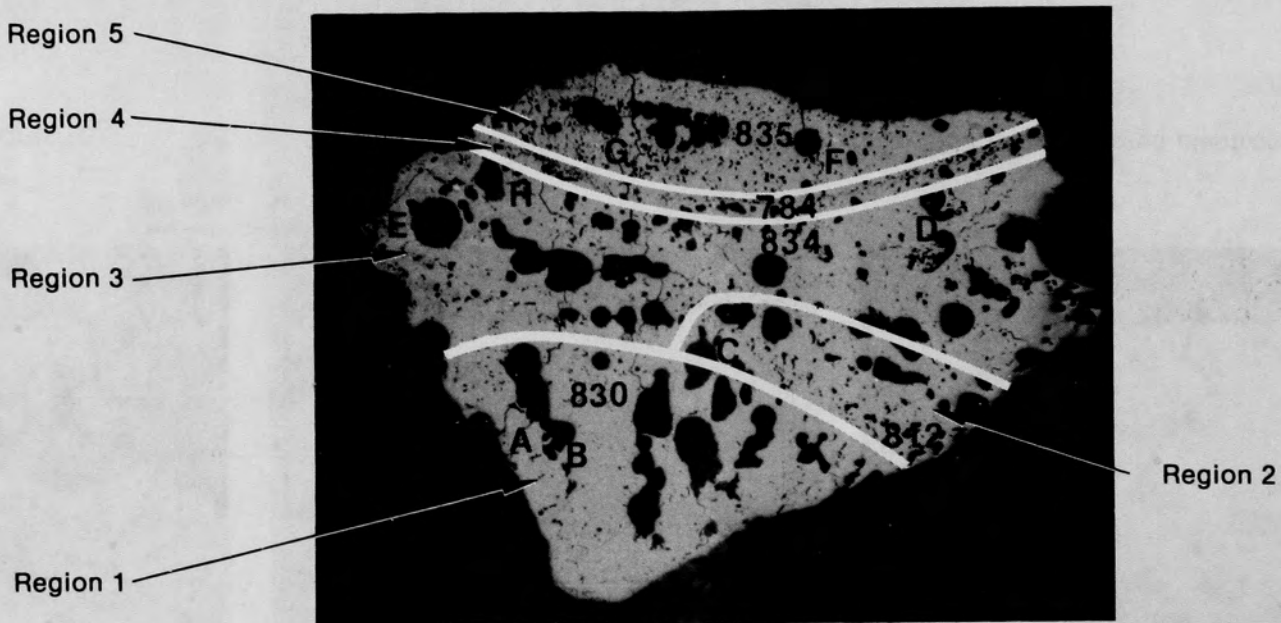
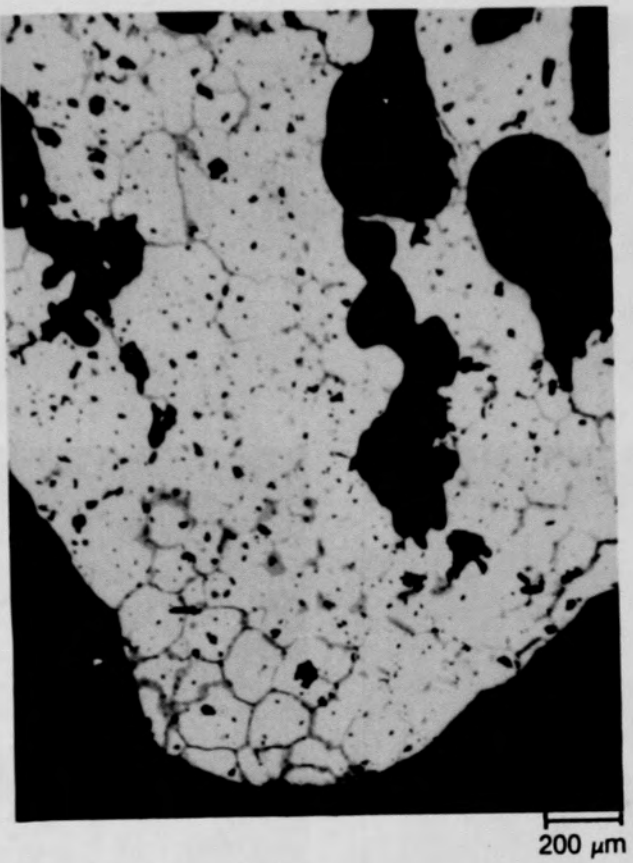
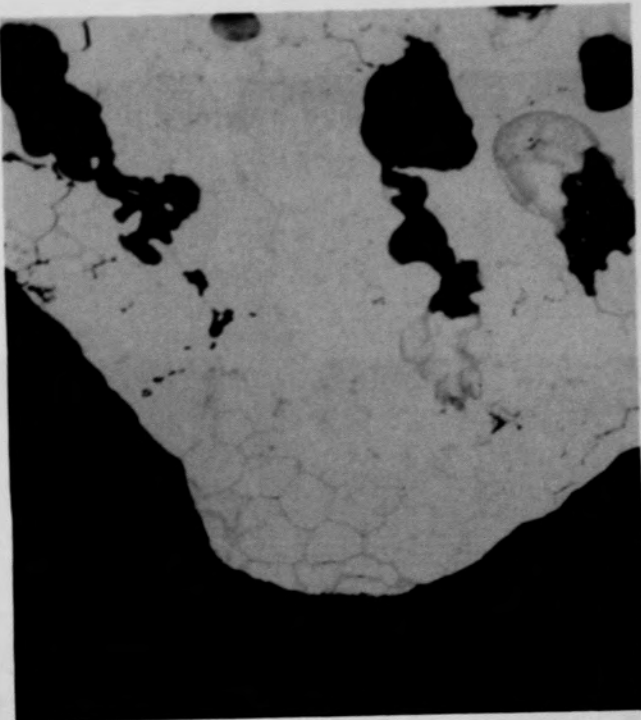


Figure C-177. Photomacrograph of Particle 8E (H8, 70 cm) showing 5 regions based on void morphology and chemical composition.

C-231



(a) Photomicrograph



(b) SEM backscattered electron image

Figure C-178. Photographs of material from Region 1 of Particle 8E (H8, 70 cm).

C-232

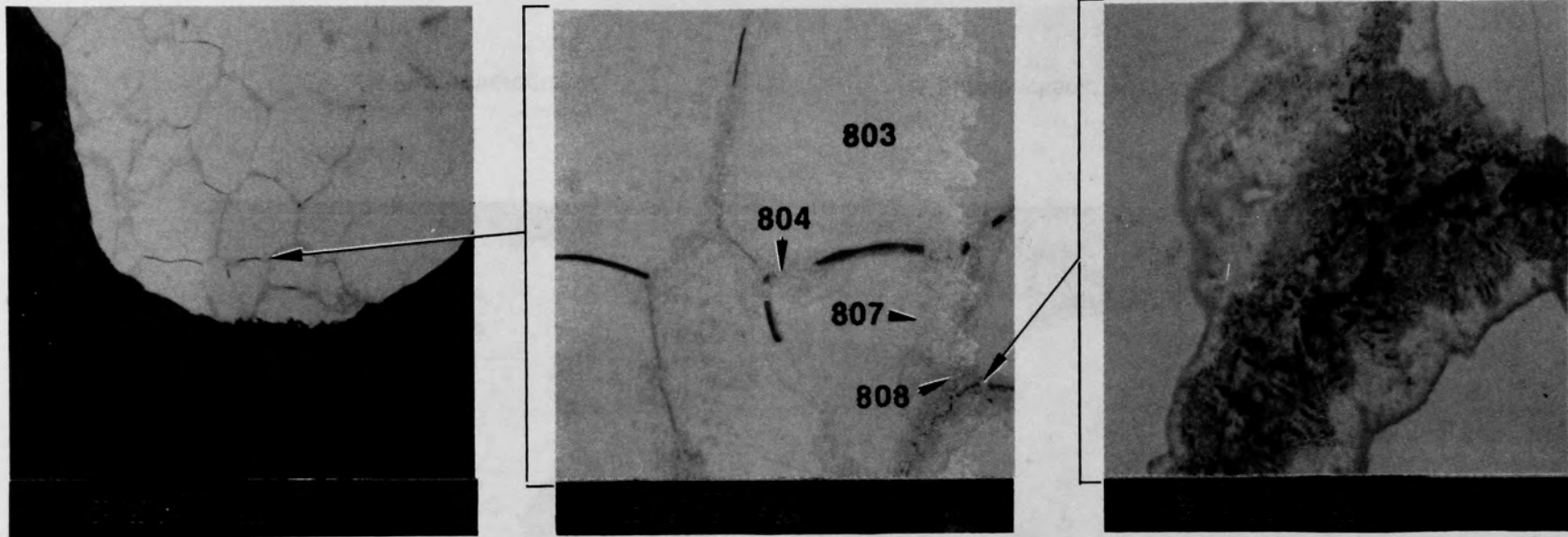
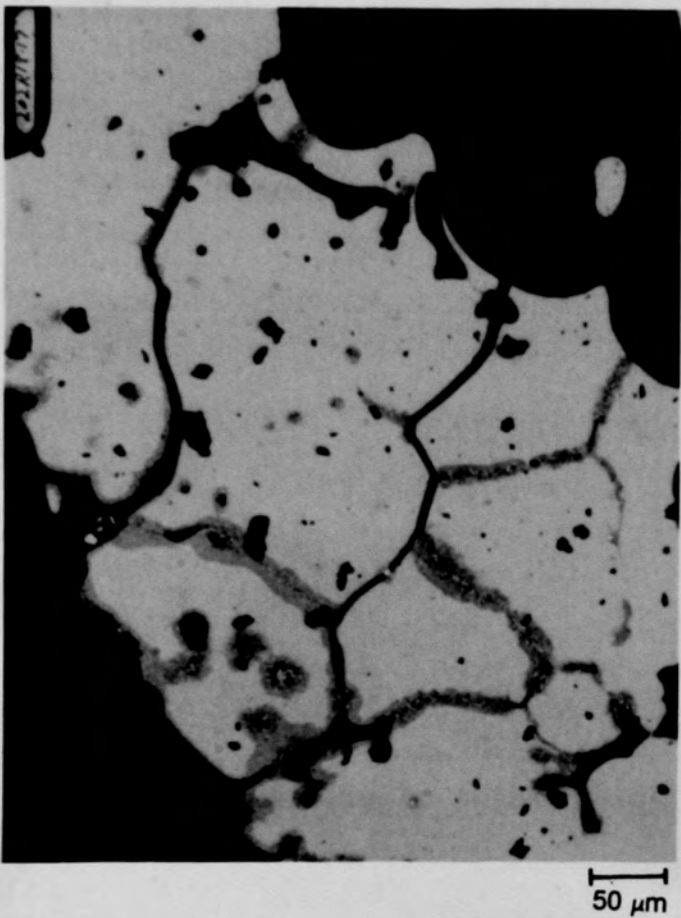
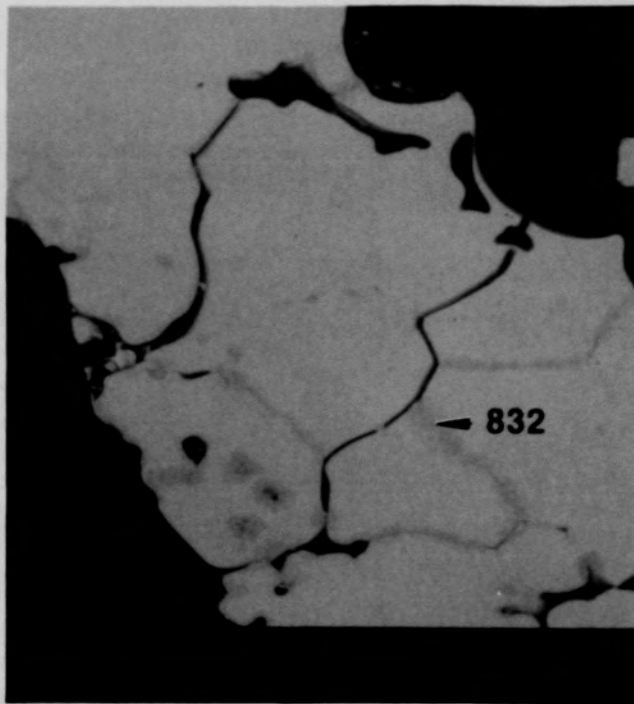


Figure C-179. SEM backscattered electron images of Region 1 of Particle 8E
(H8, 70 cm).

C-233



(a) Photomicrograph



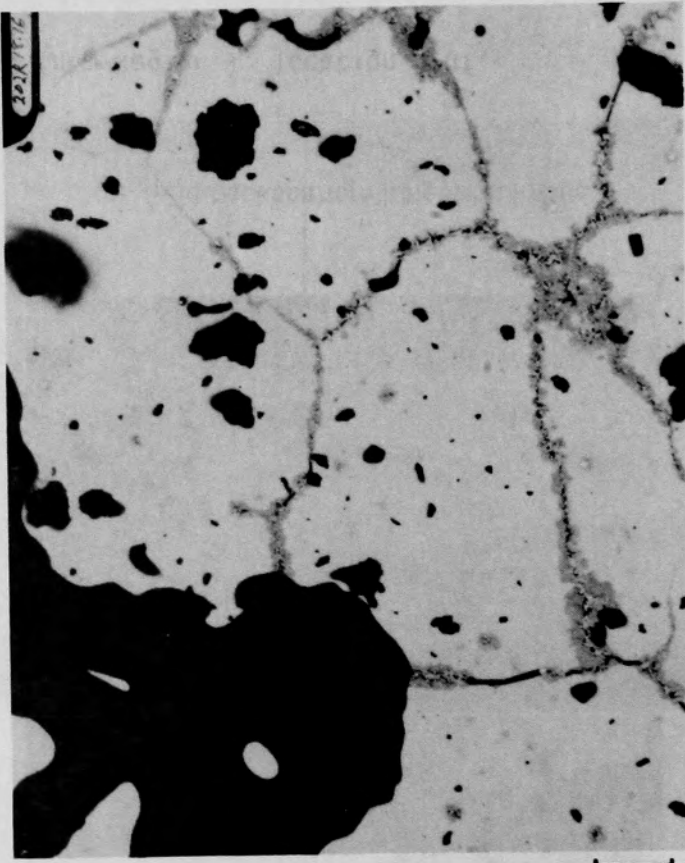
(b) SEM backscattered electron image

Figure C-180. Photographs of material from Region 1, location A of Particle 8E (H8, 70 cm).

C-234



(a) Unetched



(b) Etched

Figure C-181. Photomicrographs of material from Region 1, location B of Particle 8E (H8, 70 cm).

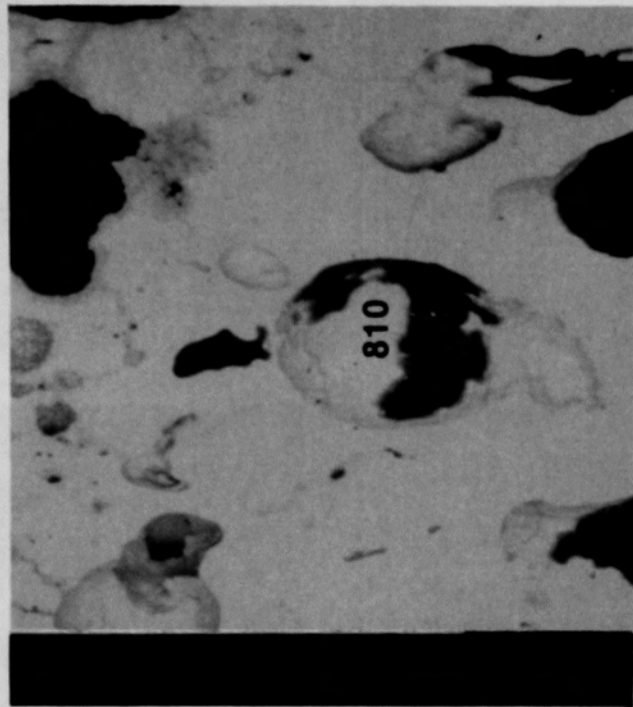


Figure C-182. SEM backscattered electron image of Region 1, location C of Particle 8E (H8, 70 cm).

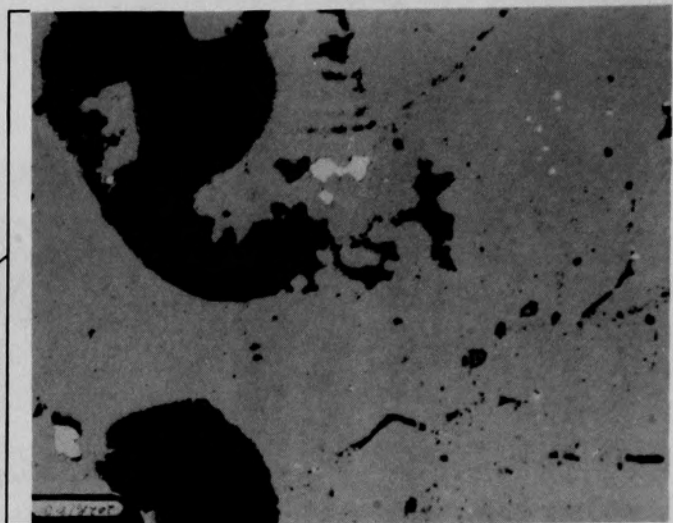
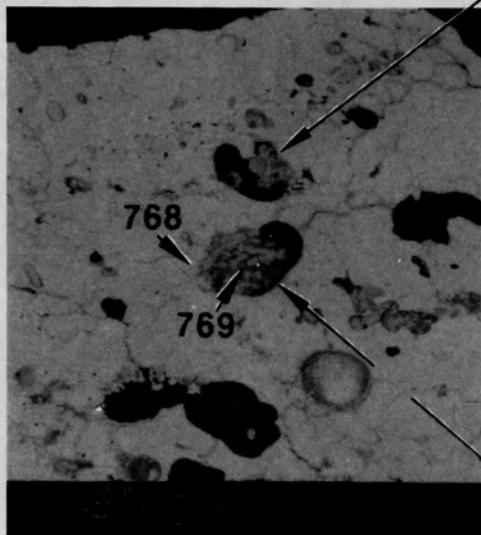


Figure C-183. Photographs of material from Region 3, location D of Particle 8E (H8, 70 cm).

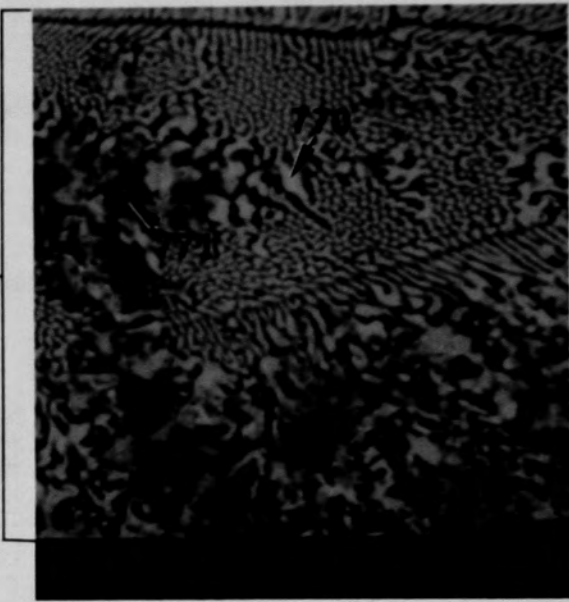
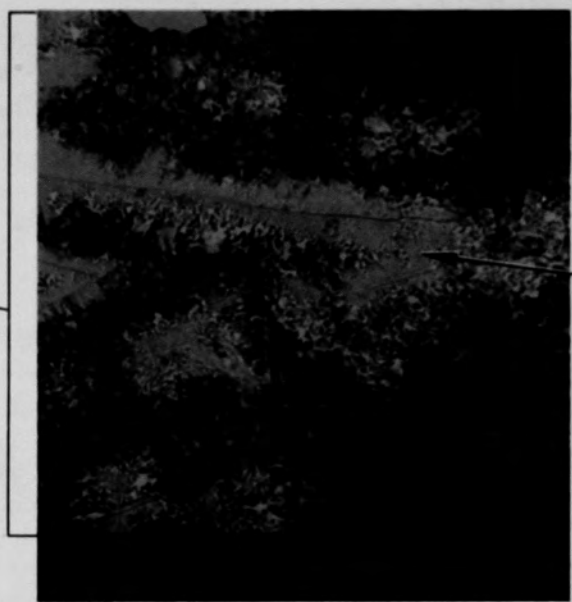
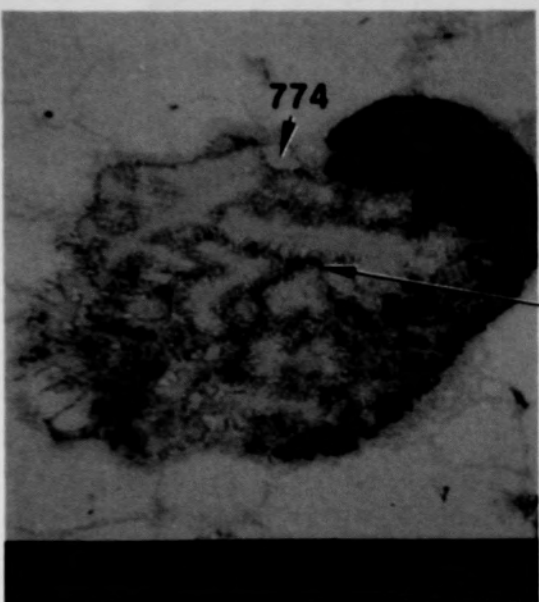


Figure C-184. SEM backscattered electron images of material from Region 3
location D of Particle 8E (H8, 70 cm).

C-238

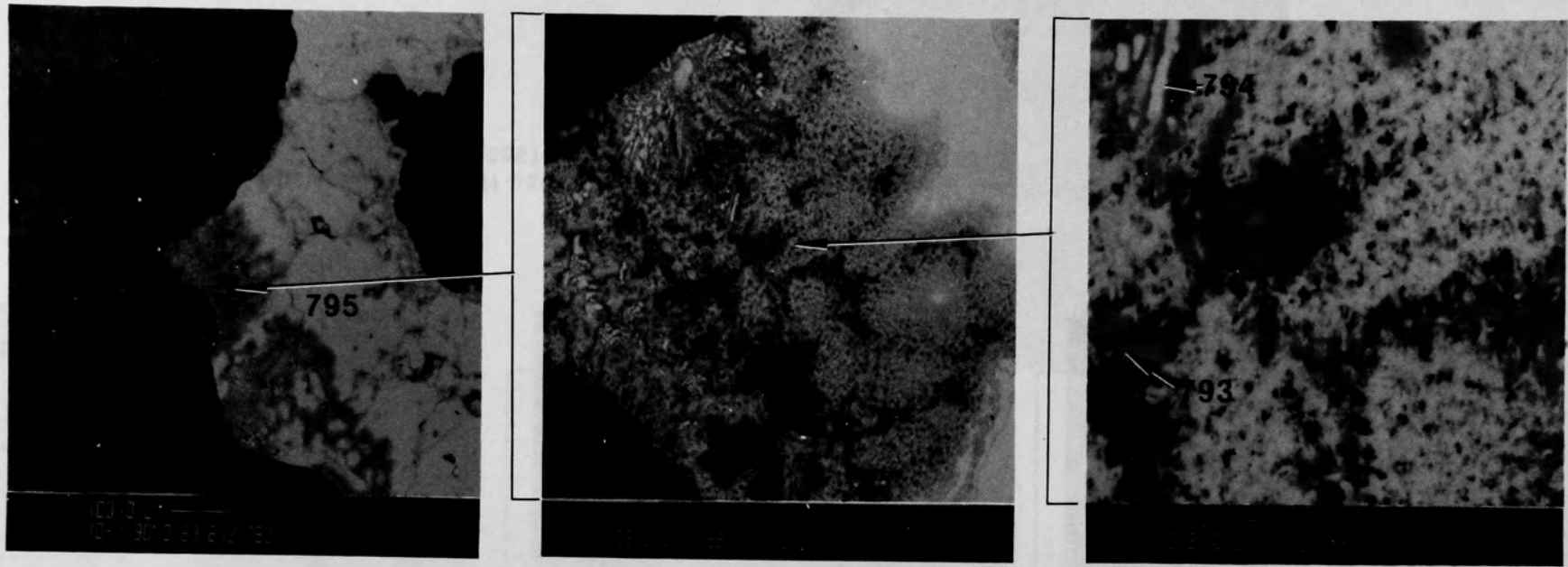
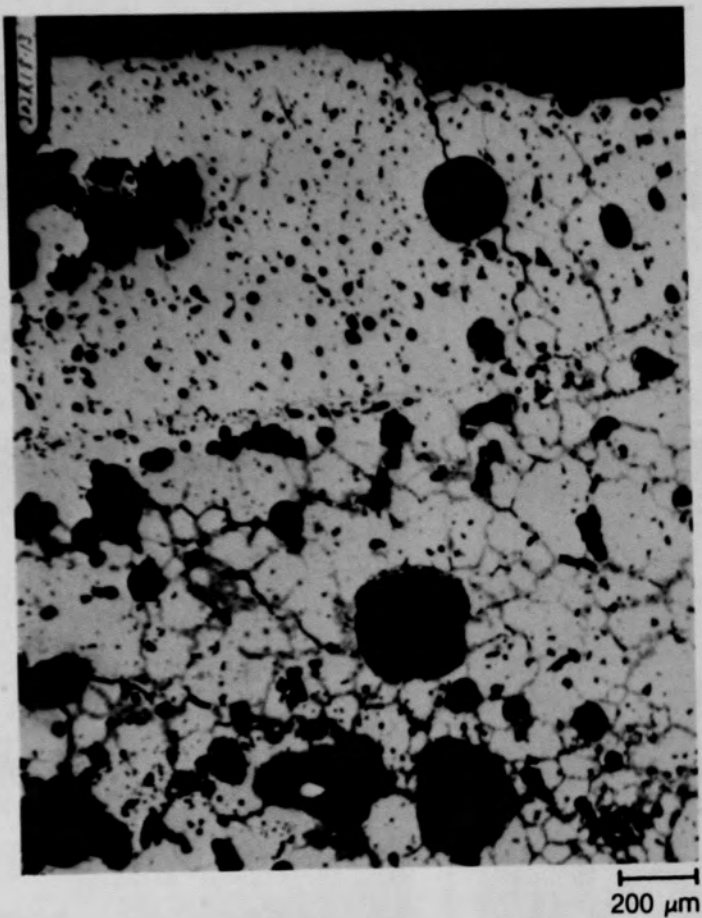
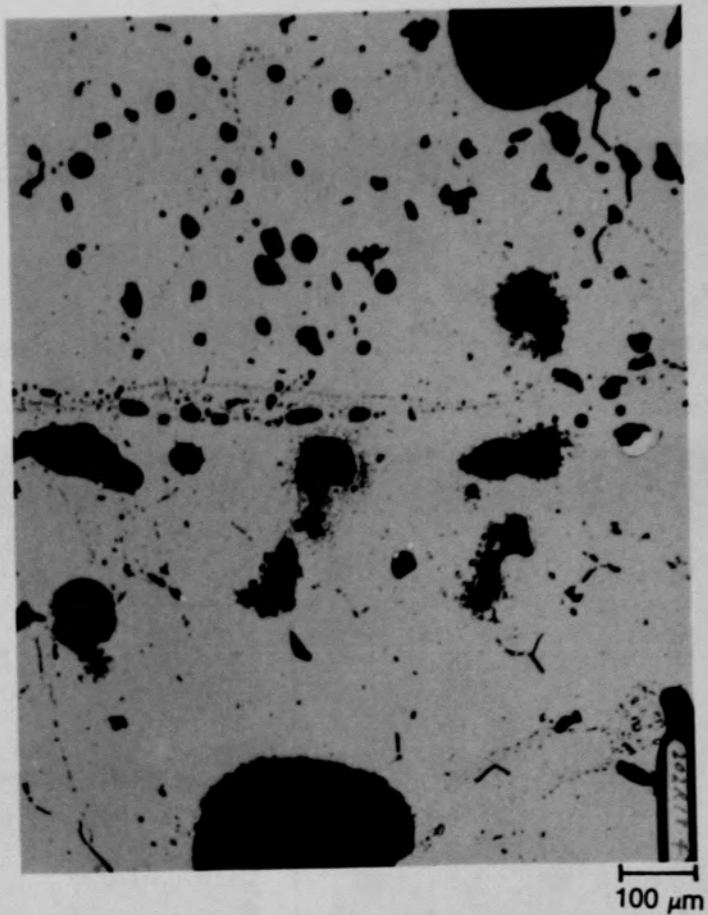


Figure C-185. SEM backscattered electron images of material from Region 3,
location E of Particle 8E (H8, 70 cm).

C-239



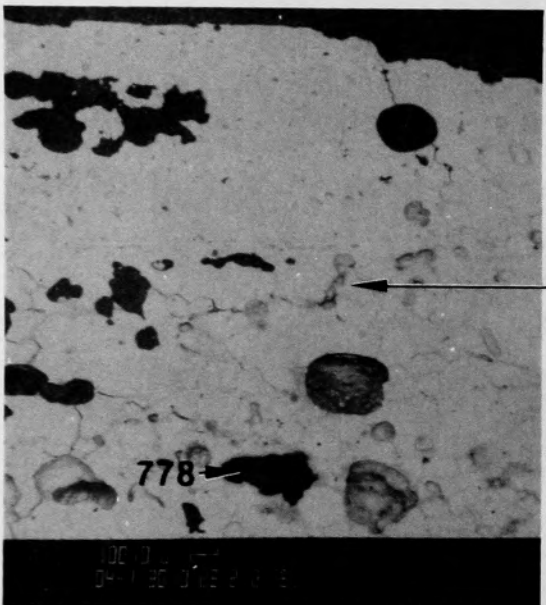
(a) Includes Regions 2 through 5



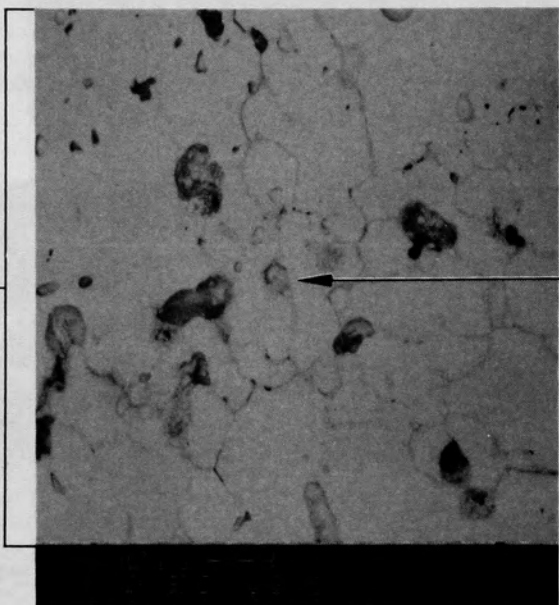
(b) Includes Regions 3 through 5

Figure C-186. Photomicrographs of region interfaces from location F of Particle 8E (H8, 70 cm).

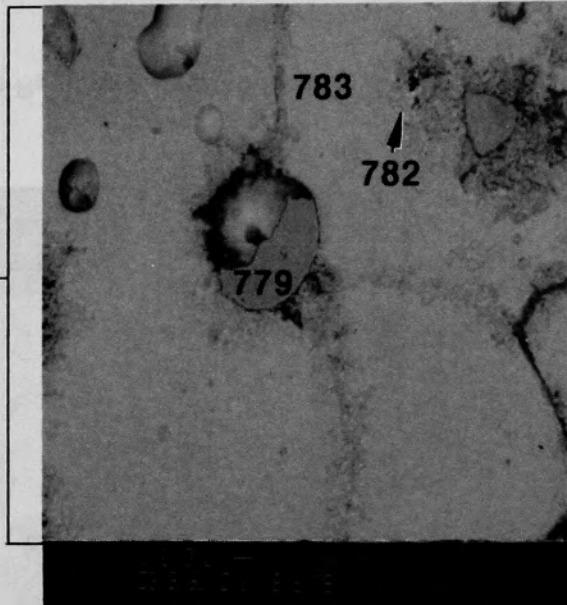
C-240



(a) Includes Regions 2 through 5



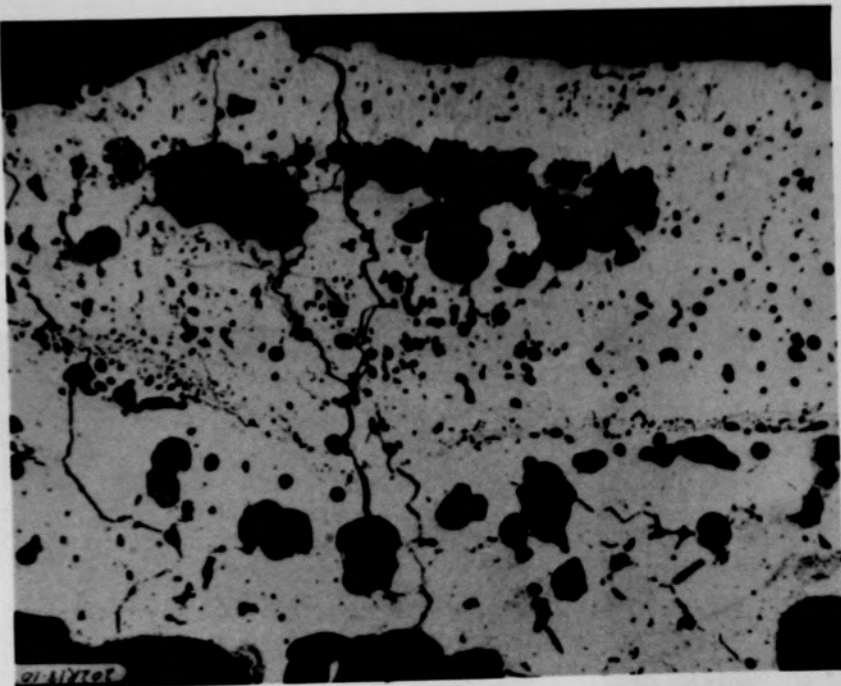
(b) Includes Regions 3 and 4



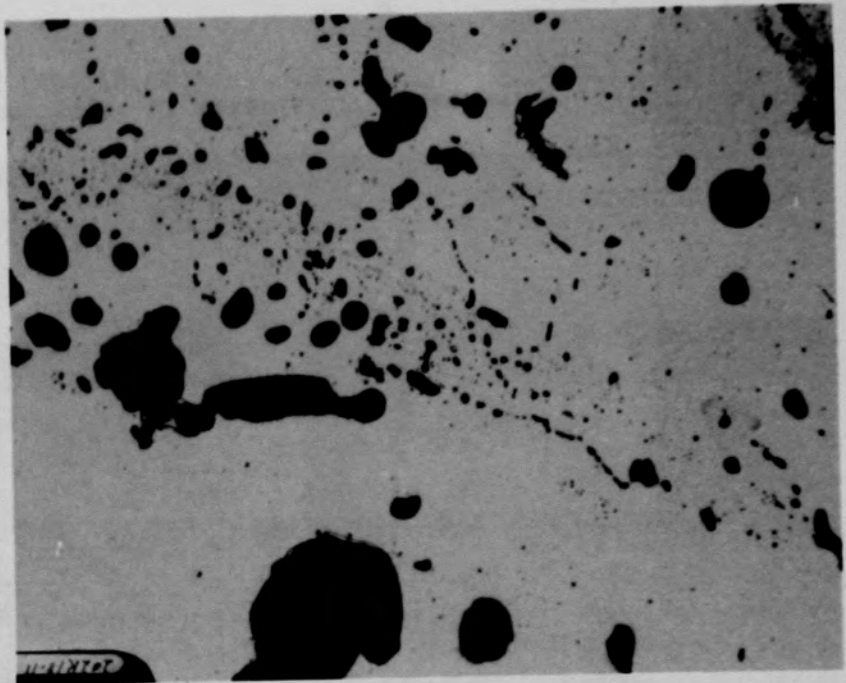
(c) Region 4 inclusion

Figure C-187. SEM backscattered electron images of location F region interfaces of Particle 8E (H8, 70 cm).

C-241



(a) Region 3 through 5



(b) Regions 3 through 5

Figure C-188. Photomicrograph of material from location G of Particle 8E
(H8, 70 cm).

C-242

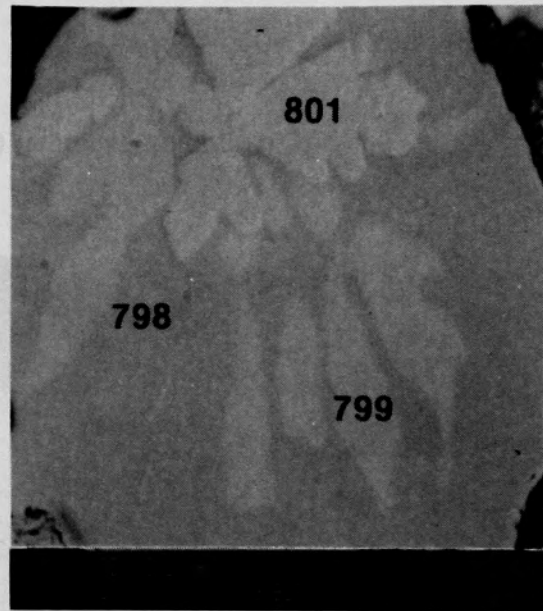
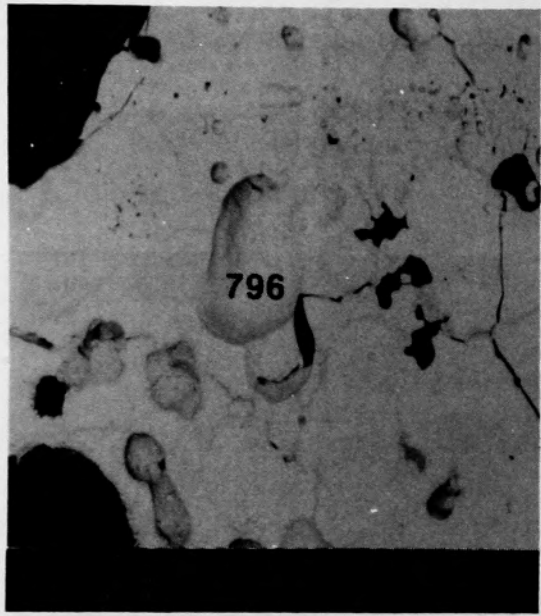


Figure C-189. SEM backscattered electron images of material from Region 3,
location H of Particle 8E (H8, 70 cm).

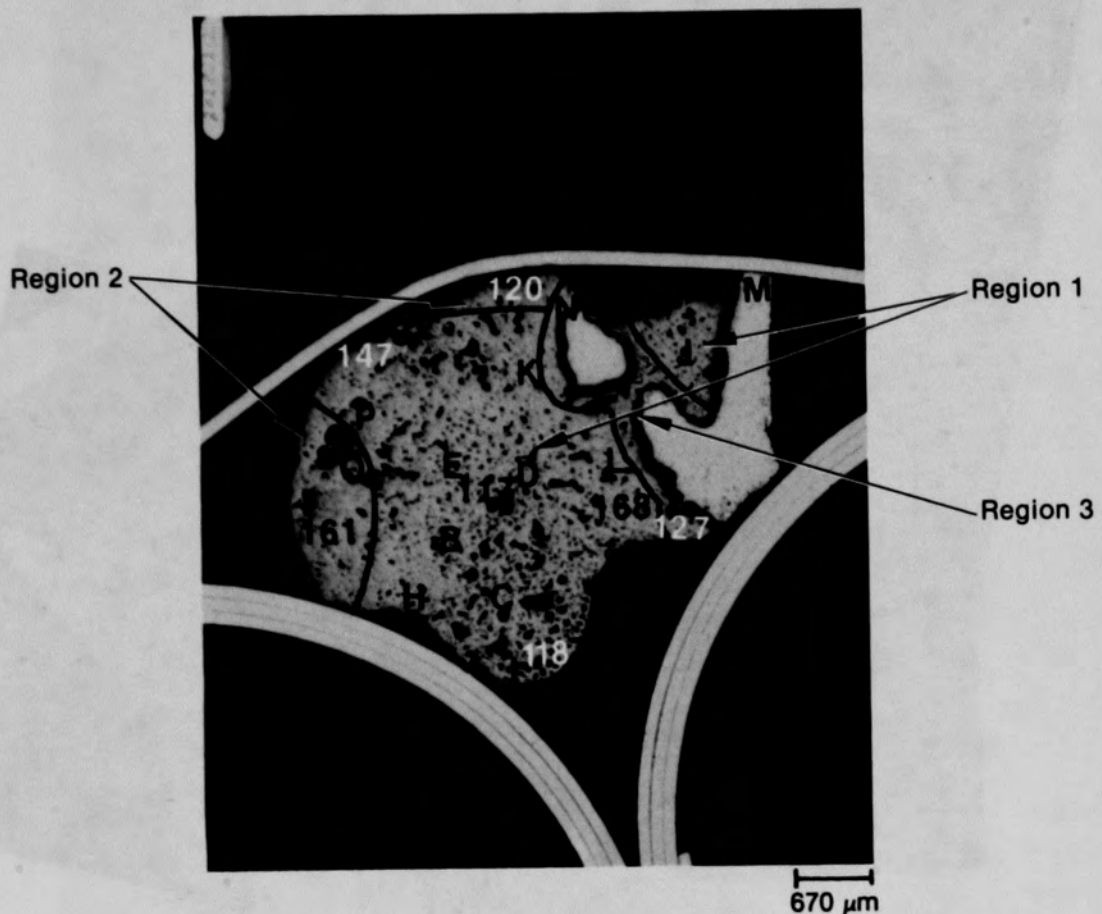


Figure C-190. Photomacrograph of Particle 8H (H8, 70 cm) showing three regions based on Zr,U ratios.

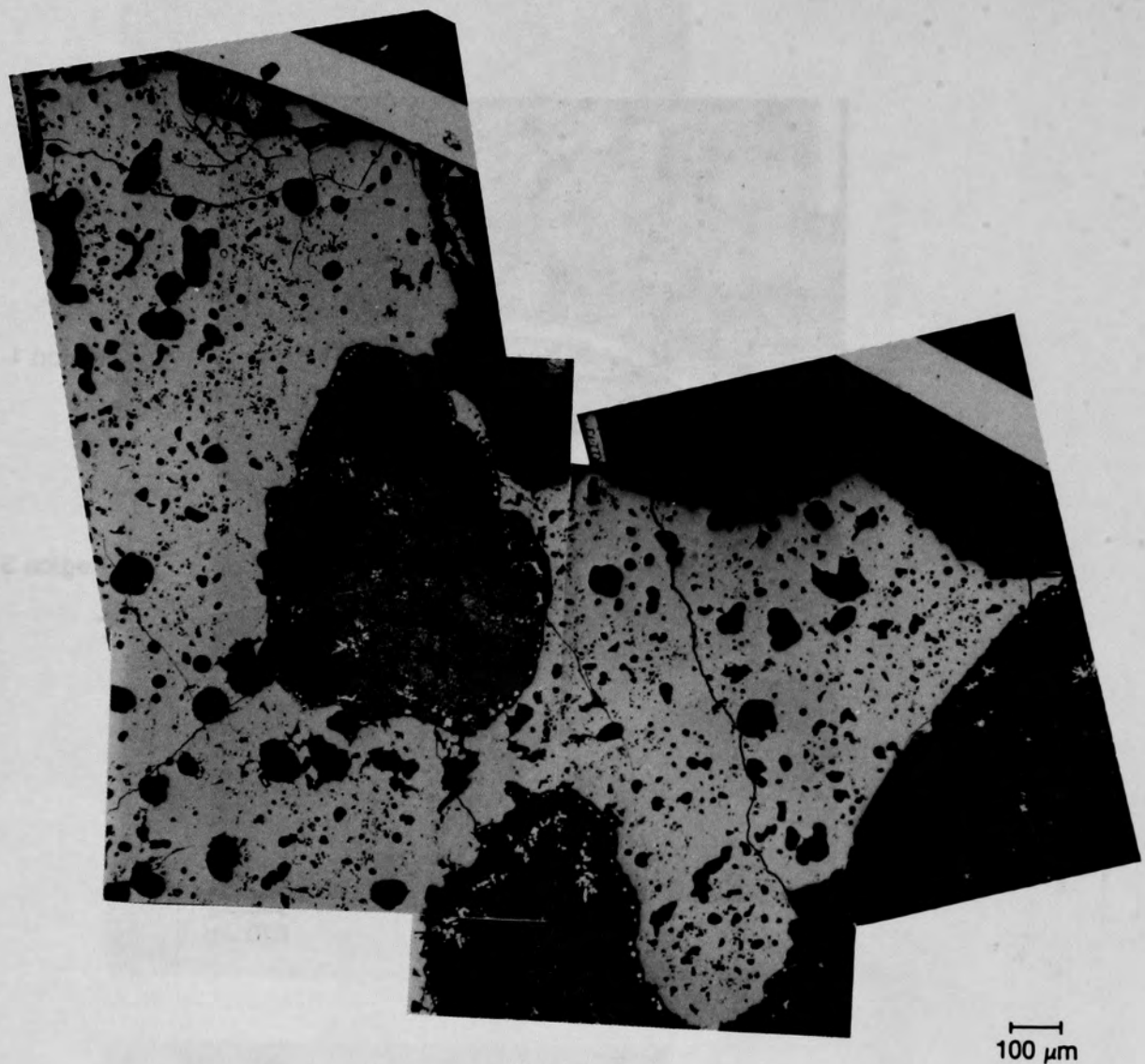
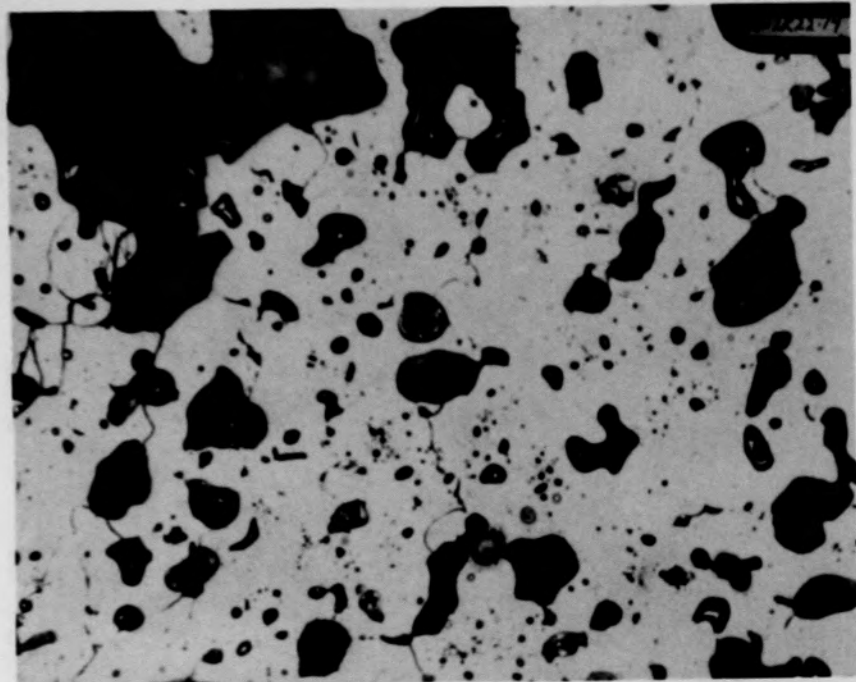
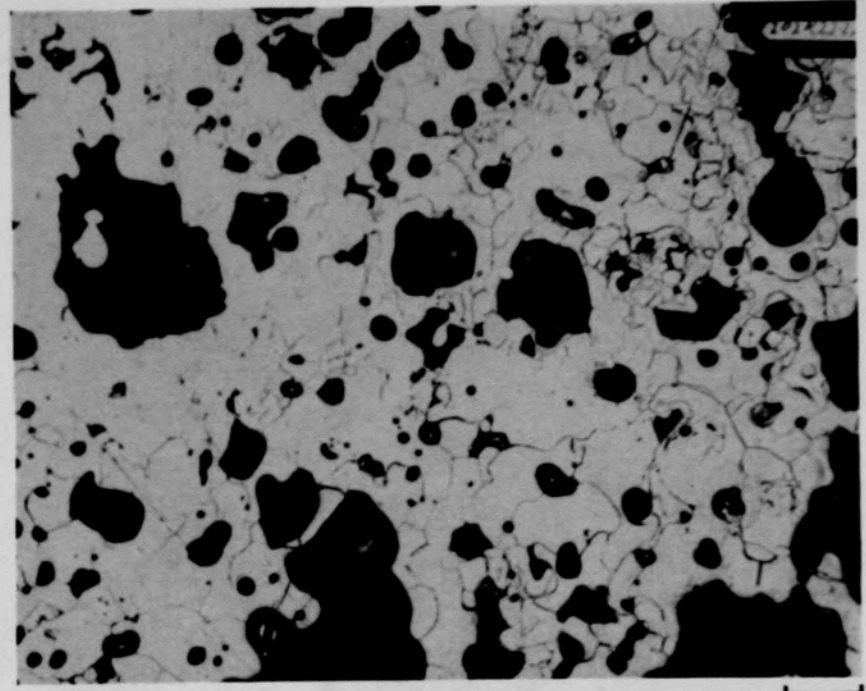


Figure C-191. Photomicrographs of galvanic etch in polisher of Particle 8H (H8, 70 cm).

C-245



(a) Location B, fuel etch

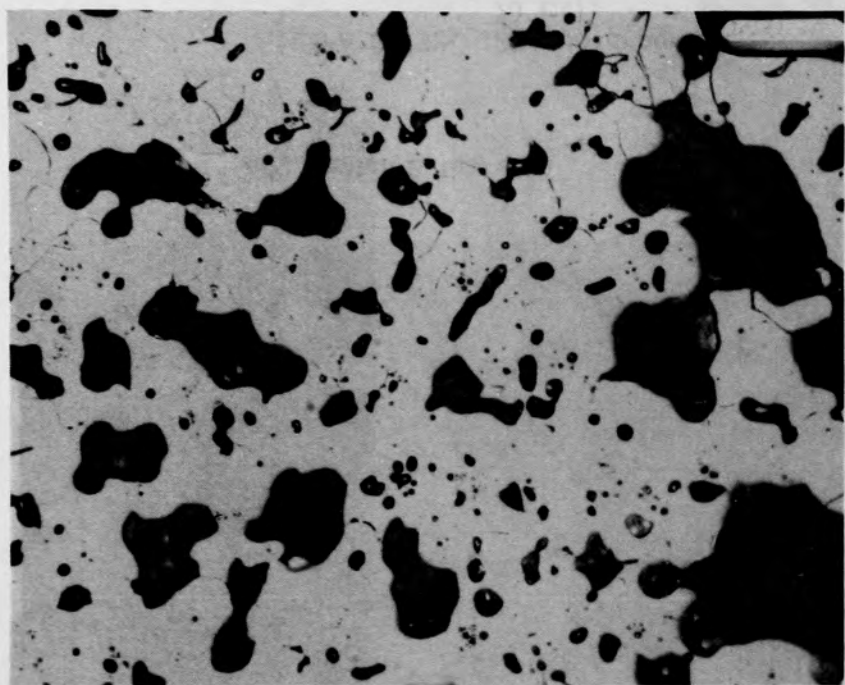


(b) Location C, cladding etch

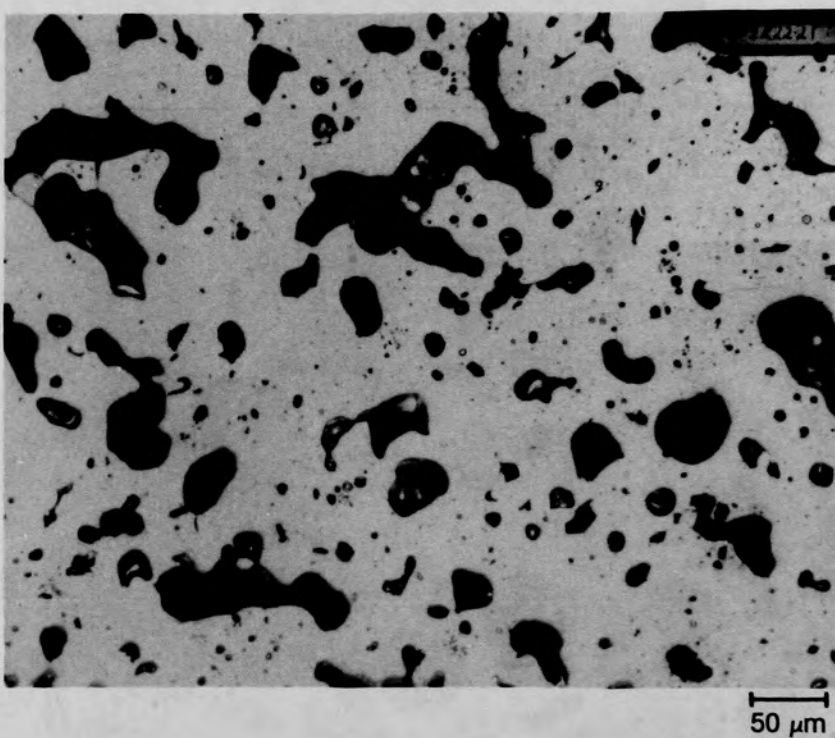
50 μm

Figure C-192. Photomicrographs of material in Region 1 of Particle 8H (H8,
70 cm).

C-246



(a) Cladding etch



(b) Fuel etch

Figure C-193. Photomicrographs of material from Region 1, location E of Particle 8H (H8, 70 cm).

C-247

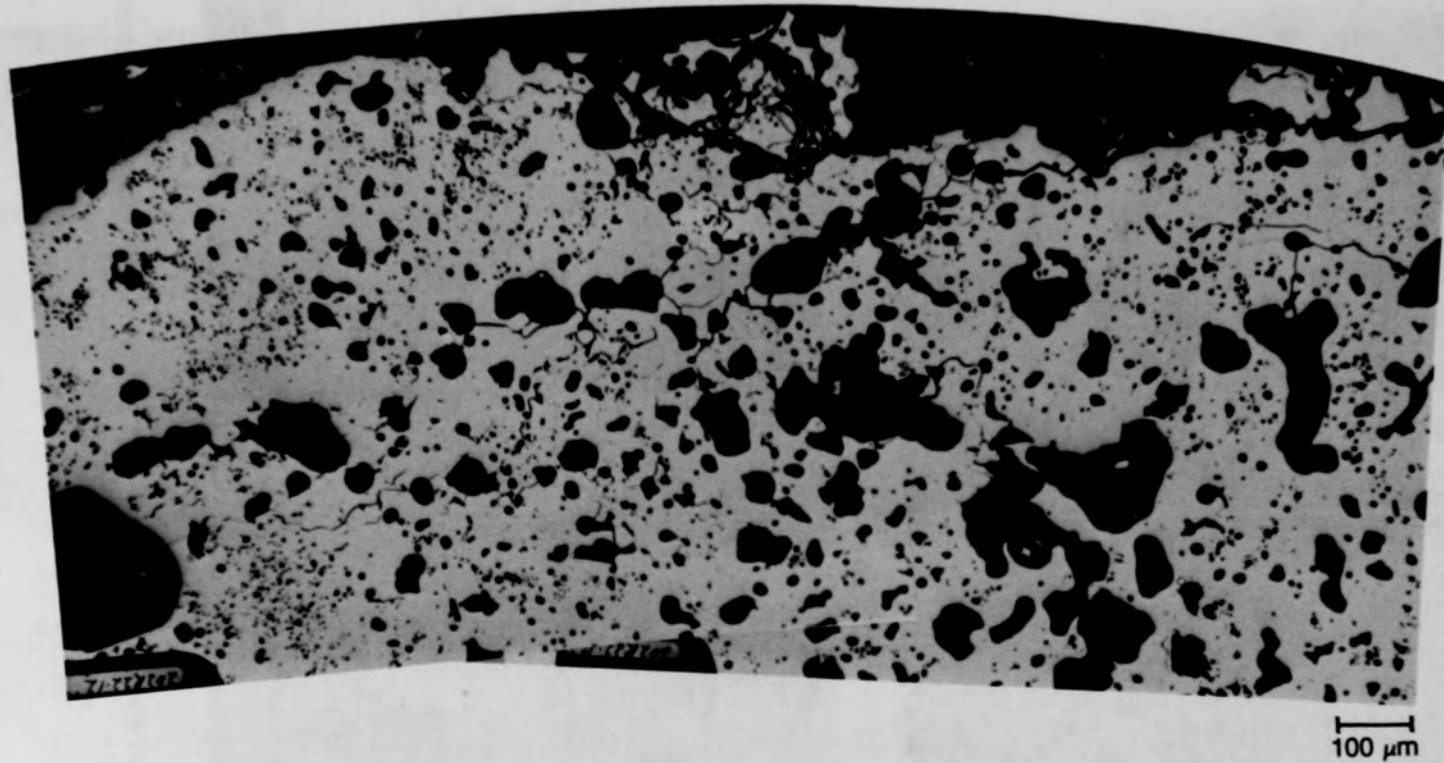
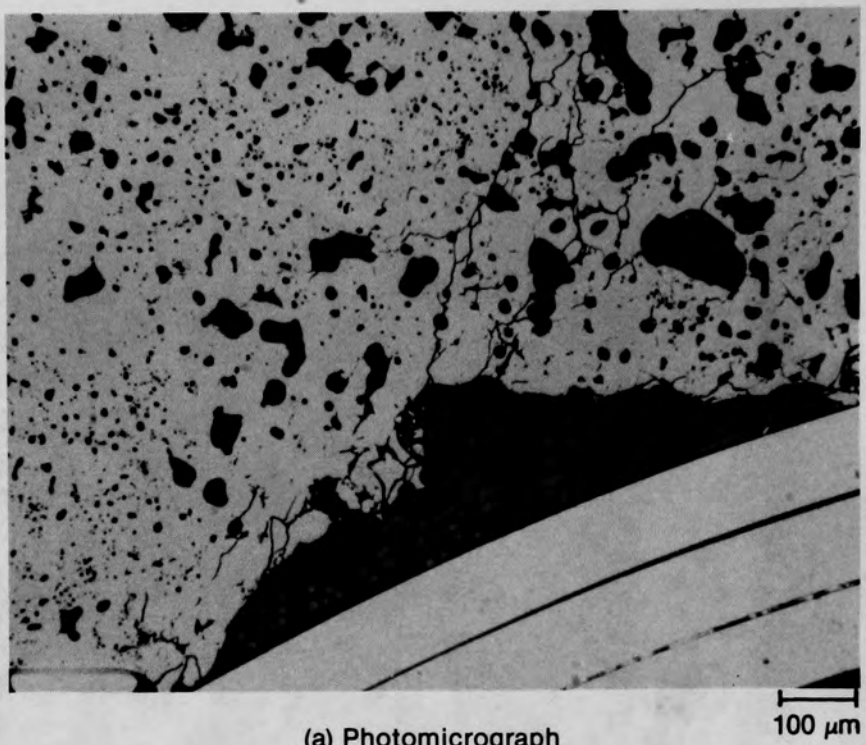


Figure C-194. Photomicrographs of material from Region 1, location G of Particle 8H (H8, 70 cm).

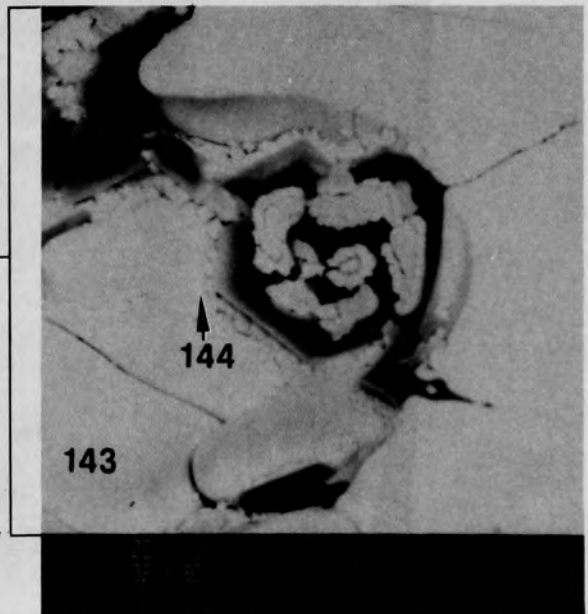


(a) Photomicrograph

100 μm



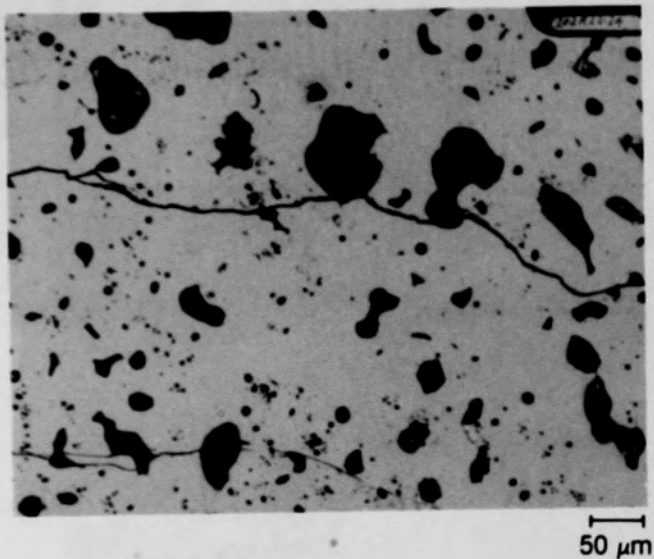
(b) SEM backscattered electron image



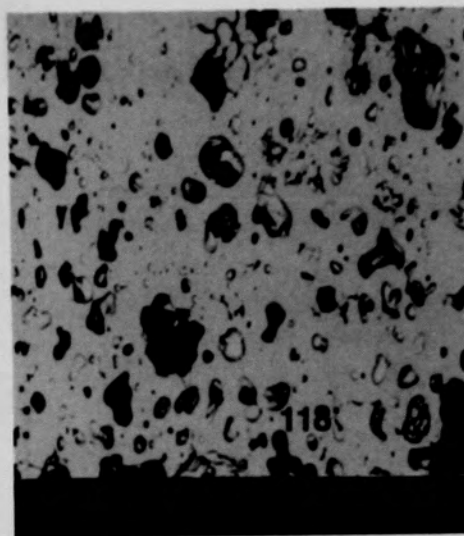
(c) SEM backscattered electron image

Figure C-195. Photographs of material from Region 1, location H of Particle 8H (H8, 70 cm).

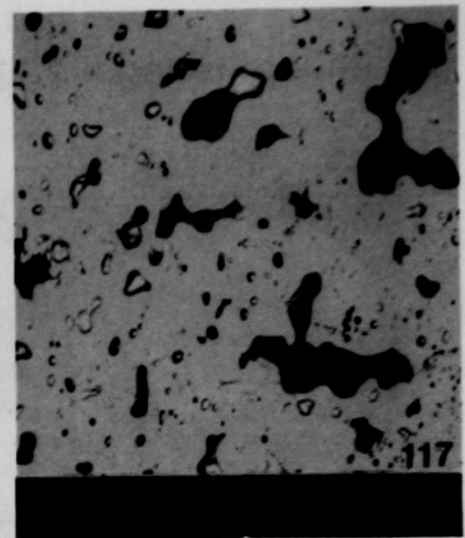
C-249



(a) Location J



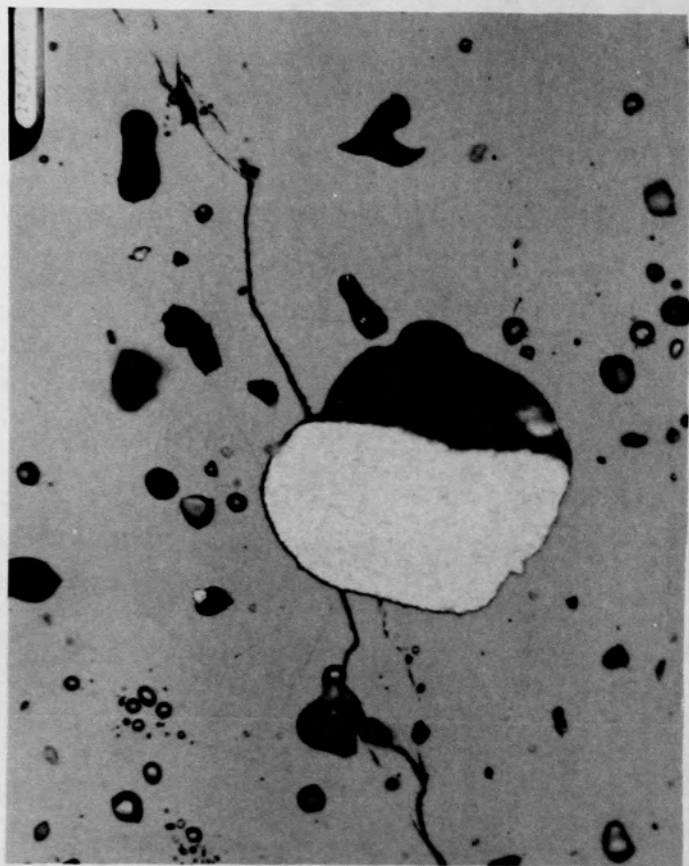
(b) Location I



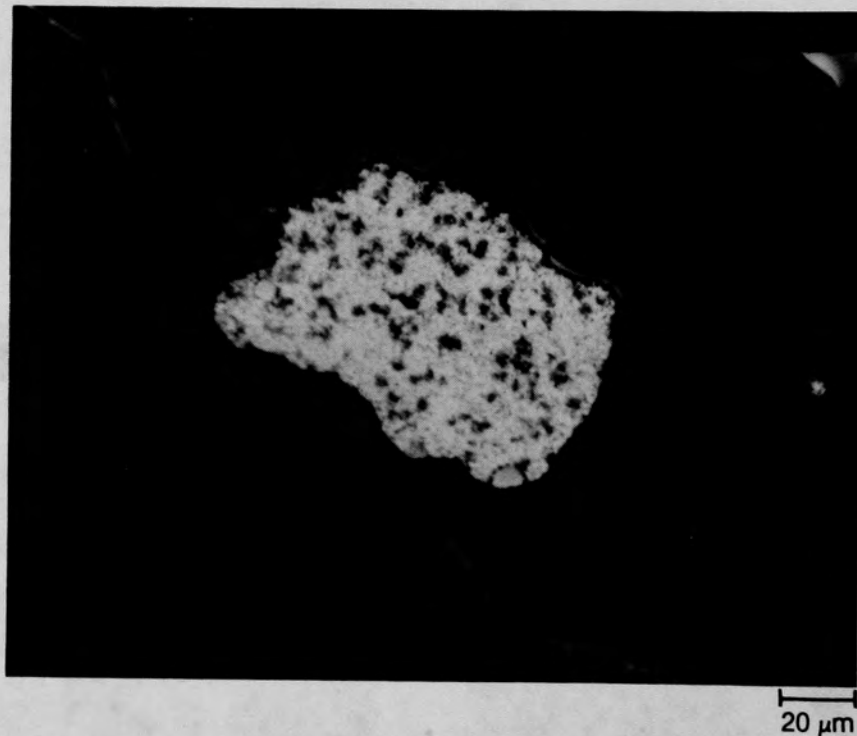
(c) Location D

Figure C-196. Photographs of material from Region 1 of Particle 8H (H8, 70 cm).

C-250



(a) Unetched



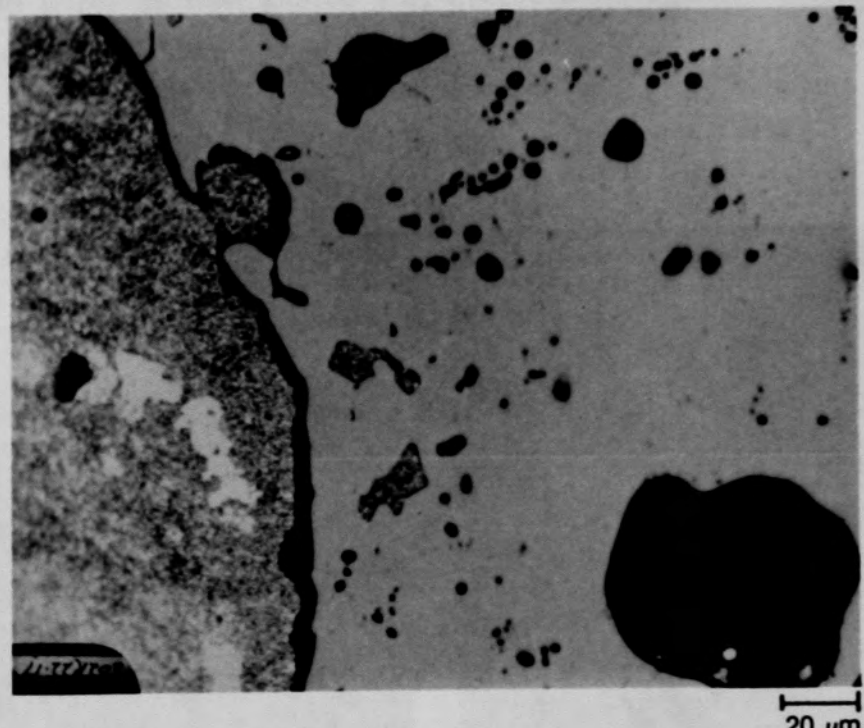
(b) Oxalic etch

Figure C-197. Photomicrographs of material from Region 1, location K of Particle 8H (H8, 70 cm).

C-251



(a) Unetched



(b) Ag etch

Figure C-198. Photomicrographs of Region 3 of Particle 8H (H8, 70 cm)
showing Ag melt interface.

C-252

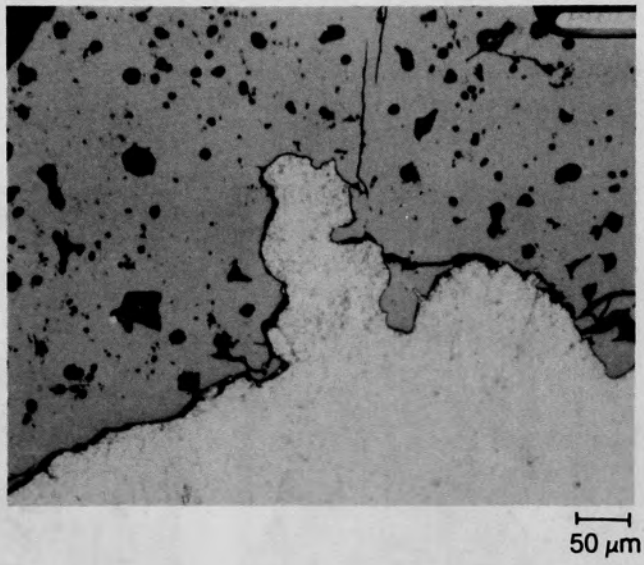
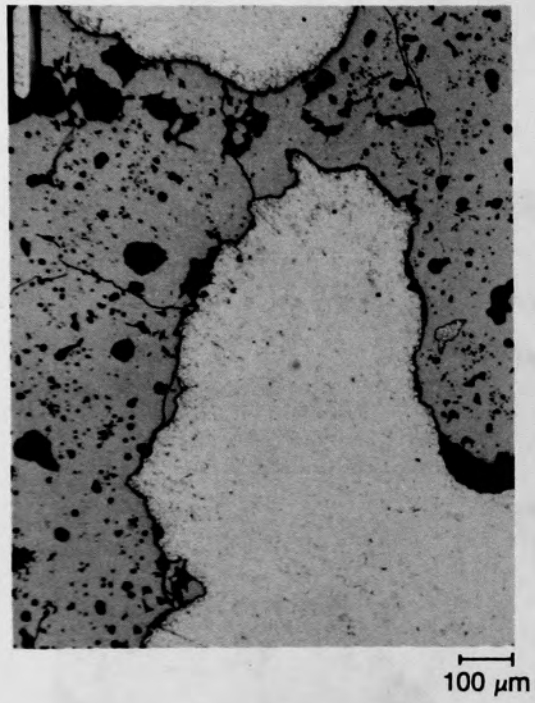


Figure C-199. Photomicrographs of material from Region 3 of Particle 8H
(H8, 70 cm) showing Ag melt interface.

C-253

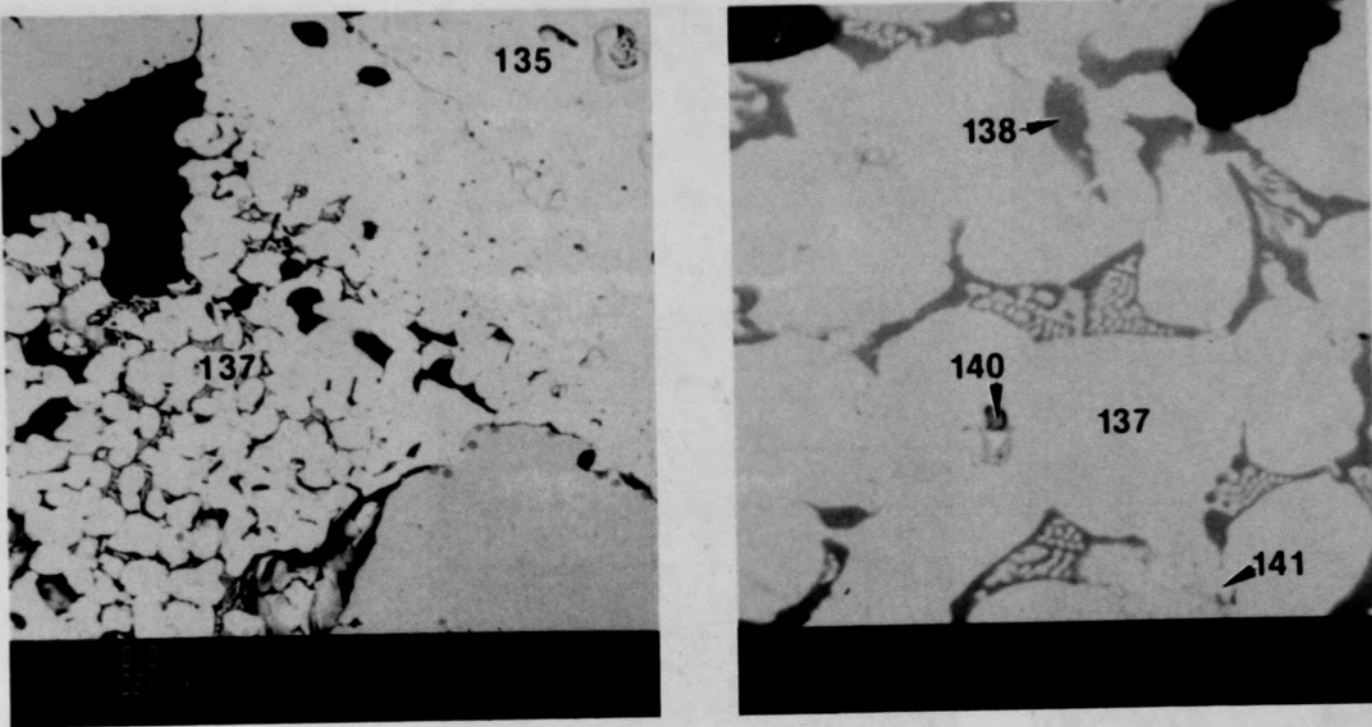
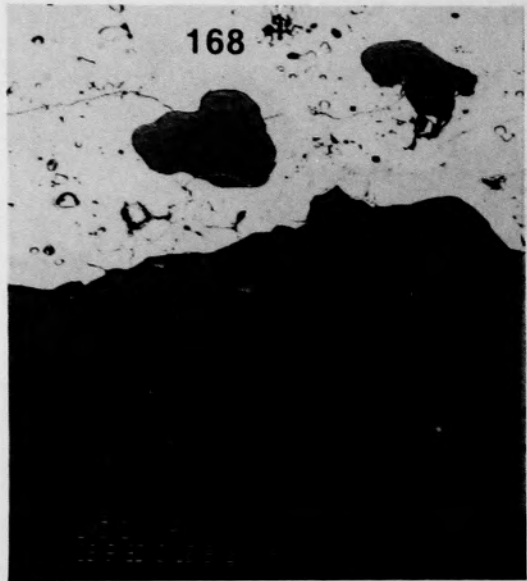


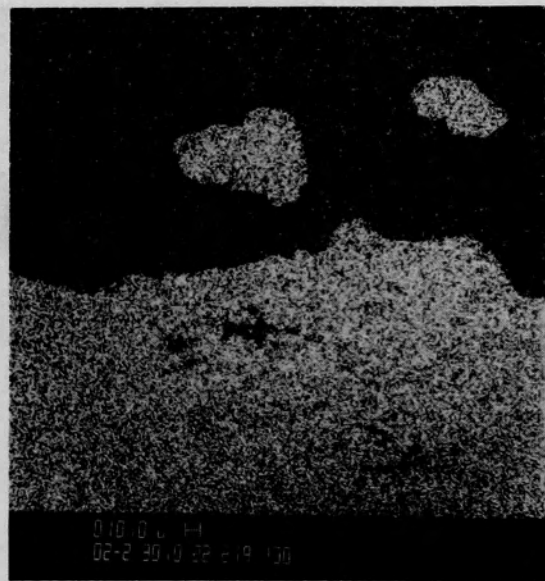
Figure C-200. SEM backscattered electron images of material from Region 3 of Particle 8H (H8, 70 cm).



(a) SEM backscattered electron image



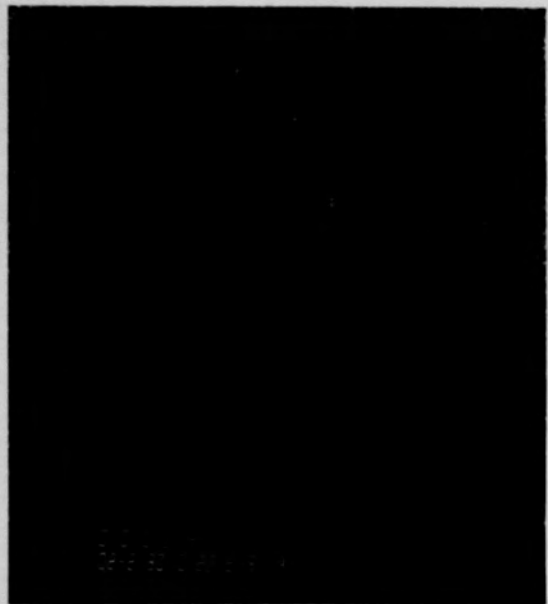
(b) X-ray dot map of Ni



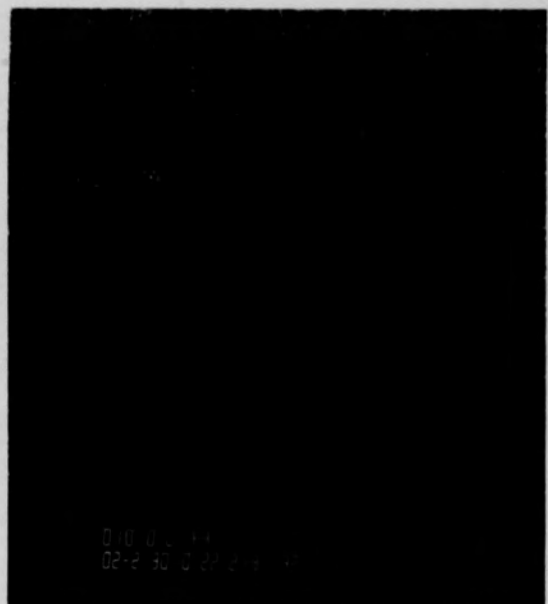
(c) X-ray dot map of Ag

Figure C-201. Photographs of material from Region 1, Region 3 and Ag interface of Particle 8H (H8, 70 cm).

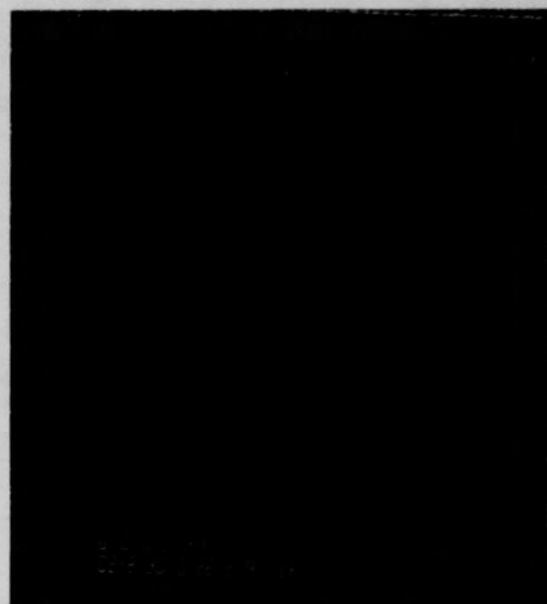
C-255



(a) Zr



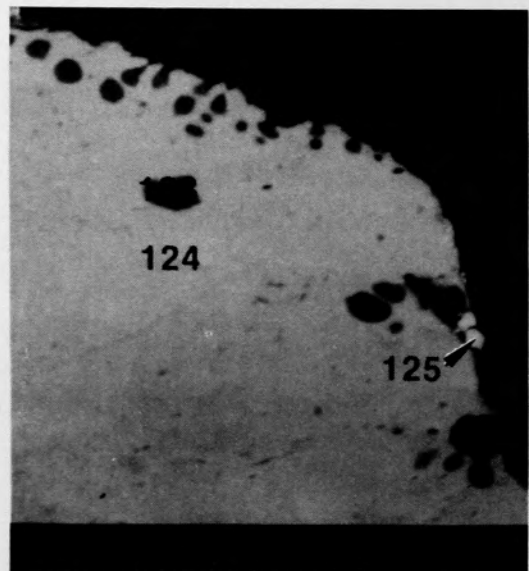
(b) U



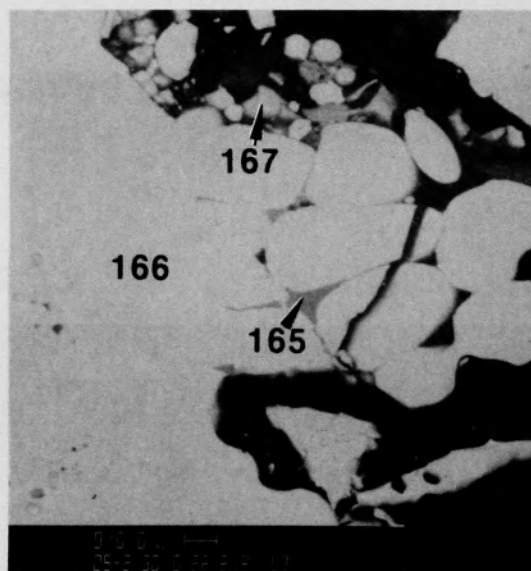
(c) Sn

Figure C-202. X-ray dot maps of Figure C-201a of Particle 8H (H8, 70 cm).

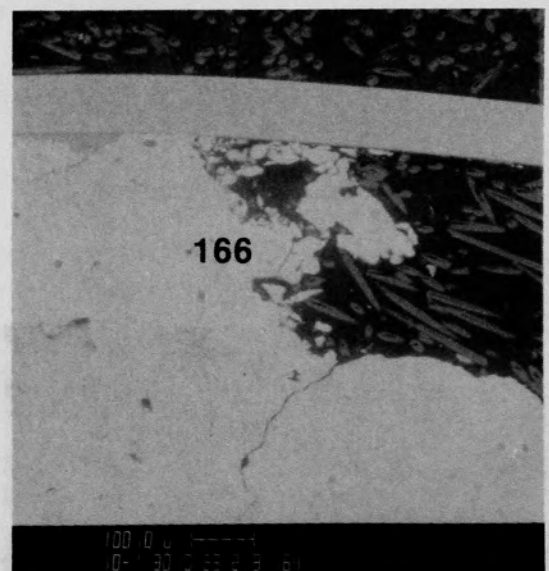
C-256



(a) Location M

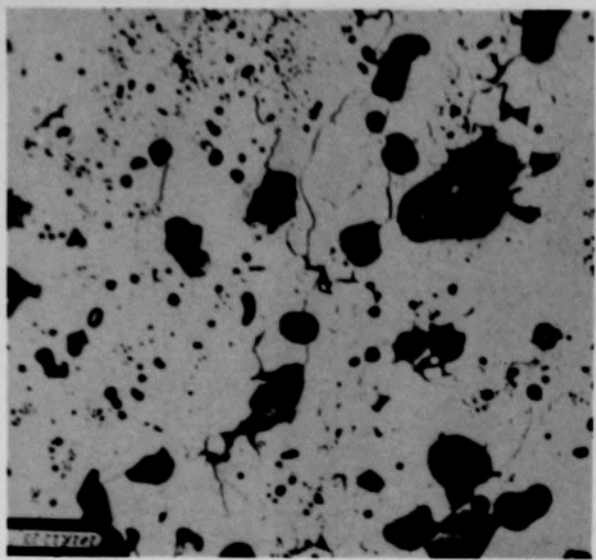


(b) Region 3, location N

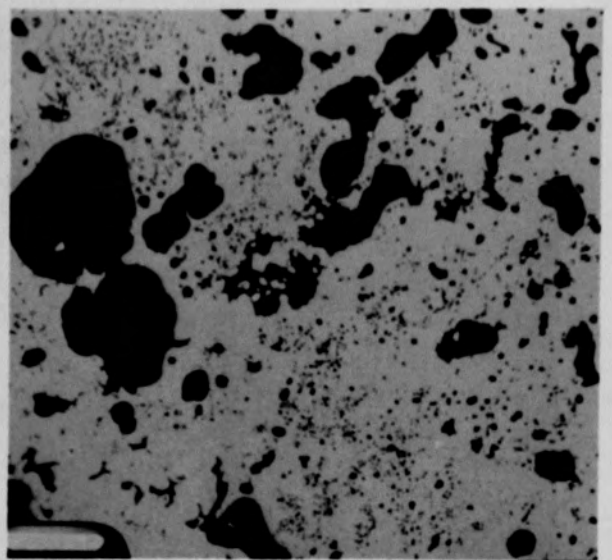


(c) Region 3, location N

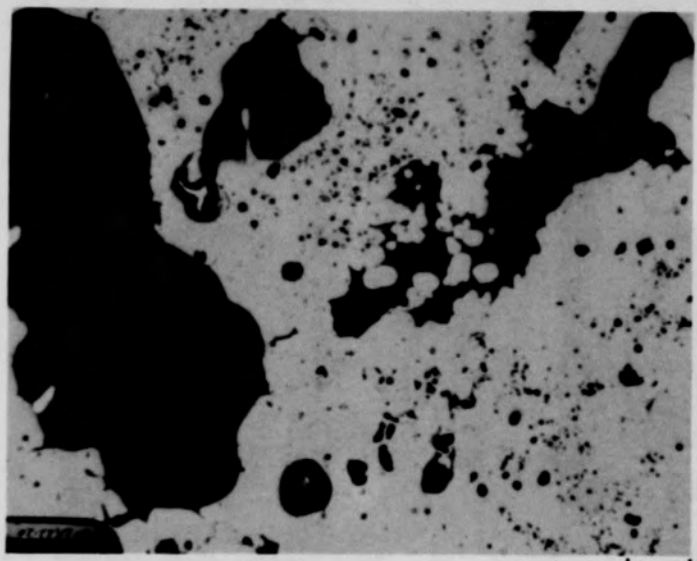
Figure C-203. SEM backscattered electron images of Particle 8H (H8, 70 cm).



(a) Location P, cladding etch



(b) Location O, unetched



(c) Location O, fuel etch

Figure C-204. Photomicrographs of material from Region 1, Region 2 interface of Particle 8H (H8, 70 cm).

C-258

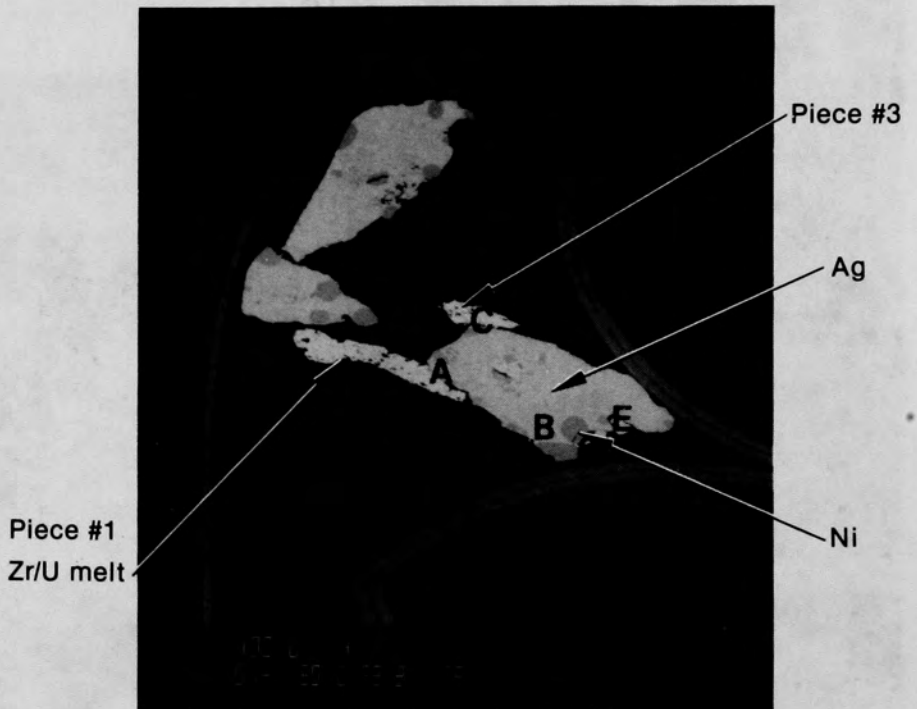
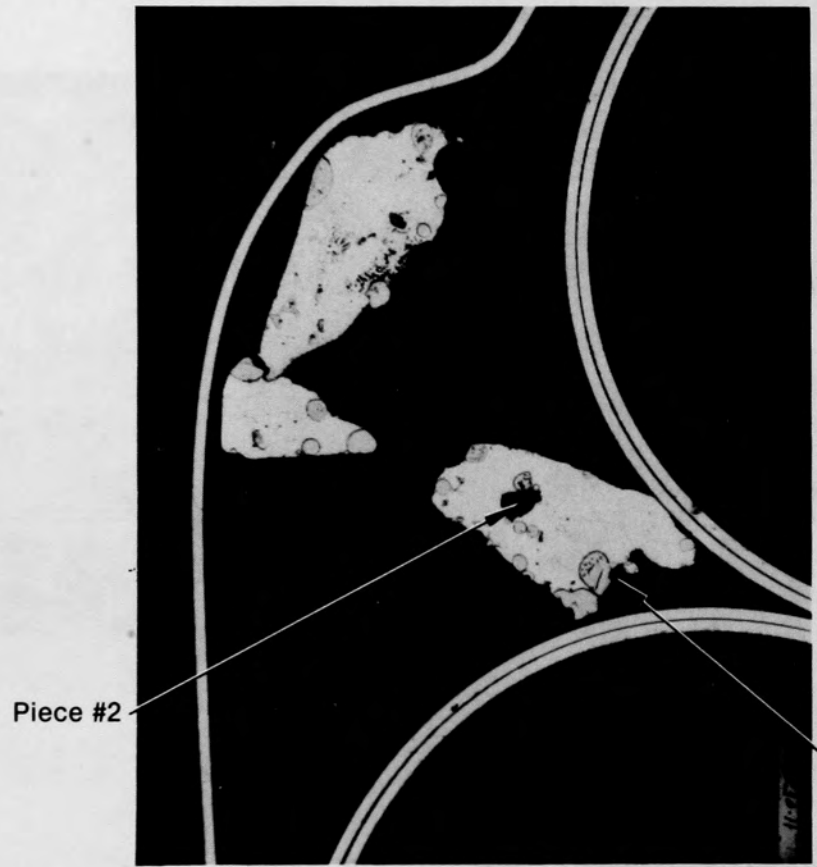
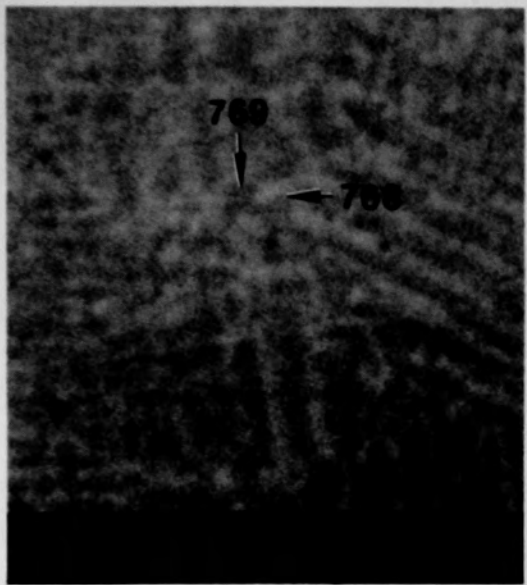
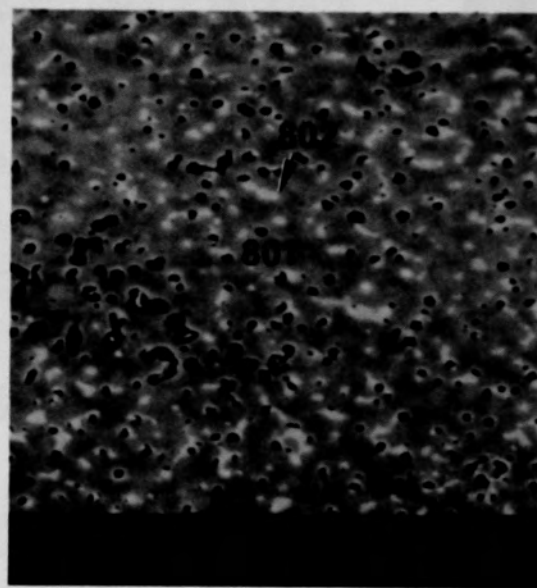


Figure C-205. Macrographs of Particle 9D (H8, 77 cm).

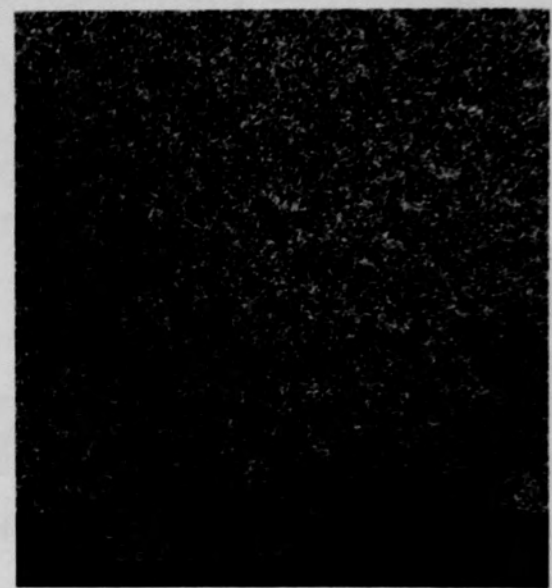
C-259



(a) Location A



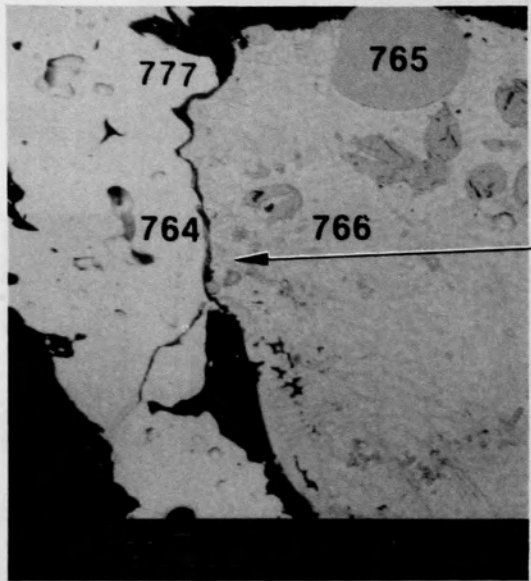
(b) Location B



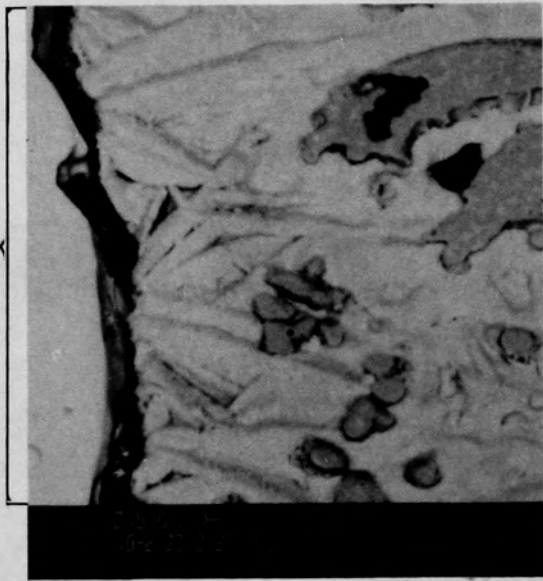
(c) X-ray dot map of (b) for Sn

Figure C-206. Photographs of material from Ag region of Particle 9D (H8, 77 cm).

C-260



(a) SEM backscattered electron image



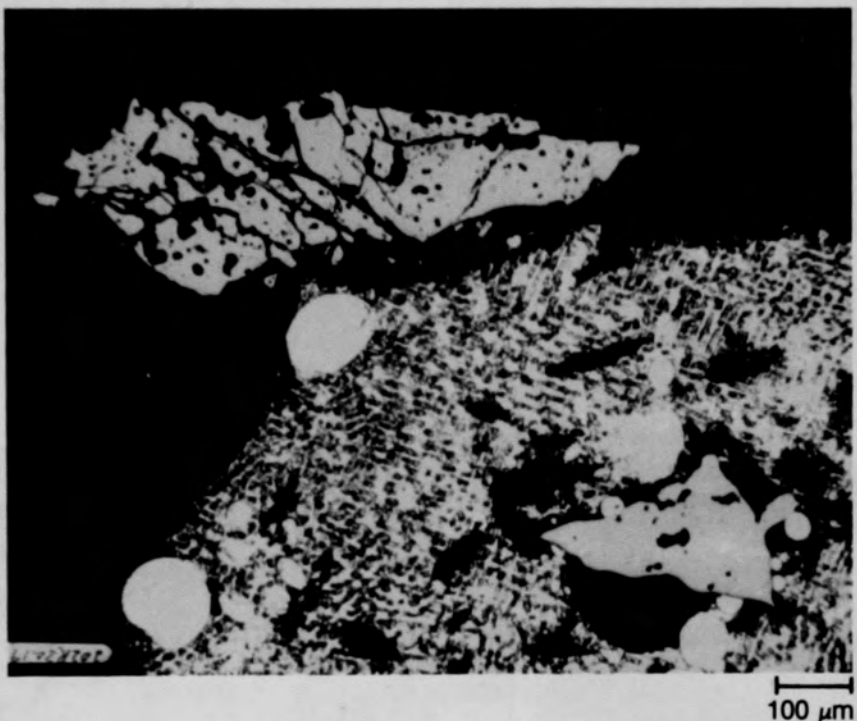
(b) SEM backscattered electron image



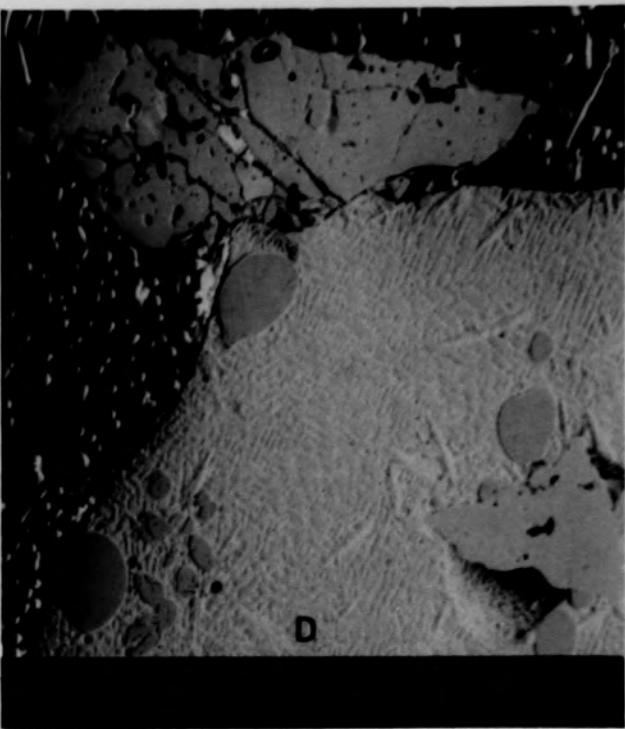
(c) SEM secondary electron image

Figure C-207. SEM electron images of material from location A of Particle 9D (H8, 77 cm).

C-261



(a) Photomicrograph (etched)



(b) SEM backscattered electron image

Figure C-209. Photographs of material from location C of Particle 9D (H8, 77 cm).

C-262

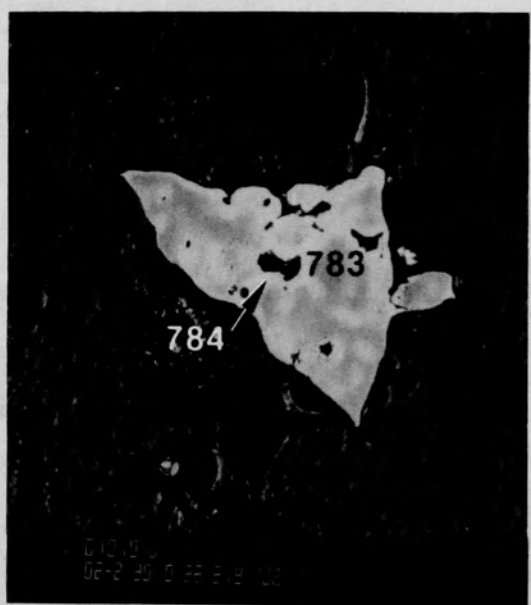
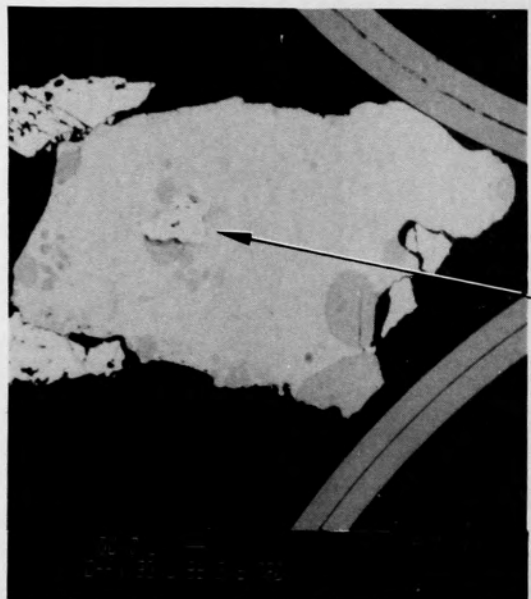


Figure C-208. SEM backscattered electron images of material from lower right Ag region of Particle 9D (H8, 77 cm).

C-263

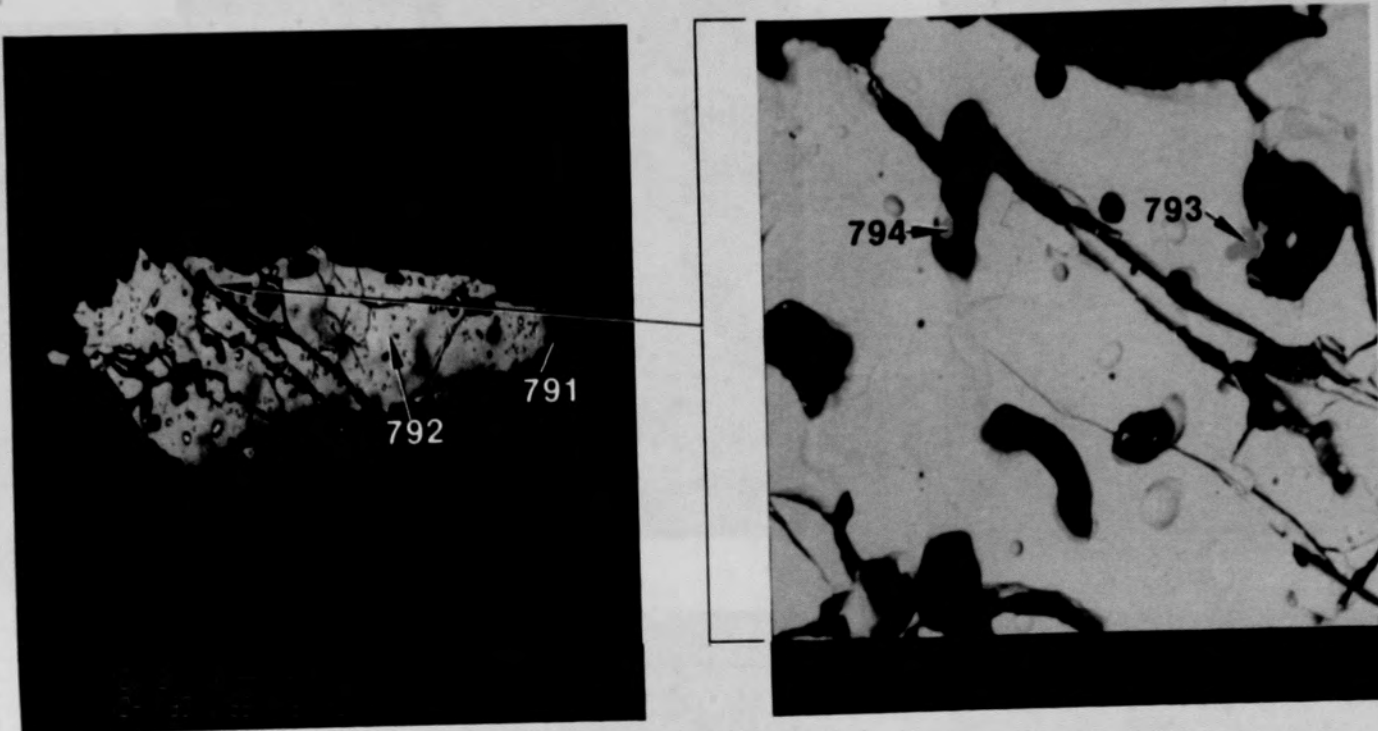
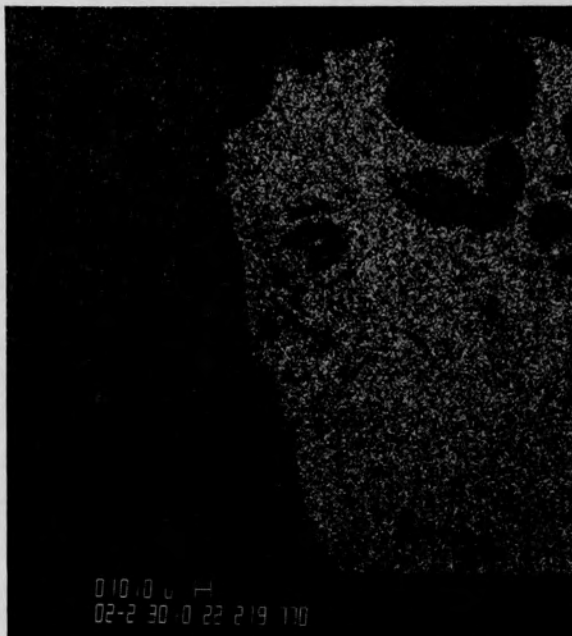
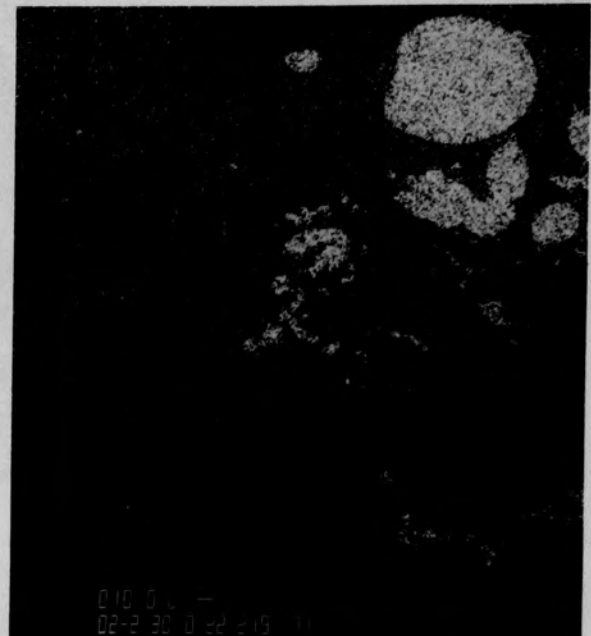


Figure C-210. SEM backscattered electron images of material from location C of Particle 9D (H8, 77 cm).



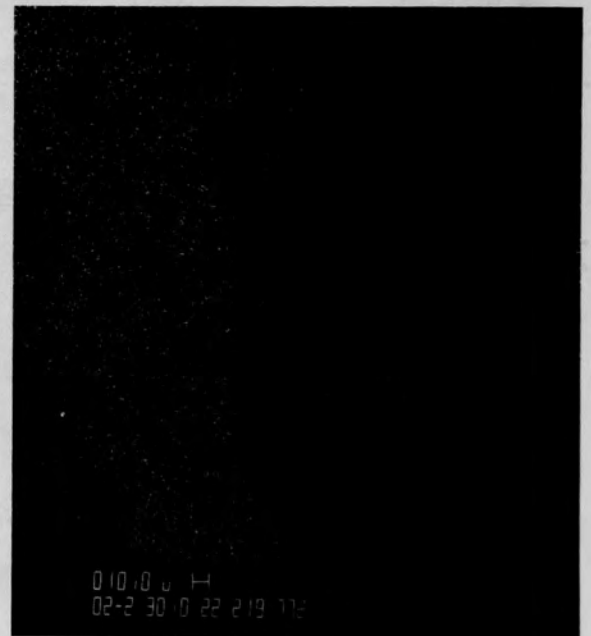
(a) Ag



(b) Ni



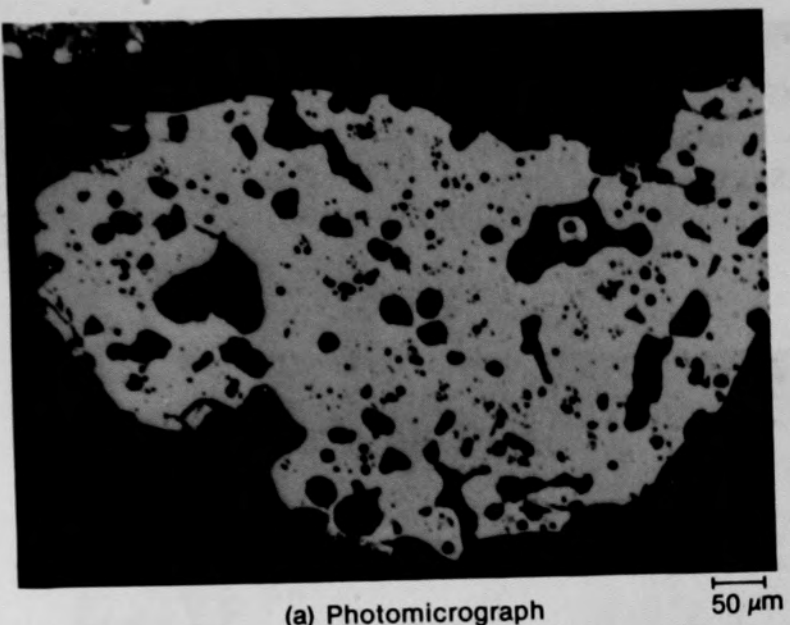
(c) Zr



(d) U

Figure C-211. X-ray dot maps of material from location D (see Figures C-207 and C-209).

* C-265



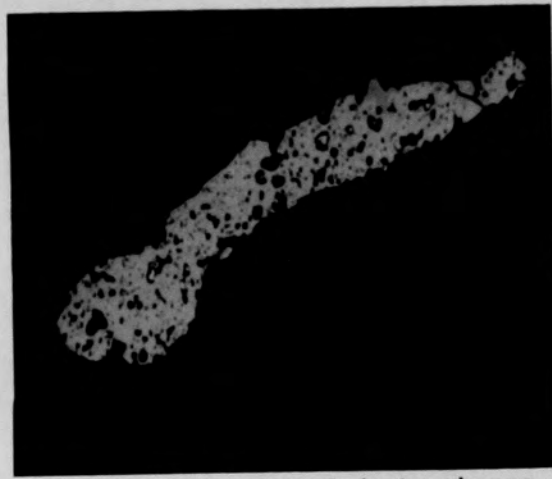
(a) Photomicrograph

50 μm



(b) Photomicrograph

50 μm



(c) SEM backscattered electron image

Figure C-212. Photographs of ceramic material from the lower left region
of Particle 9D (H8, 77 cm).

C-266

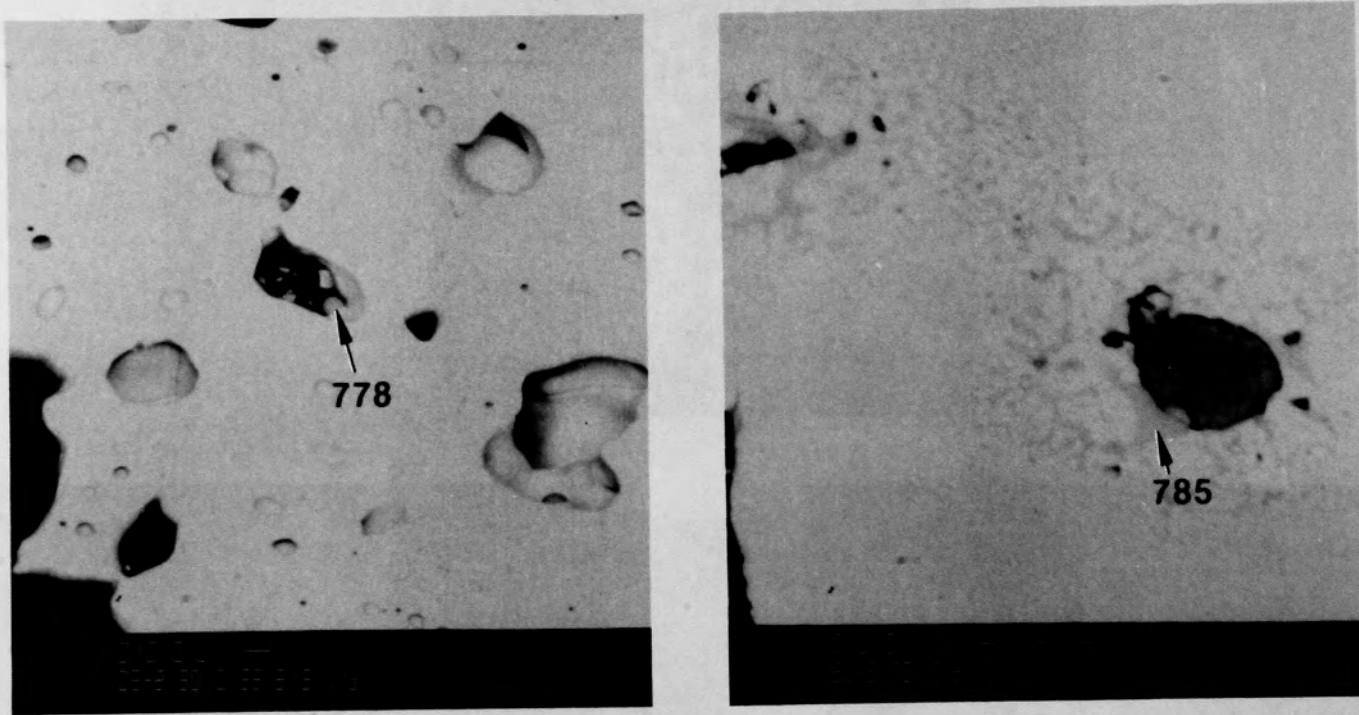
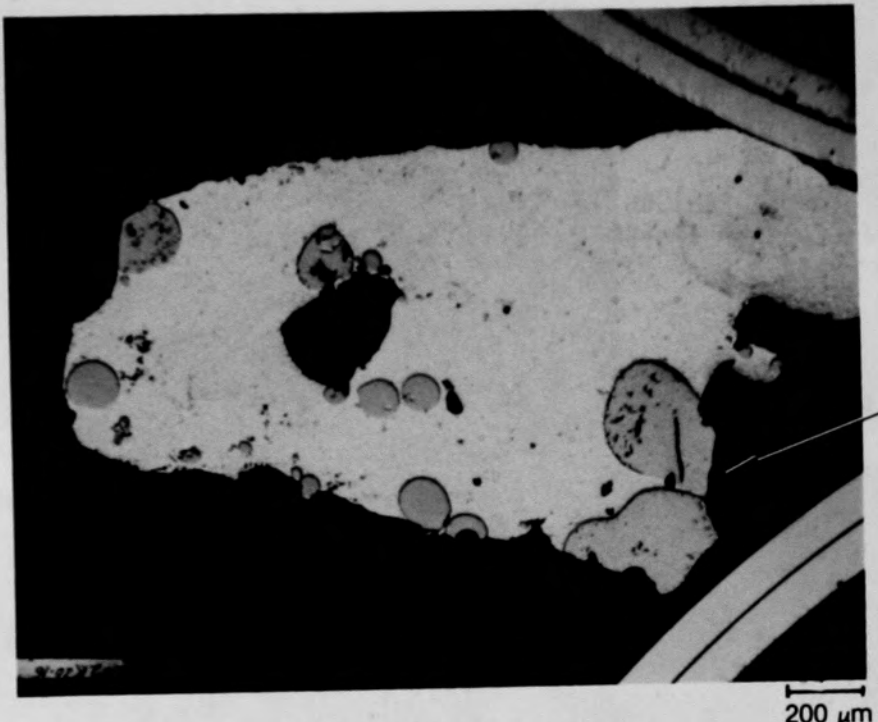
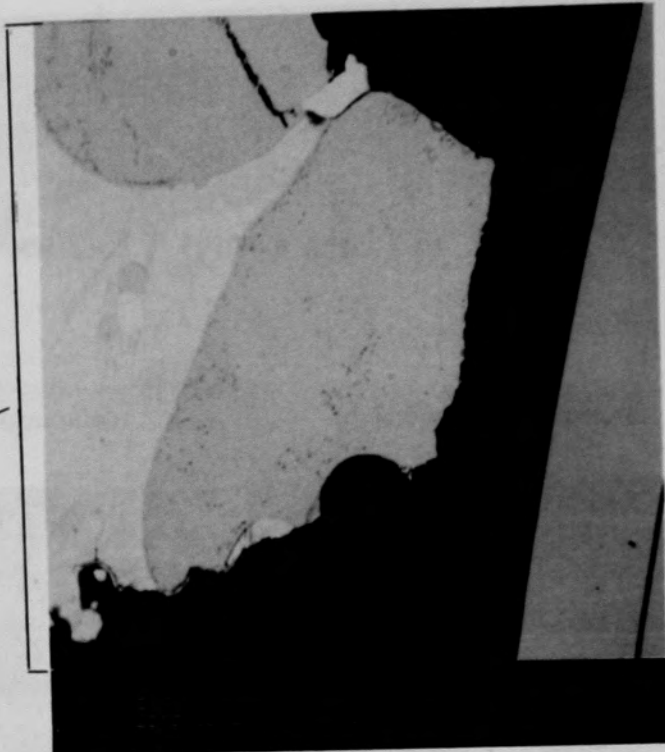


Figure C-213. SEM backscattered electron images of ceramic material from the lower left region of Particle 9D (H8, 77 cm).

C-267



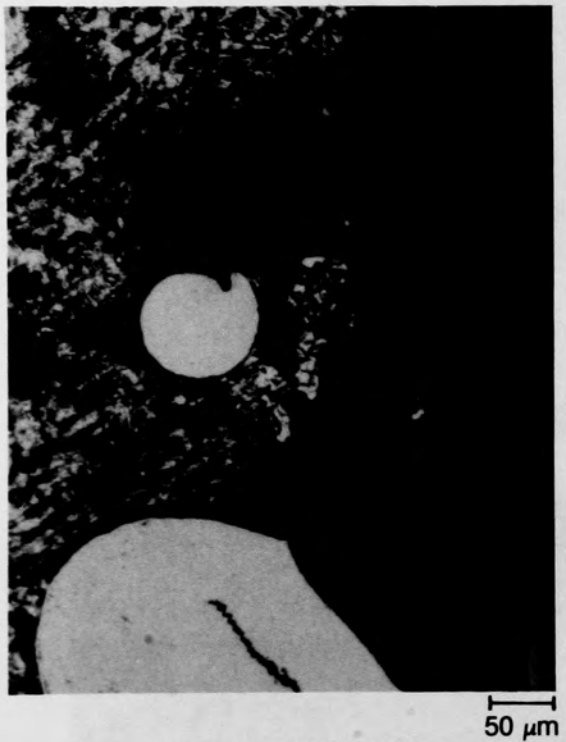
(a) Photomicrograph



(b) SEM backscattered selectron image

Figure C-214. Photographs of material from the lower right Ag region of Particle 9D (H8, 77 cm).

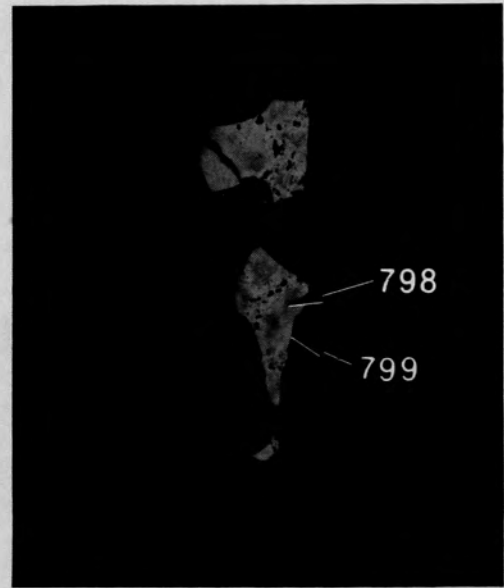
C-268



(a) Photomicrograph



(b) SEM backscattered electron image



(c) Higher contrast of (b)

Figure C-215. Photographs of material from location E (Figure C-205) of Particle 9D (H8, 77 cm).

C-269

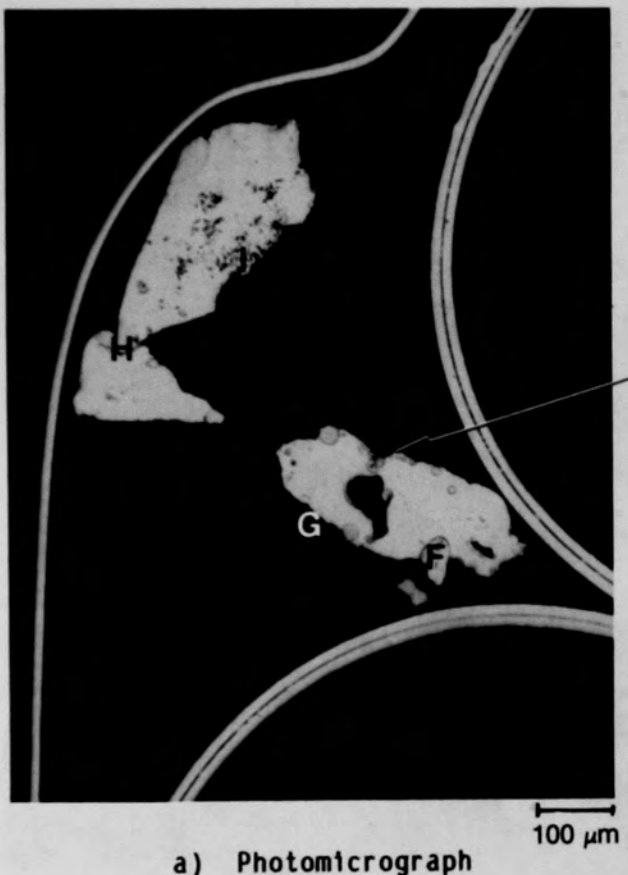


Figure C-216. Photographs of lower right Ag region of Particle 9D (H8, 77 cm).

C-270

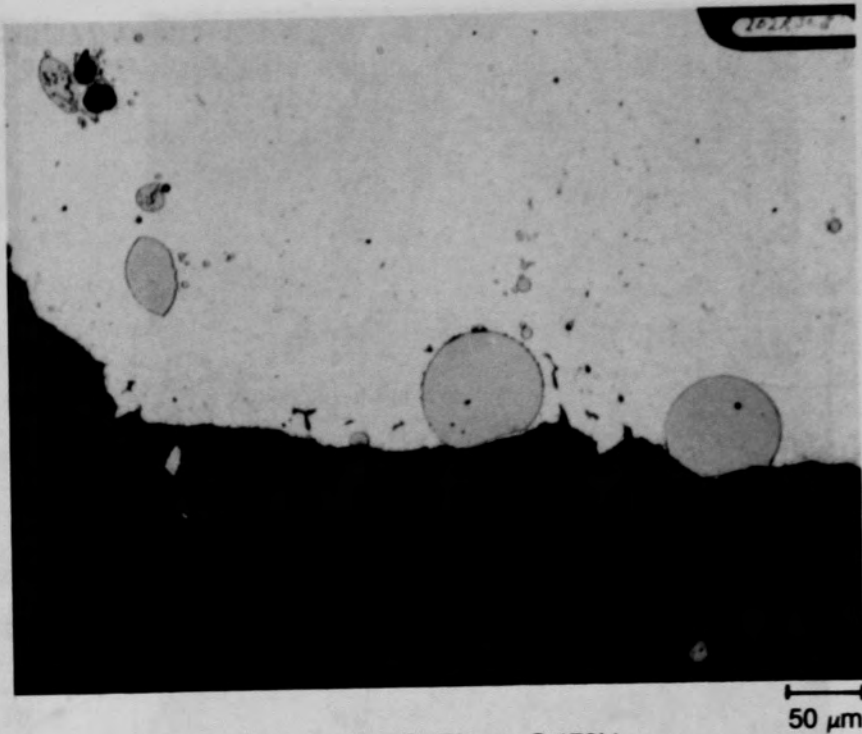


Figure C-217. Photomicrographs of material from location F, Figure C-216a, of Particle 9D (H8, 77 cm).

C-271



(a) Location H (Figure C-170a)



(b) Location G (Figure C-170b)

Figure C-218. Photomicrographs of Ag regions of Particle 9D (H8, 77 cm).

C-272

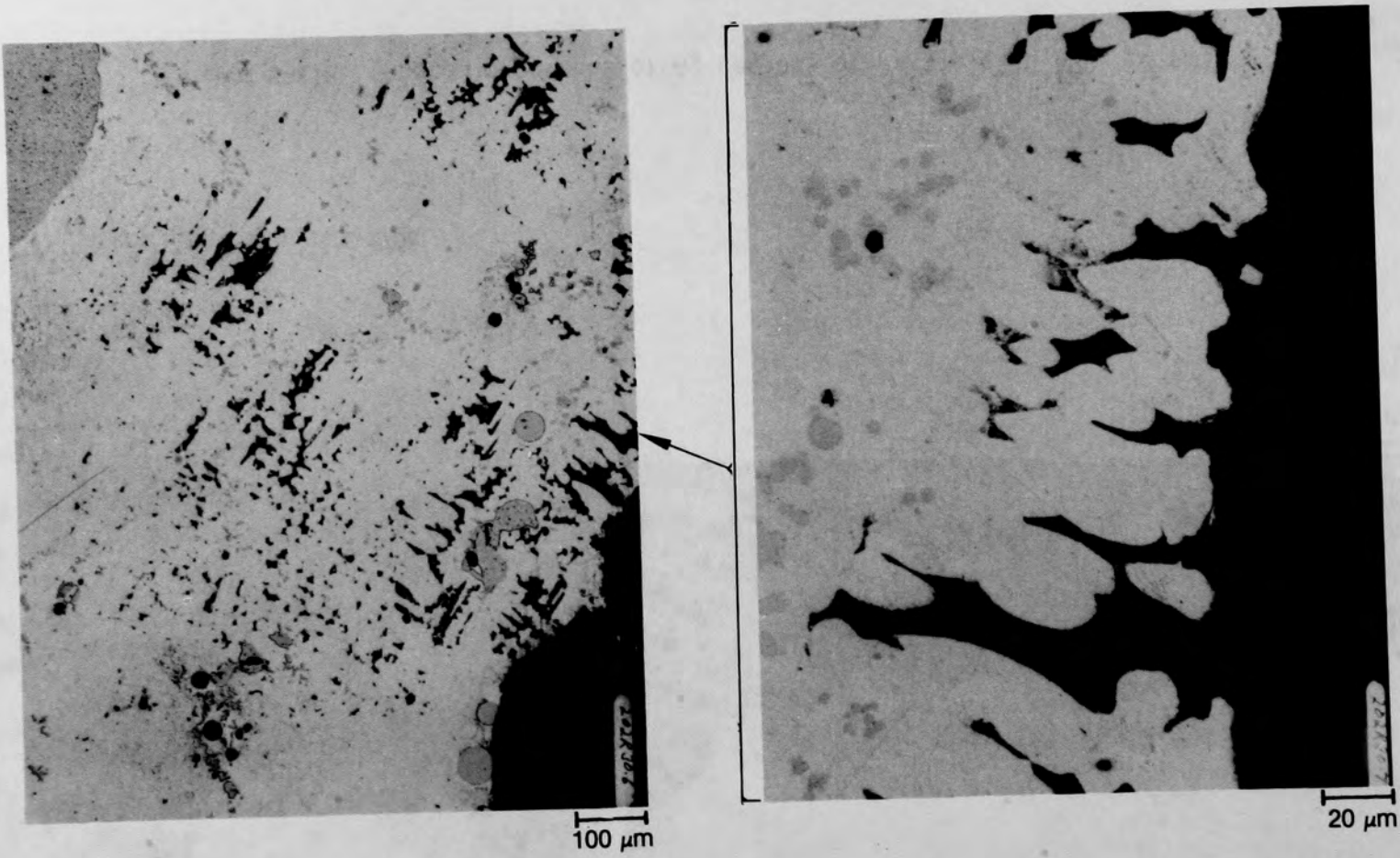


Figure C-219. Photomicrographs of material from location I, Figure C-216a,
of Particle 9D (H8, 77 cm).

C-273

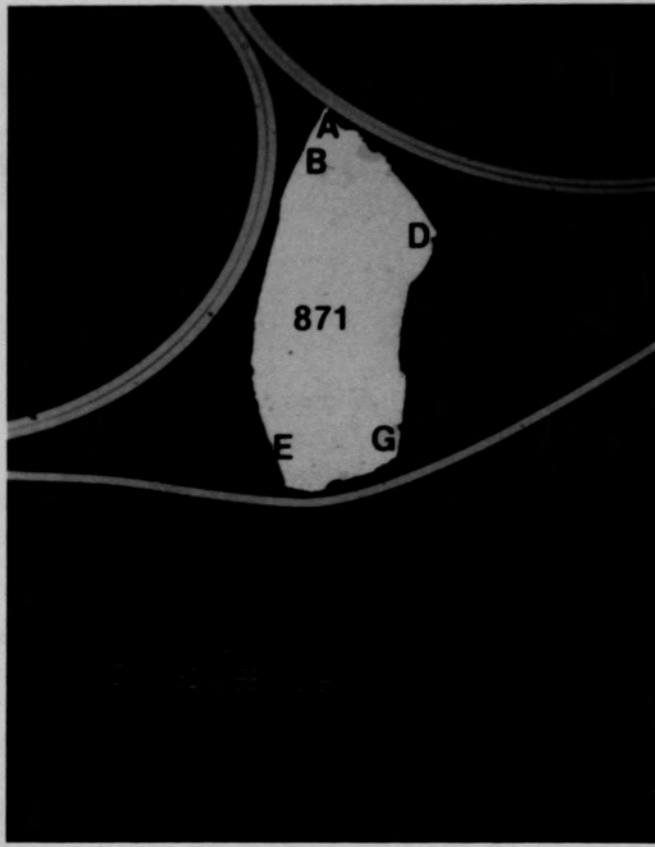
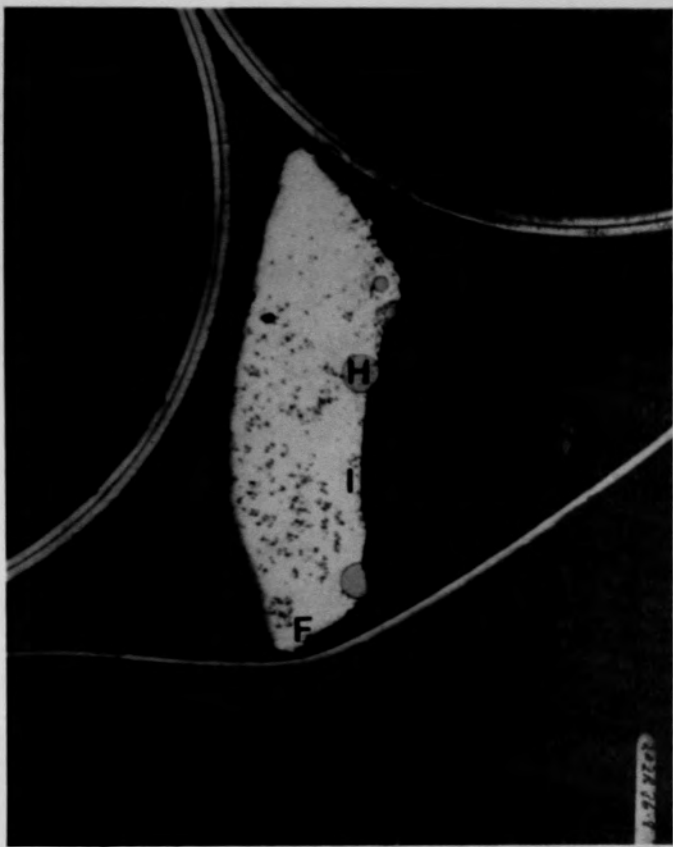
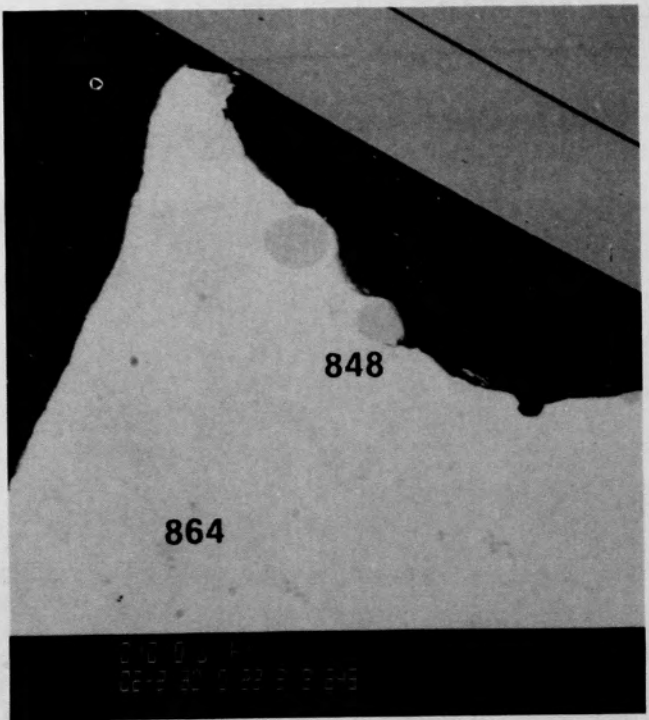
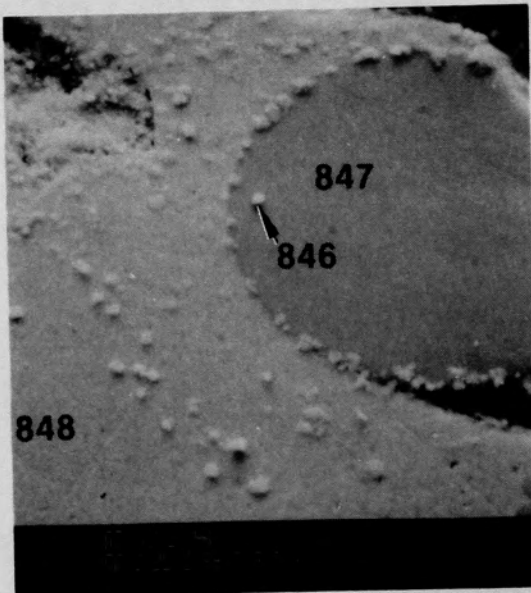


Figure C-220. Photomacrographs of overall view of Particle 9G (H8, 77 cm).

C-274

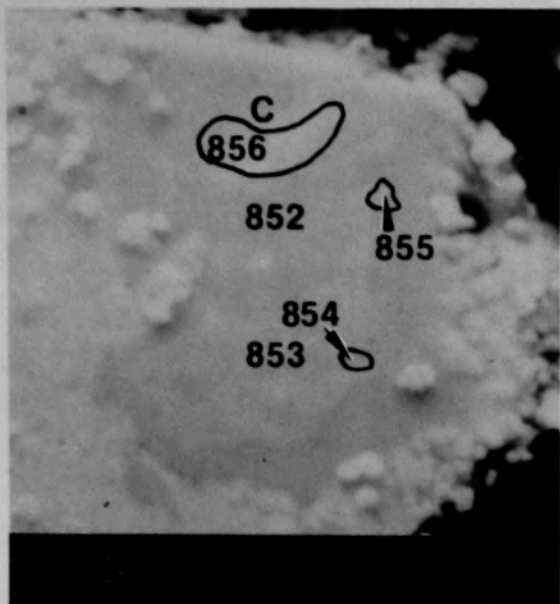


(a) SEM backscattered electron image



(b) SEM secondary electron image

Figure C-221. SEM backscattered electron images of material from location A of Particle 9G (H8, 77 cm).



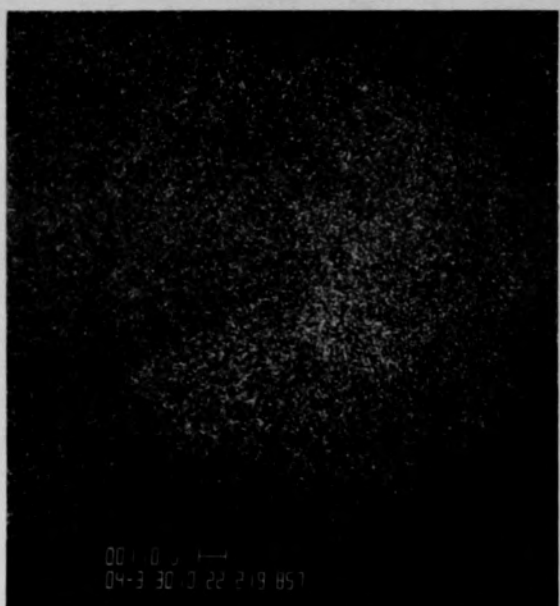
(a) SEM secondary electron image



(b) X-ray dot map of Ni



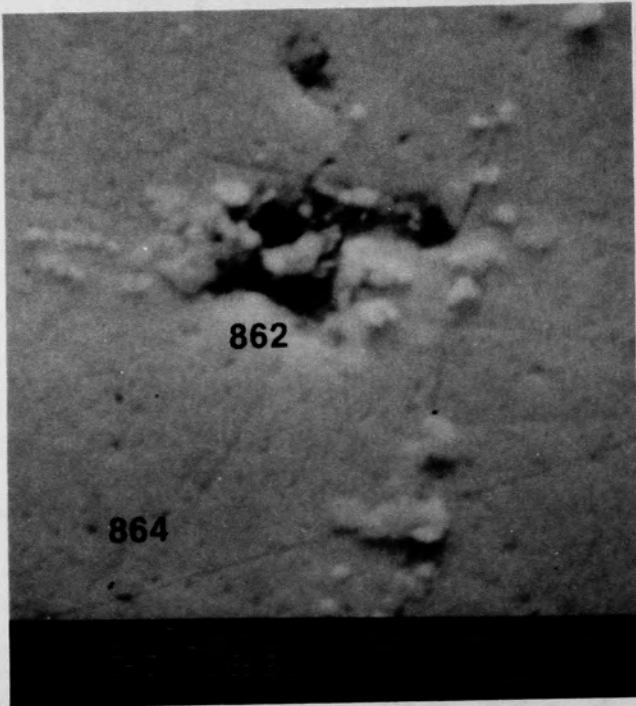
(c) X-ray dot map of Ag



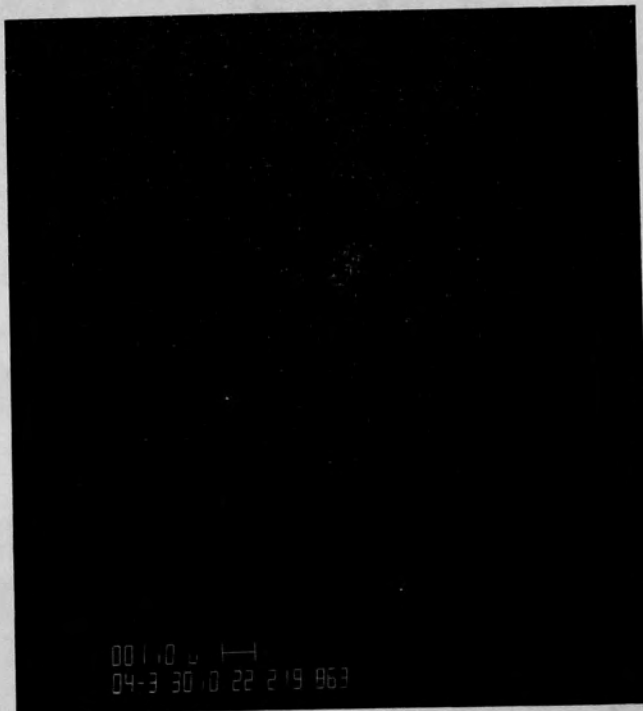
(d) X-ray dot map of Sn

Figure C-222. Photographs of material from location B of Particle 9G (H8, 77 cm).

C-276



(a) SEM secondary electron image



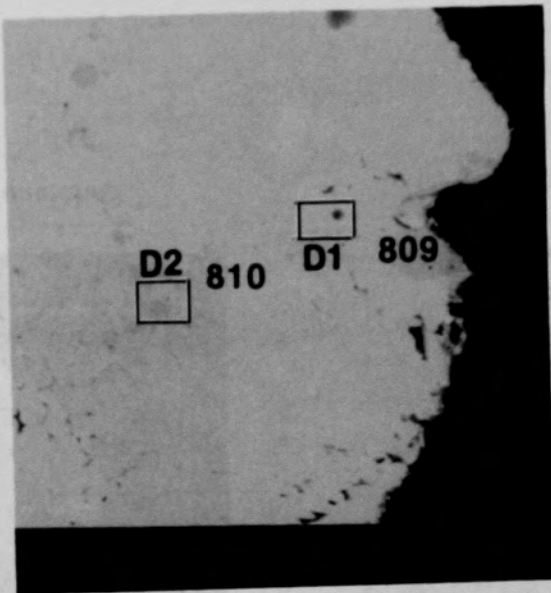
(b) X-ray dot map of Ti

Figure C-223. Photographs of material from location C, Figure C-222a, of Particle 9G (H8, 77 cm).

C-277



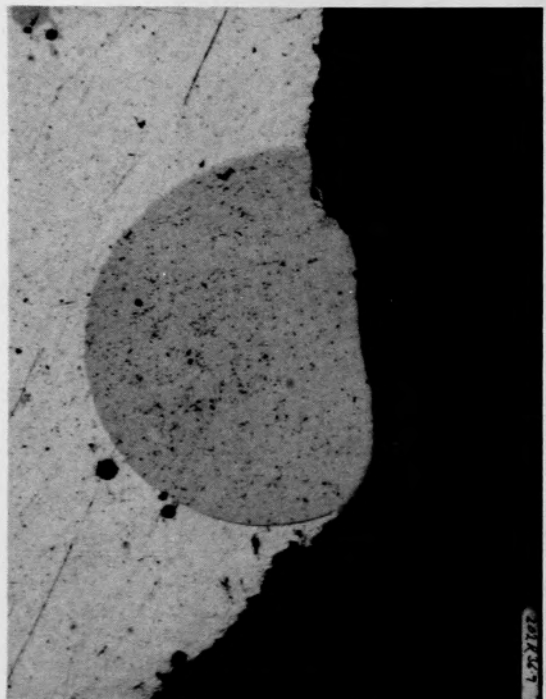
(a) Photomicrograph



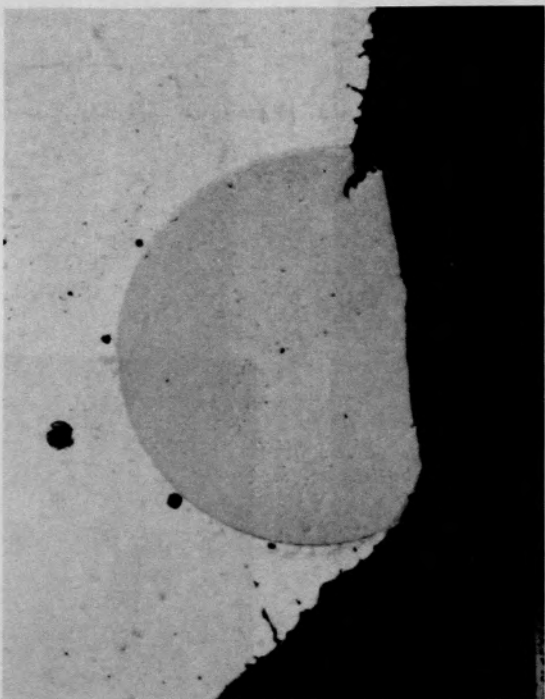
(b) SEM backscattered electron image

Figure C-224. Photographs of material from location D of Particle 9G (H8, 77 cm).

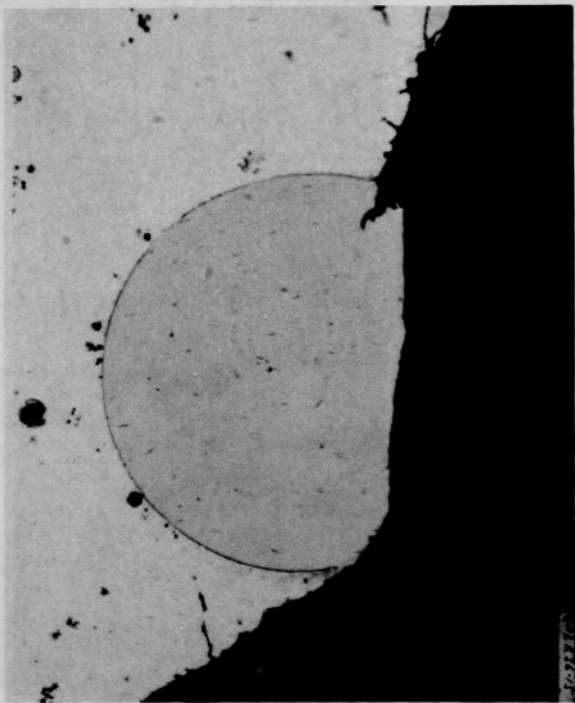
C-278



(a) As-polished, unetched



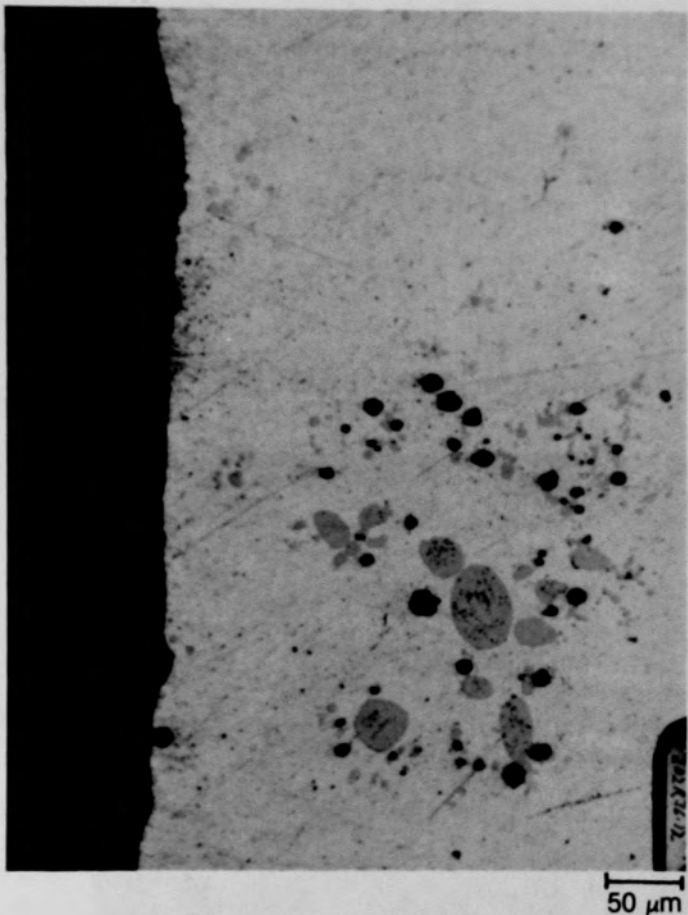
(b) Re-polished, unetched



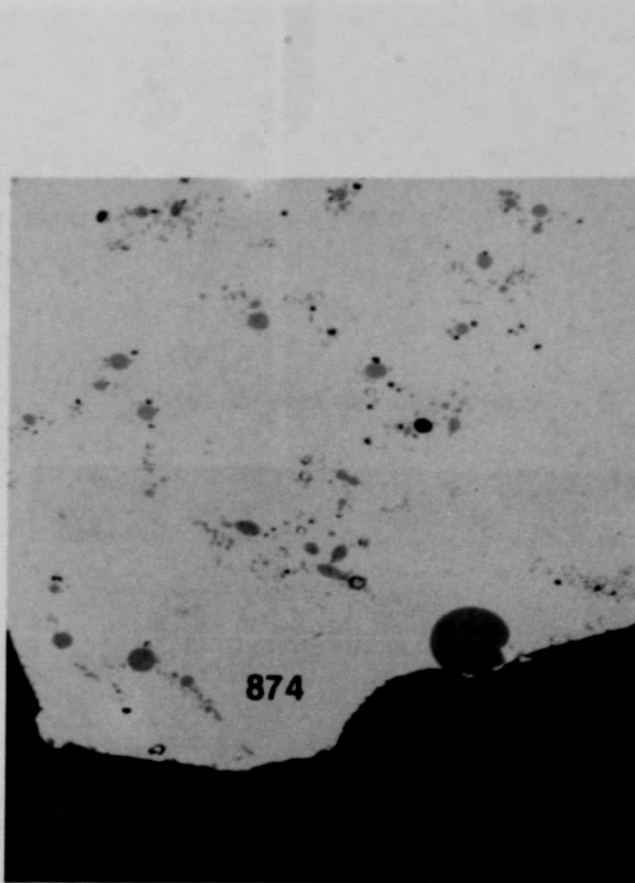
(c) Silver etch

Figure C-225. Photomicrographs of material from location H of Particle 9G (H8, 77 cm).

C-279



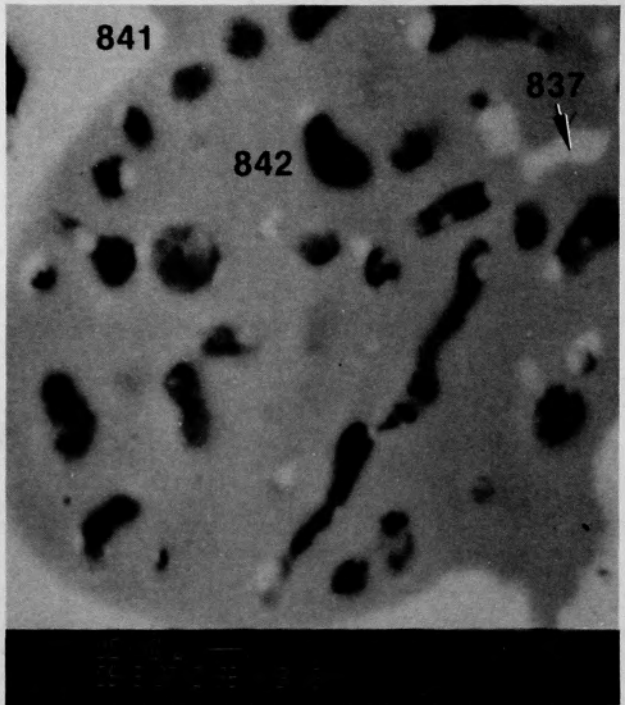
(a) Photomicrograph location E



(b) SEM backscattered electron image location F

Figure C-226. Photographs of Particle 9G (H8, 77 cm).

C-280



(a) SEM backscattered electron image



(b) Ag X-ray dot map of (a)

Figure C-227. Photographs of material from location D2, Figure C-224b, of Particle 9G (H8, 77 cm).

C-281

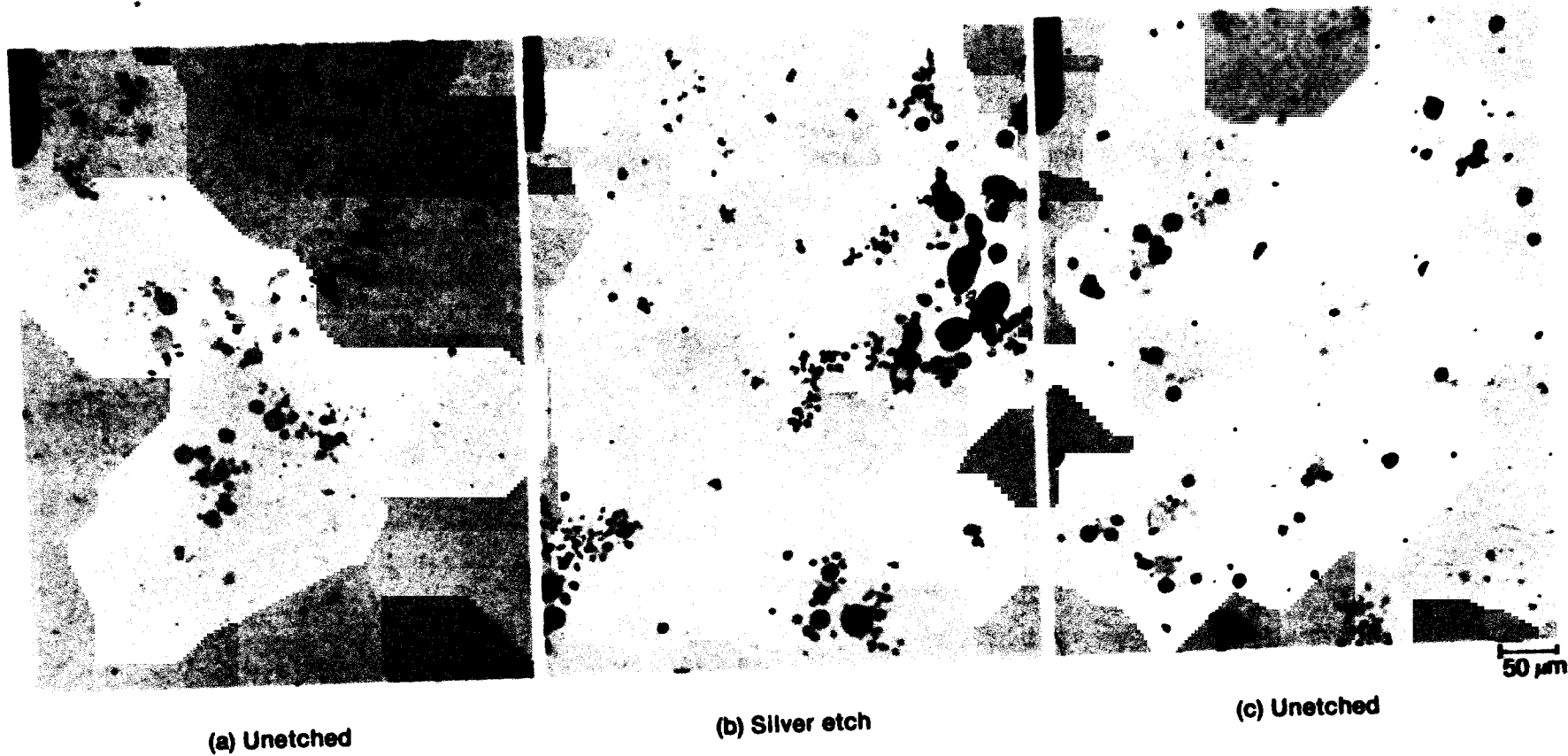
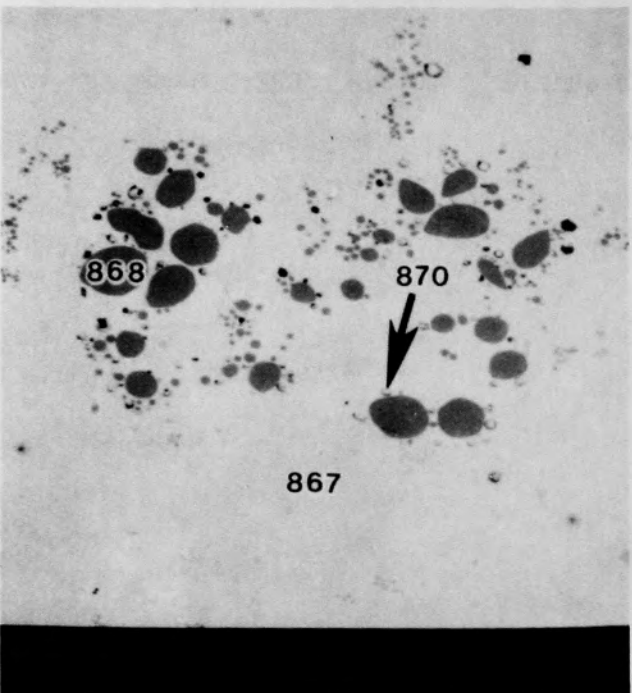
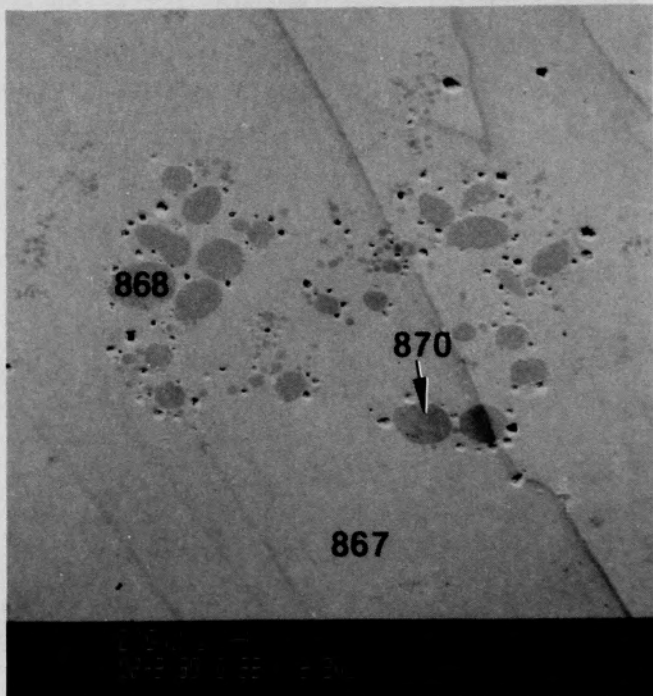


Figure C-228. Photomicrographs of material near the center of Particle 9G
(H8, 77 cm).

C-282



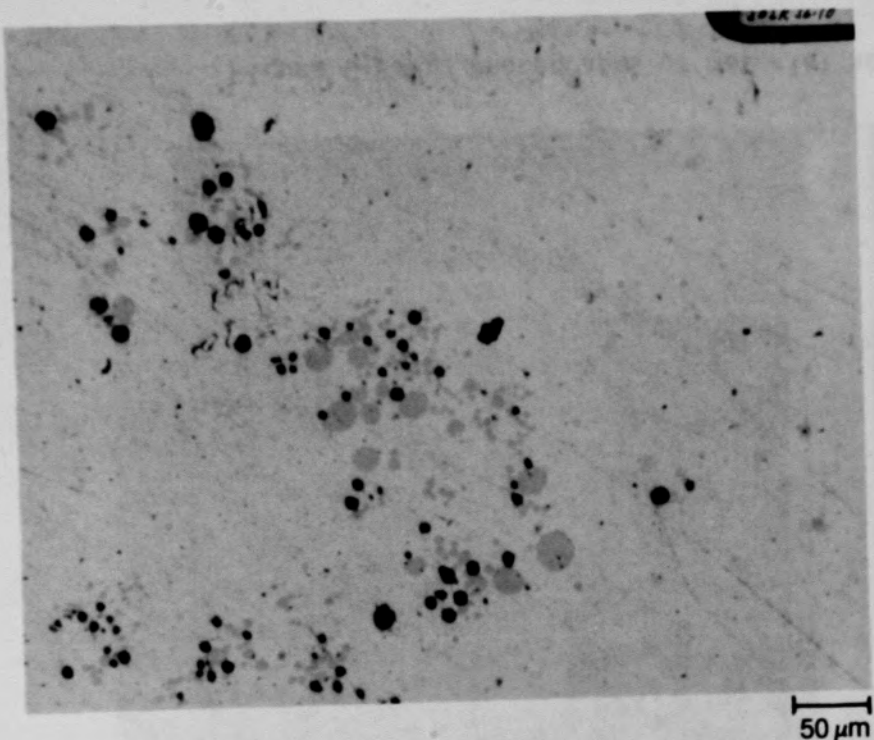
(a) SEM backscattered electron image



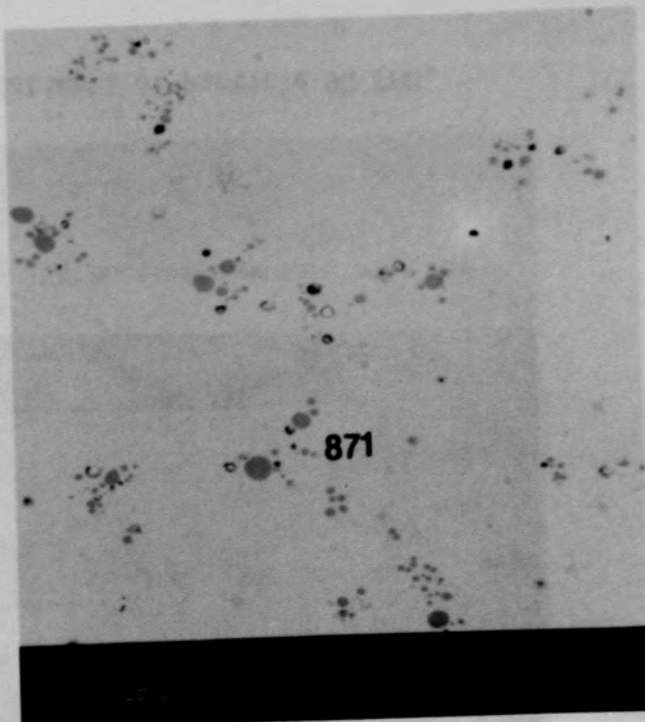
(b) SEM secondary electron image

Figure C-229. SEM backscattered electron images of material from location B of Particle 9G (H8, 77 cm).

C-283



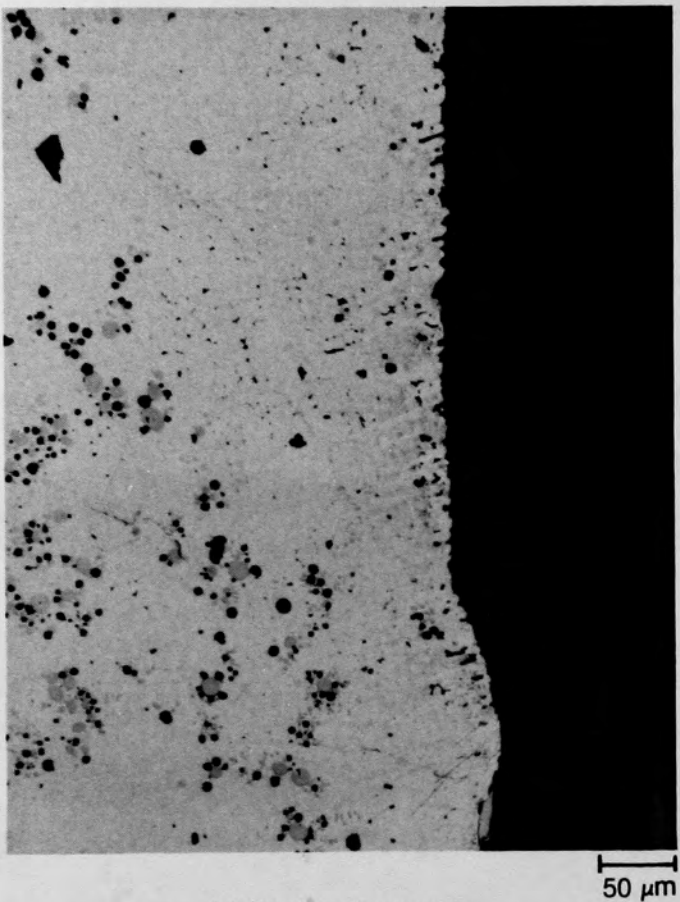
(a) Photomicrograph



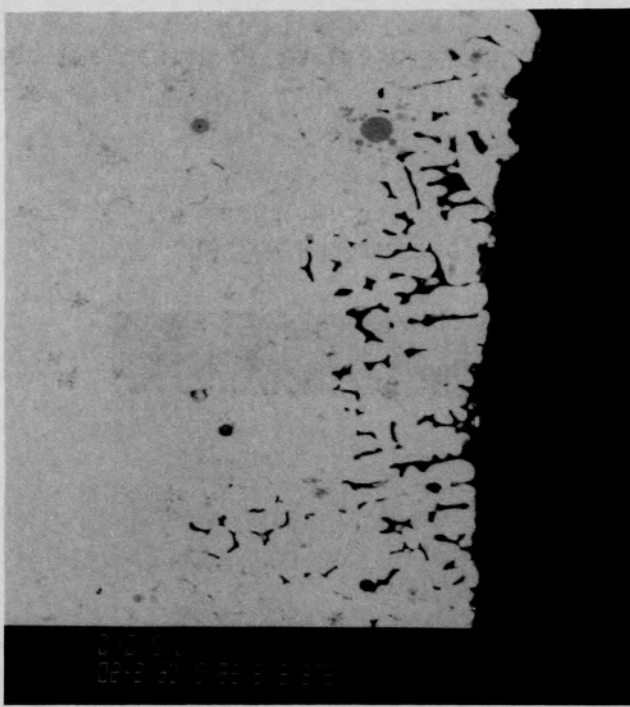
(b) SEM backscattered electron image

Figure C-230. Photographs of material near the center of Particle 9G (H8,
77 cm).

C-284



(a) Photomicrograph

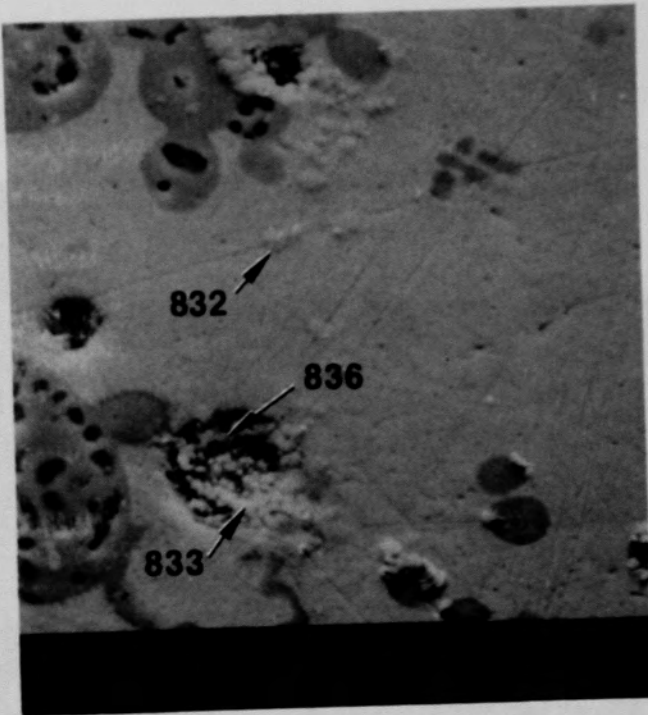


(b) SEM backscattered electron image

Figure C-231. Photographs of material near location I of Particle 9G (H8, 77 cm).



(a) Location D1



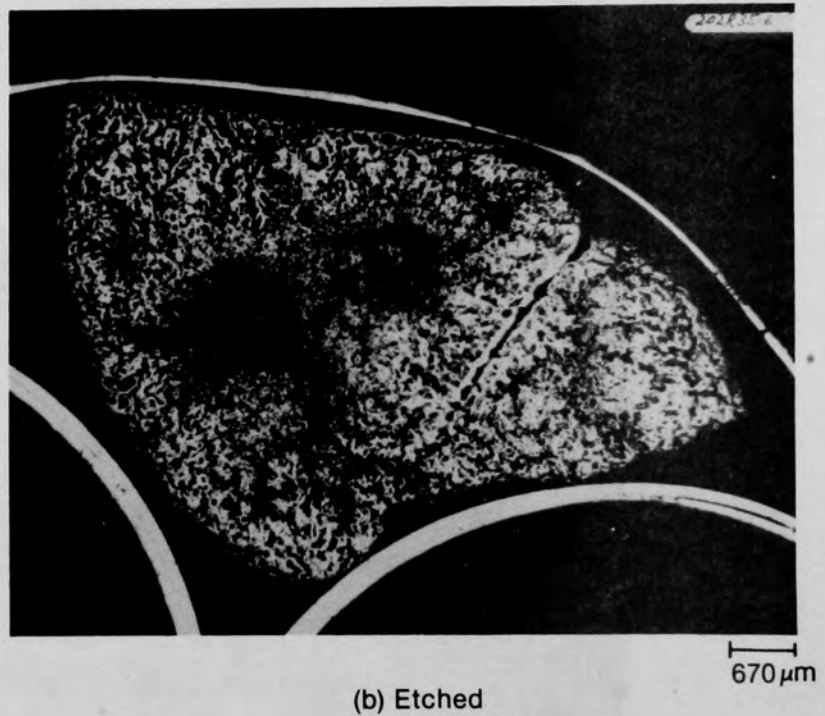
(b) Location D2

Figure C-232. SEM secondary electron images of material from location D of Particle 9G (H8, 77 cm).

C-286



(a) Unetched



(b) Etched

Figure C-233. Photomacrographs of Particle 10A (E9, 74 cm).

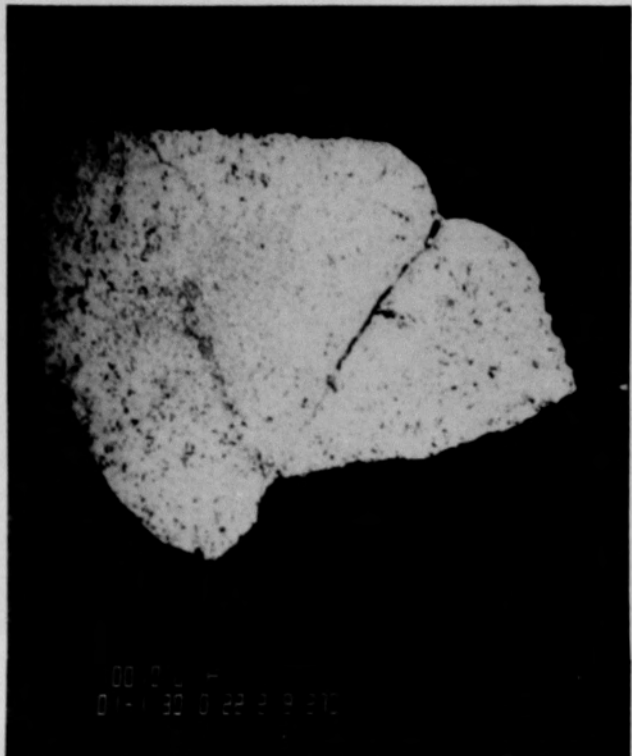


Figure C-234. SEM backscattered electron image of Particle 10A (E9, 74 cm)
after repolishing.

C-288

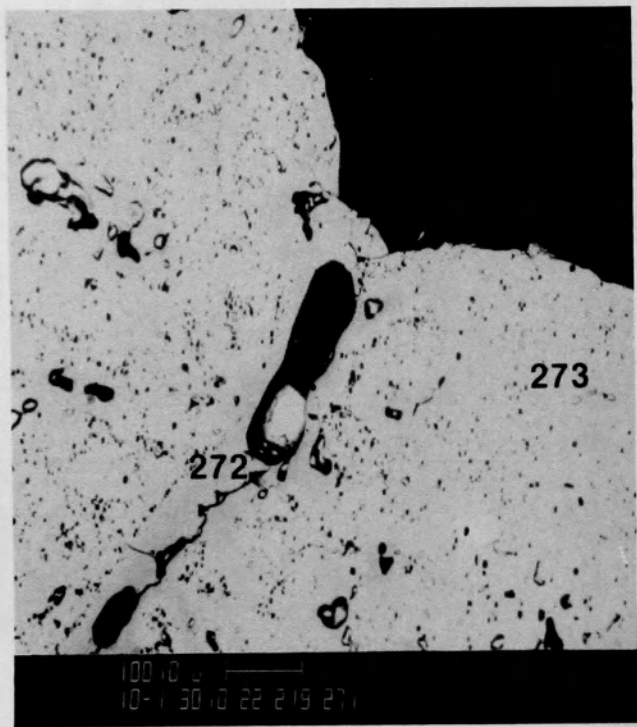
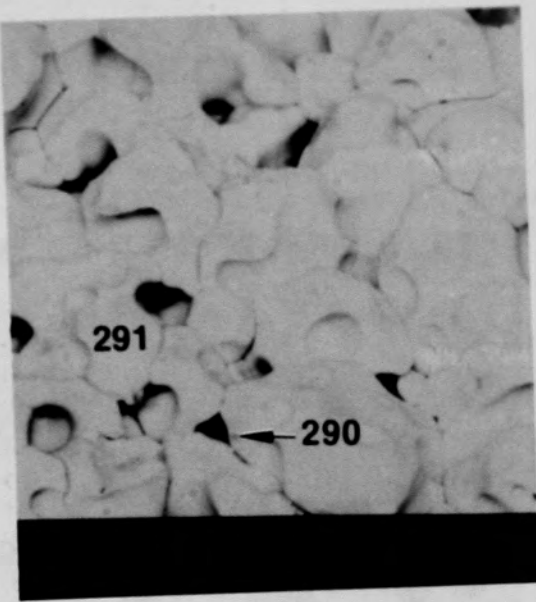
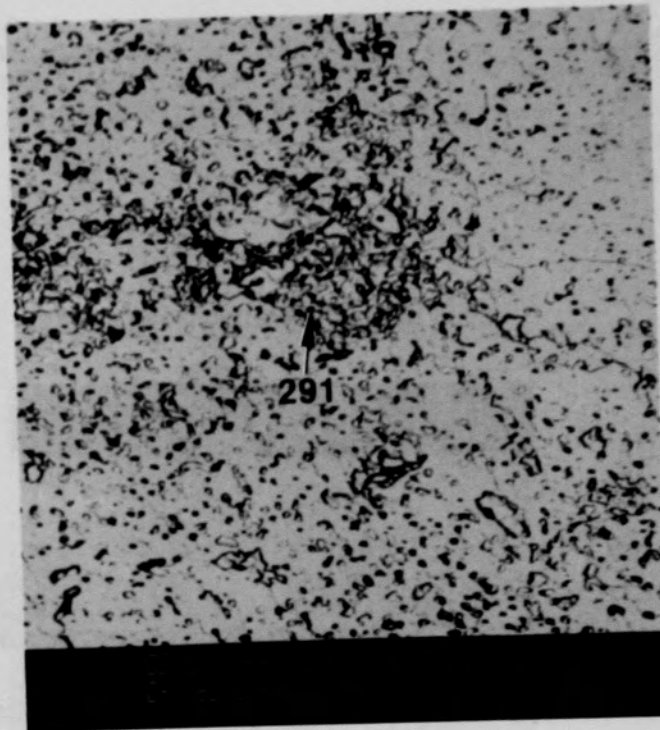


Figure C-235. SEM backscattered electron image of material from Region 1 of Particle 10A (E9, 74 cm).



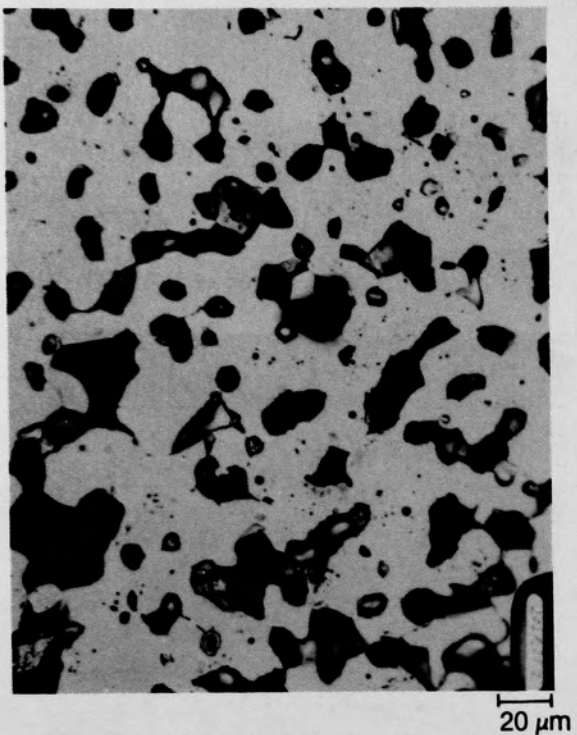
(a) SEM secondary electron image



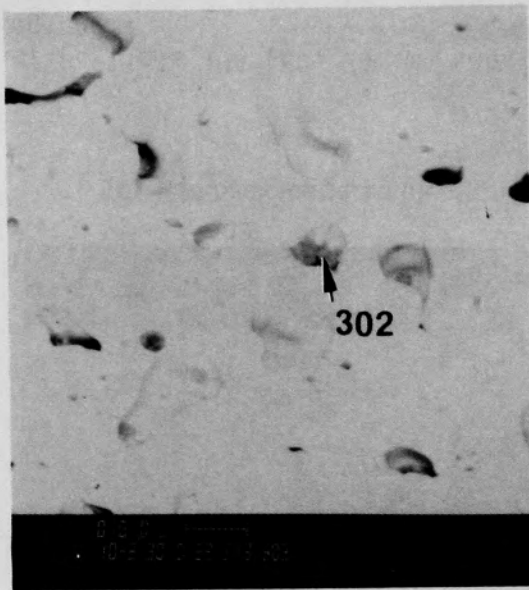
(b) SEM backscattered electron image

Figure C-236. SEM electron images of Particle 10A (E9, 74 cm) showing a grain structure in Region 2.

C-290



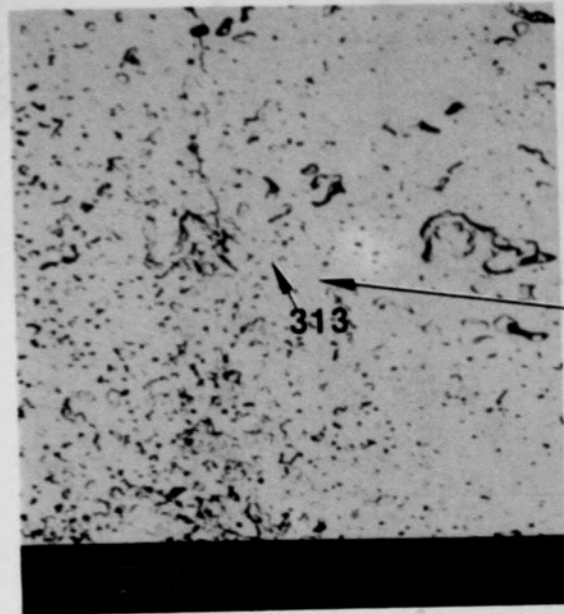
(a) Photomicrograph



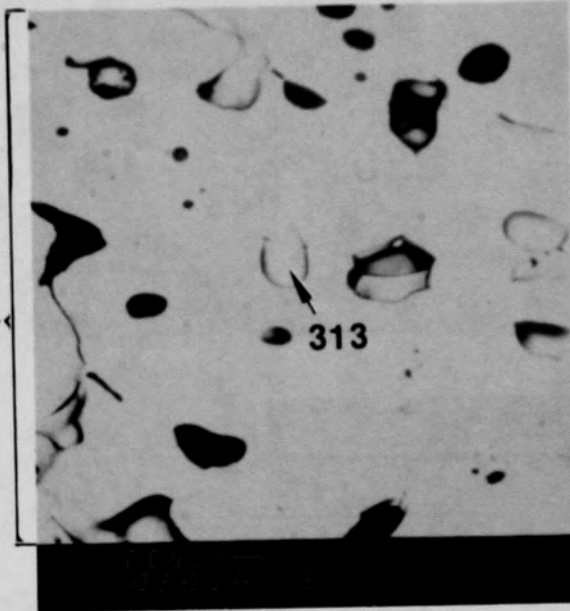
(b) SEM backscattered electron image

Figure C-237. Photographs of material from Region 2, location A of Particle 10A (E9, 74 cm).

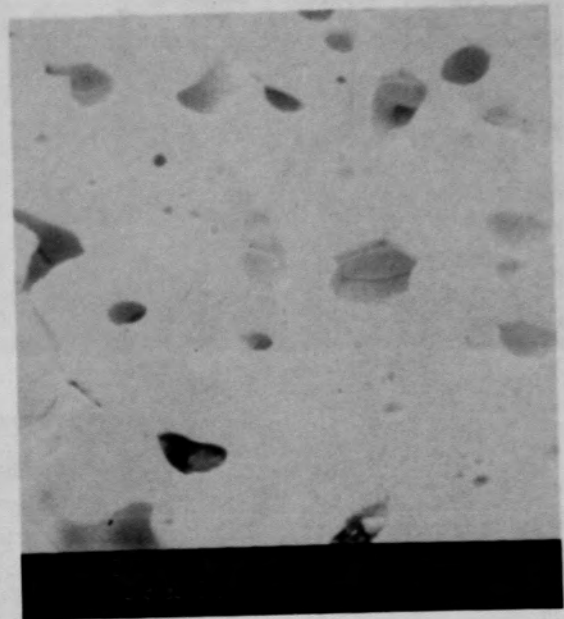
C-291



(a) SEM backscattered electron image



(b) SEM backscattered electron image



(c) SEM secondary electron image

Figure C-238. SEM electron images of material from Region 1, location B of Particle 10A (E9, 74 cm).

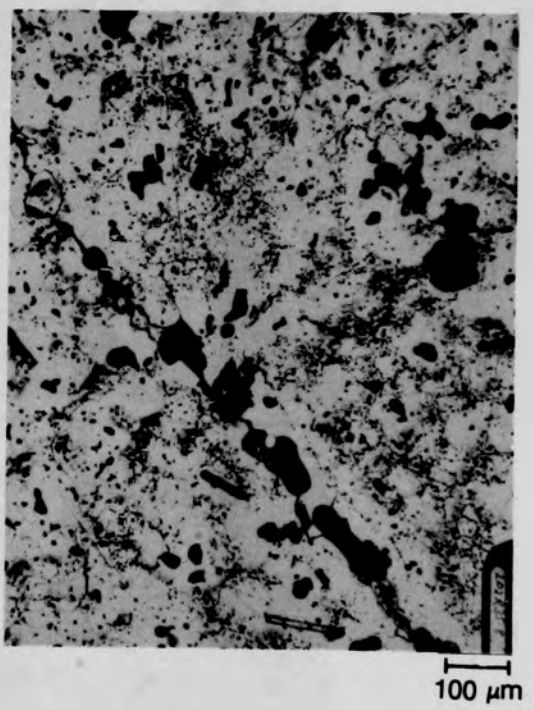
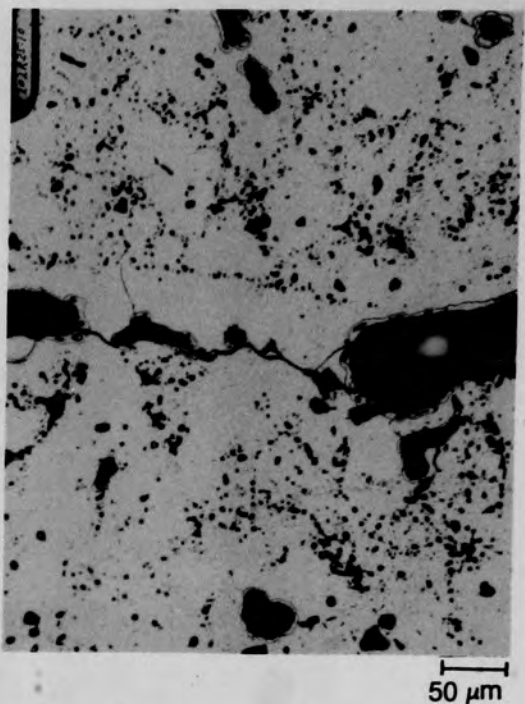
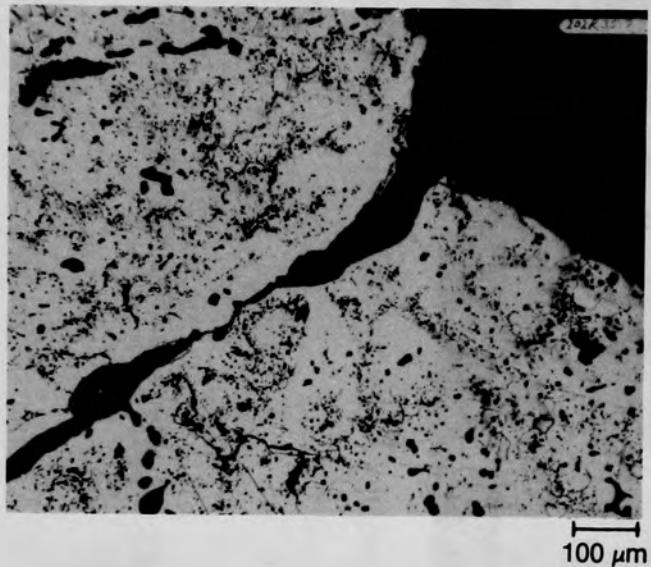


Figure C-239. Photomicrographs of etched material from Region 1,
location C of Particle 10A (E9, 74 cm).

C-293

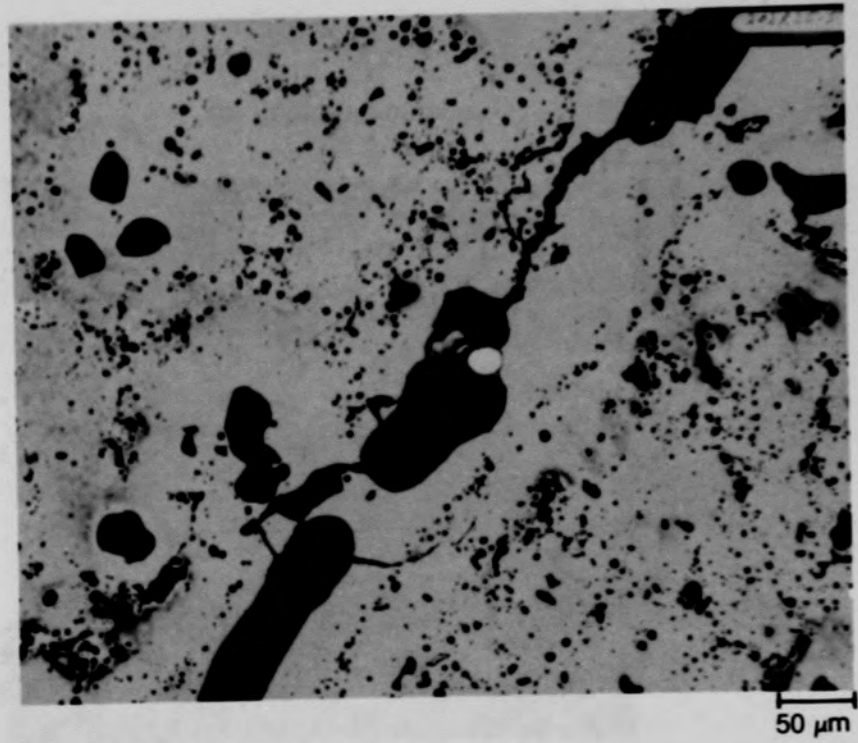
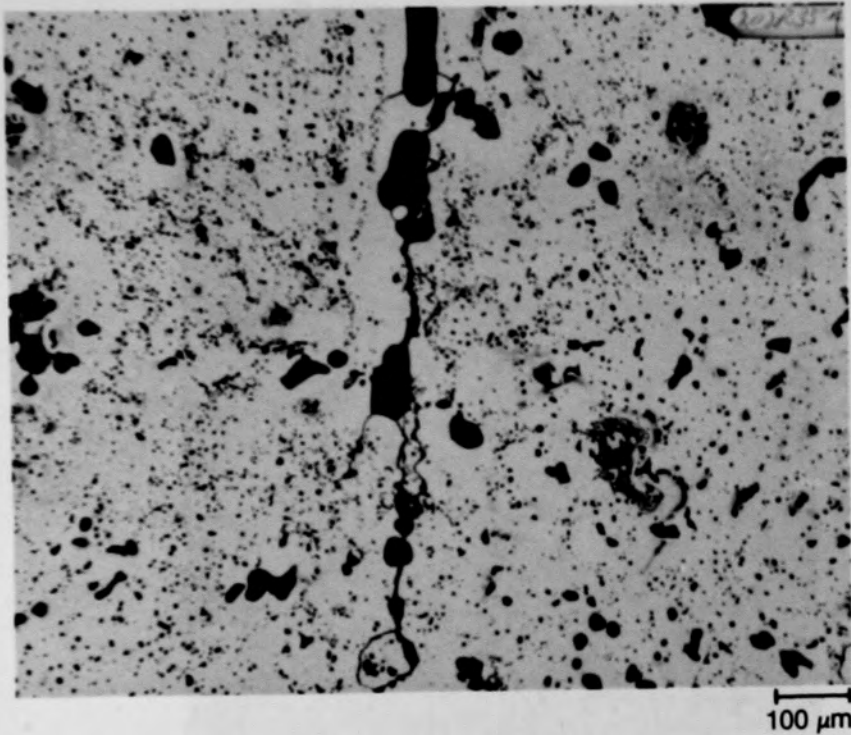
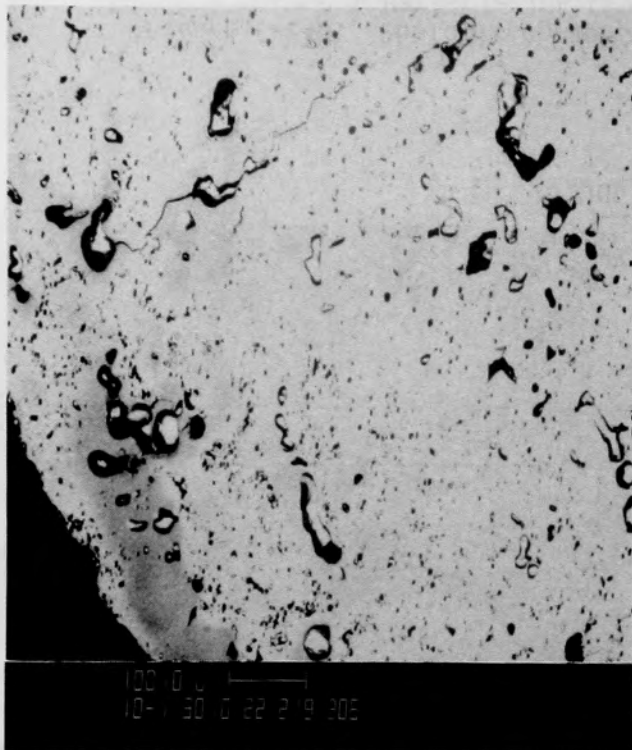


Figure C-240. Photomicrographs of material from Region 1, location D of Particle 10A (E9, 74 cm).

C-294



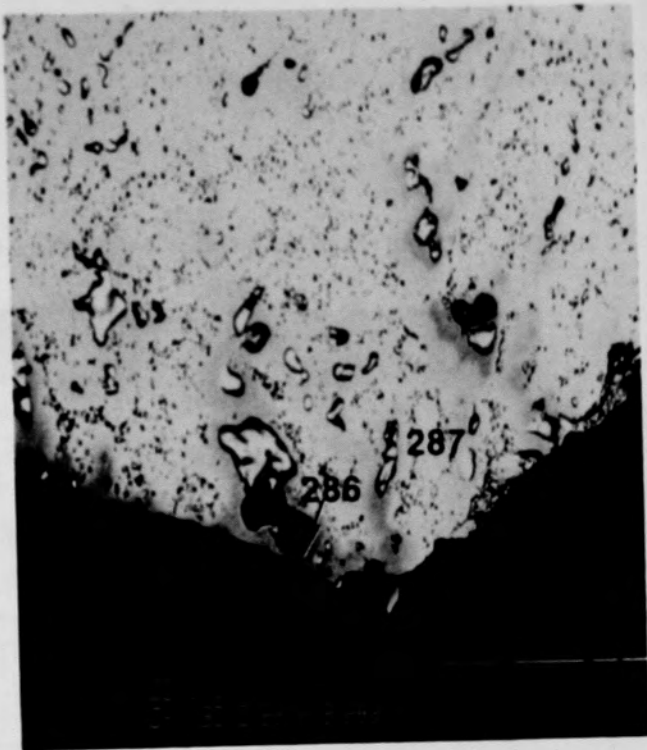
(a) SEM backscattered electron image



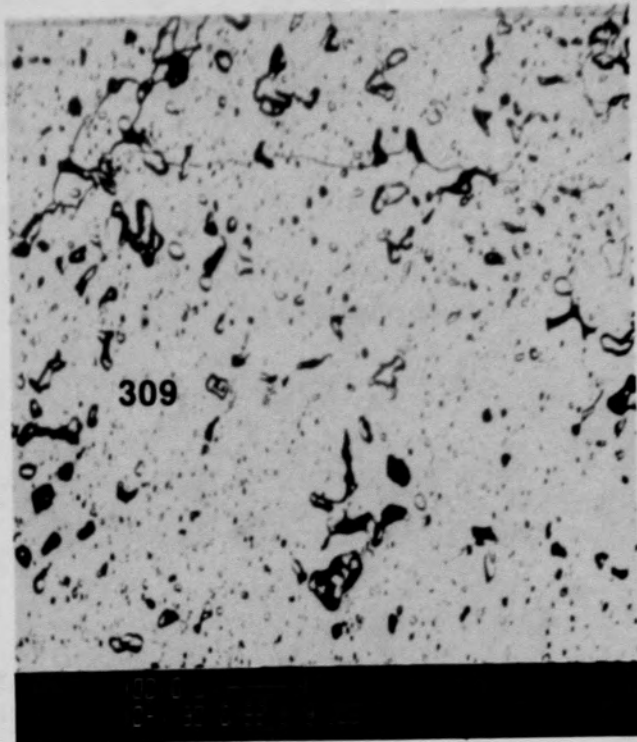
(b) Photomicrograph

Figure C-241. Photographs of material from Region 2, location E of Particle 10A (E9, 74 cm).

C-295



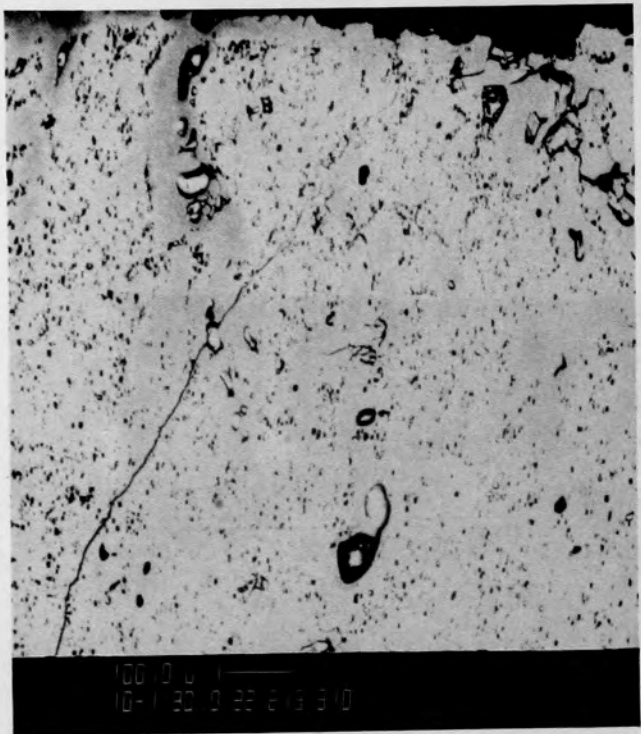
(a) Location F



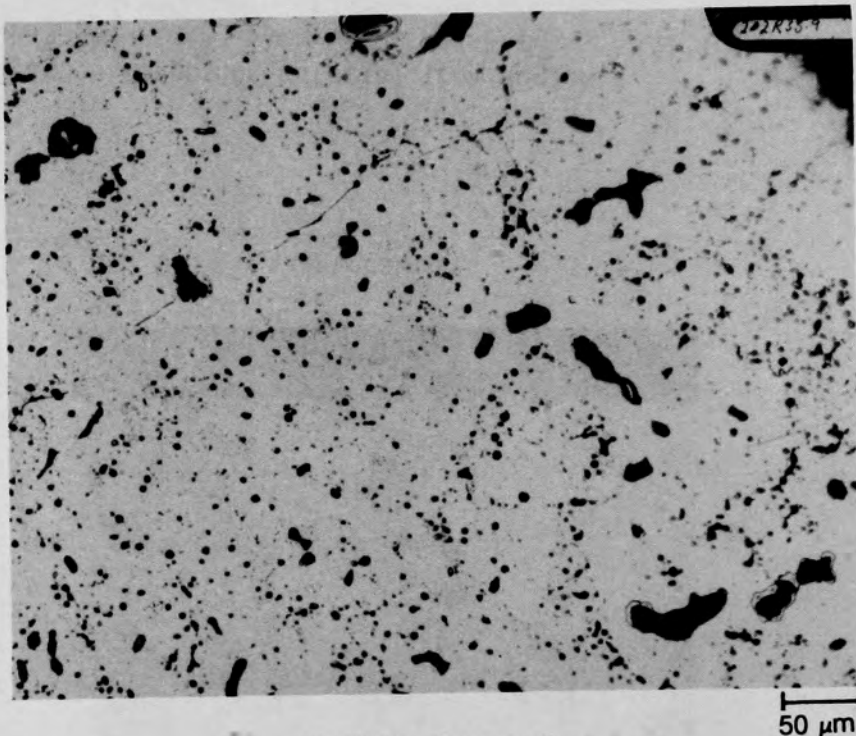
(b) Location G

Figure C-242. SEM backscattered electron images of material from Region 1
of Particle 10A (E9, 74 cm).

C-296



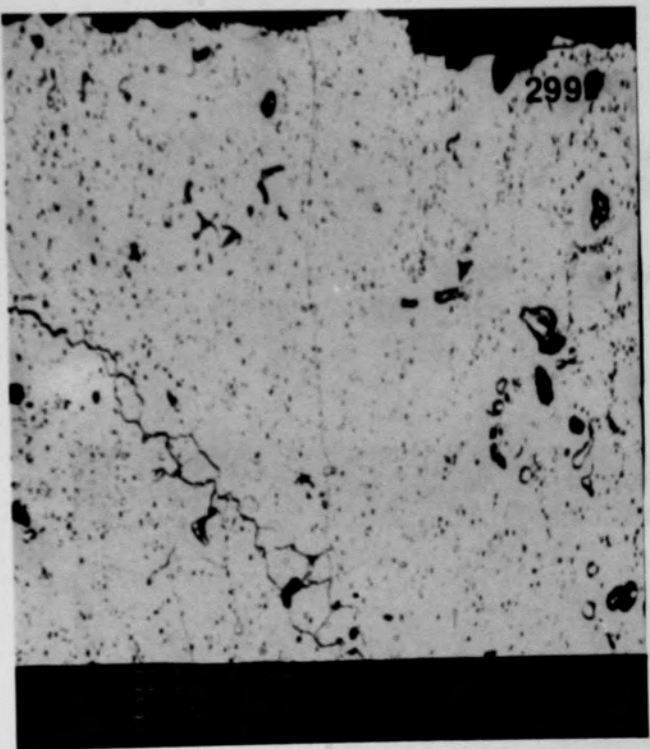
(a) SEM backscattered electron image



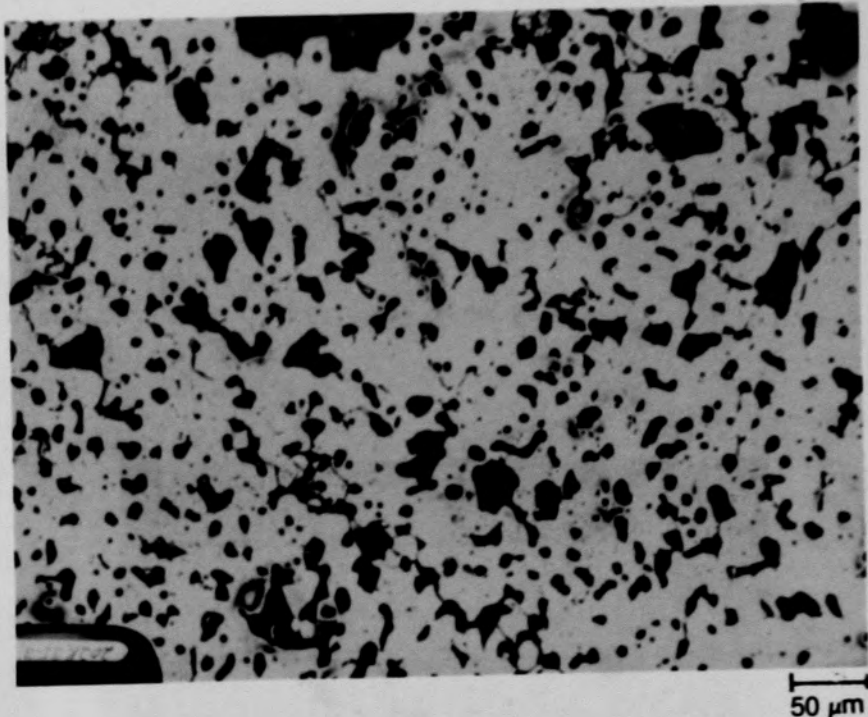
(b) Photomicrograph

Figure C-243. Photographs of material from Region 1, location B of Particle 10A (E9, 74 cm).

C-297



(a) SEM backscattered electron image
of location H



(b) Photomicrograph of location I

Figure C-244. Photographs of material from Region 1 of Particle 10A (E9,
74 cm).

C-298

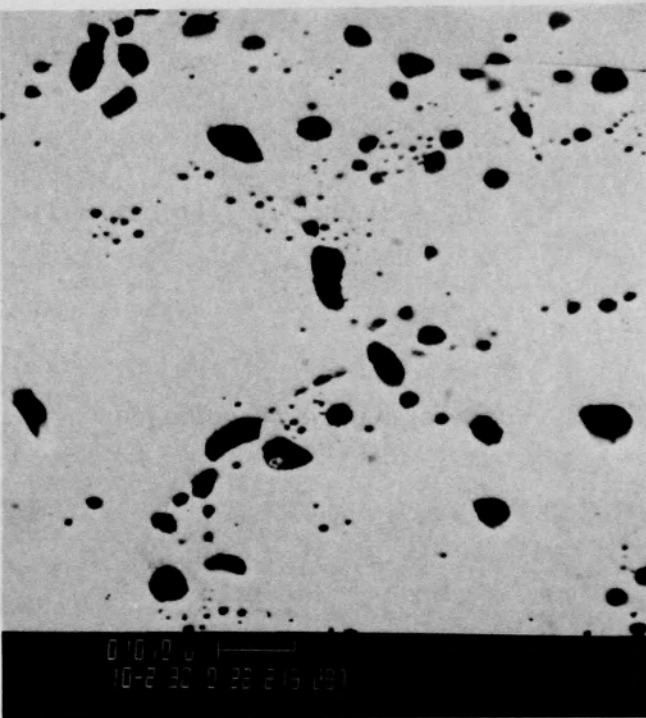
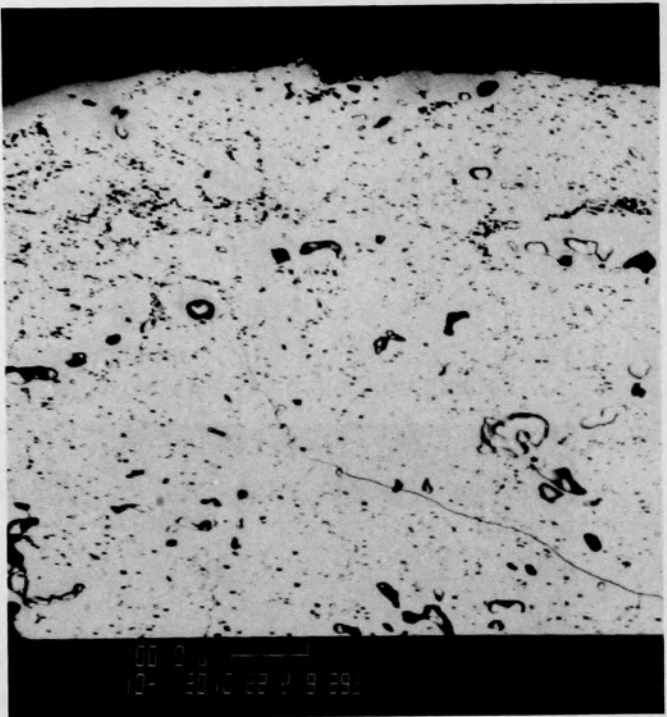
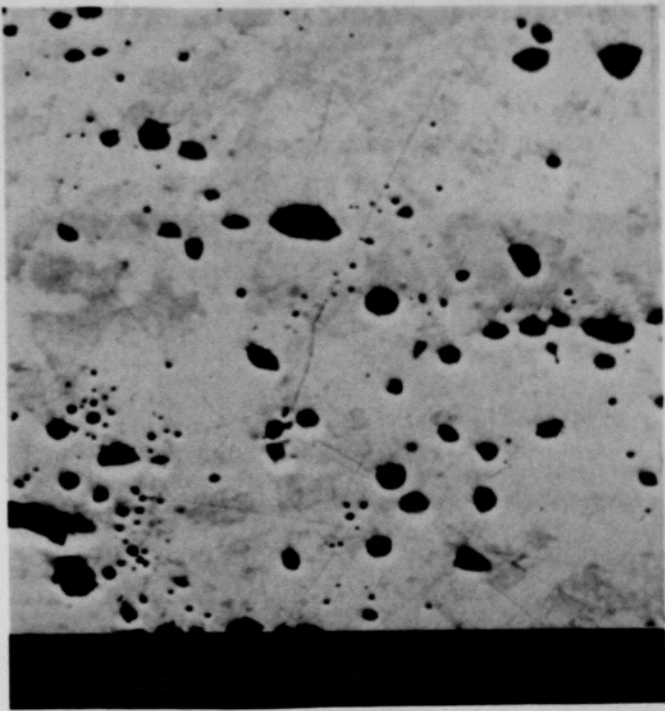
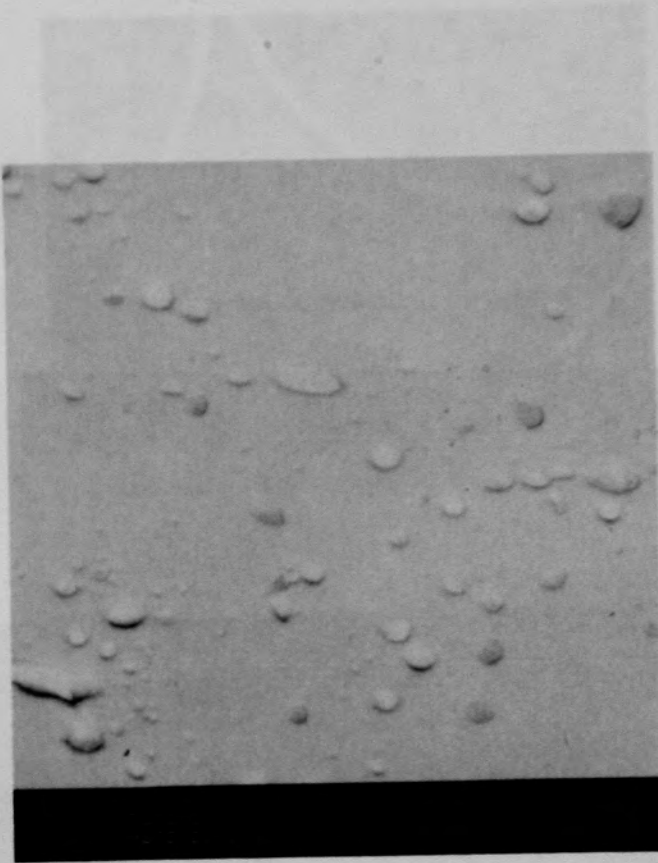


Figure C-245. SEM backscattered electron image of material from Region 1,
location J of Particle 10A (E9, 74 cm).



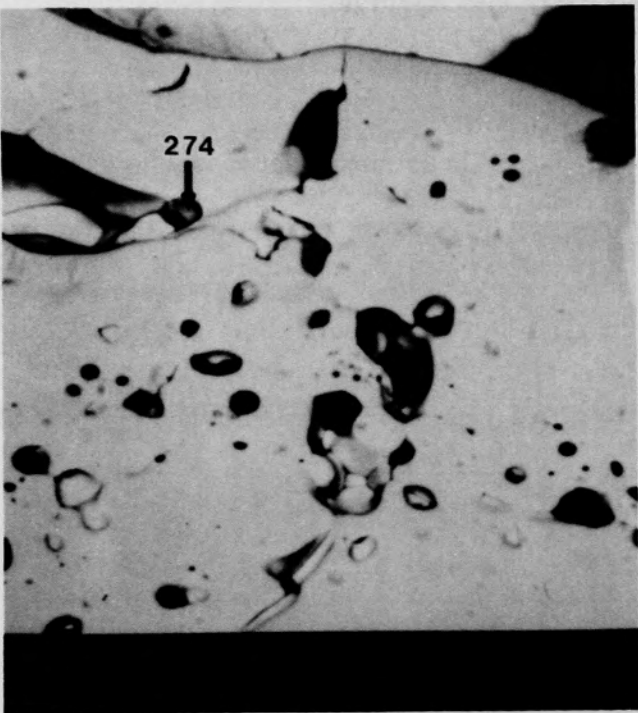
(a) SEM secondary electron image



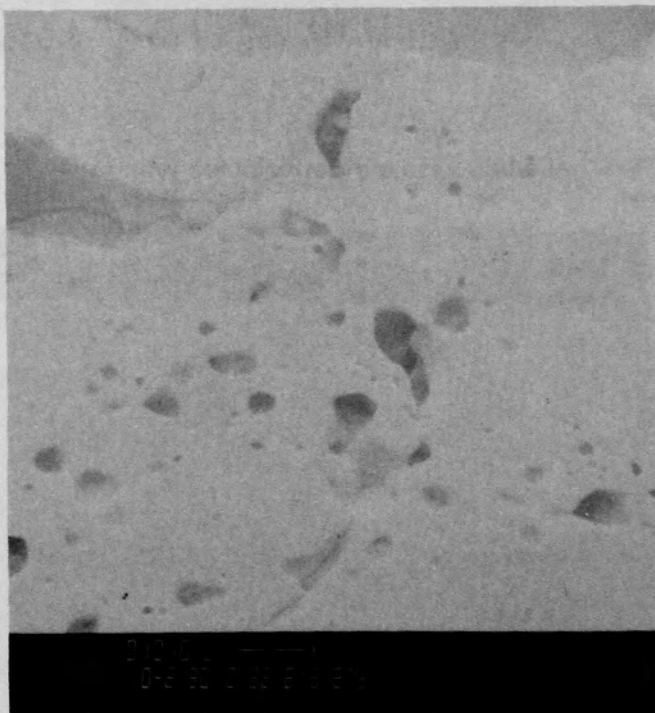
(b) SEM backscattered electron image

Figure C-246. SEM electron images of material from Region 1, location K of Particle 10A (E9, 74 cm).

C-300



(a) SEM backscattered electron image

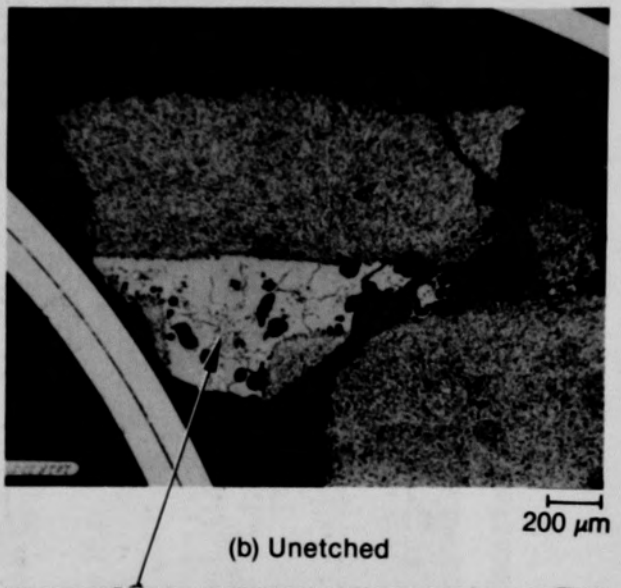


(b) SEM secondary electron image

Figure C-247. Photomicrographs of Particle 10A (E9, 74 cm).



(a) Unetched



(b) Unetched



(c) Fuel etched

Figure C-248. Photomicrographs of Particle 10E (E9, 74 cm).

C-302

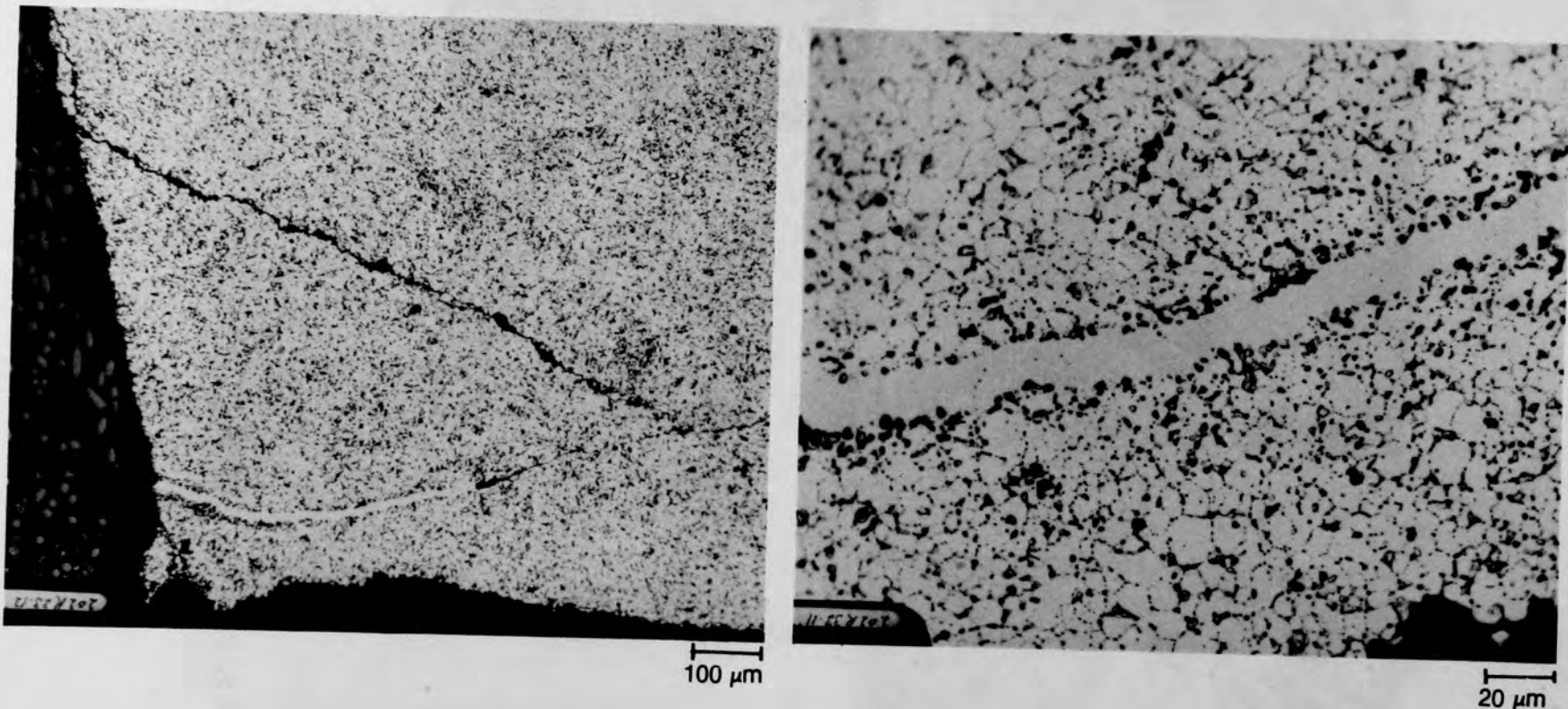
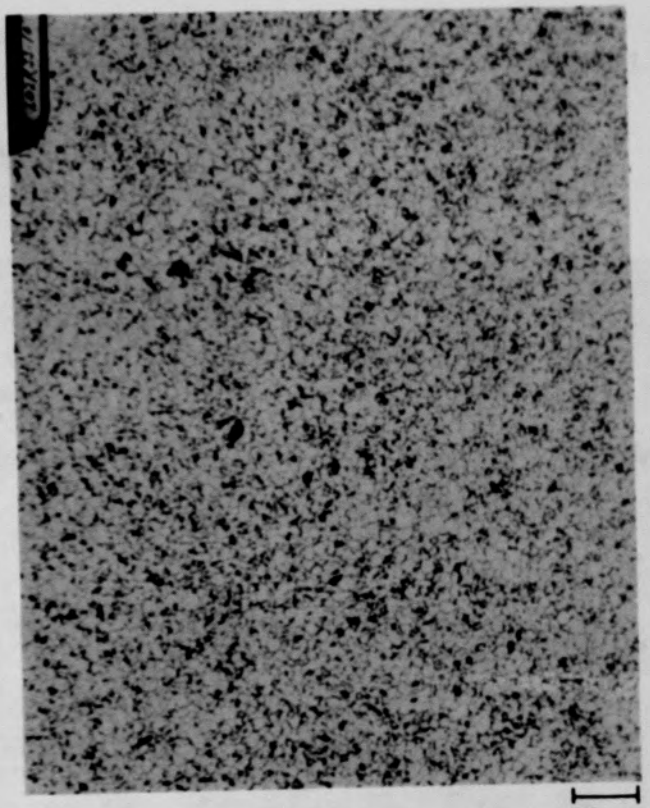
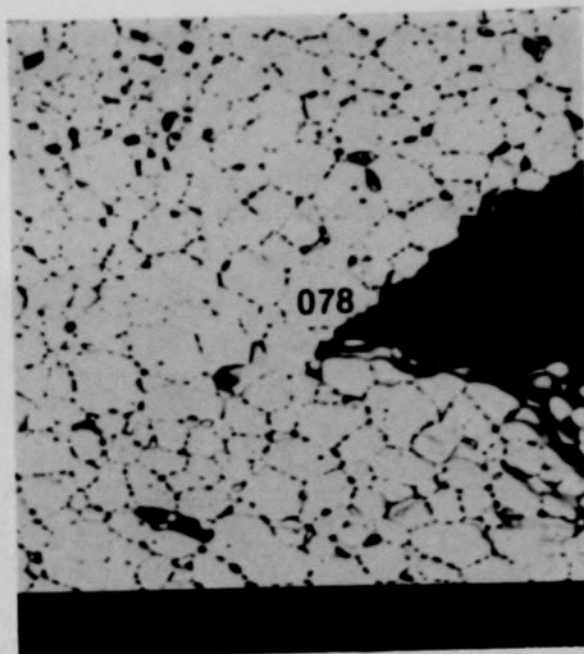


Figure C-249. Photomicrographs of material from location A of Particle 10E
(E9, 74 cm).

C-303

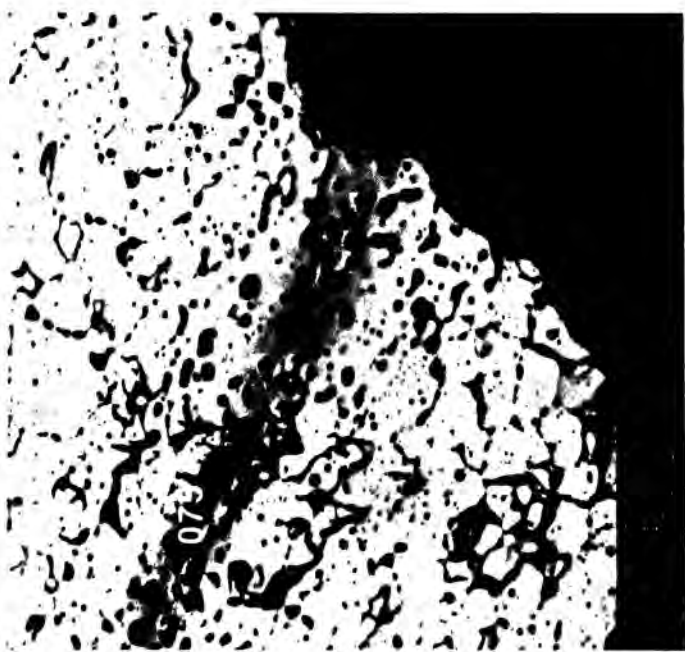


(a) Photomicrograph

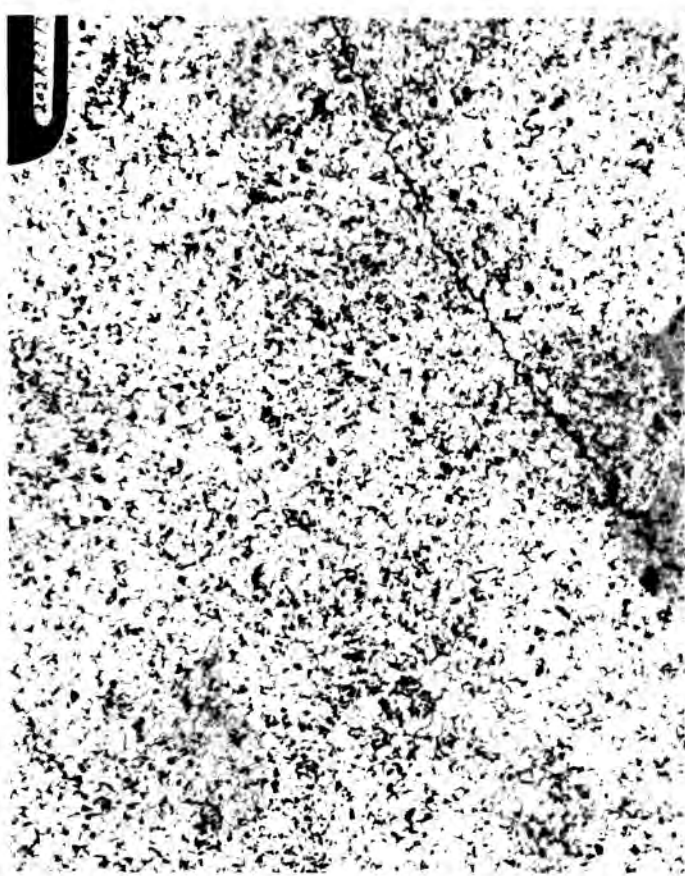


(b) SEM backscattered electron image

Figure C-250. Photographs of material from location B of Particle 10E (E9,
74 cm).



(a) SEM backscattered electron image

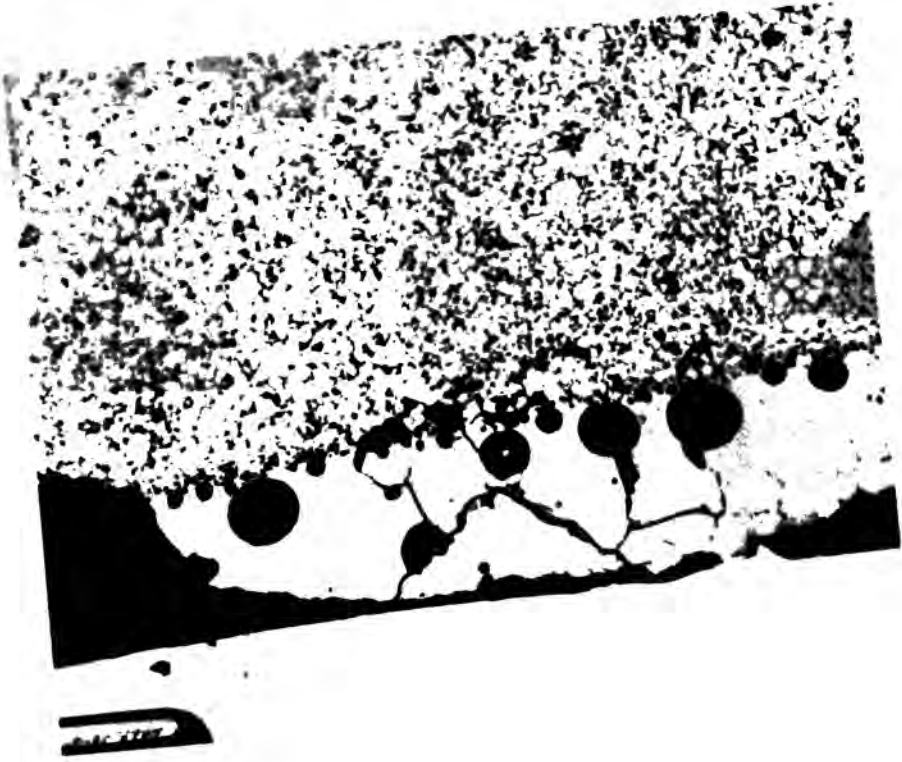


(b) Photomicrograph

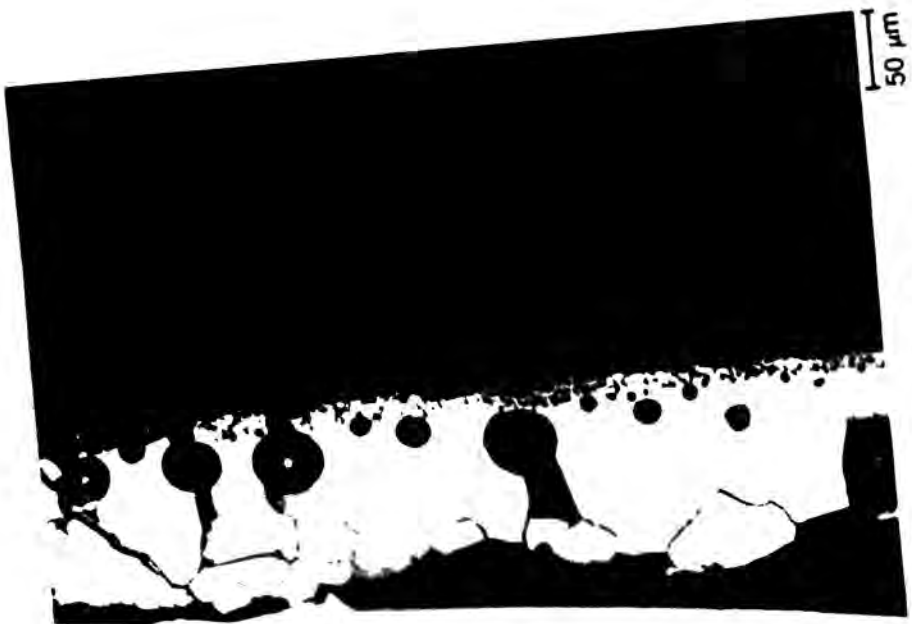
Figure C-251. Photographs of material from location C of Particle 10E (E9, 74 cm).

Figure C-252. Photomicrographs of material from location D of Particle 10E
(E9, 74 cm).

(a) Unetched



(b) Fuel etch



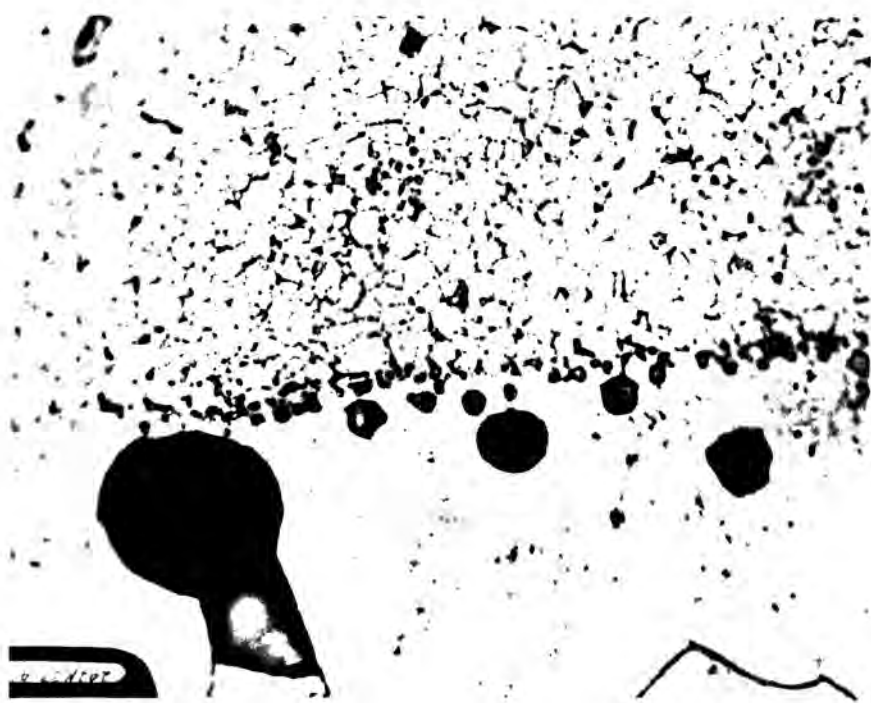


Figure C-253. Photomicrographs of material from location D of particle 10E (E9, 74 cm).



Figure C-254. Photomicrograph of material from location E of Particle 10E (E9, 74 cm).

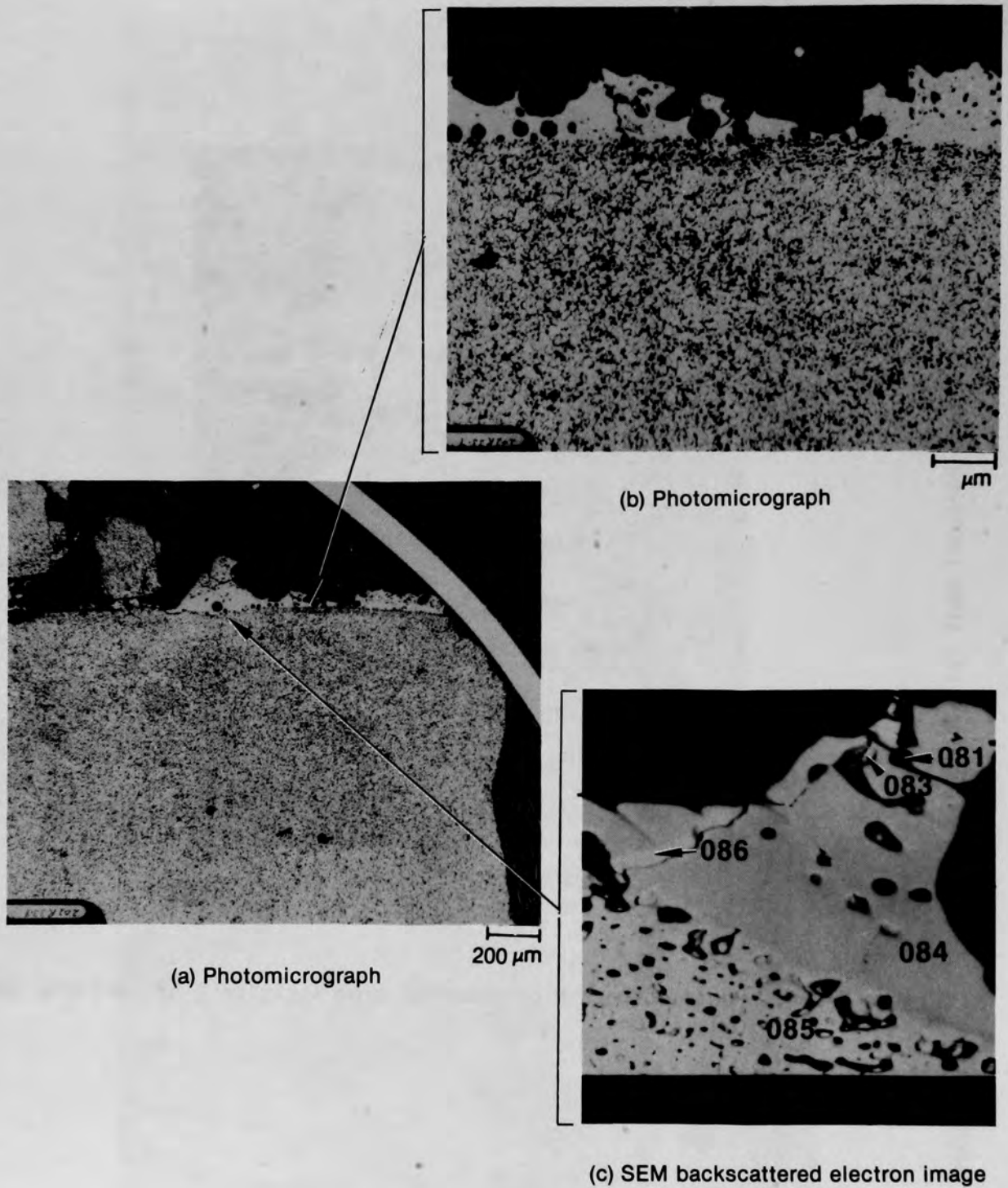
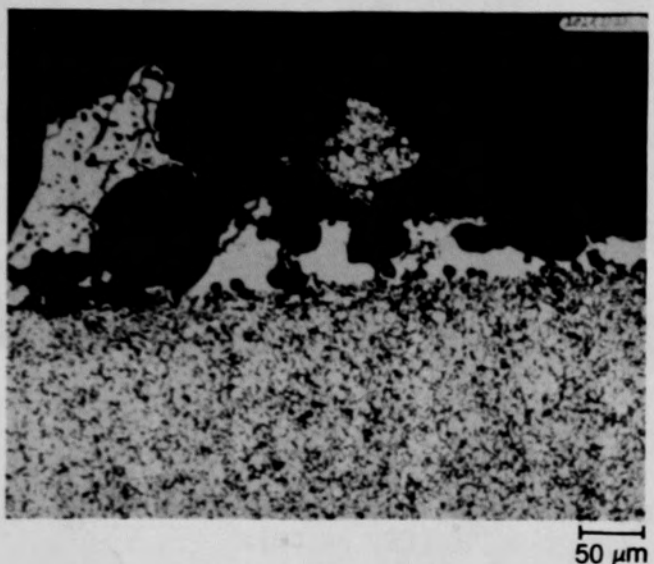
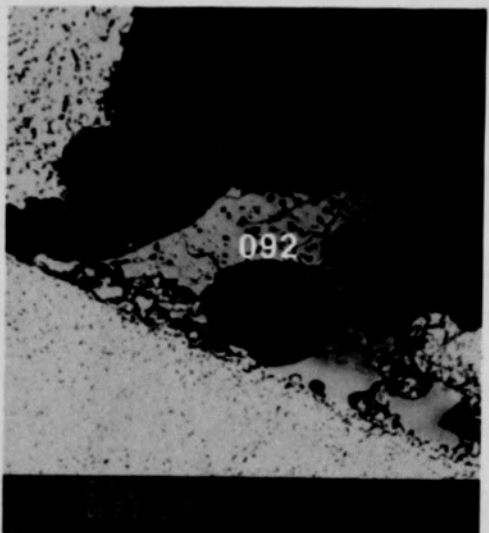


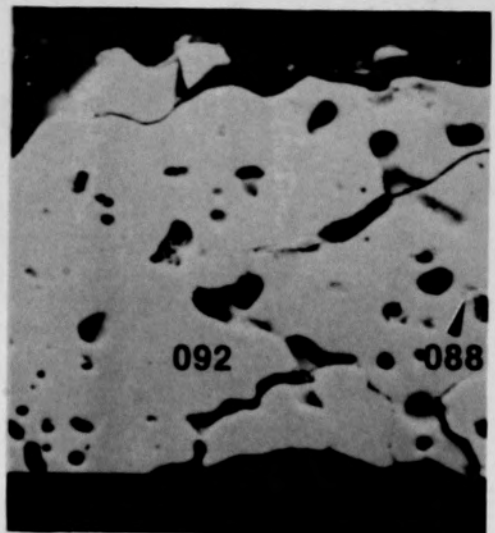
Figure C-255. Photographs of material from location F of Particle 10E (E9, 74 cm).



(a) Photomicrograph



(b) SEM backscattered electron image



(c) SEM secondary electron image

Figure C-256. Photographs of material from location F of Particle 10E (E9, 74 cm).

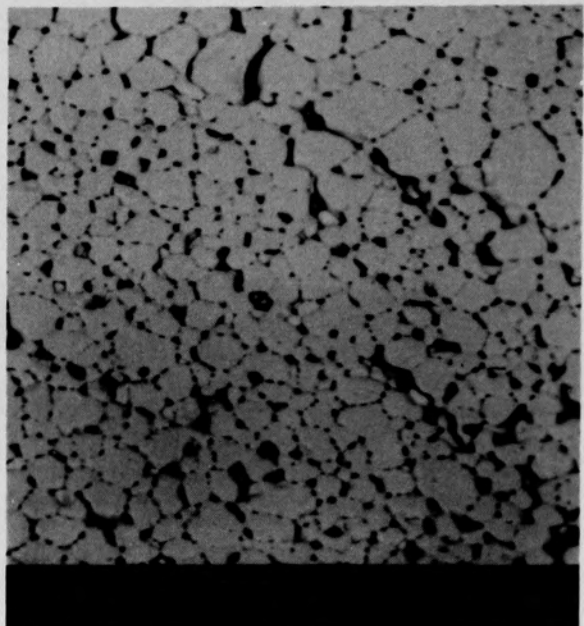
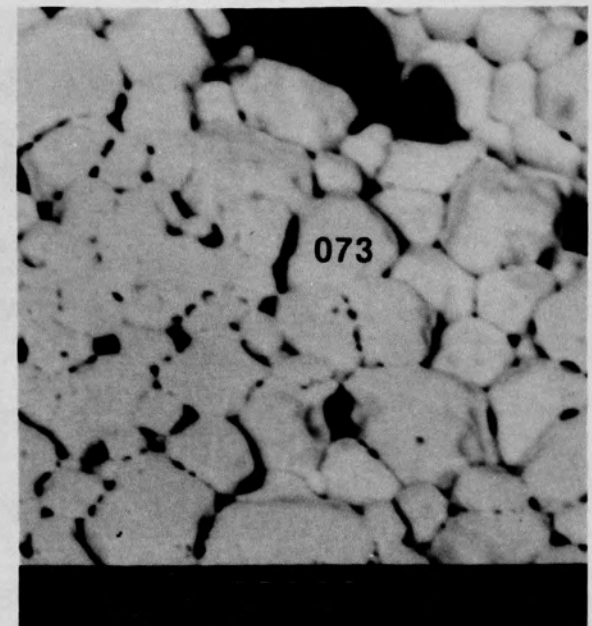
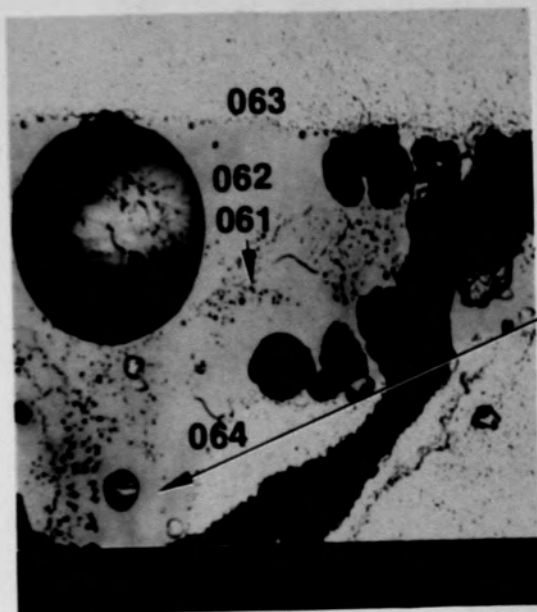


Figure C-257. SEM backscattered electron images of material from location G of Particle 10E (E9, 74 cm).

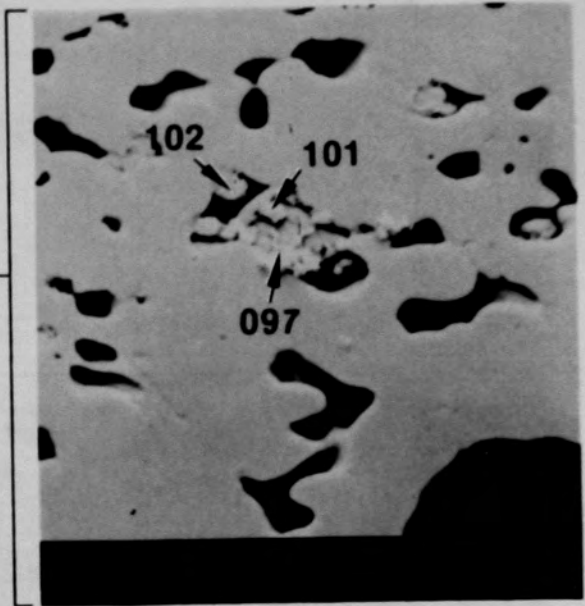
C-311



(a) SEM backscattered electron image



(b) SEM backscattered electron image



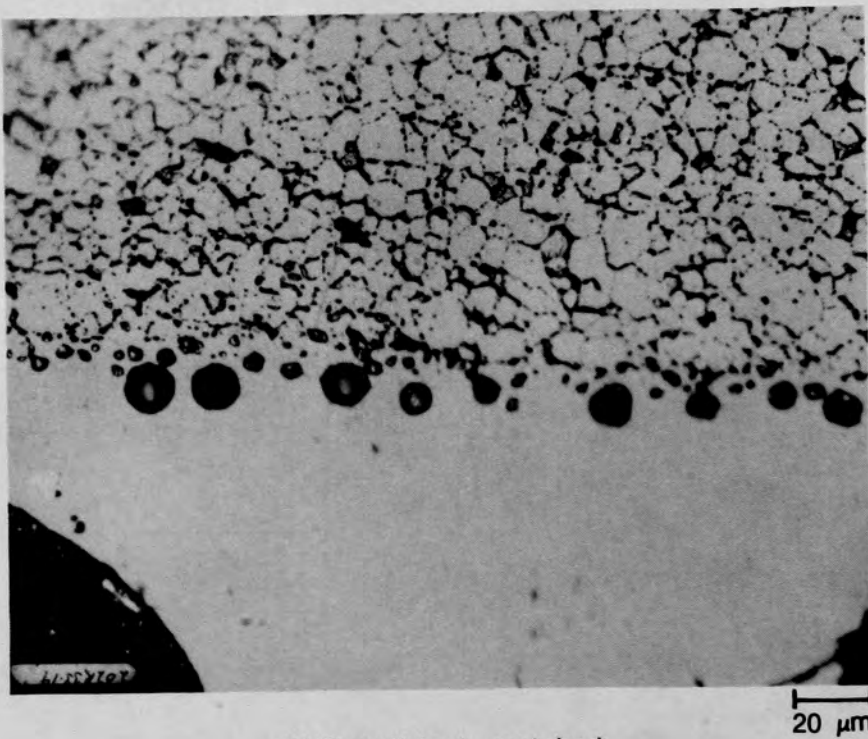
(c) SEM secondary electron image

Figure C-258. SEM electron images of material from location H of Particle 10E (E9, 74 cm).

C-312



(a) Cladding etch



(b) Repolished, unetched

Figure C-259. Photomicrographs of material from location H of Particle 10E (E9, 74 cm).

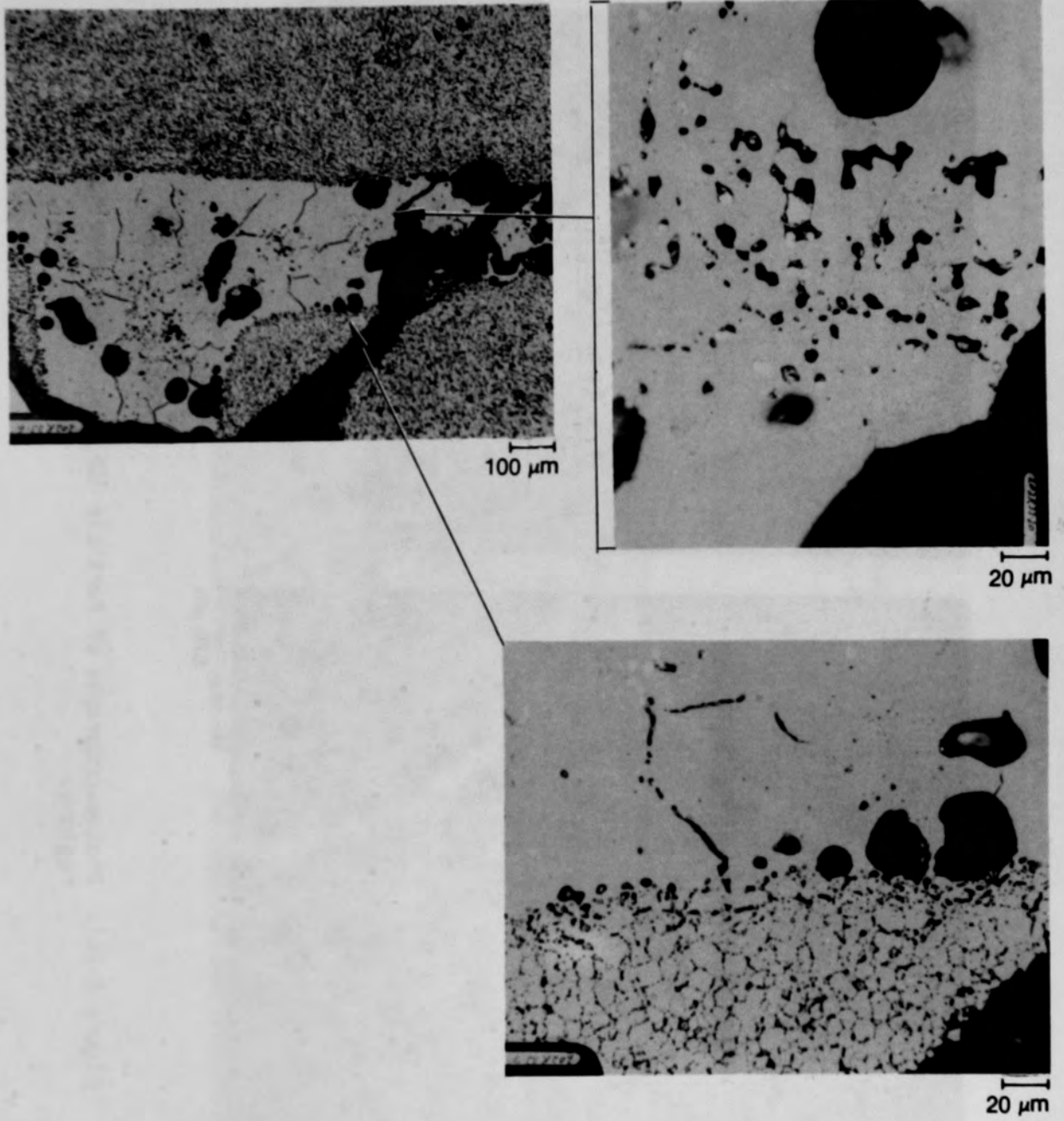


Figure C-260. Photomicrographs of material from location H of Particle 10E (E9, 74 cm).

C-314

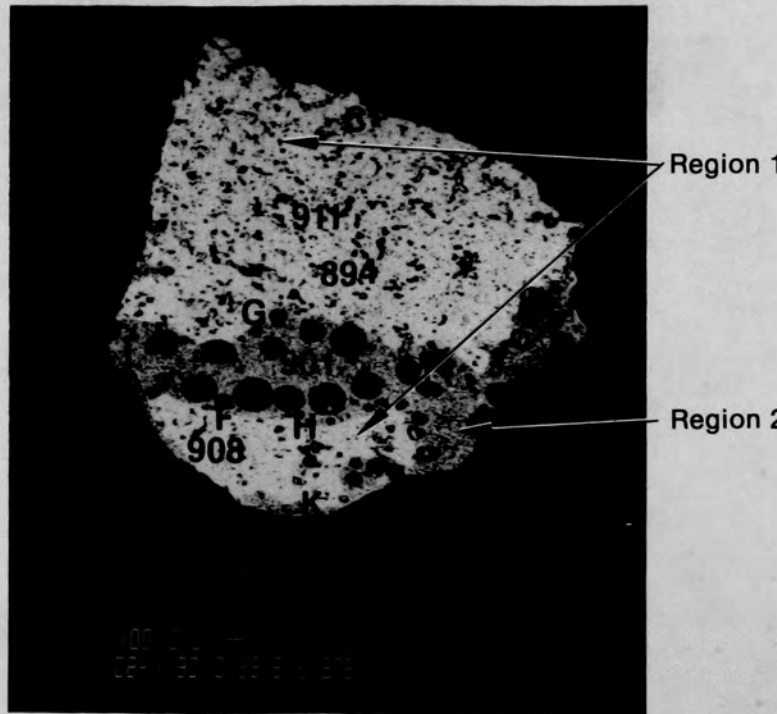
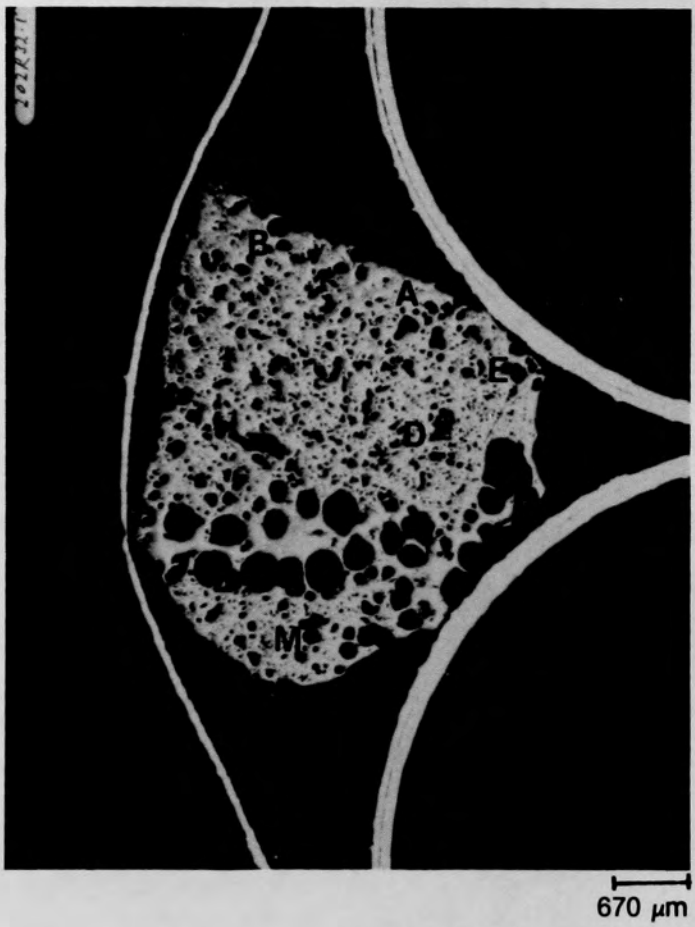
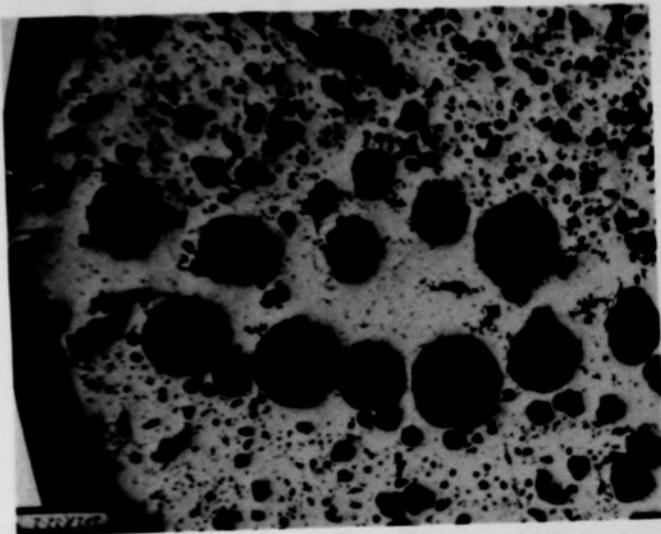
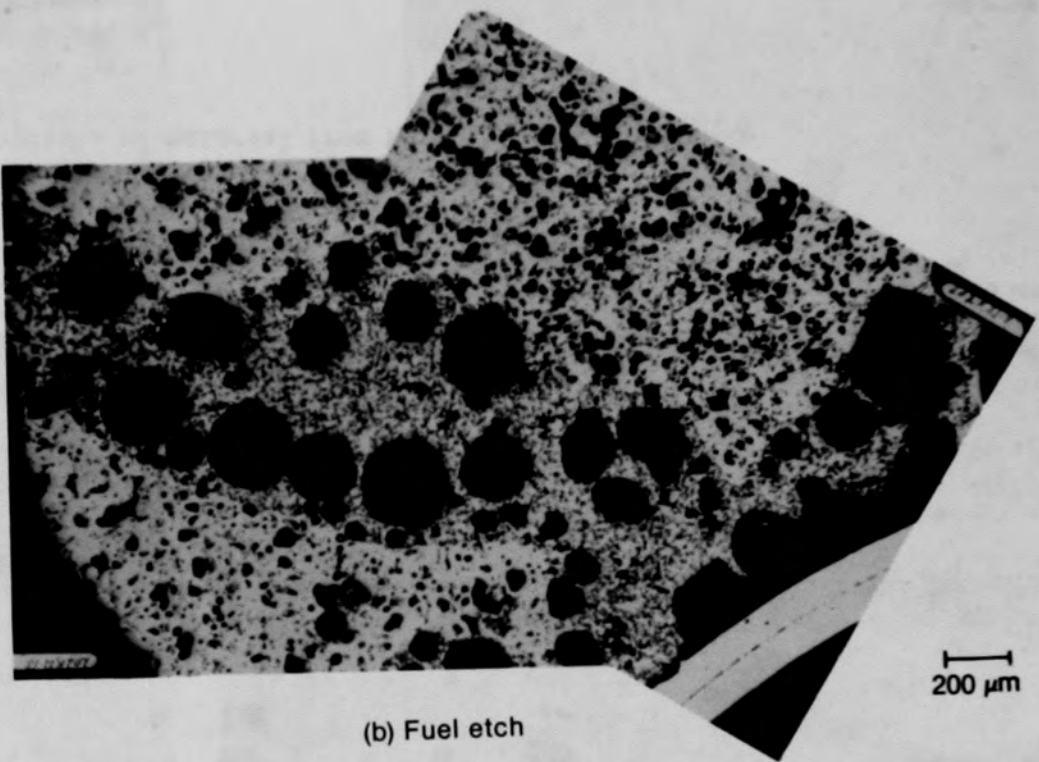


Figure C-261. Photomacrographs of Particle 10F (E9, 74 cm) showing two regions.

C-315



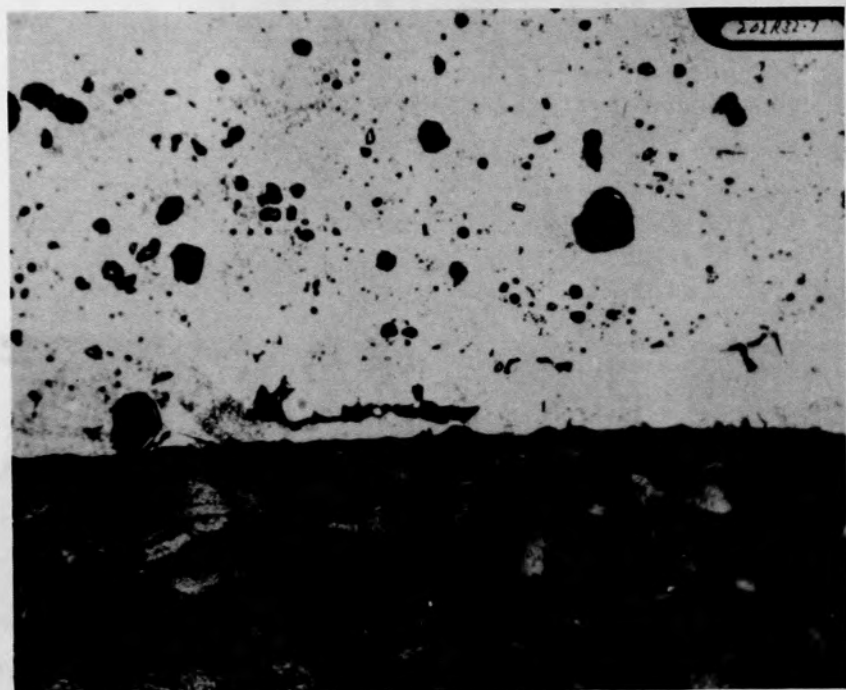
(a) Unetched



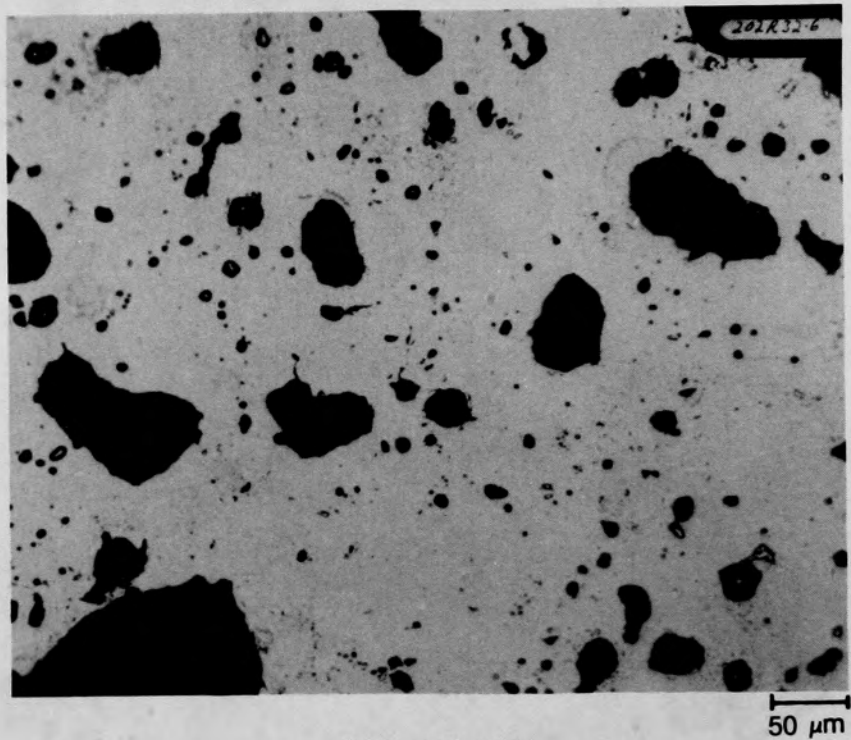
(b) Fuel etch

Figure C-262. Photomicrographs of material from Region 2 of Particle 10F
(E9, 74 cm) showing effects of etch.

C-316



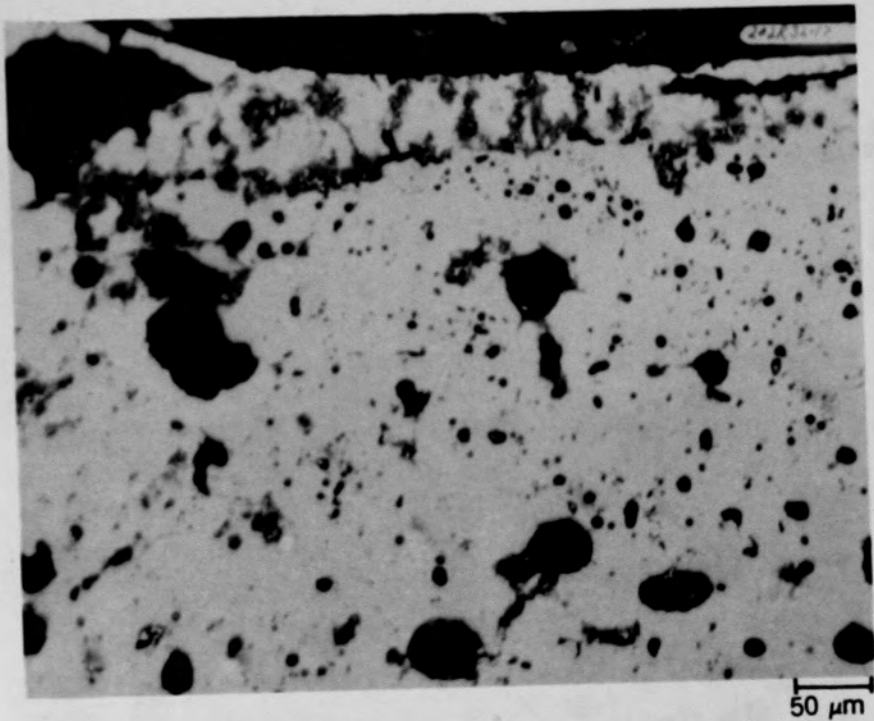
(a) Location A



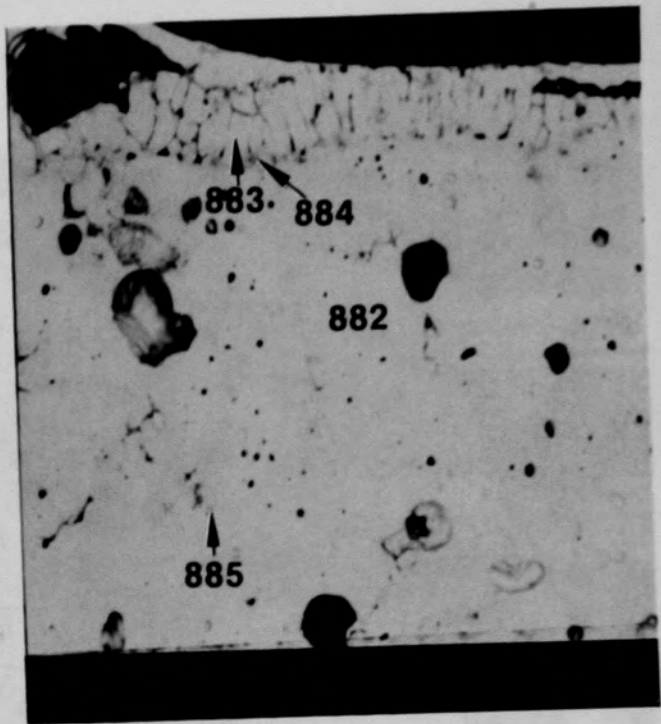
(b) Location B

Figure C-263. Photomicrographs of material from Region 1 of Particle 10F (E9, 74 cm).

C-317



(a) Photomicrograph



(b) SEM backscattered electron image

Figure C-264. Photographs of material from Region 1, location C of Particle 10F (E9, 74 cm).

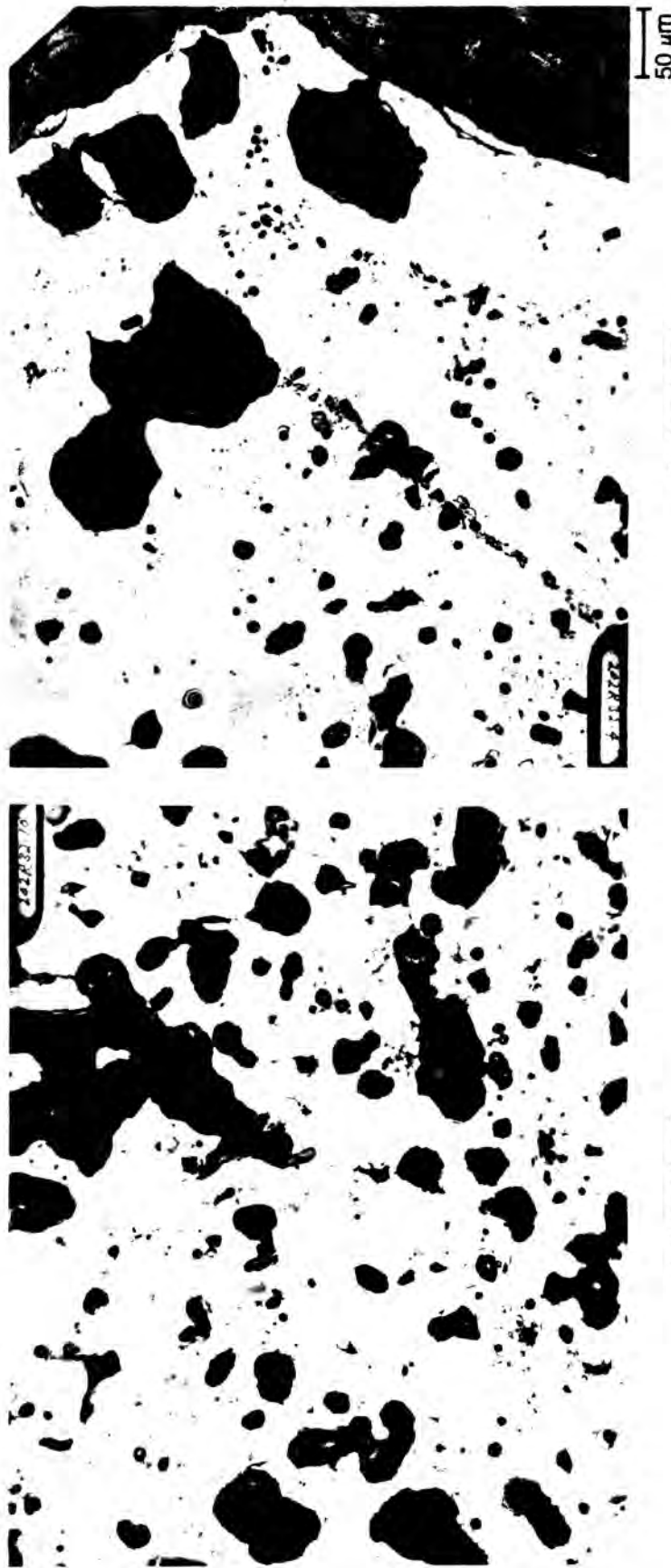
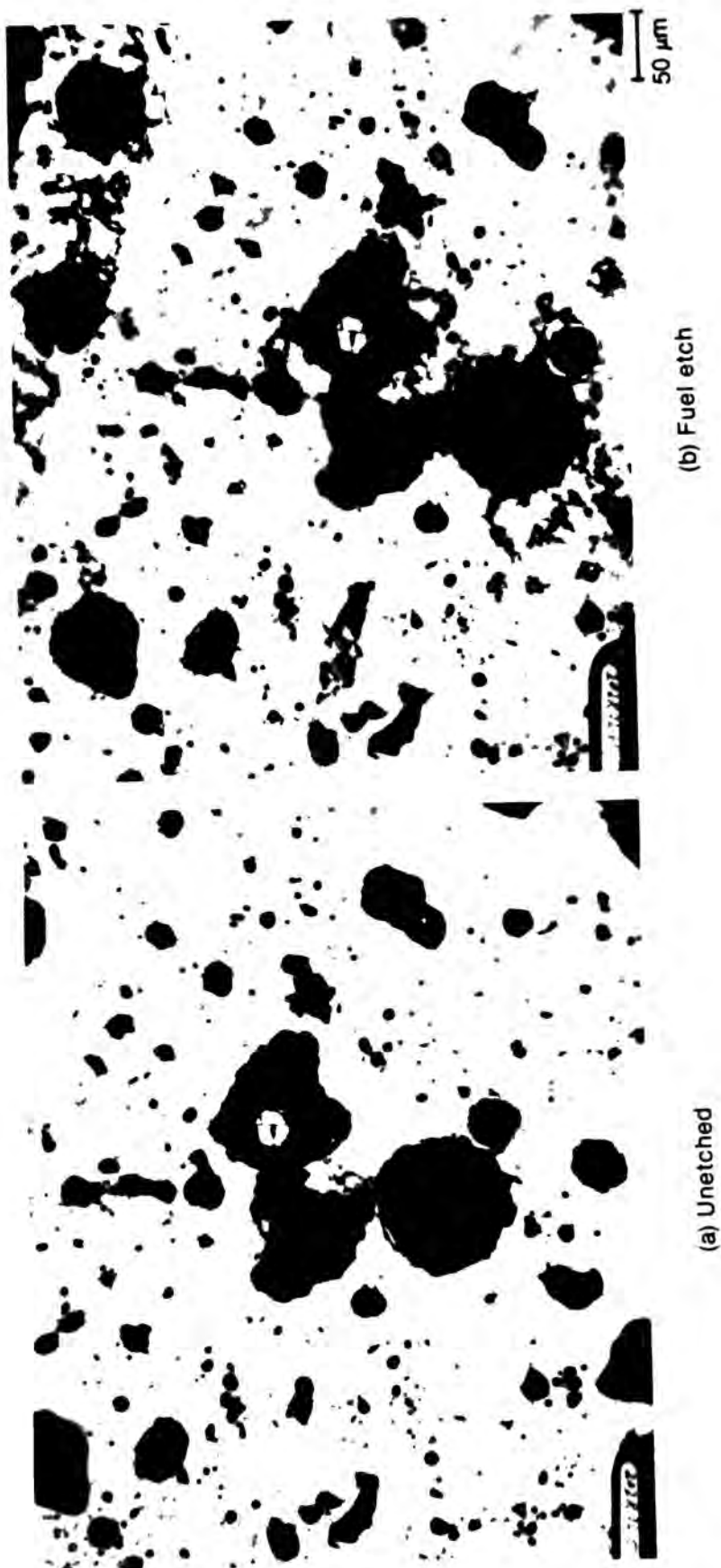
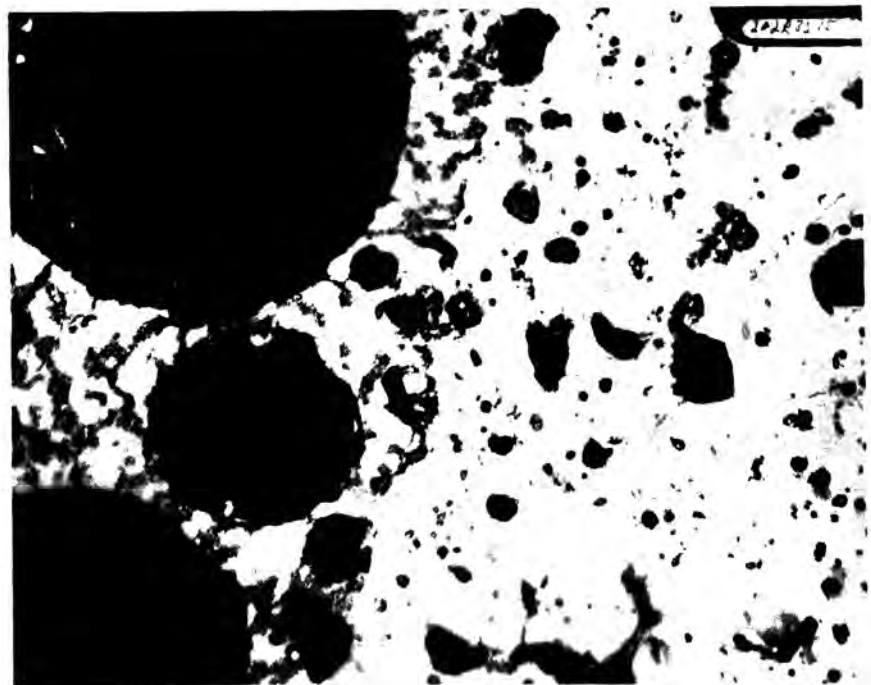


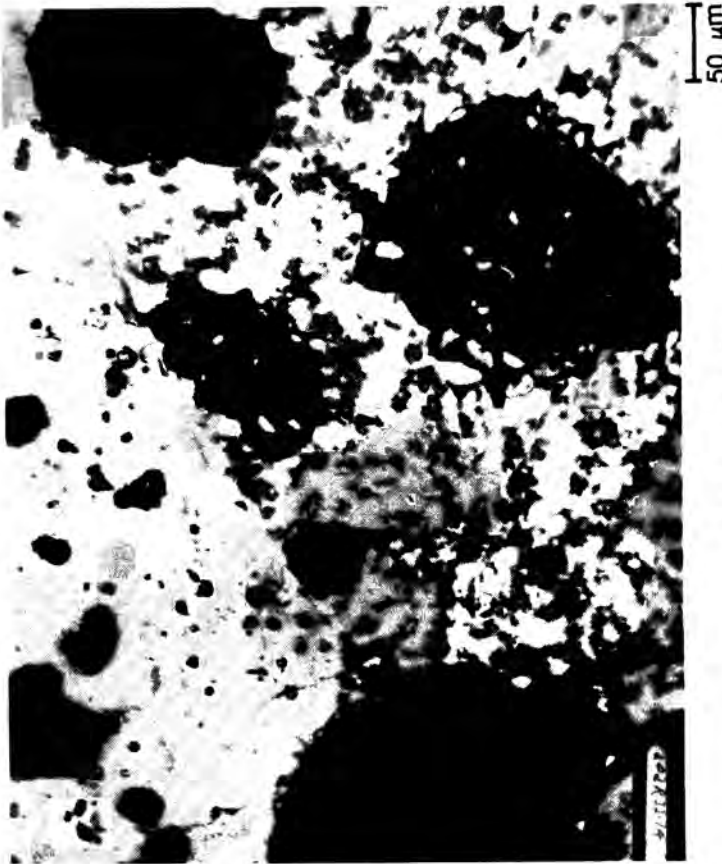
Figure C-265. Photomicrographs of material from Region 1 of Particle 10F (E9, 74 cm).

Figure C-266. Photomicrographs of material from Region 1 location M of Particle 10F (E9, 74 cm).





(a) Location F



(b) Location G

Figure C-267. Photomicrographs of etched material from Region 2 of Particle 10F (E9, 74 cm).

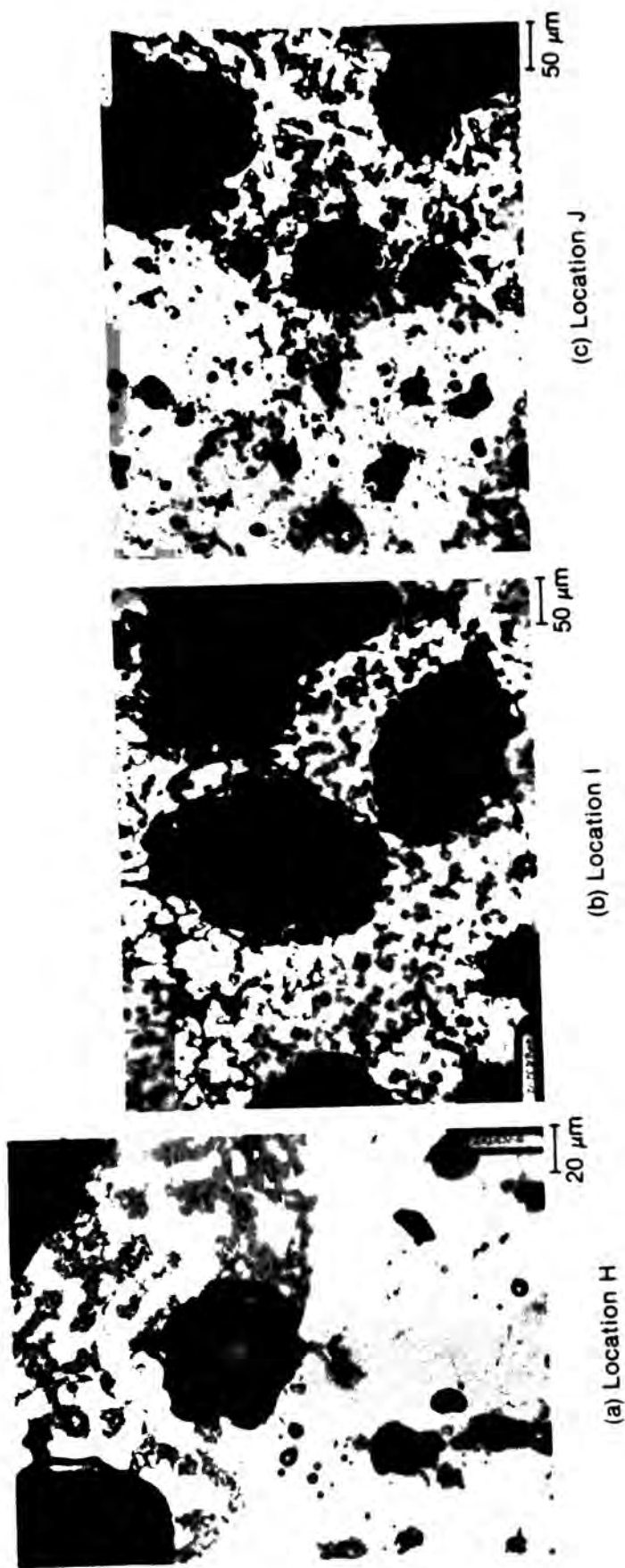


Figure C-268. Photomicrographs of etched material from Region 2 of Particle 10F (E9, 74 cm).

C-322

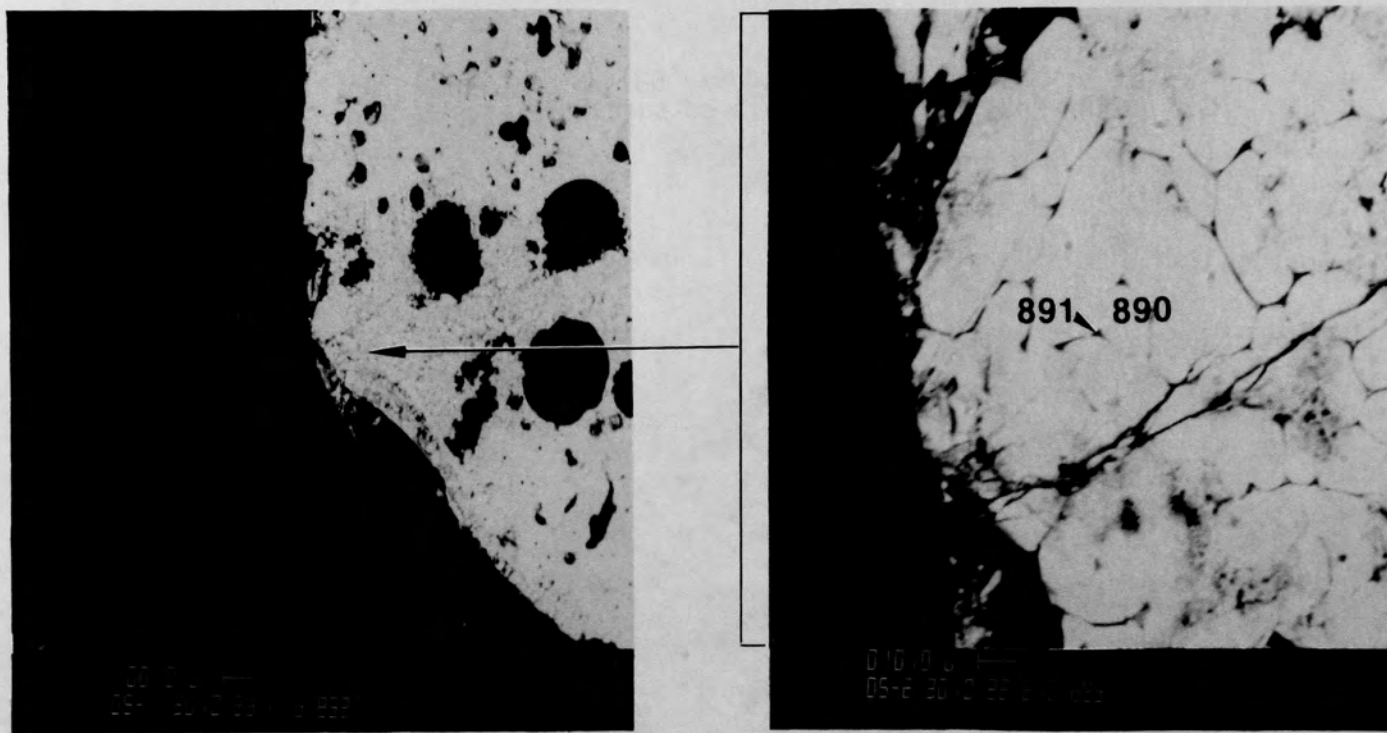
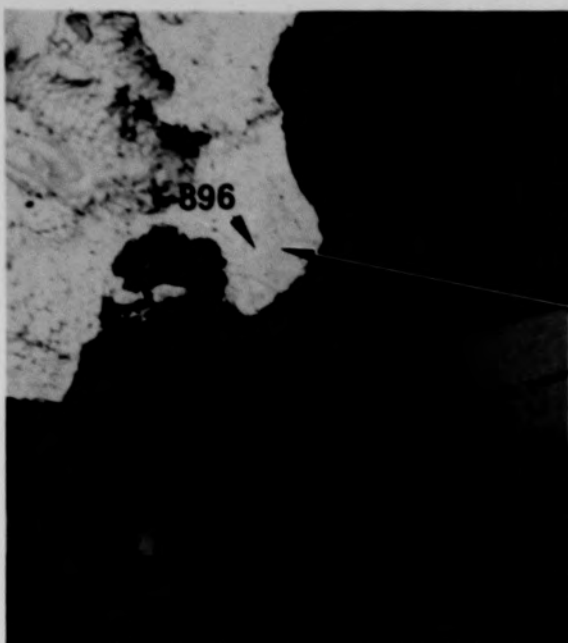
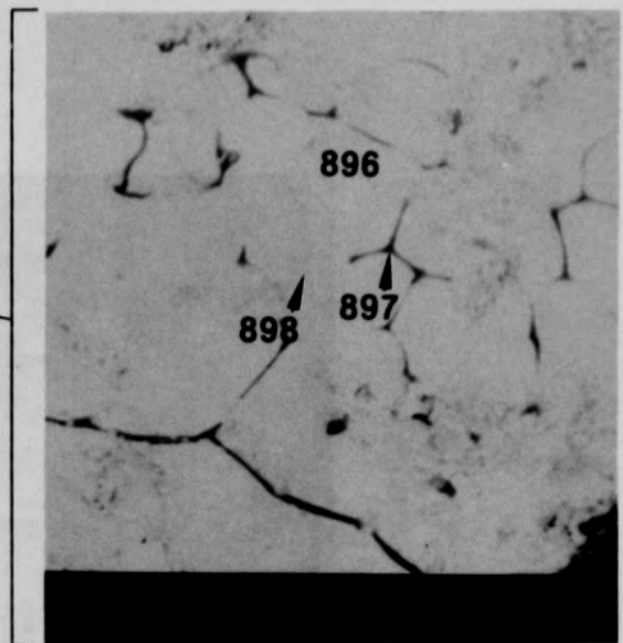


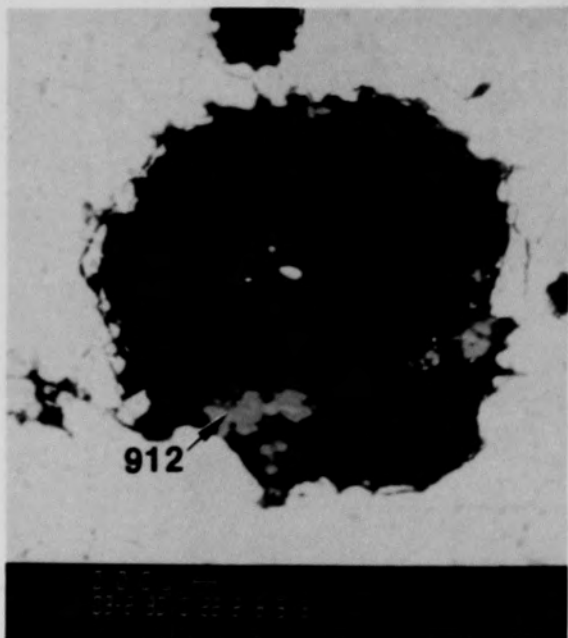
Figure C-269. SEM backscattered electron images of Region 2, location L of Particle 10F (E9, 74 cm).



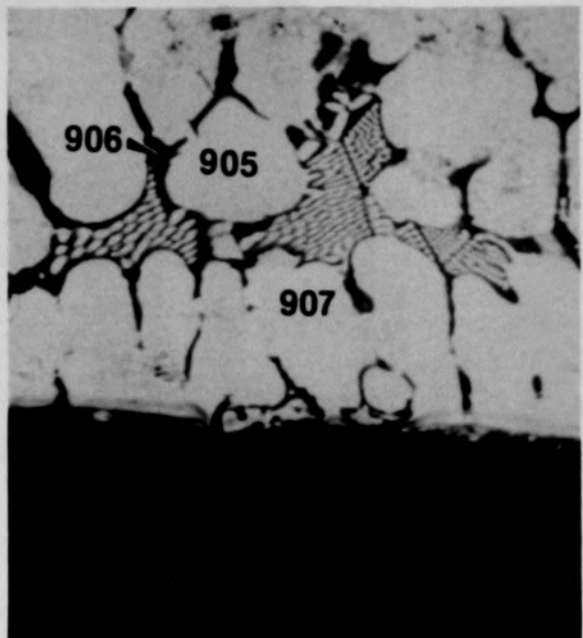
(a) Region 2, location J



(b) Higher magnification of (a)



(c) Region 2, location I

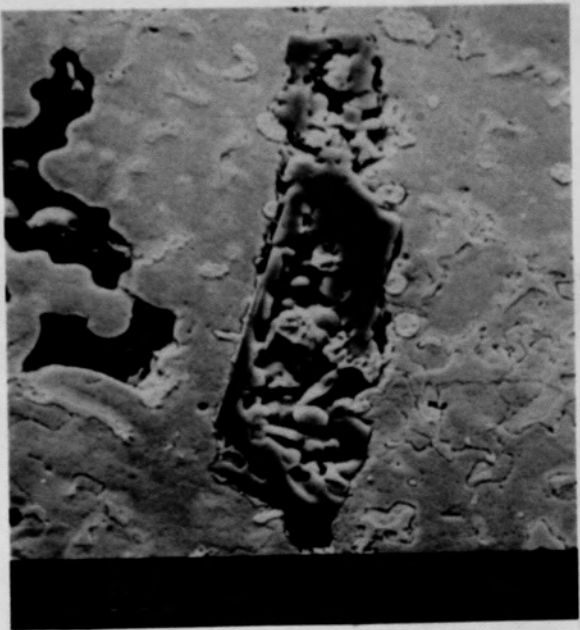


(d) Region I, location K

Figure C-270. SEM backscattered electron images of Particle 10F (E9, 74 cm).



Figure C-271. Photomacrograph of Particle 11B (E9, 94 cm).



(a) SEM secondary electron image



(b) SEM backscattered electron image

Figure C-272. SEM electron images of material from location A of Particle 11B (E9, 94 cm).

C-326

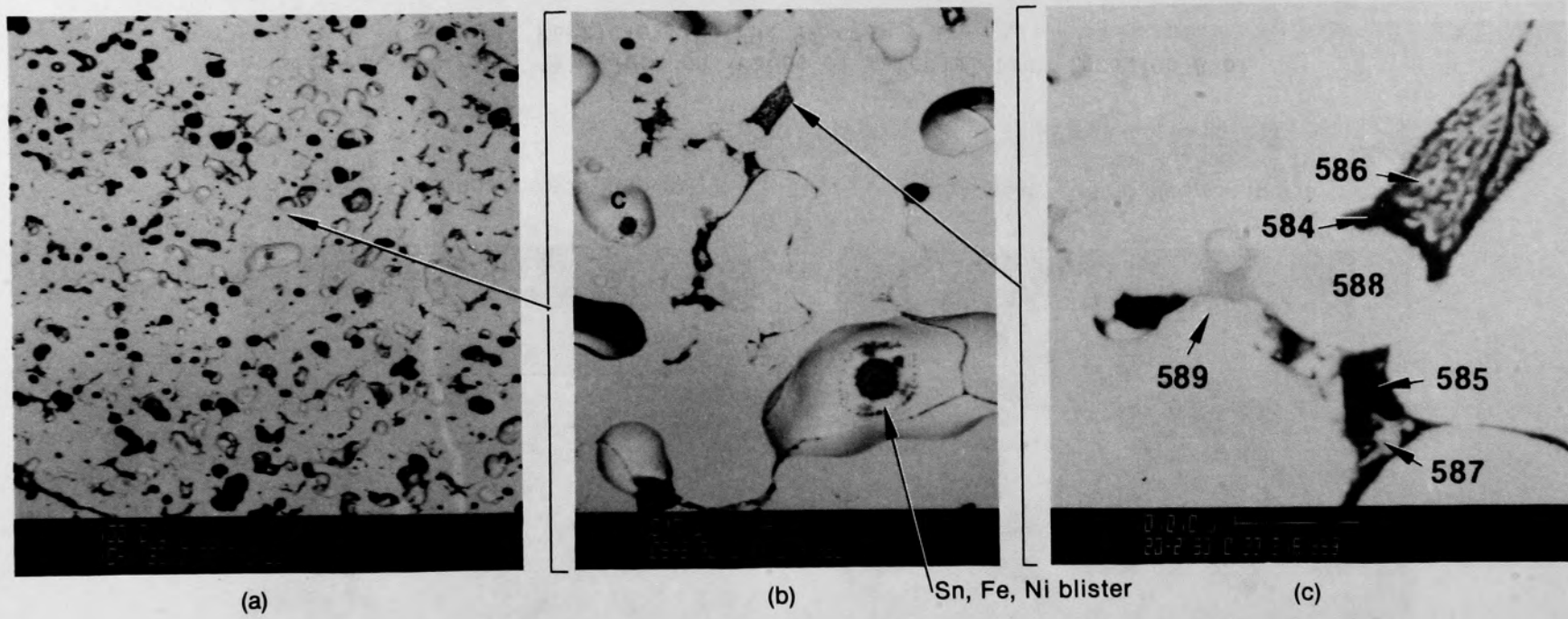


Figure C-273. SEM backscattered electron images of material from location B of Particle 11B (E9, 94 cm) showing inclusions in the ceramic material.

C-327

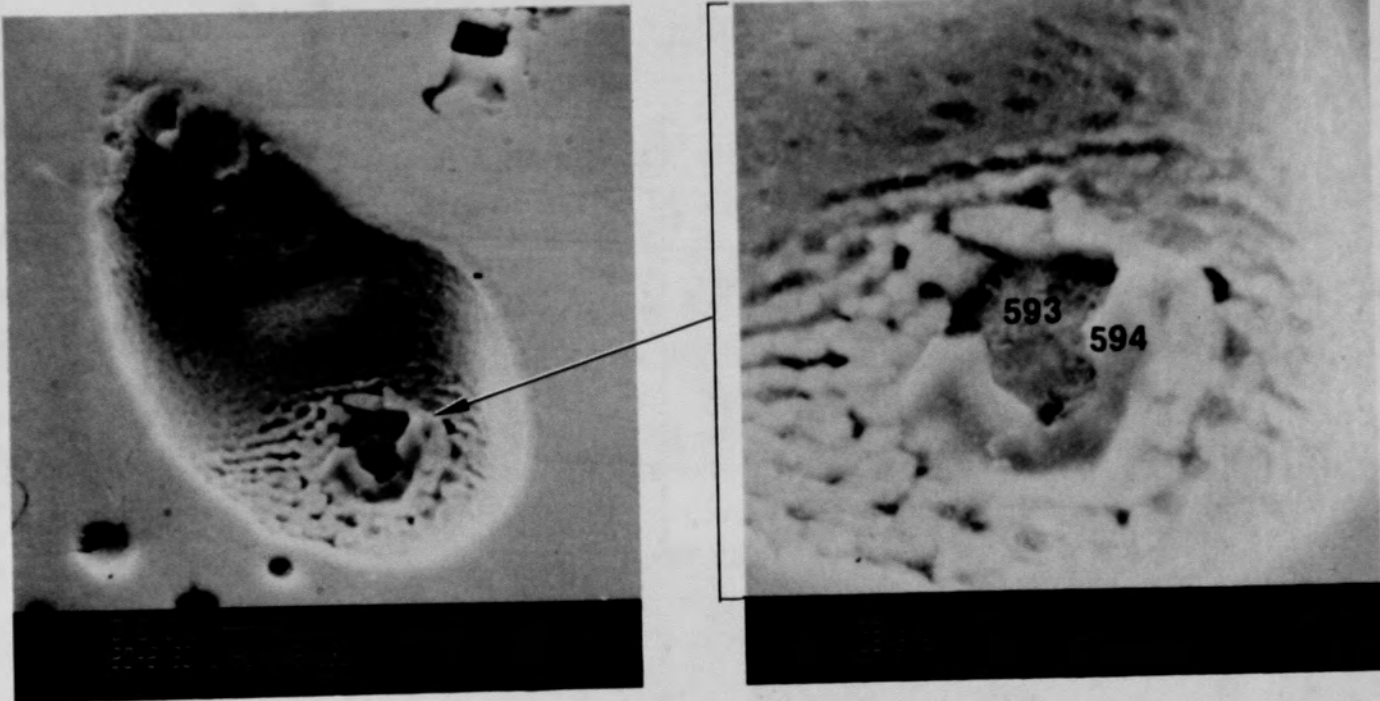
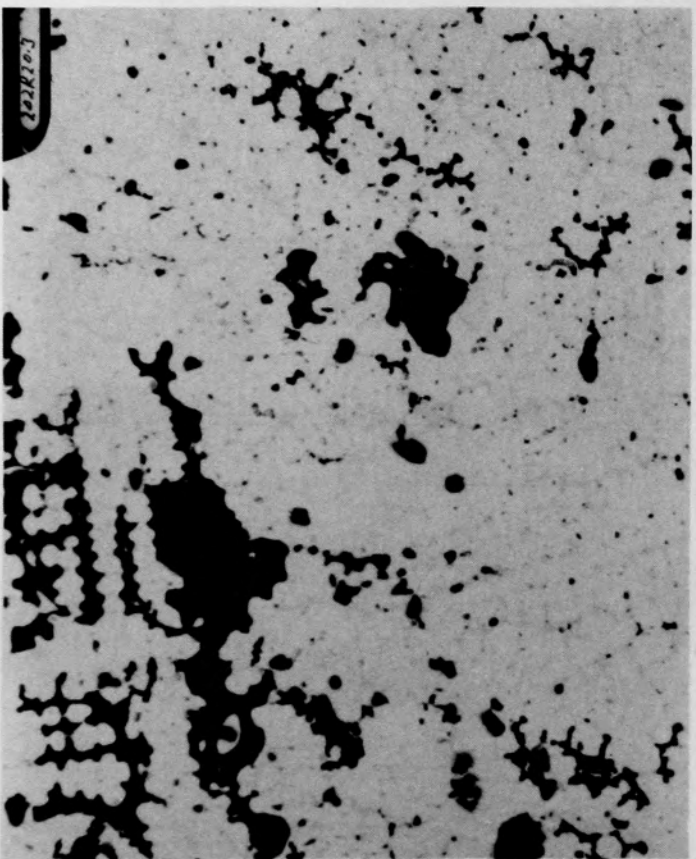
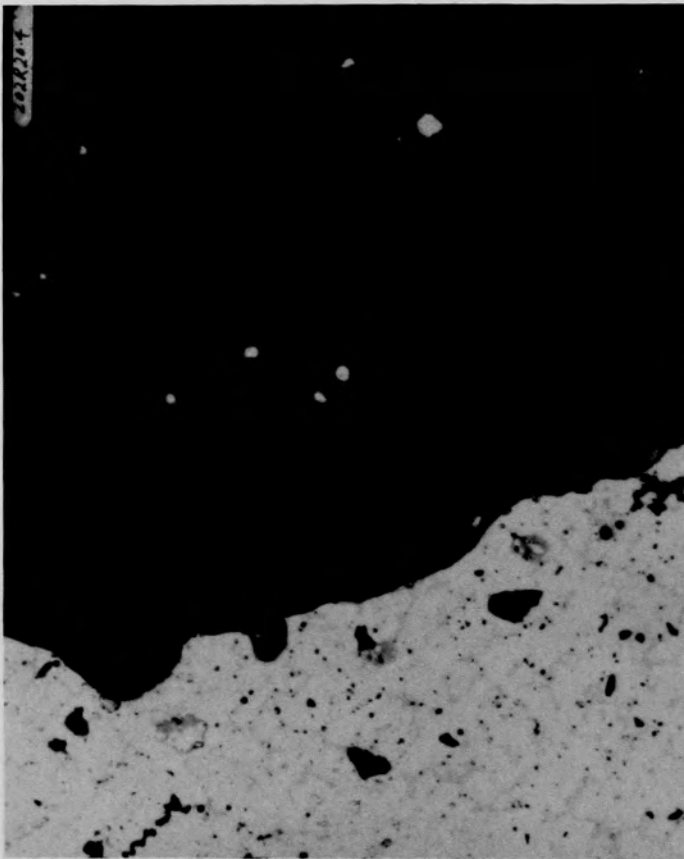


Figure C-274. SEM secondary electron images of material from location C,
Figure C-273b, of Particle 11B (E9, 94 cm).

C-328



(a) Location D



(b) Location E

Figure C-275. Photomicrographs of material from metallic and interface regions of Particle 11B (E9, 94 cm).

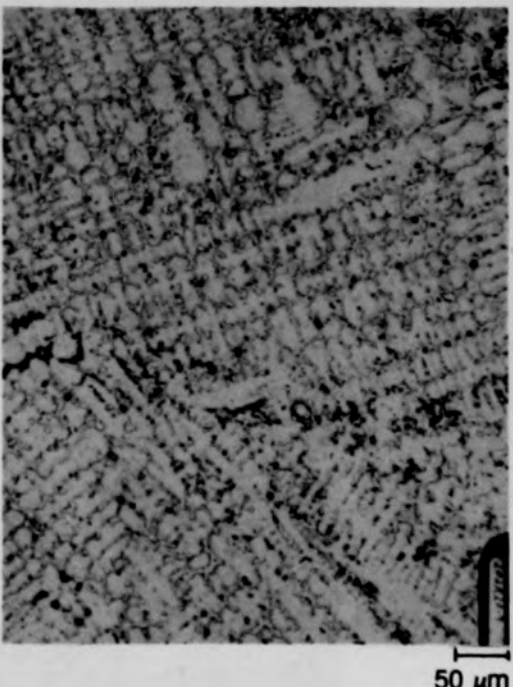
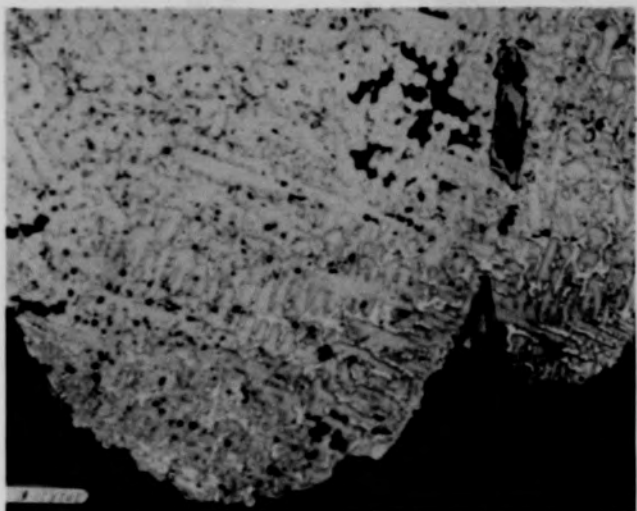
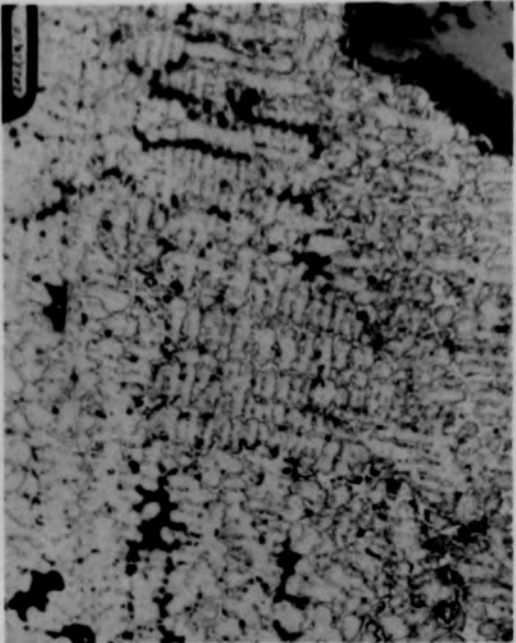
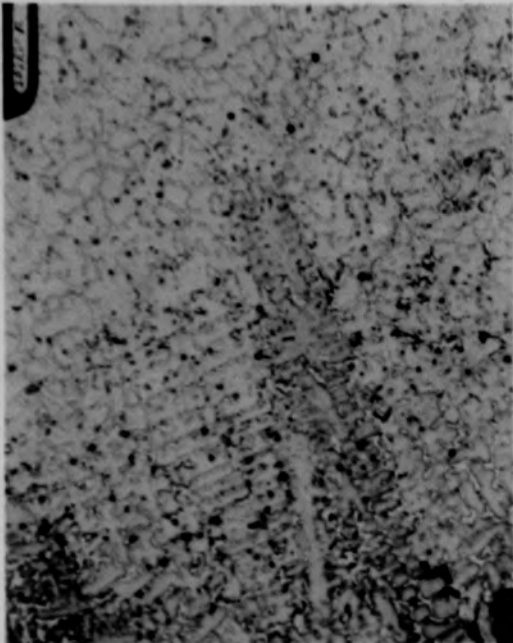


Figure C-276. Photomicrographs of Ag etched material from the metallic region of Particle 11B (E9, 94 cm).

C-330

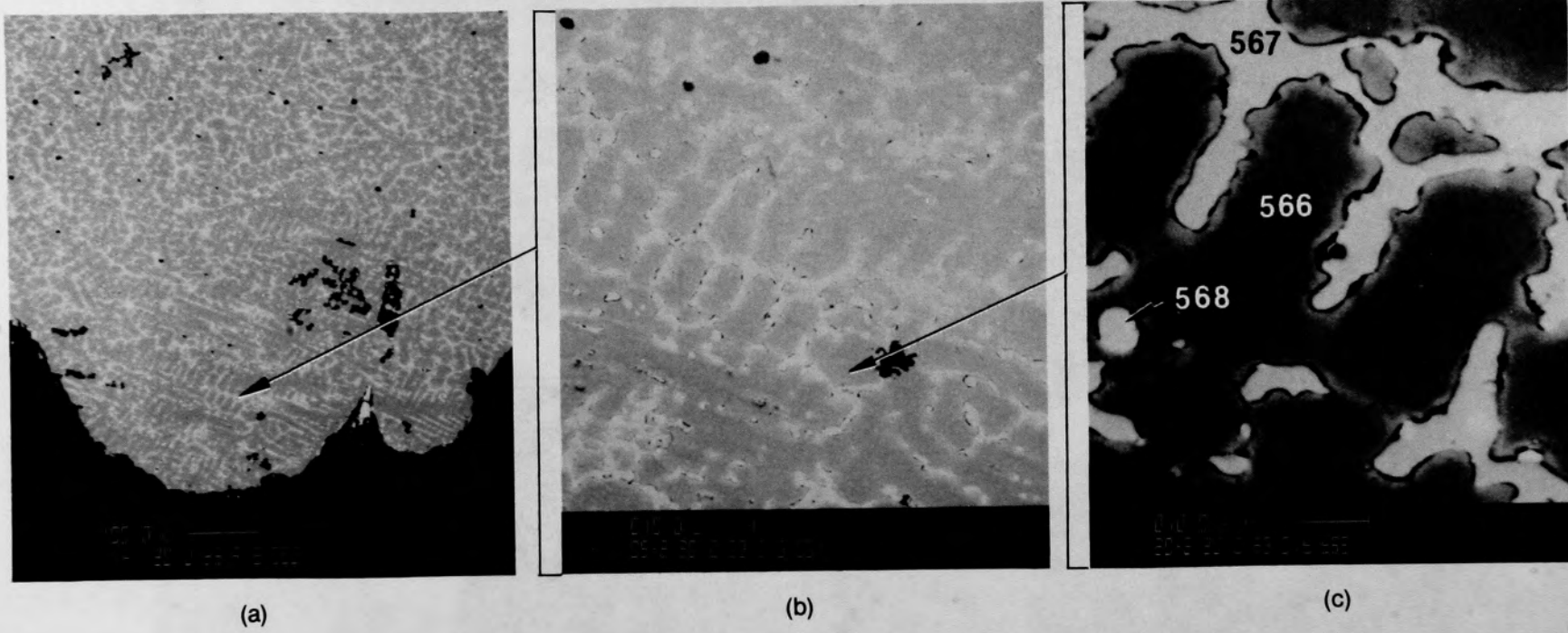


Figure C-277. SEM backscattered electron images of material from location H of Particle 11B (E9, 94 cm).



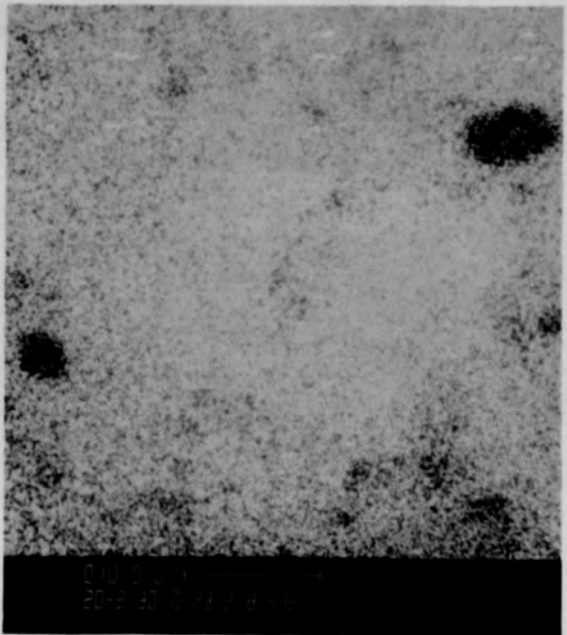
(a) Sn



(b) Ag



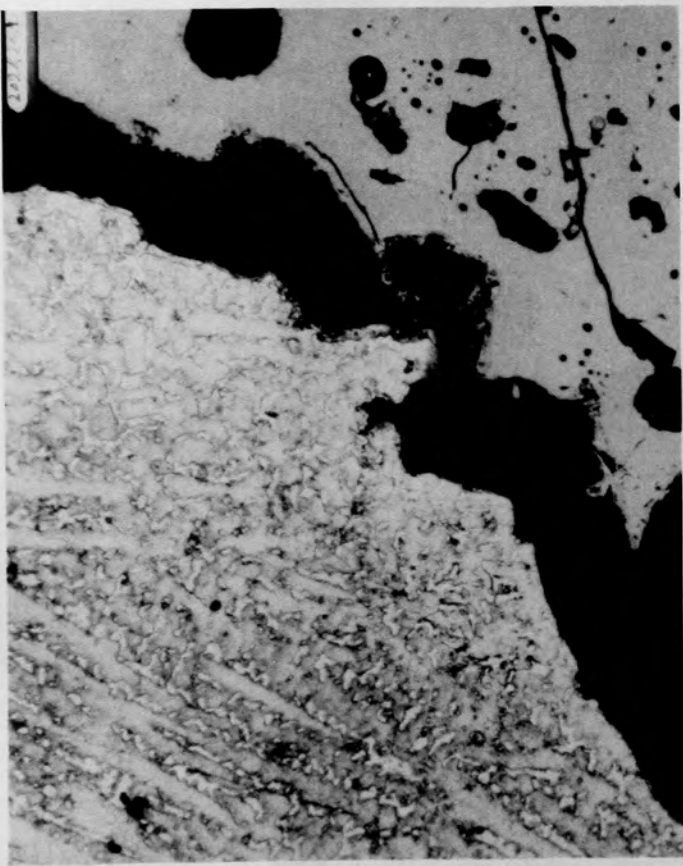
(c) Fe



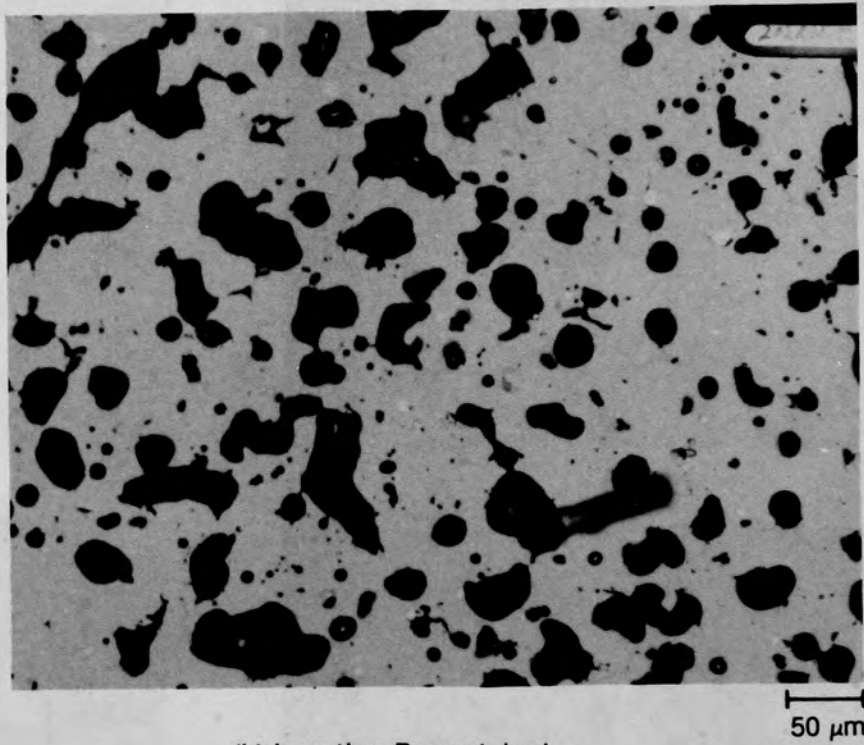
(d) Ni

Figure C-278. X-ray dot maps of material from location H, Figure C-277c, of Particle 11B (E9, 94 cm).

C-332



(a) Location F ,Ag etched



(b) Location B , unetched

Figure C-279. Photomicrographs of material from the ceramic and interface regions of Particle 11B (E9, 94 cm).

C-333

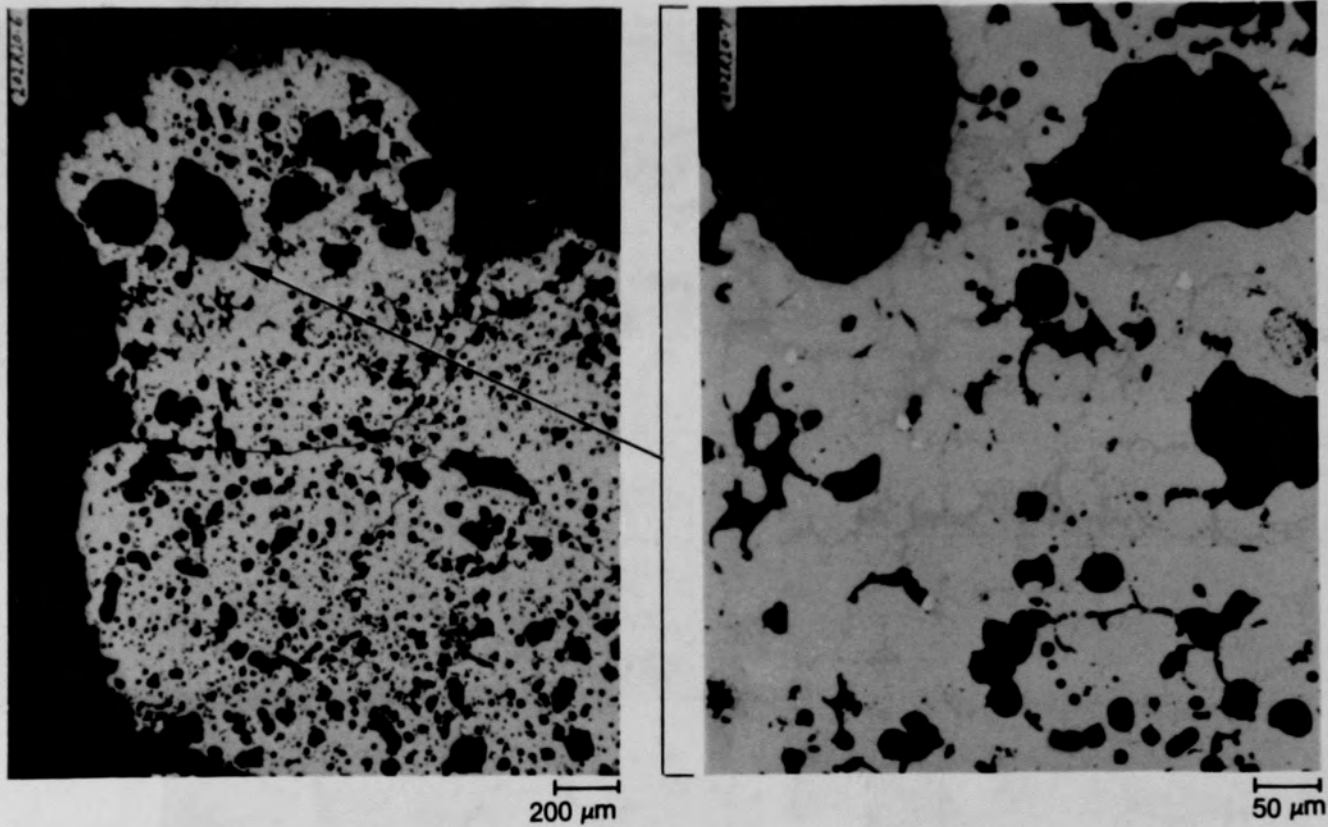


Figure C-280. Photomicrographs of material from location G of Particle 11B
(E9, 94 cm).

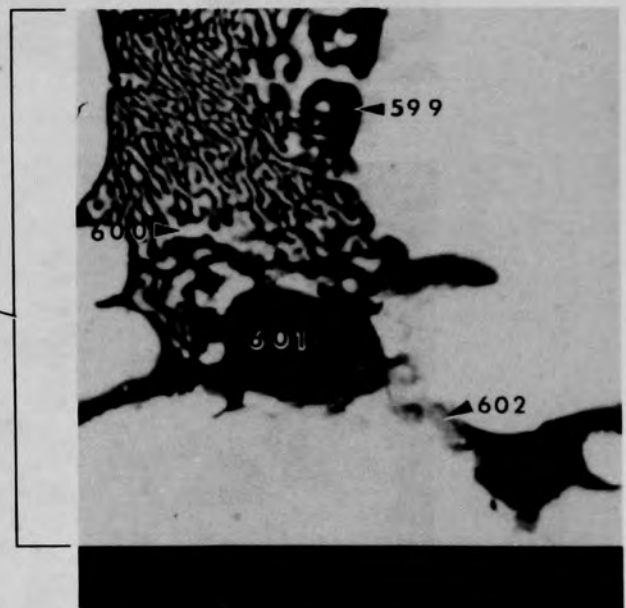
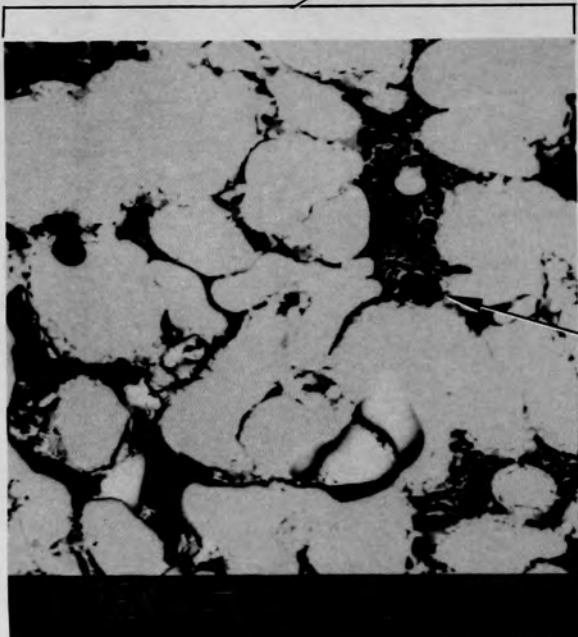
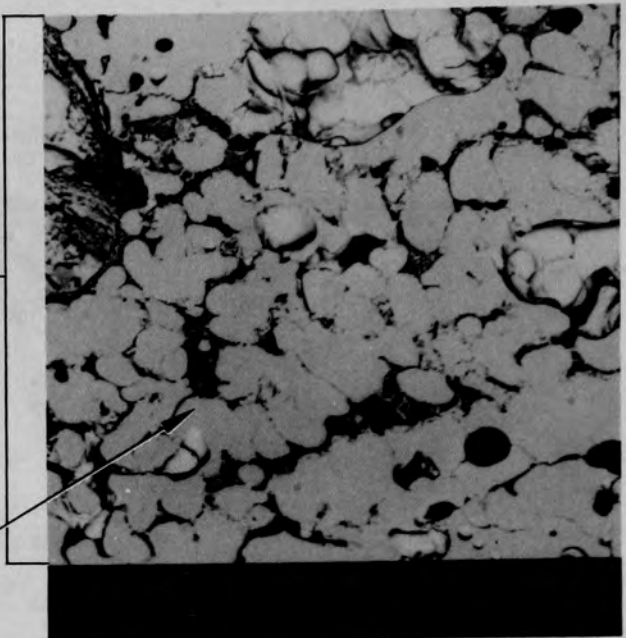
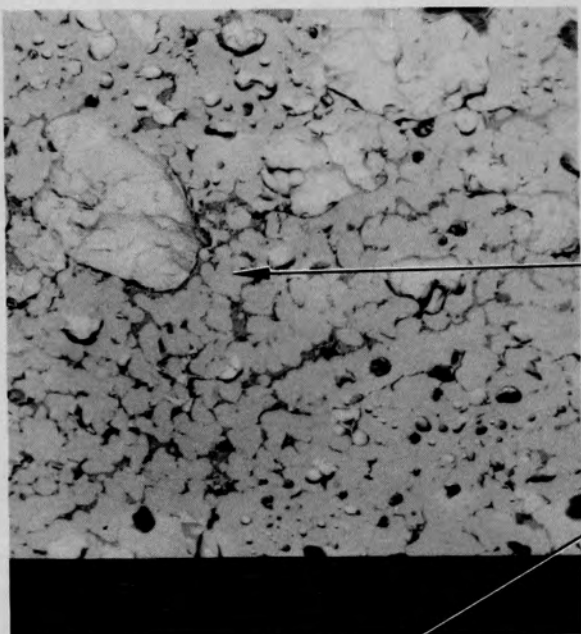
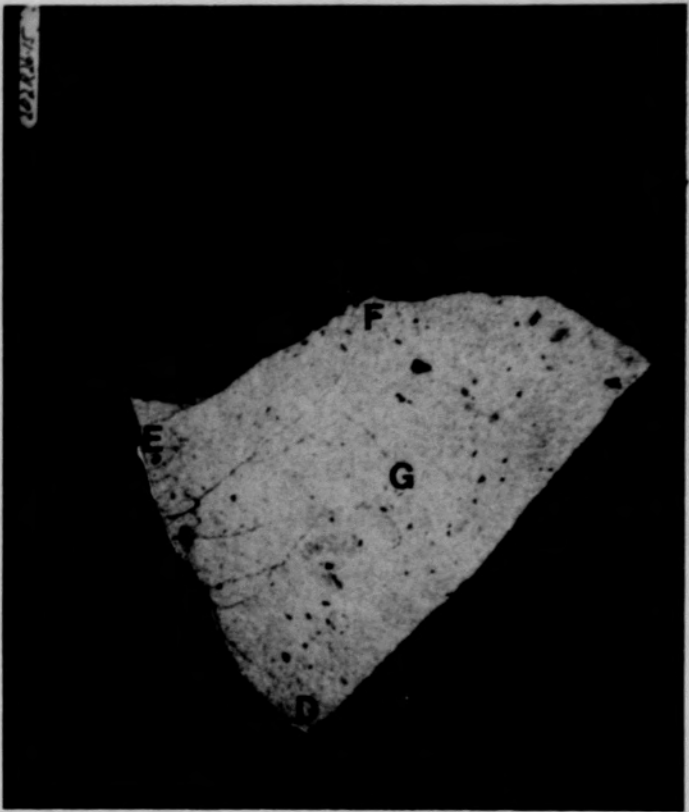


Figure C-281. SEM backscattered electron images of material from location G of Particle 11B (E9, 94 cm).

C-335



After regrinding

670 μm

Figure C-282. Photomacrographs of Particle 11C (E9, 94 cm).

C-336

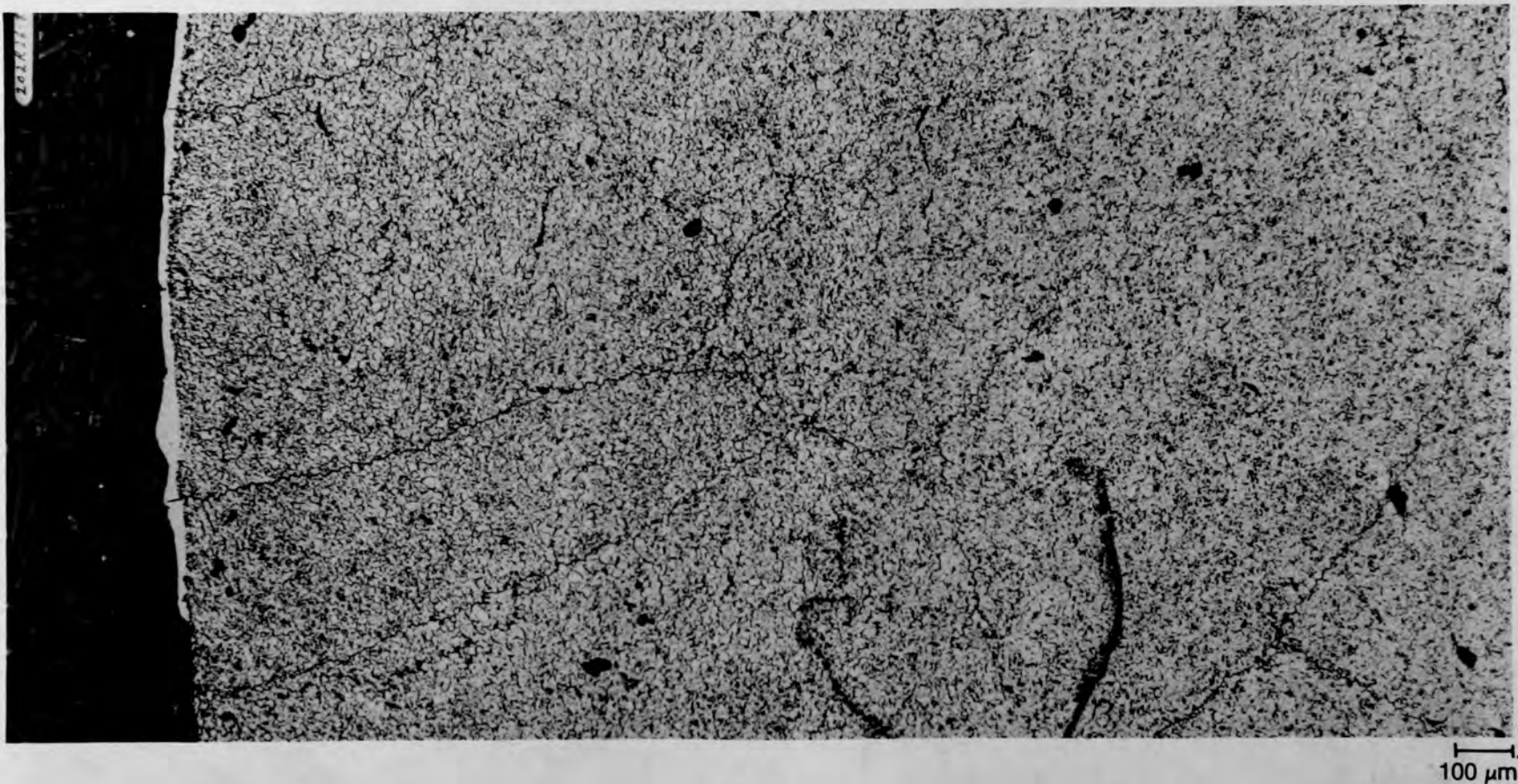


Figure C-283. Photomicrographs of a cross section of Particle 11C (E9, 94 cm) showing uniformity of grain size.

C-337

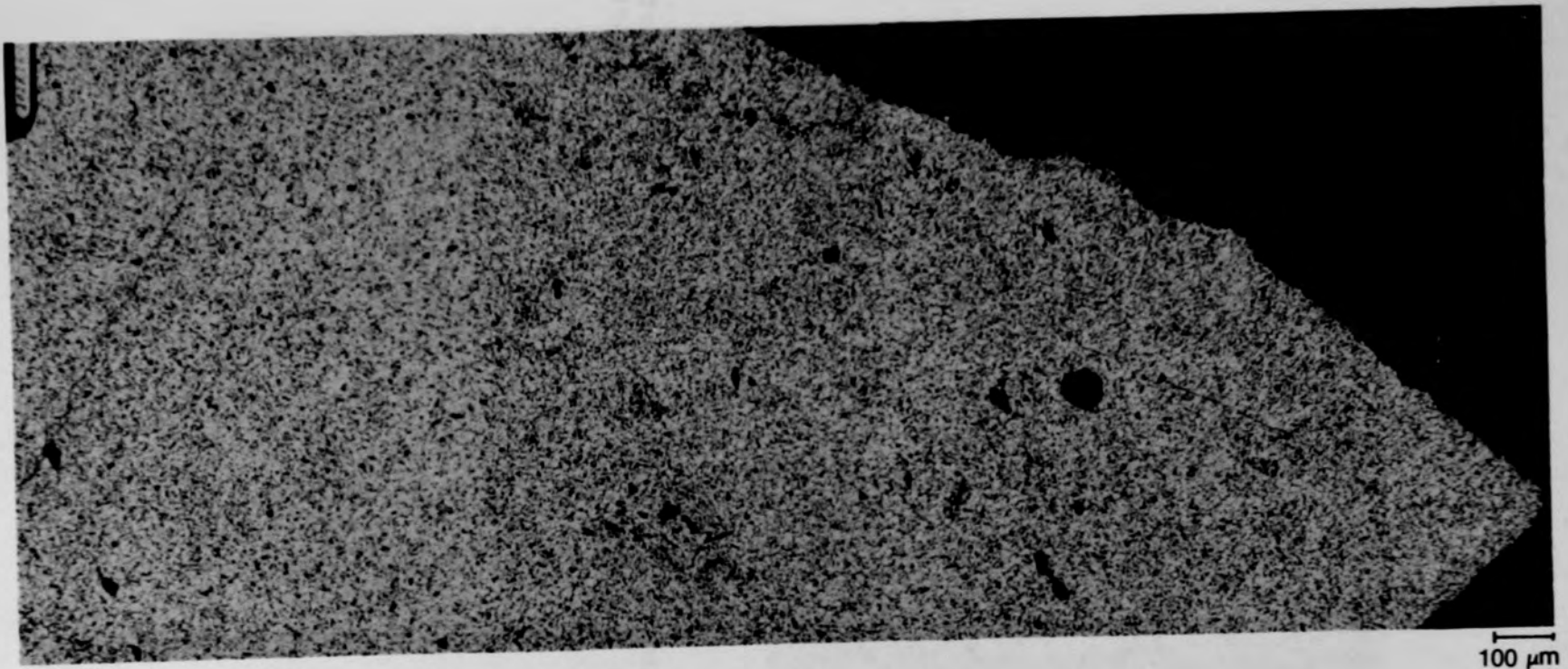


Figure C-284. Photomicrographs of a cross section of Particle 11C (E9, 94 cm) showing uniformity of grain size.

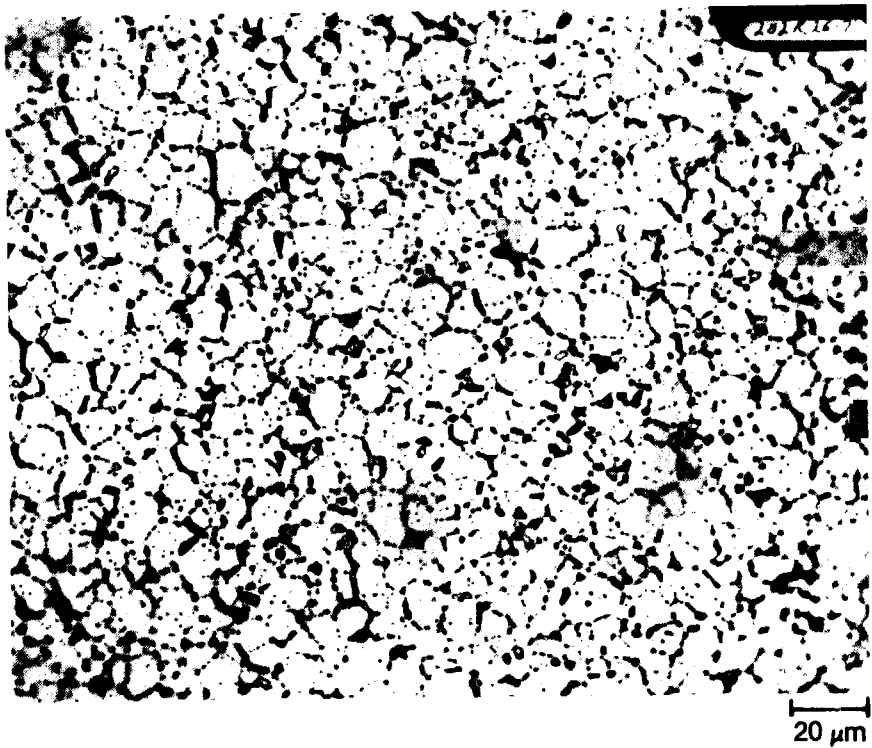
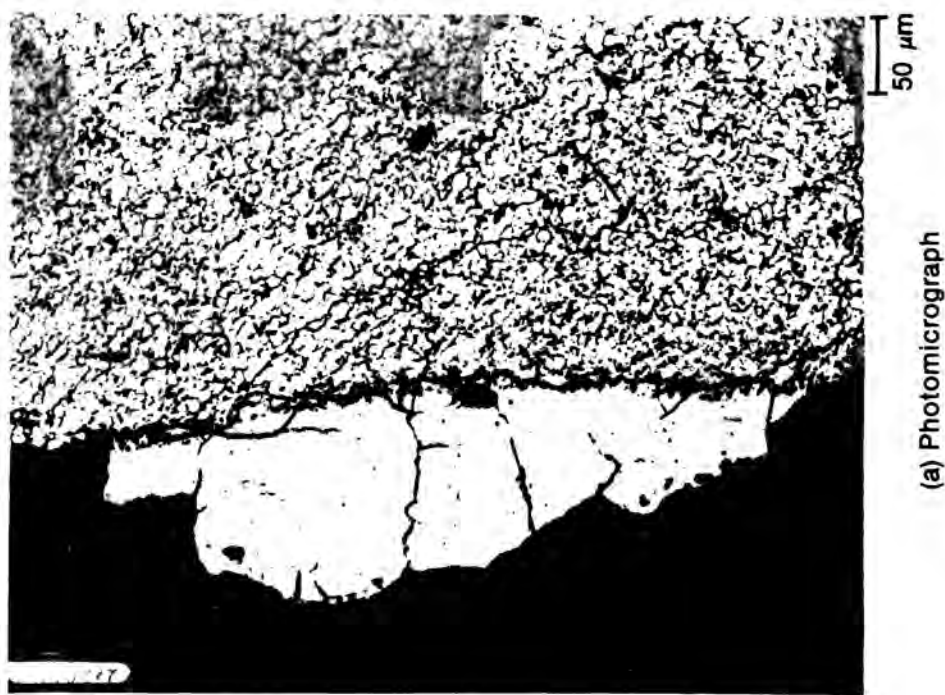


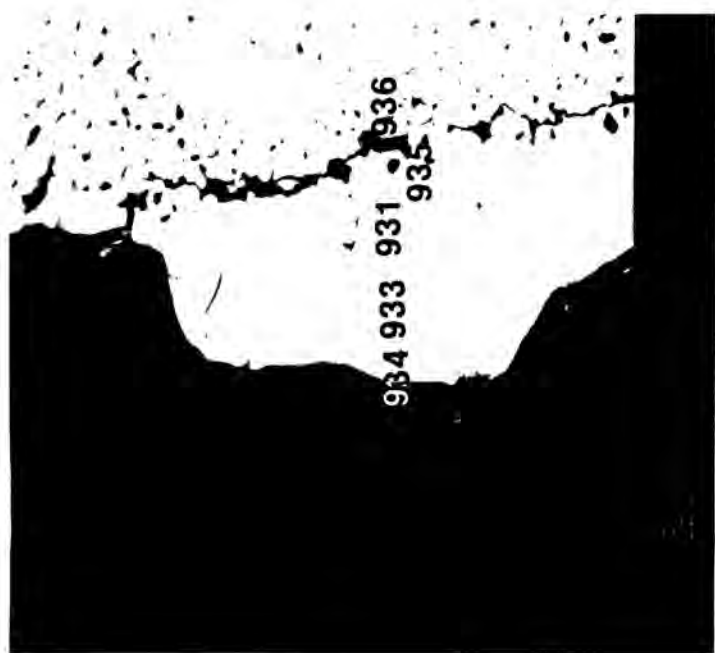
Figure C-285. Photomicrograph of material from location A of Particle 11C (E9, 94 cm) showing high porosity at grain boundaries.



Figure C-286. Photomicrographs of material from location B of Particle 11C
(E9, 94 cm).



(a) Photomicrograph



(b) SEM backscattered electron image

Figure C-287. Photographs of material from location C of Particle 11C (E9, 94 cm).

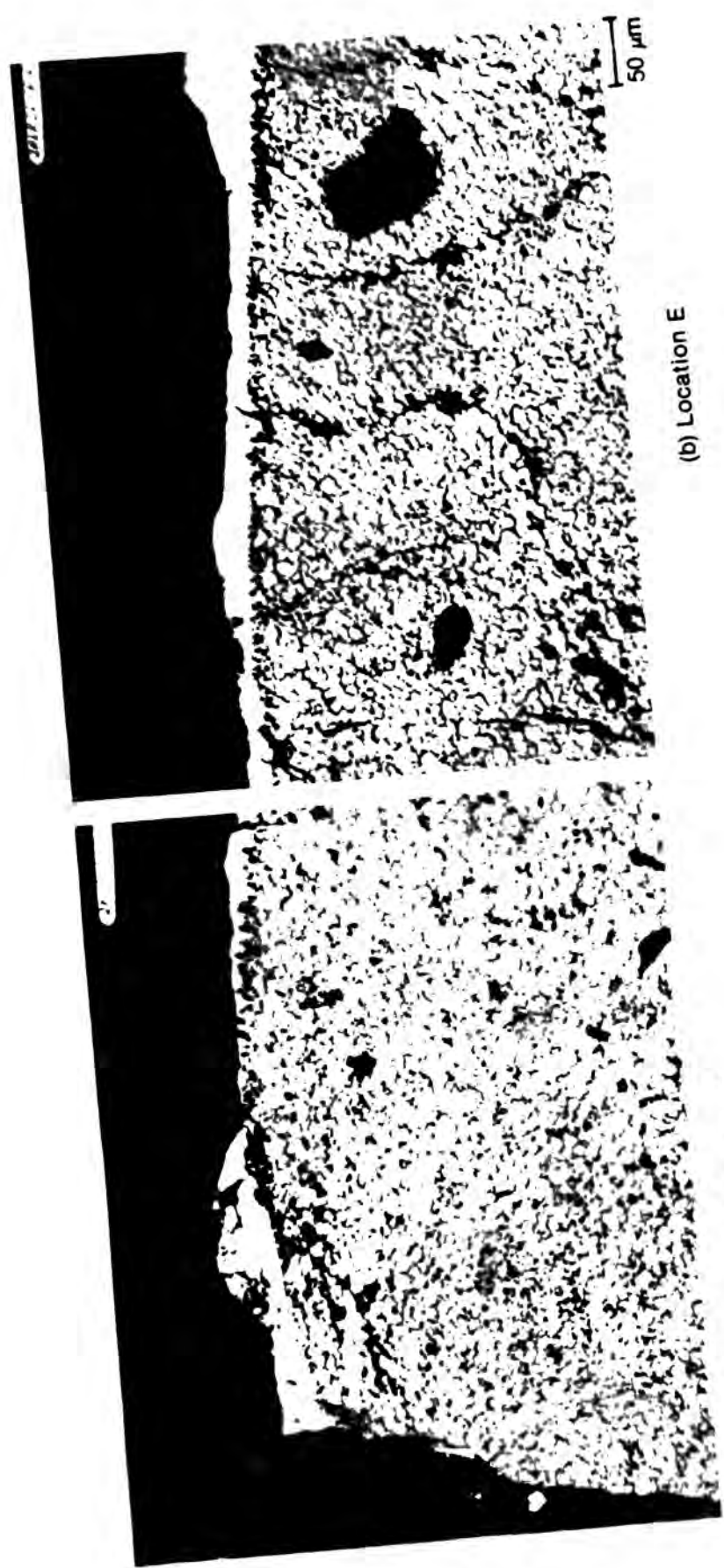


Figure C-288. Photomicrographs of material from edge of Particle 11C(E9,
94 cm).

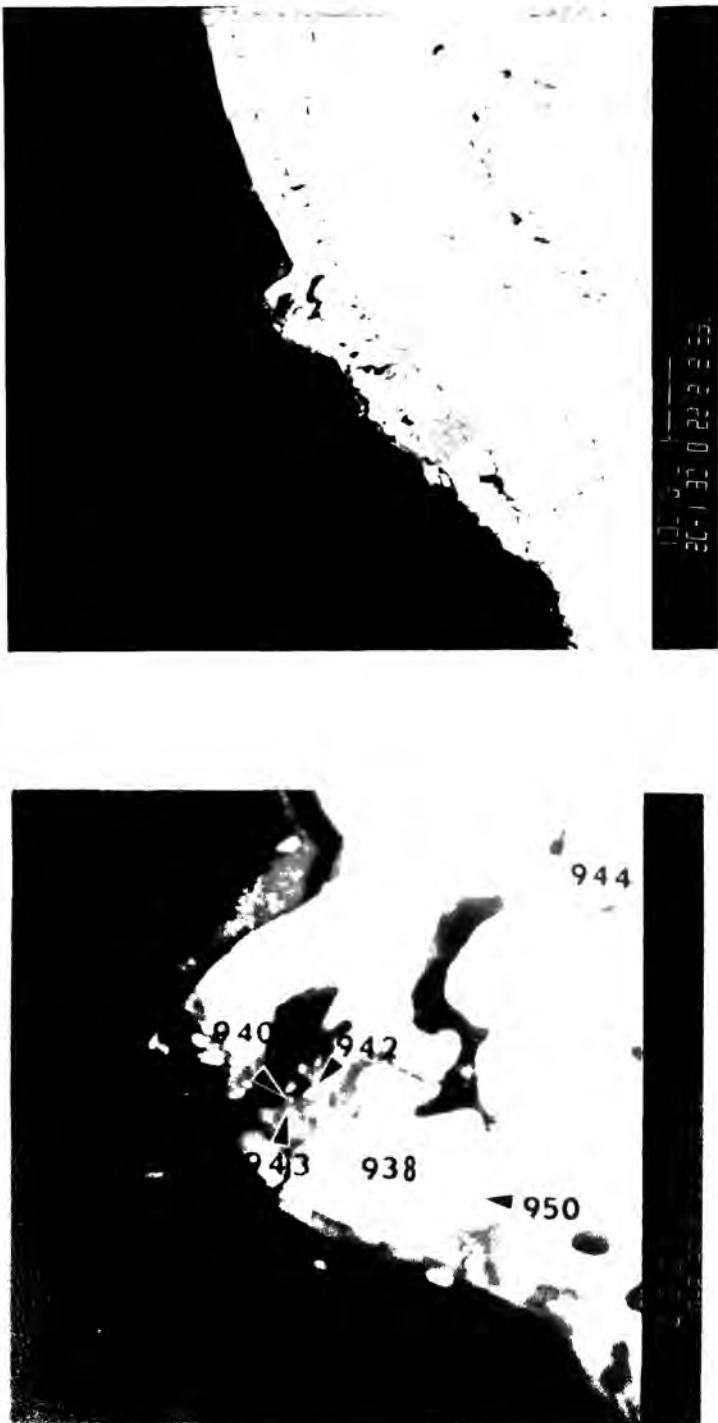
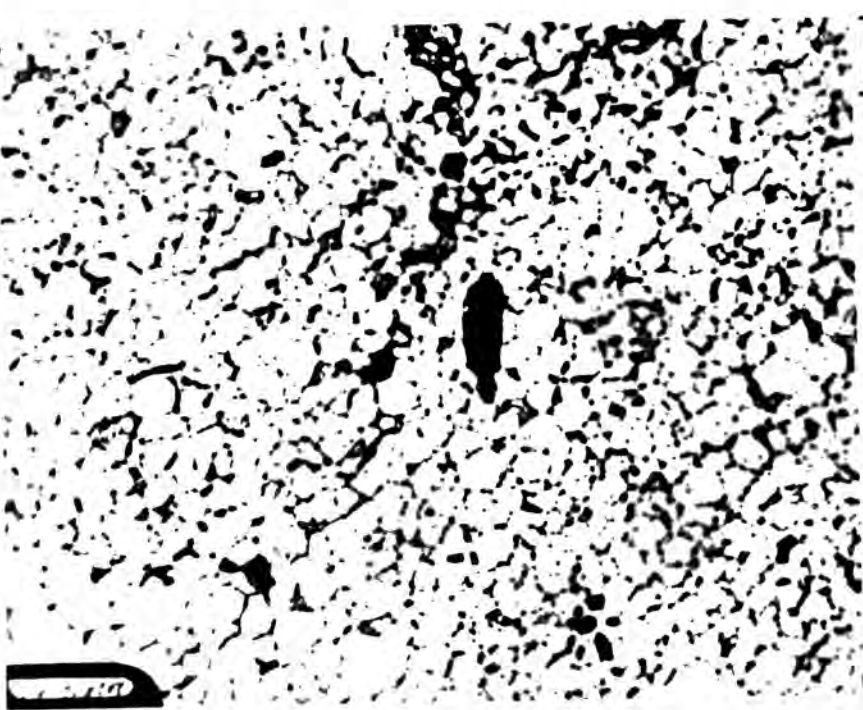


Figure C-289. SEM backscattered electron image of material from location F of Particle 11C (E9, 94 cm).

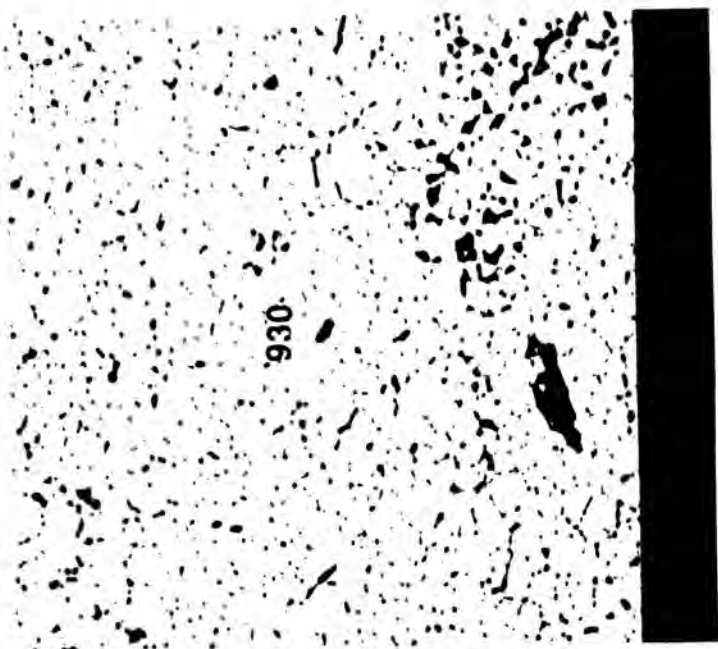
Figure C-29U. Photographs of material from location G of Particle 11C (E9, 94 cm).

(a) Photomicrograph



20 μm

(b) SEM backscattered electron image



20 μm

APPENDIX D

ELEMENTAL ANALYSIS

APPENDIX D

ELEMENTAL ANALYSIS

This Appendix presents results of the elemental analysis performed on the LMI-2 core debris grab samples, using inductively coupled plasma spectroscopy. The analysis was performed on the non-volatile dissolved portions of particles and aliquots. The results are given in mg element/g sample.

The uncertainties are large (~50%) for some analyses. These uncertainties were determined by comparing the fissile/fertile material content (Appendix E) and the elemental analysis results. The large uncertainties are caused by the small (<10 mg) sample portions and possible losses during the dissolution and analysis. Analysis of small portions was required because of high radiation levels associated with some samples.

TABLE U-i. RESULTS OF ELEMENTAL ANALYSIS OF SAMPLE 1
(mg element/g sample)

Element	Particle Size Fraction (μm)						1680-4000 Particle 16	1680-4000 Particle 14
	>4000 Particle 1A	>4000 Particle 1B	>4000 Particle 1C	>4000 Particle 1D	>4000 Particle 1E	>4000 Particle 1F		
Ag	<0.0	<5.0 E-1	5.0 E-1	<8 E-1	2.3	1.1	1.1	3.4
Al	<0.0	<7.0 E-1	4.0	1.2 E+1	4.0	3.0	7.5	<1.0
B	<0.0	<6 E-1	<6 E-1	<1.0 E-1	<4.0 E-1	<6.0 E-1	<8.0 E-1	<4.0 E-1
Ca	<0.0	3.0 E-1	<1.0 E-1	2.0 E-1	1.0 E-1	<1.0 E-1	<1.0 E-1	<8.0 E-2
Cr	<0.0	8.0 E-1	<4.0 E-1	3.0	4.7	5.0	4.4	2.6
Cu	<0.0	3.3 E-1	<3.0 E-1	1.0	4.0 E-1	5.0 E-1	8. E-1	<1.9 E-1
Fe	<0.0	4.0	1.0 E-1	4.4	7.5	5.0 E-1	1.95 E+1	3.3
Ge	<0.0	9.0 E-1	8.0 E-1	<1.0	<5.0 E-1	7.0 E-1	<1.0	5.0 E-1
In	<0.0	<4.0 E-1	<7.0	<6.0	<2.0	3.0	<5.0	7.2
Mn	<0.0	2.0 E-1	<1.0 E-1	2.0 E-1	2.0 E-1	3.3 E-1	5.2 E-1	1.1 E-1
Mo	<0.0	<1.0	<1.0	<2.0	<8.0 E-1	<1.0	<8.0 E-1	<8.0 E-1
Ni	<0.0	1.0	<6.0 E-1	<1.0	8.0 E-1	1.0	<8.0 E-1	4.1
Nb	<0.0	4.0	4.0	<6.0	<2.0	<3.0	5.0	<2.0
Si	<0.0	7.0	<9.0 E-1	7.8	5.5	4.1	2.3	3.9
Sn	<0.0	<2.0	<6.0	2.0 E+1	7.6	<5.0	<8.0	<4.0
Te	<0.0	5.0	<2.0	<4.0	3.0	4.0	<3.0	3.0
U	<0.0	8.31 E+2	9.78 E+1	2.64 E+2	1.78 E+2	5.70 E+2	5.73 E+2	4.72 E+2
Zr	<0.0	1.3 E+1	1.42 E+1	1.6 E+1	6.56 E+2	1.37 E+2	1.38 E+2	3.67 E+2
<hr/>								
1000-1680 ^a		1000-1680	1000-1680	707-1000	297-707	'49-297	74-149	30-74
Particle 11		Particle 1J	Particle 1K	Aliquot	Aliquot	Aliquot	Aliquot	Aliquot
Ag	1.5 E+1	8.0 E-1	9.0 E-1	6.0 E-1	9.0 E-1	1.5	1.3	1.8
Al	1.1	5.5	6.7	3.0	3.3	4.0	6.0	8.0
B	<2.0	<5.0 E-1	<6.0 E-1	<4.0 E-1	<4.0 E-1	<6.0 E-1	<1.0	<1.3
Ca	0.7	<1.0 E-1	<1.0 E-1	<1.0 E-1	4.6 E-1	4.7	3.7	4.8
Cr	6.4	7.3	3.4	6.8	6.3	6.9	1.10 E+1	<6.3 E-1
Cu	1.8	<2.7 E-1	<3.3 E-1	4.0 E-1	4.0 E-1	<3.1 E-1	<4.8 E-1	4.13 E+1
Fe	1.6 E+1	1.46 E+1	2.0	1.02 E+1	1.12 E+1	1.91 E+1	2.19 E+1	
Ge	<2.0	<8.0 E-1	<8.0 E-1	<6.0 E-1	<6.0 E-1	<9.0 E-1	<1.3	<1.8
In	3.9 E+1	<3.0	<4.0	5.0	4.0	<4.0	<6.0	<7.0
Mn	1.6	4.9 E-1	3.5 E-1	3.6 E-1	3.9 E-1	5.5 E-1	5.2 E-1	1.00
Nb	<4.0	<1.0	<1.0	<1.0	<1.0	<1.0	<2.0	<3.0
Si	5.4	1.8	1.0	4.01 E+1	3.3	7.1	8.8	9.8
Sn	<1.1 E+1	<3.0	<4.0	1.4	<2.0	<4.0	<6.0	<8.0
Te	<7.0	<5.0	<7.0	8.6	7.0	<6.0	1.9 E+1	2.5 E+1
U	<6.1 E+1	6.40 E+2	5.66 E+2	5.19 E+2	5.32 E+2	4.54 E+2	4.11 E+2	3.65 E+2
Zr	3.85 E+2	1.46 E+2	1.31 E+2	1.01 E+2	1.68 E+2	3.30 E+2	3.23 E+2	3.40 E+2

a. Uncertainty is 30-50% because of problems associated with the analysis.

b. Not reported because of analysis problems.

TABLE U-2. RESULTS OF ELEMENTAL ANALYSIS OF SAMPLE 3
(mg element/g sample)

Element	Particle Size fraction (μm)						1680-4000 ^a Particle 3f	1680-4000 ^a Particle 3e	1680-4000 ^a Particle 3d	1680-4000 ^a Particle 3c	1680-4000 ^a Particle 3b	1680-4000 ^a Particle 3a	
	>4000 ^b	4000- ^b	4000- ^b	4000- ^b	4000- ^b	4000- ^b							
A9	4.1 E-1	2.7	--D	2.0 E-1	8.1 E-1	<7.0 E-1	<8.0 E-1	<6.0 E-1					
Al	4.0 E-1	6.0	--D	<5.0 E-1	<5.0 E-1	<1.0 E-1	<4.0	6.0	6.0	6.0	6.0	6.0	
B	<9.0 E-2	1.0	--D	<1.0 E-1	<1.0 E-1	<2.0 E-2	<4.0 E-1	<1.0 E-1					
Ca	<2.0 E-2	<2.0 E-1	--D	<5.0 E-2	<2.0 E-2	<7.0 E-2	<2.0 E-1						
Cr	4.0 E-1	4.4	--D	<7.0 E-2	<2.0 E-1	<6.1 E-2	<2.0 E-1	<6.0 E-1					
Cu	<9.0 E-2	<5.2 E-1	--D	<6.1 E-2	<6.1 E-2	<5.0 E-2	<5.0 E-1						
Fe	<7.7 E-1	5.5	--D	<5.0 E-2	<5.0 E-2	<5.0 E-2	<5.0 E-1						
Ga	2.7 E-1	<2.0	--D	<5.4 E-1	<5.4 E-1	<6.8 E-1	<6.8 E-1	<6.0	<6.0	<6.0	<6.0	<6.0	
In	1.0	<6.0	--D	1.0	<1.0 E-1	<1.0 E-1	<1.0 E-1	<2.0 E-1					
Ni	<7.7 E-2	<1.0 E-1	--D	5.9 E-2	<1.0 E-1	<1.0 E-1	<1.0 E-1	<2.0 E-1					
Po	5.3 E-1	2.0	--D	6.0 E-1	1.0	<1.0 E-1							
Nr	<9.0 E-2	<1.0	--D	<1.0 E-1	<1.0 E-1	<2.0 E-1							
U	<9.0 E-1	<6.0	--D	8.8 E-1	1.3	<6.0 E-1							
Y	1.7	<3.17 E+1	--D	3.8 E-1	8.1 E-1	<1.0 E-1	<1.0 E-1	<1.0 E-1	<1.0 E-1	<1.0 E-1	<1.0 E-1	<1.0 E-1	
Zn	2.0	<1.0 E+1	--D	<1.0 E-1	<1.0 E-1	2.4	<9.0	<9.0	<9.0	<9.0	<9.0	<9.0	
Tl	4.0 E-1	8.0	--D	5.0 E-1	<5.0 E-1	<5.0 E-1	<4.0	<4.0	<4.0	<4.0	<4.0	<4.0	
As	<3.82 E+1	<3.6 E+1	--D	4.60 E-1	7.24 E-1	7.24 E-1	1.00 E+3	2.26 E+2	4.46 E+2	3.80 E+1	1.0 E+2	1.0 E+2	
Te	<7.31 E+1	7.10 E+1	--D	9.32	2.28 E+1	5.00 E+1	5.00 E+1	3.80 E+1					
<hr/>													
<hr/>													
<hr/>													
Element	1680-1600 ^a Particle 3j						1000-1600 ^a Particle 3j	707-1000 Particle 3j	297-707 Aliquot	149-297 Aliquot	74-149 ^a Aliquot	30-74 ^a Aliquot	<30 Aliquot
Element	>4000-1600 ^b Particle 3j	4000-1600 ^b Particle 3j	4000-1600 ^b Particle 3j	4000-1600 ^b Particle 3j	4000-1600 ^b Particle 3j	4000-1600 ^b Particle 3j	4000-1600 ^b Particle 3j	4000-1600 ^b Particle 3j	4000-1600 ^b Particle 3j	4000-1600 ^b Particle 3j	4000-1600 ^b Particle 3j	<30 Aliquot	
A9	4.0 E-1	1.0	8.2 E-1	1.4	1.7	1.8	1.8	6.0	6.0	6.0	6.0	6.0	6.0
Al	2.0	2.0	1.8	2.0	2.0	2.3	2.3	4.2	4.2	4.2	4.2	4.2	4.2
B	4.0 E-1	<3.0 E-1	<2.0 E-1	4.0 E-1	<6.0 E-1	<1.0 E-1	<1.0 E-1	<0.7	<0.7	<0.7	<0.7	<0.7	<0.7
Ca	<7.0 E-1	<6.0 E-2	<7.0 E-2	1.0 E-1	2.0 E-1	1.0	1.0	1.9	1.9	1.9	1.9	1.9	1.9
Cr	4.6	<2.0 E-1	<3.8 E-1	9.98	5.7	7.4	7.4	8.0	8.0	8.0	8.0	8.0	8.0
Cu	<2.0 E-1	<2.0 E-1	2.0 E-1	<1.9 E-1	2.8 E-1	2.0 E-1	2.0 E-1	<3.5 E-1	<3.5 E-1	<3.5 E-1	<3.5 E-1	<3.5 E-1	<3.5 E-1
In	6.7	1.5	4.16	1.26 E+1	1.26 E+1	1.26 E+1	1.26 E+1	1.89 E+1					
Te	4.0 E-1	4.0 E-1	5.2 E-1	<5.0 E-1	<8.0 E-1	<3.9 E-1	<3.9 E-1	<1.0	<1.0	<1.0	<1.0	<1.0	<1.0
Ga	2.0	2.0	<1.0	5.0	7.0	3.4	3.4	4.4	4.4	4.4	4.4	4.4	4.4
Mo	4.0 E-1	<3.0 E-1	2.0 E-1	<4.0 E-1	<3.7 E-1	<4.0 E-1	<4.0 E-1	<4.7 E-1					
Ni	8.0 E-1	6.0 E-1	4.0 E-1	1.80 E+1	2.0	7.6	7.6	8.0	8.0	8.0	8.0	8.0	8.0
W	<2.0	<2.0	<1.0	<2.0	<3.0	<8.0 E-1	<8.0 E-1	<4.4	<4.4	<4.4	<4.4	<4.4	<4.4
S1	3.0	5.8	3.0	2.7	5.4	3.9	3.9	2.1	2.1	2.1	2.1	2.1	2.1
Sn	4.0	5.9	3.7	<4.0	<6.0	4.03	4.03	<6.9	<6.9	<6.9	<6.9	<6.9	<6.9
Te	<2.0	<1.0	<7.0 E-1	<1.0	<2.0	<6.0 E-1	<6.0 E-1	<7.0	<7.0	<7.0	<7.0	<7.0	<7.0
U	5.59 E+2	1.12 E+2	4.80 E+1	5.79 E+1	4.7 E+2	3.72 E+1	3.72 E+1	3.54 E+2	3.17 E+2				
Zr	5.56 E+2	2.69 E+2	9.23 E+1	1.95 E+1	8.14 E+1	1.75 E+1	1.75 E+1	3.2 E+2	3.55 E+2	3.55 E+2	3.55 E+2	3.55 E+2	3.55 E+2

a. Uncertainty is 30-50% because of problem, dissociated with the analysis.

b. not reported because of analysis problems.

TABLE D-3. RESULTS OF ELEMENTAL ANALYSIS OF SAMPLE 4
(mg element/g sample)

Element	Particle Size Fraction (μm)				>4000 Particle 4E
	>4000 Particle 4A	>4000 ^a Particle 4B	>4000 Particle 4C	>4000 ^a Particle 4D	
Ag	1.4	<0.7	4.6 E-1	--b	1.2
Al	5.1	5.6	2.0	--b	5.0
B	<0.6	<0.9	<3.0 E-1	--b	<8.3 E-1
Cd	<0.1	3.7 E-1	<7.0 E-2	--b	3.3 E-1
Cr	5.1	2.4	3.8	--b	2.2
Cu	1.6	<4.6 E-1	<1.6 E-1	--b	<4.2 E-1
Fe	1.3 E+1	1.5	3.0	--b	3.0
Gd	<0.8	<1.3	9.2 E-1	--b	<1.0
In	<3.0	1.1 E+1	<2.0	--b	<5.0
Mn	1.8 E-1	9.0 E-2	7.0 E-2	--b	<8.0 E-2
Mo	<1.0	<1.9	<7.0 E-1	--b	<1.7
Ni	5.9	1.9	2.1	--b	<8.3 E-1
Nb	<3.0	<6.0	<2.0	--b	<5.0
Si	4.0	26.0 E+1	7.70	--b	1.0 E+1
Sn	1.1 E+1	<9.3	<3.3	--b	<8.0
Te	4.6	<3.7	2.6	--b	6.7
U	9.38 E+2	5.83 E+2	5.14 E+2	--b	8.83 E+2
Zr	1.34 E+2	1.8 E+1	1.23 E+1	--b	2.62 E+1

a. Uncertainty is 30-50% because of problems associated with the analysis.

b. Not reported because of analysis problems.

TABLE D-4. RESULTS OF ELEMENTAL ANALYSIS OF SAMPLE 5
(mg element/g sample)

Element	Particle Size Fraction (μm)					
	<u>>4000^a</u> Particle Sz	<u>>4000</u> Particle Sz	<u><4000^b</u> Particle Sz	<u>>4000^b</u> Particle Sz	<u><4000^c</u> Particle Sz	<u>>1680-4000^d</u> Particle Sz
Al	1.0	6.7 E-1	5.0 E-1	9.2 E-1	-d	-d
	5.0	2.9	2.0	4.0	-d	-d
B	8.0 E-1	0.5	1.1	1.3	-d	-d
Ca	42.0 E-1	1.9 E-1	7.0 E-2	1.0 E-1	-d	-d
Cr	2.4	1.1	1.3	2.1	-d	-d
Co	4.1 E-1	0.7	4.0 E-1	3.3 E-1	-d	-d
Fe	1.3	1.3	1.1	5.3 E-1	-d	-d
Li	1.0	7.0 E-1	6.0 E-1	9.2 E-1	-d	-d
N	1.0 E+1	3.0	4.0	7.9	-d	-d
Si	8.2 E-1	1.0 E-1	7.0 E-2	7.0 E-2	-d	-d
Sn	2.0	2.7	7.0 E-1	1.3	-d	-d
Te	1.0	2.8	7.0 E-1	6.6 E-1	-d	-d
Zn	5.0	3.0	4.2 E-1	4.0	-d	-d
	2.05 E+	1.56 E+1	5.0	2.0	-d	-d
Ba	8.0	6.0	7.1	1.3 E+1	-d	-d
Ca	1.0	2.0	3.0	2.6	-d	-d
Fe	1.0	8.52 E+2	5.74 E+2	8.96 E+2	-d	-d
Li	1.0	4.14 E+2	3.9 E+2	4.1	-d	-d
Al	1680-4000 Particle Sz	1680-4000 Particle Sz	1000-1680 ^e Particle Sz	1000-1680 Particle Sz	1680-4000 Aiquot	
	-d	2.4 E-1	-d	-d	2.0	
B	-d	7.1 E-1	-d	-d	2.0	
Ca	-d	1.0 E-1	-d	-d	4.0 E-1	
Cr	-d	7.0 E-2	-d	-d	1.0 E-1	
Co	-d	5.2 E-1	-d	-d	8.0 E-1	
Fe	-d	1.0 E-1	-d	-d	1.9 E-1	
Li	-d	1.1	-d	-d	3.74	
N	-d	4.2 E-1	-d	-d	6.0 E-1	
Si	-d	7.0 E-1	-d	-d	2.0	
Sn	-d	2.0 E-2	-d	-d	3.9 E-1	
Te	-d	2.0 E-1	-d	-d	8.0 E-1	
Zn	-d	3.6 E-1	-d	-d	1.03 E+1	
	-d	7.0 E-1	-d	-d	2.0	
	-d	2.0	-d	-d	9.75	
	-d	2.4	-d	-d	7.7 E-1	
	-d	9.0 E-1	-d	-d	1.0	
	-d	1.72 E+2	-d	-d	3.13 E+2	
	-d	8.40 E+1	-d	-d	2.87 E+1	

a. Uncertainty is 30-50% because of problems associated with the analysis.

b. Not reported because of analysis problems.

TABLE D-5. RESULTS OF ELEMENTAL ANALYSIS OF SAMPLE 6
(mg element/g Sample)

Element	Particle Size Fraction (μm)									
	4000 ^a			4000			4000 ^a			1680-4000 ^a
	Particle 6A	Particle 6B	Particle 6C	Particle 6D	Particle 6E	Particle 6F	Particle 6G	Particle 6H	Particle 6I	Particle 6J
Aq	1.0 <4.0	1.2 <2.0	2.6 <2.0	8.0 E-1 <6.0 E-1	5.1 <6.0 E-1	2.1 <4.0 E-1	8.1 E-1 <3.0 E-1	6.4 E-1 <7.0 E-1	6.0 E-1 <2.0 E-1	6.4 E-1 <1.0 E-1
Al	9.0 E-1	1.0 <2.0 E-1	2.83 E+1 <2.0 E-1	3.0 <2.0 E-1	3.0 <4.0 E-1	3.0 <3.3 E-1	3.0 <8.0 E+1	<7.0 E-1 <7.0 E-2	<6.0 E-1 <3.0 E-2	<6.0 E-1 <9.0 E-2
B	4.0 E-1	1.0 <1.0 E-1	2.0 E-1 <5.0 E-2	6.0 E-1 <2.0 E-1	4.0 E-1 <3.0 E-1	4.0 E-1 <2.8 E-1	4.0 E-1 <3.0 E-1	<2.0 E-1 <2.2 E-1	<2.0 E-1 <2.2 E-1	<1.0 E-1 <9.0 E-2
Cd	4.0 E-1	1.0 <1.0 E-1	2.0 E-1 <1.0 E-1	6.0 E-1 <1.0 E-1	4.0 E-1 <2.8 E-1	4.0 E-1 <3.0 E-1	4.0 E-1 <4.0 E-1	<2.0 E-1 <2.2 E-1	<2.0 E-1 <2.2 E-1	<3.0 E-2 <7.3 E-2
Cr	5.0 E-1	1.0 <1.0 E-1	2.0 E-1 <1.2 E-1	6.0 E-1 <1.2 E-1	4.0 E-1 <2.0 E-1	4.0 E-1 <2.0 E-1	4.0 E-1 <3.0 E-1	<2.0 E-1 <2.2 E-1	<2.0 E-1 <2.2 E-1	<3.0 E-2 <7.3 E-2
Cu	4.6 E-1	1.4 <2.0 E-2	1.0 <3.0 E-1	1.0 <3.0 E-1	1.0 <2.0 E-1	1.0 <2.0 E-1	1.0 <2.0 E-1	<1.0 E-1 <1.0 E-1	<1.0 E-1 <1.0 E-1	<6.0 E-2 <6.0 E-2
Fe	2.7	2.6 <5.0	3.0 <1.0 E-1	3.0 <1.0 E-1	3.0 <1.0 E-1	3.0 <1.0 E-1	3.0 <1.0 E-1	<6.0 E-1 <6.0 E-1	<6.0 E-1 <6.0 E-1	<6.0 E-1 <6.0 E-1
Ga	2.6 <5.0	1.0 <1.0 E-1	2.0 <1.0 E-1	2.0 <1.0 E-1	2.0 <1.0 E-1	2.0 <1.0 E-1	2.0 <1.0 E-1	<3.0 E-1 <3.0 E-1	<3.0 E-1 <3.0 E-1	<9.0 E-1 <9.0 E-1
In	2.0 E-1 <2.0	1.8 <4.0	1.0 <2.5 E-1	1.0 <2.5 E-1	1.0 <6.0 E-2	1.0 <5.8 E-2	1.0 <6.0 E-2	<7.0 E-1 <6.3 E-1	<7.0 E-1 <6.3 E-1	<6.7 E-2 <6.7 E-2
Mn	3.3 <2.0	3.0 <4.0	1.0 <5.0 E-1	1.0 <5.0 E-1	1.0 <1.0 E-1	1.0 <1.0 E-1	1.0 <6.0 E-1	<8.7 E-1 <8.7 E-1	<8.7 E-1 <9.4 E-1	<1.0 E-1 <1.0 E-1
Mo	3.3 <5.0	3.0 <1.0	1.0 <2.0 E-1	1.0 <2.0 E-1	1.0 <3.0 E-1	1.0 <3.0 E-1	1.0 <3.0 E-1	<2.0 E-1 <2.0 E-1	<2.0 E-1 <2.0 E-1	<1.0 E-1 <1.0 E-1
Ni	2.7 <9.0	1.72 E+1 <7.4 E+1	5.0 <1.0 E-1	5.0 <6.0 E-1	5.6 E-1 <2.0 E+1	5.6 E-1 <2.59 E+1	5.6 E-1 <2.59 E+1	3.0 <8.7 E-1	3.0 <8.7 E-1	1.0 <1.0 E-1
Nb	4.0 U	6.02 E+3 <4.0 E+1	3.40 E+2 <6.2 E+2	3.40 E+2 <5.9 E+1	8.14 E+1 <2.0 E+1	8.14 E+1 <2.0 E+1	8.14 E+1 <2.0 E+1	<1.5 E+1 <1.5 E+1	<1.5 E+1 <1.5 E+1	<6.0 E-1 <6.0 E-1
Si	2.49 Zr	2.49 E+1 <2.40 E+2	7.63 E+2 <3.40 E+2	7.63 E+2 <3.40 E+2	8.1 <8.1	1.45 E+3 <1.45 E+3	1.45 E+3 <6.00 E+2	6.00 E+2 <4.92	6.00 E+2 <4.92	7.06 E-1 <3.70
<hr/>										
1000-1680 ^a Particle 6I										
1000-1680 Particle 6J			1000-1680 Particle 6K			707-1000 Aliquot			297-707 ^a Aliquot	
Aq	1.4	1.8	2.0	2.82	1.02 E+1	3.7 E-1	3.7 E-1	2.36 E+1	2.68 E+1	
Al	5.0 <3.0	1.0 E-1	3.0 <1.0 E-1	1.3 <1.0 E-1	3.55 <1.0 E-1	3.54 E-1	3.54 E-1	1.9 <1.0 E-1	1.54 E+1	
B	3.0 E-1	3.0 E-1	5.0 E-1	1.0 E-1	1.0 E-1	1.0 E-1	1.0 E-1	3.0 E-1	6.0 E-1	
Cd	2.9	3.0 E-1	3.0 E-1	2.0 <1.0 E-1	3.0 <1.0 E-1	3.0 <1.0 E-1	3.0 <1.0 E-1	1.5 <1.0 E-1	2.2 <1.0 E-1	
Cr	6.2	3.0 E-1	3.0 E-1	2.0 <1.0 E-1	5.56 <1.0 E-1	8.51 <1.0 E-1	7.71 <1.0 E-1	6.90 <1.0 E-1	5.0 <1.0 E-1	
Cu	5.2 E-1	8.8 E-2	2.7 <1.0 E-1	1.0 E-1	5.1 E-2 <1.0 E-1	7.0 E-2 <1.37 E+1	7.0 E-2 <1.56 E-1	1.0 E-1 <1.45 E+1	6.0 E-1 <1.79 E+1	
Fe	2.26 E+1	3.0 E-1	2.7 <7.6	8.46 <4.4 E-1	8.46 <4.5 E-1	8.46 <2.74 E-1	8.46 <3.18 E-1	8.46 <5.11 E-1	8.46 <3.8 E-1	
Gd	<4.0 E-1	<3.0 E-1	<7.0	<6.0 E-1						
In	8.52	<1.0	2.1 <5.0 E-1	2.1 <5.0 E-1	2.1 <4.0 E-1	2.1 <4.0 E-1	2.1 <4.0 E-1	2.1 <3.3 E-1	2.1 <4.0 E-1	
Ir	2.6 E-1	3.0 E-2	<3.0 E-1	<5.0 E-1	4.8 E-1	<2.0 E-1	3.4 E-1	6.6 E-1	<1 E-1	
Mo	<6.0 E-1	<3.0 E-1	<2.0 E-1	5.0 E-1	1.51 E+1	4.08 <7.34	7.34 <7.20	7.20 <7.4	7.4 <7.4	
Ni	3.2 E+1	<2.0 E-1	<2.0	<1.0	1.0 <1.3	8.8 E-1 <1.3	8.8 E-1 <1.3	8.8 E-1 <1.3	<4.0 E-1	
Nd	<2.0	<1.0	1.2 <4.4	2.3 <4.4	2.3 <4.4	2.3 <4.4	2.3 <4.4	2.3 <3.87	3.87 <3.87	
Si	1.6	4.87 <1.24 E+1	<3.0	4.66 <1.0	4.66 <4.0 E-1	2.1 <4.0 E-1	2.1 <3.0 E-1	2.1 <2.7	2.7 <2.65	
Sn	<1.0	1.0 <1.29 E+2	7.02 E+2 <5.38 E+2	7.45 E+2 <1.52 E+2	7.45 E+2 <4.46 E+2					
Te	1.13 E+2	1.29 E+2 <2.20 E+2	7.02 E+2 <5.38 E+2	7.45 E+2 <1.52 E+2	7.45 E+2 <4.46 E+2					
<hr/>										
30-74 ^a Aliquot										
Aq	1.4	1.8	2.0	2.82	1.02 E+1	3.7 E-1	3.7 E-1	2.36 E+1	2.68 E+1	
Al	5.0 <3.0	1.0 E-1	3.0 <1.0 E-1	1.3 <1.0 E-1	3.55 <1.0 E-1	3.54 E-1	3.54 E-1	1.9 <1.0 E-1	1.54 E+1	
B	3.0 E-1	3.0 E-1	5.0 E-1	1.0 E-1	1.0 E-1	1.0 E-1	1.0 E-1	3.0 E-1	6.0 E-1	
Cd	2.9	3.0 E-1	3.0 E-1	2.0 <1.0 E-1	5.56 <1.0 E-1	8.51 <1.0 E-1	7.71 <1.0 E-1	6.90 <1.0 E-1	5.0 <1.0 E-1	
Cr	6.2	3.0 E-1	3.0 E-1	2.0 <1.0 E-1	5.1 E-2 <1.0 E-1	7.0 E-2 <1.37 E+1	7.0 E-2 <1.56 E-1	1.0 E-1 <1.45 E+1	6.0 E-1 <1.79 E+1	
Cu	5.2 E-1	8.8 E-2	2.7 <1.0 E-1	1.0 E-1	8.46 <4.4 E-1	8.46 <4.5 E-1	8.46 <2.74 E-1	8.46 <3.18 E-1	8.46 <5.11 E-1	
Fe	2.26 E+1	3.0 E-1	2.7 <7.6	8.46 <4.4 E-1	8.46 <4.5 E-1	8.46 <2.74 E-1	8.46 <3.18 E-1	8.46 <5.11 E-1	8.46 <3.8 E-1	
Gd	<4.0 E-1	<3.0 E-1	<7.0	<6.0 E-1						
In	8.52	<1.0	2.1 <5.0 E-1	2.1 <5.0 E-1	2.1 <4.0 E-1	2.1 <4.0 E-1	2.1 <4.0 E-1	2.1 <3.3 E-1	2.1 <4.0 E-1	
Ir	2.6 E-1	3.0 E-2	<3.0 E-1	<5.0 E-1	4.8 E-1	<2.0 E-1	3.4 E-1	6.6 E-1	<1 E-1	
Mo	<6.0 E-1	<3.0 E-1	<2.0 E-1	5.0 E-1	1.51 E+1	4.08 <7.34	7.34 <7.20	7.20 <7.4	7.4 <7.4	
Ni	3.2 E+1	<2.0 E-1	<2.0	<1.0	1.0 <1.3	8.8 E-1 <1.3	8.8 E-1 <1.3	8.8 E-1 <1.3	<4.0 E-1	
Nd	<2.0	<1.0	1.2 <4.4	2.3 <4.4	2.3 <4.4	2.3 <4.4	2.3 <4.4	2.3 <3.87	3.87 <3.87	
Si	1.6	4.87 <1.24 E+1	<3.0	4.66 <1.0	4.66 <4.0 E-1	2.1 <4.0 E-1	2.1 <3.0 E-1	2.1 <2.7	2.7 <2.65	
Sn	<1.0	1.0 <1.29 E+2	7.02 E+2 <5.38 E+2	7.45 E+2 <1.52 E+2	7.45 E+2 <4.46 E+2					
Te	1.13 E+2	1.29 E+2 <2.20 E+2	7.02 E+2 <5.38 E+2	7.45 E+2 <1.52 E+2	7.45 E+2 <4.46 E+2					

a. Uncertainty is 30–50% because of problems associated with the analysis.

TABLE D-6. RESULTS OF ELEMENTAL ANALYSIS OF SAMPLE 7
(mg element/g sample)

as uncertainty is usually because of problems associated with the analysis.

b. Not reported because of analysis problems.

TABLE D-7. RESULTS OF ELEMENTAL ANALYSIS OF SAMPLE 8
(mg element/g sample)

Element	Particle Size Fraction (μm)								1000-1680 ^a				
	>4000 ^a Particle 8A	>4000 Particle 8B	>4000 Particle 8C	>4000 Particle 8D	>4000 Particle 8E	>4000 ^a Particle 8F	>4000 ^a Particle 8G	>4000 ^a Particle 8H	1680-4000 ^a Particle 8E	1680-4000 ^a Particle 8F	1680-4000 ^a Particle 8G	1680-4000 ^a Particle 8H	1000-1680 ^a Particle 8I
A9	<2.0	<8.0 E-1	-b	-b	4.0	2.0	<3.0	<2.0	<8.0 E-1	1.0 E+1	1.0 E+1	1.0 E+1	6.0
A1	2.0 E+1	<4.0	-b	-b	2.0 E+1	9.0	3.7 E+1	<2.0	<2.0	1.0 E+1	1.0 E+1	1.0 E+1	6.0
B	<3.0	<1.0	-b	-b	<3.0	<2.0	<4.2	<4.0 E-1	<4.0 E-1	<2.0 E-1	<2.0 E-1	<2.0 E-1	<1.0 E-1
Cd	<5.0 E-1	<2.0 E-1	-b	-b	<6.0 E-1	<3.0 E-1	<8.3 E-1	<3.0 E-1	<3.0 E-1	<6.0 E-1	<6.0 E-1	<6.0 E-1	<1.0 E-1
Cr	6.5	1.0	-b	-b	7.5	3.0	1.1 E+1	3.0	2.1	2.0	2.0	2.0	1.0
Cu	3.0	1.0	-b	-b	5.0	2.0	1.1 E+1	5.0	2.1	2.0	2.0	2.0	1.0
Fe	2.0	<4.0 E-1	-b	-b	5.0	2.4 E+1	1.7 E+1	1.7 E+1	1.7 E+1	1.1 E+1	1.1 E+1	1.1 E+1	6.3
Gd	<4.0	<1.0	-b	-b	<4.0	<2.0	<5.8	<2.0	<3.0	<1.0	<1.0	<1.0	<1.0
In	<2.0 E+1	<6.0	-b	-b	<2.0 E+1	<9.0	3.0 E-1	<2.5 E+1	<2.5 E+1	<1.0 E+1	<1.0 E+1	<1.0 E+1	<6.0 E-1
Mn	<3.0 E+1	<1.0 E-1	-b	-b	6.0 E-1	3.0 E-1	8.3 E-1	4.0 E-1	4.0 E-1	3.1 E-1	3.1 E-1	3.1 E-1	3.1 E-1
Mo	<5.0	<2.0	-b	-b	<6.0	<3.0	<8.3	<4.0	<4.0	<2.0	<2.0	<2.0	<2.0
Ni	5.0	<1.0	-b	-b	<3.0	6.3	1.1 E+1	6.3	1.1 E+1	<1.0	<1.0	<1.0	<1.0
Nb	<2.0 E+1	<6.0	-b	-b	<2.0 E+1	<9.0	3.1 E+1	<2.5 E-1	<2.5 E-1	<1.0 E+1	<1.0 E+1	<1.0 E+1	<6.0 E-1
Si	5.15 E+1	2.28 E+1	-b	-b	5.5 E+1	7.0	1.1 E+1	7.0 E+1	7.0 E+1	4.9 E+1	4.9 E+1	4.9 E+1	3.17 E+1
Sn	<3.0 E+1	<1.0 E+1	-b	-b	<2.0 E+1	<2.0	4.1 E+1	<2.0 E+1	<2.0 E+1	<1.0 E+1	<1.0 E+1	<1.0 E+1	<1.0 E+1
Te	<1.0 E+1	<4.0	-b	-b	<1.0 E+1	<6.0	1.6 E+1	<1.6 E+1	<1.6 E+1	<9.0	<9.0	<9.0	<4.0
U	7.15 E+2	8.12 E+2	-b	-b	9.66 E+2	5.52 E+2	7.84 E+2	5.52 E+2	7.84 E+2	1.62 E+2	1.62 E+2	1.62 E+2	5.0 E+1
Zr	8.0 E+1	-b	-b	-b	5.0 E+2	3.0 E+2	1.62	1.62	1.62	8.0 E+1	8.0 E+1	8.0 E+1	5.0 E+1
1000-1680 ^a													Sweepings ^a
A9	<0.0	<1.0	<2.0	<3.0	8.1	5.4	<3.0	<1.1 E+1	<1.1 E+1	1.1 E+1	1.1 E+1	1.1 E+1	4.0
A1	6.0 E+1	1.0 E+1	2.0 E+1	<5.0	2.0 E+1	1.1 E+1	2.0 E+1	<2.0 E-1	<2.0 E-1	2.9 E+1	2.9 E+1	2.9 E+1	1.3 E+1
B	<1.0 E+1	4.0	5.0	<6.0	5.0 E-1	1.5	0.0	<0.0	<0.0	2.0	2.0	2.0	2.1
Ca	<4.0 E-1	<5.0	<6.0 E-1	<6.0	1.3 E+1	4.9	3.3	7.0 E+1	7.0 E+1	2.2	2.2	2.2	1.4 E+1
Cr	2.9 E+1	8.8	9.6	1.3 E+1	5.0 E	1.0	1.8	4.0	4.0	1.0	1.0	1.0	3.0
Cu	1.0 E+1	<9.0 E-1	4.0	5.0 E	6.3	1.7 E+1	2.65 E+1	6.0	6.0	1.9 E+1	1.9 E+1	1.9 E+1	2.9 E+1
Fe	3.4 E+1	<1.5 E+1	7.2	<4.0	<2.0 E+1	<1.0	<6.0	<6.0	<6.0	<6.0	<6.0	<6.0	<4.0 E+1
Gd	<1.0 E+1	<3.0	<3.0	<2.0 E+1	<2.0 E+1	<7.0	<4.0	<2.0 E+1	<2.0 E+1	1.0 E+1	1.0 E+1	1.0 E+1	4.0 E+1
In	<6.0 E+1	<1.0 E+1	<1.0 E+1	<6.0 E-1	6.0 E-1	3.9 E-1	7.2 E-1	<1.0	<1.0	3.8 E-1	3.8 E-1	3.8 E-1	1.6
Mn	2.0	4.0 E-1	5.0 E-1	<6.0	<2.0 E+1	<2.0	<1.0	<7.0	<7.0	<6.0	<6.0	<6.0	<6.0
Mo	<2.0 E+1	<4.0	<5.0	<6.0	<6.0	<1.0	<1.0	<7.0	<7.0	6.5	6.5	6.5	6.0
Ni	<1.0 E+1	<2.0	5.0	6.0	8.6	8.9	1.5 E+1	<2.0 E+1	<2.0 E+1	<2.0 E+1	<2.0 E+1	<2.0 E+1	<2.0 E+1
Nb	6.0 E+1	<1.0 E+1	<1.0 E+1	<2.0 E+1	<2.0 E+1	<7.0	<4.0	<2.0 E+1	<2.0 E+1	7.0	7.0	7.0	<2.0 E+1
Si	3.76 E+2	5.76 E+1	6.58 E+1	9.50 E+1	9.50 E+1	1.61 E+1	1.61 E+1	<1.0 E+1	<1.0 E+1	2.98 E+1	2.98 E+1	2.98 E+1	8.52 E+1
Sn	<1.0 E+2	<2.0	4.8 E+1	<3.0 E+1	<1.0 E+1	<7.0	<4.0	<2.0 E+1	<2.0 E+1	1.0 E+1	1.0 E+1	1.0 E+1	6.0 E+1
Te	<4.0 E+1	<7.0	<1.0 E+1	<1.0 E+1	<5.0	<3.0	<1.0	<1.0 E+1	<1.0 E+1	1.0 E+1	1.0 E+1	1.0 E+1	<1.0 E+1
U	6.3 E+2	8.10 E+2	2.80 E+2	4.21 E+2	3.18 E+2	4.77 E+2	4.77 E+2	4.28 E+2	4.28 E+2	4.87 E+2	4.87 E+2	4.87 E+2	3.97 E+2
Zr	5.0 E+2	2.0 E+2	3.08 E+2	3.9 E+1	1.84 E+2	2.60 E+2	2.74 E+2	2.60 E+2	2.74 E+2	3.97 E+2	3.97 E+2	3.97 E+2	1.30 E+2

a. Uncertainty is 30-50% because of problems associated with the analysis.

- b. Not reported because of analysis problems.

TABLE U-8. RESULTS OF ELEMENTAL ANALYSIS OF SAMPLE 9
(mg element/g sample)

3. Uncertainty is 30-50% because of problems associated with the analysis.

not reported because of sensitivity problems.

TABLE D-9. RESULTS OF ELEMENTAL ANALYSIS OF SAMPLE 10
(mg element/g sample)

Element	Particle Size Fraction ^a										Particle Size Fraction ^b			
	1000 Particle 10A		>4000 Particle 10B		>4000 Particle 10C		>4000 Particle 10D		>4000 Particle 10E		1680-4000 Particle 10F		1680-4000 Particle 10G	
Ag	<0.0	9.1 E-1	6.3 E-1	5.6 E-1	1.1	<9.0 E-1	<4.0	<1.0	<4.0	<1.0	8.0 E-1	3.0	<1.0	<1.0
Al	<0.0	<8.0 E-1	<4.0 E-1	<1.0	<3.0 E-1	<2.0 E-1	<1.0	<2.0 E-1	<1.0	<3.0 E-1	<0.0 E-1	<0.0 E-1	<5.0	<1.0
B	<0.0	<2.0 E-1	<9.0 E-2	<5.0 E-2	<5.0 E-2	<5.0 E-2	9.0 E-2	2.0 E-1	6.0 E-1	6.0 E-1	<1.0 E-1	3.0 E-1	<3.0 E-1	<1.0
Cd	<0.0	<4.0 E-2	<2.0 E-2	<6.0 E-2	<6.0 E-2	<6.0 E-2	3.0 E-1	3.0 E-1	6.0 E-1	6.0 E-1	<5.0 E-1	3.2	2.0	<1.0
Cr	<0.0	1.9	<6.0 E-2	<6.0 E-2	<6.0 E-2	<6.0 E-2	3.0 E-1	2.0 E-1	<5.0 E-1	<4.0 E-1	<3.0 E-1	4.1	1.3	E+
Cu	<0.0	2.0 E-1	9.0 E-2	3.0 E-1	<1.0 E-1	<1.0 E-1	1.4	6.0	2.4	2.4	<8.0 E-1	<8.0 E-1	<2.0	<1.0
Fe	<0.0	<4.0 E-2	<4.0 E-2	<1.0 E-1	7.2 E-1	6.1 E-1	<1.0	<1.0	<1.0	<1.0	<6.0	<6.0	<8.0	<1.0
Gd	<0.0	1.2	9.0 E-1	6.0 E-1	3.0 E-1	3.0 E-1	3.0	3.0	3.0	3.0	<2.0 E-1	2.0 E-1	3.0	<1.0
In	<0.0	2.0	<6.0 E-1	<6.0 E-1	1.2 E-1	1.2 E-1	1.6 E-1	1.1 E-1	1.1 E-1	1.1 E-1	<2.0 E-1	<2.0 E-1	<3.0 E-1	<3.0 E-1
Mn	<0.0	2.3 E-1	<2.0 E-1	<2.0 E-1	<5.0 E-1	<5.0 E-1	<4.0 E-1	<4.0 E-1	<4.0 E-1	<4.0 E-1	<2.0 E-1	<2.0 E-1	<3.0 E-1	<3.0 E-1
Mo	<0.0	<4.0 E-1	<4.0 E-1	2.0 E-1	<3.0 E-1	<3.0 E-1	1.3	2.0	2.0	2.0	<8.0 E-1	<8.0 E-1	5.8	<1.0
Ni	<0.0	3.5	<6.0 E-1	<6.0 E-1	<2.0	<2.0	<1.0	<6.0	<6.0	<6.0	<5.0	<5.0	<8.0	<1.0
Nb	<0.0	<1.0	<6.0 E-1	4.8	9.5 E-1	2.5	1.2	3.1	2.3	2.3	4.1	4.1	1.2	E+
Si	<0.0	4.8	9.5 E-1	1.9	<3.0	4.4	<1.0	<1.0	<1.0	<1.0	<8.0	<8.0	<1.0	E+
Sn	<0.0	<2.0 E-1	<2.0 E-1	<1.0	<9.0 E-1	<4.0	<4.0	<4.0	<4.0	<4.0	<2.0	<2.0	<5.0	<1.0
Te	<0.0	8.83 E+2	7.09 E+2	3.28	7.54 E+1	6.49 E+2	6.31 E+2	6.31 E+2	6.31 E+2	6.31 E+2	6.84 E+2	6.84 E+2	3.53 E+2	2.4 E+1
U	<0.0	6.93 E+1									3.96 E+1	3.96 E+1	3.89 E+1	
Zr	<0.0													
Ag	1000-1680 Particle 10J	1000-1680 Particle 10K	707-1000 Aliquot	297-707 Aliquot	149-297 Aliquot	\$4-149 ^a Aliquot	3U-74 ^a Aliquot	3U-74 ^a Aliquot	20-30 Aliquot	Sweepings				
Al	<1.0	<1.0	1.2	<1.0	<4.0	4.0	6.6	6.6	5.5	2.5	E+			
B	8.0	<6.0	3.4	1.0 E+1	3.0 E+1	1.0 E+1	8.4	8.4	8.0	8.0	E-1		5.0	E+
Cd	<3.0 E-1	6.0 E-1	3.0 E-1	7.0 E-2	<3.0 E-1	<6.0	<2.0	<2.0	<2.0	<8.0 E-1	<8.0 E-1	<4.0	<4.0	
Cr	2.0	<8.0 E-1	4.6	<1.0	<1.0	<1.0	<3.0	<3.0	<3.0	1.0	1.0	8.0	E-1	<8.0
Cu	1.0	<7.0 E-1	6.9 E-1	<8.0 E-1	6.0	6.0	<8.0 E-1	<8.0 E-1	<8.0 E-1	<8.0 E-1	<4.0 E-1	3.3	E-1	<2.0
Fe	3.0	2.0	7.27	9.8	3.0 E+1	9.9	1.80 E+1	1.80 E+1	1.80 E+1	1.80 E+1	1.4 E+1	1.4 E+1	2.6	E+
Ga	<2.0	<2.0	<5.0 E-1	<2.0	<2.0	<8.0	<2.0	<2.0	<2.0	<2.0	<1.0	<1.0	<5.0	<1.0
In	<8.0	<8.0	<2.0	<1.0 E+1	<3.0 E+1	<1.0 E+1	<1.0 E+1	<1.0 E+1	<1.0 E+1	<1.0 E+1	<5.0	<5.0	<2.0	E+
Mn	<1.0 E-1	3.0 E-1	1.9 E-1	3.0 E-1	2.6	2.6	3.0 E-1	3.0 E-1	3.0 E-1	4.2 E-1	3.3	E-1	8.0	E-1
Mo	<3.0	<3.0	<7.0 E-1	<3.0	<3.0	<3.0	<1.0 E+1	<1.0 E+1	<1.0 E+1	<2.0	<2.0	<2.0	<8.0	
Ni	<1.0	7.2	1.4	<2.0	<2.0	<2.0	<2.0	<2.0	<2.0	<2.0	5.3	4.9	8.0	
No	<8.0	<8.0	<1.0 E+1	<1.0 E+1	<1.0 E+1	<1.0 E+1	<1.0 E+1	<1.0 E+1	<1.0 E+1	<1.0 E+1	<5.0	<5.0	<2.0	E+
Si	1.4 E+	1.0 E+1	9.60	3.97 E+1	1.51 E+2	4.67 E+1	6.72	6.72	6.72	6.72	2.34 E+1	2.34 E+1	1.19 E+2	
Sn	<1.0 E+1	<1.0 E+1	6.9	<2.0 E+1	<6.0 E+1	<2.0 E+1	<8.0	<8.0	<8.0	<8.0	<4.0 E+1	<4.0 E+1	<4.0 E+1	
Te	<5.0	<6.0	<1.0	<7.0	<7.0	<7.0	<7.0	<7.0	<7.0	<7.0	<3.0	<3.0	<2.0	
U	5.37 E+2	9.67 E+2	6.43 E+2	3.77 E+2	3.30 E+2	1.71 E+2	3.67 E+2	3.67 E+2	3.67 E+2	3.67 E+2	4.68 E+2	4.68 E+2	6.1 E+2	
Zr	8.59 E+1	5.6	2.10 E+2	6.50 E+1	2.24 E+2	1.26 E+2	1.63 E+2	1.63 E+2	1.63 E+2	1.63 E+2	4.24 E+2	4.24 E+2		

a. Uncertainty is 30-50% because of problems associated with the analysis.

b. Not reported because of analysis problems.

TABLE V-10. RESULTS OF ELEMENTAL ANALYSIS OF SAMPLE 11
(mg element/g sample)

[REDACTED]

D. 4.1 Refining process of analysis problems.

APPENDIX E

RADIOCHEMICAL ANALYSES

APPENDIX E

RADIOCHEMICAL ANALYSES

This Appendix presents results of the radiochemical analyses of the TMI-2 core debris grab samples. All analyses were performed on the same portions of each sample. Gamma emitting radionuclides measured by gamma spectroscopy were ^{60}Co , ^{106}Ru , $^{110\text{m}}\text{Ag}$, ^{125}Sb , ^{134}Sc , ^{137}Cs , ^{144}Ce , ^{154}Eu , and ^{155}Eu . Results of the ^{90}Sr analysis were obtained by radiochemical separation and subsequent beta emitter analysis. The ^{129}I and fissile/fertile material results were obtained by neutron activation analysis, with subsequent gamma spectroscopy and delayed neutron analysis, respectively. Results of all analyses are reported in $\mu\text{Ci/g}$ sample, except for the fissile/fertile material contents which are reported in mg. All activities are decay corrected to April 1, 1984.

TABLE E-1. RESULTS OF RADIONUCLIDE ANALYSIS OF SAMPLE 1 ($\mu\text{Ci/g}$ sample)

a. Uncertainty is ~30% because of problems associated with the analysis.

b. Not detected.

TABLE E--. RESULTS OF RADIONUCLIDE ANALYSIS OF SAMPLE 3
(μ Ci/g sample)

Radionuclide	Particle Size Fraction					
	4000 ^a	4000 ^a				
⁸⁸ Br	4.67 ± 0.27 E+1	5.94 ± 0.41 E+1	1.30 ± 0.05 E+1	2.03 ± 0.29	1.33 ± 0.24	2.20 ± 0.30
⁹⁰ Sr	7.5 ± 0.4 E+3	2.6 ± 0.1 E+1	5.3 ± 0.3 E+3	4.1 ± 0.1 E+3	8.4 ± 0.4 E+3	9.2 ± 0.4 E+3
¹⁰³ Ru	6.25 ± 0.36 E+1	3.76 ± 0.35	4.03 ± 0.24 E+2	1.46 ± 0.08 E+3	1.43 ± 0.08 E+3	1.73 ± 0.10 E+3
¹¹³ In-Ag	1.00 ± 0.08 E+1	1.00 ± 0.08 E+1	1.00 ± 0.13 E+1	1.34 ± 0.08 E+2	1.25 ± 0.08 E+2	6.40 ± 0.73 E+1
¹³⁷ Cs	1.1 ± 0.5 E-5	5.8 ± 1.9 E-4	1.06 ± 0.08	8.4 ± 0.3 E-5	1.43 ± 0.04 E-3	2.4 ± 0.3 E-4
¹³⁴ S	3.45 ± 0.26	5.00 ± 0.42 E+1	2.23 ± 0.18	5.06 ± 0.32 E+1	5.19 ± 0.30 E+1	7.93 ± 0.35 E+1
¹³⁵ S	5.87 ± 0.34 E+1	1.17 ± 0.08 E+1	4.65 ± 0.28 E+1	9.49 ± 0.52 E+1	8.36 ± 0.47 E+1	5.00 ± 0.60 E+1
¹³⁷ Cl	1.77 ± 0.12 E+3	5.79 ± 0.52 E+3	1.75 ± 0.11 E+3	5.94 ± 0.25 E+3	4.67 ± 0.25 E+3	4.67 ± 0.53 E+3
¹³⁷ Br	3.00 ± 0.19 E+1	7.15 ± 0.75 E+1	2.24 ± 0.14 E+1	6.67 ± 0.41 E+1	6.83 ± 0.42 E+1	7.87 ± 0.43 E+1
¹³⁵ Eu	7.4 ± 1.5 E+1	2.92 ± 0.59	6.04 ± 0.43 E+1	1.54 ± 0.32 E+2	1.36 ± 0.27 E+2	2.07 ± 0.46 E+2
 1660-1660 ^a						
⁸⁸ Br	1000-1660 ^a	1000-1660 ^a				
⁸⁸ Br	6.41 ± 0.75	6.14 ± 0.71	7.13 ± 0.49 E+1	7.29 ± 0.27 E+1	6.41 ± 0.41	6.41 ± 0.59 E+1
⁹⁰ Sr	1.10 ± 0.05 E+3	2.8 ± 0.1 E+3	3.8 ± 0.2 E+3	1.89 ± 0.09 E+1	3.5 ± 0.1 E+2	4.4 ± 0.2 E+3
¹⁰³ Ru	1.81 ± 0.21 E+2	3.61 ± 0.47 E+1	2.39 ± 0.17 E+2	2.05 ± 0.24 E+2	4.17 ± 0.28 E+1	2.07 ± 0.14 E+2
¹¹³ In-Ag	1.68 ± 0.22 E+1	4.4 ± 1.3	4.45 ± 0.36 E+1	2.39 ± 0.30 E+1	9.00 ± 0.81	3.37 ± 0.25 E+1
¹²⁵ Sr	1.5 ± 0.3 E-4	3.1 ± 0.7 E-4	6.57 ± 0.71 E+1	6.48 ± 0.78	2.0 ± 0.3 E-4	2.0 ± 0.3 E-4
¹³⁴ S	1.06 ± 0.12 E+1	6.57 ± 0.71 E+1	4.80 ± 0.33 E+1	6.48 ± 0.78	1.16 ± 0.07 E+1	3.10 ± 0.20 E+1
¹³⁵ S	2.95 ± 0.45 E+2	1.73 ± 0.13 E+3	3.32 ± 0.63 E+2	1.03 ± 0.12 E+3	2.05 ± 0.12 E+2	5.40 ± 0.34 E+2
¹³⁷ Cl	3.10 ± 0.69 E+1	1.55 ± 0.19 E+3	4.55 ± 0.19 E+3	1.31 ± 0.18 E+3	4.53 ± 0.16 E+3	2.38 ± 0.16 E+3
¹³⁷ Br	4.34 ± 0.55	2.54 ± 0.30 E+1	4.29 ± 0.31 E+1	2.33 ± 0.28 E+1	4.69 ± 0.28 E+1	4.46 ± 0.30 E+1
¹³⁵ Eu	2.82 ± 0.33 E+1	5.6 ± 1.1 E+1	1.13 ± 0.23 E+2	5.72 ± 0.66 E+1	1.10 ± 0.22 E+2	1.00 ± 0.20 E+2
 297-307						
⁸⁸ Br	149-297 Aliquot	149-297 Aliquot	74-149 Aliquot	74-149 Aliquot	30-74 ^b Aliquot	30-74 ^b Aliquot
⁸⁸ Br	2.21 ± 0.18 E+1	6.61 ± 0.37 E+1	8.59 ± 0.61 E+1	1.40 ± 0.14 E+2	1.02 ± 0.26 E+2	1.02 ± 0.26 E+2
⁹⁰ Sr	3.1 ± 0.2 E+3	6.6 ± 0.09 E+3	2.9 ± 0.2 E+3	3.6 ± 0.2 E+3	9.0 ± 0.2 E+3	9.0 ± 0.2 E+3
¹⁰³ Ru	1.19 ± 0.09 E+1	3.09 ± 0.17 E+2	2.33 ± 0.17 E+1	6.50 ± 0.44 E+1	1.46 ± 0.63 E+1	1.46 ± 0.63 E+1
¹¹³ In-Ag	1.93 ± 0.19 E+1	1.09 ± 0.06 E+2	1.93 ± 0.14 E+2	2.21 ± 0.15 E+1	1.78 ± 0.46 E+2	1.78 ± 0.46 E+2
¹²⁵ Sr	1.6 ± 0.2 E-4	1.6 ± 0.2 E-4	7.6 ± 0.3 E-4	8.6 ± 0.4 E-4	1.17 ± 0.01 E-3	1.17 ± 0.01 E-3
¹³⁴ S	3.50 ± 0.27 E+1	4.31 ± 0.4 E+1	5.15 ± 0.37 E+1	5.16 ± 0.35 E+1	2.87 ± 0.74 E+1	2.87 ± 0.74 E+1
¹³⁵ S	8.90 ± 0.60 E+2	6.6 ± 1.7 E+2	8.35 ± 0.65 E+2	9.00 ± 0.49 E+2	9.05 ± 0.64 E+2	9.05 ± 0.64 E+2
¹³⁷ Cl	1.69 ± 0.15 E+1	1.64 ± 0.10 E+1	1.48 ± 0.12 E+1	1.19 ± 0.09 E+1	7.5 ± 2.0 E+2	7.5 ± 2.0 E+2
¹³⁷ Br	1.73 ± 0.14 E+1	1.05 ± 0.28 E+1	3.16 ± 0.26 E+1	2.59 ± 0.16 E+1	2.30 ± 0.19 E+1	2.30 ± 0.19 E+1
¹³⁵ Eu	4.9 ± 1.0 E+1	3.07 ± 0.79 E+1	3.83 ± 0.31 E+1	8.2 ± 1.6 E+1	6.3 ± 1.3 E+1	6.3 ± 1.3 E+1

a. Uncertainty is ± 0.02 because of problems associated with the analysis.

b. Not detected.

TABLE E-3. RESULTS OF RADIONUCLIDE ANALYSIS OF SAMPLE 4
 $(\mu\text{Ci}/\text{g sample})$

Radionuclide	Particle 4A	Particle 4B ^a	Particle 4C	Particle 4D ^a	Particle 4E ^a
⁶⁰ Co	6.45 + 0.73 E+1	5.33 + 0.33 E+1	2.51 + 0.17 E+2	1.77 + 0.33	1.99 + 0.20 E+1
⁹⁰ Sr	5.9 + 0.3 E+3	9.4 + 0.4 E+1	1.9 + 0.1 E+3	5.4 + 0.3 E+3	9.2 + 0.5 E+3
¹⁰⁶ Ru	1.52 + 0.17 E+3	1.12 + 0.71 E+3	6.00 + 0.41 E+2	9.4 + 1.2 E+2	1.37 + 0.15 E+3
^{110m} Ag	-b	-b	-b	-b	-b
¹²⁵ Sb	9.9 + 1.1 E+1	3.21 + 0.25 E+1	4.94 + 0.38 E+1	9.7 + 1.2 E+1	6.43 + 0.72 E+2
¹²⁹ I	1.0 + 0.2 E-4	2.7 + 0.6 E-5	4.9 + 1.3 E-5	7.8 + 3.0 E-4	-b
¹³⁴ Cs	4.64 + 0.54 E+1	8.16 + 0.61	1.34 + 0.10 E+1	1.13 + 0.14 E+2	2.44 + 0.26 E+1
¹³⁷ Cs	7.77 + 0.86 E+2	1.68 + 0.10 E+2	3.65 + 0.24 E+2	2.52 + 0.31 E+3	4.00 + 0.42 E+2
¹⁴⁴ Ce	3.91 + 0.46 E+3	3.65 + 0.25 E+3	2.51 + 0.19 E+3	2.96 + 0.38 E+3	3.80 + 0.41 E+3
¹⁵⁴ Eu	6.82 + 0.77 E+1	4.39 + 0.28 E+1	2.03 + 0.16 E+1	3.89 + 0.50 E+1	6.34 + 0.68 E+1
¹⁵⁵ Eu	1.43 + 0.29 E+2	1.40 + 0.28 E+2	1.07 + 0.21 E+2	3.99 + 0.77 E+1	1.29 + 0.14 E+2

a. Uncertainty is ~30% because of problems associated with the analysis.

b. Not detected.

TABLE E-4. RESULTS OF RADIONUCLIDE ANALYSIS OF SAMPLE D
($\mu\text{Ci/g}$ sample)

Radionuclide	Particle Size Fraction (μm)					
	>4000 ^a		>4000 ^a		>4000 ^a	
Particle 5A	Particle 5B	Particle 5C	Particle 5D	Particle 5E	Particle 5F	
^{60}Co	2.06 ± 0.36 E+1	4.51 ± 0.31 E+1	3.94 ± 0.28 E+1	2.81 ± 0.25	1.20 ± 0.09 E+2	2.07 ± 0.19
^{90}Sr	6.2 ± 0.3 E+3	4.0 ± 0.2 E+3	4.5 ± 0.2 E+3	6.2 ± 0.3 E+3	3.2 ± 0.2 E+2	8.2 ± 0.4 E+1
^{138}Cs	1.20 ± 0.21 E+3	1.15 ± 0.08 E+3	1.04 ± 0.07 E+3	5.40 ± 0.36 E+2	1.19 ± 0.08 E+3	5.58 ± 0.34 E+2
^{137}Cs	-	-	-	-	-	-
^{135}Cs	9.11 ± 0.16 E+1	1.47 ± 0.10 E+2	2.47 ± 0.24 E+1	3.86 ± 0.28 E+1	3.00 ± 0.22 E+2	6.35 ± 0.40 E+1
^{129}I	1.1 ± 0.2 E-4	-	3.0 ± 0.9 E-5	1.9 ± 0.3 E-4	-	1.3 ± 0.3 E-3
^{134}Cs	1.27 ± 0.23 E+2	1.53 ± 0.11 E+1	9.55 ± 0.75	2.25 ± 0.15 E+1	6.78 ± 0.55	2.92 ± 0.18 E+1
^{144}Ce	2.14 ± 0.38 E+2	2.95 ± 0.20 E+2	1.64 ± 0.11 E+2	6.89 ± 0.45 E+2	1.48 ± 0.11 E+2	7.90 ± 0.47 E+2
^{154}Eu	3.60 ± 0.65 E+3	3.84 ± 0.27 E+3	3.15 ± 0.24 E+3	1.81 ± 0.13 E+3	2.13 ± 0.17 E+3	1.86 ± 0.12 E+3
^{155}Eu	6.54 ± 0.11 E+1	5.45 ± 0.42 E+1	4.27 ± 0.35 E+1	1.58 ± 0.12 E+1	3.82 ± 0.29 E+1	1.73 ± 0.12 E+1
^{148}Eu	1.48 ± 0.29 E+2	1.33 ± 0.27 E+2	1.35 ± 0.27 E+2	8.1 ± 1.6 E+1	9.9 ± 2.0 E+1	7.4 ± 1.5 E+1
	1680-4000 ^a					
	Particle 5H					
^{60}Co	3.10 ± 0.18 E+1	-	6.57 ± 0.40 E-1	1.09 ± 0.18	<1000 ^a	5.53 ± 0.34 E+1
^{90}Sr	5.0 ± 0.2 E+1	-	3.9 ± 0.1 E+3	2.9 ± 0.1 E+3	-	-
^{138}Cs	6.93 ± 0.38 E+2	-	1.44 ± 0.09 E+3	1.29 ± 0.09 E+3	-	6.53 ± 0.40 E+2
^{137}Cs	-	-	-	-	-	-
^{129}I	1.32 ± 0.11 E+1	-	1.02 ± 0.07 E+2	1.16 ± 0.08 E+2	-	8.01 ± 0.55 E+1
^{134}Cs	5.5 ± 0.8 E-4	-	-	5.4 ± 0.9 E-5	-	-
^{137}Cs	2.86 ± 0.26	-	3.17 ± 0.20 E+1	3.29 ± 0.23 E+1	-	9.85 ± 0.59 E+1
^{144}Ce	3.78 ± 0.21 E+1	-	5.08 ± 0.31 E+2	5.36 ± 0.37 E+2	-	1.71 ± 0.10 E+3
^{154}Eu	2.36 ± 0.14 E+3	-	3.36 ± 0.25 E+3	3.40 ± 0.26 E+3	-	2.24 ± 0.17 E+3
^{155}Eu	2.94 ± 0.18 E+1	-	6.26 ± 0.42 E+1	6.23 ± 0.45 E+1	-	3.54 ± 0.25 E+1
	1.02 ± 0.20 E+2	-	1.62 ± 0.32 E+2	1.39 ± 0.26 E+2	-	1.06 ± 0.20 E+2
	1680-4000 ^a					
	Particle 5J					
^{60}Co	3.10 ± 0.18 E+1	-	6.57 ± 0.40 E-1	1.09 ± 0.18	<1000 ^a	5.53 ± 0.34 E+1
^{90}Sr	5.0 ± 0.2 E+1	-	3.9 ± 0.1 E+3	2.9 ± 0.1 E+3	-	-
^{138}Cs	6.93 ± 0.38 E+2	-	1.44 ± 0.09 E+3	1.29 ± 0.09 E+3	-	6.53 ± 0.40 E+2
^{137}Cs	-	-	-	-	-	-
^{129}I	1.32 ± 0.11 E+1	-	1.02 ± 0.07 E+2	1.16 ± 0.08 E+2	-	8.01 ± 0.55 E+1
^{134}Cs	5.5 ± 0.8 E-4	-	-	5.4 ± 0.9 E-5	-	-
^{137}Cs	2.86 ± 0.26	-	3.17 ± 0.20 E+1	3.29 ± 0.23 E+1	-	9.85 ± 0.59 E+1
^{144}Ce	3.78 ± 0.21 E+1	-	5.08 ± 0.31 E+2	5.36 ± 0.37 E+2	-	1.71 ± 0.10 E+3
^{154}Eu	2.36 ± 0.14 E+3	-	3.36 ± 0.25 E+3	3.40 ± 0.26 E+3	-	2.24 ± 0.17 E+3
^{155}Eu	2.94 ± 0.18 E+1	-	6.26 ± 0.42 E+1	6.23 ± 0.45 E+1	-	3.54 ± 0.25 E+1
	1.02 ± 0.20 E+2	-	1.62 ± 0.32 E+2	1.39 ± 0.26 E+2	-	1.06 ± 0.20 E+2

a. Uncertainty is ~30% because of problems associated with the analysis.

b. not detected.

c. Not reported because a portion of the sample was lost in analysis.

TABLE E-5. RESULTS OF RADIONUCLIDE ANALYSIS OF SAMPLE 6
($\mu\text{Ci/g}$ sample)

Radionuclide	Particle Size Fraction (μm)									
	>4000		>4000		>4000		>4000		>4000	
	Particle 6A	Particle 6B	Particle 6C	Particle 6D	Particle 6E	Particle 6F	Particle 6G	Particle 6H	Particle 6I	Particle 6J
^{60}Co	6.07 + 0.67	1.66 + 0.09	3.34 + 0.23	2.3 + 0.1 E+1	1.24 + 0.09	4.89 + 0.35	9.3 + 2.1 E-1	- ^b	- ^b	- ^b
^{90}Sr	3.5 + 0.2 E+3	7.9 + 0.7 E+1	2.7 + 0.2 E+2	9.15 + 0.62 E+2	3.8 + 0.4 E+1	1.5 + 0.2 E+2	1.4 + 0.1 E+1	1.19 + 0.06 E+2	1.4 + 0.1 E+1	1.05 + 0.45 E+2
^{106}Ru	1.07 + 0.11 E+3	2.39 + 0.23	1.16 + 0.07 E+2	9.15 + 0.62 E+2	1.32 + 0.14	7.0 + 1.0	1.03 + 0.06 E+3	8.05 + 0.45 E+2	- ^b	- ^b
^{110}Ag	- ^b	- ^b	- ^b	- ^b	- ^b	- ^b	- ^b	- ^b	- ^b	- ^b
^{125}Sb	9.74 + 0.99 E+1	3.05 + 0.17 E+2	4.22 + 0.26 E+1	6.95 + 0.53 E+1	2.40 + 0.16 E+1	1.46 + 0.11 E+1	9.97 + 0.66 E+1	8.16 + 0.50 E+1	- ^b	- ^b
^{129}I	1.16 + 0.6 E-3	4.8 + 0.7 E-3	2.2 + 0.8 E-5	6.64 + 0.07 E-3	2.9 + 0.9 E-5	1.6 + 0.4 E-4	3.5 + 0.6 E-5	4.47 + 0.06 E-4	- ^b	- ^b
^{134}Cs	3.90 + 0.39 E+1	7.11 + 0.40	9.73 + 0.59	5.47 + 0.38 E+1	2.22 + 0.15	3.25 + 0.20 E+1	1.69 + 0.09 E+2	4.67 + 0.26 E+1	- ^b	- ^b
^{137}Cs	1.19 + 0.12 E+3	1.24 + 0.07 E+3	1.82 + 0.11 E+2	1.30 + 0.09 E+3	4.41 + 0.29 E+1	6.22 + 0.38 E+2	3.79 + 0.21 E+3	1.07 + 0.06 E+3	- ^b	- ^b
^{144}Ce	3.65 + 0.38 E+3	2.84 + 0.98 E+3	1.96 + 0.17 E+2	2.66 + 0.21 E+3	1.91 + 0.38	1.84 + 0.35 E+1	3.06 + 0.20 E+3	2.50 + 0.16 E+3	- ^b	- ^b
^{154}Eu	2.88 + 0.30 E+1	0.30 E+1	2.93 + 0.25	3.25 + 0.25 E+1	1.16 + 0.23 E+2	- ^b	- ^b	4.34 + 0.28 E+1	2.46 + 0.16 E+1	- ^b
^{155}Eu	1.51 + 0.30 E+2	2.21 + 0.88 E+1	1.03 + 0.07 E+1	1.16 + 0.23 E+2	- ^b	- ^b	- ^b	1.37 + 0.27 E+2	- ^b	- ^b
 1000-1680										
^{60}Co	2.74 + 0.16 E+2	7.33 + 0.43	6.87 + 0.55	1.43 + 0.08 E+2	5.15 + 0.29 E+1	9.21 + 0.59 E+1	1.11 + 0.06 E+2	1.25 + 0.09 E+2	- ^b	- ^b
^{90}Sr	3.8 + 0.2 E+2	1.4 + 0.6 E+3	4.2 + 0.2 E+3	8.9 + 0.4 E+1	1.14 + 0.05 E+2	2.5 + 0.1 E+3	2.3 + 0.1 E+3	2.6 + 0.1 E+3	- ^b	- ^b
^{106}Ru	2.64 + 0.16 E+3	2.92 + 0.16 E+2	5.81 + 0.35 E+2	4.20 + 0.23 E+2	2.19 + 0.13 E+2	2.94 + 0.17 E+2	3.74 + 0.21 E+2	5.23 + 0.37 E+2	- ^b	- ^b
^{110}Ag	- ^b	- ^b	- ^b	- ^b	- ^b	- ^b	- ^b	- ^b	- ^b	- ^b
^{125}Sb	8.28 + 0.49 E+1	1.78 + 0.11 E+1	8.15 + 0.59 E+1	8.77 + 0.52 E+1	9.77 + 0.57 E+1	1.46 + 0.08 E+2	1.89 + 0.11 E+2	1.67 + 0.12 E+2	- ^b	- ^b
^{129}I	9.49 + 0.03 E-4	2.1 + 0.1 E-5	1.27 + 0.03 E-3	5.60 + 0.1 E-4	4.77 + 0.05 E-4	6.7 + 0.3 E-4	1.92 + 0.02 E-3	2.4 + 0.1 E-3	- ^b	- ^b
^{134}Cs	2.08 + 0.34	4.97 + 0.57 E-1	1.76 + 0.10 E+2	5.66 + 0.31 E+1	5.82 + 0.32 E+1	5.36 + 0.30 E+1	4.81 + 0.27 E+1	5.00 + 0.35 E+1	- ^b	- ^b
^{137}Cs	2.98 + 0.18 E+1	1.10 + 0.06 E+1	4.06 + 0.24 E+3	1.23 + 0.07 E+3	1.13 + 0.06 E+3	1.07 + 0.06 E+3	9.58 + 0.53 E+2	9.54 + 0.67 E+2	- ^b	- ^b
^{144}Ce	3.20 + 0.34 E+2	6.90 + 0.44 E+2	3.48 + 0.24 E+3	2.29 + 0.15 E+3	2.11 + 0.15 E+3	1.40 + 0.09 E+3	1.27 + 0.09 E+3	1.11 + 0.09 E+3	- ^b	- ^b
^{154}Eu	5.04 + 0.64	1.34 + 0.08 E+1	5.07 + 0.34 E+1	3.63 + 0.22 E+1	3.55 + 0.22 E+1	2.16 + 0.22 E+1	2.14 + 0.14 E+1	1.83 + 0.14 E+1	- ^b	- ^b
^{155}Eu	- ^c	- ^c	- ^c	- ^c	- ^c	- ^c	- ^c	- ^c	- ^c	- ^c
 149-297 ^a										
^{60}Co	1000-1680	1000-1680	1000-1680	707-1000	297-707 ^a	149-297 ^a	74-149 ^a	30-74	Aliquot	
^{90}Sr	2.74 + 0.16 E+2	7.33 + 0.43	6.87 + 0.55	1.43 + 0.08 E+2	5.15 + 0.29 E+1	9.21 + 0.59 E+1	1.11 + 0.06 E+2	1.25 + 0.09 E+2	Aliquot	
^{106}Ru	2.64 + 0.16 E+3	2.92 + 0.16 E+2	5.81 + 0.35 E+2	4.20 + 0.23 E+2	2.19 + 0.13 E+2	2.94 + 0.17 E+2	3.74 + 0.21 E+2	5.23 + 0.37 E+2	Aliquot	
^{110}Ag	- ^b	- ^b	- ^b	- ^b	- ^b	- ^b	- ^b	- ^b	Aliquot	
^{125}Sb	8.28 + 0.49 E+1	1.78 + 0.11 E+1	8.15 + 0.59 E+1	8.77 + 0.52 E+1	9.77 + 0.57 E+1	1.46 + 0.08 E+2	1.89 + 0.11 E+2	1.67 + 0.12 E+2	Aliquot	
^{129}I	9.49 + 0.03 E-4	2.1 + 0.1 E-5	1.27 + 0.03 E-3	5.60 + 0.1 E-4	4.77 + 0.05 E-4	6.7 + 0.3 E-4	1.92 + 0.02 E-3	2.4 + 0.1 E-3	Aliquot	
^{134}Cs	2.08 + 0.34	4.97 + 0.57 E-1	1.76 + 0.10 E+2	5.66 + 0.31 E+1	5.82 + 0.32 E+1	5.36 + 0.30 E+1	4.81 + 0.27 E+1	5.00 + 0.35 E+1	Aliquot	
^{137}Cs	2.98 + 0.18 E+1	1.10 + 0.06 E+1	4.06 + 0.24 E+3	1.23 + 0.07 E+3	1.13 + 0.06 E+3	1.07 + 0.06 E+3	9.58 + 0.53 E+2	9.54 + 0.67 E+2	Aliquot	
^{144}Ce	3.20 + 0.34 E+2	6.90 + 0.44 E+2	3.48 + 0.24 E+3	2.29 + 0.15 E+3	2.11 + 0.15 E+3	1.40 + 0.09 E+3	1.27 + 0.09 E+3	1.11 + 0.09 E+3	Aliquot	
^{154}Eu	5.04 + 0.64	1.34 + 0.08 E+1	5.07 + 0.34 E+1	3.63 + 0.22 E+1	3.55 + 0.22 E+1	2.16 + 0.22 E+1	2.14 + 0.14 E+1	1.83 + 0.14 E+1	Aliquot	
^{155}Eu	- ^c	- ^c	- ^c	- ^c	- ^c	- ^c	- ^c	- ^c	Aliquot	

a. Uncertainty is ~30% because of problems associated with the analysis.

b. Not detected.

c. Not reported because of problems associated with the analysis.

TABLE I-6. RESULTS OF KAURI-NUCLEIC ACID ANALYSIS OF SAMPLE 7 (UCI/g sample)

a. Uncertainty is ~30% because of problems associated with the analysis.

D. S. G. DE LIMA

TABLE E-7. RESULTS OF GAMMA SPECTROSCOPY ANALYSIS OF SAMPLE 8
($\mu\text{Ci/g}$ sample)

Radionuclide	>4000 ^a		>4000		>4000 ^a		>4000		>4000		
	Particle 9A	Particle 9B	Particle 9C	Particle 9D	Particle 9E	Particle 9F	Particle 9G	Particle 9H	Particle 9I	Particle 9J	
60Co	5.55 \pm 0.11 E+1	-D	6.72 \pm 0.43	9.18 \pm 0.43	5.15 \pm 0.08 E+1	2.54 \pm 0.05 E+1					
90Sr	5.67 \pm 0.61 E+3	-D	1.37 \pm 0.15 E+4	-C	5.31 \pm 0.51 E+3	1.59 \pm 0.14 E+3					
106Ru	8.29 \pm 0.14 E+2	-D	4.35 \pm 0.56 E+1	3.370 \pm 0.004 E+3	6.60 \pm 0.28 E+1	1.97 \pm 0.14 E+1					
125Sb	-C	-D	2.09 \pm 0.26 E+1	2.11 \pm 0.24 E+1	3.23 \pm 0.15 E+1	5.37 \pm 0.67					
129I	-C	-D									
134Cs	5.19 \pm 0.12 E+1	-D	4.98 \pm 0.11 E+1	5.60 \pm 0.09 E+1	1.06 \pm 0.03 E+1	1.64 \pm 0.12					
137Cs	9.85 \pm 0.04 E+2	-D	8.93 \pm 0.04 E+2	9.85 \pm 0.03 E+2	2.84 \pm 0.01 E+2	3.67 \pm 0.04 E+1					
144Ce	3.26 \pm 0.15 E+3	-D	2.02 \pm 0.15 E+3	2.95 \pm 0.15 E+3	1.65 \pm 0.09 E+3	9.94 \pm 0.62 E+2					
154Eu	5.41 \pm 0.51 E+1	-D	3.98 \pm 0.31 E+1	5.41 \pm 0.31 E+1	1.33 \pm 0.20 E+1	1.43 \pm 0.10 E+1					
155Eu	-C	-D	7.7 \pm 2.5 E+1	1.13 \pm 0.37 E+2	6.7 \pm 2.2 E+1	5.7 \pm 1.9 E+1					
<hr/>											
1680-4000 ^a		1000-1680 ^a		1000-1680 ^a		1000-1680 ^a		1000-1680 ^a		707-100u	
Particle 86		Particle 8H		Particle 8I		Particle 8J		Particle 8K		Aliquot	
60Co	6.40 \pm 0.75	3.95 \pm 0.11 E+1	1.53 \pm 0.14 E+1	12.3 \pm 0.4 E+1	1.07 \pm 0.05 E+1	5.14 \pm 0.08 E+1					
90Sr	9.62 \pm 1.0 E+3	5.47 \pm 0.61 E+3	1.19 \pm 0.09 E+3	8.10 \pm 0.81 E+3	1.03 \pm 0.10 E+4	2.43 \pm 0.20 E+3					
106Ru	7.44 \pm 1.26 E+1	9.41 \pm 0.14 E+2	8.86 \pm 1.92 E+1	7.3 \pm 1.7	3.51 \pm 0.42 E+1	5.76 \pm 0.28 E+1					
125Sb	5.36 \pm 0.66 E+1	5.72 \pm 0.32 E+1	3.82 \pm 0.91 E+1	6.15 \pm 0.91	1.87 \pm 0.26 E+1	2.49 \pm 0.15 E+1					
129I	-C	-C	5.08 \pm 1.86 E-5								
134Cs	3.83 \pm 1.34 E-4	1.36 \pm 0.03 E+2	1.36 \pm 0.03 E+2	1.37 \pm 0.03 E+1	3.00 \pm 0.82 E+1	7.32 \pm 0.35					
137Cs	1.31 \pm 0.02 E+2	1.25 \pm 0.71 E+1	1.25 \pm 0.13 E+3	2.54 \pm 0.01 E+2	5.28 \pm 0.01 E+2	1.80 \pm 0.01 E+2					
144Ce	2.350 \pm 0.09 E+3	2.07 \pm 0.02 E+2	2.51 \pm 0.13 E+3	2.54 \pm 0.5 E+3	5.28 \pm 0.62 E+2	2.48 \pm 0.15 E+3					
154Eu	3.11 \pm 0.31 E+3	3.73 \pm 0.15 E+3	1.18 \pm 0.11 E+1	8.27 \pm 0.12 E+2	4.70 \pm 0.41 E+1	2.55 \pm 0.20 E+1					
155Eu	5.41 \pm 0.61 E+1	6.84 \pm 0.5 E+1	4.60 \pm 0.11 E+2	3.11 \pm 1.02 E+2	1.56 \pm 0.52 E+1	1.00 \pm 0.33 E+2					
	1.15 \pm 0.38 E+2	1.47 \pm 0.48 E+2									
<hr/>											
297-707 ^a		149-297		74-149		30-74		20-30 ^a		Sweepings ^a	
Aliquot		Aliquot		Aliquot		Aliquot		Aliquot		Aliquot	
60Co	2.63 \pm 0.53 E+1	4.48 \pm 0.11 E+1	9.39 \pm 0.21 E+1	8.86 \pm 0.10 E+1	8.86 \pm 0.15	7.68 \pm 0.21 E+1					
90Sr	4.81 \pm 0.51 E+3	3.26 \pm 0.34 E+3	5.45 \pm 0.57 E+3	5.74 \pm 0.67 E+3	1.52 \pm 0.10 E+4	3.85 \pm 0.40 E+3					
106Ru	4.78 \pm 0.28 E+1	1.62 \pm 0.07 E+2	1.29 \pm 0.06 E+2	1.77 \pm 0.06 E+2	2.92 \pm 0.01 E+1	4.49 \pm 0.11 E+2					
125Sb	6.05 \pm 0.73	-C	9.43 \pm 0.36 E+1	3.18 \pm 0.06 E+2	1.59 \pm 0.03 E+2	1.75 \pm 0.05 E+2					
129I	-C	-C	1.89 \pm 0.07 E-3	1.26 \pm 0.12 E-3	1.80 \pm 0.29 E-3	6.81 \pm 0.38 E-4					
134Cs	3.66 \pm 0.24	-C	2.92 \pm 0.09 E+1	4.60 \pm 0.12 E+1	3.79 \pm 0.08 E+1	4.30 \pm 0.12 E+1					
137Cs	6.60 \pm 0.06 E+1	5.69 \pm 0.03 E+2	9.65 \pm 0.04 E+2	7.70 \pm 0.04 E+2	8.950 \pm 0.004 E+1	7.32 \pm 0.12 E+1					
144Ce	1.30 \pm 0.08 E+3	1.37 \pm 0.12 E+3	1.85 \pm 0.14 E+3	1.37 \pm 0.11 E+3	1.57 \pm 1.33 E+2	2.02 \pm 0.15 E+3					
154Ce	2.55 \pm 0.20 E+1	2.15 \pm 0.41 E+1	3.47 \pm 0.41 E+1	2.15 \pm 0.31 E+1	2.92 \pm 0.43	3.06 \pm 0.51 E+1					
155Eu	5.3 \pm 1.7 E+1	4.8 \pm 1.6 E+1	7.5 \pm 2.5 E+1	4.6 \pm 1.5 E+1	-C	6.8 \pm 2.2 E+1					

a. Uncertainty is ~30% because of problems associated with the analysis.

b. Not reported because of problems associated with the analysis.

c. Not detected.

TABLE E-6. RESULTS OF RADIONUCLIDE ANALYSIS OF SAMPLE 9
(μ Ci/g sample)

Radionuclide	Particle 9A		Particle 9B		Particle 9C		Particle 9D		Particle 9E		Particle 9F	
	4000	Stable	4000	Stable	4000	Stable	4000	Stable	4000	Stable	4000	Stable
1680-4000												
^{60}Co	4.41 ± 0.07 E+1	9.80 ± 0.93 E+1	3.42 ± 0.11 E+1	8.86 ± 0.43 E+1	5.72 ± 0.16 E+1	4.48 ± 0.07 E+1						
^{90}Sr	5.57 ± 0.51 E+3	6.13 ± 0.61 E+3	4.69 ± 0.45 E+3	1.85 ± 0.17 E+3	1.74 ± 0.10 E+3	6.36 ± 0.6 E+3						
^{106}Ru	5.21 ± 0.03 E+2	2.54 ± 0.06 E+2	1.04 ± 0.01 E+2	4.65 ± 0.03 E+2	7.57 ± 0.02 E+2	4.96 ± 0.08 E+2						
^{125}Sb	1.08 ± 0.11 E+1	7.81 ± 1.48	7.44 ± 0.40 E+1	5.64 ± 0.06 E+1	6.65 ± 0.44 E+1	1.30 ± 0.30 E+1						
^{129}I	9.23 ± 1.35 E-4				3.70 ± 0.08 E-3							
^{134}Cs	3.30 ± 0.40 E+0	5.42 ± 0.40 E+0	1.58 ± 0.08 E+1	2.06 ± 0.10 E+1	1.37 ± 0.06 E+1							
^{37}Cs	5.70 ± 0.59 E+1	9.77 ± 0.08 E+1	2.65 ± 0.02 E+1	1.52 ± 0.30 E+1	3.50 ± 0.02 E+1	2.61 ± 0.02 E+2						
^{44}Ca	2.17 ± 0.11 E+1	1.94 ± 0.10 E+1	3.57 ± 0.15 E+1	3.73 ± 0.25 E+1	2.79 ± 0.02 E+2							
^{154}Eu	3.71 ± 0.24 E+1	2.60 ± 0.06 E+1	0.72 ± 0.51 E+1	6.86 ± 0.73 E+1	4.29 ± 0.41 E+1							
^{155}Eu	1.84 ± 2.59 E+1	7.48 ± 2.46 E+1	1.51 ± 0.50 E+1	1.48 ± 0.48 E+1	1.17 ± 0.39 E+1							
1680-4000												
$^{1680-4000}$		$^{1680-4000}$		$^{1680-4000}$		$^{1680-4000}$		$^{1680-4000}$		$^{1680-4000}$		
^{88}Se	5.76 ± 0.24 E+1	1.94 ± 0.07 E+1	8.00 ± 0.01 E+1	2.77 ± 0.11 E+1	—	—				6.62 ± 0.21		
^{90}Sr	1.60 ± 0.16 E+3	2.93 ± 0.34 E+3	1.08 ± 0.11 E+3	5.45 ± 0.51 E+3	—	—				4.18 ± 0.38 E+3		
^{106}Ru	1.77 ± 0.01 E+4	3.55 ± 0.93 E+2	9.69 ± 0.14 E+2	1.67 ± 0.03 E+3	—	—				3.93 ± 0.14 E+3		
^{125}Sb	1.61 ± 0.02 E+3	1.69 ± 0.16 E+1	—	—	—	—				2.71 ± 0.11 E+1		
^{149}I	1.12 ± 0.44 E-3	—	—	—	—	—				—		
^{151}Cs	2.71 ± 1.17 E+1	7.97 ± 0.11 E+1	4.01 ± 0.83 E+1	3.42 ± 0.12 E+1	—	—				9.68 ± 0.24		
^{147}La	—	4.46 ± 0.53 E+1	6.07 ± 0.10 E+1	6.40 ± 0.04 E+1	—	—				7.60 ± 0.009 E+1		
^{152}Eu	1.65 ± 0.14 E+1	1.65 ± 0.14 E+1	4.97 ± 0.31 E+1	4.97 ± 0.31 E+1	—	—				1.61 ± 0.08 E+1		
^{155}Eu	2.95 ± 0.04 E+1	7.76 ± 0.71 E+1	8.48 ± 0.61 E+1	—	—	—				2.76 ± 0.20 E+1		
$^{297-307}$		$^{149-197}$		$^{74-149}$		$^{30-74}$		$^{20-30}$		<20		
Aliquot		Aliquot		Aliquot		Aliquot		Aliquot		Aliquot		
^{60}Co	4.70 ± 0.21 E+1	4.03 ± 0.06 E+1	1.71 ± 0.03 E+1	1.07 ± 0.07 E+1	6.03 ± 0.08 E+1	7.04 ± 0.21 E+1				6.83 ± 0.11 E+1		
^{90}Sr	3.74 ± 0.40 E+3	6.07 ± 0.51 E+3	2.89 ± 0.29 E+3	2.89 ± 0.29 E+3	2.28 ± 0.23 E+3	4.55 ± 0.51 E+3				3.85 ± 0.40 E+3		
^{106}Ru	7.72 ± 1.69 E+1	7.44 ± 0.26 E+1	5.71 ± 2.00 E+1	4.45 ± 0.07 E+2	2.05 ± 0.04 E+2	4.49 ± 0.14 E+2				1.87 ± 0.07 E+2		
^{125}Sb	—	—	4.29 ± 0.11 E+1	1.49 ± 0.03 E+2	1.03 ± 0.02 E+2	—				1.47 ± 0.04 E+2		
^{129}I	—	—	—	—	—	—				—		
^{134}Cs	3.16 ± 0.05 E+2	2.01 ± 0.03 E+1	1.14 ± 0.30 E+1	3.46 ± 0.07 E+1	3.52 ± 0.06 E+1	8.85 ± 0.23 E+1				6.75 ± 0.06 E+1		
^{137}Cs	5.98 ± 0.02 E+3	3.87 ± 0.01 E+2	2.35 ± 0.04 E+2	7.06 ± 0.03 E+2	7.87 ± 0.04 E+2	2.140 ± 0.008 E+3				5.77 ± 0.03 E+3		
^{144}Ce	7.30 ± 1.55 E+2	7.30 ± 0.47 E+2	4.71 ± 0.40 E+2	1.10 ± 0.01 E+2	9.78 ± 0.62 E+2	2.17 ± 0.15 E+3				1.26 ± 0.11 E+3		
^{145}Ce	1.33 ± 0.31 E+1	1.12 ± 0.10 E+1	2.25 ± 0.31 E+1	1.33 ± 0.31 E+1	2.25 ± 0.31 E+1	1.33 ± 0.51 E+1				2.86 ± 0.51 E+1		
^{155}Eu	2.68 ± 0.88 E+1	2.40 ± 0.79 E+1	1.54 ± 0.51 E+1	5.40 ± 1.80 E+1	3.2 ± 1.1 E+1	7.7 ± 2.5 E+1				4.2 ± 1.4 E+1		

a. Not detected.

b. Associated uncertainty is 30-50%.

c. Not reported because of problems associated with the analysis.

TABLE E-9. RESULTS OF RADIONUCLIDE ANALYSIS OF SAMPLE 10
(μ Ci/g sample)

Radionuclide	4000 Particle 10A		4000 Particle 10B		4000 Particle 10C		4000 Particle 10D		4000 Particle 10E		4000 Particle 10F	
	Aliquot	Aliquot	Aliquot	Aliquot	Aliquot	Aliquot	Aliquot	Aliquot	Aliquot	Aliquot	Aliquot	Aliquot
Particle Size Fraction (μ m)												
60Co	9.07 ± 0.53	1.95 ± 0.08 E+1	6.19 ± 0.60 E+3	-b	--c	1.28 ± 0.11 E+1	9.60 ± 0.45					
90Sr	2.22 ± 0.23 E+4	9.67 ± 0.92 E+3	5.62 ± 0.28 E+2	5.62 ± 0.14 E+2	--c	4.62 ± 0.53 E+3	1.59 ± 0.76 E+3					
106Ru	6.76 ± 0.11 E+2	8.57 ± 0.14 E+2	9.94 ± 0.93 E+1	9.94 ± 0.37 E+1	--c	1.3b ± 0.03 E+3	7.37 ± 0.10 E+2					
125Sb	2.91 ± 0.24 E+1	5.40 ± 0.37 E+1	7.53 ± 0.48 E-5	1.32 ± 0.11 E-3	--c	2.24 ± 0.13 E+2	4.85 ± 0.24 E+1					
129I	-b	1.39 ± 0.08 E+1	1.57 ± 0.02 E+2	4.38 ± 0.01 E+3	--c	9.25 ± 0.12 E-4	-					
134Cs	1.12 ± 0.05 E+1	2.63 ± 0.02 E+2	1.86 ± 0.15 E+3	1.74 ± 0.31 E+1	--c	2.55 ± 0.05 E+2	1.08 ± 0.07 E+1					
137Cs	2.50 ± 0.02 E+2	2.95 ± 0.15 E+3	4.39 ± 0.51 E+1	5.7 ± 1.9 E+1	--c	4.00 ± 0.01 E+3	1.84 ± 0.01 E+2					
144Ce	2.03 ± 0.14 E+3	2.86 ± 0.81 E+1	1.52 ± 0.50 E+2	5.7 ± 1.9 E+1	--c	3.88 ± 0.31 E+3	2.21 ± 0.11 E+3					
154Eu	1.31 ± 0.43 E+2	1.680-4000 Particle 10G	1.680-4000 Particle 10H	1000-1680 ^a Particle 10I	1000-1680 ^a Particle 10J	1000-1680 ^a Particle 10K	1000-1680 ^a Particle 10L	1000-1680 ^a Particle 10M	1000-1680 ^a Particle 10N	1000-1680 ^a Particle 10O	1000-1680 ^a Particle 10P	1000-1680 ^a Aliquot
155Eu	-	-	-	-	-	-	-	-	-	-	-	707-1000
Aliquot												
60Co	3.63 ± 0.11 E+1	6.65 ± 0.35 E+1	2.33 ± 0.20 E+3	2.63 ± 0.20 E+3	1.28 ± 0.04 E+1	7.04 ± 0.21 E+1	3.35 ± 0.96 E+1					
90Sr	9.11 ± 1.0 E+1	3.15 ± 0.07 E+1	5.75 ± 0.05 E+2	5.75 ± 0.18 E+1	1.19 ± 0.01 E+3	1.23 ± 0.11 E+4	5.78 ± 0.58 E+3					
106Ru	6.94 ± 0.13 E+2	5.90 ± 1.80 E+1	2.68 ± 0.13 E+1	1.49 ± 0.05 E+2	1.49 ± 0.05 E+2	1.19 ± 0.01 E+3	4.19 ± 1.1 E+2					
125Sb	2.75 ± 0.27 E+1	-b	1.16 ± 0.54 E-4	-	-	-	3.29 ± 0.31 E+1					
129I	-c	8.59 ± 1.63 E-5	1.36 ± 0.17	7.60 ± 0.03	1.79 ± 0.99 E+1	3.49 ± 0.11 E+1						
134Cs	-c	1.63 ± 0.02 E+2	2.37 ± 0.01 E+1	1.45 ± 0.01 E+2	3.15 ± 0.03 E+2	8.07 ± 0.03 E+2						
137Cs	-c	3.26 ± 0.15 E+3	1.16 ± 0.07 E+3	1.47 ± 0.07 E+3	3.11 ± 0.15 E+3	1.88 ± 0.14 E+3						
144Ce	-c	4.70 ± 0.41 E+1	1.79 ± 0.41 E+1	2.40 ± 0.41 E+1	4.80 ± 0.41 E+1	2.45 ± 0.41 E+1						
154Eu	-c	1.43 ± 0.47 E+2	5.60 ± 1.85 E+1	7.10 ± 2.35 E+1	1.48 ± 0.49 E+2	7.4 ± 2.4 E+1						
155Eu	-	-	-	-	-	-	-	-	-	-	-	
Aliquot												
297-707	149-297 Aliquot	149-297 Aliquot	74-149 Aliquot	30-74 Aliquot	<30 Aliquot	Sweepings ^a						
60Co	3.54 ± 0.06 E+1	4.27 ± 0.11 E+1	4.83 ± 0.08 E+1	9.07 ± 0.21 E+1	9.18 ± 0.21 E+1	1.55 ± 0.02 E+1						
90Sr	3.29 ± 0.38 E+3	2.23 ± 0.20 E+3	2.17 ± 0.29 E+3	3.42 ± 0.32 E+3	5.86 ± 0.58 E+3	6.07 ± 0.68 E+3						
106Ru	3.03 ± 0.04 E+2	1.57 ± 0.07 E+2	2.40 ± 0.06 E+2	5.27 ± 0.11 E+2	8.57 ± 0.14 E+2	6.46 ± 0.14 E+1						
125Sb	2.42 ± 0.01 E+2	8.87 ± 0.34 E+1	-b	1.06 ± 0.04 E+2	-b	2.75 ± 0.07 E+1						
129I	1.69 ± 0.54 E-4	3.69 ± 1.07 E-4	-b	2.98 ± 2.23 E-4	5.05 ± 1.70 E-4	9.23 ± 1.35 E-4						
134Cs	1.59 ± 0.06 E+1	3.20 ± 0.09 E+1	2.11 ± 0.59 E+1	3.52 ± 0.11 E+1	3.55 ± 0.11 E+1	7.56 ± 0.12 E+1						
137Cs	3.04 ± 0.01 E+2	6.71 ± 0.03 E+2	4.30 ± 0.02 E+2	7.20 ± 0.40 E+2	7.77 ± 0.40 E+2	1.71 ± 0.61 E+2						
144Ce	1.53 ± 0.07 E+3	8.85 ± 0.93 E+2	-b	1.86 ± 0.15 E+3	2.17 ± 0.15 E+3	3.57 ± 0.15 E+2						
154Eu	2.11 ± 0.50 E+1	1.23 ± 0.31 E+1	2.15 ± 0.20 E+1	2.76 ± 0.41 E+1	3.68 ± 0.51 E+1	5.21 ± 0.71						
155Eu	5.25 ± 1.75 E+1	2.96 ± 0.97 E+1	-b	6.9 ± 2.3 E+1	7.5 ± 2.5 E+1	1.17 ± 0.39 E+1						

a. Uncertainty is 30 to 50% because of problems associated with the analysis.

b. Not detected.

c. Not reported because of problems associated with the analysis.

TABLE E-10. RESULTS OF RADIONUCLIDE ANALYSIS OF SAMPLE 11
(μ Ci/g sample)

		Particle Size Fraction (μm)						1680-4000 ^a Aliquot					
Radionuclide	Particle 11A	4000			4000			4000			1000-1680		
		Particle 11B	Particle 11C	Particle 11D	Particle 11E	Particle 11F	Particle 11G	Particle 11H	Particle 11I	Particle 11J	Particle 11K	Particle 11L	Particle 11M
⁶⁰ Co	2.73 ± 0.05 E+1	1.98 ± 0.05 E+1	-D	-D	-D	-D	-D	-D	-D	-D	2.46 ± 0.29 E+3	1.94 ± 0.06 E+1	2.94 ± 0.03 E+4
⁹⁰ Sr	3.37 ± 0.34 E+2	3.74 ± 0.40 E+4	-D	-D	-D	-D	-D	-D	-D	-D	2.16 ± 0.08 E+2	2.66 ± 0.06 E+2	3.19 ± 0.16 E+1
¹⁰⁶ Ru	4.37 ± 0.06 E+2	2.49 ± 0.04 E+2	-D	-D	-D	-D	-D	-D	-D	-D	4.02 ± 0.28 E+1	5.05 ± 0.40 E+4	2.57 ± 1.12 E+5
¹²⁵ Sr	9.18 ± 0.17 E+1	2.10 ± 0.10 E+1	-C	-C	-C	-C	-C	-C	-C	-C	3.23 ± 0.08 E+1	1.10 ± 0.05 E+1	1.10 ± 0.01 E+2
¹³⁷ Cs	-C	-C	-C	-C	-C	-C	-C	-C	-C	-C	1.850 ± 0.005 E+3	-C	1.32 ± 0.08 E+3
¹³⁴ Sr	2.95 ± 0.24 E+1	9.21 ± 0.35 E+1	-D	-D	-D	-D	-D	-D	-D	-D	2.14 ± 0.05 E+3	7.35 ± 1.55 E+0	7.35 ± 1.55 E+0
¹⁴¹ Nd	1.880 ± 0.007 E+1	1.73 ± 0.01 E+1	-D	-D	-D	-D	-D	-D	-D	-D	-C	-C	-C
¹⁴⁷ Pm	1.46 ± 0.07 E+1	1.06 ± 0.06 E+1	-D	-D	-D	-D	-D	-D	-D	-D	-C	-C	-C
¹⁵⁵ Tb	1.62 ± 0.10 E+1	8.0 ± 1.4 E+0	-D	-D	-D	-D	-D	-D	-D	-D	-C	-C	-C
 1680-4000		 1680-4000						 1680-4000					
Particle 11G		1680-4000			1680-4000			1680-4000			1680-4000		
Radionuclide	Particle 11G	Particle 11H			Particle 11I			Particle 11J			Particle 11K		
		1.60 ± 0.32 E-1	7.26 ± 0.32 E-1	-C	7.64 ± 0.74 E+3	-C	-C	7.64 ± 0.74 E+3	1.56 ± 0.05 E+3	1.56 ± 0.05 E+3	5.06 ± 0.58 E+3	4.65 ± 0.08 E+2	2.43 ± 0.64 E+2
⁶⁰ Co	-C	1.40 ± 0.13 E+3	6.74 ± 0.14 E+4	-C	3.79 ± 0.05 E+2	-C	-C	2.48 ± 0.09 E+2	-C	-C	6.61 ± 0.25 E+1	3.00 ± 0.53 E+1	3.00 ± 0.53 E+1
⁹⁰ Sr	9.13 ± 0.14 E+1	6.74 ± 0.14 E+1	-C	4.11 ± 0.42 E+1	-C	-C	-C	-C	-C	-C	-C	-C	-C
¹⁰⁶ Ru	125 ± 20	3.72 ± 0.28 E-4	4.44 ± 0.32 E-4	-C	1.89 ± 0.23 E+1	-C	-C	5.08 ± 0.83 E+2	9.48 ± 0.51 E+2	9.48 ± 0.51 E+2	1.73 ± 0.51 E+4	1.02 ± 0.42 E+2	1.02 ± 0.16 E+2
¹²⁵ Sr	6.4 ± 0.12 E+1	9.96 ± 0.12 E+1	-C	3.48 ± 0.51 E+1	-C	-C	2.30 ± 0.11 E+1	3.26 ± 0.42 E+3	3.26 ± 0.42 E+3	3.03 ± 0.02 E+2	2.17 ± 0.05 E+1	2.17 ± 0.05 E+1	
¹³⁴ Sr	1.640 ± 0.007 E+3	8.96 ± 0.05 E+2	-C	2.30 ± 0.15 E+3	-C	-C	2.30 ± 0.11 E+1	3.26 ± 0.42 E+3	3.26 ± 0.42 E+3	1.33 ± 0.20 E+1	-C	-C	
¹⁴¹ Nd	6.64 ± 0.15 E+3	2.66 ± 0.05 E+3	-C	2.04 ± 0.41 E+1	-C	-C	4.80 ± 0.20 E+1	6.0 ± 0.01 E+1	6.0 ± 0.01 E+1	1.33 ± 0.20 E+1	-C	-C	
¹⁴⁷ Pm	3.42 ± 0.51 E+1	8.7 ± 2.6 E+1	-C	-C	-C	-C	-C	-C	-C	-C	-C	-C	-C
¹⁵⁵ Tb	-C	-C	-C	-C	-C	-C	-C	-C	-C	-C	-C	-C	-C
 297-7078		 297-7078			149-297			74-149			30-74		
Aliquot		Aliquot			Aliquot			Aliquot			Aliquot		
Radionuclide	Aliquot	1.01 ± 0.02 E+2	8.86 ± 0.51 E+1	-C	1.59 ± 0.03 E+2	-C	-C	2.61 ± 0.04 E+2	-C	-C	2.61 ± 0.04 E+2	3.12 ± 0.53 E+1	3.12 ± 0.67 E+3
		6.33 ± 0.76 E+3	3.04 ± 0.29 E+3	-C	3.05 ± 0.29 E+2	-C	-C	3.64 ± 0.40 E+3	5.90 ± 0.14 E+2	5.90 ± 0.14 E+2	4.05 ± 0.34 E+3	1.54 ± 0.04 E+3	1.54 ± 0.04 E+3
⁶⁰ Co	6.40 ± 0.21	4.42 ± 0.09 E+1	-C	1.10 ± 0.04 E+1	-C	-C	1.81 ± 0.05 E+1	2.0 ± 0.05 E+2	2.0 ± 0.05 E+2	3.83 ± 0.11 E+2	8.26 ± 0.16 E+1	8.26 ± 0.16 E+1	
⁹⁰ Sr	-D	5.11 ± 0.36 E+1	4.60 ± 0.11 E+1	-C	5.90 ± 0.12 E+1	-C	-C	2.6 ± 1.1 E-5	1.17 ± 0.11 E-3	1.17 ± 0.11 E-3	6.05 ± 1.90 E-3	2.67 ± 0.05 E+1	2.67 ± 0.05 E+1
¹⁰⁶ Ru	8.15 ± 0.28 E+1	4.42 ± 0.09 E+1	-C	1.10 ± 0.04 E+1	-C	-C	1.81 ± 0.05 E+1	2.0 ± 0.05 E+2	2.0 ± 0.05 E+2	3.83 ± 0.11 E+2	8.26 ± 0.16 E+1	8.26 ± 0.16 E+1	
¹²⁵ Sr	1.23 ± 0.08 E+1	1.10 ± 0.04 E+1	-C	-C	-C	-C	5.43 ± 0.53 E-4	-C	-C	-C	-C	-C	
¹²⁹ I	-C	-C	-C	-C	-C	-C	-C	-C	-C	-C	-C	-C	-C
¹³⁴ Sr	5.11 ± 0.36 E+1	4.60 ± 0.11 E+1	-C	1.02 ± 0.04 E+1	-C	-C	5.90 ± 0.12 E+1	8.42 ± 0.05 E+2	8.42 ± 0.05 E+2	1.00 ± 0.00 E+3	4.98 ± 0.02 E+2	4.98 ± 0.02 E+2	
¹³⁷ Cs	1.010 ± 0.007 E+2	1.020 ± 0.004 E+3	-C	-C	-C	-C	1.54 ± 0.14 E+3	1.38 ± 0.15 E+3	1.38 ± 0.15 E+3	1.29 ± 0.20 E+3	1.15 ± 0.06 E+3	1.15 ± 0.06 E+3	
¹⁴¹ Nd	1.47 ± 0.47 E+1	2.25 ± 0.41 E+1	-C	-C	-C	-C	2.35 ± 0.41 E+1	1.43 ± 0.61 E+1	1.43 ± 0.61 E+1	1.43 ± 0.61 E+1	1.43 ± 0.20 E+1	1.43 ± 0.20 E+1	
¹⁴⁷ Pm	1.74 ± 0.10 E+1	5.3 ± 1.3 E-1	-C	-C	-C	-C	5.8 ± 1.9 E+1	4.8 ± 1.65 E+1	4.8 ± 1.65 E+1	4.9 ± 1.6 E+1	5.9 ± 1.7 E+1	5.9 ± 1.7 E+1	

a. Uncertainty is 30 to 50% because of problems associated with the analysis.

b. It reported because of problems associated with the analysis.

卷之三

TABLE E-11. FISSILE/FERTILE MATERIAL CONTENT OF TMI-2 CORE DEBRIS GRAB SAMPLES

Particle Size Fraction (μm)	Particle/Aliquot	Fissile (mg)	Fertile (mg)	Enrichment (wt%)	Particle/Aliquot Weight (mg)
<u>Sample 1</u>					
>4000	Particle 1A	2.4 + 0.1 E-1	7.5 + 0.1	3.0 + 0.4	84
>4000	Particle 1B	2.2 + 0.1 E-1	1.10 + 0.07 E+1	2.0 + 0.2	15
>4000	Particle 1C	1.4 + 0.1 E-1	5.2 + 0.9	2.6 + 0.5	15
>4000	Particle 1D	1.4 + 0.1 E-1	5.4 + 1.0	2.4 + 0.5	7
>4000	Particle 1E	1.4 + 0.1 E-1	5.0 + 0.9	2.6 + 0.5	29
1680-4000	Particle 1F	2.6 + 0.1 E-1	1.08 + 0.09 E+1	2.3 + 0.2	20
1680-4000	Particle 1G	1.6 + 0.1 E-1	7.9 + 1.0	2.0 + 0.3	15
1680-4000	Particle 1H	4.2 + 0.2 E-1	1.5 + 0.1 E+1	2.7 + 0.2	33
1000-1680	Particle 1I	-- ^a	-- ^a	-- ^a	-- ^a
1000-1680	Particle 1J	3.2 + 0.1 E-1	1.48 + 0.9 E+1	2.2 + 0.2	24
1000-1680	Particle 1K	2.5 + 0.1 E-1	9.8 + 0.09	2.4 + 0.3	19
707-1000	Aliquot	3.7 + 0.1 E-1	1.68 + 0.09 E+1	2.2 + 0.2	26
297-707	Aliquot	4.0 + 0.2 E-1	1.65 + 0.09 E+1	2.4 + 0.2	35
149-297	Aliquot	2.1 + 0.2 E-1	8.8 + 0.9	2.3 + 0.3	23
149-149	Aliquot	1.2 + 0.1 E-1	4.8 + 0.8	2.2 + 0.4	12
30-74	Aliquot	7.5 + 0.1 E-2	3.2 + 0.8	2.3 + 0.7	10
<u>Sample 3</u>					
>4000	Particle 3A	6.2 + 0.4 E-1	2.2 + 0.1 E+1	2.7 + 0.2	56
>4000	Particle 3B	<1.6 E-2	<0.7	-- ^a	23
>1000	Particle 3C	-- ^a	-- ^a	-- ^a	39
>4000	Particle 3D	1.9 + 0.03	8.3 + 0.3 E+1	2.23 + 0.06	97
>4000	Particle 3E	1.3 + 0.02	5.8 + 0.2 E+1	2.2 + 0.1	69
1680-4000	Particle 3F	3.8 + 0.1 E-1	2.8 ^c	-- ^b	15
1680-4000	Particle 3G	8.2 + 0.1 E-2	4.8 + 1.0	2.8	10
1680-4000	Particle 3H	9.8 + 0.1 E-2	-- ^b	2.0 + 0.5	14
1000-1680	Particle 3I	4.6 + 0.1 E-1	3.9 + 0.8	-- ^b	25
1000-1680	Particle 3J	1.1 + 0.1 E-1	2.9 + 0.1 E+1	2.7 + 0.6	17
1000-1680	Particle 3K	6.4 + 0.2 E-1	-- ^b	2.2 + 0.1	45
707-1000	Aliquot	4.3 + 0.1 E-1	1.9 E+1 ^c	2.3 ^c	30
297-707	Aliquot	2.2 + 0.1 E-1	8.7 ^c	2.4 ^c	18
149-297	Aliquot	1.15 + 0.02	-- ^b	-- ^b	114
149-149	Aliquot	1.7 + 0.1 E-1	7.0 ^c	2.3	22
30-74	Aliquot	1.8 + 0.1 E-1	6.4 + 1.0	2.6 + 0.4	25
20-30	Aliquot	1.5 + 1.2 E-2	<1	-- ^b	4

TABLE I-11. (continued)

Particle Size Fraction (um)	Particle/Aliquot	Fissile (mg)	Fertile (mg)	Enrichment (wt%)	Particle/Aliquot Weight (mg)
<u>Sample 4</u>					
<400	Particle 4A	4.6 ± 0.2 E-1	1.86 E+1C	2.4C	22
400-500	Particle 4B	2.1 ± 0.2 E-1	5.6 ± 0.9	2.3 ± 0.1	7
500-600	Particle 4C	5.9 ± 0.1 E-1	1.93 E+1C	3.0C	38
600-700	Particle 4D	2.8 ± 0.1 E-1	1.05 E+1C	2.6C	14
700-800	Particle 4E	3.2 ± 0.1 E-1	1.4 E+1C	2.2C	15
<u>Sample 5</u>					
≤400	Particle 5A	2.3 ± 0.1 E-1	8.7 ± 1.0	2.6 ± 0.3	11
400-500	Particle 5B	5.5 ± 0.2 E-1	2.4 ± 0.1 E+1	2.3 ± 0.1	26
500-600	Particle 5C	5.5 ± 0.1 E-1	1.9 E+1C	2.66C	24
600-700	Particle 5D	5.4 ± 0.1 E-1	1.9 E+1C	2.75C	27
700-800	Particle 5E	2.3 ± 0.1 E-1	7.4 ± 0.9	3.1 ± 0.4	21
≤400	Particle 5F	6.5 ± 0.3 E-1	2.2 ± 0.1 E+1	2.9 ± 0.2	39
400-500	Particle 5G	4.1 ± 0.1 E-1	1.7 E+1b	2.4b	89
500-600	Particle 5H	4.1 ± 0.1 E-1	1.7 E+1b	2.4b	6
600-700	Particle 5I	4.1 ± 0.1 E-1	1.7 E+1b	2.4b	37
700-800	Particle 5J	4.1 ± 0.1 E-1	1.7 E+1b	2.4b	24
≤1000	Aliquot	8.1 ± 0.2 E-1	2.8 ± 0.1 E+1	2.8 ± 0.1	43
<u>Sample 6</u>					
<400	Particle 6A	4.5 ± 0.2 E-1	1.2 ± 0.1 E+1	2.9 ± 0.4	12
400-500	Particle 6B	4.0 ± 0.1 E-1	1.1 ± 0.1 E+1	2.6 ± 0.1	65
500-600	Particle 6C	5.7 ± 0.1 E-2	1.9 ± 0.2 E+1	2.8 ± 0.2	40
600-700	Particle 6D	5.6 ± 0.1 E-1	1.9 ± 0.1 E+1	2.8 ± 0.2	25
700-800	Particle 6E	4.0 ± 0.1 E-1	1.1 ± 0.1 E+1	2.7 ± 0.1	26
≤400	Particle 6F	2.16 ± 0.03	7.7 ± 0.2 E+1	2.7 ± 0.1	33
400-500	Particle 6G	2.43 ± 0.03	9.1 ± 0.2 E+1	2.6 ± 0.1	94
500-600	Particle 6H	2.43 ± 0.03	9.1 ± 0.2 E+1	2.6 ± 0.1	101
600-700	Particle 6I	1.2 ± 0.1 E-1	3.3 ± 0.8	3.4 ± 0.9	41
700-800	Particle 6J	2.8 ± 0.1 E-1	8.7 ± 0.9	3.1 ± 0.4	71
≤1000	Particle 6K	9.2 ± 0.2 E-1	3.3 ± 0.1 E+1	2.7 ± 0.1	43
1000-1600	Aliquot	2.08 ± 0.02	8.1 ± 0.2 E+1	2.5 ± 0.1	139
1000-1600	Aliquot	1.72 ± 0.03	7.3 ± 0.2 E+1	2.3 ± 0.1	130
1000-1600	Aliquot	1.36 ± 0.05	5.1 ± 0.2 E+1	2.6 ± 0.1	135
1000-1600	Aliquot	7.9 ± 0.02 E-1	3.3 ± 0.1 E+1	2.3 ± 0.1	87
1000-1600	Aliquot	1.5 ± 0.1 E-1	5.1 ± 0.9	2.9 ± 0.5	22

TABLE E-11. (continued)

Particle Size Fraction (μm)	Particle/Aliquot	Fissile (mg)	Fertile (mg)	Enrichment (wt%)	Particle/Aliquot Weight (mg)
<u>Sample 7</u>					
>4000	Particle 7A	1.1 + 0.1 E-1	4.8 + 0.8	2.2 + 0.4	7
>4000	Particle 7B	2.4 + 0.1 E-1	9.2 + 0.8	2.5 + 0.2	11
>4000	Particle 7C	1.1 + 0.1 E-1	4.6 + 0.7	2.2 + 0.4	6
>4000	Particle 7D	-c	-c	-c	11
>4000	Particle 7E	-c	-c	-c	4
1680-4000	Particle 7F	1.9 + 0.1 E-2	9.2 + 6.6 E-1	2.0 + 0.2	3
1680-4000	Particle 7G	1.8 + 0.1 E-1	8.5 + 0.7	2.0 + 0.2	13
1680-4000	Particle 7H	3.2 + 0.1 E-1	1.00 + 0.08 E+1	3.1 + 0.3	14
1000-1680	Particle 7I	2.6 + 0.1 E-2	1.5 + 0.7	1.7 + 1.1	3
1000-1680	Particle 7J	7.8 + 0.1 E-2	3.5 + 0.7	2.2 + 0.5	5
1000-1680	Particle 7K	1.6 + 0.1 E-1	6.6 + 0.7	2.3 + 0.3	10
707-1000	Aliquot	2.6 + 0.1 E-1	1.21 + 0.08 E+1	2.2 + 0.2	29
707-707	Aliquot	5.2 + 0.1 E-2	3.6 + 0.7	1.4 + 0.4	7
149-297	Aliquot	-d	-d	-d	6
74-149	Aliquot	5.2 + 0.1 E-2	3.4 + 0.7	1.5 + 0.4	4
30-74	Aliquot	1.3 + 0.1 E-2	1.1 + 0.7	1.2 + 1.2	2
20-30	Aliquot	5.4 + 0.1 E-2	2.4 + 0.7	2.2 + 0.8	4
<20	Aliquot	1.6 + 0.1 E-2	<1	-d	2
<u>Sample 8</u>					
>4000	Particle 8A	9.9 + 0.1 E-2	5.3 + 0.8	1.8 + 0.3	13
>4000	Particle 8B	3.0 + 0.1 E-1	1.05 + 0.08 E+1	2.8 + 0.2	13
>4000	Particle 8C	5.9 + 0.1 E-2	2.3 + 0.7	2.5 + 0.9	6
>4000	Particle 8D	7.7 + 0.1 E-2	4.1 + 0.7	1.8 + 0.4	4d
>4000	Particle 8E	1.3 + 0.1 E-1	5.9 + 0.8	2.1 + 0.3	5d
1680-4000	Particle 8F	1.1 + 0.1 E-1	5.0 + 0.8	2.0 + 0.4	7
1680-4000	Particle 8G	5.2 + 0.1 E-2	3.3 + 0.7	1.5 + 0.5	3d
1680-4000	Particle 8H	1.1 + 0.1 E-1	5.4 + 0.8	2.0 + 0.4	5d
1000-1680	Particle 8I	5.1 + 0.1 E-2	3.8 + 0.8	1.3 + 0.4	11
1000-1680	Particle 8J	1.0 + 1.2 E-2	1.8 + 0.7	-c	5
1000-1680	Particle 8K	1.2 + 0.1 E-1	4.9 + 0.7	2.4 + 0.4	8
707-1000	Aliquot	4.2 + 1.2 E-2	2.3 + 0.7	1.8 + 0.8	5
297-707	Aliquot	4.9 + 1.2 E-2	3.0 + 0.7	1.6 + 0.6	6
149-297	Aliquot	7.7 + 1.2 E-2	3.4 + 0.8	2.2 + 0.8	8
74-149	Aliquot	2.3 + 0.1 E-1	9.1 + 0.8	2.5 + 0.3	19
30-74	Aliquot	3.4 + 1.2 E-2	1.9 + 0.7	1.7 + 0.9	4
20-30	Aliquot	6.4 + 1.2 E-2	1.9 + 0.8	3.3 + 1.4	7
<20	Aliquot	1.6 + 0.1 E-1	6.2 + 0.8	2.5 + 0.4	9
Sweepings				5.6 + 0.3	9

Table E-11. (continued)

Particle Size Fraction μm	Particle/Aliquot	Fissile (mg)	Fertile (mg)	Enrichment (wt%)	Particle/Aliquot Weight (mg)
<u>Sample 9</u>					
4.0-4.5	Particle 9A	2.6 ± 0.1 E-1	9.7 ± 0.8	2.6 ± 0.4	20
4.0-4.5	Particle 9B	5.3 ± 0.1 E-1	2.0 ± 0.9 E+1	2.6 ± 0.4	33
4.0-4.5	Particle 9C	1.46 ± 0.03	5.8 ± 0.1 E+1	2.46 ± 0.07	64
4.0-4.5	Particle 9D	1.46 ± 0.03	<1	2.46 ± 0.07	7
4.0-4.5	Particle 9E	6.6 ± 0.1 E-2	2.4 ± 0.1 E+1	2.7 ± 0.1	30
4.0-4.5	Particle 9F	1.7 ± 0.1 E-1	7.5 ± 0.8	2.2 ± 0.3	4
4.0-4.5	Particle 9G	4.0 ± 0.1 E-1	1.2 ± 0.7	2.0 ± 0.4	5
4.0-4.5	Particle 9H	9.7 ± 0.1 E-2	4.7 ± 0.8	2.0 ± 0.4	9
1000-1680	Particle 9I	1.1 ± 0.1 E-1	3.8 ± 0.8	3.0 ± 0.6	28
1000-1680	Particle 9J	1.3 ± 0.1 E-1	6.7 ± 0.8	2.0 ± 0.3	28
1000-1680	Particle 9K	1.4 ± 0.1 E-1	<1	2.0 ± 0.3	28
1000-1680	Aliquot	1.0 ± 0.1 E-1	3.2 ± 0.8	3.1 ± 0.8	9
247-7297	Aliquot	0.1	1.3 ± 0.7	2.4 ± 0.4	2
4.0-4.5	Aliquot	4.0 ± 0.1 E-2	2.0 ± 0.7	1.9 ± 0.9	8
74-149	Aliquot	6.4 ± 0.1 E-2	2.5 ± 0.7	2.5 ± 0.8	7
35-73	Aliquot	1.2 ± 0.1 E-1	4.7 ± 0.7	2.4 ± 0.4	12
20-30	Aliquot	4.8 ± 0.1 E-2	1.8 ± 0.7	2.6 ± 1.2	7
<20	Aliquot	1.6 ± 0.1 E-1	7.5 ± 0.8	2.0 ± 0.3	10
Sweepings	--	5.5 ± 1.2 E-2	3.2 ± 0.7	1.7 ± 0.5	7
<u>Sample 10</u>					
>4000	Particle 10A	2.06 ± 0.03	1.10 ± 0.02 E+2	1.83 ± 0.05	131
>4000	Particle 10B	1.53 ± 0.03	5.2 ± 0.1 E+1	2.86 ± 0.09	66
>4000	Particle 10C	3.21 ± 0.05	1.21 ± 0.03 E+2	2.58 ± 0.06	153
>4000	Particle 10D	1.14 ± 0.02	3.8 ± 0.1 E+1	2.9 ± 0.1	44
>4000	Particle 10E	1.11 ± 0.02	4.5 ± 0.1 E+1	2.41 ± 0.08	58
1000-4000	Particle 10F	1.4 ± 0.01 E-1	7.7 ± 0.8	1.8 ± 0.2	12
1000-4000	Particle 10G	4.7 ± 0.1 E-1	1.6 ± 0.09 E+1	2.8 ± 0.2	18
1000-4000	Particle 10H	4.0 ± 0.1 E-1	1.74 ± 0.08 E+1	2.2 ± 0.1	22
1000-1680	Particle 10I	8.0 ± 1.0 E-2	5.8 ± 0.8	1.4 ± 0.3	10
1000-1680	Particle 10J	1.5 ± 0.1 E-1	5.4 ± 0.7	2.8 ± 0.4	10
1000-1680	Particle 10K	2.7 ± 0.1 E-1	1.13 ± 0.08 E+1	2.3 ± 0.2	12
707-1000	Aliquot	6.3 ± 0.2 E-1	2.67 ± 0.9 E+1	2.4 ± 0.1	41
297-707	Aliquot	9.7 ± 1.2 E-2	3.6 ± 0.7	2.6 ± 0.6	8
147-149	Aliquot	1.2 ± 1.2 E-2	1.7 ± 0.7	2.4 ± 3.2	2
147-149	Aliquot	4.0 ± 1.2 E-2	9.1 ± 7.2 E-1	4.2 ± 3.2	7
50-74	Aliquot	2.4 ± 0.1 E-1	9.5 ± 0.8	2.4 ± 0.2	17
20-30	Aliquot	3.0 ± 1.2 E-2	1.01 ± 0.08 E+1	2.3 ± 0.2	15
Sweepings	--	--	1.6 ± 0.7	1.7 ± 0.9	14

TABLE E-11. (continued)

Particle Size Fraction (μm)	Particle/Aliquot	Fissile (mg)	Fertile (mg)	Enrichment (wt%)	Particle/Aliquot Weight (mg)
<u>Sample 11</u>					
>4000	Particle 11A	1.8 + 0.1 E-1	6.4 + 0.7	2.8 + 0.4	6 ^d
	Particle 11B	2.4 + 0.1 E-1	1.08 + 0.08 E+1	2.2 + 0.2	15
>4000	Particle 11C	1.1 + 0.1 E-1	6.4 + 0.7	1.6 + 0.3	5 ^d
>4000	Particle 11D	3.1 + 1.2 E-2	2.4 + 0.7	1.2 + 0.6	7
>4000	Particle 11E	1.3 ± 0.1 E-1	5.7 ± 0.7	2.2 ± 0.3	
1680-4000	Particle 11F	3.7 + 0.1 E-1	1.46 + 0.08 E+1	2.5 + 0.2	20
1680-4000	Particle 11G	2.6 + 0.1 E-1	9.4 + 0.8	2.7 + 0.3	10
1680-4000	Particle 11H	3.4 + 0.1 E-1	1.21 ± 0.08 E+1	2.8 ± 0.2	15
1000-1680	Particle 11I	1.0 + 0.1 E-1	5.3 + 0.7	1.8 + 0.3	6
1000-1680	Particle 11J	2.6 + 0.1 E-1	1.04 + 0.08 E+1	2.5 + 0.2	10
1000-1680	Particle 11K	1.9 ± 0.1 E-1	8.1 ± 0.8	2.3 ± 0.3	9
707-1000	Aliquot	<0.01	1.9 + 0.7	-- ^a	3
597-707	Aliquot	6.7 + 1.2 E-2	3.5 + 0.7	1.9 + 0.5	8
149-597	Aliquot	7.5 + 1.2 E-2	2.8 + 0.7	2.6 + 0.8	7
74-149	Aliquot	5.3 + 1.2 E-2	3.3 + 0.7	1.6 + 0.5	5
50-74	Aliquot	5.5 + 1.2 E-2	2.7 + 0.8	2.0 + 0.7	6
20-50	Aliquot	3.4 + 1.2 E-2	2.2 + 0.7	1.5 + 0.7	3
Sweepings		1.0 ± 0.1 E-1	4.2 ± 0.7	2.4 ± 0.5	8

a. Not measured.

b. Not reported because of problems associated with the analysis.

c. Calculated based on mass spectrometry enrichment analysis.

d. Uncertainty is ~50% because of small sample weights.

TABLE E-12. RADIONUCLIE CONCENTRATIONS OF THE INSOLUBLE PORTIONS OF THE RECOMBINED BULK SAMPLES FROM THE H8 AND E9 CORE LOCATIONS ($\mu\text{Ci/g}$ insoluble material)

Sample No.	H8 Location		E9 Location		Sample 9 (1.60 g) ^a
	Sample 1 (0.43 g) ^a	Sample 7 (1.60 g) ^a	Sample 5 (1.54 g) ^a	Sample 10 (1.60 g) ^a	
16010	3.91 : 0.05 E+1	-D	1.49 : 0.04 E+1	1.97 : 0.04	1.36 : 0.03
16010 16010	3.36 : 0.24 E+1	-D	1.88 : 0.04 E+1	7.06 : 0.21	1.93 : 0.04 E+1
16010 16010	6.35 : 0.47	-D	1.10 : 0.04	1.61 : 0.20 E-1	8.09 : 0.39 E+1
13410	3.2 : 1.0 E-1	-D	9.0 : 1.4 E-2	5.82 : 0.37 E-2	2.81 : 0.16 E-1
13710	9.52 : 0.19	-D	2.54 : 0.03	1.27 : 0.02	5.74 : 0.05
14110	1.74 : 0.14 E+1	-D	1.31 : 0.08 E+2	4.06 : 0.38 E+1	1.76 : 0.28 E+1
15410	2.12 : 0.22	-D	2.21 : 0.07	4.81 : 0.31 E-1	2.51 : 0.25 E+1
15210	5.3 : 1.8	-D	3.4 : 1.1	1.77 : 0.37	5.2 : 1.7 E+1
<hr/>					
Sample 4 (0.90 g) ^a	Sample b		Sample 10		Sample 11 (1.5 g) ^a
1.4) : 0.06 E+1	-D	3.09 : 0.13	5.27 : 0.06	2.15 : 0.04	
2.6) : 0.01 E+1	-D	7.13 : 0.05 E+1	1.34 : 0.01 E+1	2.14 : 0.04 E+1	
1.37 : 0.15 E+1	-D	7.41 : 0.32	3.28 : 0.06	2.49 : 0.06	
1.37 : 0.15 E+1	-C	-C	1.19 : 0.03	2.76 : 0.18 E-1	
13710	3.17 : 0.35	-D	4.72 : 0.12	2.59 : 0.01 E+1	5.67 : 0.05
14110	6.4 : 0.31 E+1	-D	2.00 : 0.22 E+2	2.59 : 0.34 E+1	6.29 : 0.53 E+1
15410	1.0) : 0.03 E+1	-D	2.61 : 0.26	2.66 : 0.35 E+1	7.46 : 0.42 E-1
15210	1.9) : 0.6) E+1	-D	6.9 : 2.3	6.6 : 2.2 E-1	1.76 : 0.58

a. Urans of insoluble material.

b. No insoluble material.

c. Not detected.

APPENDIX F

TMI-2 CORE MODULAR ORIGEN2 CALCULATIONS

APPENDIX F

TMI-2 CORE NODULAR ORIGEN-2 CALCULATIONS²

Core inventory calculations using the ORIGEN- code have been made based on the average burnup estimates for the TMI-2 core.^b Therefore, to provide a more accurate estimate of radionuclide inventories and concentrations in the core, the 177 individual assembly power histories were obtained from GPU Nuclear Inc. Figure F-1 shows the grid location, identification, and initial enrichment at each location.

It was determined from the initial data that a burnup summary map could be developed for the TMI-2 core. For this analysis, the Axial core height (~3.9 m) was divided into seven arbitrary axial zones, each 55.6 cm in height. The average burnup then was calculated for each of the seven axial zones of each assembly, a total of 1239 nodes.

The burnup nodes were then divided into four subgroups for each initial enrichment group (1.98%, 2.65%, and 2.98% ^{235}U enrichment). Table F-1 shows the number of burnup nodes in each subgroup, the initial enrichment, number of metric tones of uranium ($^{235}\text{U} + ^{238}\text{U}$) in each group, the average burnup (MWd/MTU) for each group and the maximum and minimum burnup zones for each group. Figures F-2 through F-8 show the burnup zones for all fuel assemblies in the seven axial burnup zones.

Table F-2 lists the full core and initial enrichment zone radionuclide inventories for April 1, 1984, the date used for decay correction purposes for the measured radionuclide concentration. Table F-3 contains the average radionuclide concentrations for the entire core and each enrichment group. Tables F-4 through F-6 give the radionuclide concentrations for each of the individual burnup subgroups.

a. B. G. Schnitzler and J. B. Briggs, TMI-2 Isotopic Inventory Calculations, EGG-PBS-6798, August 1985.

b. R. J. Davis et al., Radionuclide Mass Balance for the TMI-2 Accident: Data through 1979 and Preliminary Assessment of Uncertainties, GEND-INF-047, November 1984.

	1	2	3	4	5									
	A-6	A-7	A-8	A-9	A-10									
	2.96%	2.96%	2.96%	2.96%	2.96%									
	6	7	8	9	10	11	12	13	14					
	B-4	B-5	B-6	B-7	B-8	B-9	B-10	B-11	B-12					
	2.96%	2.96%	2.96%	2.64%	2.96%	2.64%	2.96%	2.96%	2.96%					
	15	16	17	18	19	20	21	22	23	24	25			
	C-3	C-4	C-5	C-6	C-7	C-8	C-9	C-10	C-11	C-12	C-13			
	2.96%	2.96%	1.98%	2.64%	1.96%	2.64%	1.98%	2.64%	1.98%	2.64%	2.96%			
	26	27	28	29	30	31	32	33	34	35	36	37	38	
	D-2	D-3	D-4	D-5	D-6	D-7	D-8	D-9	D-10	D-11	D-12	D-13	D-14	
	2.96%	2.96%	1.98%	2.64%	1.98%	2.64%	1.98%	2.64%	1.98%	2.64%	1.98%	2.96%	2.96%	
	39	40	41	42	43	44	45	46	47	48	49	50	51	
	E-2	E-3	E-4	E-5	E-6	E-7	E-8	E-9	E-10	E-11	E-12	E-13	E-14	
	2.96%	1.98%	2.64%	1.98%	2.64%	1.98%	2.64%	1.98%	2.64%	1.98%	2.64%	1.98%	2.96%	
	52	53	54	55	56	57	58	59	60	61	62	63	64	65
	F-1	F-2	F-3	F-4	F-5	F-6	F-7	F-8	F-9	F-10	F-11	F-12	F-13	F-14
	2.96%	2.96%	2.64%	1.98%	2.64%	1.98%	2.54%	1.96%	2.64%	1.93%	2.64%	1.98%	2.64%	2.96%
	67	68	69	70	71	72	73	74	75	76	77	78	79	80
	G-1	G-2	G-3	G-4	G-5	G-6	G-7	G-8	G-9	G-10	G-11	G-12	G-13	G-14
	2.96%	2.64%	1.98%	2.64%	1.98%	2.54%	1.98%	2.64%	1.98%	2.64%	1.98%	2.64%	1.98%	2.96%
	82	83	84	85	86	87	88	89	90	91	92	93	94	95
	H-1	H-2	H-3	H-4	H-5	H-6	H-7	H-8	H-9	H-10	H-11	H-12	H-13	H-14
	2.96%	2.96%	2.64%	1.98%	2.64%	1.98%	2.64%	2.64%	1.98%	2.64%	1.98%	2.64%	2.96%	2.96%
	97	98	99	100	101	102	103	104	105	106	107	108	109	110
	K-1	K-2	K-3	K-4	K-5	K-6	K-7	K-8	K-9	K-10	K-11	K-12	K-13	K-14
	2.96%	2.64%	1.98%	2.64%	1.98%	2.64%	1.98%	2.64%	1.98%	2.64%	1.98%	2.64%	1.98%	2.96%
	112	113	114	115	116	117	118	119	120	121	122	123	124	125
	L-1	L-2	L-3	L-4	L-5	L-6	L-7	L-8	L-9	L-10	L-11	L-12	L-13	L-14
	2.96%	2.96%	1.98%	2.64%	1.98%	2.64%	1.98%	2.64%	1.98%	2.64%	1.98%	2.64%	1.98%	2.96%
	127	128	129	130	131	132	133	134	135	136	137	138	139	
	M-2	M-3	M-4	M-5	M-6	M-7	M-8	M-9	M-10	M-11	M-12	M-13	M-14	
	2.96%	1.98%	2.64%	1.98%	2.64%	1.98%	2.64%	1.98%	2.64%	1.98%	2.64%	1.98%	2.96%	
	140	141	142	143	144	145	146	147	148	149	150	151	152	
	N-2	N-3	N-4	N-5	N-6	N-7	N-8	N-9	N-10	N-11	N-12	N-13	N-14	
	2.96%	2.96%	1.98%	2.64%	1.98%	2.64%	1.98%	2.64%	1.98%	2.64%	1.98%	2.96%	2.96%	
	153	154	155	156	157	158	159	160	161	162	163			
	O-3	O-4	O-5	O-6	O-7	O-8	O-9	O-10	O-11	O-12	O-13			
	2.96%	2.96%	1.98%	2.54%	1.98%	2.64%	1.98%	2.64%	1.98%	2.96%	2.96%			
	164	165	166	167	168	169	170	171	172					
	P-4	P-5	P-6	P-7	P-8	P-9	P-10	P-11	P-12					
	2.96%	2.96%	2.96%	2.64%	2.96%	2.64%	2.96%	2.96%	2.96%					
	173	174	175	176	177									
	R-6	R-7	R-8	R-9	R-10									
	2.96%	2.96%	2.96%	2.96%	2.96%									

Element Number
 Entity Location
 Enrichment

Figure F-1. TM1-2 element location and enrichment map.

TABLE F-1. TMI-2 REACTOR CORE FUEL NODE SUMMARY

<u>Fuel Group</u>	<u>Number of Fuel Nodes</u>	<u>Initial Enrichment (wt%)</u>	<u>Initial Uranium (metric ton)</u>	<u>Average Burnup (MWd/MTU)</u>	<u>Minimum Burnup (MWd/MTU)</u>	<u>Maximum Burnup (MWd/MTU)</u>
1	72	1.98	4.7684	1863	1436	2240
2	68	1.98	4.5035	2746	2488	3158
3	152	1.98	10.067	3637	3190	4021
4	100	1.98	6.6228	4391	4087	4905
5	105	2.64	6.9540	2239	1647	2741
6	76	2.64	5.0334	3552	2810	3890
7	230	2.64	15.233	4315	3907	4952
8	16	2.64	1.0597	5465	5227	6213
9	136	2.96	9.0071	1548	910	2020
10	164	2.96	10.861	2644	2100	3143
11	76	2.96	5.0334	3554	3261	4192
12	44	2.96	2.9140	4878	4453	5572

Figure F-2. TMI-2 burnup for Axial Level 1 of 7 (levels numbered from top of core).

Figure F-3. TMI-2 burnup for Axial Level 2 of 7 (levels numbered from top of core).

		1	2	3	4	5					
		10	10	11	10	10					
		2632	3053	3738	3054	2632					
		6	7	8	9	10	11	12	13	14	
		10	11	12	7	12	7	12	11	10	
		2107	3401	4603	4387	5551	4387	4603	3402	2108	
		15	16	17	18	19	20	21	22	23	25
		10	10	3	7	4	7	4	7	3	10
		2220	3142	3630	4342	4370	4832	4371	4303	3630	3143
		26	27	28	29	30	31	32	33	34	35
		10	10	3	7	3	7	3	7	3	7
		2108	3142	3560	4188	3862	4480	3920	4480	3862	4189
		39	40	41	42	43	44	45	46	47	48
		11	3	7	4	7	4	7	4	7	3
		3402	3604	4127	4197	4589	4421	4774	4485	4589	4198
		52	53	54	55	56	57	58	59	60	61
		10	12	7	3	7	4	7	4	7	3
		2632	4666	4301	3794	4470	4559	4933	4675	4933	4559
		67	68	69	70	71	72	73	74	75	76
		10	7	4	7	4	7	4	8	4	7
		3053	4276	4395	4494	4393	4921	4836	5236	4836	4921
		82	83	84	85	86	87	88	89	90	91
		11	12	7	3	7	4	8	8	8	4
		3738	5550	4831	3919	4773	4574	5235	6009	5235	4674
		97	98	99	100	101	102	103	104	105	106
		10	7	4	7	4	7	4	8	4	7
		3053	4276	4394	4494	4418	4920	4835	5234	4834	4920
		112	113	114	115	116	117	118	119	120	121
		10	12	7	3	7	4	7	4	7	4
		2632	4666	4212	3793	4468	4557	4931	4673	4931	4557
		127	128	129	130	131	132	133	134	135	136
		11	3	7	4	7	4	7	4	7	4
		3401	3602	4126	4195	4586	4452	4771	4473	4585	4195
		140	141	142	143	144	145	146	147	148	149
		10	10	3	7	3	7	3	7	3	7
		2107	3141	3558	4186	3859	4476	3916	4476	3858	4185
		153	154	155	156	157	158	159	160	161	162
		10	10	3	7	4	7	4	7	3	10
		2218	3141	3627	4279	4367	4828	4367	4277	3626	3139
		164	165	166	167	168	169	170	171	172	
		10	11	12	7	12	7	12	11	10	
		2106	3799	4522	4387	5547	4383	4599	3338	2105	
		173	174	175	176	177					
		10	10	11	10	10					
		2630	3050	3734	3050	2623					

Element Number

Fuel Group

MW, NT

Figure F-4. TMI-2 burnup for Axial Level 3 of 7 (levels numbered from top of core).

		1 10 2617	2 11 3380	3 11 3734	4 11 3381	5 10 2618										
		6 10 2101	7 11 3347	8 12 4567	9 7 4384	10 12 5572	11 7 4385	12 12 4568	13 11 3348	14 10 2102						
		15 10 2170	16 10 3122	17 3 3478	18 7 4016	19 4 4264	20 7 4794	21 4 4264	22 2 4063	23 3 3479	24 10 3124	25 10 2171				
		26 10 2102	27 10 3123	28 3 3413	29 6 3818	30 2 2925	31 7 4224	32 3 3790	33 7 4225	34 2 2925	35 6 3819	36 3 3413	37 10 3124	38 10 2102		
		39 11 3347	40 3 3401	41 6 3712	42 3 3805	43 4207	44 1 4501	45 7 4723	46 4 4350	47 7 4208	48 3 3806	49 6 3713	50 3 3401	51 3 3348		
		52 10 2616	53 12 4598	54 7 4035	55 2 4567	56 4 4195	57 4435	58 4936	59 4748	60 4936	61 4436	62 4195	63 2867	64 3984	65 4598	66 3618
		67 11 3380	68 7 4384	69 4 4265	70 3 4208	71 7 4294	72 4 4952	73 4 4904	74 5 5421	75 4 4904	76 4 4952	77 4 4314	78 4 4208	79 4 4265	80 4 4324	81 4 3381
		82 11 3794	83 12 5572	84 7 4793	85 3 3789	86 7 4722	87 4 4747	88 4 5421	89 4 6213	90 4 5421	91 4 4747	92 7 4722	93 3 3789	94 7 4793	95 3 5572	96 7 3794
		97 11 3360	98 7 4324	99 4 4265	100 3 4208	101 7 4315	102 4 4951	103 8 4904	104 4 5421	105 8 4904	106 4 4951	107 4 4320	108 7 4207	109 3 4265	110 7 4324	111 3 3380
		112 10 2618	113 12 4597	114 7 3227	115 2 2866	116 7 4193	117 4 4471	118 7 4934	119 4 4746	120 7 4334	121 4 4433	122 7 4193	123 2 3865	124 7 4046	125 2 4597	126 7 2618
		127 11 3347	128 3 3400	129 6 3711	130 3 3804	131 7 4205	132 4 4295	133 7 4720	134 4 4286	135 7 4205	136 3 3804	137 6 3710	138 3 3400	139 6 3346		
		140 10 2101	141 10 3122	142 3 3411	143 6 3816	144 2 2922	145 7 4222	146 3 3787	147 7 4221	148 2 2922	149 6 3815	150 3 3411	151 7 3121	152 3 2101		
		153 10 2170	154 10 3121	155 3 3476	156 7 4010	157 4 4261	158 7 4730	159 4 4261	160 7 3982	161 3 3476	162 10 3120	163 10 2169				
		164 10 2100	165 11 3345	166 12 4565	167 7 4382	168 4 5569	169 7 4361	170 4 4565	171 11 3344	172 10 3100						
						173 10 2616	174 11 3373	175 11 3791	176 11 3373	177 10 2615						

Element Number

Fuel Group

MWH/MT

Figure F-5. TMI-2 burnup for Axial Level 4 of / (levels numbered from top of core).

			1 10	2 11	3 11	4 11	5 10				
			2522	3321	3717	3321	2523				
			6 9	7 11	8 12	9 7	10 12	11 7	12 12	13 11	14 9
			2020	3295	4455	4264	5500	4264	4456	3296	2021
			15 10	16 10	17 3	18 7	19 4	20 7	21 4	22 7	23 3
			2131	3040	3361	3906	4106	4611	4106	3926	3362
			2131	3040	3265	3645	2855	4067	3401	4067	2855
			26 9	27 10	28 3	29 6	30 2	31 7	32 3	33 7	34 2
			2020	3040	3265	3645	2855	4067	3401	4067	2855
			39 11	40 3	41 6	42 3	43 7	44 4	45 7	46 4	47 7
			3295	3310	3612	3635	4049	4167	4529	4186	4050
			52 10	53 12	54 6	55 2	56 7	57 4	58 7	59 4	60 7
			2523	4479	3890	2829	4024	4263	4714	4572	4714
			67 11	68 7	69 4	70 7	71 4	72 7	73 4	74 8	75 4
			3321	4252	4133	4036	4147	4804	4739	5228	4739
			82 11	83 12	84 7	85 3	86 7	87 4	88 8	89 8	90 4
			3717	5500	4611	3400	4528	4572	5228	6117	5228
			97 11	98 7	93 4	100 7	101 4	102 7	103 4	104 8	105 4
			3321	4252	4132	4036	4185	4804	4738	5227	4738
			112 10	113 12	114 6	115 2	116 7	117 4	118 7	119 4	120 7
			2523	4478	3839	2828	4023	4261	4713	4571	4713
			127 11	128 3	129 6	130 3	131 7	132 4	133 7	134 4	135 7
			3295	3309	3611	3634	4047	4124	4527	4157	4047
			140 9	141 10	142 3	143 6	144 2	145 7	146 3	147 7	148 2
			2020	3039	3264	3644	2853	4064	3398	4064	2852
			153 10	154 10	155 3	156 6	157 4	158 7	159 4	160 6	161 3
			2130	3039	3359	3872	4103	4609	4103	3864	3359
			164 9	165 11	166 12	167 7	168 12	169 7	170 12	171 11	172 9
			2019	3039	4453	4262	5429	4261	4453	3293	2019
			173 10	174 11	175 11	176 11	177 10	178 10	179 11	180 9	181 10
			2521	3019	3715	3519	2521				

Element
Number

Fuel
Group

Mw/Mt

Figure F-6. TMI-2 burnup for Axial Level 5 of 7 (levels numbered from top of core).

	1 10 2290	2 10 2370	3 11 3410	4 10 2971	5 10 2290						
	6 9 1845	7 10 3075	8 11 4163	9 7 3966							
	15 9 1996	16 10 2837	17 3 3194	18 6 3856	19 3 3840	20 7 4261	21 3 3840	22 6 3811	23 3 3194	24 10 2838	25 9 1997
	26 9 1845	27 10 2937	28 2 3064	29 6 3615	31 3 3419	32 7 3939	33 2 3061	34 7 3940	35 3 3419	36 6 3615	37 2 3065
	36 10 3075	39 3 3192	41 6 3625	42 3 3645	43 7 4014	44 3 3891	45 7 4147	46 3 3909	47 6 4014	48 3 3646	49 6 3625
	52 10 2290	53 11 4192	54 6 3790	55 3 3416	56 7 3921	57 3 3950	58 4 4274	59 7 4148	60 4 4274	61 3 3950	62 7 3921
	67 10 2970	68 7 3949	69 3 3927	70 7 3925	71 3 3878	72 4 4384	73 4 4270	74 7 4678	75 4 4270	76 3 4385	77 3 3875
	82 11 3409	83 12 5163	84 7 4260	85 2 3060	86 4 4146	87 7 4147	88 7 4678	89 5 5571	90 4 4678	91 4 4147	92 7 4146
	97 10 2970	98 7 3945	99 3 3917	100 7 3925	101 3 3904	102 7 4384	103 4 4270	104 7 4677	105 4 4270	106 3 4384	107 3 3865
	112 10 2290	113 11 4191	114 6 3791	115 3 3415	116 7 3900	117 3 3949	118 7 4273	119 4 4147	120 7 4973	121 3 3949	122 7 7918
	127 10 3075	128 3 3191	129 6 3624	130 3 3645	131 7 4012	132 3 3870	133 7 4145	134 3 3932	135 7 4012	136 3 3645	137 6 3623
	140 9 1844	141 10 2837	142 2 3064	143 6 3613	144 3 3417	145 7 3937	146 2 3058	147 7 3937	148 3 3417	149 6 3612	150 2 3063
	153 9 1995	154 10 2836	155 3 7192	156 6 3768	157 3 3838	158 7 4058	159 3 3878	160 7 3725	161 3 3192	162 10 2836	163 9 1995
	164 9 1845	165 10 3074	166 11 4161	167 7 3964	168 3 5161	169 7 3964	170 7 4161	171 11 3913	172 10 1845		Element Number
	173 10 2838	174 9 3964	175 10 3968	176 11 2954	177 10 3286						Fuel Rod #
	178 10 2838	179 9 3964	180 10 3968	181 11 2954	182 10 3286						MW ₁ -MT

Figure F-7. TMI-2 burnup for Axial Level 6 of 7 (levels numbered from top of core).

			1 9 1416	2 9 1984	3 10 2134	4 9 1984	5 9 1416											
			6 9 1205	7 9 1936	8 10 2681	9 5 2582	10 11 3263	11 5 2582	12 10 2682	13 9 1936	14 9 1205							
			15 9 1279	16 9 1895	17 1 2125	18 5 2591	19 2 2548	20 6 2811	21 2 2548	22 5 2612	23 1 2125	24 9 1895	25 9 1279					
			26 9 1205	27 9 1895	28 1 2039	29 5 2514	30 2 2582	31 5 2726	32 1 2240	33 5 2726	34 2 2582	35 5 2515	36 1 2039	37 9 1895	38 9 1205			
			39 9 1936	40 1 2107	41 5 2454	42 2 2489	43 5 2741	44 2 2547	45 5 2735	46 2 2569	47 5 2741	48 2 2489	49 5 2454	50 1 2108	51 9 1936			
52 9 1416	53 10 2683	54 5 2593	55 2 2569	56 5 2740	57 2 2586	58 6 2819	59 2 2689	60 6 2819	61 2 2586	62 5 2740	63 2 2569	64 5 2548	65 2 2683	66 10 1416				
67 9 1984	68 5 2552	69 2 2594	70 5 2728	71 2 2606	72 6 2847	73 2 2735	74 6 3042	75 2 2734	76 6 2847	77 2 2578	78 5 2728	79 2 2593	80 5 2552	81 9 1984				
82 10 2134	83 11 3262	84 6 2811	85 1 2240	86 5 2735	87 2 2688	88 6 3042	89 6 3464	90 2 3042	91 6 2688	92 5 2735	93 1 2240	94 6 2811	95 1 3262	96 10 2134				
97 9 1984	98 5 2552	99 2 2593	100 5 2728	101 2 2553	102 6 2847	103 2 2734	104 6 3041	105 2 2734	106 6 2846	107 2 2603	108 5 2728	109 2 2593	110 5 2552	111 9 1984				
112 9 1416	113 10 2683	114 5 2565	115 2 2568	116 5 2739	117 2 2585	118 6 2819	119 2 2688	120 6 2819	121 2 2585	122 5 2739	123 2 2568	124 5 2583	125 2 2683	126 10 1416				
			127 9 1936	128 1 2107	129 5 2453	130 2 2488	131 5 2740	132 2 2580	133 5 2734	134 2 2567	135 5 2740	136 2 2488	137 5 2453	138 1 2107	139 9 1936			
			140 9 1204	141 1 1894	142 5 2038	143 2 2514	144 5 2581	145 1 2725	146 1 2240	147 5 2725	148 2 2581	149 5 2513	150 1 2039	151 9 1895	152 9 1204			
			153 9 1278	154 9 1894	155 1 2124	156 5 2589	157 2 2547	158 6 2810	159 2 2547	160 5 2593	161 1 2124	162 9 1894	163 9 1278					
							164 9 1204	165 9 1935	166 10 2680	167 5 2581	168 11 3261	169 5 2581	170 10 2680	171 9 1935	172 9 1204			
								173 9 1416	174 9 1983	175 10 2133	176 9 1953	177 9 1415						

Element Number
Fuel Group
Mwd/MT

Figure F-8. TMI-2 burnup for Axial Level 7 of 7 (levels numbered from top of core).

TABLE F-2 TMI-2 ISOTOPIC ACTIVITY SUMMARY (CURIES)
FOR FULL CORE (MARCH 1984).

FULL CORE ALL 1.98% ALL 2.64% ALL 2.96%

TH231	3.899E+00	9.256E-01	1.373E+00	1.601E+00
TH434	2.662E+01	8.529E+00	4.231E+00	9.059E+00
PA233	1.200E+00	4.536E-01	4.638E-01	2.827E-01
PA234M	2.682E+01	8.529E+00	9.231E+00	9.059E+00
U234	9.758E-02	3.179E-02	3.057E-02	2.721E-02
U235	3.899E+00	9.256E-01	1.373E+00	1.601E+00
U236	3.303E+00	1.010E+00	1.313E+00	9.812E-01
U237	4.704E+02	2.261E+02	1.768E+02	6.754E-03
U238	2.662E+01	8.529E+00	9.231E+00	9.059E+00
NP237	1.200E+00	4.536E-01	4.638E-01	2.827E-01
NP239	4.059E-01	2.342E-01	1.387E-01	3.563E-02
PU236	6.217E-02	2.719E-02	2.411E-02	1.0839E+02
PU238	1.055E+03	4.612E+02	4.739E+02	1.0839E+03
PU239	9.336E+03	3.644E+03	3.450E+03	2.392E+03
PU240	2.860E+03	1.228E+03	1.086E+03	5.456E+02
PU241	1.91E+05	9.217E+04	7.206E+04	2.753E+04
PU242	3.302E-01	1.751E-01	1.180E-01	3.617E-02
AM241	1.761E+03	8.468E+02	6.617E+02	2.528E+02
AM242M	7.286E-01	3.801E-01	2.645E-01	8.353E-02
AM242	7.286E-01	3.762E-01	2.632E-01	8.353E-02
AR243	4.085E-01	2.342E-01	1.367E-01	3.563E-02
CM242	1.547E+00	8.192E-01	5.661E-01	1.71E-01
CM243	1.110E-01	5.305E-02	3.745E-02	9.601E-03
CM244	4.342E+00	2.662E+00	1.370E+00	3.092E+00
SRR75	3.196E+03	1.073E+03	1.251E+03	9.933E+02
SRR86	5.542E+03	2.231E+04	2.779E+04	2.021E+04
SSR89	7.031E-04	2.509E-04	3.170E-04	2.332E-04
SSR90	6.625E+05	2.099E+05	2.621E+05	1.915E+05
YY90	6.627E+05	2.090E+05	2.621E+05	1.916E+05
YY91	2.886E-02	9.056E-03	1.141E+00	4.787E+00
ZR93	1.675E+01	5.350E+00	6.612E+00	1.060E+00
ZR93M	3.710E+00	1.186E+00	1.464E+00	1.785E-02
ZR95	2.034E-01	6.530E-02	1.022E-02	5.784E-01
NPC5P	4.515E-01	1.450E-01	1.781E-01	1.284E-01
NPC5	1.509E-03	4.44E-04	5.951E-04	4.292E-04
TC59	1.200E+02	3.895E+01	4.721E+01	3.380E+01
RH103	6.165E+07	2.110E+07	2.411E+07	1.687E+04
RH106	1.149E+05	4.391E+04	4.410E+04	2.687E+04
PD107	3.771E-01	1.484E-01	1.441E-01	9.458E-02
AG110	2.783E-01	1.266E-01	1.063E+00	4.333E+00
AG110M	2.092E-01	9.522E-01	7.992E+00	3.408E+00
CN113MM	2.422E+02	9.041E+01	9.204E+01	5.071E+01
CN119MM	1.908E+02	7.310E+00	7.567E+00	5.004E+00
CN121M	9.562E-01	3.428E-01	3.726E-01	2.408E-01
CN123	5.303E+00	1.903E+00	2.033E+00	1.367E+00
SB125	3.598E+04	1.351E+04	1.413E+04	9.336E+03
TE125M	9.024E+03	3.297E+03	3.449E+03	2.278E+03
SN126	5.338E+00	1.908E+00	2.054E+00	1.375E+00
SB126	7.474E-01	2.672E-01	2.876E+00	1.926E-01
SN126M	5.338E+00	1.908E+00	1.054E+00	1.375E+00
TE127	3.072E+00	1.092E+00	1.188E+00	7.918E-01
TE127M	3.136E+00	1.115E+00	1.213E+00	8.083E-01
C127	2.294E-01	7.301E-02	8.958E-02	6.182E-02
C134	3.609E+04	1.403E+04	1.517E+04	7.793E+03
C135	3.308E+00	9.396E-01	1.236E+00	1.132E+00
C137	7.505E+05	2.476E+05	2.995E+05	2.134E+05
CE137M	7.194E+05	2.343E+05	2.633E+05	2.018E+05
CE144	2.752E+05	8.821E+04	1.036E+05	7.404E+04
PR144	2.752E+05	8.822E+04	1.066E+05	7.840E+04
PR144M	3.303E+03	1.059E+03	1.303E+03	9.408E+02
PM147	3.366E+05	2.665E+05	3.278E+05	2.423E+05
CF151	1.039E+04	3.173E+03	3.918E+03	3.294E+03
FU152	4.319E+01	1.411E+01	1.720E+01	1.188E+01
G153	3.351E-01	1.316E-01	1.305E-01	6.499E-02
EU154	6.385E+03	2.526E+03	2.580E+03	1.279E+03
FU155	1.612E+04	5.566E+03	6.139E+03	4.395E+03

TABLE F-3 TH1-2 SPECIFIC ACTIVITY SUMMARY (CURIES/GRAM U)
FOR FULL CURE (MARCH 1984).

FULL CURE ALL 1.98% ALL 2.64% ALL 2.96%

TH231	4.77E-08	3.586E-08	4.805E-08	5.779E-08
TH234	3.286E-07	3.305E-07	3.284E-07	3.271E-07
PA233	1.470E-08	1.757E-08	1.650E-08	1.021E-08
PA234M	3.286E-07	3.305E-07	3.284E-07	3.271E-07
U234	1.19E-09	1.232E-09	1.372E-09	9.826E-10
U235	4.778E-08	3.586E-08	4.805E-08	5.779E-08
U236	4.048E-08	3.912E-08	4.670E-08	3.543E-08
U237	5.764E-10	8.761E-10	6.289E-10	2.439E-10
U238	3.286E-07	3.305E-07	3.284E-07	3.271E-07
NP237	1.470E-08	1.757E-08	1.650E-08	1.021E-08
NP239	5.005E-09	9.074E-09	4.933E-09	1.286E-09
PU236	7.51E-10	1.053E-09	8.579E-10	3.925E-10
PU238	1.290E-05	1.787E-05	1.451E-05	6.639E-06
PU239	1.144E-04	1.354E-04	1.222E-04	8.636E-05
PU240	3.504E-05	4.759E-05	3.864E-05	1.470E-05
PU241	2.350E-03	3.571E-03	2.564E-03	9.941E-04
PU242	4.046E-09	6.784E-09	4.230E-09	1.306E-09
AM241	2.015E-05	3.281E-05	2.354E-05	9.128E-06
AM242M	8.927E-09	1.473E-08	9.409E-09	3.031E-09
AM242	8.883E-09	1.466E-08	9.362E-09	3.016E-09
AM243	5.005E-09	9.074E-09	4.933E-09	1.286E-09
CM242	1.695E-08	3.174E-08	1.979E-08	6.193E-09
CM243	1.360E-09	2.478E-09	1.332E-09	3.466E-10
CM244	5.320E-08	1.032E-07	4.876E-08	1.116E-08
H3	3.916E-05	4.157E-05	4.450E-05	3.150E-05
SE79	4.340E-08	4.493E-08	4.952E-08	3.586E-08
SKR85	8.616E-04	8.646E-04	9.886E-04	7.299E-04
SKR69	7.811E-12	9.721E-12	1.128E-11	8.420E-12
SP90	5.118E-03	8.094E-03	9.324E-03	6.916E-03
YY90	8.122E-03	8.096E-03	9.327E-03	6.918E-03
ZY91	3.536E-10	3.520E-10	4.060E-10	3.018E-10
ZP93	2.052E-07	2.073E-07	2.352E-07	1.729E-07
NB93M	4.545E-08	4.594E-08	5.210E-08	3.826E-08
ZR95	2.492E-09	2.530E-09	2.854E-09	2.089E-09
NR95	5.533E-09	5.618E-09	6.336E-09	4.638E-09
NB95M	1.849E-11	1.877E-11	2.117E-11	1.550E-11
TC99	1.470E-06	1.509E-06	1.680E-06	1.221E-06
KU103	7.554E-15	6.174E-15	8.577E-15	5.939E-15
RU106	1.408E-03	1.701E-03	1.569E-03	9.703E-04
RH106	1.408E-03	1.701E-03	1.569E-03	9.703E-04
PE1C7	4.621E-09	5.750E-09	5.128E-09	3.054E-09
AG110	3.410E-09	4.907E-09	3.782E-09	1.637E-09
AG110M	2.564E-07	3.689E-07	2.843E-07	1.231E-07
CD113M	2.967E-06	3.503E-06	3.275E-06	2.156E-06
SN119M	2.436E-07	3.832E-07	2.692E-07	1.807E-07
SN121M	1.172E-08	1.328E-08	1.326E-08	8.694E-09
SN123	6.498E-08	7.374E-08	7.233E-08	4.937E-08
SB125	4.531E-04	5.234E-04	5.028E-04	3.371E-04
TE125M	1.106E-04	1.277E-04	1.227E-04	8.226E-05
SN126	6.541E-08	7.394E-08	7.309E-08	4.966E-08
SB125	9.157E-09	1.035L-08	1.023E-08	6.952E-09
SB126M	6.541E-08	7.394E-08	7.309E-08	4.966E-08
TE127	3.764E-08	4.230E-08	4.227E-08	2.859E-08
TE127M	3.843E-08	4.319E-08	4.316E-08	2.918E-08
I129	2.811E-09	3.022E-09	3.187E-09	2.232E-09
CS134	4.533E-04	5.436E-04	5.398E-04	2.814E-04
CS135	4.053E-08	3.641E-08	4.397E-08	4.088E-08
CS137	9.316E-03	9.544E-03	1.065E-02	7.704E-03
BA137M	8.815E-03	9.076E-03	1.008E-02	7.288E-03
CE144	3.372E-03	3.418E-03	3.864E-03	2.831E-03
PR144	3.372E-03	3.418E-03	3.864E-03	2.831E-03
PR144M	4.047E-05	4.101E-05	4.637E-05	3.397E-05
PM147	1.025E-02	1.032E-02	1.166E-02	8.749E-03
SM151	1.272E-04	1.229E-04	1.394E-04	1.189E-04
EU152	5.292E-07	5.467E-07	6.121E-07	4.288E-07
GU153	4.106E-09	5.101E-09	4.928E-09	2.346E-09
EU154	7.824E-05	9.788E-05	9.179E-05	4.617E-05
EU155	1.975E-04	2.157E-04	2.191E-04	1.587E-04

TABLE F-4 TMI-2 SPECIFIC ACTIVITY SUMMARY (CURIES/GRAM U)
FOR 1.98% INITIAL ENRICHMENT ZONES (MARCH 1984).

	ALL 1.98%	GR CUP 1	GROUP 2	GROUP 3	GROUP 4
TH231	3.586E-08	3.868E-08	3.694E-08	3.529E-08	3.396E-08
TH234	3.305E-07	3.301E-07	3.303E-07	3.305E-07	3.307E-07
PA233	1.757E-08	8.721E-09	1.359E-08	1.619E-08	2.416E-08
PA234M	3.305E-07	3.301E-07	3.303E-07	3.305E-07	3.307E-07
U234	1.232E-09	6.567E-10	9.868E-10	1.338E-08	1.652E-09
U235	3.586E-08	3.868E-08	3.695E-08	3.529E-08	3.396E-08
U236	3.912E-03	2.333E-08	3.312E-08	4.235E-08	4.970E-08
U237	2.761E-10	1.719E-10	4.763E-10	9.655E-10	1.522E-09
U239	3.305E-07	3.301E-07	3.303E-07	3.305E-07	3.307E-07
NP237	1.757E-08	8.721E-09	1.369E-08	1.919E-08	2.416E-08
NP239	9.074E-09	4.073E-10	2.458E-09	8.790E-09	2.026E-09
PU236	1.053E-09	2.036E-10	6.494E-10	1.160E-09	1.715E-09
PU238	1.787E-05	4.986E-06	1.102E-05	1.068E-05	2.910E-05
PU239	1.354E-04	8.694E-05	1.185E-04	1.458E-04	1.659E-04
PU240	4.759E-05	1.764E-05	3.391E-05	5.299E-05	7.033E-05
PU241	3.571E-03	7.008E-04	1.942E-03	3.936E-03	6.203E-03
PU242	6.764E-09	6.419E-10	2.630E-09	7.098E-09	1.358E-08
AM241M	3.281E-05	6.437E-06	1.784E-05	3.615E-05	5.699E-05
AM242M	1.473E-08	1.652E-09	5.282E-09	1.576E-09	2.833E-09
AM243	1.466E-08	1.644E-09	6.250E-09	1.568E-09	2.824E-09
CM242	9.074E-09	4.073E-10	2.458E-09	8.790E-09	2.026E-09
CH243	3.174E-08	3.198E-09	1.274E-08	3.348E-08	6.268E-08
CH244	2.478E-09	1.115E-10	6.727E-10	2.402E-09	5.534E-09
H3	1.032E-07	2.155E-09	1.910E-08	9.055E-08	2.527E-07
SE79	4.157E-05	2.257E-05	3.372E-05	4.522E-05	5.510E-05
KP05	4.483E-08	2.515E-08	3.690E-08	4.869E-08	5.958E-08
SR09	8.646E-04	4.960E-04	7.190E-04	9.379E-04	1.119E-03
SR90	9.721E-12	5.678E-12	8.149E-12	1.053E-11	1.244E-11
YY90	5.094E-03	4.672E-03	6.750E-03	8.778E-03	1.045E-02
YY91	8.096E-03	4.673E-03	6.752E-03	8.790E-03	1.045E-02
ZP03	3.520E-10	2.042E-10	2.942E-10	3.817E-10	4.533E-10
NB93M	2.073E-07	1.180E-07	1.718E-07	2.250E-07	2.691E-07
NB95	4.594E-08	2.612E-08	3.505E-08	4.986E-08	5.968E-08
NB05	2.530E-09	1.431E-09	2.091E-09	2.747E-09	3.295E-09
NB95M	5.618E-09	3.178E-09	4.642E-09	6.098E-09	7.315E-09
TC69	1.877E-11	1.062E-11	1.551E-11	2.039E-11	2.444E-11
RU103	1.509E-06	8.453E-07	1.242E-06	1.639E-06	1.973E-06
RU1C6	9.174E-15	4.267E-15	6.522E-15	8.910E-15	1.100E-14
RH106	1.701E-03	7.724E-04	1.260E-03	1.865E-03	2.410E-03
PD107	5.750E-09	2.490E-09	4.245E-09	6.315E-09	8.272E-09
AG110	4.307E-09	1.137E-09	2.782E-09	5.373E-09	8.370E-09
AG110M	3.699E-07	8.546E-08	2.092E-07	4.040E-07	6.293E-07
CD113M	3.503E-06	1.850E-06	2.803E-06	3.813E-06	4.703E-06
SN119M	2.832E-07	1.543E-07	2.299E-07	3.030E-07	3.751E-07
SN121M	1.322E-08	6.293E-09	1.001E-08	1.455E-08	1.933E-08
SN123	7.374E-09	4.038E-08	6.000E-08	8.018E-08	9.739E-08
SB125	5.234E-04	2.798E-04	4.217E-04	5.698E-04	6.982E-04
TE125M	1.277E-04	6.829E-05	1.029E-04	1.391E-04	1.704E-04
SN126	7.394E-03	3.945E-08	5.953E-08	9.051E-08	1.087E-08
SB126M	1.035E-08	5.523E-09	8.334E-09	1.127E-08	1.382E-08
TE127	7.394E-08	3.945E-08	5.952E-08	8.051E-08	9.871E-08
TE127M	4.230E-08	2.200E-08	3.369E-08	4.612E-08	5.704E-08
TE127M	4.319E-08	2.246E-08	3.440E-08	4.709E-08	5.823E-08
I129	3.022E-09	1.017E-09	2.437E-09	3.291E-09	4.029E-09
CS134	5.436E-04	1.649E-04	3.467E-04	6.011E-04	8.619E-04
CS135	3.641E-03	2.960E-08	3.439E-08	3.793E-08	4.038E-08
CS137	9.594E-03	5.321E-03	7.052E-03	1.043E-02	1.260E-02
BA137M	9.076E-03	5.033E-03	7.433E-03	9.633E-03	1.192E-02
CE144	3.418E-03	1.935E-03	2.825E-03	3.710E-03	4.449E-03
PR144	3.416E-03	1.935E-03	2.825E-03	3.710E-03	4.449E-03
FR144M	4.101E-05	2.322E-05	3.390E-05	4.452E-05	5.334E-05
PR147	1.032E-02	6.127E-03	8.728E-03	1.118E-02	1.314E-02
SN151	1.229E-04	9.049E-05	1.130E-04	1.301E-04	1.422E-04
SE152	5.467E-07	3.104E-07	4.742E-07	6.023E-07	6.824E-07
SN153	5.101E-09	1.318E-09	3.178E-09	5.710E-09	8.219E-09
CE154	9.786E-05	2.806E-05	6.112E-05	1.079E-04	1.582E-04
LW155	2.157E-04	1.251E-04	1.797E-04	2.334E-04	2.786E-04

TABLE F-5 TAI-2 SPECIFIC ACTIVITY SUMMARY (CURIES/GRAM U)
FOR 2.64% INITIAL ENRICHMENT ZONES (MARCH 1984).

	ALL 2.64%	GROUP 5	GROUP 6	GROUP 7	GROUP 8
TH231	4.385E-08	5.191E-08	4.913E-08	4.760E-08	4.537E-08
TH234	3.284E-07	3.261E-07	3.284E-07	3.286E-07	3.269E-07
PA233	1.650E-09	3.654E-09	1.536E-08	1.974E-08	2.699E-08
PA234M	3.284E-07	3.281E-07	3.284E-07	3.286E-07	3.249E-07
U234	1.372E-09	3.056E-10	1.302E-09	1.606E-09	2.090E-09
U235	4.895E-08	5.191E-08	4.913E-08	4.759E-08	4.537E-08
U236	4.670E-08	2.946E-08	4.512E-08	5.376E-08	6.620E-08
U237	6.289E-10	1.455E-10	5.025E-10	8.316E-10	1.501E-09
U238	3.264E-07	3.261E-07	3.284E-07	3.286E-07	3.229E-07
NP237	1.650E-08	3.654E-09	1.536E-08	1.974E-08	2.699E-08
NP239	4.933E-09	3.060E-10	2.725E-09	6.739E-09	1.997E-08
PU236	9.579E-10	2.701E-10	7.231E-10	1.103E-09	1.952E-09
PU238	1.451E-05	2.592E-06	1.223E-05	1.864E-05	3.128E-05
PU239	1.228E-04	8.223E-05	1.201E-04	1.393E-04	1.650E-04
PU240	3.864E-05	1.580E-05	3.500E-05	4.815E-05	6.968E-05
PL241	2.564E-03	5.930E-04	2.048E-03	3.390E-03	6.120E-03
PU242	2.230E-09	5.115E-10	2.840E-09	5.759E-09	1.336E-08
AM241	2.354E-05	5.445E-06	1.881E-05	3.113E-05	5.620E-05
AM242M	9.409E-09	1.315E-09	6.649E-09	1.278E-08	2.738E-08
AM242	9.362E-09	1.309E-09	6.616E-09	1.272E-08	2.724E-08
AM243	9.033E-09	3.060E-10	2.725E-09	6.739E-09	1.997E-08
CM242	1.979E-08	2.534E-09	1.355E-08	2.691E-08	6.059E-08
CM243	1.332E-09	8.317E-11	7.379E-10	1.821E-09	5.371E-09
CM244	4.767E-08	2.526E-09	2.170E-08	6.555E-08	2.474E-07
H3	4.450E-05	2.635E-05	4.242E-05	5.196E-05	6.655E-05
SE79	4.952E-08	3.0000E-08	4.744E-08	5.754E-08	7.270E-08
KR85	9.886E-04	6.080E-04	9.499E-04	1.145E-03	1.433E-03
SR89	1.128E-11	7.021E-12	1.086E-11	1.302E-11	1.618E-11
TF90	9.324E-03	5.759E-03	9.967E-03	1.079E-02	1.347E-02
YY91	7.327E-03	5.760E-03	9.970E-03	1.079E-02	1.347E-02
ZF93	4.060E-10	2.516E-10	3.907E-10	4.693E-10	5.347E-10
NB93M	2.352E-07	1.440E-07	2.258E-07	2.727E-07	3.424E-07
ZR95	5.210E-08	3.186E-08	5.000E-08	6.041E-08	7.587E-08
NR95	2.854E-09	1.740E-09	2.737E-09	3.311E-09	4.168E-09
NB95M	6.336E-09	3.863E-09	6.078E-09	7.352E-09	9.254E-09
TC99	2.117E-11	1.291E-11	2.031E-11	2.457E-11	3.092E-11
RU103	1.680E-06	1.018E-06	1.609E-06	1.952E-06	2.464E-06
RU106	8.577E-15	4.937E-15	8.133E-15	1.058E-14	1.310E-14
RH106	1.569E-03	8.040E-04	1.455E-03	1.886E-03	2.599E-03
PD107	1.569E-03	8.040E-04	1.455E-03	1.886E-03	2.599E-03
AG110	5.122E-09	2.517E-09	4.719E-09	6.209E-09	8.719E-09
AG110M	3.782E-09	1.056E-08	3.098E-09	4.917E-09	6.672E-09
CD113M	2.843E-07	7.943E-08	2.329E-07	3.697E-07	5.520E-07
SN119M	2.275E-06	1.382E-06	3.101E-06	3.648E-06	5.326E-06
SN121M	2.692E-07	1.583E-07	2.563E-07	3.148E-07	4.051E-07
SN123	1.326E-08	7.107E-09	1.240E-08	1.580E-08	2.128E-08
SB125	7.233E-03	4.282E-08	6.896E-08	9.447E-08	1.032E-07
TE125M	5.028E-04	2.923E-04	4.776E-04	5.955E-04	7.629E-04
SN120	1.227E-04	7.133E-05	1.166E-04	1.439E-04	1.862E-04
SB126	7.309E-08	4.253E-08	6.945E-08	8.568E-08	1.100E-07
SA126M	1.023E-09	5.954E-09	9.723E-09	1.199E-08	1.551E-08
TF127	7.309E-08	4.253E-08	6.945E-08	8.568E-08	1.108E-07
TE127M	4.227E-03	2.416E-03	4.003E-03	4.974E-03	6.493E-08
I129	4.316E-08	2.466E-08	4.087E-08	5.078E-08	6.628E-08
CS134	3.187E-09	1.868E-09	3.033E-09	3.730E-09	4.802E-09
CS135	5.398E-04	1.889E-04	4.645E-04	6.860E-04	1.089E-03
CS137	4.397E-08	3.687E-08	4.385E-08	4.681E-08	5.044E-08
BA137M	1.065E-02	6.409E-03	1.019E-02	1.240E-02	1.573E-02
CC144	1.008E-02	6.063E-03	9.641E-03	1.173E-02	1.488E-02
PR144	3.864E-03	2.357E-03	3.707E-03	4.493E-03	5.642E-03
PR144M	3.864E-03	2.357E-03	3.707E-03	4.493E-03	5.642E-03
PM147	4.637E-05	2.828E-05	4.449E-05	5.380E-05	6.770E-05
SM151	1.166E-02	7.407E-03	1.129E-02	1.341E-02	1.642E-02
SL152	1.394E-04	1.076E-04	1.387E-04	1.522E-04	1.687E-04
GI153	6.121E-07	3.626E-07	6.039E-07	7.134E-07	8.364E-07
EU154	4.928E-09	1.449E-09	4.219E-09	6.387E-09	1.023E-08
EU155	9.179E-05	3.083E-05	7.866E-05	1.172E-04	1.903E-04
	2.191E-04	1.387E-04	2.111E-04	2.521E-04	3.134E-04

TABLE F-6 TMI-2 SPECIFIC ACTIVITY SUMMARY (CURIES/GRAM U)
FDF 2.96% INITIAL ENRICHMENT ZONES (MARCH 1984).

	ALL 2.96%	GROUP 9	GROUP 10	GROUP 11	GROUP 12
TH231	5.779E-06	6.030E-08	5.784E-08	5.587E-08	5.312E-08
TH234	3.271E-07	3.267E-07	3.271E-07	3.274E-07	3.277E-07
PA233	1.021E-08	5.071E-09	9.671E-09	1.410E-08	2.144E-08
PA234M	3.271E-07	3.267E-07	3.271E-07	3.274E-07	3.277E-07
UU234	9.826E-10	5.586E-10	9.591E-10	1.304E-09	1.831E-09
UU235	5.779E-08	6.030E-08	5.784E-08	5.587E-08	5.312E-08
UU236	3.543E-08	2.011E-08	3.518E-08	4.635E-08	6.165E-08
UU237	2.439E-10	3.024E-11	1.742E-10	3.085E-10	8.310E-10
UU238	3.271E-07	3.267E-07	3.271E-07	3.274E-07	3.277E-07
NP237	1.021E-08	5.071E-09	9.671E-09	1.410E-08	2.144E-08
NP239	1.266E-09	3.165E-11	4.212E-10	1.729E-09	7.656E-09
PU236	3.925E-10	1.022E-10	3.174E-10	6.028E-10	1.211E-09
PU235	6.639E-06	1.735E-06	5.377E-06	1.019E-05	2.04E-05
PU239	8.636E-05	5.422E-05	6.681E-05	1.110E-04	1.416E-04
PU240	1.970E-05	6.699E-06	1.773E-05	2.968E-05	5.024E-05
PU241	9.941E-04	1.558E-04	7.102E-04	1.544E-03	3.633E-03
PU242	1.306E-09	8.442E-11	6.559E-10	1.687E-09	6.356E-09
AP241	9.126E-06	1.457E-06	6.521E-06	1.454E-05	3.339E-05
AM242M	3.031E-09	2.314E-10	1.662E-09	4.737E-09	1.390E-08
AM242	3.016E-09	2.302E-10	1.653E-09	4.714E-09	1.383E-08
AM243	1.266E-09	3.165E-11	4.212E-10	1.729E-09	7.656E-09
CK242	6.193E-09	4.301E-10	3.224E-09	9.526E-09	2.944E-08
CM243	3.466E-10	8.597E-12	1.141E-10	4.670E-10	2.059E-09
CP244	1.116E-08	9.823E-11	2.244E-09	1.248E-08	7.666E-08
CH3	3.150E-05	1.786E-05	3.087E-05	4.189E-05	5.820E-05
SC79	3.586E-08	2.072E-08	3.532E-08	4.741E-08	6.449E-08
KP85	7.259E-04	4.269E-04	7.211E-04	9.612E-04	1.304E-03
SP89	8.420E-12	4.973E-12	8.339E-12	1.105E-11	1.488E-11
SR90	6.916E-03	4.058E-03	6.538E-03	9.098E-03	1.231E-02
YY90	6.911E-03	4.059E-03	6.640E-03	9.100E-03	1.231E-02
YY91	3.011E-10	1.777E-10	2.967E-10	3.967E-10	5.355E-10
ZP43	1.729E-07	1.007E-07	1.706E-07	2.279E-07	3.101E-07
ZP43M	3.926E-09	2.228E-08	3.775E-08	5.455E-08	6.866E-08
ZP45	2.089E-09	1.213E-09	2.060E-09	2.757E-09	3.760E-09
NB79	4.633E-09	2.694E-09	4.574E-09	6.121E-09	8.349E-09
NB95	1.550E-11	9.002E-12	1.529E-11	2.045E-11	2.790E-11
TC99	1.221E-06	7.052E-07	1.202E-06	1.613E-06	2.208E-06
RU103	5.939E-15	3.287E-15	5.788E-15	7.960E-15	1.125E-14
RU106	9.703E-04	4.797E-04	9.202E-04	1.342E-03	2.039E-03
RH106	9.703E-04	4.797E-04	9.202E-04	1.342E-03	2.039E-03
FD107	3.054E-09	1.639E-09	2.565E-09	4.276E-09	6.661E-09
AG110	1.637E-09	3.777E-10	1.269E-09	2.532E-09	5.374E-09
AG110M	1.231E-07	2.840E-08	9.542E-08	1.904E-07	4.041E-07
CO113M	2.156E-06	1.190E-06	2.097E-06	2.891E-06	4.107E-06
SN119M	1.907E-07	1.018E-07	1.767E-07	2.408E-07	3.367E-07
SN121M	8.594E-09	4.509E-09	8.343E-09	1.188E-08	1.751E-08
SEN123	4.937E-08	2.796E-08	4.836E-08	6.570E-08	9.143E-08
SR125	3.371E-04	1.878E-04	3.289E-04	4.508E-04	6.347E-04
TE125M	8.226E-05	4.594E-05	6.027E-05	1.100E-04	1.549E-04
SN126	4.666E-08	2.771E-08	4.847E-08	6.638E-08	9.335E-08
SN126M	6.952E-09	3.040E-09	6.780E-09	9.293E-09	1.330E-08
SR126M	4.966E-08	2.771E-08	4.847E-08	6.638E-08	9.335E-08
TF127	2.859E-08	1.570E-08	2.700E-08	3.840E-08	5.457E-08
TF127M	2.918E-08	1.603E-08	2.838E-08	3.920E-08	5.572E-08
T129	2.232E-09	1.255E-09	2.184E-09	2.977E-09	4.161E-09
CS134	2.314E-04	8.286E-05	2.390E-04	4.292E-04	8.008E-04
CC135	4.088E-08	3.290E-08	4.104E-08	4.673E-08	5.195E-08
CS137	7.704E-03	4.427E-03	7.577E-03	1.020E-02	1.404E-02
RA137M	7.288E-03	4.188E-03	7.168E-03	9.652E-03	1.328E-02
CE144	2.931E-03	1.645E-03	2.792E-03	3.736E-03	5.094E-03
PR144	2.831E-03	1.645E-03	2.792E-03	3.736E-03	5.094E-03
PR144M	3.397E-05	1.474E-05	3.351E-05	4.483E-05	6.113E-05
PM147	8.749E-03	5.259E-03	8.710E-03	1.142E-02	1.512E-02
SM151	1.159E-04	8.604E-05	1.221E-04	1.435E-04	1.667E-04
SEU152	4.288E-07	2.079E-07	4.332E-07	6.030E-07	7.970E-07
GU153	2.346E-02	4.876E-10	1.876E-09	3.752E-09	7.440E-09
GU154	4.617E-05	1.314E-05	3.860E-05	7.050E-05	1.351E-04
EU155	1.587E-04	9.638E-05	1.578E-04	2.060E-04	2.740E-04

APPENDIX G

SURFACE AREA CALCULATION FOR PARTICLE SIZE GROUPS

APPENDIX G

SURFACE AREA CALCULATION FOR PARTICLE SIZE FRACTIONS

Surface area ratios were calculated for particle size fractions sieved from the TMI-2 core debris grab samples. The results of the calculation were used for evaluating the correlation between the surface area of particle size fractions and element fission product concentrations measured for the samples. For the calculational model, particles were assumed to have similar shapes and a constant particle density. The specific surface area ratio difference between the minimum particle size fraction (30 to 74 μm) and the maximum (1680 to 4000 μm) fraction is approximately a factor of 50.

Assumptions for Surface Area Calculation

Assumptions

1. Particle shapes are approximated to be similar.
2. Particle density is constant for individual particles.
3. Particle size distribution is described to be logarithmically linear for cumulative weight fraction and particle size.
4. Effective diameter represents particle size.

Nomenclature

- F = Cumulative weight fraction for a certain particle size
- R = Particle size (effective diameter) in μm
- S = Surface area of distinct particle (cm^2)

W = Weight of distinct particle (mg)

D = Effective particle density used in the relationship between W and R

k = Effective surface area coefficient used in the relationship between S and R

a,b = Particle size distribution coefficients used in the relationship between F and R

T = Total weight of all particle size fractions (mg)

N_x^y = Number of particles in the diameter range from x to y

A_x^y = Surface area of particles in the diameter range from x to y (cm^2)

i = Identification for a certain particle size fraction

A_i = Average specific surface area for a certain particle size fraction i (cm^2)

C = Average specific surface area for all particle size fractions (cm^2).

Formulation

From Assumption 3, the relationship between F (cumulative weight fraction) and R (effective diameter) can be described as

$$F = aR^b \quad (1)$$

where a and b are determined from the relationship between F and R.

The weight (W) and surface area (S) of a particle with diameter R can be approximated as follows:

$$W = DR^3 \quad (2)$$

$$S = kR^2 \quad (3)$$

where D and k are assumed to be constant.

The number of particles included in the diameter range from R to R + dR is derived from Equations 1 and 2, and the total sample weight (T).

$$\begin{aligned} dF &= abR^{b-1}dR \\ N_R^{R+dR} &= \frac{TdF}{dR^3} \\ &= \frac{Tab}{D} R^{b-4}dR \end{aligned} \quad (4)$$

The surface area of particles included in the above diameter range is described as

$$\begin{aligned} A_R^{R+dR} &= kR^2 \cdot N_R^{R+dR} \\ &= \frac{kTab}{D} R^{b-2}dR \end{aligned}$$

The average specific surface area for particle size fraction i can be derived as follows:

$$A_i = A_{r_{i1}}^{r_{i2}} / T[F(r_{i2}) - F(r_{i1})]$$

$$= \int_{r_{i1}}^{r_{i2}} \frac{k T_{ab}}{b} R^{b-2} dR / Ta(r_{i2}^b - r_{i1}^b)$$

$$= \frac{k}{D} \cdot \frac{b}{r_{i2}^b - r_{i1}^b} \int_{r_{i1}}^{r_{i2}} R^{b-2} dR .$$

When $b = 1$,

$$A_i = \frac{k}{D} \cdot \frac{\log(r_{i2}/r_{i1})}{r_{i2} - r_{i1}} \quad (6)$$

and when $b \neq 1$,

$$A_i = \frac{k}{D} \cdot \frac{b}{b-1} \cdot \frac{r_{i2}^{b-1} - r_{i1}^{b-1}}{r_{i2}^b - r_{i1}^b} \quad (7)$$

where r_{i1} and r_{i2} indicate the diameter range of the particle size fraction i .

The specific surface area averaged for all particle size fractions may be used as a normalization standard.

When $b = 1$,

$$C = \frac{k}{D} \cdot \frac{\log(r_{\max}/r_{\min})}{r_{\max} - r_{\min}}$$

$$A_i/C = \frac{\log(r_{i2}/r_{i1})}{\log(r_{\max}/r_{\min})} \cdot \frac{r_{\max} - r_{\min}}{r_{i2} - r_{i1}} . \quad (8)$$

When $b \neq 1$,

$$C = \frac{k}{D} \cdot \frac{b}{b-1} \cdot \frac{\frac{r_{\max}^{b-1} - r_{\min}^{b-1}}{r_{\max}^b - r_{\min}^b}}$$

$$A_i/C = \frac{\frac{r_{i2}^{b-1} - r_{i1}^{b-1}}{r_{\max}^{b-1} - r_{\min}^{b-1}} \cdot \frac{r_{\max}^b - r_{\min}^b}{r_{i2}^b - r_{i1}^b}}{(9)}$$

Application to Grab Sample Particle Size Distribution

The particle size distribution coefficient b in Equation (1) can be determined for the core debris grab samples (See Figure 15 of Reference G-1) by

$$A_i/C = \frac{\frac{r_{i2}^{0.59} - r_{i1}^{0.59}}{r_{\max}^{0.59} - r_{\min}^{0.59}} \cdot \frac{r_{\max}^{1.59} - r_{\min}^{1.59}}{r_{i2}^{1.59} - r_{i1}^{1.59}}}{(9)}$$

Results of the application to the core debris grab sample particle size distribution are shown in the Table G-1.

TABLE G-1. NORMALIZED SURFACE AREA FOR TMI-2 CORE DEBRIS GRAB SAMPLES

Particle Size Range (μm)		Normalized Surface Area per Unit Mass	
r_{i1}	r_{i2}	$(30 \mu\text{m})^a$	$(20 \mu\text{m})^b$
1680	4000	0.57	0.56
1000	1680	1.18	1.17
707	1000	1.85	1.83
297	707	3.21	3.17
149	297	7.16	7.07
74	149	14.3	14.1
30	74	31.0	30.6
20	30	--	62.4

a. For samples sieved to 30 μm .

b. For samples sieved to 20 μm .

Reference

- G-1. D. W. Akers and B. A. Cook, Draft Preliminary Report: TMI-2 Core Debris Grab Samples--Analysis of First Group of Samples, EGG-TMI-6630, June 1984, draft.

APPENDIX H

THERMAL ANALYSIS OF TMI-2 CORE DEBRIS SAMPLES

J. R. Jewett

Rockwell Hanford Operations

Rockwell Hanford Operations

SUPPORTING DOCUMENT		Number SD-WM-TRP-009	Rev Ltr / Chg No. Rev. 0	Page 1 of Total Pages 13
PROGRAM WASTE MANAGEMENT				
Document Title Thermal Analysis of TMI-2 Core Debris Samples		Baseline Document <input type="checkbox"/> Yes <input checked="" type="checkbox"/> No		
Key Words Zirconium, Core Debris, TMI, DTA, Pyrophoricity		WBS No. or Work Package No. X762B		
THIS DOCUMENT IS FOR USE IN PERFORMANCE OF WORK UNDER CONTRACTS WITH THE U.S. DEPARTMENT OF ENERGY BY PERSONS OR FOR PURPOSES WITHIN THE SCOPE OF THESE CONTRACTS. DISSEMINATION OF ITS CONTENTS FOR ANY OTHER USE OR PURPOSE IS EXPRESSLY FORBIDDEN.		Prepared by (Name and Dept. No.) J. R. Jewett/65450		Date 10/10/84
Abstract Differential thermal analyses (DTA) were conducted on samples of Three Mile Island core debris. The samples generally showed little thermal activity; however, one sample gave a large broad exotherm starting at 550°C.		See reverse side for additional approvals		
		• Distribution Name Mail Address		
		<p>Department of Energy Richland Operations Office</p> <ul style="list-style-type: none"> * M. Dayani Fed/700 * J. D. White Fed/700 <p>EG&G Idaho (TMI) Middletown, Pennsylvania</p> <ul style="list-style-type: none"> * G. J. Quinn * H. M. Burton (10) + Joe Carlson Department of Energy TMI Site <p>* W. W. Bixby</p> <p>Rockwell Hanford Operations</p> <ul style="list-style-type: none"> * J. N. Appel 2750E/200E * J. S. Buckingham MO-037/200W * B. D. Bullough MO-922/200E * T. D. Cooper 234-5Z/200W * J. O. Henrie (3) 2750E/200E * J. R. Jewett (3) MO-037/200W * J. P. Sloughter 2704S/200W 		
		(Continued on reverse side)		
		*COMPLETE DOCUMENT (No asterisk, title page/summary or revision page only)		
		Release Stamp		
Prepared By: _____				
Used By: _____				

1974-10-10

19

Rockwell Hanford Operations

Page 2	Number SD-WM-TRP-009	SUPPORTING DOCUMENT		
Approvals		* Distribution	Name	Mail Address
<input checked="" type="checkbox"/> <u>H. E. McGuire</u> Program Office				
<input checked="" type="checkbox"/> <u>J. O. Henrie</u> Research and Engineering				
<input type="checkbox"/> <u>Plant Operations</u>				
<input type="checkbox"/> <u>Health, Safety and Environment</u>				
<input type="checkbox"/> <u>Quality Assurance</u>				
<input type="checkbox"/> <u>Training</u>				
<input type="checkbox"/> <u>End Function</u>				
<input type="checkbox"/> <u>End Function</u>				
<input type="checkbox"/>				
<input checked="" type="checkbox"/> <u>J. S. Buckingham</u> Approval Authority				

A-6400-073B (2-83)

Rockwell Hanford Operations

SUPPORTING DOCUMENT	Number	Rev. Ltr./Chg. No.	Page
	SD-WM-TRP-009	Rev. 0	3

THERMAL ANALYSIS OF TMI-2 CORE DEBRIS SAMPLES

Differential thermal analyses (DTA) have been conducted on seven samples of core debris from Three Mile Island Unit 2 (TMI-2). The samples were received from D. W. Akers of EG&G Idaho on August 23, 1984. The attached table summarizes the appearances of the samples.

Each sample was heated from 40°C to 1000°C at 10 deg/min while monitoring the heat energy being absorbed or produced by the sample, using a Perkin-Elmer DTA 1700 DTA System. Each sample was packaged separately in a small glass vial and weighed in the range 10-20 mg. Each sample was consumed completely in the test, leaving a dark powder residue.

The attached figures give the DTA results. The samples generally showed little or no thermal activity. In exception, sample #262 gave a large broad exotherm of 761 cal/g, spanning nearly 500 degrees, starting at about 550°C. This exotherm is at much greater temperatures than those observed for samples of zirconium powder and partially oxidized zirconium powder (Reference). If the exotherm is due to the oxidation of zirconium, the zirconium must be coated with a thick non-combustible (oxide?) layer which protects it at lower temperatures.

Samples #245 and Sp1 #5 both showed about 100 cal/g of exothermic activity in the 200-600°C region, with most of it occurring in a peak from about 550°C to 600°C. Similar activity, but greatly reduced in magnitude, was also observed in sample #247.

"Blank" runs, conducted in the same way (except without samples) have been included in the figures to demonstrate the baseline and run-to-run variation inherent in the measurement method.

TABLE

Appearance of Sample Materials As Received

<u>Sample</u>	<u>Appearance</u>
#245	single, black, obsidian-like particle
#246	one large black particle plus black fines
#247	single, black, obsidian-like particle
#258	single brownish shard
#262	single black particle
#265	single black obsidian-like particle
Spl #5	single black particle plus black fines

26.00

TMI 262

WT. 18.70 mg

SCRATE: 10.00 deg/min

ATMOSPHERE: AIR 0 cc/min

<ENDO

MCAL/SEC

18.00

8.00

PEAK FROM: 540
TO: 880
ONSET: 702.8
CAL/GRAM: -760.98
MAX: 825

50.00 148.00 236.00 324.00 412.00 480.00 568.00 656.00 744.00 832.00 920.00

JKW

FILE: 262PK.DT

TEMPERATURE (C)

DTA

DATE: 84/09/20

TIME: 12:04

5.00

TMI #245

WT: 13.90 mg

SCAN RATE: 10.00 deg/min

ATMOSPHERE: AIR 0 cc/min

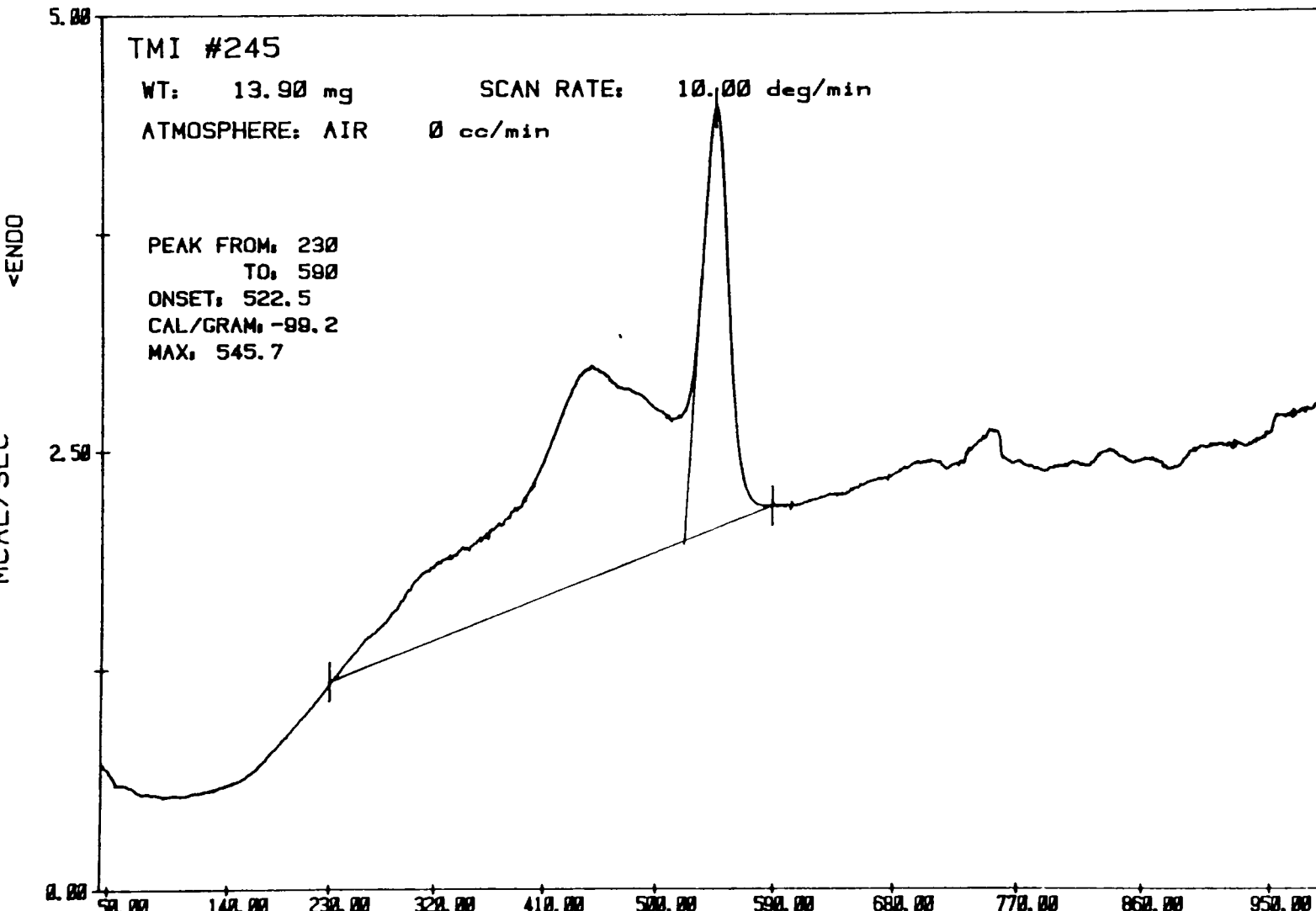
<ENDO

MCAL/SEC

2.50

0.00

PEAK FROM: 230
TO: 590
ONSET: 522.5
CAL/GRAM: -88.2
MAX: 545.7



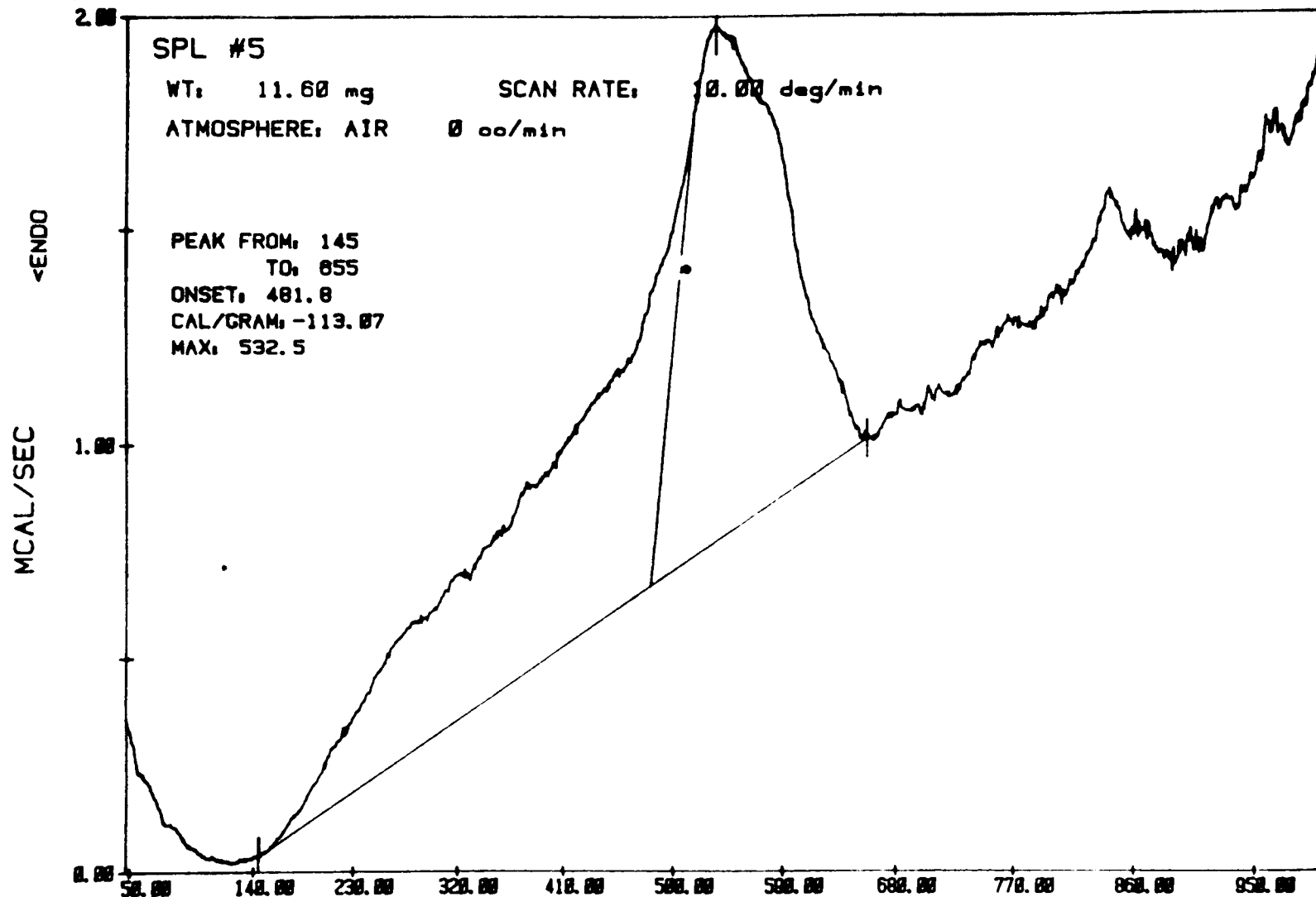
JKW

FILE: TM245.DT

TEMPERATURE (C)

DTA

-- 01/20/07 TIME 14:34



JWW

FILE: TMS.DT

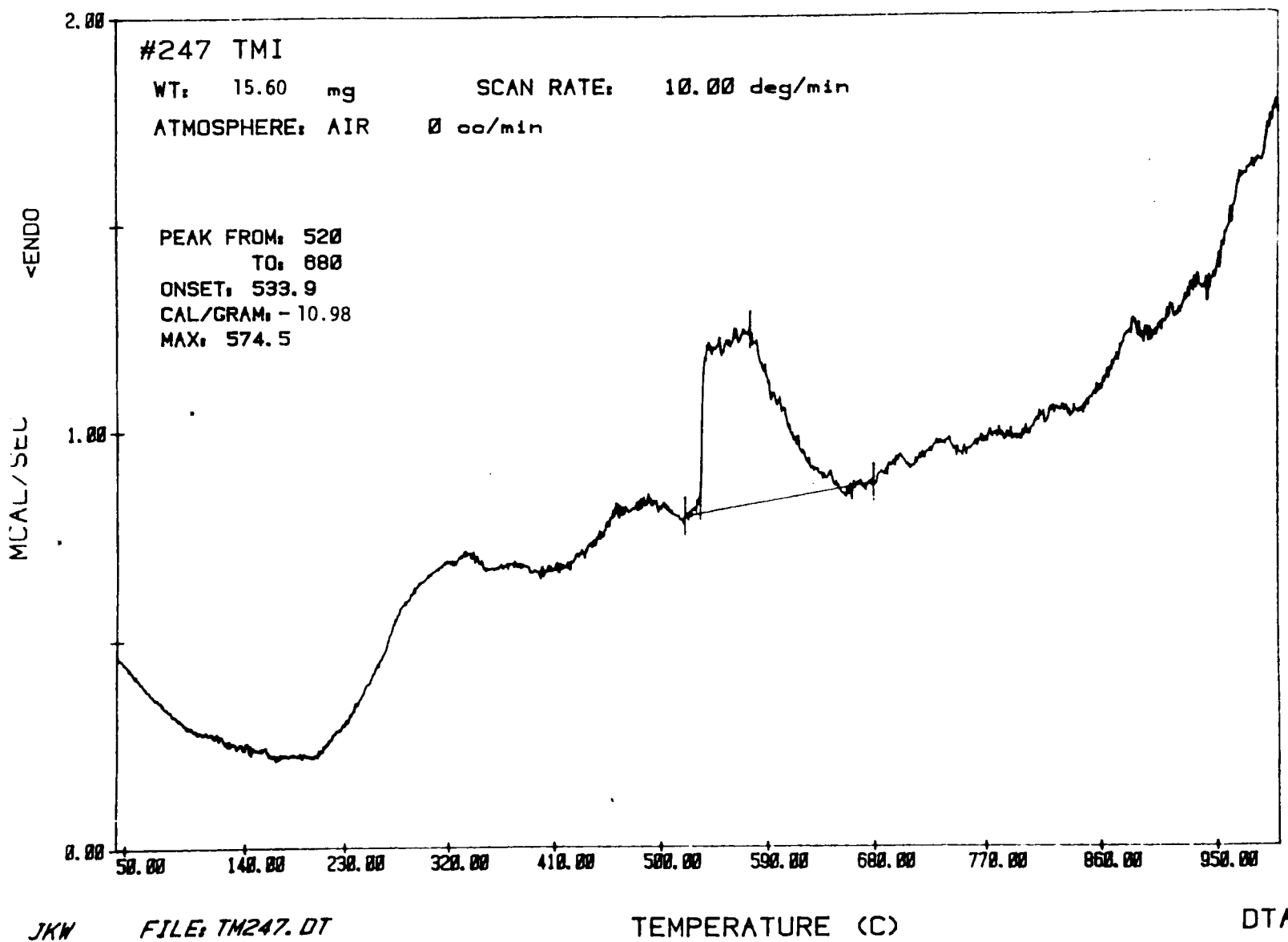
DATE:

01/10/21

TIME: 08:03

TEMPERATURE (C)

DTA



2.00

TMI #246

WT: 17.40 mg

SCAN RATE: 10.00 deg/min

ATMOSPHERE: AIR 0 cc/min

<ENDO

MCAL/SEC

1.00

0.00

50.00 140.00 230.00 320.00 410.00 500.00 590.00 680.00 770.00 860.00 950.00

II-H

TEMPERATURE (C)

JKW

FILE: TM246.DT

DTA

14.09

2.00

TMI #265

WT: 14.70 mg

SCAN RATE: 10.00 deg/min

ATMOSPHERE: AIR 0 cc/min

<ENDO

MICAL/SEC

1.00

0.00

60.00

150.00

240.00

330.00

420.00

510.00

600.00

690.00

780.00

870.00

960.00

H-12

JKW

FILE: 265.DT

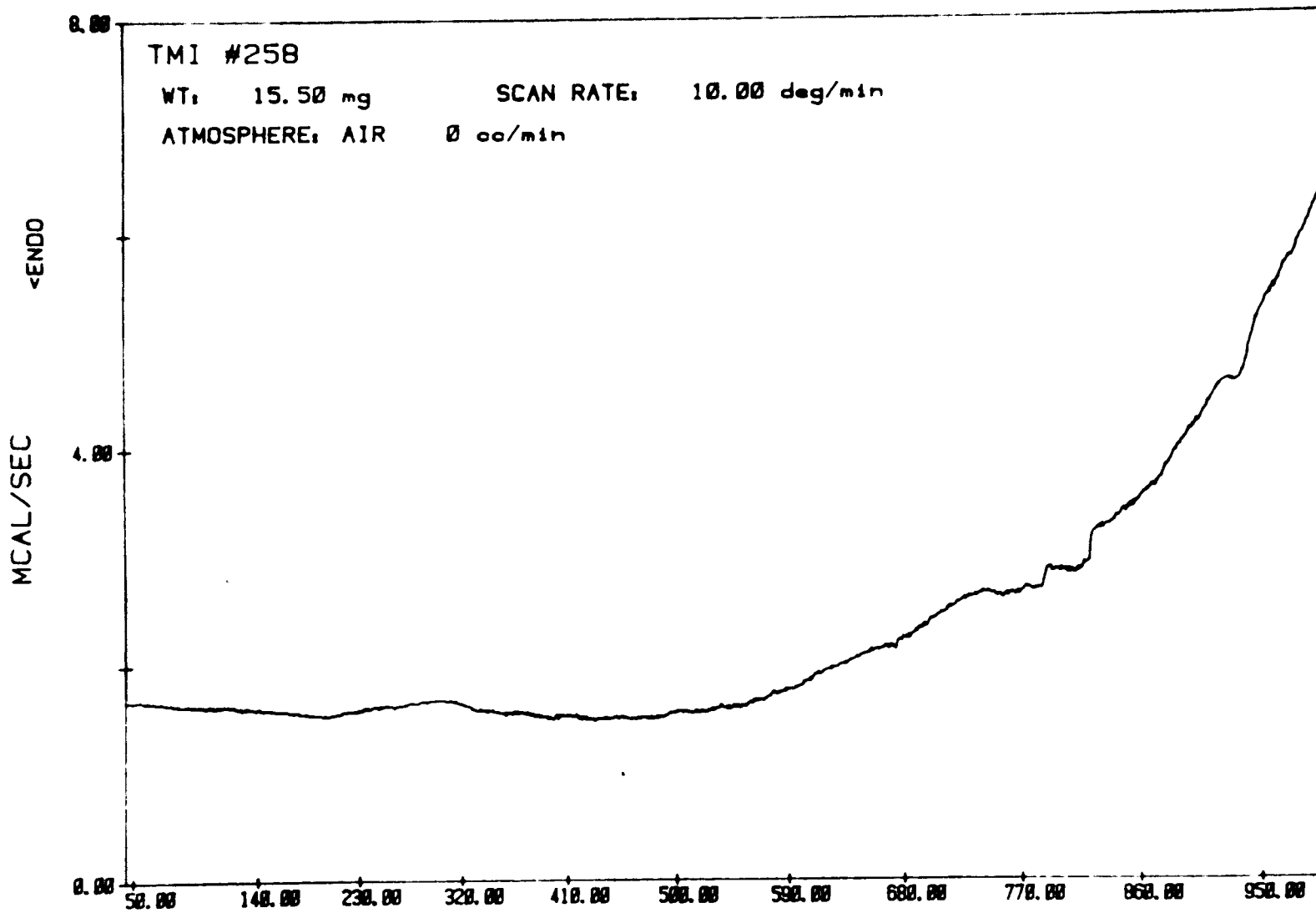
TEMPERATURE (C)

DTA

DATE

01/09/85

TIME: 14:49



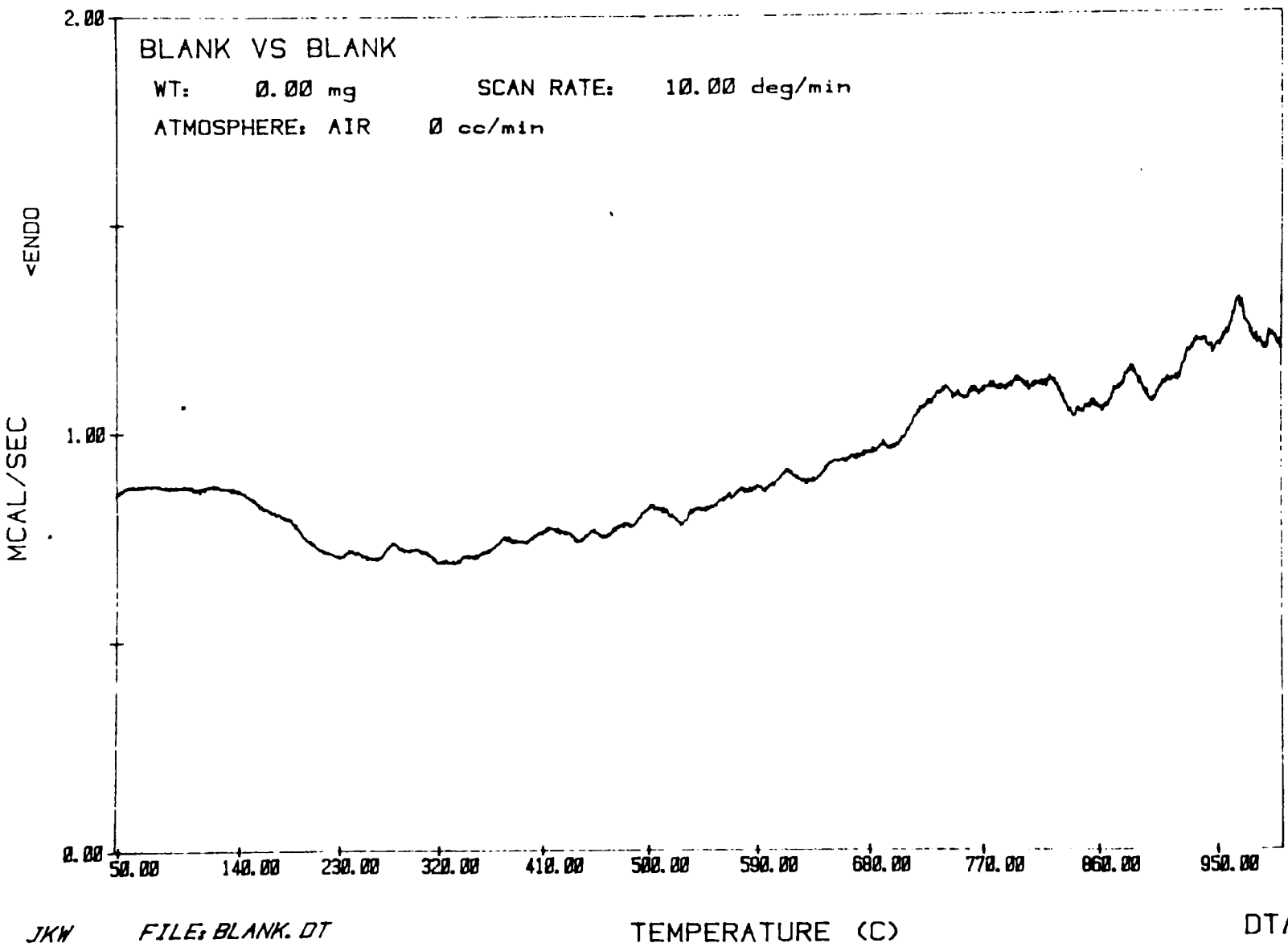
JKW

FILE, TM258. DT

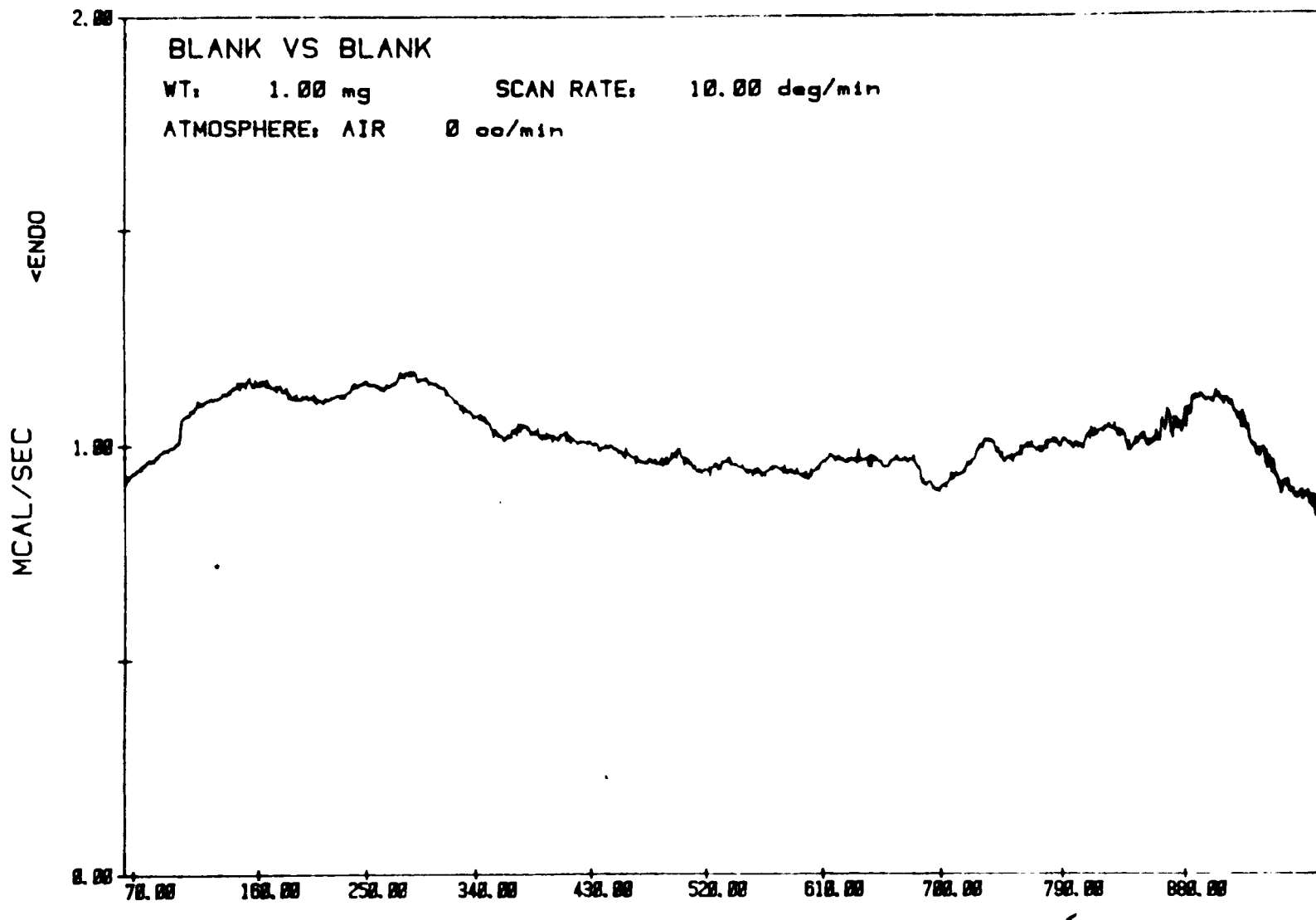
TEMPERATURE (C)

DTA

-- **2010-02-22** **12:44**



SI-H



JKW FILE: 2BLK.DT

DATE: 01/00/11 TIME: 09:21

TEMPERATURE (C)

